

Pediatric Radiology Casebase

Charles A. James

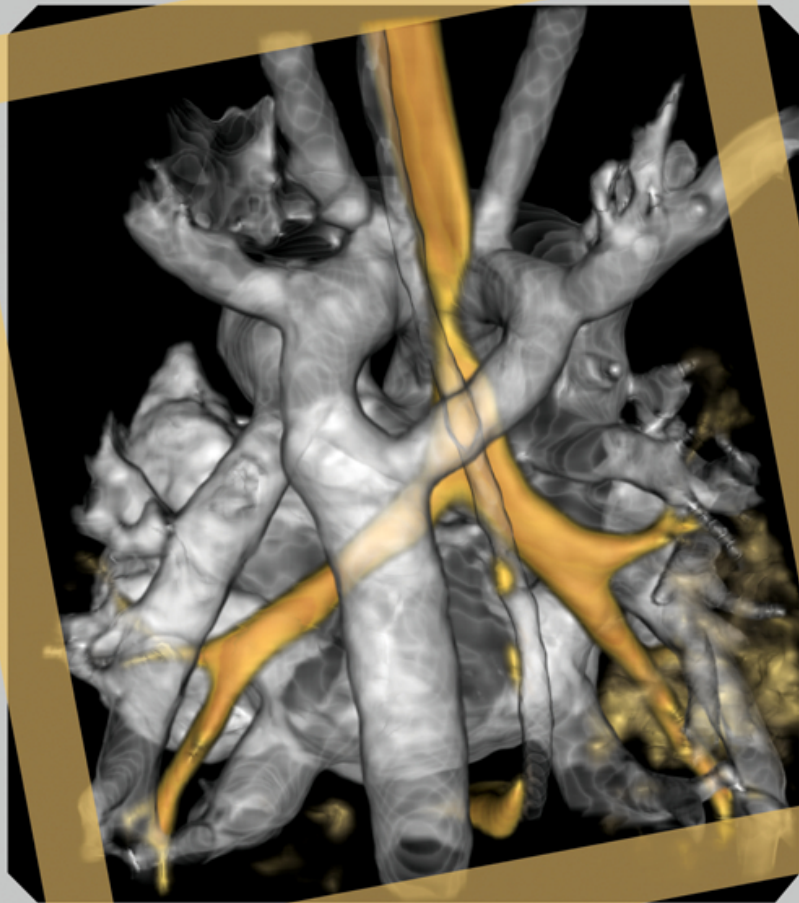
Leah E. Braswell

Charles M. Glasier

S. Bruce Greenberg

Joanna J. Seibert

2nd Edition



MediaCenter.thieme.com
includes videos online



Thieme

Access videos of dynamic imaging findings on MediaCenter.thieme.com!

Simply visit MediaCenter.thieme.com and, when prompted during the registration process, enter the code below to get started today.

BAF5-3PGQ-64BK-4NJ9

Pediatric Radiology Casebase

2nd Edition

Charles A. James, MD, FACR

Professor of Radiology
University of Arkansas for Medical Sciences
The Lee Roy and Melba T. Beasley Endowed Chair
in Pediatric Radiology
Arkansas Children's Hospital
Little Rock, Arkansas, USA

Leah E. Braswell, MD

Assistant Professor of Radiology
Associate Program Director, Radiology Residency
University of Arkansas for Medical Sciences
Director of Pediatric Interventional Radiology
Arkansas Children's Hospital
Little Rock, Arkansas, USA

Charles M. Glasier, MD, FACR

Professor of Radiology and Pediatrics
University of Arkansas for Medical Sciences
Director of Neurologic Imaging
Arkansas Children's Hospital
Little Rock, Arkansas, USA

S. Bruce Greenberg, MD

Professor of Radiology
University of Arkansas for Medical Sciences
Director of Cardiovascular Imaging
Arkansas Children's Hospital
Little Rock, Arkansas, USA

The Rev. Joanna J. Seibert, MD

Professor of Radiology and Pediatrics
University of Arkansas for Medical Sciences
Staff Pediatric Radiologist
Arkansas Children's Hospital
Little Rock, Arkansas, USA

Thieme

New York • Stuttgart • Delhi • Rio de Janeiro

Executive Editor: William Lamsback
Managing Editor: J. Owen Zurhellen IV
Director, Editorial Services: Mary Jo Casey
Vice President, Editorial and Electronic Product Development:
Vera Spillner
Production Editor: Barbara A. Chernow
International Production Director: Andreas Schabert
International Marketing Director: Fiona Henderson
Director of Sales, North America: Mike Roseman
International Sales Director: Louisa Turrell
Senior Vice President and Chief Operating Officer: Sarah Vanderbilt
President: Brian D. Scanlan
Compositor: Carol Pierson, Chernow Editorial Services, Inc.

Library of Congress Cataloging-in-Publication Data

Pediatric radiology casebase / [edited by] Charles A. James,
Leah E. Braswell, Charles M. Glasier, S. Bruce Greenberg,
Joanna J. Seibert. — Second edition.

p. ; cm.

Includes index.

ISBN 978-1-60406-907-5 (alk. paper) —

ISBN 978-1-60406-908-2 (eISBN)

I. James, Charles A., editor. II. Braswell, Leah E., editor.
III. Glasier, Charles M., editor. IV. Greenberg, S. Bruce, editor.
V. Seibert, Joanna J., editor.

[DNLM: 1. Diagnostic Imaging—Case Reports. 2. Child.
3. Diagnosis, Differential—Case Reports. 4. Infant. WN 240]
RJ51.D5

618.92'00754—dc23

2015003160

Important note: Medicine is an ever-changing science undergoing continual development. Research and clinical experience are continually expanding our knowledge, in particular our knowledge of proper treatment and drug therapy. Insofar as this book mentions any dosage or application, readers may rest assured that the authors, editors, and publishers have made every effort to ensure that such references are in accordance with **the state of knowledge at the time of production of the book.**

Nevertheless, this does not involve, imply, or express any guarantee or responsibility on the part of the publishers in respect to any dosage instructions and forms of applications stated in the book. **Every user is requested to examine carefully** the manufacturers' leaflets accompanying each drug and to check, if necessary in consultation with a physician or specialist, whether the dosage schedules mentioned therein or the contraindications stated by the manufacturers differ from the statements made in the present book. Such examination is particularly important with drugs that are either rarely used or have been newly released on the market. Every dosage schedule or every form of application used is entirely at the user's own risk and responsibility. The authors and publishers request every user to report to the publishers any discrepancies or inaccuracies noticed. If errors in this work are found after publication, errata will be posted at www.thieme.com on the product description page.

Some of the product names, patents, and registered designs referred to in this book are in fact registered trademarks or proprietary names even though specific reference to this fact is not always made in the text. Therefore, the appearance of a name without designation as proprietary is not to be construed as a representation by the publisher that it is in the public domain.

Copyright ©2016 by Thieme Medical Publishers, Inc.
Thieme Publishers New York
333 Seventh Avenue, New York, NY 10001
USA +1 800 782 3488, customerservice@thieme.com

Thieme Publishers Stuttgart
Rüdigerstrasse 14, 70469 Stuttgart, Germany
+49 [0]711 8931 421, customerservice@thieme.de

Thieme Publishers Delhi
A-12, Second Floor, Sector-2, Noida-201301
Uttar Pradesh, India
+91 120 45 566 00, customerservice@thieme.in

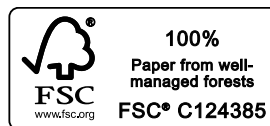
Thieme Publishers Rio de Janeiro, Thieme Publicações Ltda.
Argentina Building 16th floor, Ala A,
228 Praia do Botafogo
Rio de Janeiro 22250-040 Brazil
+55 21 3736-3631

Printed in China by Everbest Printing Ltd.

5 4 3 2 1

ISBN 978-1-60406-907-5

Also available as an e-book:
eISBN 978-1-60406-908-2



This book, including all parts thereof, is legally protected by copyright. Any use, exploitation, or commercialization outside the narrow limits set by copyright legislation without the publisher's consent is illegal and liable to prosecution. This applies in particular to photostat reproduction, copying, mimeographing or duplication of any kind, translating, preparation of microfilms, and electronic data processing and storage.

To our children, who remind us to treat each patient as our own family.

To our spouses, who support educational efforts that extend beyond the workday.

To the radiology residents and fellows at the University of Arkansas for Medical Sciences,
who challenge us to stay current in our subspecialty as we learn from and teach them.

To the pediatricians, pediatric subspecialty staff, pediatric radiology department, and Arkansas Children's Hospital staff,
who support us in our efforts to provide high-quality integrated care of children.

Finally, to our patients and their families. May we get the right answer and improve their care and outcome.

Contents

Menu of Accompanying Videos	xiii
Foreword <i>by Marilyn J. Goske</i>	xv
Preface	xvii
Acknowledgments	xix

Section I Brain

Raghu H. Ramakrishnaiah

1 Vein of Galen Malformation	3
2 Sagittal Craniosynostosis	5
3 Periventricular Leukomalacia	7
4 Septo-Optic Dysplasia	9
5 Craniopharyngioma	11
6 Coronal Craniosynostosis	13
7 Child Abuse: Cerebral Injury	15
8 Subependymal Gray Matter Heterotopias	17
9 Cytomegalovirus Encephalitis	19
10 Holoprosencephaly	21
11 Agenesis of the Corpus Callosum	23
12 Occipital Encephalocele	25
13 Polymicrogyria	27
14 Neurofibromatosis Type 1	29
15 Canavan Disease	31
16 Mitochondrial Disease: Leigh Disease	33
17 Subdural Empyema	35
18 Hypothalamic Astrocytoma	37
19 Ependymoma	39
20 Lissencephaly	41
21 Moyamoya Disease	43
22 Subependymal/Intraventricular Hemorrhage	45
23 Nasal Dermal Sinus/Dermoid Cyst	47
24 Schizencephaly	49
25 Sturge-Weber Syndrome	51
26 Brain Abscess	53
27 Medulloblastoma	55
28 Cerebellar Pilocytic Astrocytoma	57
29 Tuberous Sclerosis	59

Section II Spine

Sumit Singh

30 Brachial Plexopathy: Birth Injury	63
31 Epidural Abscess	65

32	Currarino Triad	67
33	Neurofibromatosis Type 1	69
34	Traumatic Atlanto-Occipital Dislocation	71
35	Sacroccygeal Teratoma	73
36	Chance Fracture	75
37	Down Syndrome: Atlantoaxial Instability	77
38	Vertebral Osteomyelitis	79
39	Myelomeningocele/Chiari II Malformation	81
40	Diastematomyelia	83
41	Tethered Spinal Cord	85
42	Vertebra Plana	87
43	Neurofibromatosis Type 2	89
44	Dermal Sinus with Intraspinal Epidermoid/Infection	91
45	Spinal Cord Tumor: Astrocytoma	93

Section III Head and Neck

Ruba Khasawneh

46	Orbital Cellulitis	97
47	Choanal Atresia	99
48	Infectious Mononucleosis	101
49	Branchial Cleft Cyst Type II	103
50	External Auditory Canal Atresia	105
51	Orbital Metastasis: Leukemia	107
52	Fibromatosis Colli	109
53	Juvenile Nasopharyngeal Angiofibroma	111
54	Retropharyngeal Abscess	113
55	Rhabdomyosarcoma	115
56	Antrochoanal Polyp	117
57	Hemangioma	119
58	Epiglottitis	121
59	Middle Ear Cholesteatoma	123
60	Croup	125
61	Temporal Bone Fracture	127
62	Thyroglossal Duct Cyst	129

Section IV Gastrointestinal

Scott A. Lile and Ananth Ravi

63	Intussusception	133
64	Foreign Body Ingestion	137
65	Meconium Ileus	141
66	Pyloric Stenosis	143
67	Small Bowel Atresia	145
68	Hirschsprung Disease	147
69	Meconium Plug Syndrome	149
70	Duplication Cyst	151

71	Meckel's Diverticulum	153
72	Imperforate Anus	155
73	Appendicitis	159
74	Choledochal Cyst	161
75	Necrotizing Enterocolitis	163
76	Biliary Atresia	165
77	Duodenal Atresia	167
78	Esophageal Atresia with Tracheoesophageal Fistula	169
79	Duodenal Hematoma	173
80	Crohn's Disease	175
81	Malrotation with Midgut Volvulus	177
82	Hepatoblastoma	181

Section V Genitourinary

Leann E. Linam and Nadir Khan

83	Torsion of the Appendix Testis	185
84	Adrenal Hemorrhage	187
85	Wilms' Tumor	189
86	Collecting System Duplication/Ectopic Ureter/Ureterocele	191
87	Posterior Urethral Valves	195
88	Urachal Anomalies	199
89	Hydrocolpos	203
90	Ovarian Cyst	205
91	Neuroblastoma	207
92	Autosomal Recessive Polycystic Kidney Disease	211
93	Vesicoureteral Reflux	213
94	Ovarian Torsion	217
95	Urolithiasis	219
96	Megaureter	221
97	Acute Pyelonephritis	223
98	Mesoblastic Nephroma	225
99	Ureteropelvic Junction Obstruction	227
100	Cortical Scarring	231
101	Autosomal Dominant Polycystic Kidney Disease	233
102	Rhabdomyosarcoma	235
103	Multicystic Dysplastic Kidney	237
104	Testicular Torsion	241

Section VI Bone

Robert F. Buchmann and Mary B. Moore

105	Elbow Fracture	245
106	Langerhans Cell Histiocytosis	247
107	Tarsal Coalition	249
108	Ewing Sarcoma	251
109	Developmental Dysplasia of the Hip	253

110	Toddler Fracture	255
111	Juvenile Idiopathic Arthritis.....	257
112	Legg-Calvé-Perthes Disease	261
113	Child Abuse.....	263
114	Chondroblastoma	267
115	Osteomyelitis	269
116	Slipped Capital Femoral Epiphysis	271
117	Physal Fracture	273
118	Osteosarcoma.....	275

Section VII Chest

Shilpa V. Hegde and Chetan C. Shah

119	Foreign Body Aspiration	279
120	Respiratory Distress Syndrome	283
121	Lymphoma	285
122	Congenital Pulmonary Airway Malformation	287
123	Round Pneumonia.....	289
124	Pulmonary Sequestration	291
125	Bronchogenic Cyst.....	293
126	Posterior Mediastinal Mass: Neuroblastoma.....	295
127	Teratoma	297
128	Cystic Fibrosis.....	299
129	Congenital Diaphragmatic Hernia	301
130	Sickle Cell Disease: Acute Chest Syndrome	303
131	Meconium Aspiration	305
132	Congenital Lobar Overinflation.....	307

Section VIII Cardiac

Sadaf T. Bhutta

133	Double Aortic Arch	311
134	Ventricular Septal Defect	313
135	Tetralogy of Fallot	317
136	Cardiomyopathy	319
137	D-Transposition of the Great Vessels	323
138	Hypoplastic Left Heart Syndrome.....	325
139	Pulmonary Sling	327
140	Total Anomalous Pulmonary Venous Return.....	329
141	Bicuspid Aortic Valve	331
142	Heterotaxy	333
143	Coarctation of the Aorta	335

Section IX Interventional Radiology

Leah E. Braswell

144	Percutaneous Cecostomy	339
145	Abscess Drainage.....	341

146	Embolization of Hemoptysis	343
147	Sclerotherapy: Venous Malformation	345
148	Gastrojejunostomy	347
149	Osteoid Osteoma Ablation	349
150	Parapneumonic Pleural Effusion.....	353
151	Peripherally Inserted Central Venous Catheter.....	355
152	Renovascular Hypertension	357
153	Sclerotherapy: Lymphatic Malformation	359
154	Percutaneous Nephrostomy.....	361
155	Septic Arthritis.....	363

Section X Syndromes

Chinar Lath and Joanna J. Seibert

156	Achondroplasia	367
157	Osteopetrosis	369
158	Cleidocranial Dysplasia	371
159	Thanatophoric Dysplasia.....	373
160	Osteogenesis Imperfecta.....	375
161	Mucopolysaccharidosis Type I.....	379
162	Chondrodysplasia Punctata	381
163	Chondroectodermal Dysplasia.....	383
164	Myositis Ossificans Progressiva.....	385
165	Thrombocytopenia–Absent Radius	387
166	Polyostotic Fibrous Dysplasia.....	389
167	Noonan Syndrome	393
	Index.....	395

Menu of Accompanying Videos

Video 1.1a–d A 6-year-old boy with macrocephaly and headaches. Lateral (**Video 1.1a**) and anteroposterior (AP) (**Video 1.1b**) right internal carotid artery angiograms show dilated anterior circulation feeders and arteriovenous shunting into an enlarged vein of Galen malformation. Lateral (**Video 1.1c**) and AP (**Video 1.1d**) left vertebral artery angiograms show enlarged posterior circulation feeders supplying the vein of Galen malformation and retrograde sagittal sinus contrast flow.

Video 7.1 Head computed tomography (CT) with three-dimensional (3D) reconstruction in a 16-month-old boy with forearm fracture and retinal hemorrhages. Complex left parietal bone fracture is seen, with fracture lines extending into the coronal, squamosal, and lambdoid sutures delineated in this projection.

Video 21.1 A 2-year-old boy with past history of seizures and surgical treatment for moyamoya disease. AP angiogram of the left internal carotid artery (LICA) shows intracranial LICA occlusion, adjacent small-vessel collateral artery branches, and postsurgical transcalvarial arterial flow via the left external carotid artery branches.

Video 41.1 Normal conus: longitudinal spine ultrasound in a 7-week-old boy with sacral dimple shows normal mobility of the conus which is located at the lower limits of normal (L2–L3 level).

Video 41.2 Tethered cord: longitudinal spine ultrasound in a 2-day-old boy with cloacal anomaly. The low-lying spinal cord (L4 vertebra level) is fixed in a dorsal location consistent with a tethered spinal cord.

Video 52.1 A 6-week-old girl with right neck mass. Ultrasound shows enlargement and heterogeneity of the midportion of the right sternocleidomastoid muscle.

Video 53.1a,b Lateral external carotid artery angiogram (same patient as in the book's **Fig. 53.1**) shows a lobular vascular mass arising from enlarged branches of the distal internal maxillary artery (**Video 53.1a**). Lateral external carotid artery angiogram in this same patient following microcatheter embolization (**Video 53.1b**) with 300- to 500- μ m polyvinyl alcohol particles shows that the vascular mass has been devascularized.

Video 63.1a,b A 10-month-old girl with vomiting and dehydration. Transverse ultrasound through the lesion (**Video 63.1a**) shows a circular hypoechoic thickened bowel layer surrounding a central crescent of echogenicity. Tangential-view ultrasound (**Video 63.1b**) shows longitudinal bowel thickening continuous with an oval obstructing intraluminal lesion.

Video 66.1 Normal pylorus: ultrasound shows nonobstructed flow of echogenic gastric contents through a morphologically normal pylorus.

Video 66.2 Pyloric stenosis: ultrasound shows the lack of gastric content passage through an abnormally thickened and elongated pylorus.

Video 73.1a,b A 3-year-old boy with fever, vomiting, and severe lower abdomen pain. Transverse ultrasound image of the right pelvis (**Video 73.1a**) shows a circular noncompressible dilated appendix with surrounding echogenic edema. Localized hypoechoic ascites anterior to the dilated appendix, mass effect on the lateral bladder wall, and echogenic debris in the bladder lumen are noted. Color flow ultrasound at the same site (**Video 73.1b**) shows hyperemic inflammatory changes medial to the iliac vessels surrounding the dilated appendix. Perforated appendicitis was confirmed at laparoscopic appendectomy.

Video 97.1 A 12-year-old girl with meningitis and urinary tract infection (UTI). Color flow ultrasound images show increased echogenicity and decreased vascularity of the left lower pole, consistent with acute pyelonephritis.

Video 104.1 Transverse scrotal ultrasound shows absence of color flow vascularity within an enlarged left testicle, consistent with testicular torsion. Normal color flow vascularity in the right testicle and small left hydrocele are noted.

Video 109.1 Transverse hip ultrasound with stress application in a 3-week-old girl with a history of breech delivery. Increased hip subluxation with stress application is seen in this newborn with developmental dysplasia of the hip.

Video 111.1a,b A 10-year-old girl with bilateral knee-joint swelling and pain. Color flow ultrasound of the right knee (**Video 111.1a**) shows thickened hyperemic synovium. Contrast injected under roadmap fluoroscopy (**Video 111.1b**) outlines irregular synovium prior to knee-joint steroid injection.

Video 111.2 Ultrasound-guided elbow-joint injection in a different 17-year-old patient with juvenile idiopathic arthritis (JIA) shows echogenic intra-articular needle and joint-capsule distention with steroid injection.

Video 132.1 Coronal reformatted cine images of the chest (same patient as in the book's **Fig. 132.1**) show mediastinal shift secondary to a hyperinflated left upper lobe. The left upper lobe has decreased parenchymal density with attenuated vessels.

Video 133.1a,b A 5-day-old with respiratory distress. Axial computed tomography angiography (CTA) images (**Video 133.1a**) show a double aortic arch with localized tracheal narrowing. Three-dimensional volume-rendered CTA (**Video 133.1b**) shows the vascular ring encircling the trachea.

Video 139.1a,b A 10-year-old boy with cough, dysphagia, intermittent wheezing, and recurrent pneumonias (same patient as in the book's **Fig. 139.1**). Axial CTA images (**Video 139.1a**)

show anomalous origin of the left pulmonary artery from the right pulmonary artery and associated mass effect on the airway. Three-dimensional reformats of dynamic pulmonary imaging (**Video 139.1b**) demonstrate distal tracheomalacia and proximal left main bronchomalacia.

Video 143.1 Three-dimensional reformats of CTA in an 18-year-old woman with bicuspid aortic valve. There is coarctation of the aorta with post-stenotic dilatation. The ascending aorta and left subclavian artery are also dilated.

Video 144.1a,b A 17-year-old girl has fecal incontinence and chronic constipation secondary to spina bifida. Fluoroscopic contrast injection through a micropuncture dilator (**Video 144.1a**) confirms intraluminal cecal location. Two retention sutures are deployed through the dilator with guidewire advancement (**Video 144.1b**).

Video 144.2 Fluoroscopic image in another patient with mature cecostomy tract shows distal coil formation of a low-profile Chait trapdoor cecostomy tube with guidewire removal.

Video 145.1 A 14-year-old girl with fever and left pelvic complex fluid collection. Procedural ultrasound imaging guides echogenic guidewire advancement within the abscess. Following 10-French drain placement, 120 mL of purulent fluid was aspirated.

Video 147.1 Intraoperative ultrasound image shows a linear echogenic needle/laser fiber within an oval hypoechoic venous malformation. Dynamic echogenic treatment response near the laser tip with interstitial laser therapy is displayed.

Video 151.1 A 5-year-old girl with pneumonia and respiratory failure needs stable long-term venous access. Transverse ultrasound imaging of the left arm guides echogenic needle puncture and advancement within the left basilic vein. Acoustic fall-off deep to the needle and pulsating left brachial artery lateral to the basilic vein are noted.

Foreword

In 2007, I was studying for renewal of my Certificate of Added Qualification exam in Pediatric Radiology as part of the process of recertification by the American Board of Radiology. One of the first references I turned to was *Pediatric Radiology Casebase*, first edition, edited by Dr. Joanna J. Seibert and Dr. Charles A. James from Arkansas Children's Hospital. I reviewed the cases in CD-ROM format because the ABR exam was transitioning to computerized testing, and I felt the consistency of presentation would be beneficial to my study. I found this educational resource to be straightforward and fun. The cases presented in the books were "classics," by which I mean those diagnoses that all pediatric radiologists should be mastering. The book and CD were manageable for my crazy schedule. Instead of thousands of pages of esoteric diagnoses, the number of cases to be reviewed could fit easily into my busy days. The cases ranged from simple to complex and were perfect as a study guide. Further, I knew, admired, and respected Joanna Seibert, Past President of the Society for Pediatric Radiology and a highly regarded educator, radiologist, and ultrasonographer. I was also familiar with the pediatric interventional radiology leadership of Charles James, as I had supervised his Pediatric IR committee contributions during my term as President of the Society for Pediatric Radiology. On completing my Pediatric Radiology recertification exam, I felt that this type of textbook should be available to learners for many years into the future.

This second edition of *Pediatric Radiology Casebase* is truly an improvement. The cases are selected to provide the full range of pediatric disorders, including congenital, developmental, and metabolic disorders. This concise and practical book was revised with attention to greater consistency of the

text and improved image quality. Every image in the book has been updated to the highest quality. There are new digital movie files that enhance the display of dynamic findings, such as bowel motion and vascular flow. Three-dimensional surface-rendered images are used effectively in the cardiac imaging section. The text is written by 15 contributing authors with years of varied experience and 5 editors with established subspecialty expertise. All of the text has either been rewritten or is new to this edition.

What I find most valuable is that the book is casebased. Each case is presented in a well-organized fashion that allows the reader to interact with the case as is most meaningful for adult learners. The self-study format allows the learner to garner as much information as needed prior to making a diagnosis and then comparing it to that of the experts. The book is divided into 10 sections based on anatomy and includes highlights on a wide variety of diseases, including focused discussions on the genitourinary, gastrointestinal, pulmonary, cardiac, musculoskeletal, and nervous systems. Special attention is paid to the key role that interventional radiology now plays in pediatric disease and treatment.

I highly recommend this book. It will provide medical students and radiology trainees a highly efficient review for radiology board preparation and can be used by practicing radiologists as well.

Marilyn J. Goske, MD
Professor of Radiology and Pediatrics
Corning Benton Chair for Radiology Education, Emeritus
Cincinnati Children's Hospital Medical Center
Cincinnati, Ohio, USA

Preface

In the late 1980s, *Casebase Pediatric Radiology*, first edition, was written to provide a practical textbook to guide radiology students and those imaging children in daily practice. All text documents were produced on a typewriter, and all images were submitted to the publisher as 5×7-inch glossy prints. Between 2000 and 2010 growing interest for a second edition was identified, and an enthusiastic team of university-based pediatric radiologists at Arkansas Children's Hospital was assembled to undertake it. The goal from the start of this project was to update all text content, to seek current/pertinent references, and to include all new images with improved and consistent image quality.

As in the first edition, cases are divided into nine anatomic sections and are organized by clinical presentation, radiographic findings, diagnosis, discussion/differential diagnosis, pearls, pitfalls, and references. Cases cover a wide range of congenital anomalies, infections, trauma, tumors, syndromes, and metabolic conditions encountered when caring for pediatric patients. We believe this new and improved edition will aid in preparing radiology residents and pediatric radiology fellows for certification examinations, and will aid experienced pediatric radiology practitioners who are seeking recertification. The diagnosis is deliberately excluded from the first page

of each case, so that the reader can review the clinical information with the characteristic images provided and try to arrive at a correct diagnosis before reading the explanation in the subsequent text. For general radiologists and pediatricians, a quick review of a comprehensive variety of cases seen in daily pediatric radiology practice is provided.

This new edition features the contributions of many more authors and editors than did the first edition, as the field of radiology has become increasingly subspecialized. All images in this edition were acquired directly in digital format from the picture archiving and communicating system (PACS) that has replaced hardcopy film since the first edition was published. Also, this new edition is available in both the popular hardcopy print version and in digital format for mobile electronic devices. The latter format includes motion files to better display the morphology of some disease entities and to more directly display physiologic states such as altered blood flow and dynamic morphologic changes such as a collapsing trachea.

We hope that this resource will enhance readers' lifelong learning with pediatric disease pattern recognition and provide practical teaching points that are useful during and well beyond the training years.

Acknowledgments

We would like to thank the team at Thieme for maintaining communication and trust with our educational team for nearly two decades. This includes Timothy Hiscock's belief in, and persistence in acquiring, a second edition of this book, the ongoing project supervision of William Lamsback, the capable/accessible project management of Owen Zurhellen and Heather Allen, and the summer intern work of Steven Behm. Luke James restored and converted the previous edition's hardcopy text into an updated digital format, providing the authors with an initial starting point to begin their work on the new edition. Susan Rose offered diligent secretarial support throughout the entire project, particularly in her efficient formatting of all text documents for the second edition. She provided

authors with requested references and dependably formatted the cited references, always working with a smile. Early in the project, Chetan Shah initiated a process for image acquisition from PACS that was utilized by all contributors. Radiology resident Sam McMurphy contributed valuable expertise with AVI file management. We could not have accomplished a primary goal of this project, consistent high-quality images, without the tireless image management work of Donna Ashlock. She processed every TIFF file in this edition, labeling images where directed by the authors, in a conscientious and professional fashion. Finally, we thank Barbara Chernow for efficiently formatting the work into book format and facilitating our review to project completion.

Contributors

Leah E. Braswell, MD

Assistant Professor of Radiology
Associate Program Director, Radiology Residency
University of Arkansas for Medical Sciences
Director of Pediatric Interventional Radiology
Arkansas Children's Hospital
Little Rock, Arkansas, USA

Sadaf T. Bhutta, MBBS

Associate Professor of Radiology
University of Washington
Seattle Children's Hospital
Seattle, Washington, USA

Robert F. Buchmann, DO

Associate Professor of Radiology
University of Arkansas for Medical Sciences
Director of Body Imaging
Arkansas Children's Hospital
Little Rock, Arkansas, USA

Charles M. Glasier, MD, FACP

Professor of Radiology and Pediatrics
University of Arkansas for Medical Sciences
Director of Neurologic Imaging
Arkansas Children's Hospital
Little Rock, Arkansas, USA

S. Bruce Greenberg, MD

Professor of Radiology
University of Arkansas for Medical Sciences
Director of Cardiovascular Imaging
Arkansas Children's Hospital
Little Rock, Arkansas, USA

Shilpa V. Hegde, MBBS, FRCR

Clinical Instructor
University of Arkansas for Medical Sciences
Director of Pulmonary Imaging
Arkansas Children's Hospital
Little Rock, Arkansas, USA

Charles A. James, MD, FACP

Professor of Radiology
University of Arkansas for Medical Sciences
The Lee Roy and Melba T. Beasley Endowed Chair
in Pediatric Radiology
Arkansas Children's Hospital
Little Rock, Arkansas, USA

Nadir Khan, MBBS, FRCR

Consultant Paediatric Radiologist
Royal Stoke University Hospital
University Hospitals of North Midlands NHS Trust
Stoke-on-Trent, Staffordshire, UK

Ruba Khasawneh, MD

Assistant Professor of Radiology
Jordan University of Science and Technology
King Abdullah University Hospital
Irbid, Jordan

Chinar Lath, MD

Instructor in Radiology
Medical College of Wisconsin
Milwaukee, Wisconsin, USA

Scott A. Lile, MD

Assistant Professor of Radiology
University of Arkansas for Medical Sciences
Staff Pediatric Radiologist
Arkansas Children's Hospital
Little Rock, Arkansas, USA

Leann E. Linam, MD

Assistant Professor of Radiology
University of Arkansas for Medical Sciences
Chief of Pediatric Radiology
Arkansas Children's Hospital
Little Rock, Arkansas, USA

Mary B. Moore, MD

Associate Professor of Radiology
University of Arkansas for Medical Sciences
Staff Pediatric Radiologist
Arkansas Children's Hospital
Little Rock, Arkansas, USA

Raghu H. Ramakrishnaiah, MBBS, FRCR

Assistant Professor of Radiology
Program Director, Pediatric Radiology Fellowship
University of Arkansas for Medical Sciences
Arkansas Children's Hospital
Little Rock, Arkansas, USA

Ananth Kumar Ravi, MBBS

Radiology Resident (PEDRAP)
University of Arkansas for Medical Sciences
Arkansas Children's Hospital
Little Rock, Arkansas, USA

The Rev. Joanna J. Seibert, MD

Professor of Radiology and Pediatrics
University of Arkansas for Medical Sciences
Staff Pediatric Radiologist
Arkansas Children's Hospital
Little Rock, Arkansas, USA

Chetan Chandulal Shah, MBBS, B Tech, MBA

Pediatric Neuroradiologist
Nemours, Wolfson Children's Hospital
Faculty, Mayo Clinic
Jacksonville, Florida, USA

Sumit Singh, MD

Assistant Professor of Radiology
University of Arkansas for Medical Sciences
Staff Pediatric Radiologist
Arkansas Children's Hospital
Little Rock, Arkansas, USA

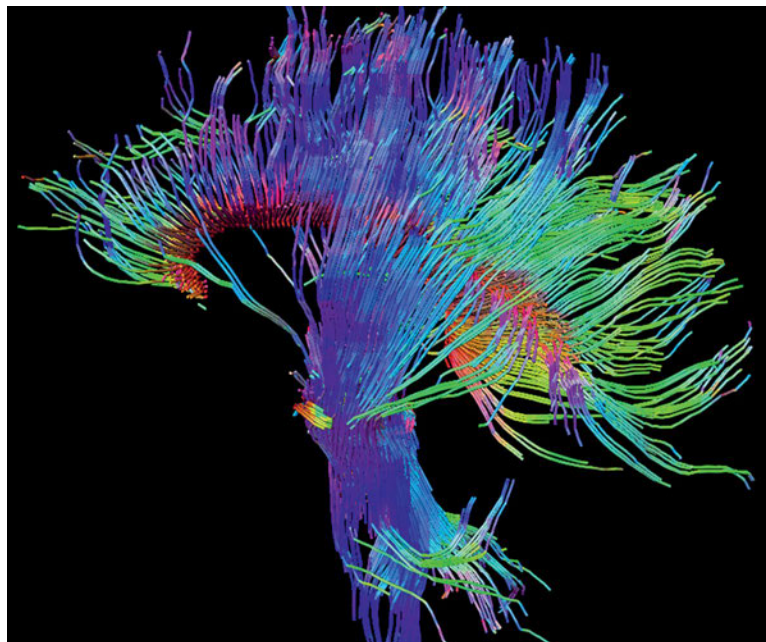
Brain

Section Editor

Charles M. Glasier

Author

Raghu H. Ramakrishnaiah



Case 1

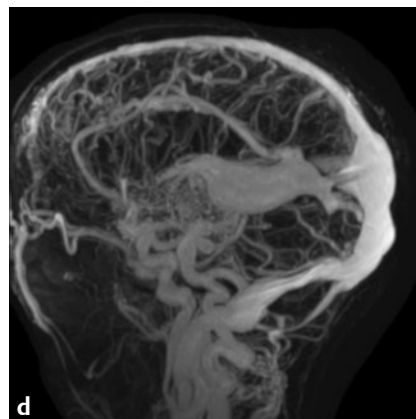
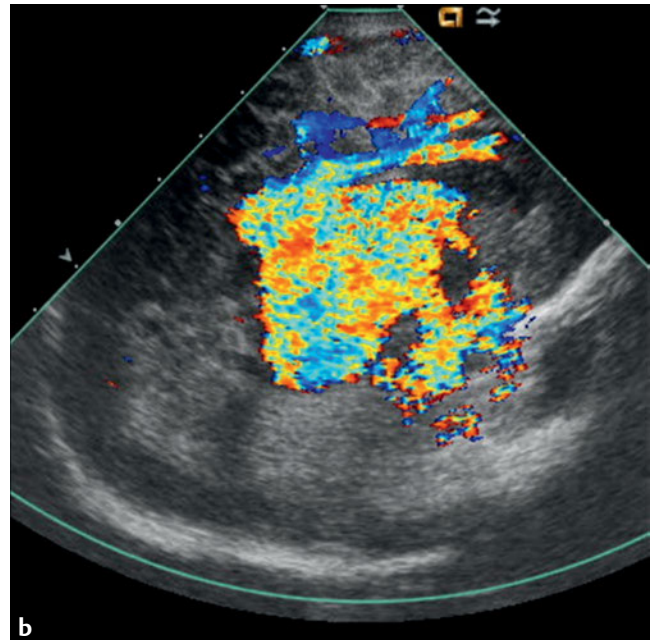
■ Clinical Presentation

A newborn with congestive heart failure.

■ Radiographic Studies

Initial chest radiograph (**Fig. 1.1a**) shows marked cardiomegaly. Sagittal midline color flow ultrasound image (**Fig. 1.1b**, anterior to the right) shows dilated vein of Galen with high flow. Axial T2-weighted magnetic resonance imaging (MRI) (**Fig. 1.1c**) demonstrates bilateral arterial feeders, marked en-

largement of the vein of Galen (*arrows*), and hydrocephalus. Magnetic resonance angiography (MRA) (**Fig. 1.1d**) confirms the vein of Galen malformation with dilated venous outflow. Internal carotid artery angiogram prior to embolization documents the noninvasive imaging findings (**Fig. 1.1e**).



■ Diagnosis

Vein of Galen Malformation



■ Discussion and Differential Diagnosis

Vein of Galen malformations can be divided into direct arteriovenous fistulae and arteriovenous malformations that have venous drainage into the galenic system. Many patients have persistence of fetal drainage such as the persistent falcine vein seen in this case.¹ Patients with vein of Galen malformations usually present in infancy with cardiomegaly, high-output heart failure, and cranial bruit. Older infants and children may present with hydrocephalus secondary to obstruction of the aqueduct of Sylvius. The neonatal cranial Doppler demonstrates extensive aliasing artifacts in the dilated vein of Galen due to turbulence and high flow velocity.¹ Imaging findings on computed tomography angiography (CTA) and MRA include dilated feeding arteries of both the anterior and posterior circulation.

The surrounding brain parenchyma may show encephalomalacia secondary to ischemic changes. Current therapy consists of neurointerventional procedures, including arterial and/or venous embolization using liquid embolic agents or coils.² Ventricular shunting is avoided for treating hydrocephalus in patients with vein of Galen malformation, as this may alter hemodynamics and increase the incidence of intraventricular hemorrhage and complications related to cerebral ischemia.³ Noninvasive imaging studies including cranial ultrasound with color flow/Doppler and MRI/MRA are used to establish the diagnosis. Cerebral angiography is typically reserved for performance of neurointerventional procedures.

Pearl

- ◆ Vein of Galen malformation should be considered in the differential diagnosis of neonates with high-output cardiac failure.

Pitfall

- ◆ Duplex Doppler differentiates congenital cystic masses such as cyst of the superior vermian cistern from high-flow vein of Galen malformations.

References

1. Jones BV, Ball WS, Tomsick TA, Millard J, Crone KR. Vein of Galen aneurysmal malformation: diagnosis and treatment of 13 children with extended clinical follow-up. *AJNR Am J Neuroradiol* 2002;23:1717–1724. [PubMed](#)
2. Mitchell PJ, Rosenfeld JV, Dargaville P, et al. Endovascular management of vein of Galen aneurysmal malformations presenting in the neonatal period. *AJNR Am J Neuroradiol* 2001;22:1403–1409. [PubMed](#)
3. Schneider SJ, Wisoff JS, Epstein FJ. Complications of ventriculoperitoneal shunt procedures or hydrocephalus associated with vein of Galen malformations in childhood. *Neurosurgery* 1992;30:706–708. [PubMed](#)

Case 2

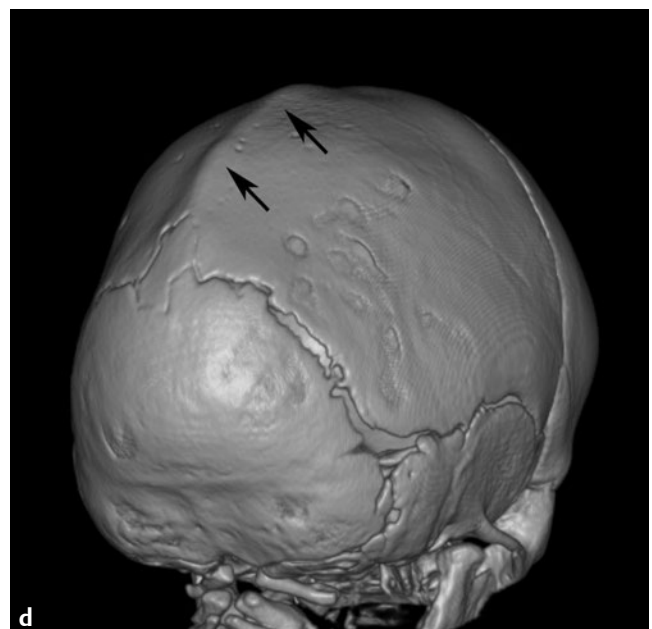
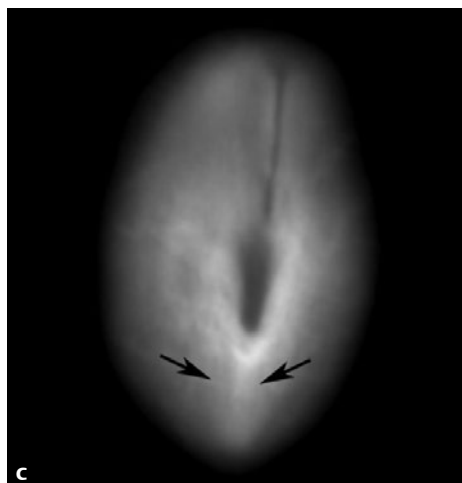
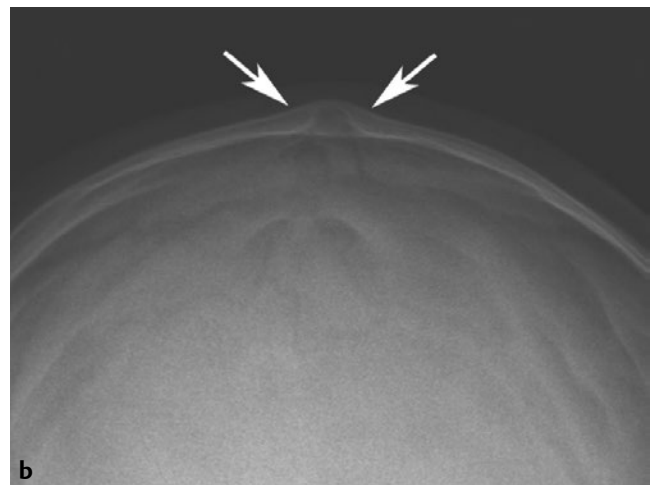
■ Clinical Presentation

An infant with elongated calvaria and palpable bony ridge.

■ Radiographic Studies

Lateral skull radiograph (**Fig. 2.1a**) shows anteroposterior elongation of the calvaria. Towne projection radiograph (**Fig. 2.1b**) shows the bony sutural bar with associated midsagittal ridge (*arrows*). Axial computed tomography (CT) image (**Fig.**

2.1c) near the apex shows straight, knife edge-like suture anteriorly with linear bony sutural fusion posteriorly (*arrows*). Oblique three-dimensional (3D) reconstruction (**Fig. 2.1d**) of the skull clearly demonstrates the midsagittal ridge (*arrows*).



■ Diagnosis

Sagittal Craniosynostosis

■ Discussion and Differential Diagnosis

Sagittal synostosis is the most common form of craniosynostosis with arrest of lateral calvarial growth and continued anteroposterior calvarial growth.¹ This growth asymmetry leads to deformity of the skull known as dolichocephaly (scaphocephaly). Skull radiography in infants with suspected sagittal synostosis is performed to document the clinical diagnosis. Skull shape is key to which sutures are closed. Low-dose CT with 3D reconstruction is performed to better delineate the findings and for surgical planning. Surgical cranioplasty is the treatment.²

A common cause of dolichocephaly not related to sagittal synostosis is positional molding producing mild dolichocephaly in premature infants. This probably relates to long periods of time in the supine position with the head turned to the side on respiratory support in the neonatal nursery.³ Positional molding is not associated with bony bridging of the sagittal suture. Premature sutural closure may be seen secondary to extensive encephalomalacia related to hypoxic-ischemic encephalopathy or following decompression of hydrocephalus. In these patients, sutural hyperostosis is usually absent.

Pearls

- ◆ Normal sutures are never perfectly straight.
- ◆ Most patients with sagittal synostosis are developmentally normal.

Pitfall

- ◆ Closure of all cranial sutures is usually secondary to cerebral atrophy or treated hydrocephalus rather than primary craniosynostosis.

References

1. Medina LS. Three-dimensional CT maximum intensity projections of the calvaria: a new approach for diagnosis of craniosynostosis and fractures. *AJNR Am J Neuroradiol* 2000;21:1951–1954 [PubMed](#)
2. Kirmi O, Lo SJ, Johnson D, Anslow P. Craniosynostosis: a radiological and surgical perspective. *Semin Ultrasound CT MR* 2009;30:492–512 [PubMed](#)
3. Nagaraja S, Anslow P, Winter B. Craniosynostosis. *Clin Radiol* 2013;68:284–292 [PubMed](#)

Case 3

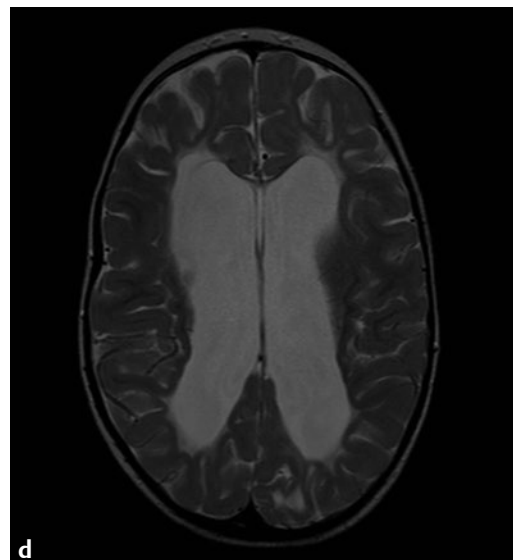
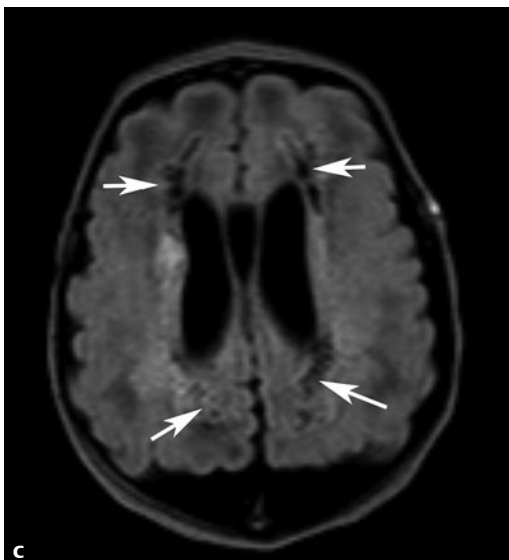
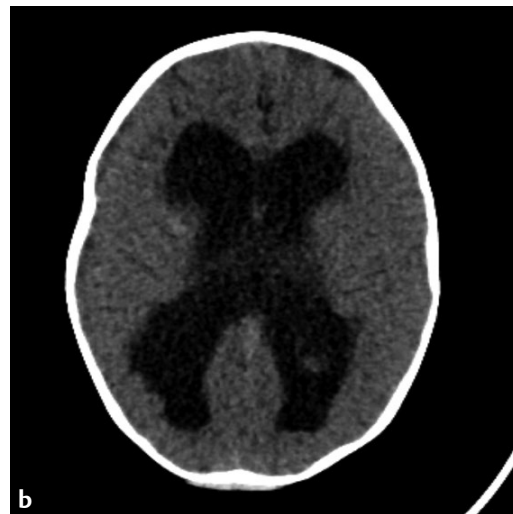
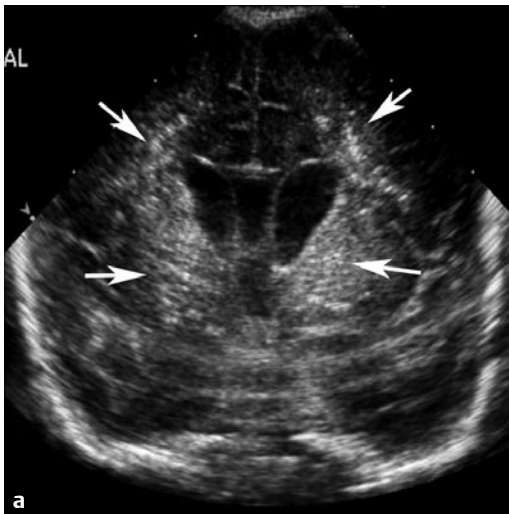
■ Clinical Presentation

A 32-week-gestation, 1,000-g neonate with hyaline membrane disease.

■ Radiographic Studies

Coronal image from cranial ultrasound examination at 1 week of age shows increased clumpy echogenicity in the periventricular white matter and basal ganglia bilaterally (**Fig. 3.1a**, *arrows*). Subsequent CT examination 6 months later shows severe periventricular white matter thinning, ventricular enlargement, and undulation of the ventricular wall secondary to white matter loss (**Fig. 3.1b**). Follow-up MRI shows discrete

cyst formation on fluid-attenuated inversion recovery (FLAIR) sequence (**Fig. 3.1c**, *arrows*) in the periventricular white matter corresponding to the echogenic areas seen in the previous ultrasound examination. Axial T2-weighted MRI demonstrates an irregularly enlarged outline of the lateral ventricles secondary to white matter volume loss (**Fig. 3.1d**); high signal in the periventricular white matter represents gliosis.



■ Diagnosis

Periventricular Leukomalacia

■ Discussion and Differential Diagnosis

Periventricular leukomalacia (PVL) is typically found in preterm infants (less than 33 weeks of gestation/less than 1,500-g birth weight), particularly in those requiring ventilatory support and with cardiopulmonary instability.¹ Damage to the periventricular white matter in PVL is probably related to the vascular border zones in the frontal and peritrigonal white matter and to episodes of hypoxia and hypotension that invariably occur in sick preterm infants. Diffuse cerebral edema is most frequently seen in asphyxiated full-term newborns and usually lacks the “clumpy” appearance of echoden-

sities seen with typical PVL.² Diagnostic considerations in infants with periventricular white matter echodensities on cranial sonography include diffuse cerebral edema and TORCH (toxoplasmosis, other agents, rubella, cytomegalovirus, herpes simplex) infections. TORCH infections are less commonly seen in the preterm infant and may show striations in the basal ganglia and thalamus, subependymal cysts, and focal periventricular echodensities with posterior shadowing representing calcification. A significant percentage of infants with PVL develop cerebral palsy, delayed milestones, and vision deficit.^{2,3}

Pearls

- ◆ Focal, dense increased echogenicity in the periventricular white matter may be the earliest sonographic sign of PVL.
- ◆ Cystic PVL at birth denotes intrauterine injury.
- ◆ MRI is the most sensitive imaging examination.

Pitfalls

- ◆ Serial ultrasound scans may be necessary for diagnosis.
- ◆ Small subependymal cysts should not be confused with PVL, which by definition involves the periventricular white matter.

References

1. Barkovich AJ, Truwit CL. Brain damage from perinatal asphyxia: correlation of MR findings with gestational age. *AJNR Am J Neuroradiol* 1990;11:1087–1096 [PubMed](#)
2. Sie LT, van der Knaap MS, van Wezel-Meijler G, Taets van Amerongen AH, Lafeber HN, Valk J. Early MR features of hypoxic-ischemic brain injury in neonates with periventricular densities on sonograms. *AJNR Am J Neuroradiol* 2000;21:852–861 [PubMed](#)
3. Flodmark O, Lupton B, Li D, et al. MR imaging of periventricular leukomalacia in childhood. *AJR Am J Roentgenol* 1989;152:583–590 [PubMed](#)

Case 4

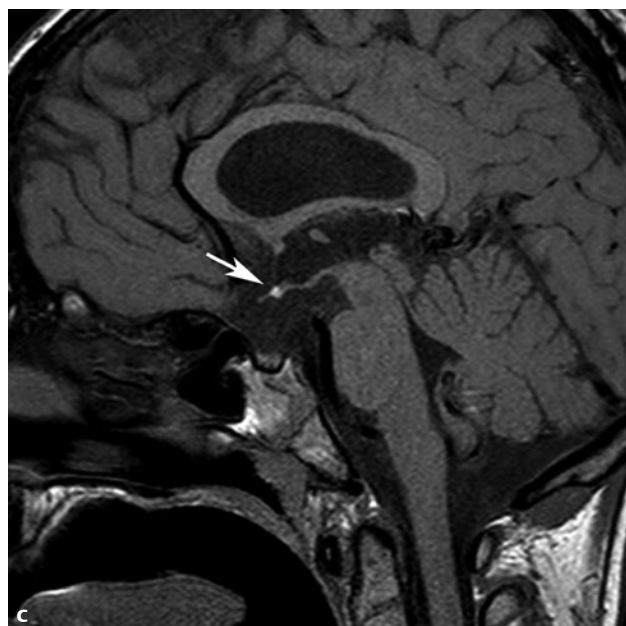
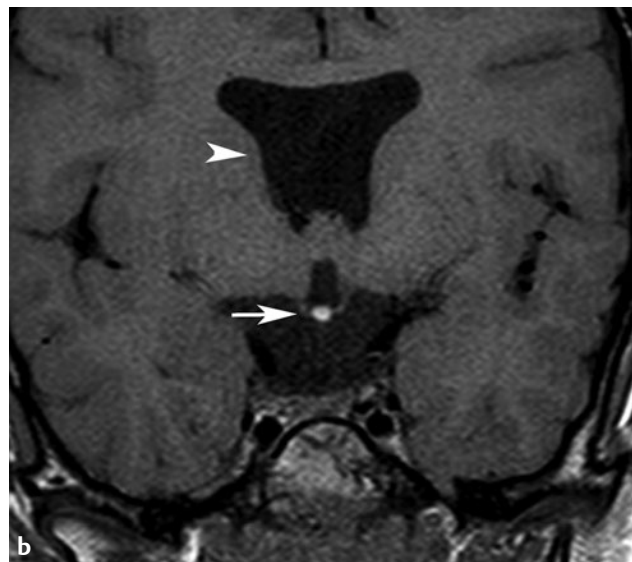
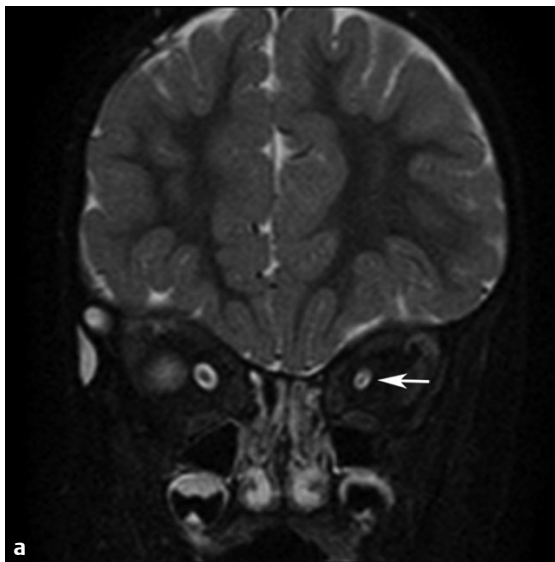
■ Clinical Presentation

A 5-year-old girl with bilateral decreased visual acuity.

■ Radiographic Studies

Coronal fat-suppressed T2-weighted MRI through the orbits shows severely hypoplastic left optic nerve (**Fig. 4.1a, arrow**). Coronal T1-weighted MRI at the level of the suprasellar cistern (**Fig. 4.1b**) demonstrates confluent frontal horns with absence of the septum pellucidum (**arrowhead**) and an ectopic posterior

pituitary bright spot at the hypothalamus (**arrow**). Midline sagittal T1-weighted MRI (**Fig. 4.1c**) shows an ectopic posterior pituitary bright spot (**arrow**) at the hypothalamus and absence of the pituitary infundibulum.



■ Diagnosis

Septo-Optic Dysplasia

■ Discussion and Differential Diagnosis

Optic nerve hypoplasia may occur as an isolated abnormality but frequently occurs in the presence of other cerebral abnormalities, especially absent septum pellucidum, absent/ectopic posterior pituitary, neuronal migration anomalies such as schizencephaly, and perinatal cerebral hemispheric injury.^{1,2} Thinning of the corpus callosum is present in some patients. Patients with absent/ectopic posterior pituitary, absent pituitary infundibulum, and, to a lesser extent, absence of the septum pellucidum, have an increased incidence of neuroendocrine abnormalities.^{1–3} Optic nerve hypoplasia is usually diagnosed by fundoscopic evaluation. High-resolution cranial MRI is used to confirm optic nerve or chiasm hypoplasia as well as to detect associated intracranial abnormalities such as absent/ectopic posterior pituitary and other anomalies.

Pearl

- ◆ High-resolution coronal imaging is necessary to reliably diagnose optic nerve hypoplasia; high-resolution sagittal imaging is needed to evaluate the pituitary.¹

Pitfall

- ◆ Absent septum pellucidum may be seen without optic nerve hypoplasia or other anomalies. Absent septum pellucidum may be an acquired condition in patients with severe hydrocephalus, especially those who have undergone multiple cerebrospinal fluid diversion procedures with damage to septal tissue from shunt catheter placement.

References

1. Ramakrishnaiah RH, Shelton JB, Glasier CM, Phillips PH. Reliability of magnetic resonance imaging for the detection of hypopituitarism in children with optic nerve hypoplasia. *Ophthalmology* 2014;121:387–391. [PubMed](#)
2. Brodsky MC, Glasier CM, Pollock SC, Angtuango EJ. Optic nerve hypoplasia. Identification by magnetic resonance imaging. *Arch Ophthalmol* 1990; 108:1562–1567. [PubMed](#)
3. Phillips PH, Spear C, Brodsky MC. Magnetic resonance diagnosis of congenital hypopituitarism in children with optic nerve hypoplasia. *J AAPOS* 2001;5: 275–280. [PubMed](#)

Case 5

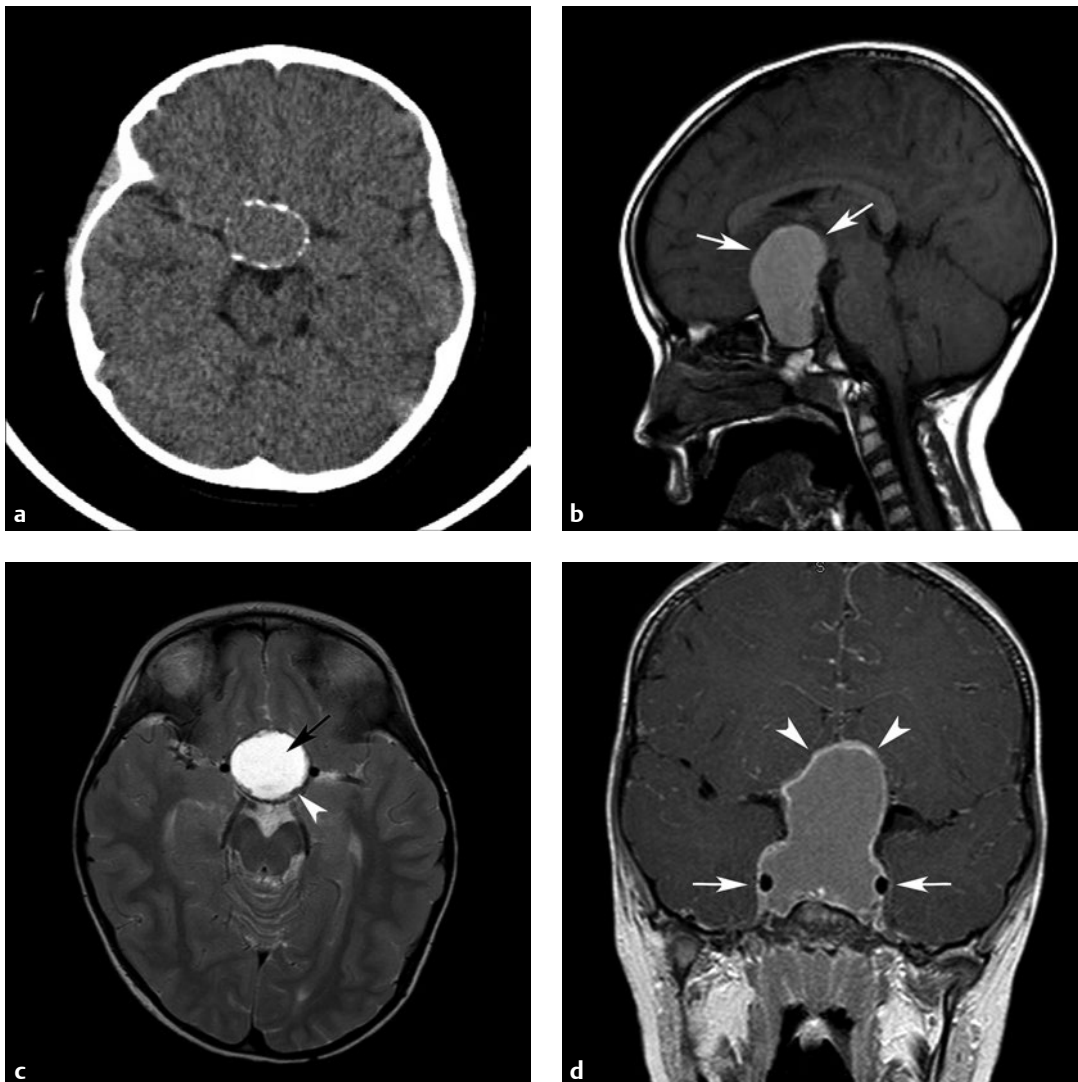
■ Clinical Presentation

A 7-year-old boy with headache, endocrine dysfunction, and visual disturbance.

■ Radiographic Studies

Axial noncontrast head CT shows a suprasellar mass with rim calcification (**Fig. 5.1a**). Sagittal T1-weighted MRI demonstrates a hyperintense mass (*arrows*) arising in the sella with extent into the suprasellar cistern (**Fig. 5.1b**). Axial T2-weighted MRI (**Fig. 5.1c**) shows that most of the mass is cystic and hyperintense to gray matter (*arrow*). The peripheral ir-

regular low signal rim (*arrowhead*) of the mass corresponds to the wall calcification seen on CT. Coronal postgadolinium T1-weighted MRI (**Fig. 5.1d**) shows rim enhancing sellar/suprasellar mass (*arrowheads*) encasing the cavernous internal carotid arteries (*arrows*).



■ Diagnosis

Craniopharyngioma

■ Discussion and Differential Diagnosis

Craniopharyngioma is the most common suprasellar mass in children.¹ Craniopharyngioma has a bimodal pattern of incidence, with an initial peak between the ages of 10 and 15 years and a second peak in middle age. Craniopharyngiomas in children are usually of adamantinomatous type and in adults are usually papillary types.² Up to 90% of craniopharyngiomas are calcified on CT and demonstrate a large cystic component. Calcification is less common in the papillary-type craniopharyngioma which is predominantly solid.¹ High-resolution MRI prior to surgical resection is performed to demonstrate the relationship of the tumor to the optic chiasm, hypothalamus, and adjacent circle of Willis vasculature.^{1,2} Craniopharyngioma cysts are usually hyperintense on T1-weighted MRI sequences. Gadolinium images frequently show

enhancement of the solid components of the tumor and variable rim enhancement of the cyst.^{2,3} Postresection complication includes local tumor recurrence and pseudoaneurysm of the internal carotid arteries.

Suprasellar lesions, including optic/hypothalamic gliomas, germ cell tumors, Rathke cleft cysts, and arachnoid cysts, need to be distinguished from craniopharyngioma. Langerhans cell histiocytosis may present as a mass in the pituitary infundibulum that rarely enlarges to fill the suprasellar cistern. Unusual suprasellar masses include ectopic posterior pituitary tissue, lipomas, and hamartomas of the tuber cinereum, which are typically found in children with precocious puberty. Pituitary macroadenomas, meningiomas, and aneurysms are much less common in children than in adults.

Pearl

- ◆ A calcified suprasellar mass in a child is highly suggestive of craniopharyngioma.¹

Pitfall

- ◆ Calcification may rarely occur in the wall of a Rathke cleft cyst, simulating findings more typically seen in craniopharyngioma.

References

1. Eldevik OP, Blaivas M, Gabrielsen TO, Hald JK, Chandler WF. Craniopharyngioma: radiologic and histologic findings and recurrence. *AJNR Am J Neuroradiol* 1996;17:1427–1439 [PubMed](#)
2. Sartoretti-Schefer S, Wichmann W, Aguzzi A, Valavanis A. MR differentiation of adamantinous and squamous-papillary craniopharyngiomas. *AJNR Am J Neuroradiol* 1997;18:77–87 [PubMed](#)
3. Petito CK. Craniopharyngioma: prognostic importance of histologic features. *AJNR Am J Neuroradiol* 1996;17:1441–1442 [PubMed](#)

Case 6

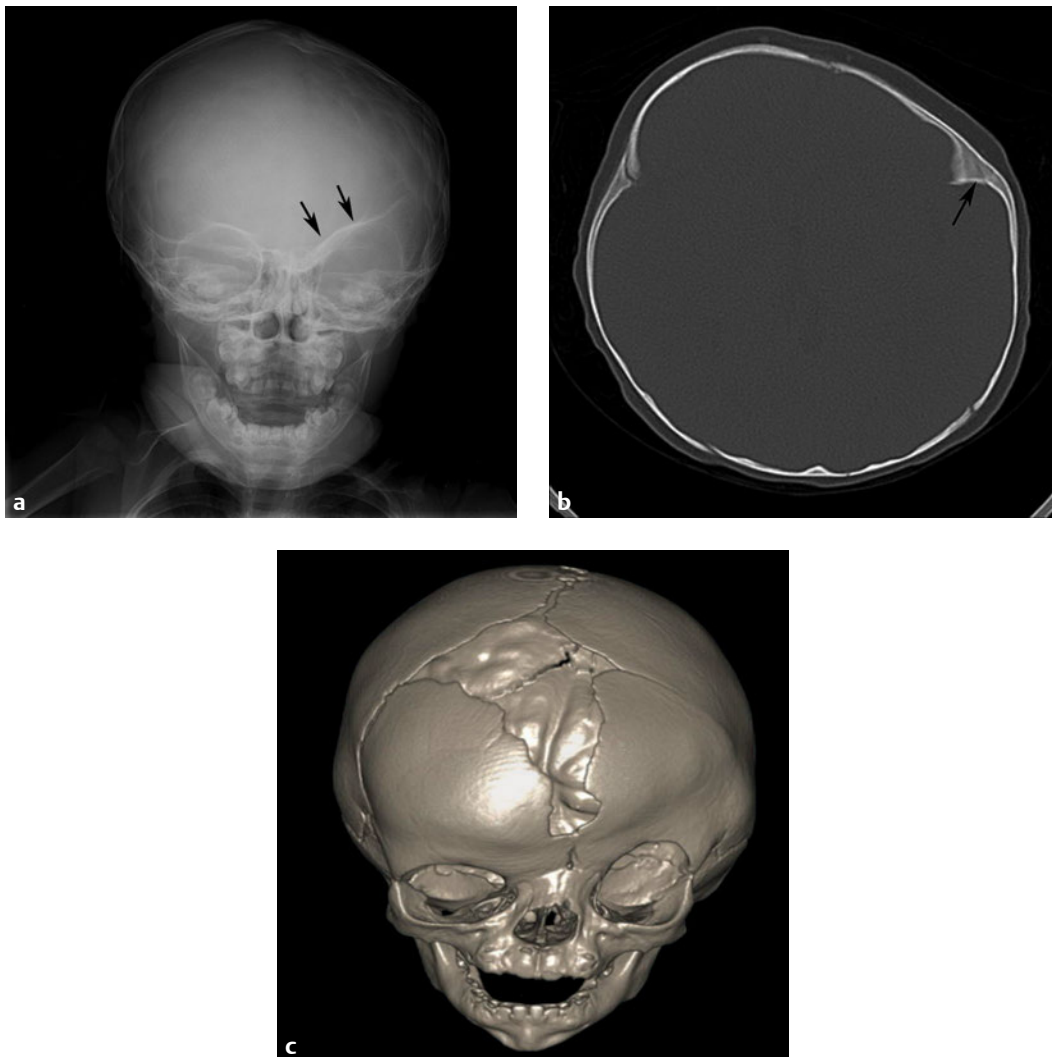
■ Clinical Presentation

A 3-month-old girl with flattening of the left forehead.

■ Radiographic Studies

Frontal skull radiograph (**Fig. 6.1a**) shows asymmetric frontal skull deformity (plagiocephaly) with elevation of the left sphenoid wing and orbital roof, forming the “harlequin eye” deformity (*arrows*). Axial “bone window” CT image demonstrates a small left anterior cranial fossa, elevation of the left

orbital roof and sphenoid wing, and sclerosis of the left coronal suture (**Fig. 6.1b**, *arrow*). Three-dimensional CT reconstruction of the skull (**Fig. 6.1c**) demonstrates partially closed left coronal suture, left orbital abnormality, and plagiocephaly.



■ Diagnosis

Coronal Craniosynostosis

■ Discussion and Differential Diagnosis

Unilateral coronal craniosynostosis is typically idiopathic and should be distinguished from bilateral coronal craniosynostosis, which is frequently syndromic.¹ Premature closure of one coronal suture results in loss of the normal serrated appearance of the suture with sclerosis of the sutural margins.¹ There may be compensatory bulging of the contralateral posterior parieto-occipital skull. Imaging findings include decreased volume of the anterior cranial fossa and shallow orbit as well as elevation of the superolateral corner of the orbital roof producing a “harlequin eye” deformity.^{1,2} Surgical management is

by cranioplasty usually in the first year of life and is necessary to avoid restriction of brain growth and raised intracranial pressure.³

The most common craniofacial syndromes associated with bilateral coronal craniosynostosis are Crouzon (craniofacial dysostosis) and Apert (acrocephalosyndactyly). Patients with Crouzon syndrome may be developmentally normal, whereas patients with Apert syndrome are usually developmentally delayed. In Apert syndrome, syndactyly of the hands and feet is characteristic.¹

Pearl

- ◆ Coronal synostosis is the second most common isolated suture closure, following sagittal craniosynostosis.

Pitfall

- ◆ Postural flattening is a frequent cause of occipital calvarial asymmetry and should not be confused with plagiocephaly secondary to primary sutural closure.

References

1. Badve CA, K MM, Iyer RS, Ishak GE, Khanna PC. Craniosynostosis: imaging review and primer on computed tomography. *Pediatr Radiol* 2013;43: 728–742, quiz 725–727 [PubMed](#)
2. Nagaraja S, Anslow P, Winter B. Craniosynostosis. *Clin Radiol* 2013;68: 284–292 [PubMed](#)
3. Kirmi O, Lo SJ, Johnson D, Anslow P. Craniosynostosis: a radiological and surgical perspective. *Semin Ultrasound CT MR* 2009;30:492–512 [PubMed](#)

Case 7

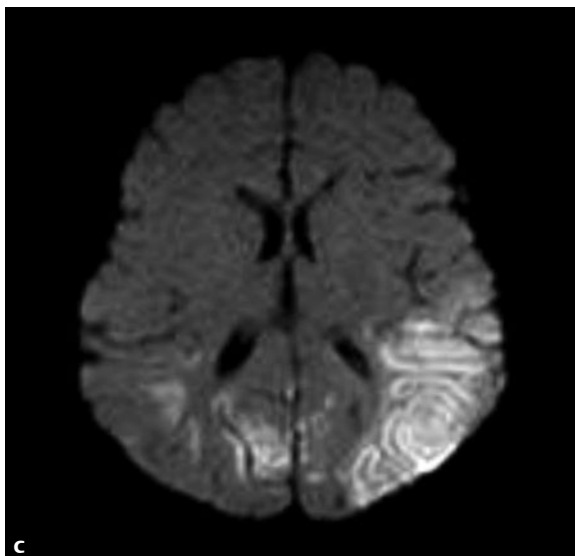
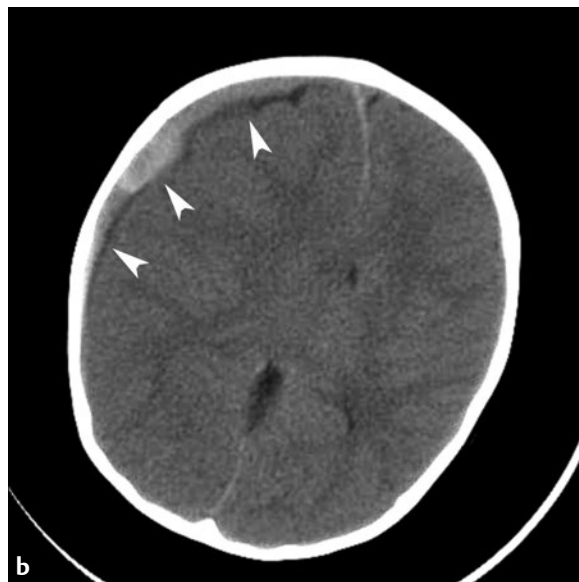
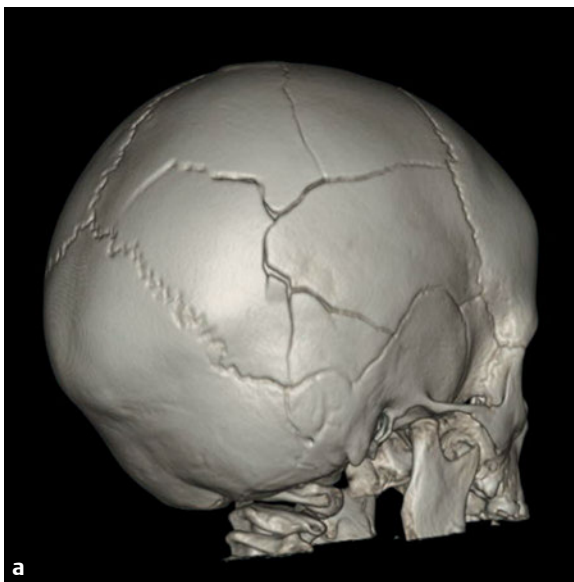
■ Clinical Presentation

An 8-month-old infant was brought to the emergency department after “turning blue.” The baby was in status epilepticus.

■ Radiographic Studies

A 3D CT reconstruction of the skull (**Fig. 7.1a**) shows a comminuted right parietal bone fracture. Axial CT image (**Fig. 7.1b**) shows a right frontoparietal subdural hemorrhage (*arrowheads*) with mass effect and midline shift to left. Note the effacement of the ventricles and hemorrhage along the falx

cerebri. Axial diffusion-weighted MRI (**Fig. 7.1c**) of a different patient shows restricted diffusion in the bilateral parieto-occipital region. Sagittal T1-weighted MRI (**Fig. 7.1d**) shows subdural hemorrhage distributed posteriorly in the lumbar spine (*arrows*).



■ Diagnosis

Child Abuse: Cerebral Injury



■ Discussion and Differential Diagnosis

Child abuse is one of the leading causes of death in the first year of life, and craniocerebral injury is the leading cause of death in abused infants.^{1,2} Shaking and/or direct blows to the head cause subdural hemorrhage and parenchymal contusions. Skull fractures may or may not be associated with cerebral injury. Asphyxia or status epilepticus may compound the

direct traumatic injuries and lead to ischemic change.² Differential diagnosis includes accidental trauma and various coagulopathies. CT is the primary diagnostic tool in acute craniocerebral injury in abused infants. MRI of the head and spine is used to evaluate the complete extent of central neuraxis injuries.^{3,4}

Pearl

- ◆ A subdural hematoma in an infant, especially without history of significant head trauma, is suggestive of abusive injury.¹

Pitfalls

- ◆ Focal or diffuse increased attenuation of the extra-axial fluid in infants should be considered suspicious for subdural hemorrhage.
- ◆ Although MRI is definitive for the extent of cerebral injury in abused infants, CT is still the preferred initial diagnostic modality to exclude head injury in infants with suspected abuse.

References

1. Harwood-Nash DC. Abuse to the pediatric central nervous system. *AJNR Am J Neuroradiol* 1992;13:569–575 [PubMed](#)
2. Rajaram S, Batty R, Rittley CD, Griffiths PD, Connolly DJ. Neuroimaging in non-accidental head injury in children: an important element of assessment. *Postgrad Med J* 2011;87:355–361 [PubMed](#)
3. Choudhary AK, Bradford RK, Dias MS, Moore GJ, Boal DK. Spinal subdural hemorrhage in abusive head trauma: a retrospective study. *Radiology* 2012;262:216–223 [PubMed](#)
4. Kadom N, Khademian Z, Vezina G, Shalaby-Rana E, Rice A, Hinds T. Usefulness of MRI detection of cervical spine and brain injuries in the evaluation of abusive head trauma. *Pediatr Radiol* 2014;44:839–848 [PubMed](#)

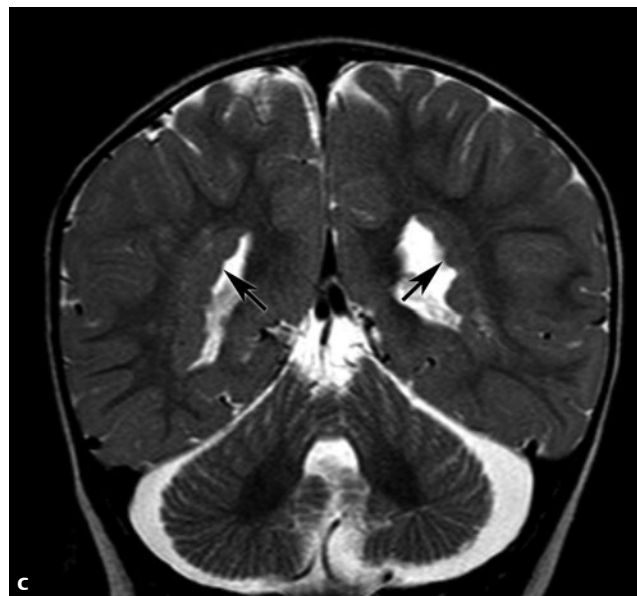
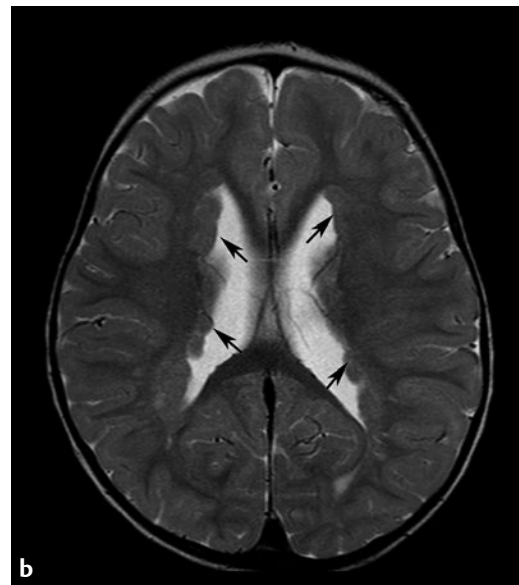
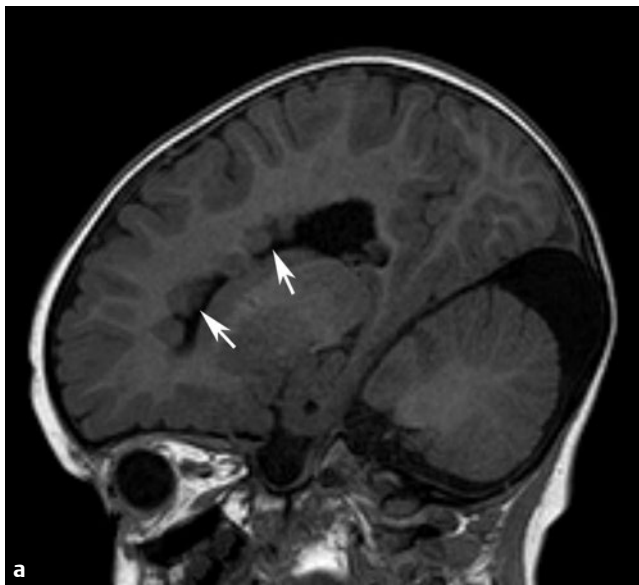
Case 8

■ Clinical Presentation

A 2-year-old girl with seizures.

■ Radiographic Studies

T1-weighted sagittal (**Fig. 8.1a**), T2-weighted axial (**Fig. 8.1b**), and T2-weighted coronal (**Fig. 8.1c**) MRI scans show lumpy gray matter intensity nodules (*arrows*) protruding into the lateral ventricles. The nodules are isointense to gray matter on all sequences.



■ Diagnosis

Subependymal Gray Matter Heterotopias

■ Discussion and Differential Diagnosis

Gray matter heterotopias can be categorized on imaging as subependymal, focal subcortical, and diffuse heterotopias such as band heterotopias.¹ Patients with gray matter heterotopias typically present with seizure disorder.¹ Heterotopic gray matter is typically isodense to gray matter on CT and iso-intense to normal gray matter on all MRI sequences. The heterotopic gray matter does not enhance following contrast administration.^{2,3} Gray matter heterotopias may be associated

with other anomalies of the brain, such as agenesis of the corpus callosum and schizencephaly.³ Other lesions that should not be confused with subependymal heterotopias include subependymal tubers of tuberous sclerosis and the periventricular calcifications of the various TORCH infections. Prominent dependent glomus of the choroid plexus and hemorrhage into the occipital horns of the lateral ventricles are other entities that could simulate subependymal lesions.

Pearls

- ◆ The contour of the ventricular lining should be smooth. Any nodularity in the subependymal area is abnormal.
- ◆ Subependymal abnormalities may be more clearly seen on sagittal or coronal imaging.

Pitfalls

- ◆ The subependymal nodules of tuberous sclerosis and ependymal veins should not be confused with subependymal heterotopias. Contrast administration may be helpful.
- ◆ Body or the tail of the caudate nucleus and the fornices should not be confused with heterotopias, which are focal and nodular.

References

1. Barkovich AJ, Gressens P, Evrard P. Formation, maturation, and disorders of brain neocortex. *AJNR Am J Neuroradiol* 1992;13:423–446 [PubMed](#)
2. Barkovich AJ. Morphologic characteristics of subcortical heterotopia: MR imaging study. *AJNR Am J Neuroradiol* 2000;21:290–295 [PubMed](#)
3. Barkovich AJ, Kjos BO. Gray matter heterotopias: MR characteristics and correlation with developmental and neurologic manifestations. *Radiology* 1992;182:493–499 [PubMed](#)

Case 9

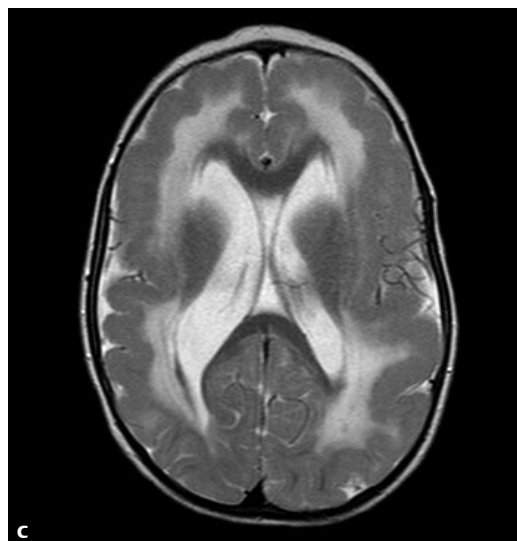
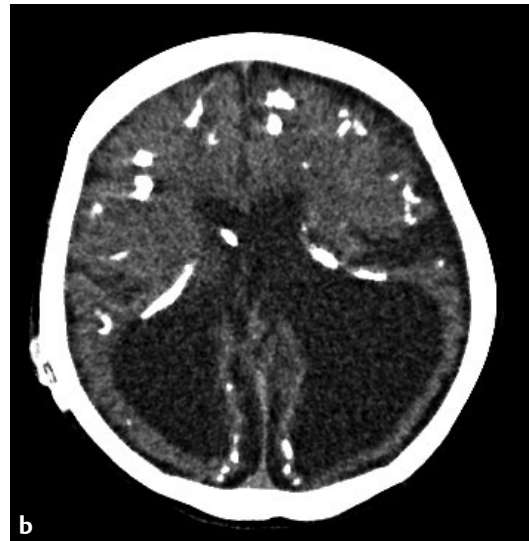
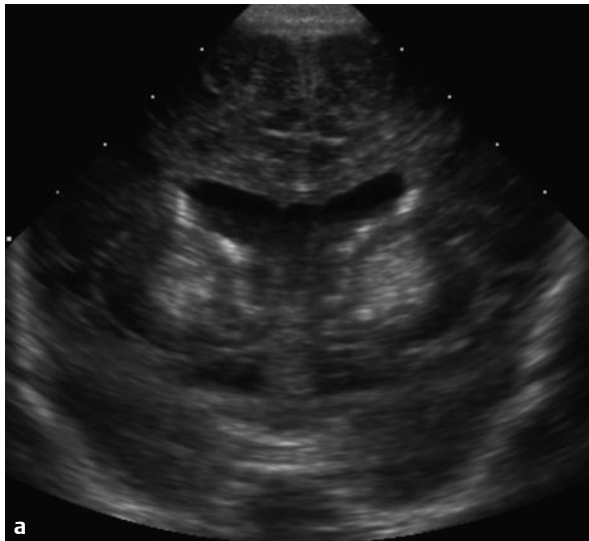
■ Clinical Presentation

A term newborn with hepatosplenomegaly and petechial skin rash.

■ Radiographic Studies

Coronal cranial ultrasound image shows punctate areas of increased echogenicity in the periventricular white matter and basal ganglia compatible with calcifications (**Fig. 9.1a**). Follow-up noncontrast CT image (**Fig. 9.1b**) shows periven-

tricular and subcortical calcifications. Axial T2-weighted MRI in another patient demonstrates bilateral thick cortex, polymicrogyria, and abnormal increased white matter signal intensity (**Fig. 9.1c**).



■ Diagnosis

Cytomegalovirus Encephalitis

■ Discussion and Differential Diagnosis

Cytomegalovirus (CMV) infection is the most common of the TORCH group of congenital infections. Infants with CMV infection typically present with seizures, chorioretinitis, hepatosplenomegaly, and petechial hemorrhage.^{1,2} Central nervous system manifestations of CMV disease are thought to depend on the stage at which the fetus is infected. Fetuses with infection during the first two trimesters, when neuronal migration is active, may demonstrate microcephaly and extensive corti-

cal neuronal migration anomalies. Extensive encephalomalacia, ventriculomegaly, delayed myelination, and periventricular calcifications may be present. It is important to identify infants with neuronal migration anomalies secondary to CMV infection because genetic counseling is not necessary in these patients, in contrast to patients with noninfectious neuronal migration anomalies.^{2,3}

Pearl

- ◆ For congenital infections, remember “TORCH”: T, toxoplasmosis; O, other (i.e., syphilis); R, rubella; C, cytomegalovirus; and H, herpes simplex virus.

Pitfall

- ◆ The periventricular calcifications of TORCH infections should not be confused with calcified subependymal tubers of tuberous sclerosis.

References

1. Malinge G, Lev D, Zahalka N, et al. Fetal cytomegalovirus infection of the brain: the spectrum of sonographic findings. *AJNR Am J Neuroradiol* 2003;24:28–32 [PubMed](#)
2. Barkovich AJ, Lindan CE. Congenital cytomegalovirus infection of the brain: imaging analysis and embryologic considerations. *AJNR Am J Neuroradiol* 1994;15:703–715 [PubMed](#)
3. Fink KR, Thapa MM, Ishak GE, Pruthi S. Neuroimaging of pediatric central nervous system cytomegalovirus infection. *Radiographics* 2010;30:1779–1796 [PubMed](#)

Case 10

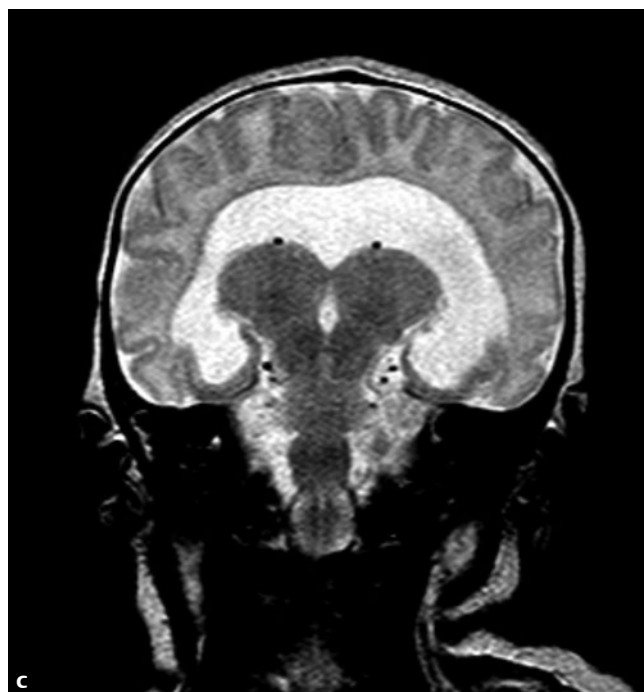
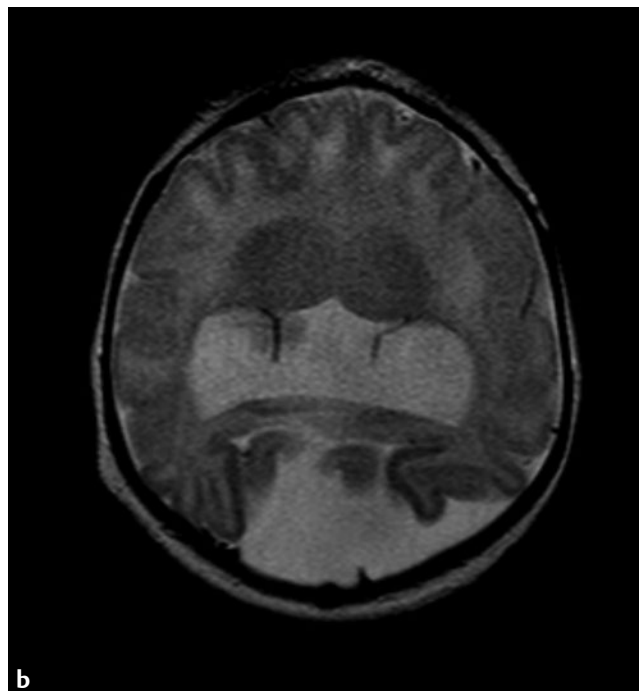
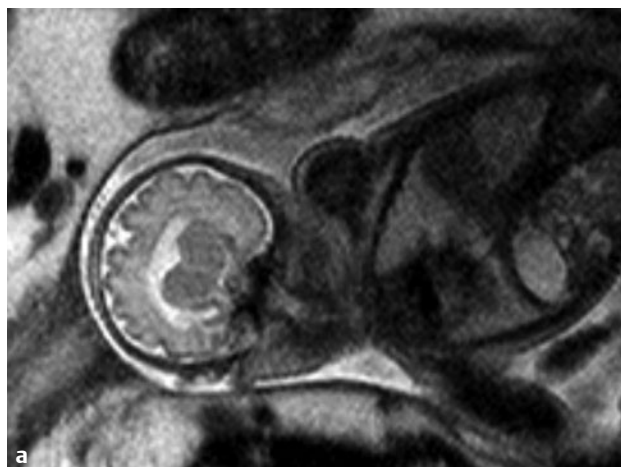
■ Clinical Presentation

A newborn infant with poor feeding and abnormal temperature control.

■ Radiographic Studies

T2-weighted coronal fetal MRI (**Fig. 10.1a**) shows fusion of the thalami and cerebral hemispheres with a monoventricle. Axial T2-weighted MRI (**Fig. 10.1b**) shows fusion of the thalami and a dorsal cyst. Coronal T2-weighted MRI (**Fig. 10.1c**) shows

midline fusion of the cerebral hemispheres with a monoventricle. The corpus callosum, hippocampus, and interhemispheric fissure are absent.



■ Diagnosis

Holoprosencephaly

■ Discussion and Differential Diagnosis

Holoprosencephaly represents a failure of normal formation and separation of the cerebral hemispheres and diencephalon.¹ The subtypes of holoprosencephaly are a continuum of imaging findings including alobar, semilobar, and lobar types. Alobar holoprosencephaly is the most severe form and often has associated facial malformations, including midline facial clefts and hypotelorism.² The condition is usually lethal, often related to neuroendocrine dysfunction. Chromosomal abnor-

malities may be associated with holoprosencephaly, especially trisomy 13. This malformation develops during the first weeks of embryogenesis and may be diagnosed on fetal sonography/MRI in the second or third trimester. The alobar form is associated with a thin “pancake” of cerebral cortex anteriorly with a large monoventricle and dorsal cyst. The less severe semilobar and lobar forms have better development, but still lack normal separation of the cerebral hemispheres.^{2,3}

Pearls

- ◆ Partial or complete contiguity of brain across the midline is required for the diagnosis of holoprosencephaly.
- ◆ Coronal imaging most clearly shows the thalamic fusion and monoventricle.

Pitfall

- ◆ Hydranencephaly and severe forms of schizencephaly may be confused with holoprosencephaly. Proper differentiation is important because holoprosencephaly may be associated with various syndromes and chromosomal abnormalities.

References

1. Dubourg C, Bendavid C, Pasquier L, Henry C, Odent S, David V. Holoprosencephaly. *Orphanet J Rare Dis* 2007;2:8 [PubMed](#)
2. Hahn JS, Barnes PD, Clegg NJ, Stashinko EE. Septopreoptic holoprosencephaly: a mild subtype associated with midline craniofacial anomalies. *AJNR Am J Neuroradiol* 2010;31:1596–1601 [PubMed](#)
3. Barkovich AJ, Simon EM, Clegg NJ, Kinsman SL, Hahn JS. Analysis of the cerebral cortex in holoprosencephaly with attention to the sylvian fissures. *AJNR Am J Neuroradiol* 2002;23:143–150 [PubMed](#)

Case 11

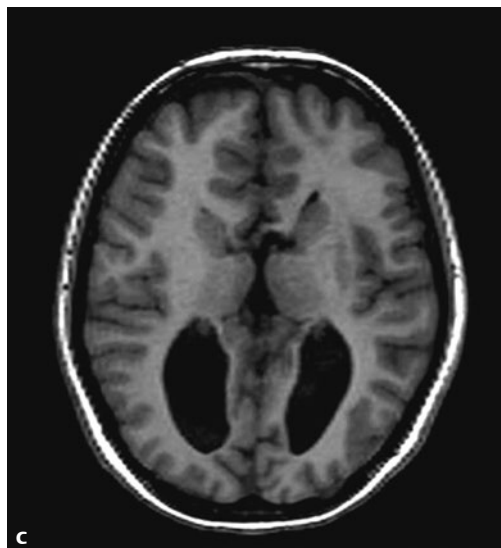
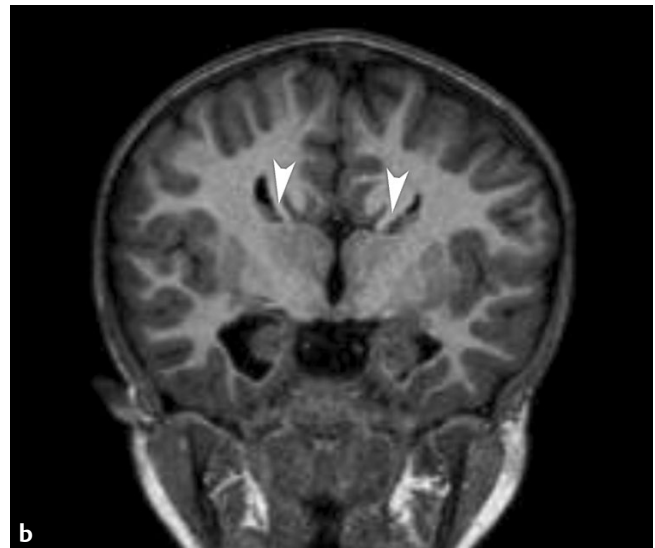
■ Clinical Presentation

A 2-month-old infant with seizures.

■ Radiographic Studies

Sagittal T1-weighted MRI (**Fig. 11.1a**) shows absent corpus callosum with central gyral radiation (*arrowheads*). Coronal T1-weighted MRI (**Fig. 11.1b**) illustrates the “candelabra” appearance of the lateral ventricles and low-riding interhemispheric fissure. Probst bundles (*arrowheads*) represent white matter bundles that would have formed the normal

corpus callosum. The temporal horns are dilated secondary to hypoplasia of the mesial temporal lobe structures. Axial T1-weighted MRI (**Fig. 11.1c**) shows parallel configuration of lateral ventricles with dilatation of the occipital horns (colpocephaly).



■ Diagnosis

Agensis of the Corpus Callosum

■ Discussion and Differential Diagnosis

Callosal agenesis may be partial or complete.¹ When partially absent, the splenium is most frequently involved, especially in patients with Chiari II malformation. Partial absence of the anterior corpus callosum is seen only in patients with holoprosencephaly.^{1,2} Callosal agenesis may be an isolated anomaly but is often associated with intracranial lipomas, neuronal migra-

tion anomalies, and interhemispheric cysts.^{2,3} Clinical presentation in callosal agenesis includes mental retardation (60%), visual problems (33%), and seizures (25%).⁴ Patients with isolated callosal agenesis may be neurologically normal.⁴ Neonatal or prenatal sonography is frequently diagnostic, but MRI is preferred to detect other cerebral anomalies.⁵

Pearls

- ◆ In cases of partial callosal agenesis, absence of the splenium is more commonly found than absence of the genu.
- ◆ Although agenesis of the corpus callosum may be seen as an incidental finding, other cerebral anomalies are often present.

Pitfall

- ◆ A thinned corpus callosum in patients with periventricular leukomalacia may simulate agenesis of the corpus callosum. These patients lack the characteristic findings of callosal agenesis (central radiation of gyri, Probst bundles).

References

1. Kier EL, Truwit CL. The normal and abnormal genu of the corpus callosum: an evolutionary, embryologic, anatomic, and MR analysis. *AJNR Am J Neuroradiol* 1996;17:1631–1641 [PubMed](#)
2. Georgy BA, Hesselink JR, Jernigan TL. MR imaging of the corpus callosum. *AJR Am J Roentgenol* 1993;160:949–955 [PubMed](#)
3. Barkovich AJ, Simon EM, Walsh CA. Callosal agenesis with cyst: a better understanding and new classification. *Neurology* 2001;56:220–227 [PubMed](#)
4. Schell-Apacik CC, Wagner K, Bihler M, et al. Agenesis and dysgenesis of the corpus callosum: clinical, genetic and neuroimaging findings in a series of 41 patients. *Am J Med Genet A* 2008;146A:2501–2511 [PubMed](#)
5. Barkovich AJ. Apparent atypical callosal dysgenesis: analysis of MR findings in six cases and their relationship to holoprosencephaly. *AJNR Am J Neuroradiol* 1990;11:333–339 [PubMed](#)

Case 12

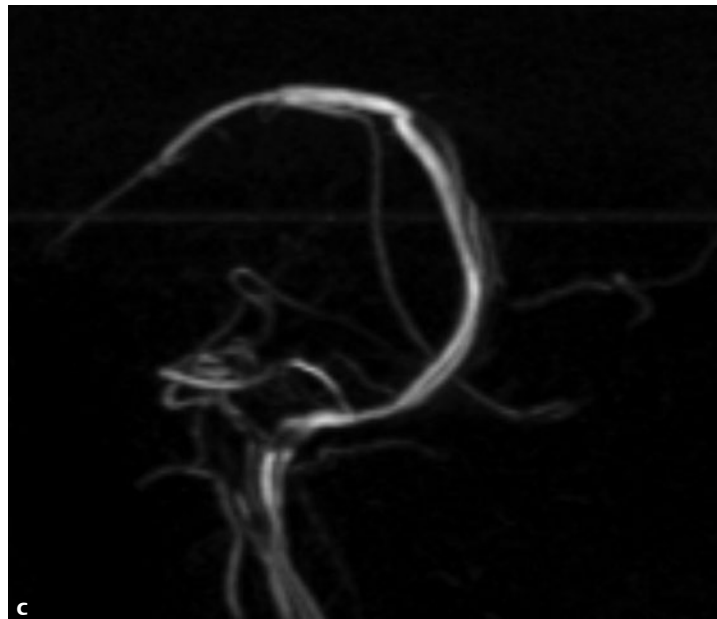
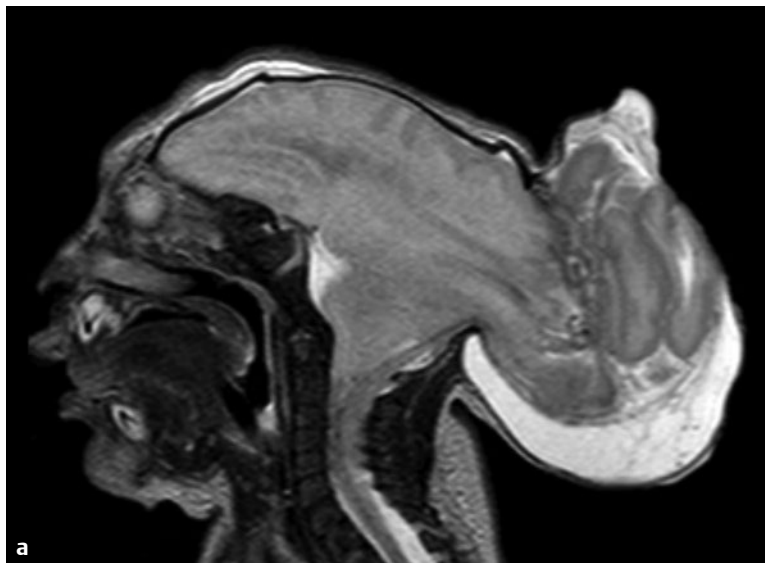
■ Clinical Presentation

A newborn infant with large occipital skin covered mass.

■ Radiographic Studies

Sagittal and axial T2-weighted MRI (**Fig. 12.1a,b**) scans show a midline occipital skull defect with herniation of the cerebral parenchyma and meninges. The corpus callosum is absent.

Magnetic resonance venogram image (**Fig. 12.1c**) shows associated extracranial venous channels.



■ Diagnosis

Occipital Encephalocele

■ Discussion and Differential Diagnosis

The majority of encephaloceles (1 to 3 in 100,000 births) in the Western Hemisphere are located in the occipital region. The second most common location is anteriorly, including naso-frontal, nasoethmoidal, or naso-orbital.^{1,2} Anterior cephaloceles are the most frequent form in South Asian populations. Cephaloceles may contain meninges only; meninges and cerebrospinal fluid (CSF); or meninges, CSF, and brain. Basal cephaloceles also occur anteriorly and may protrude into the sphenoid sinus, pharynx, or temporal bone. Other intracranial anomalies are frequently present, and the majority of the pa-

tients have abnormal neurologic development. The herniated brain is usually nonfunctioning and may have extensive neuronal migrational anomalies, gliosis, and fibrosis. Occipital encephalocele may occur as an isolated abnormality or be a part of various syndromes. Occipital encephaloceles may occur in Meckel-Gruber syndrome, Walker-Warburg syndrome, and as part of Chiari III malformation. Preoperative neuroimaging is crucial to define anomalous vascular anatomy and associated intracranial anomalies.

Pearl

- ◆ Preoperative imaging is critical for defining bony and vascular anatomy.

Pitfall

- ◆ Magnetic resonance imaging of the spine is required in patients with low occipital or high cervical encephaloceles because anomalies of the brainstem and the upper cervical spinal cord are often present.³

References

1. Morón FE, Morriss MC, Jones JJ, Hunter JV. Lumps and bumps on the head in children: use of CT and MR imaging in solving the clinical diagnostic dilemma. *Radiographics* 2004;24:1655–1674 [PubMed](#)
2. Khanna G, Sato Y, Smith RJ, Bauman NM, Nerad J. Causes of facial swelling in pediatric patients: correlation of clinical and radiologic findings. *Radiographics* 2006;26:157–171 [PubMed](#)
3. Castillo M, Quencer RM, Dominguez R. Chiari III malformation: imaging features. *AJNR Am J Neuroradiol* 1992;13:107–113 [PubMed](#)

Case 13

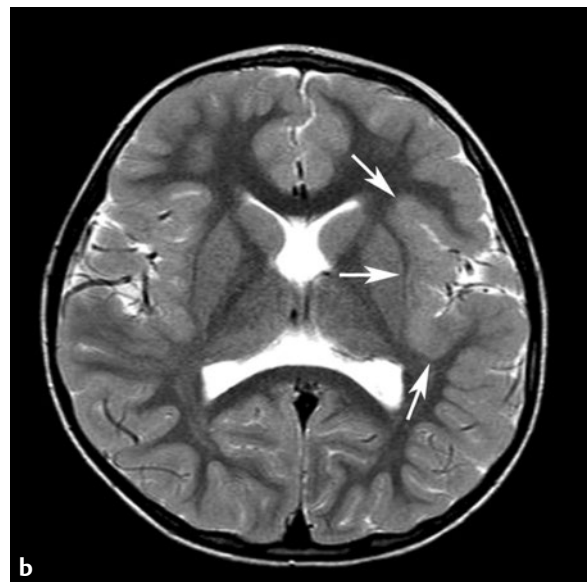
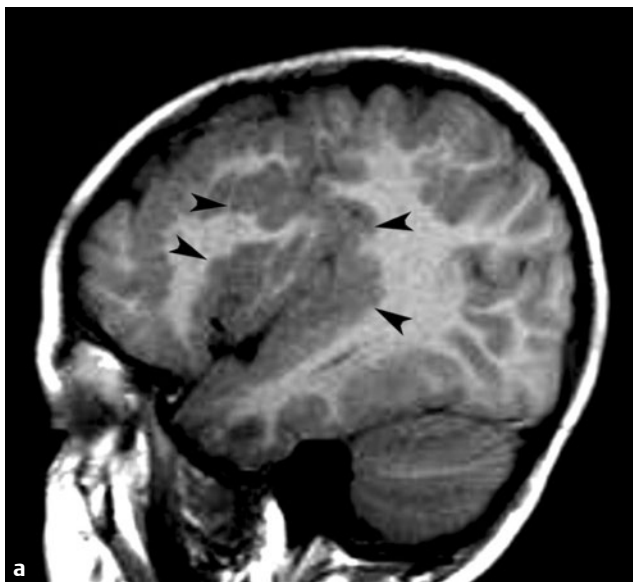
■ Clinical Presentation

A 3-year-old boy with developmental delay and seizures.

■ Radiographic Studies

Sagittal T1-weighted MRI (**Fig. 13.1a**) shows small nodular gyri appearance in the peripheral perisylvian cortex (*arrow-heads*). Axial T2-weighted MRI (**Fig. 13.1b**) demonstrates lack

of normal sulcation and gray matter cortical thickening in the left perisylvian region (*arrows*).



■ Diagnosis

Polymicrogyria

■ Discussion and Differential Diagnosis

Neuronal migration disorders are characterized by dysmorphic gray matter with signal generally isointense to more normal-appearing gray matter. Increased thickness of otherwise normal-appearing gray matter distinguishes a focal area of pachygyria from a tumor. Neuronal migration anomalies do not enhance after administration of intravenous contrast material.^{1,2} Areas of pachygyria may be interspersed with areas of agyria (lissencephaly) or polymicrogyria in the same pa-

tient.^{2,3} Patients with neuronal migration anomalies frequently present with seizures. Given high contrast resolution and multiplanar capability, MRI is the study of choice for detection of neuronal migration anomalies. In polymicrogyria, MRI shows numerous small gyri, with typically bumpy with blurred margins of the gray matter–white matter junction; the underlying white matter may have altered signal.³

Pearl

- ◆ Cortically based neuronal migration disorders are usually recognized because of focal or diffuse areas of abnormal smoothness (lissencephaly), cortical thickening (pachygyria), irregularity (polymicrogyria), or gray matter–lined clefts (schizencephaly).²

Pitfall

- ◆ Anomalous clusters of cortical veins, frequently found in patients with dysplastic cortex, should not be confused with vascular malformations.³

References

1. Barkovich AJ. Current concepts of polymicrogyria. *Neuroradiology* 2010; 52:479–487 [PubMed](#)
2. Takanashi J, Barkovich AJ. The changing MR imaging appearance of polymicrogyria: a consequence of myelination. *AJNR Am J Neuroradiol* 2003;24:788–793 [PubMed](#)
3. Barkovich AJ, Hevner R, Guerrini R. Syndromes of bilateral symmetrical polymicrogyria. *AJNR Am J Neuroradiol* 1999;20:1814–1821 [PubMed](#)

Case 14

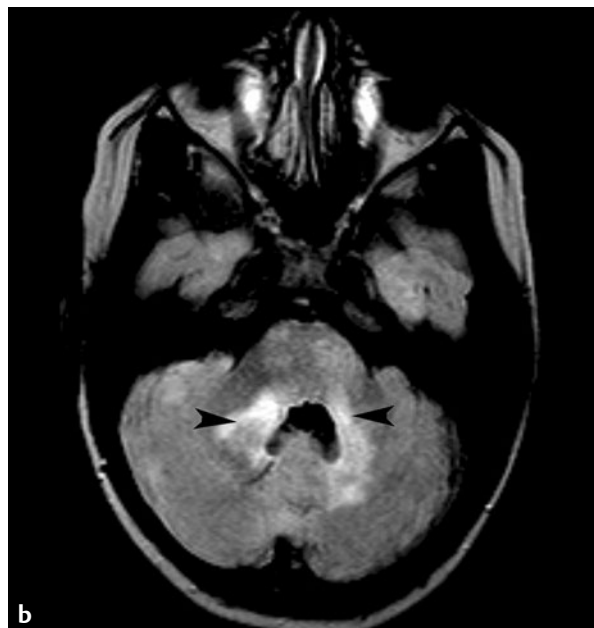
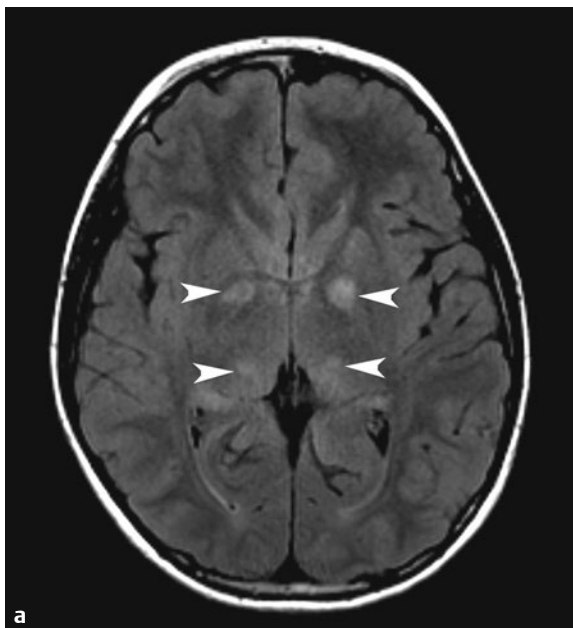
Clinical Presentation

A 7-year-old girl with café-au-lait skin lesions and family history of tumors.

Radiographic Studies

Axial FLAIR MRI (**Fig. 14.1a,b**) shows multiple areas of high signal in the globus pallidus, thalamus, pons, and middle cerebellar peduncles (*arrowheads*). Axial postcontrast fat-saturated T1-weighted MRI (**Fig. 14.1c**) shows bilateral enlarged and enhancing optic nerves (*arrows*), suggesting optic nerve gliomas.

Axial postcontrast fat-saturated T1-weighted MRI (**Fig. 14.1d**) in a different patient shows an enlarged right globe and an enhancing lateral right orbital mass (*arrows*) extending into the right cavernous sinus.



■ Diagnosis

Neurofibromatosis Type 1

■ Discussion and Differential Diagnosis

Neurofibromatosis type 1 (NF1) is the most common of the phakomatoses.¹ It is inherited in an autosomal dominant pattern, but there is a high rate of spontaneous mutation. The defect is carried on chromosome 17. Characteristic skin lesions include café-au-lait spots and axillary freckling. Lisch nodules in the iris, osseous lesions, family history, and the presence of neurofibromas or optic glioma are diagnostic criteria for NF1. There is little pathological material to indicate the nature of the characteristic high-signal lesions seen on MRI in the basal

ganglia, brainstem, and cerebellum in patients with NF1. These signal abnormalities are present in most children between 1 year of age and adulthood, but are less commonly seen in infants and adults with NF1.^{1,2} Brain tumors occur commonly in patients with NF1. In addition to optic gliomas, astrocytomas of the hypothalamus, cerebellum, and brainstem are seen with increased frequency in patients with NF1. Orbital imaging features include sphenoid wing dysplasia, optic nerve glioma, and an enlarged globe.³

Pearl

- ◆ Optic glioma is the most common intracranial neoplasm in children with NF1.

Pitfall

- ◆ Differentiation of high-signal hamartomas from gliomas may be difficult or impossible with imaging alone.

References

1. Herron J, Darrah R, Quaghebeur G. Intra-cranial manifestations of the neurocutaneous syndromes. *Clin Radiol* 2000;55:82–98 [PubMed](#)
2. Aoki S, Barkovich AJ, Nishimura K, et al. Neurofibromatosis types 1 and 2: cranial MR findings. *Radiology* 1989;172:527–534 [PubMed](#)
3. Jacquemin C, Bosley TM, Svedberg H. Orbit deformities in craniofacial neurofibromatosis type 1. *AJNR Am J Neuroradiol* 2003;24:1678–1682 [PubMed](#)

Case 15

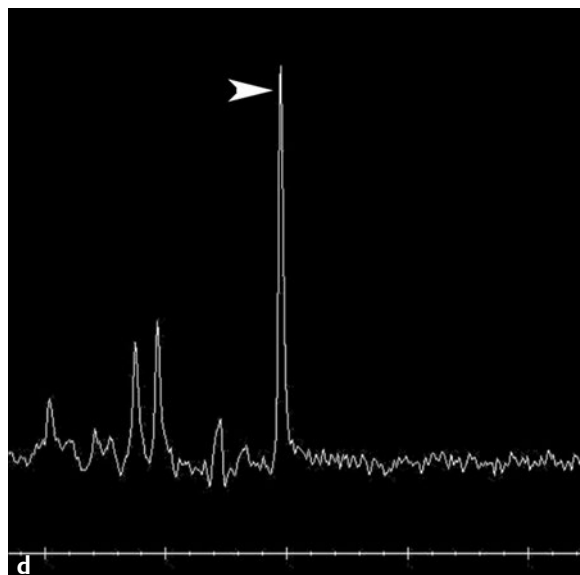
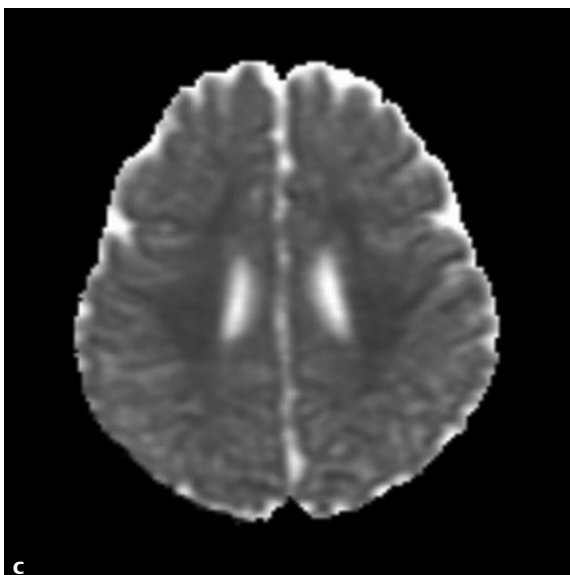
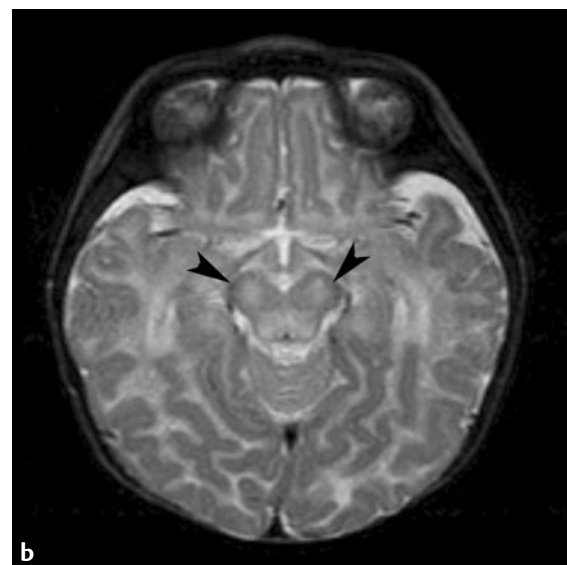
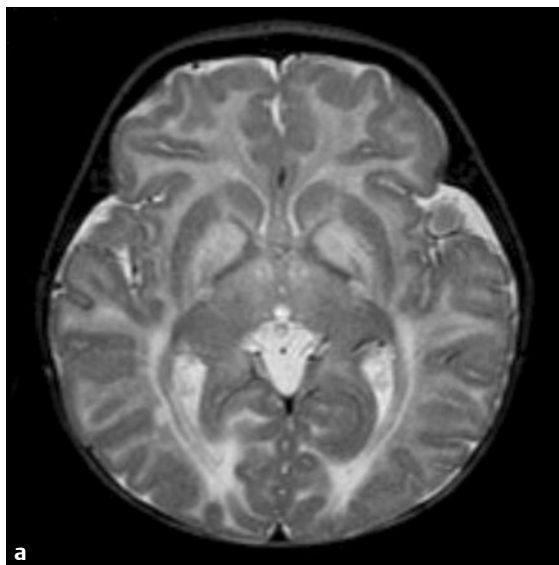
■ Clinical Presentation

A 2-year-old with developmental delay and increased head circumference.

■ Radiographic Studies

T2-weighted axial MRI (**Fig. 15.1a,b**) shows diffuse high signal hypomyelination of the white matter including the subcortical U-fibers. Note the high signal hypomyelination of the corticospinal tracts in the cerebral peduncles (*arrowheads*). An apparent diffusion coefficient (ADC) map of a diffusion-weighted

MRI sequence (**Fig. 15.1c**) shows low signal intensity in the white matter, suggesting restricted diffusion. Long TE single voxel magnetic resonance spectroscopy (**Fig. 15.1d**) shows a markedly elevated *N*-acetylaspartate (NAA) metabolite peak (*arrowhead*) and an elevated NAA/creatinine ratio.



■ Diagnosis

Canavan Disease

■ Discussion and Differential Diagnosis

Canavan disease is an autosomal recessive disorder of amino acid metabolism due to deficiency of the enzyme aspartoacylase leading to accumulation of NAA.¹ This disease more frequently affects people of Ashkenazi Jewish origin. Patients with Canavan disease tend to present in infancy with hypotonia, increased head circumference, seizures, and developmental delay. Urinalysis for acetylaspartic acid is usually diagnostic.

The characteristic signal abnormalities on MRI include diffuse hypomyelination in a centripetal distribution starting in from the subcortical U-fibers and followed by deep white matter with relative sparing of the internal capsule, external

capsule, and corpus callosum.^{1,2} Internal capsule and corticospinal tract involvement is usually seen with disease progression. Abnormal T2 hyperintensity is seen in the globus pallidus with sparing of the putamen and caudate nucleus. Restricted diffusion is seen in the white matter in early stages of the disease due to the “gelatinous state” of the extracellular fluid space in patients with Canavan disease.³ Late-stage ventricular dilatation is seen due to white matter thinning. Magnetic resonance proton spectroscopy may provide a more specific diagnosis by demonstrating elevated NAA metabolite peak with an elevated NAA/creatine ratio.

Pearls

- ◆ Macrocephaly with diffuse centripetal hypomyelination, involvement of subcortical white matter, and relative sparing of the internal/external capsule is characteristic of Canavan disease.^{1,2}
- ◆ T2 hyperintensity of the globus pallidus with sparing of the putamen and caudate nucleus is typically seen.

Pitfall

- ◆ Features of various leukodystrophies with macrocrania such as Alexander disease and vacuolating leukoencephalopathies may have overlapping imaging findings with Canavan disease in the early stages. Significant elevation of NAA peak on magnetic resonance spectroscopy is helpful for accurate diagnosis of Canavan disease.

References

1. Brismar J, Brismar G, Gascon G, Ozand P. Canavan disease: CT and MR imaging of the brain. *AJNR Am J Neuroradiol* 1990;11:805–810 [PubMed](#)
2. McAdams HP, Geyer CA, Done SL, Deigh D, Mitchell M, Ghaed VNCT. CT and MR imaging of Canavan disease. *AJNR Am J Neuroradiol* 1990;11:397–399. [PubMed](#)
3. Sener RN. Canavan disease: diffusion magnetic resonance imaging findings. *J Comput Assist Tomogr* 2003;27:30–33 [PubMed](#)

Case 16

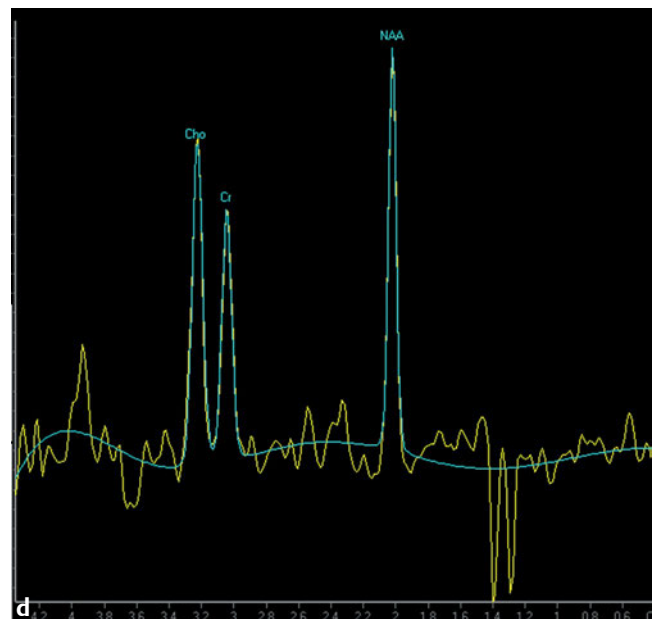
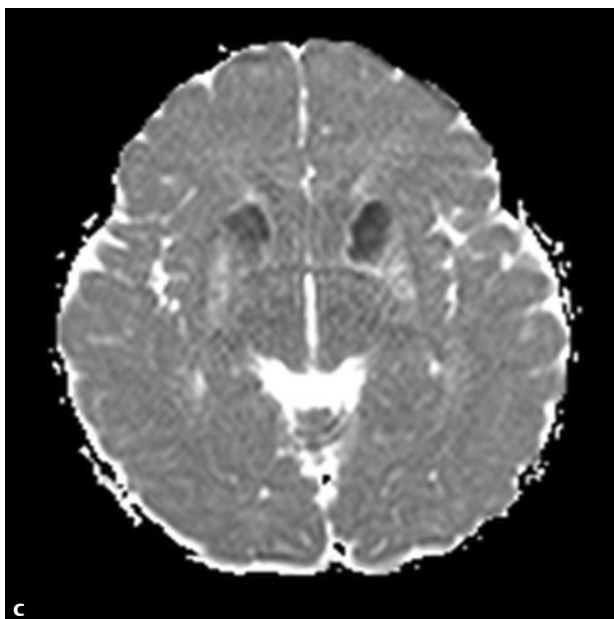
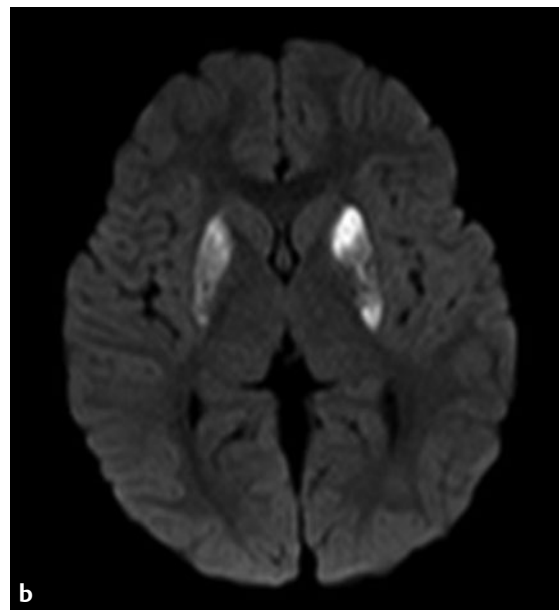
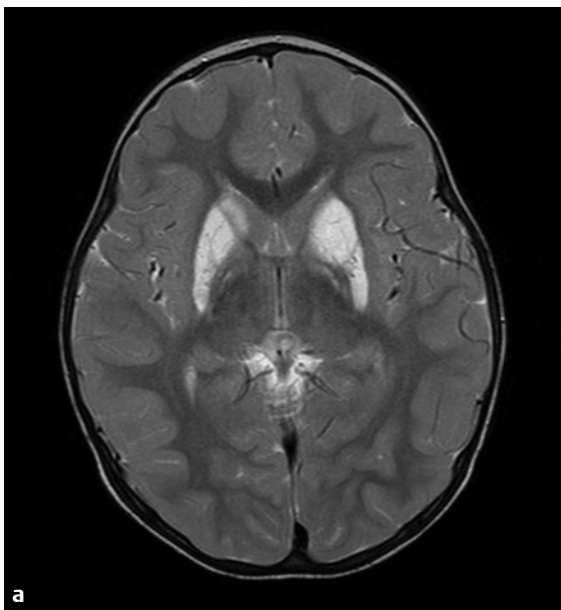
■ Clinical Presentation

A 12-month-old infant with hypotonia and ophthalmoplegia.

■ Radiographic Studies

Axial T2-weighted MRI (**Fig. 16.1a**) shows abnormal high signal in the lentiform nuclei and medial thalamus. Axial diffusion-weighted MRI (**Fig. 16.1b**) and ADC map (**Fig. 16.1c**) show

bilateral restricted diffusivity in the lentiform nuclei. Single voxel proton magnetic resonance spectroscopy (TR = 144 ms, **Fig. 16.1d**) shows an inverted lactate doublet.



■ Diagnosis

Mitochondrial Disease: Leigh Disease

■ Discussion and Differential Diagnosis

Leigh disease is actually not one disorder but the manifestation of one of several metabolic abnormalities caused by enzyme deficiencies secondary to mutations of mitochondrial DNA.¹ Patients with Leigh disease tend to present in infancy with ataxia, hypotonia, cranial nerve abnormalities, and seizures. Elevated lactate levels can be found in the serum and in

the spinal fluid. The characteristic signal abnormalities on MRI and low attenuation in the basal ganglia and brainstem on CT suggest the diagnosis in infants with characteristic clinical abnormalities.^{1,2} MRI proton spectroscopy may provide a more specific diagnosis by demonstrating elevated central nervous system (CNS) lactate.

Pearl

- ◆ Low-attenuation changes on CT and long T1 and T2 signal in the basal ganglia and brainstem on MRI are characteristic in infants with Leigh disease.

Pitfall

- ◆ Other mitochondrial encephalopathies as well as profound asphyxia may demonstrate similar imaging findings on CT and MRI.

References

1. Barkovich AJ, Good WV, Koch TK, Berg BO. Mitochondrial disorders: analysis of their clinical and imaging characteristics. *AJNR Am J Neuroradiol* 1993;14:1119–1137 [PubMed](#)
2. Valanne L, Ketonen L, Majander A, Suomalainen A, Pihko H. Neuroradiologic findings in children with mitochondrial disorders. *AJNR Am J Neuroradiol* 1998;19:369–377 [PubMed](#)

Case 17

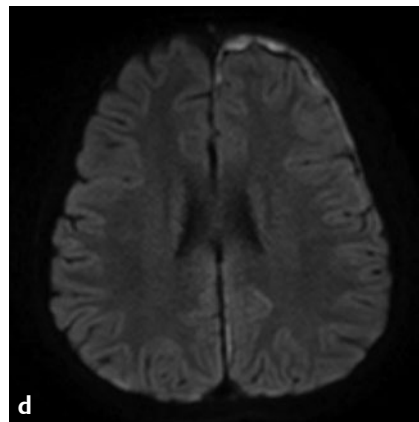
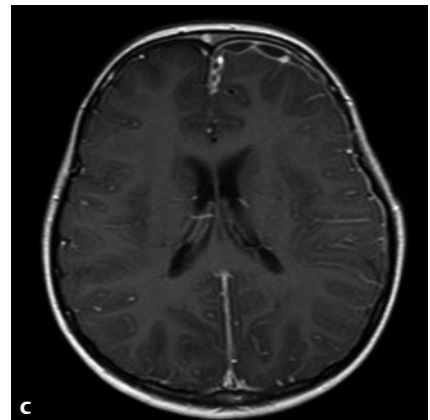
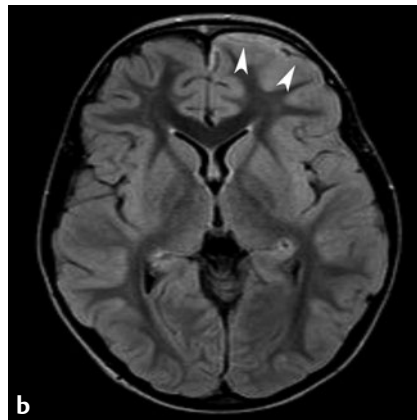
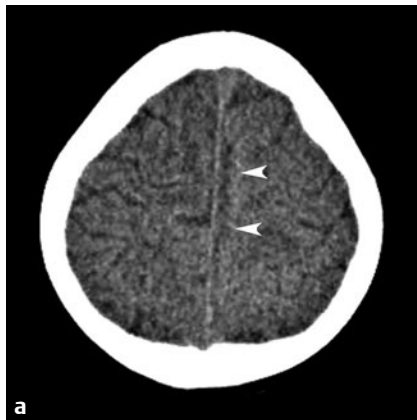
■ Clinical Presentation

A 9-year-old girl with headaches and recent onset of seizure activity.

■ Radiographic Studies

Noncontrast CT image (**Fig. 17.1a**) shows subtle asymmetry and prominence of the interhemispheric fissure on the left side of the falx cerebri (*arrowheads*). Axial FLAIR MRI (**Fig. 17.1b**) shows hyperintense rim of subdural fluid collection in the left frontal convexity (*arrowheads*). Postcontrast T1-weighted MRI (**Fig. 17.1c**) shows peripheral enhancement of

the subdural fluid collection in the left frontal convexity. The subdural fluid shows restricted diffusivity on B1000 MRI (**Fig. 17.1d**). Noncontrast CT image of the paranasal sinus (**Fig. 17.1e**) shows mucosal thickening in the left maxillary/ethmoid sinus. The sinus wall thickening suggests chronic sinus disease.



■ Diagnosis

Subdural Empyema

■ Discussion and Differential Diagnosis

Subdural empyema is typically seen in adolescents secondary to direct spread of infection from the paranasal sinuses or mastoid air cells.¹ In infants, subdural empyema is usually a complication of bacterial meningitis. Congenital defects such as dermal sinus and cephaloceles may present a direct pathway for intracranial spread of infection. Patients with subdural empyema typically present with headache, focal neurologic deficit, and seizures.¹ Noncontrast CT findings may be very subtle. Careful attention to any subdural collection with associated sulcal effacement in patients with paranasal sinus dis-

ease helps in early detection of empyema. MRI is much more sensitive than CT for detection of subdural empyema.² FLAIR images show hyperintense fluid in the subdural space with peripheral enhancement on postgadolinium images. Restricted diffusion within the purulent collection is virtually always present.^{2,3} Adjacent cerebral parenchyma may show edema, or enhancement suggestive of focal cerebritis. Venous sinus thrombosis with associated parenchymal infarction is a potential complication appropriately evaluated by magnetic resonance venography.

Pearl

- ◆ Peripheral enhancing subdural fluid with restricted diffusivity in a patient with acute paranasal sinus disease is diagnostic of subdural empyema.^{2,3}

Pitfall

- ◆ Subtle subdural collections with mild sulcal effacement on non-contrast CT can be easily missed.

References

1. Kombogiorgas D, Seth R, Athwal R, Modha J, Singh J. Suppurative intracranial complications of sinusitis in adolescence. Single institute experience and review of literature. *Br J Neurosurg* 2007;21:603–609. [PubMed](#)
2. Wong AM, Zimmerman RA, Simon EM, Pollock AN, Bilaniuk LT. Diffusion-weighted MR imaging of subdural empyemas in children. *AJNR Am J Neuroradiol* 2004;25:1016–1021. [PubMed](#)
3. Fanning NF, Laffan EE, Shroff MM. Serial diffusion-weighted MRI correlates with clinical course and treatment response in children with intracranial pus collections. *Pediatr Radiol* 2006;36:26–37. [PubMed](#)

Case 18

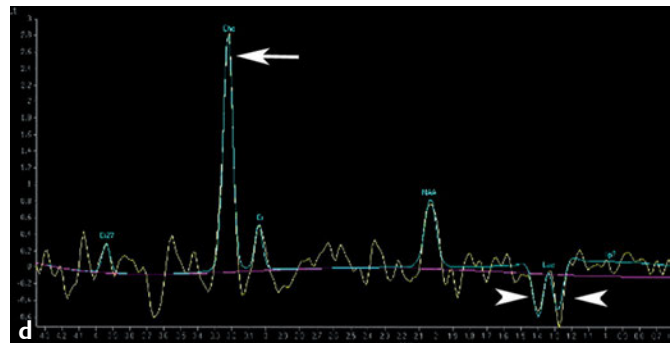
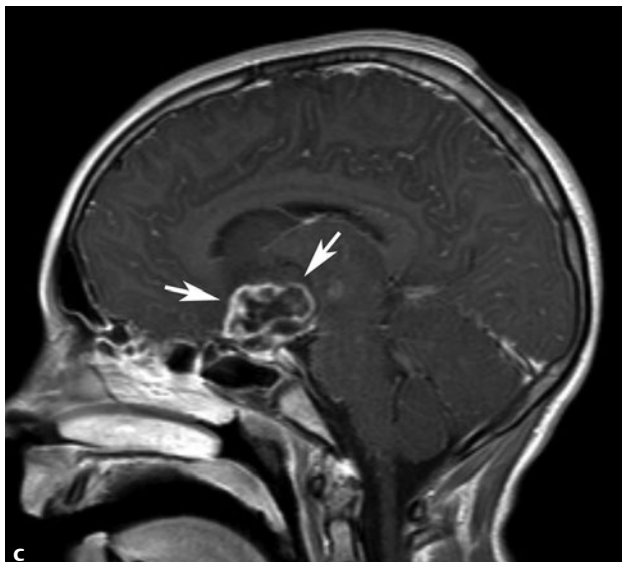
Clinical Presentation

A 5-year-old boy with headache, vomiting, pallor, and emaciation. Workup for gastrointestinal disease was normal.

Radiographic Studies

Sagittal T1-weighted MRI shows low signal lobulated mass in the suprasellar and interpeduncular cistern displacing the third ventricle superiorly and brainstem posteriorly (**Fig. 18.1a**, arrows). Axial T2-weighted MRI shows the tumor to be markedly hyperintense (**Fig. 18.1b**, arrows). There is irregular pe-

ripheral tumor enhancement on the sagittal T1-weighted MRI (**Fig. 18.1c**, arrows) following administration of contrast. Single voxel magnetic resonance spectroscopy with TE = 144 ms (**Fig. 18.1d**) of the tumor shows an elevated choline peak (arrow) and an inverted lactate doublet (arrowheads).



■ Diagnosis

Hypothalamic Astrocytoma

■ Discussion and Differential Diagnosis

Suprasellar masses in children include craniopharyngiomas, hypothalamic/optic pathway gliomas, germ cell tumors, Langerhans cell histiocytosis, and tuber cinereum hamartomas. Clinical presentation of hypothalamic gliomas includes changes in visual acuity and endocrine abnormalities.¹ Hypothalamic gliomas are typically low-grade, slow-growing, pilocytic astrocytomas and account for 10 to 15% of suprasellar tumors. Up to 50% of the patients with hypothalamic glioma have a positive family history of neurofibromatosis type 1. These lesions tend to be bulky, and are hypointense to gray matter on T1-weighted images, hyperintense on T2-weighted images, and show variable enhancement.² The optic nerves and visual

pathways are frequently enlarged. Children with both germ cell tumors and histiocytosis frequently present with diabetes insipidus. Germ cell tumors tend to be large and may have associated masses in the pineal region as well as leptomeningeal spread of tumor. In histiocytosis, the pituitary infundibulum is abnormally prominent, but large masses are infrequent. Patients with histiocytosis often have lytic lesions in the calvaria, skull base, or elsewhere in the skeleton. Children with hamartoma of the tuber cinereum present with seizure and precocious puberty.¹ Hamartomas are isointense to gray matter on all pulse sequences and rarely enhance.

Pearl

- ◆ Hypothalamic/optic chiasm gliomas occur with an increased incidence in patients with neurofibromatosis type 1.²

Pitfall

- ◆ To distinguish craniopharyngioma from hypothalamic/optic pathway glioma, look for hyperintensity in the tumor on T1-weighted images as well as focal low signal suggestive of calcification, findings frequently present in craniopharyngioma but uncommonly in gliomas.³

References

1. Saleem SN, Said AH, Lee DH. Lesions of the hypothalamus: MR imaging diagnostic features. *Radiographics* 2007;27:1087–1108. [PubMed](#)
2. Kornreich L, Blaser S, Schwarz M, et al. Optic pathway glioma: correlation of imaging findings with the presence of neurofibromatosis. *AJNR Am J Neuroradiol* 2001;22:1963–1969. [PubMed](#)
3. Sartoretti-Schefer S, Wichmann W, Aguzzi A, Valavanis A. MR differentiation of adamantinous and squamous-papillary craniopharyngiomas. *AJNR Am J Neuroradiol* 1997;18:77–87. [PubMed](#)

Case 19

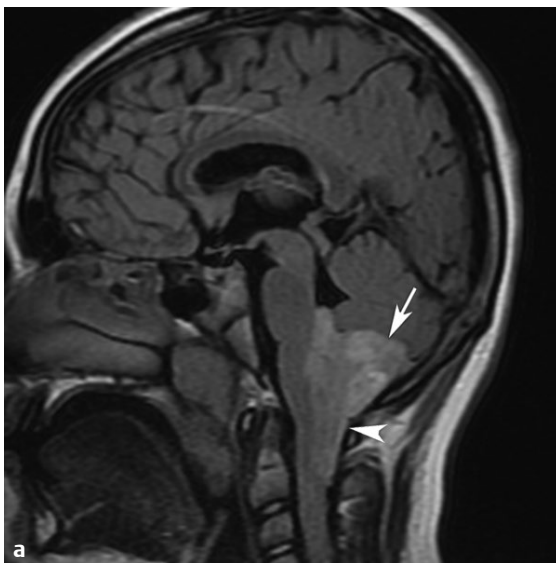
■ Clinical Presentation

A 6-year-old boy with recent history of headaches, vomiting, and papilledema.

■ Radiographic Studies

Sagittal FLAIR MRI (**Fig. 19.1a**) shows an intermediate signal intensity mass within the fourth ventricle extending through the foramen of Magendie into the cisterna magna (*arrow*) and upper cervical canal (*arrowhead*). Axial T2-weighted MRI (**Fig. 19.1b**) demonstrates an intermediate signal intensity

mass with extraventricular extension through the foramen of Luschka (*arrow*). Postcontrast sagittal and coronal T1-weighted MRI scans (**Fig. 19.1c,d**) show heterogeneous contrast enhancement of the mass and significant mass effect on the cervicomedullary junction.



■ Diagnosis

Ependymoma

■ Discussion and Differential Diagnosis

Ependymoma is the third most common posterior fossa tumor in childhood (12%) following medulloblastoma and pilocytic astrocytoma.^{1,2} It is a glial tumor arising from the ependymal cells lining the ventricular wall or the central canal of the spinal cord. Ependymoma can occur anywhere in the neuraxis (supratentorial, posterior fossa, and spinal cord) with posterior fossa being the most common location (70%) in children. Posterior fossa ependymoma typically occurs in the first decade of life with a peak age of 6 years with signs and symptoms of raised intracranial pressure such as headache, nausea, and vomiting.^{1,2}

Posterior fossa ependymoma presents as a fourth ventricular mass arising from the ventricular floor. Ependymoma are soft plastic tumors that show characteristic extension out of

the fourth ventricle through the foramina of Magendie and Luschka. Hydrocephalus is usually present secondary to obstruction at the level of the fourth ventricle and its outlet. On CT, ependymoma is usually hypodense to gray matter and contrast enhancement is expected.² Intratumoral hemorrhage, calcification, and cyst formation may occur. On MRI, the tumor tends to be hypointense on T1-weighted sequences, and hyperintense on T2-weighted and FLAIR sequences.² Ependymomas show variable restricted diffusivity compared with the intense restricted diffusivity seen in medulloblastoma.³ Postcontrast MRI of the entire spine is performed before surgery to rule out leptomeningeal metastases, which are often present in patients with ependymoma.

Pearls

- ◆ Ependymomas are soft and plastic tumors often with extension through the foramina of Magendie and Luschka.^{1,2}
- ◆ Leptomeningeal metastases are frequent with ependymoma. Systemic metastases are rare.

Pitfall

- ◆ Medulloblastomas may also fill the fourth ventricle, but typically show intensely restricted diffusion and uncommonly extend into the upper cervical spinal canal.

References

1. Poretti A, Meoded A, Huisman TA. Neuroimaging of pediatric posterior fossa tumors including review of the literature. *J Magn Reson Imaging* 2012;35:32–47. [PubMed](#)
2. Rasalkar DD, Chu WC, Paunipagar BK, Cheng FW, Li CK. Paediatric intra-axial posterior fossa tumours: pictorial review. *Postgrad Med J* 2013;89:39–46. [PubMed](#)
3. Rumboldt Z, Camacho DL, Lake D, Welsh CT, Castillo M. Apparent diffusion coefficients for differentiation of cerebellar tumors in children. *AJNR Am J Neuroradiol* 2006;27:1362–1369. [PubMed](#)

Case 20

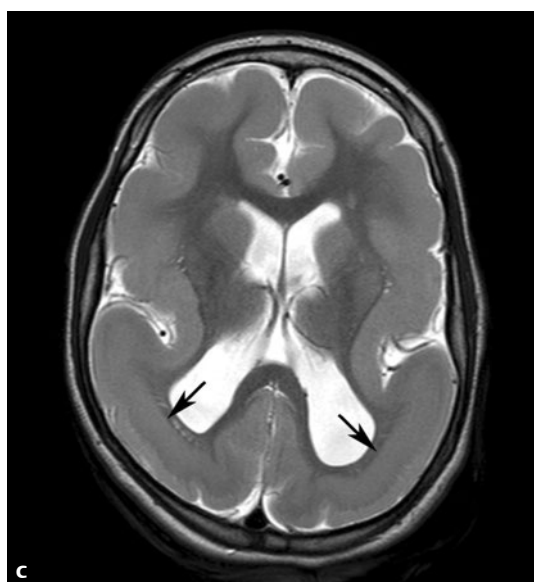
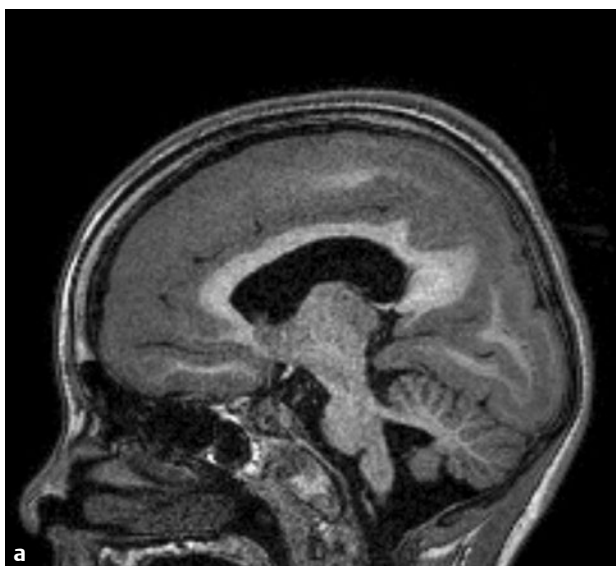
■ Clinical Presentation

A 9-month-old infant with severe developmental delay and seizures.

■ Radiographic Studies

Sagittal T1-weighted (**Fig. 20.1a**) and coronal T2-weighted (**Fig. 20.1b**) MRI shows smooth, thickened cortex with absence of normal sulcation, and hypoplasia of the inferior cerebellar

vermis. Axial T2-weighted MRI (**Fig. 20.1c**) shows ventriculomegaly and gray matter band heterotopia (*arrows*) deep to the abnormally thickened and smooth cerebral cortex.



■ Diagnosis

Lissencephaly

■ Discussion and Differential Diagnosis

Lissencephaly or agyria is a severe disorder of brain structure categorized as the most severe anomaly of neuronal migration.¹ Children with lissencephaly are almost always severely developmentally delayed. There is lack of formation of normal cortical gyri and sulci. A few sulci may be present or the cortical surface may be nearly completely smooth. The sylvian fissures are usually shallow and vertically oriented, providing an “hour glass” appearance on the axial imaging.^{1,2} There are several different types of lissencephaly. Classic lissencephaly (type 1) may be isolated without a known mutation or could

be associated with various mutations of *LIS1* or *DCX* genes. Type 2 lissencephalies are a group of disorders associated with muscular dystrophy (Walker-Warburg syndrome, Fukuyama muscular dystrophy, and muscle-eye-brain disease).² Patients with Walker-Warburg syndrome usually present with various optic disk anomalies, lissencephaly, hydrocephalus, and characteristic posterior fossa malformations. Lissencephaly with underlying dysmorphic strands and nodules of heterotopic gray matter (cobblestone lissencephaly) is typical of type 2 lissencephaly.^{2,3}

Pearls

- ◆ Lissencephaly may be localized to one area of the cortical surface.
- ◆ A smooth “agyric” cortex is a developmental finding in extremely premature infants and should not be confused with lissencephaly.

Pitfall

- ◆ Diffuse polymicrogyria/lissencephaly with a “knobby” appearance of the cerebral cortical surface, often with associated cerebral calcifications, is seen in infants with cytomegalovirus infection. It is important to recognize this “variant” of lissencephaly because it does not carry the possible genetic implications of some lissencephaly syndromes.

References

1. Barkovich AJ, Gressens P, Evrard P. Formation, maturation, and disorders of brain neocortex. *AJNR Am J Neuroradiol* 1992;13:423–446 [PubMed](#)
2. Abdel Razek AA, Kandell AY, Elsorogy LG, Elmongy A, Basett AA. Disorders of cortical formation: MR imaging features. *AJNR Am J Neuroradiol* 2009;30:4–11 [PubMed](#)
3. Ghai S, Fong KW, Toi A, Chitayat D, Pantazi S, Blaser S. Prenatal US and MR imaging findings of lissencephaly: review of fetal cerebral sulcal development. *Radiographics* 2006;26:389–405 [PubMed](#)

Case 21

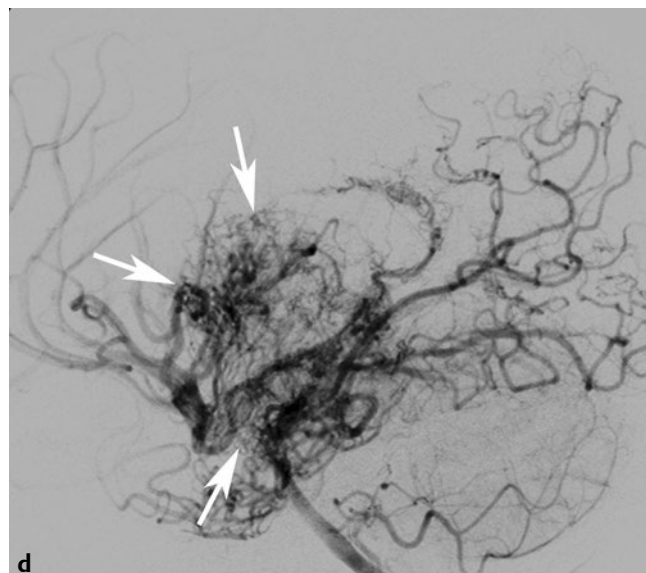
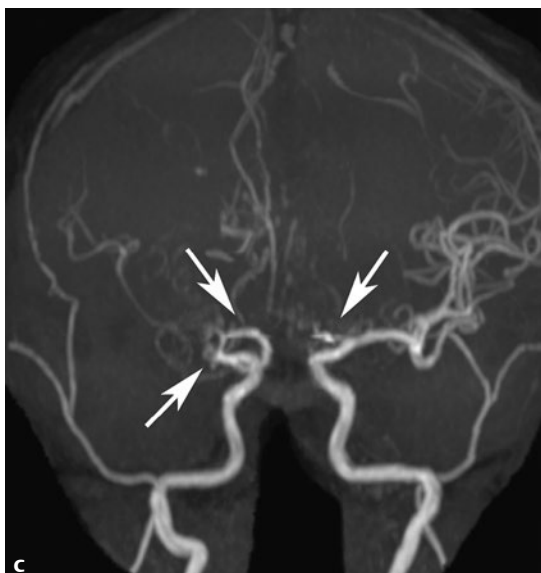
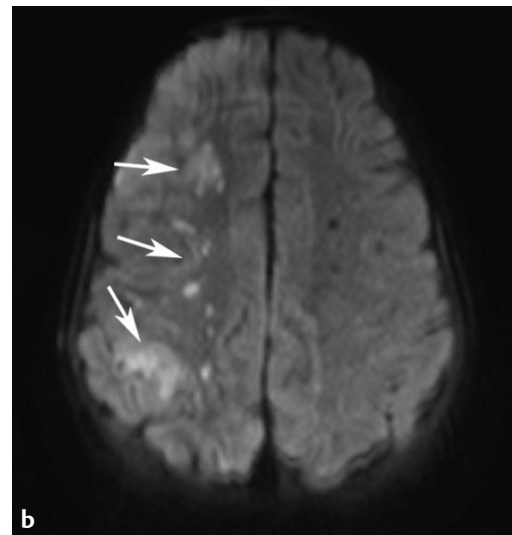
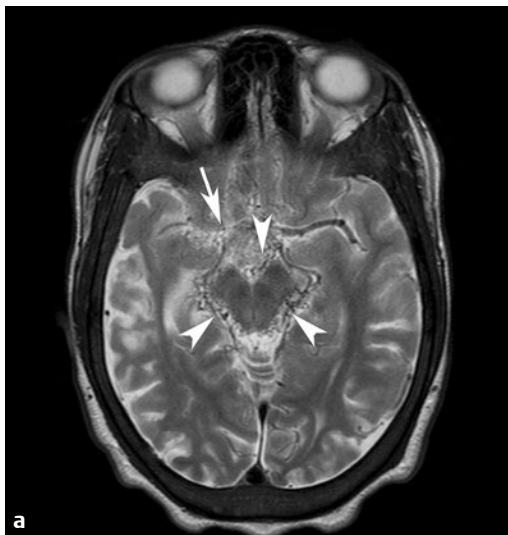
■ Clinical Presentation

A 7-year-old boy with sickle cell disease with acute onset of left hemiparesis.

■ Radiographic Studies

Axial T2-weighted MRI (**Fig. 21.1a**) shows multiple small collateral vessels in the basal cistern and ambient cistern (*arrowheads*). There is high signal in the right temporal lobe with cortical volume loss. Note the absence of the signal void within the right middle cerebral artery (*arrow*). Axial diffusion-weighted MRI (**Fig. 21.1b**) shows multifocal infarcts in the

right frontoparietal region (*arrows*). MRA shows proximal occlusion of the right middle cerebral artery and bilateral anterior cerebral arteries (**Fig. 21.1c**, *arrows*). Selective right internal carotid artery angiogram (**Fig. 21.1d**) shows proximal occlusion of the right middle cerebral artery and extensive parenchymal and leptomeningeal collateral vessels (*arrows*).



■ Diagnosis

Moyamoya Disease



■ Discussion and Differential Diagnosis

Moyamoya disease is a cerebrovascular disorder with progressive stenosis or occlusion of the internal carotid artery bifurcation with associated parenchymal, leptomeningeal, and transdural collaterals.¹ Patients present with recurrent transient ischemic attacks, strokes, headaches, and seizures; chronic dementia may result. The characteristic angiographic appearance with numerous parenchymal collaterals mimicking a “puff of smoke” led to the Japanese description of moyamoya.¹

Though moyamoya disease is most often idiopathic, the angiographic appearance may be seen in other conditions such as neurofibromatosis type 1, Down syndrome, systemic lupus erythematosus, cranial irradiation, and sickle cell disease.^{1,2}

Supraclinoid arterial occlusive disease is a common complication of sickle cell disease, with stroke occurring in 17% of patients.² Early detection of cerebral vasculopathy in sickle cell disease is performed using noninvasive diagnostic tools of transcranial Doppler and MRI/MRA. Erythrocytapheresis and hypertransfusion therapy are being studied in an attempt to prevent progressive cerebral vasculopathy and neurologic deterioration in sickle cell patients.³ In addition to parenchymal findings of ischemia/infarction, MRI occasionally shows pial collateral vessels as sulcal hyperintensity (ivy sign) on the FLAIR sequence.^{4,5}

Pearls

- ◆ Cerebral infarction in patients with sickle cell disease is primarily related to large vessel vasculopathy with occlusions of the supraclinoid internal carotid artery, middle cerebral artery, and anterior cerebral artery.²
- ◆ Surgical intervention (superficial temporal artery pial synangiosis) is performed in selected patients with idiopathic moyamoya disease to improve cerebral blood flow.¹

Pitfall

- ◆ Transient focal cerebral edema related to encephalitis or an active seizure focus may be difficult to differentiate from an acute infarction on imaging studies.

References

1. Robertson RL, Burrows PE, Barnes PD, Robson CD, Poussaint TY, Scott RM. Angiographic changes after pial synangiosis in childhood moyamoya disease. *AJNR Am J Neuroradiol* 1997;18:837–845 [PubMed](#)
2. Mugikura S, Takahashi S, Higano S, et al. The relationship between cerebral infarction and angiographic characteristics in childhood moyamoya disease. *AJNR Am J Neuroradiol* 1999;20:336–343 [PubMed](#)
3. Burke GM, Burke AM, Sherma AK, Hurley MC, Batjer HH, Bendok BR. Moyamoya disease: a summary. *Neurosurg Focus* 2009;26:E11 [PubMed](#)
4. Fujiwara H, Momoshima S, Kuribayashi S. Leptomeningeal high signal intensity (ivy sign) on fluid-attenuated inversion-recovery (FLAIR) MR images in moyamoya disease. *Eur J Radiol* 2005;55:224–230 [PubMed](#)
5. Yoon HK, Shin HJ, Chang YW. “Ivy sign” in childhood moyamoya disease: depiction on FLAIR and contrast-enhanced T1-weighted MR images. *Radiology* 2002;223:384–389 [PubMed](#)

Case 22

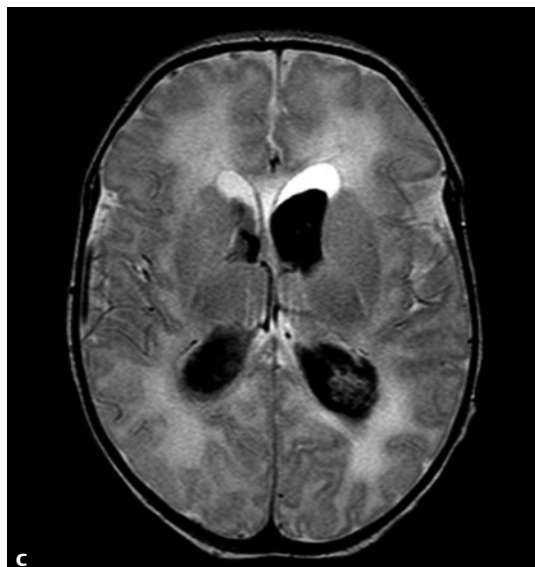
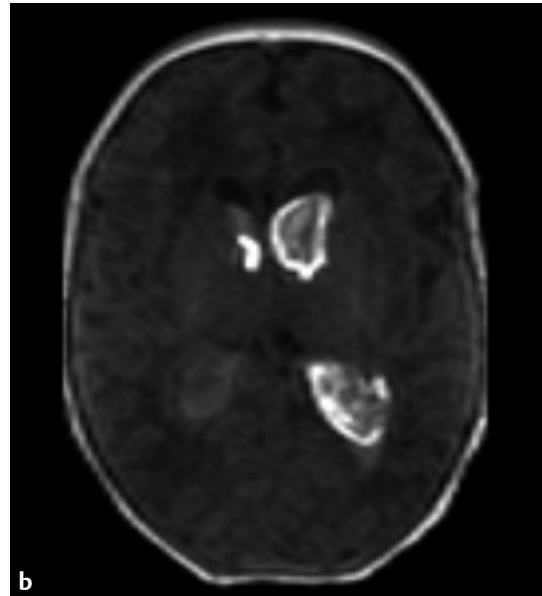
■ Clinical Presentation

Screening cranial ultrasound in a 1,250-g premature infant with hyaline membrane disease.

■ Radiographic Studies

Coronal transfontanelle ultrasound image (**Fig. 22.1a**) shows bilateral subependymal increased echogenicity. Axial T1-weighted and T2-weighted MRI scans (**Fig. 22.1b,c**) show intraventricular hemorrhage in both lateral ventricles, which

are dilated. The intraventricular hemorrhage is hyperintense on the T1-weighted image and low signal on T2-weighted image, consistent with subacute intraventricular hemorrhage.



■ Diagnosis

Subependymal/Intraventricular Hemorrhage

■ Discussion and Differential Diagnosis

Subependymal/intraventricular hemorrhage is a common problem in extremely preterm newborns. The densely vascular subependymal germinal matrix is the location of neuronal proliferation and is present until 32 weeks' gestation.^{1,2} In preterm infants, hemorrhage most commonly occurs within the substance of residual vascular germinal matrix tissue in the region of the caudothalamic groove. In older infants, hemorrhage may occur primarily within the choroid plexus. Intracranial hemorrhage is usually of increased echogenicity on ultrasound imaging. Blood (or occasionally pus) within the ventricular system may demonstrate a particulate echogenicity on sonography. Subependymal hemorrhage may occur as an isolated finding (grade 1), with intraventricular blood but without ventricular dilatation (grade 2), with intraventricular blood and dilated ventricles (grade 3), or with periventricular

intraparenchymal hemorrhage (grade 4).^{2,3} The risk factors for germinal matrix hemorrhage include low birth weight, prolonged or difficult labor, and congenital heart disease. Post-hemorrhagic hydrocephalus and damage to the periventricular white matter (PVL) are the most common complications of subependymal/intraventricular hemorrhage. There is a positive correlation between the higher grades of hemorrhage (particularly grade 4) and subsequent neurodevelopmental abnormalities.^{2,3} Portable cranial ultrasound is the imaging modality of choice in most premature infants with intracranial hemorrhage; CT or MRI is reserved for unusual or complicated cases. The intraventricular hemorrhage in this case would be classified as a grade 3 hemorrhage because there is both intraventricular blood and moderate ventricular dilatation.

Pearl

- ◆ Most subependymal/intraventricular hemorrhage in premature infants occurs prior to the end of the first week of life. Screening ultrasound is most efficiently accomplished in infants aged 4 to 7 days.^{2,3}

Pitfall

- ◆ In extremely premature infants, the head of the caudate nucleus may appear echogenic on cranial sonography and should not be confused with a subependymal hemorrhage.⁴

References

1. Roland EH, Hill A. Germinal matrix-intraventricular hemorrhage in the premature newborn: management and outcome. *Neurol Clin* 2003;21: 833–851, vi–vii vi–vii [PubMed](#)
2. Taylor GA. New concepts in the pathogenesis of germinal matrix intraparenchymal hemorrhage in premature infants. *AJNR Am J Neuroradiol* 1997;18:231–232 [PubMed](#)
3. Ballabh P. Intraventricular hemorrhage in premature infants: mechanism of disease. *Pediatr Res* 2010;67:1–8 [PubMed](#)
4. Schlesinger AE, Shackelford GD, Adcock LM. Hyperechoic caudate nuclei: a potential mimic of germinal matrix hemorrhage. *Pediatr Radiol* 1998;28: 297–302 [PubMed](#)

Case 23

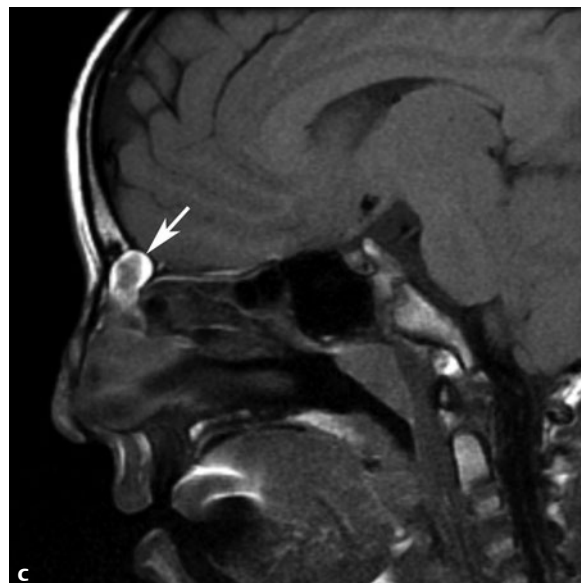
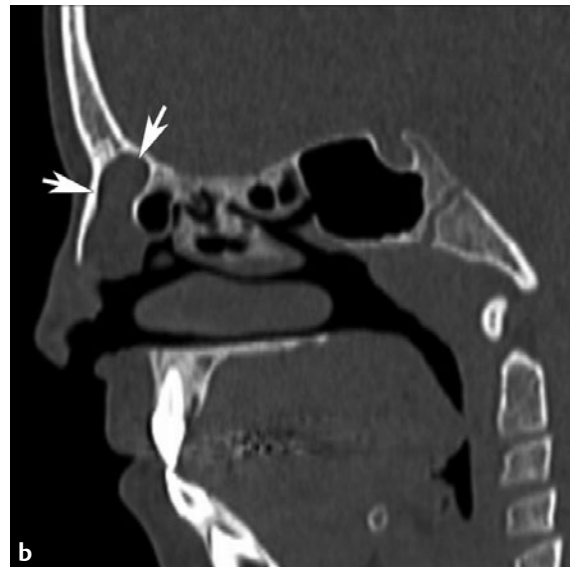
■ Clinical Presentation

A 2-year-old boy with a small pit in the skin in the midline of his nasal bridge.

■ Radiographic Studies

Axial high-resolution CT shows a midline defect in the nasal bone (**Fig. 23.1a**, arrows) with a round low attenuation mass compatible with fat. Sagittal reformatted CT image (**Fig. 23.1b**) shows the low attenuation lesion (arrows) and the bony defect

extending cranially to the anterior cranial fossa. Sagittal T1-weighted MRI shows a focal midline nasal high signal mass with cranial extension (**Fig. 23.1c**, arrow).



■ Diagnosis

Nasal Dermal Sinus/Dermoid Cyst

■ Discussion and Differential Diagnosis

The differential diagnosis of congenital nasal masses includes nasal cephalocele, nasal glioma, and nasal dermoid/dermal sinus.¹ Nasal dermoid cysts occur due to skin elements being pulled into the prenasal soft tissue along with the regressing dural diverticulum.¹ Infants with congenital nasal dermal sinuses present with a small pit, dimple, or soft tissue mass on the nose from the columella to the glabella. A sinus may end blindly in the soft tissues of the nose or extend intracranially through a bifid foramen cecum. There may be an associated

dermoid or epidermoid tumor in the sinus tract or in the midline intracranially. Some patients present with osteomyelitis of the frontal bone at the glabella, in which case the sinus tract may be obliterated. CT is useful in demonstrating bone detail in older children who have ossification of the anterior skull base. The multiplanar capability of MRI makes it the most useful preoperative imaging modality for demonstrating the skull base and dura in patients with nonossified skull base.^{2,3}

Pearl

- ◆ Any nasal mass or sinus in a child should be imaged with high-resolution MRI and possibly CT prior to surgical therapy to exclude intracranial communication or associated intracranial masses.

Pitfalls

- ◆ The normal thin, poorly ossified anterior midline skull base in the infant and young child may simulate a bony defect.
- ◆ Fat in the crista galli may simulate fatty tissue present in a dermoid tumor.

References

1. Barkovich AJ, Vandermarck P, Edwards MS, Cogen PH. Congenital nasal masses: CT and MR imaging features in 16 cases. *AJNR Am J Neuroradiol* 1991;12:105–116 [PubMed](#)
2. Hedlund G. Congenital frontonasal masses: developmental anatomy, malformations, and MR imaging. *Pediatr Radiol* 2006;36:647–662, quiz 726–727 [PubMed](#)
3. Huisman TA, Schneider JF, Kellenberger CJ, Martin-Fiori E, Willi UV, Holzmann D. Developmental nasal midline masses in children: neuroradiological evaluation. *Eur Radiol* 2004;14:243–249 [PubMed](#)

Case 24

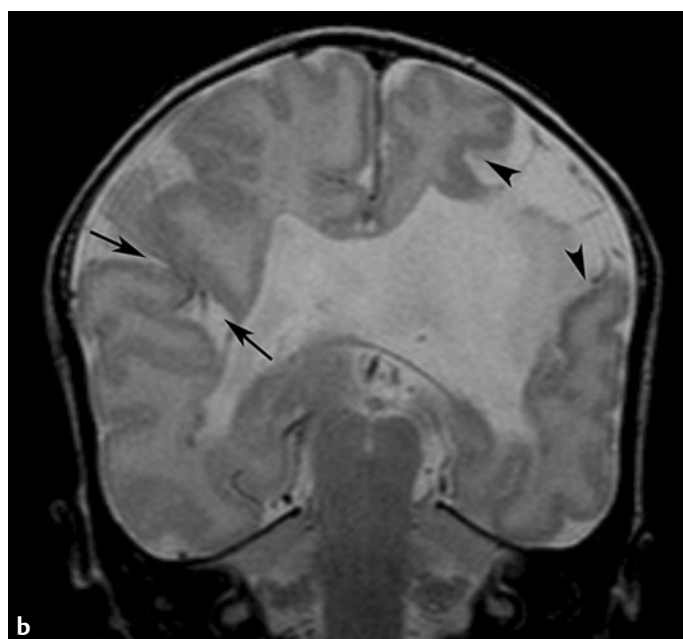
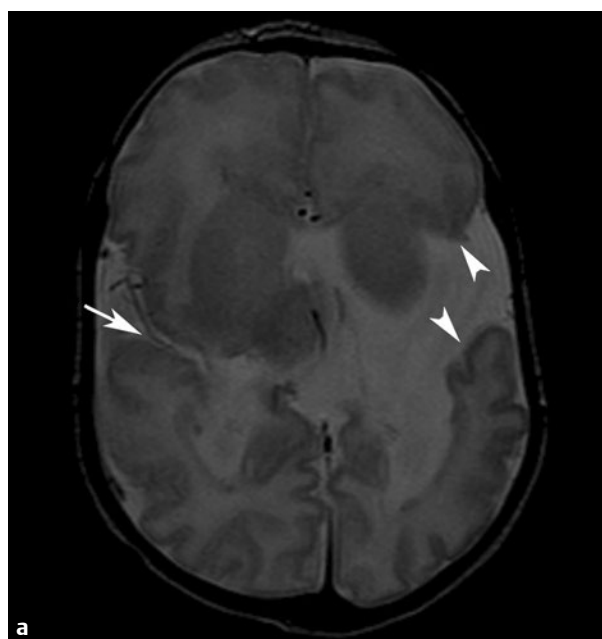
■ Clinical Presentation

A 9-month-old infant with seizures.

■ Radiographic Studies

Axial T2-weighted MRI (**Fig. 24.1a**) shows a right-sided cleft with opposed walls (*arrow*) and a left-sided, gray matter-lined, CSF-filled cleft (*arrowheads*) extending from the cerebral cortical surface to the ventricular lumen. Prominent vessels are

seen overlying the clefts, particularly on the right. Coronal T2-weighted MRI (**Fig. 24.1b**) demonstrates absence of the septum pellucidum as well as bilateral gray matter-lined clefts (closed lip, *arrow*; open lip, *arrowhead*).



■ Diagnosis

Schizencephaly

■ Discussion and Differential Diagnosis

Schizencephaly is a disorder of neuronal migration and refers to a cleft in the cerebral cortex that extends centrally toward the ventricle.¹ Patients with schizencephaly usually present with developmental delay and seizures.¹ The cleft is lined with gray matter that is dysplastic, which differentiates schizencephaly from encephaloclastic porencephaly or encephalomalacia, which is not lined by gray matter. In open-lip

schizencephaly, the cleft has a definite communication with the ipsilateral lateral ventricle and is filled with CSF. In closed-lip schizencephaly the walls of the cleft with dysplastic gray matter are in apposition.^{1–3} Schizencephaly may be unilateral or bilateral. The septum pellucidum is frequently absent. Coronal images are optimal to define the cleft, communication with the ventricular system, and associated anomalies.

Pearl

- ◆ Multiplanar imaging is optimal for demonstration of schizencephalic clefts.

Pitfall

- ◆ Closed-lip schizencephaly may be difficult to detect on ultrasound or on CT. MRI is optimal for diagnosis of this condition.

References

1. Glenn OA, Cuneo AA, Barkovich AJ, Hashemi Z, Bartha AI, Xu D. Malformations of cortical development: diagnostic accuracy of fetal MR imaging. *Radiology* 2012;263:843–855. [PubMed](#)
2. Oh KY, Kennedy AM, Frias AE Jr, Byrne JL. Fetal schizencephaly: pre- and postnatal imaging with a review of the clinical manifestations. *Radiographics* 2005;25:647–657. [PubMed](#)
3. Packard AM, Miller VS, Delgado MR. Schizencephaly: correlations of clinical and radiologic features. *Neurology* 1997;48:1427–1434. [PubMed](#)

Case 25

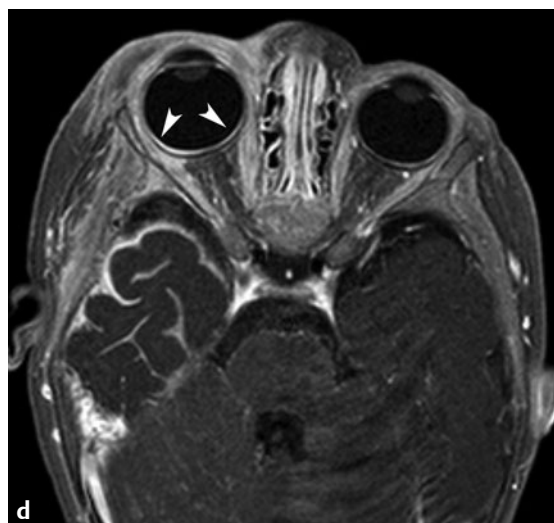
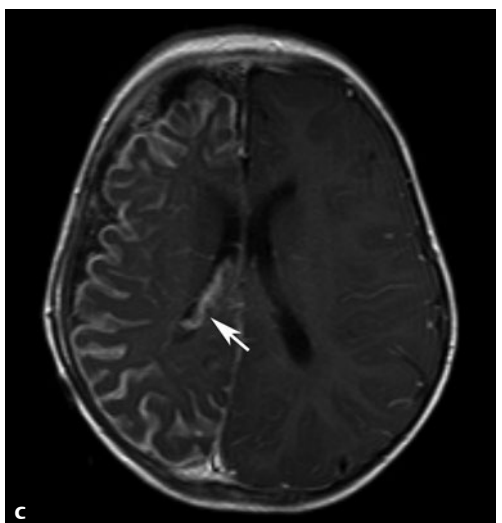
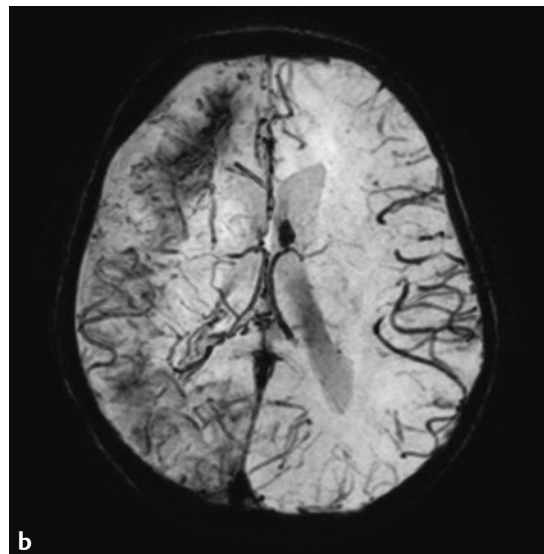
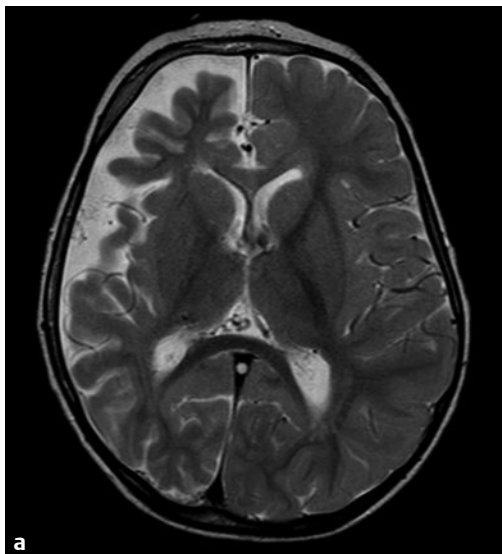
■ Clinical Presentation

A 12-year-old boy with right facial port-wine stain and seizures.

■ Radiographic Studies

Axial T2-weighted MRI (**Fig. 25.1a**) shows right cerebral hemiatrophy with subtle thickening of the right hemicranium. Axial susceptibility-weighted MRI (**Fig. 25.1b**) shows prominent abnormal vascular channels in the right hemisphere and cortical low signal secondary to dystrophic calcification in the right frontal lobe. Axial postcontrast T1-weighted MRI (**Fig. 25.1c**) shows intense surface enhancement over the right cerebral

hemisphere. There is prominent enhancement of the glomus of the right choroid plexus (*arrow*). Axial fat-suppressed T1-weighted MRI of the orbit (**Fig. 25.1d**) shows right preseptal soft tissue swelling and enhancement, which corresponds to the facial port-wine stain. There is enlargement of the right globe with retinal enhancement due to angiomas (arrowheads).



■ Diagnosis

Sturge-Weber Syndrome

■ Discussion and Differential Diagnosis

Sturge-Weber syndrome is characterized by a facial port-wine stain in association with retinal and leptomeningeal angiomatosis.¹ The facial lesion is usually ipsilateral to the retinal and cerebral lesion. The embryogenesis of the cerebral lesion is somewhat controversial, but the leptomeningeal angiomatosis is usually accompanied by abnormal superficial and deep cerebral venous drainage with associated dystrophic changes in

the cortex. Most patients present with seizures; glaucoma is frequently present.² Leptomeningeal angiomatosis results in a vascular steal phenomenon producing localized ischemia, resulting in cerebral hemiatrophy, cortical gyriform calcification, and gliosis. Enlarged medullary veins are frequently present as well as enlargement of the ipsilateral glomus of the choroid plexus.³

Pearls

- ◆ Most children with facial port-wine stains do not have ocular or leptomeningeal angiomatosis.
- ◆ Ocular enlargement with retinal angioma suggests infantile glaucoma.²

Pitfall

- ◆ CT is less sensitive than MRI in detecting cortical ischemic changes as well as leptomeningeal and cortical enhancement.

References

1. Adams ME, Aylett SE, Squier W, Chong W. A spectrum of unusual neuroimaging findings in patients with suspected Sturge-Weber syndrome. *AJNR Am J Neuroradiol* 2009;30:276–281 [PubMed](#)
2. Griffiths PD, Boodram MB, Blaser S, et al. Abnormal ocular enhancement in Sturge-Weber syndrome: correlation of ocular MR and CT findings with clinical and intracranial imaging findings. *AJNR Am J Neuroradiol* 1996;17:749–754 [PubMed](#)
3. Griffiths PD, Blaser S, Boodram MB, Armstrong D, Harwood-Nash D. Choroid plexus size in young children with Sturge-Weber syndrome. *AJNR Am J Neuroradiol* 1996;17:175–180 [PubMed](#)

Case 26

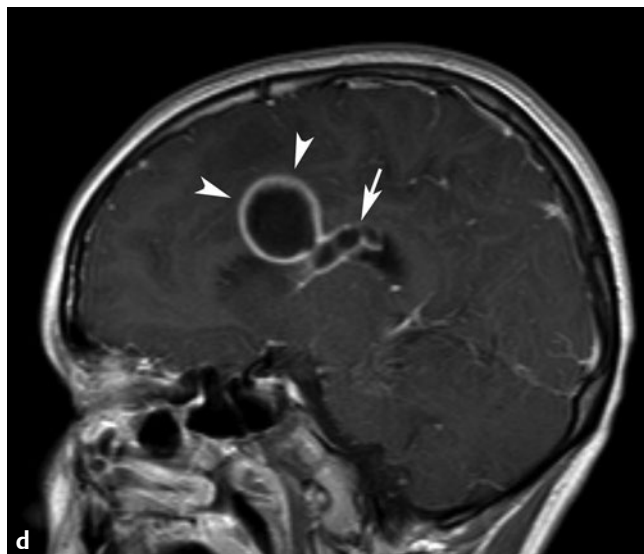
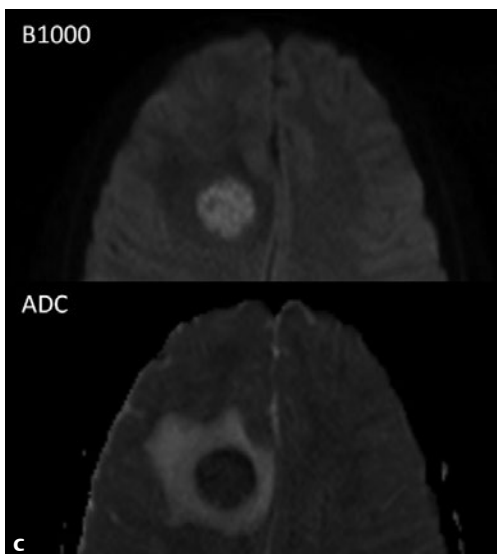
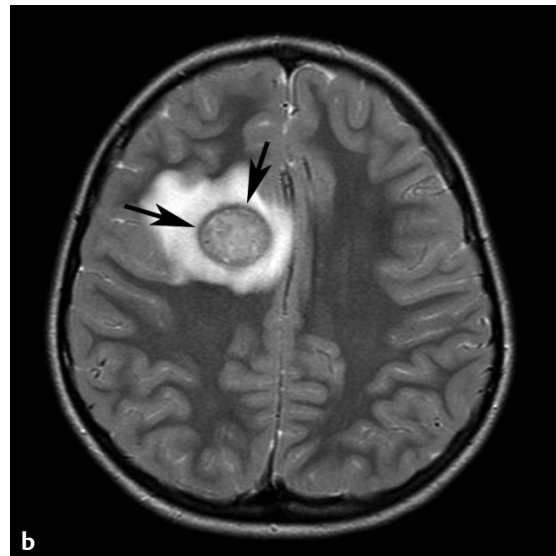
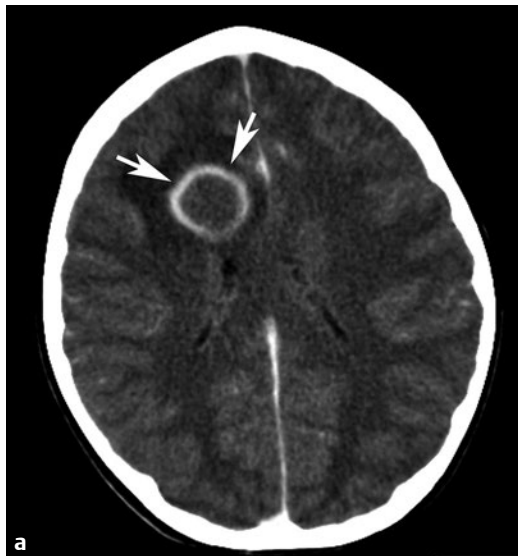
■ Clinical Presentation

A 9-year-old girl with headaches and recent onset of seizure activity.

■ Radiographic Studies

Axial postcontrast CT image (**Fig. 26.1a**) shows a rounded low attenuation mass with ring enhancement (*arrows*) in the right frontal lobe with surrounding vasogenic edema. Axial T2-weighted MRI (**Fig. 26.1b**) shows the mass is mixed hyperintense and hypointense to gray matter with a low signal intensity rim (*arrows*). Axial B1000 image (*top*) and ADC map

(*bottom*) of diffusion-weighted MRI sequence (**Fig. 26.1c**) shows restricted diffusion. Postgadolinium sagittal T1-weighted MRI (**Fig. 26.1d**) demonstrates intense rim enhancement of the periphery of the mass (*arrowheads*). Notice the intraventricular extent of the abscess (*arrow*). Stereotactic aspiration of the right frontal lobe lesion yielded purulent material.



■ Diagnosis

Brain Abscess

■ Discussion and Differential Diagnosis

Brain abscesses are more common in adolescents than in younger children. Causes of cerebral abscess include right-to-left shunting in children with cyanotic congenital heart disease, endocarditis, lung abscess, penetrating trauma, infected congenital dermal sinus, paranasal sinus disease, and mastoiditis.¹ Patients with cerebral abscess present with symptoms of raised intracranial pressure, focal neurologic deficits, and seizures. Contrast-enhanced CT characteristically shows focal edema with ring-enhancing lesion with central low-density and surrounding vasogenic edema.¹ Ependymal or leptomeningeal enhancement occurs if the abscess ruptures into the ventricle or into the subarachnoid space. Acute hydro-

cephalus is commonly seen with intraventricular decompression of the abscess and can be fatal. MRI is more sensitive than CT for early diagnosis of brain abscess.^{1,2} T1-weighted images show central low signal with peripheral ring enhancement following gadolinium administration. T2-weighted images show central hyperintensity, a peripheral low signal capsular ring, and surrounding vasogenic edema. Restricted diffusion on MRI is virtually always found within an abscess, which helps differentiate from other space-occupying lesions.^{2,3} Differential diagnosis of brain abscess includes subacute infarction, resolving hematoma, demyelinating plaque, and metastatic disease.

Pearl

- ◆ Brain abscess is a rare complication of meningitis except in newborns with gram-negative meningitis.

Pitfall

- ◆ Even appropriately treated and bacteriologically sterile brain abscesses may show ring enhancement on CT or MRI for months after diagnosis.

References

1. Haimes AB, Zimmerman RD, Morgello S, et al. MR imaging of brain abscesses. *AJR Am J Roentgenol* 1989;152:1073–1085 [PubMed](#)
2. Lai PH, Ho JT, Chen WL, et al. Brain abscess and necrotic brain tumor: discrimination with proton MR spectroscopy and diffusion-weighted imaging. *AJNR Am J Neuroradiol* 2002;23:1369–1377 [PubMed](#)
3. Nath K, Agarwal M, Ramola M, et al. Role of diffusion tensor imaging metrics and in vivo proton magnetic resonance spectroscopy in the differential diagnosis of cystic intracranial mass lesions. *Magn Reson Imaging* 2009; 27:198–206 [PubMed](#)

Case 27

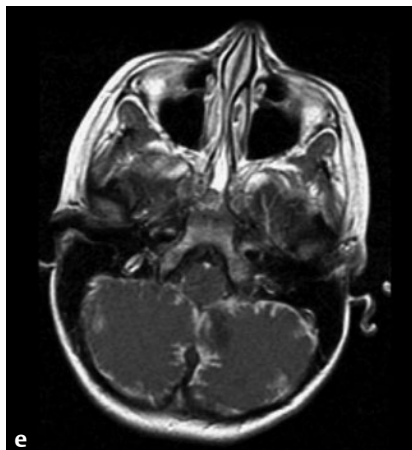
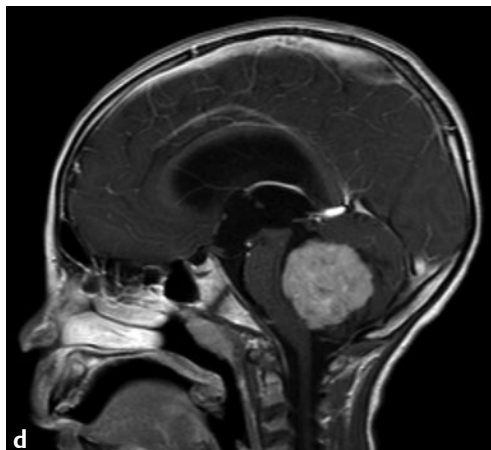
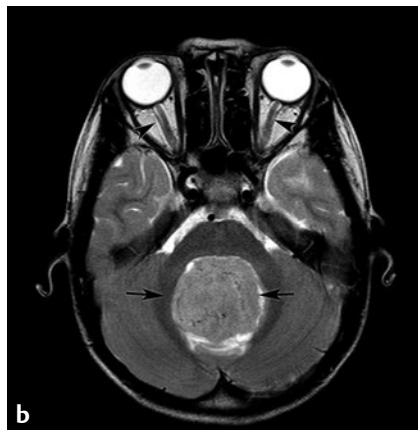
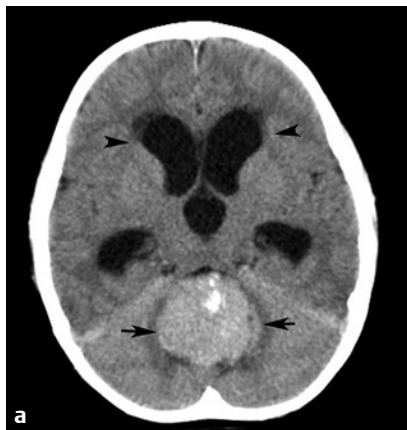
■ Clinical Presentation

A 5-year-old boy with ataxia, headaches, and papilledema.

■ Radiographic Studies

Axial noncontrast CT image (**Fig. 27.1a**) shows a hyperdense mass (*arrows*) within the fourth ventricle with focal calcification and dilated ventricles (*arrowhead*) with periventricular CSF seepage. Axial T2-weighted MRI (**Fig. 27.1b**) demonstrates a T2 isointense mass in the region of the fourth ventricle (*arrows*). There is increase CSF within the optic nerve sheath (*arrowheads*) in this patient with clinical papilledema. The tumor shows restricted diffusivity on axial B1000 diffusion-weighted

MRI sequence (**Fig. 27.1c**). Sagittal T1-weighted postcontrast MRI (**Fig. 27.1d**) shows intense contrast enhancement in the mass as well as significant mass effect on the brainstem. Axial postcontrast T1-weighted MRI (**Fig. 27.1e**) in another child illustrates extensive, enhancing leptomeningeal tumor spread along the cerebellar folia and CSF cisterns. Sagittal T1-weighted, postcontrast spine MRI shows enhancing leptomeningeal masses (**Fig. 27.1f**).



■ Diagnosis

Medulloblastoma

■ Discussion and Differential Diagnosis

Medulloblastoma is the most common posterior fossa tumor in childhood.¹ This tumor is sometimes classified as a primitive neuroectodermal tumor (PNET). Medulloblastoma most commonly occurs in the first decade of life and presents after a short history of symptoms typical of posterior fossa tumors including headache, nausea, and vomiting.¹ In young children, medulloblastoma usually presents as a midline mass arising from the vermis, growing into the fourth ventricle. Hydrocephalus is usually present secondary to fourth ventricular and aqueductal obstruction. On CT, medulloblastoma is usually hyperdense to gray matter and shows intense enhancement

after contrast administration. Calcification and cyst formation may occur within the tumor. On MRI, the tumor tends to be isointense to gray matter on both T1- and T2-weighted images and enhances with contrast administration. Restricted diffusion helps to differentiate medulloblastoma from other posterior fossa tumors, especially pilocytic astrocytoma.^{2,3} Medulloblastoma may spread locally into the cerebellopontine angles as well as via the CSF into the ventricular system, cisterns, and spinal canal. Contrast-enhanced MRI of the spine is performed to rule out “drop metastasis.”⁴

Pearls

- ◆ Systemic metastases may involve the lymphatic system and the skeleton.
- ◆ Rarely, medulloblastoma may occur in patients with Turcot, Gardner, or Cowden syndrome.⁵

Pitfall

- ◆ In older children, the desmoplastic variant of medulloblastoma tends to occur in the cerebellar hemispheres rather than in the midline.⁶

References

1. Vézina LG, Packer RJ. Infratentorial brain tumors of childhood. Neuroimaging Clin N Am 1994;4:423–436 [PubMed](#)
2. Jaremko JL, Jans LB, Coleman LT, Ditchfield MR. Value and limitations of diffusion-weighted imaging in grading and diagnosis of pediatric posterior fossa tumors. AJNR Am J Neuroradiol 2010;31:1613–1616 [PubMed](#)
3. Rumboldt Z, Camacho DL, Lake D, Welsh CT, Castillo M. Apparent diffusion coefficients for differentiation of cerebellar tumors in children. AJNR Am J Neuroradiol 2006;27:1362–1369 [PubMed](#)
4. Meyers SP, Wildenhain SL, Chang JK, et al. Postoperative evaluation for disseminated medulloblastoma involving the spine: contrast-enhanced MR findings, CSF cytologic analysis, timing of disease occurrence, and patient outcomes. AJNR Am J Neuroradiol 2000;21:1757–1765 [PubMed](#)
5. Hamada H, Kurimoto M, Endo S, Ogiuchi T, Akai T, Takaku A. Turcot's syndrome presenting with medulloblastoma and familial adenomatous polyposis: a case report and review of the literature. Acta Neurochir (Wien) 1998;140:631–632 [PubMed](#)
6. Levy RA, Blaivas M, Muraszko K, Robertson PL. Desmoplastic medulloblastoma: MR findings. AJNR Am J Neuroradiol 1997;18:1364–1366 [PubMed](#)

Case 28

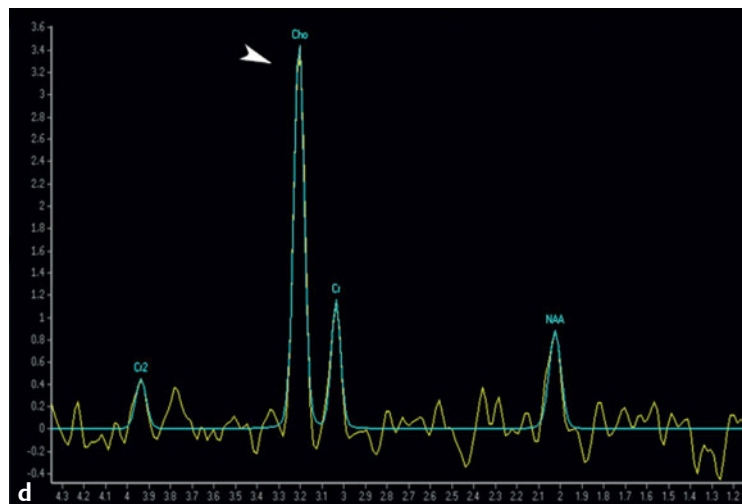
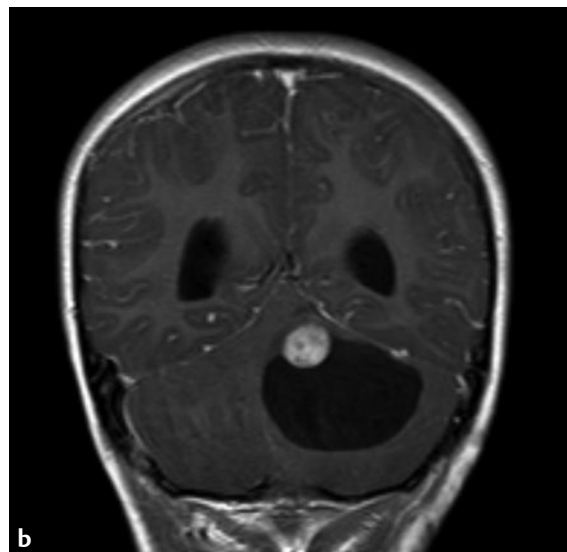
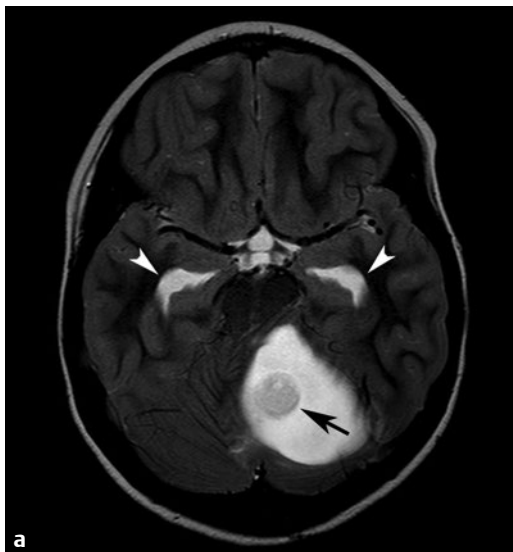
■ Clinical Presentation

A 5-year-old girl with headaches, vomiting, and papilledema.

■ Radiographic Studies

Axial T2-weighted MRI (**Fig. 28.1a**) shows a large left cerebellar cystic lesion with mural nodule (*arrow*) displacing the brainstem to the right. Note the dilated temporal horns due to obstructive hydrocephalus (*arrowheads*). Coronal and sagittal postcontrast T1-weighted MRI scans (**Fig. 28.1b,c**) show intense contrast enhancement of the tumor nodule but no en-

hancement of the cyst wall. There is loss of posterior fossa cisternal spaces with caudal herniation of the cerebellar tonsils. Long TE single voxel magnetic resonance spectroscopy (**Fig. 28.1d**) over the mural nodule shows elevated choline peak (*arrowhead*).



■ Diagnosis

Cerebellar Pilocytic Astrocytoma

■ Discussion and Differential Diagnosis

Cerebellar astrocytomas in children are commonly of the pilocytic variety, which are low grade (World Health Organization [WHO] grade 1) and have an excellent prognosis following complete surgical resection.¹ These tumors usually originate in the vermis and may extend into the cerebellar hemispheres. Hydrocephalus is present, associated with obstruction of the fourth ventricle and aqueduct of Sylvius. Typically, there is a large cyst that displaces the fourth ventricle associated with a prominent solid mural nodule, although many tumors may not have this classic appearance. The solid portion of the tumor usually enhances homogeneously on CT and MRI; typically, there is no enhancement in the cyst wall. The cyst wall is usually composed of compressed brain tissue rather than tumor. Although hemangioblastomas have a similar neuroim-

aging appearance, they uncommonly occur during the first decade of life, when cerebellar astrocytomas are most common. On CT, the mural nodule of astrocytoma is usually isodense to brain and the cyst appears similar to CSF. On MRI, the mural nodule may be isointense or hyperintense to brain on T2-weighted images and is usually isointense to slightly hypointense on T1-weighted images.^{1,2} Magnetic resonance spectroscopy over the solid component typically shows elevated choline peak and inverted lactate doublet.³ In contrast to medulloblastoma, the solid components of pilocytic astrocytoma do not show restricted diffusion. The tumor may also present as a solid mass with areas of cystic degeneration. Calcification may occur in the solid component. Leptomeningeal metastasis may occur but is very uncommon.

Pearl

- ◆ The most common posterior fossa tumors in children include (in order of decreasing frequency) medulloblastoma, cerebellar astrocytoma, brainstem glioma, and ependymoma.

Pitfall

- ◆ Hemangioblastoma may have a similar neuroimaging appearance.

References

1. Paldino MJ, Faerber EN, Poussaint TY. Imaging tumors of the pediatric central nervous system. *Radiol Clin North Am* 2011;49:589–616, v. [PubMed](#)
2. Koeller KK, Rushing EJ. From the archives of the AFIP: pilocytic astrocytoma: radiologic-pathologic correlation. *Radiographics* 2004;24:1693–1708. [PubMed](#)
3. Hwang JH, Egnaczyk GF, Ballard E, Dunn RS, Holland SK, Ball WS Jr. Proton MR spectroscopic characteristics of pediatric pilocytic astrocytomas. *AJNR Am J Neuroradiol* 1998;19:535–540. [PubMed](#)

Case 29

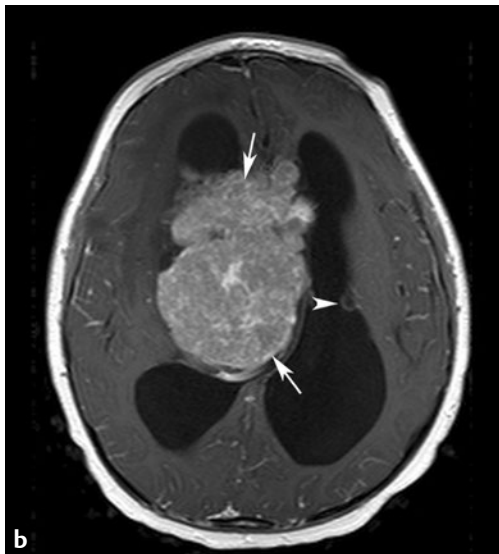
■ Clinical Presentation

A 7-year-old girl with history of seizures developed progressive headaches, nausea, and vomiting over a 2-month period.

■ Radiographic Studies

Noncontrast CT image (**Fig. 29.1a**) and postcontrast T1-weighted MRI (**Fig. 29.1b**) reveal characteristic calcified subependymal nodules (*arrowheads*) along the ventricular wall and a large enhancing mass at the right foramen of Monro (*arrows*), causing obstructive hydrocephalus. This mass was surgically resected and found to be a giant cell astrocytoma.

Axial T2-weighted MRI (**Fig. 29.1c**) shows low-signal subependymal nodules and multiple high-signal cortical tubers (*arrows*). Axial FLAIR MRI (**Fig. 29.1d**) of another patient shows transverse linear streaks (*arrows*) extending from the cortex toward the ventricles, representing the neuronal migration abnormalities seen in some patients with this disease.



■ Diagnosis

Tuberous Sclerosis

■ Discussion and Differential Diagnosis

Tuberous sclerosis (Bourneville's disease) is a condition in which imaging is essential for diagnosis and for determining the extent of disease.¹ Infants with tuberous sclerosis may not show skin manifestations of the disease, and there may not be a family history. Three of the pathognomonic diagnostic criteria for diagnosis of tuberous sclerosis are found by imaging and include subependymal nodules, cortical tubers, and multiple unilateral or bilateral renal angiomyolipomas.^{2,3} Other pathognomonic diagnostic criteria include retinal hamartomas, facial angiofibromas, ungual fibromas, and cutaneous fibrous plaques. Infants with tuberous sclerosis frequently have a type of seizure known as infantile spasms.

Imaging of children with suspected tuberous sclerosis should include cranial MRI and abdominal ultrasound. On MRI, subependymal nodules in infants are bright on T1-weighted images but later develop low signal intensity due to calcification.^{2,3} Subependymal nodules frequently enhance on MRI following contrast administration. In infants, cortical tubers and white matter lesions are hyperintense to gray matter on T1-weighted

images, but this high signal intensity diminishes with progressive myelination.³ Cortical tubers and white matter lesions may enhance after contrast administration, but enhancement is less common than in the subependymal nodules. On CT, subependymal nodules are difficult to detect in infants until the nodules calcify. White matter lesions on CT tend to be low attenuation. Subependymal nodules typically do not enhance on CT after contrast administration unless a giant cell astrocytoma is present. Giant cell astrocytomas may occur in patients with tuberous sclerosis, usually at the end of the first decade or during the second decade of life. These tumors are most commonly located at the foramen of Monro and present as obstructive hydrocephalus.^{2,3} The tumors show intense enhancement after the administration of intravenous contrast. Annual cranial MRI scans are recommended for patients with tuberous sclerosis during the first two decades of life to detect subependymal giant cell astrocytomas when the tumors are small and more easily resectable.⁴

Pearl

- ◆ The classic clinical triad found in patients with tuberous sclerosis includes mental retardation, adenoma sebaceum (cutaneous angiofibromas), and seizure disorder.

Pitfall

- ◆ The periventricular calcifications seen in patients with TORCH infections should not be confused with the subependymal calcified tubers found in tuberous sclerosis.

References

1. Baron Y, Barkovich AJ. MR imaging of tuberous sclerosis in neonates and young infants. *AJNR Am J Neuroradiol* 1999;20:907–916 [PubMed](#)
2. Arca G, Pacheco E, Alfonso I, Duchowny MS, Melnick SJ. Characteristic brain magnetic resonance imaging (MRI) findings in neonates with tuberous sclerosis complex. *J Child Neurol* 2006;21:280–285 [PubMed](#)
3. Pinto Gama HP, da Rocha AJ, Braga FT, et al. Comparative analysis of MR sequences to detect structural brain lesions in tuberous sclerosis. *Pediatr Radiol* 2006;36:119–125 [PubMed](#)
4. Braffman BH, Bilaniuk LT, Naidich TP, et al. MR imaging of tuberous sclerosis: pathogenesis of this phakomatosis, use of gadopentetate dimeglumine, and literature review. *Radiology* 1992;183:227–238 [PubMed](#)



Spine

Section Editor

Charles M. Glasier

Author

Sumit Singh



Case 30

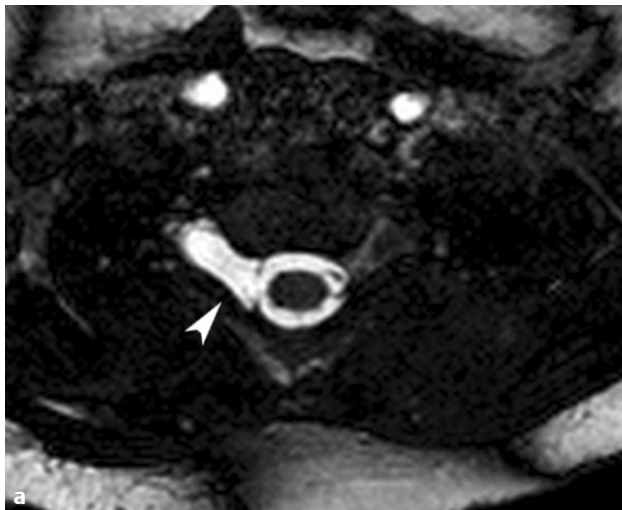
■ Clinical Presentation

A 5-month-old infant has upper extremity paralysis. The baby was 4000-g term infant of a diabetic mother delivered vaginally with a breech presentation.

■ Radiographic Studies

Axial balanced fast field echo MRI (**Fig. 30.1a**) shows discrete tubular cerebrospinal fluid collection (pseudomeningocele) in the right C7-T1 neural foramen (*arrowhead*). The adjacent right nerve roots are not seen, compared with the corresponding normal left nerve roots at this level. Sagittal T2-weighted

MRI (**Fig. 30.1b**) shows pseudomeningocele in the right C7-T1 neural foramen (*arrowhead*). Coronal short tau inversion recovery (STIR) MRI (**Fig. 30.1c**) in another patient shows hyperintensity along the right C6 nerve (*arrow*), suggesting stretching injury.



■ Diagnosis

Brachial Plexopathy: Birth Injury

■ Discussion and Differential Diagnosis

Brachial plexopathy is seen most commonly in macrosomic term infants, especially in association with breech delivery.¹ The injury is presumed to be caused by stretching of the neck during delivery with tears of the root sleeve or actual avulsion of the spinal nerve.¹ The lower cervical nerve roots (C4–C8) are most commonly injured, leading to the clinical finding of upper extremity paralysis.¹ Injury to C5 and C6 nerve roots (Erb–Duchenne palsy) affects muscles of the shoulder and proximal arm; injury to C8 and T1 nerve roots (Dejerine–Klumpke palsy) affects muscles of the forearm and hand. There may be an associated paresis of the ipsilateral hemidiaphragm.

Plain radiographs of the upper extremity and chest should be obtained to rule out clavicular or humeral fractures. Fortunately, most infants with brachial plexopathy recover sponta-

neously without surgical intervention.¹ Imaging is usually performed after 3 months of age following incomplete recovery of neurologic function. 3D MRI has largely replaced thin-slice, high-resolution CT myelography for demonstrating tiny spinal roots in infants for differentiation and surgical planning for traumatic injuries.² MRI demonstrates pseudomeningoceles, nerve root avulsion, damage to the cervical spinal cord, and paraspinal muscle intensity changes in preganglionic injury.^{2,3} In postganglionic injuries (distal to dorsal root ganglion), enhancing nodular thickening (posttraumatic neuroma) and hematoma in the vicinity of the injury can be seen.^{2,3} In a stretching injury, MRI reveals asymmetric thickening, irregularity, T2 hyperintensity, and contrast enhancement of the injured nerve.^{2,3}

Pearl

- ◆ Brachial plexus injuries may be associated with clavicle fractures, probably related to extreme traction on the shoulder during delivery.

Pitfall

- ◆ Pseudomeningoceles in the newborn are small lesions. High-resolution, motion-free imaging is necessary to reliably detect these abnormalities.

References

1. Sjöberg I, Erichs K, Bjerre I. Cause and effect of obstetric (neonatal) brachial plexus palsy. *Acta Paediatr Scand* 1988;77:357–364 [PubMed](#)
2. Aralasmak A, Karaali K, Cevikol C, Uysal H, Senol U. MR imaging findings in brachial plexopathy with thoracic outlet syndrome. *AJNR Am J Neuroradiol* 2010;31:410–417 [PubMed](#)
3. Chhabra A, Thawait GK, Soldatos T, et al. High-resolution 3T MR neurography of the brachial plexus and its branches, with emphasis on 3D imaging. *AJNR Am J Neuroradiol* 2013;34:486–497 [PubMed](#)

Case 31

■ Clinical Presentation

A 5-year-old girl with fever, back pain, and leg pain.

■ Radiographic Studies

Sagittal T2-weighted MRI (**Fig. 31.1a**) shows heterogenous hyperintensity in the posterior thoracic epidural space (*arrowheads*). Postcontrast sagittal T1-weighted MRI with fat saturation (**Fig. 31.1b**) shows a peripherally enhancing epidural collection (*arrowheads*). Axial T2-weighted MRI (**Fig. 31.1c**)

shows hyperintense collection in the posterior epidural space (*arrow*) causing anterior displacement and moderate effacement of the thecal sac. Postcontrast axial T1-weighted MRI with fat saturation (**Fig. 31.1d**) shows peripherally enhancing collection (*arrow*) consistent with abscess formation.



■ Diagnosis

Epidural Abscess

■ Discussion and Differential Diagnosis

Epidural abscess is most commonly located posteriorly in the spinal canal. The most common cause of epidural abscess is sepsis, with the infection reaching the spinal canal through the Batson plexus.¹ Anterior epidural abscesses are typically due to direct extension from diskitis or vertebral osteomyelitis.² Neurologic dysfunction is often disproportionate to the degree of compression on the spinal cord perhaps due to inflammation of the epidural venous plexus, which may compromise circulation and result in cord ischemia. Surgical decompression remains the main line of treatment.³

Magnetic resonance imaging is the modality of choice for the diagnosis of epidural abscess.⁴ Hyperintense fluid collections on T2-weighted images with peripheral rim enhancement on T1-weighted images are delineated. The epidural abscess collections show restricted diffusion. MRI may also demonstrate spinal cord edema, associated vertebral osteomyelitis/diskitis, and paraspinal abscess.

Pearl

- ◆ Children with sepsis and back pain require urgent contrast-enhanced MRI to exclude epidural abscess.

Pitfall

- ◆ Intravenous contrast administration is required to demonstrate rim enhancement of abscess collection.

References

1. Glazer PA, Hu SS. Pediatric spinal infections. *Orthop Clin North Am* 1996;27:111–123 [PubMed](#)
2. Chao D, Nanda A. Spinal epidural abscess: a diagnostic challenge. *Am Fam Physician* 2002;65:1341–1346 [PubMed](#)
3. Martin RJ, Yuan HA. Neurosurgical care of spinal epidural, subdural, and intramedullary abscesses and arachnoiditis. *Orthop Clin North Am* 1996;27:125–136 [PubMed](#)
4. Barkovich AJ, Raybaud C. *Pediatric Neuroimaging*, 5th ed. Philadelphia: Lippincott Williams & Wilkins; 2012

Case 32

■ Clinical Presentation

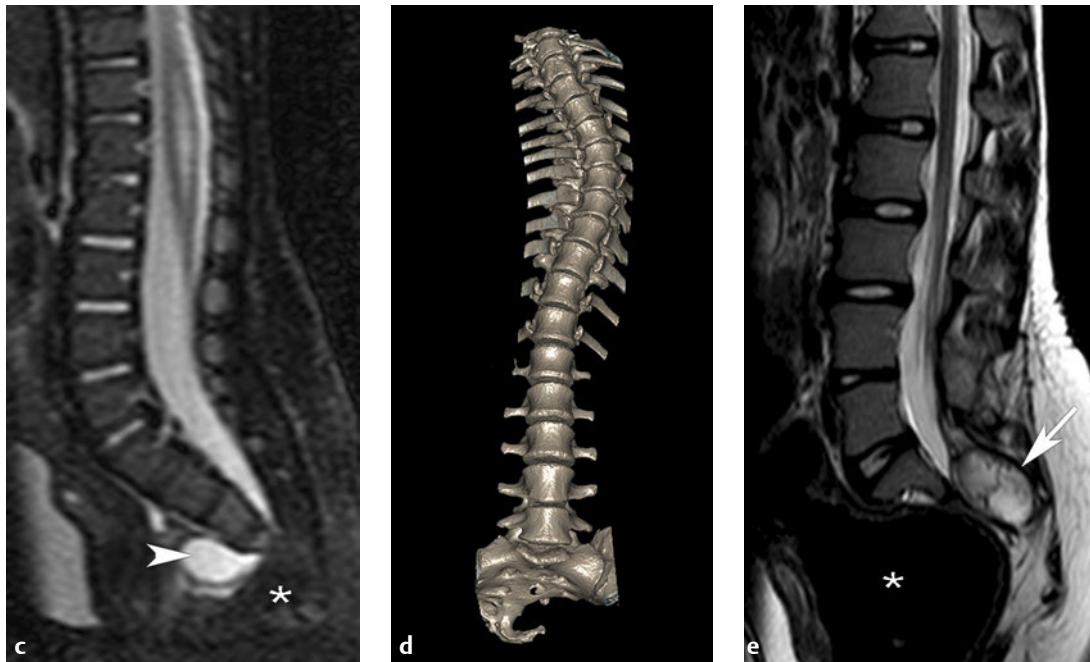
A newborn with imperforate anus.

■ Radiographic Studies

Anteroposterior (AP) radiograph (**Fig. 32.1a**) shows sickle bone deformity of the sacrum (*arrowhead*). Sagittal T1-weighted MRI (**Fig. 32.1b**) shows hypoplasia of the sacrum. There is mixed intensity presacral mass with lobular high signal component (*asterisk*) extending into the sacral canal, and a more anterior oval hypointense component (*arrowhead*). Sagittal STIR MRI (**Fig. 32.1c**) shows suppression of the T1 hyperintense fatty lesion (*asterisk*); the more anterior oval component is hyperintense (*arrowhead*), suggesting meningocele.

Note the low-lying conus medullaris, with associated syrinx versus dilated ventriculus terminalis. 3D volume-rendered CT image in another patient (**Fig. 32.1d**) shows sickle-shaped sacral anomaly. Sagittal T2-weighted MRI (**Fig. 32.1e**) in the patient shown in **Fig. 32.1d** shows sacral hypoplasia, mixed intensity oval mass in the sacral canal most consistent with dermoid (*arrow*), and dilation of the rectum (*asterisk*), suggesting rectal stenosis.





■ Diagnosis

Currarino Triad

■ Discussion and Differential Diagnosis

Currarino triad, also known as ASP (anorectal malformation, sacrococcygeal osseous defect, and presacral mass) triad, is a unique complex of caudal congenital anomalies with autosomal dominant genetic inheritance in more than 50% of cases.¹ Anorectal malformations may include anal ectopia, rectal stenosis, and imperforate anus. Bony sacral segmentation anomalies include the classic sickle-shaped sacrum. Presacral masses include meningocele, teratoma, dermoid cyst, hamartoma, and enteric duplication cyst.² Fetal ultrasound and fetal MRI can be effective in prenatal diagnosis.

Infants with anorectal anomalies should undergo screening neuroimaging of the spine in the neonatal period. Screening should include plain radiography of the spine and pelvis and spine ultrasound. If a sacral defect is seen or if spine ultrasound suggests intraspinal pathology, MRI evaluation of the spine is necessary. High-resolution MRI provides information concerning the presence of associated intraspinal anomalies such as tethered cord or lipoma and delineates any associated presacral mass.³

Pearl

- ◆ Infants with sacral agenesis or sacral anomalies have an increased incidence of tethered cord and other intraspinal anomalies.

Pitfall

- ◆ Look carefully at the “scout” radiograph in all patients undergoing barium enema examination for constipation. The presence of a “sickle deformity” of the sacrum may indicate the presence of an associated presacral mass.

References

1. Currarino G, Coln D, Votteler T. Triad of anorectal, sacral, and presacral anomalies. *AJR Am J Roentgenol* 1981;137:395–398. [PubMed](#)
2. Kocaoglu M, Frush DP. Pediatric presacral masses. *Radiographics* 2006; 26:833–857. [PubMed](#)
3. Low G, Irwin GJ, Haddock G, Maroo SV. Currarino triad: characteristic appearances on magnetic resonance imaging and plain radiography. *Australas Radiol* 2006;50:249–251. [PubMed](#)

Case 33

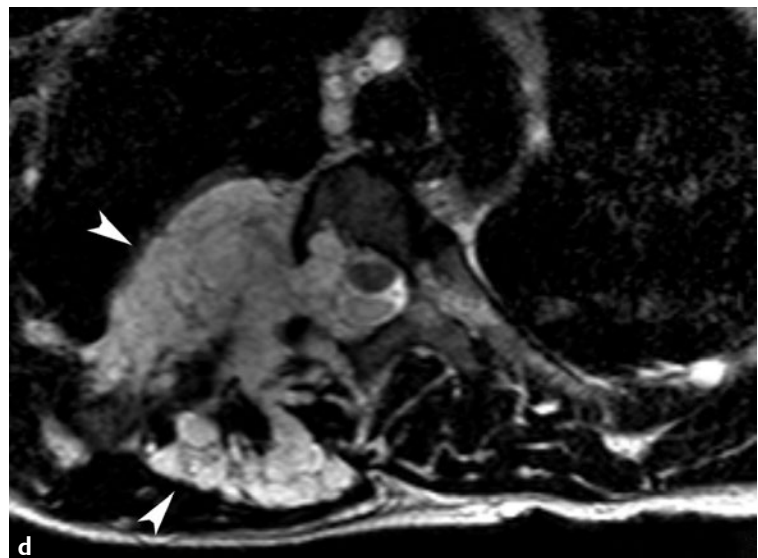
■ Clinical Presentation

A 5-year-old boy with spine deformity, multiple café-au-lait spots, and family history of tumors.

■ Radiographic Studies

Sagittal STIR MRI (**Fig. 33.1a**) shows dural ectasia with scalloping of posterior margin of the L4 vertebral body (*arrow*). Postcontrast sagittal T1-weighted MRI (**Fig. 33.1b**) shows enhancement within the lower cervical and upper thoracic neurofibromas (*arrow*). Coronal STIR MRI (**Fig. 33.1c**) shows

bilateral hyperintense tubulonodular lumbosacral lesions. Axial T2-weighted MRI (**Fig. 33.1d**) shows a large lobular plexiform neurofibroma (*arrowheads*) in the right intercostal/extrapleural, paraspinal, and intraspinal regions.



■ Diagnosis

Neurofibromatosis Type 1

■ Discussion and Differential Diagnosis

Spinal involvement is commonly seen in patients with neurofibromatosis type 1 (NF1). Most spinal tumors in these patients are neurofibromas, although in rare cases intramedullary tumors, such as astrocytomas, are seen.¹ Extrapapinal tumors may be associated with either minimal or extensive intraspinal involvement with cord compression. Dural ectasia without soft tissue mass may be associated with extensive bony deformity.² Rapid growth of an existing mass or development of a

new, enlarging mass may indicate development of a malignant nerve sheath tumor. Large heterogeneous masses (> 5 cm) with ill-defined margins, invasion of fat planes, and surrounding edema are more suggestive of malignant nerve sheath tumor.³ Fluorodeoxyglucose (FDG) positron emission tomography (PET) and PET/CT are useful and highly sensitive methods to identify malignant change in nerve sheath tumors in NF1 patients.⁴

Pearl

- ◆ Posterior vertebral body scalloping with neural foramen widening are characteristic spine findings of NF1. Acute angular kyphoscoliosis suggests the diagnosis of NF1 particularly in the presence of bony erosion and neural foramen expansion.

Pitfall

- ◆ Dural ectasia may be seen in patients without NF1 or spinal tumors.

References

1. Abul-Kasim K, Thurnher MM, McKeever P, Sundgren PC. Intradural spinal tumors: current classification and MRI features. *Neuroradiology* 2008;50:301–314. [PubMed](#)
2. Ramachandran M, Tsirikos AI, Lee J, Saifuddin A. Whole-spine magnetic resonance imaging in patients with neurofibromatosis type 1 and spinal deformity. *J Spinal Disord Tech* 2004;17:483–491. [PubMed](#)
3. Wasa J, Nishida Y, Tsukushi S, et al. MRI features in the differentiation of malignant peripheral nerve sheath tumors and neurofibromas. *AJR Am J Roentgenol* 2010;194:1568–1574. [PubMed](#)
4. Bredella MA, Torriani M, Hornicek F, et al. Value of PET in the assessment of patients with neurofibromatosis type 1. *AJR Am J Roentgenol* 2007;189:928–935. [PubMed](#)

Case 34

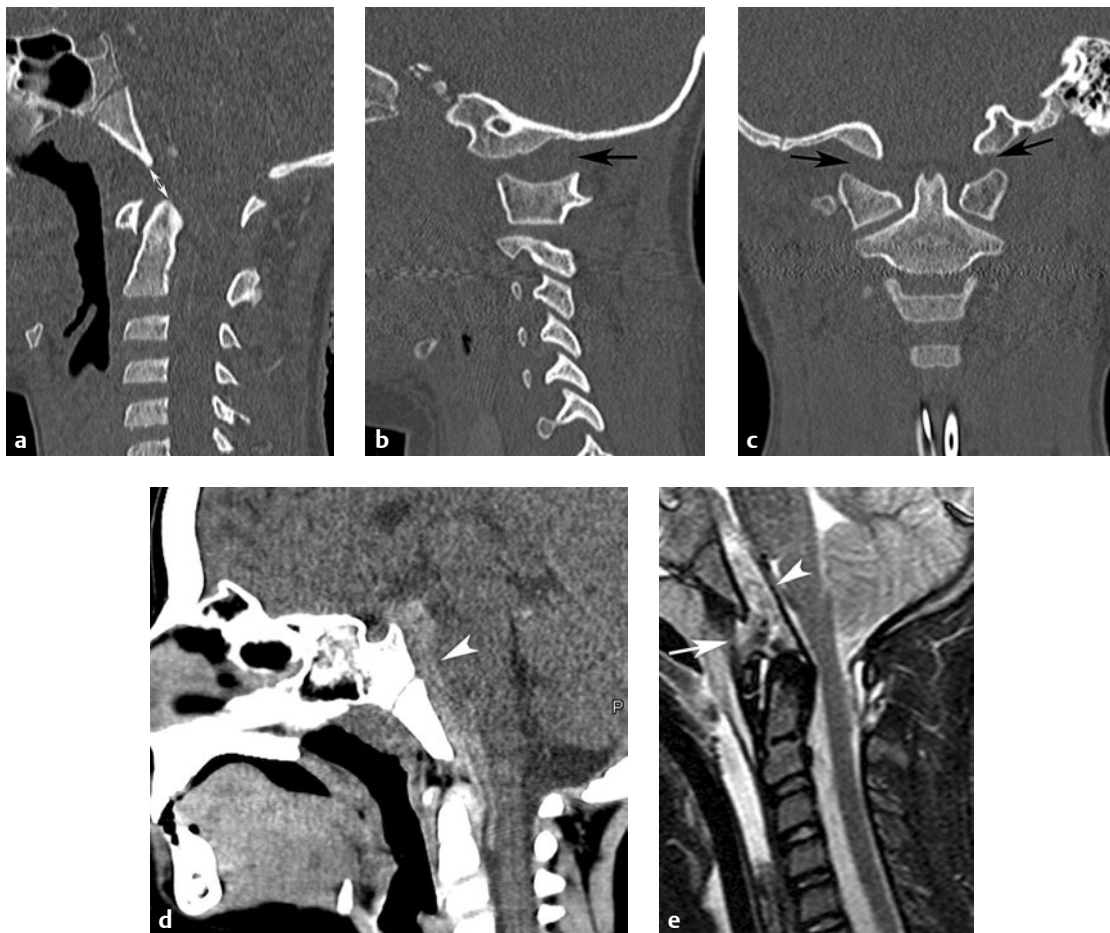
■ Clinical Presentation

A 10-year-old unrestrained passenger in a car that was in a motor vehicle accident, who sustained injuries resulting in quadriplegia.

■ Radiographic Studies

Sagittal reformatted CT image (**Fig. 34.1a**) shows increased distance (> 1.5 cm) between the basion and the tip of the odontoid process (*double arrow*). Parasagittal CT scan (**Fig. 34.1b**) and coronal CT scan (**Fig. 34.1c**) show posterior subluxation and distraction of the atlanto-occipital joint (*arrows*).

Sagittal reformatted CT image (**Fig. 34.1d**) shows clival hematoma (*arrowhead*) and adjacent subarachnoid hemorrhage. Sagittal T2-weighted MRI (**Fig. 34.1e**) shows retropharyngeal edema, ligamentous injury (*arrow*), and stripping of the tectorial membrane from clivus with clival hematoma (*arrowhead*).



■ Diagnosis

Traumatic Atlanto-Occipital Dislocation

■ Discussion and Differential Diagnosis

Traumatic atlanto-occipital dislocation (AOD) is seen most commonly in children who have been hit by a motor vehicle. Survival is not rare but is usually accompanied by severe neurologic abnormality caused by spinal cord and lower cranial nerve injury. The patients may be neurologically intact at the scene of the accident. Prompt neck immobilization and correct interpretation of properly exposed and positioned lateral neck radiographs and CT scan are essential in the care of these patients. Traumatic AOD is characterized by complete disruption of all ligaments between occiput and atlas with subluxation or complete dislocation of the occipitoatlantal facets. Anterior translation of the skull on the vertebral column is the most common presentation. Although uncommon, traumatic AOD is more prevalent in young children than in adults due to increased ligamentous laxity, the large size of the head relative to the body, and hypoplastic occipital condyles.¹

Careful attention to the relationship between the apical portion of the odontoid process and the basion (dens–basion distance) is essential in the interpretation of all posttraumatic lateral cervical spine radiographs, along with soft tissue swelling and pathological convexity of the soft tissues anterior to the C2 vertebrae (generally > 10 mm in thickness). CT imaging is increasingly preferred for initial evaluation of significant trauma. It can show subluxation more clearly, and it better defines associated fractures. CT findings of traumatic AOD are clival hematoma due to avulsion of tectorial membrane, dens–basion distance > 10 mm, predental space > 2.6 mm, and atlanto-occipital interval of > 2.5 mm.² CT scan can demonstrate subarachnoid and epidural hemorrhages. MRI is helpful in demonstrating spinal cord compression/edema and ligamentous injury.³

Pearls

- ◆ The dens–basion distance in a child should not be greater than 1 to 1.2 cm.
- ◆ Clival hematoma sometimes identified on facial bone or head CT imaging is an important indicator of significant craniocervical junction injury.

Pitfall

- ◆ CT imaging should be done for patients with significant injury to evaluate the craniocervical junction and cervical spine with high imaging confidence.

References

1. Lustrin ES, Karakas SP, Ortiz AO, et al. Pediatric cervical spine: normal anatomy, variants, and trauma. *Radiographics* 2003;23:539–560 [PubMed](#)
2. Bertozzi JC, Rojas CA, Martinez CR. Evaluation of the pediatric craniocervical junction on MDCT. *AJR Am J Roentgenol* 2009;192:26–31 [PubMed](#)
3. Warner J, Shanmuganathan K, Mirvis SE, Cerva D. Magnetic resonance imaging of ligamentous injury of the cervical spine. *Emerg Radiol* 1996;3:9–15

Case 35

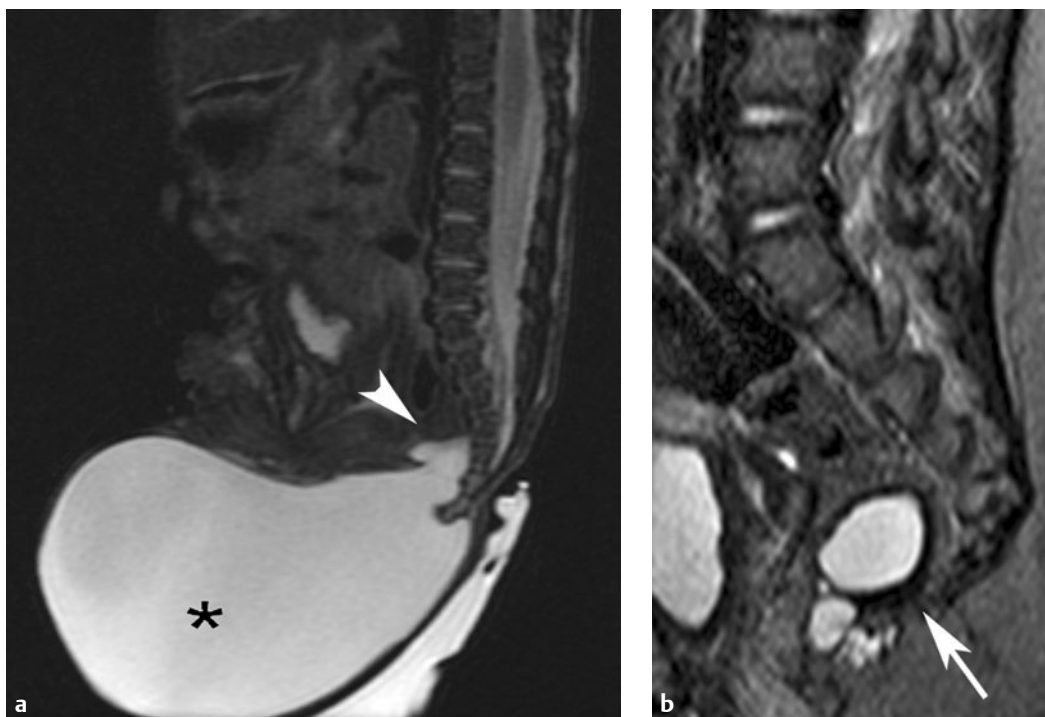
■ Clinical Presentation

A newborn with a large perineal mass.

■ Radiographic Studies

Sagittal T2-weighted MRI (**Fig. 35.1a**) shows a large cystic perineal mass (*asterisk*) with a small presacral component (*arrowhead*). In another patient, sagittal T2-weighted MRI

(**Fig. 35.1b**) shows a multilocular cystic mass (*arrow*) that is entirely presacral.



■ Diagnosis

Sacroccygeal Teratoma

■ Discussion and Differential Diagnosis

Sacroccygeal teratoma is the most common congenital solid tumor.¹ It arises from totipotential cells in the caudal cell mass and has a marked female preponderance. Teratomas may present as external masses protruding from the intergluteal cleft or perineum with a minimal presacral component or as primarily abdominal/pelvic lesions.² Histologically, these are usually mature lesions; a small percentage are immature and anaplastic carcinomas.

Most teratomas have mixed cystic and solid components. Solid components may include calcium and/or fat. Demonstration of fat with calcification on CT imaging clinches the

diagnosis. Less commonly, teratomas are predominantly cystic, which favors a benign histology.² On MRI, the solid portion of tumor is usually heterogeneous on T1- and T2-weighted sequences with enhancement postcontrast. Cystic components of teratoma show internal T2 hyperintensity and lack internal enhancement postcontrast.

Prenatal diagnosis of teratomas is now common on prenatal MRI. Delivery of a fetus with a large tumor should be by cesarean section to prevent intratumoral hemorrhage and dystocia.³ Differential diagnosis includes meningocele, anterior sacral meningocele, lipoma, duplication cyst, and chordoma.

Pearl

- ◆ MRI is essential to evaluate the relationship of tumor with abdominal and pelvic viscera.

Pitfall

- ◆ Suspect internal tumors in infants with anal stenosis and sacral anomalies (Currarino triad).

References

1. Wells RG, Sty JR. Imaging of sacroccygeal germ cell tumors. *Radiographics* 1990;10:701–713 [PubMed](#)
2. Kocaoglu M, Frush DP. Pediatric presacral masses. *Radiographics* 2006;26:833–857 [PubMed](#)
3. Danzer E, Hubbard AM, Hedrick HL, et al. Diagnosis and characterization of fetal sacroccygeal teratoma with prenatal MRI. *AJR Am J Roentgenol* 2006;187:W350–6 [PubMed](#)

Case 36

■ Clinical Presentation

A 15-year-old unrestrained passenger in motor vehicle accident, resulting in multiple spinal fractures.

■ Radiographic Studies

Sagittal reformatted CT spine image (**Fig. 36.1a**) shows horizontal L2 vertebral body compression fracture (*arrow*) with distraction of the posterior elements (*arrowhead*). L5 vertebral body fracture is also noted. Axial CT image (**Fig. 36.1b**) shows fractures of both upper lumbar facets, with loss of definition of right pedicle (*arrow*) and empty left facet (*arrow-*

head). Sagittal STIR MRI (**Fig. 36.1c**) shows high signal edema anteriorly in the L2 compression fracture (*arrow*) and throughout the posterior column ligamentous disruption (*arrowhead*). L5 vertebral body edema is also seen. Abdomen CT image (**Fig. 36.1d**) shows free fluid and thickening of the proximal small bowel wall (*arrow*), suggesting injury.



■ Diagnosis

Chance Fracture

■ Discussion and Differential Diagnosis

Chance fracture was first described by G.Q. Chance in 1948.¹ It is an unstable flexion-distraction injury causing the middle and posterior columns to fail under tension and the anterior column to fail under compression. The use of seat belts, particularly lap belts, has been associated with an increasing incidence of this injury caused by extreme hyperflexion.² In children, Chance fractures occur in the lumbar spine, probably related to the pediatric body habitus.³ There is disruption of the posterior elements of the spine, which may be osseous, ligamentous, or both, with longitudinal separation and minimal decrease in the anterior vertical height of the involved vertebral body. There is often vertebral body subluxation that may be associated with injury to the spinal cord.³ Severe compression forces may cause extensive injury to the soft abdominal viscera.

Clues to the diagnosis of the Chance fracture on AP radiographs include distraction with uncovering of the facet (plain film equivalent of empty or naked facet sign on CT), widening of the disrupted intervertebral disk space, anterior vertebral body wedging, and visualization of the horizontal fracture fragment.⁴ CT accurately demonstrates osseous injury, posterior column distraction, and any vertebral subluxation into the spinal canal. It helps to assess the spine stability, especially the critical middle column, to identify patients at risk of acute neurologic compromise.³ CT also shows associated abdominal viscera injury. MRI evaluation provides information regarding the integrity of the posterior and middle column ligaments, annulus fibrosis, and spinal cord in neurologically injured patients.⁵ MRI may also reveal the presence of epidural hematomas.

Pearls

- ◆ Chance fractures in children are frequently associated with injuries to the conus medullaris of the spinal cord.
- ◆ T2-weighted and STIR MRI sequences are best to assess soft tissue edema, bone bruises, and spinal cord injury.

Pitfall

- ◆ Lateral spine views on a backboard may “reduce” spinal subluxation. Careful, physician-supervised flexion radiographs or MRI may be necessary to demonstrate facet subluxation and interspinous ligament disruption.

References

1. Chance GQ. Note on a type of flexion fracture of the spine. *Br J Radiol* 1948; 21:452. [PubMed](#)
2. Rogers LF. Transverse fractures of the spine. In: Rogers LF, ed. *Radiology of Skeletal Trauma*. New York: Churchill Livingstone; 1982:325–328
3. Arkader A, Warner WC Jr, Tolo VT, Sponseller PD, Skaggs DL. Pediatric Chance fractures: a multicenter perspective. *J Pediatr Orthop* 2011;31:741–744. [PubMed](#)
4. Lingawi SS. The naked facet sign. *Radiology* 2001;219:366–367. [PubMed](#)
5. Groves CJ, Cassar-Pullicino VN, Tins BJ, Tyrrell PN, McCall IW. Chance-type flexion-distraction injuries in the thoracolumbar spine: MR imaging characteristics. *Radiology* 2005;236:601–608. [PubMed](#)

Case 37

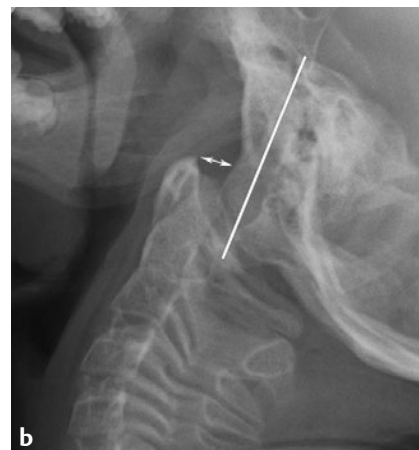
■ Clinical Presentation

A 12-year-old with Down syndrome and progressive hyperreflexia.

■ Radiographic Studies

Lateral flexion radiograph of the cervical spine (**Fig. 37.1a**) shows widening of the atlantodental joint (*arrow*) compatible with atlantoaxial subluxation. Lateral extension radiograph (**Fig. 37.1b**) shows anterior atlanto-occipital subluxation (*arrow*) with flattening of the occipital condyle and posterior displace-

ment of the posterior clival line. CT at the C1 ring level (**Fig. 37.1c**) in another patient shows severe sagittal narrowing of the spinal canal (*arrow*). Sagittal T2-weighted MRI (**Fig. 37.1d**) in the same patient shown in Fig 37.1c shows critical C1 ring stenosis with cord compression.



■ Diagnosis

Down Syndrome: Atlantoaxial Instability

■ Discussion and Differential Diagnosis

Atlantoaxial subluxation without clinical symptoms is common in patients with Down syndrome.¹ Symptomatic atlantoaxial subluxation, however, is infrequent, occurring in less than 1.5% of these children.² In children the atlantodental space is normally up to 5 mm and the AP neural canal width can be normal up to 14 mm.³ Atlantoaxial instability is suggested in Down syndrome when the atlantodental interval is 7 mm or greater. Atlanto-occipital instability is also seen with an increased incidence and suggested when there is posterior displacement of the posterior clival line. In addition to liga-

mentous laxity and subluxation, bony anomalies of the cranio-cervical junction, especially os odontoideum and C1 ring stenosis, are found in these patients.

Children with atlantoaxial or atlanto-occipital subluxation should be examined with CT of the craniocervical junction and MRI of the cervical spine prior to surgical therapy.⁴ High-resolution CT accurately delineates bony anomalies and associated spinal canal narrowing. MRI with T1- and T2-weighted images detects spinal stenosis and abnormal signal in the spinal cord related to a previous injury.

Pearls

- ◆ The upper limit of normal for the measurement of the atlantodental interval is generally considered to be 5 mm in the pediatric patient.
- ◆ Patients with bony abnormalities have a higher incidence of neurologic abnormality and should be studied carefully.

Pitfall

- ◆ In the preoperative evaluation of the child with atlantoaxial subluxation, high-resolution CT of the craniocervical junction is required to detect subtle but significant bony anomalies that may be missed on plain radiography or MRI.

References

1. Smoker WRK, Khanna G. Imaging the craniocervical junction. *Childs Nerv Syst* 2008;24:1123–1145 [PubMed](#)
2. Pueschel SM, Scola FH, Pezzullo JC. A longitudinal study of atlanto-dens relationships in asymptomatic individuals with Down syndrome. *Pediatrics* 1992;89(6 Pt 2):1194–1198 [PubMed](#)
3. Brockmeyer D. Down's syndrome and craniovertebral instability: topic review and treatment recommendations. *Nepal J Neurosci*. 2005;2:52–58
4. Menezes AH. Specific entities affecting the craniocervical region: Down's syndrome. *Childs Nerv Syst* 2008;24:1165–1168 [PubMed](#)

Case 38

■ Clinical Presentation

A 15-year-old with back pain and fever.

■ Radiographic Studies

Sagittal T1-weighted MRI of the lumbar spine (**Fig. 38.1a**) shows hypointensity in the lower half of the L2 and much of the L3 vertebral body (*arrowheads*) along with a decrease in intervertebral disk height and signal. Sagittal STIR MRI shows hyperintensity within these vertebral bodies (**Fig. 38.1b**, *arrowheads*) and decreased adjacent disk signal. Postcontrast

T1-weighted sagittal MRI (**Fig. 38.1c**) shows enhancement in the two adjacent vertebral bodies (*arrowheads*). Axial post-contrast T1-weighted MRI (**Fig. 38.1d**) shows enhancement within the vertebral body, cortical loss, and adjacent paraspinal soft tissue enhancement (*arrow*).



■ Diagnosis

Vertebral Osteomyelitis

■ Discussion and Differential Diagnosis

Vertebral osteomyelitis is frequently associated with bacteremia. Bacteria may gain access to the vertebral column via Batson's plexus.¹ Retropharyngeal infection, penetrating trauma, and recent surgery may also be causative.¹ Plain radiographs show bony change after the infectious process has been present for 2 to 3 weeks including demineralization, loss of disk height, adjacent bone destruction, kyphosis, and extrusion of bone fragments into adjacent soft tissue.² Bone destruction and soft tissue infection can be detected much earlier using CT.

Magnetic resonance imaging is the most sensitive and most specific imaging modality. The earliest finding on MRI is bone marrow edema, which produces low-signal intensity on T1-

weighted images and high signal on T2-weighted and STIR sequences within the infected vertebral bodies and related disk spaces. Contrast enhancement may be seen in the disk space, vertebral body, paraspinal soft tissues, or epidural space. Liquefied paraspinal fluid collections may be seen in pyogenic or tuberculosis spondylitis.³

Other entities that can mimic vertebral osteomyelitis include primary neoplasms or metastatic disease (particularly neuroblastoma or leukemia). Malignant destruction of the vertebral body classically spares the disk space, which is usually involved early in infectious spondylitis.^{1,3}

Pearls

- ◆ The most common organism associated with vertebral osteomyelitis is *Staphylococcus aureus*.
- ◆ Involvement of the cervical spine is uncommon.

Pitfalls

- ◆ Intraspinal spread of infection (epidural abscess, myelitis) should be considered and excluded with spine MRI in children with vertebral osteomyelitis.
- ◆ Neonatal osteomyelitis is often multifocal: nuclear scintigraphy, radiographic skeletal survey, and/or whole body MRI should be considered to exclude multiple sites of infection.

References

1. Mahboubi S, Morris MC. Imaging of spinal infections in children. *Radiol Clin North Am* 2001;39:215–222. [PubMed](#)
2. Pineda C, Espinosa R, Pena A. Radiographic imaging in osteomyelitis: the role of plain radiography, computed tomography, ultrasonography, magnetic resonance imaging, and scintigraphy. *Semin Plast Surg* 2009;23:80–89. [PubMed](#)
3. Hong SH, Choi JY, Lee JW, Kim NR, Choi JA, Kang HS. MR imaging assessment of the spine: infection or an imitation? *Radiographics* 2009;29:599–612. [PubMed](#)

Case 39

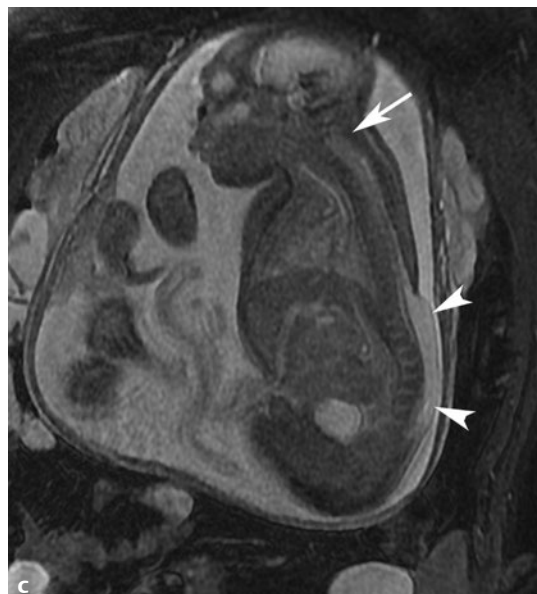
■ Clinical Presentation

A newborn with lower back mass.

■ Radiographic Studies

Sagittal T1-weighted MRI (**Fig. 39.1a**) shows dysplastic body (*arrowhead*) and absent splenium of corpus callosum, small posterior fossa with towering superior cerebellum, and inferior displacement of cerebellar tissue into the upper cervical canal (*arrow*). Tectal beaking, enlarged mass intermedia, and low-lying torcular are also seen. Axial T2-weighted MRI at the

lumbosacral junction (**Fig. 39.1b**) shows open dysraphic defect of the posterior elements with protruding myelomeningocele (*arrowheads*). Fetal MRI in another patient (**Fig. 39.1c**) shows low-lying cerebellar tonsils (*arrow*) and lumbosacral dysraphic defect with myelomeningocele (*arrowheads*).



■ Diagnosis

Myelomeningocele/Chiari II Malformation

■ Discussion and Differential Diagnosis

The Chiari II malformation is a group of neuroanatomic abnormalities seen in nearly all patients with myelomeningocele. Multiplanar MRI best displays the extensive craniocervical anomalies found in these patients, predominantly secondary to a small posterior fossa. Intracranial findings include hydrocephalus, dysgenesis of corpus callosum, fenestration of the falx with gyral interdigitation, enlarged massa intermedia, midbrain tectal beaking, low-lying torcular, and both superior extension of the cerebellum through a dysplastic tentorium and inferior displacement of the fourth ventricle and cerebellum into the upper cervical spinal canal.¹ Prenatal ultrasound can diagnose myelomeningocele, and fetal MRI may be helpful to further characterize these complex anomalies.² In Chiari II

malformation, syringohydromyelia is frequently found in association with hydrocephalus and shunt malfunction.

Differential diagnosis of Chiari II malformation includes Chiari I malformation, which occurs in patients with a more normal posterior fossa and without myelomeningocele. Chiari I refers to > 5 mm inferior displacement of the cerebellar tonsils below the foramen magnum. As in Chiari II, patients with Chiari I malformation have an increased incidence of syringohydromyelia.³ Chiari III malformation includes patients with occipital or high cervical cephaloceles containing posterior fossa structures in conjunction with intracranial findings of Chiari II malformation.⁴

Pearl

- ◆ The vast majority of infants with myelomeningocele have hydrocephalus and intracranial findings of Chiari II malformation.

Pitfalls

- ◆ Newborn infants with Chiari II malformation may not have hydrocephalus at birth but develop ventriculomegaly later.
- ◆ Serial measurement of head circumference and cranial sonography should be performed in infants with myelomeningocele who have normal or minimally enlarged ventricular size at birth.

References

1. Barkovich AJ, Raybaud C. Congenital malformations of the brain and skull. In: Barkovich AJ, Raybaud C, eds. *Pediatric Neuroimaging*, 5th ed. Philadelphia: Lippincott Williams & Wilkins. 2012:497–501
2. Coakley FV, Glenn OA, Qayyum A, Barkovich AJ, Goldstein R, Filly RA. Fetal MRI: a developing technique for the developing patient. *AJR Am J Roentgenol* 2004;182:243–252. [PubMed](#)
3. Elster AD, Chen MY. Chiari I malformations: clinical and radiologic reappraisal. *Radiology* 1992;183:347–353. [PubMed](#)
4. Wolpert SM, Anderson M, Scott RM, Kwan ES, Runge VM. Chiari II malformation: MR imaging evaluation. *AJR Am J Roentgenol* 1987;149:1033–1042. [PubMed](#)

Case 40

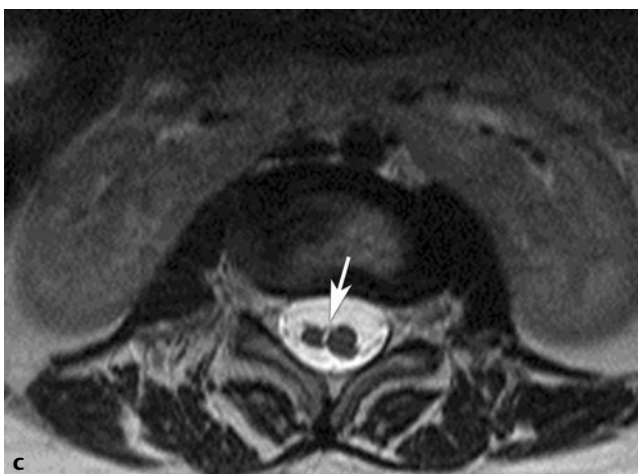
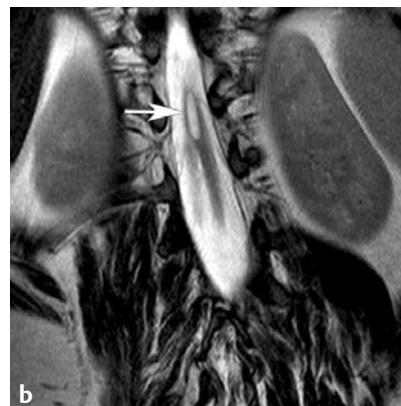
■ Clinical Presentation

A 2-year-old girl with dermal sinus and progressive urinary incontinence.

■ Radiographic Studies

Coronal T2-weighted MRI (**Fig. 40.1a**) shows the lower thoracic spinal cord split into two hemicords (*arrowheads*). Coronal T2-weighted MRI (**Fig. 40.1b**) shows a syrinx (*arrow*) just above the two hemicords. Axial T2-weighted MRI (**Fig. 40.1c**) in another patient shows two lumbar hemicords (*arrow*) in one

thecal sac. Associated prevertebral horseshoe kidney anomaly is seen. At a higher thoracic level, CT image (**Fig. 40.1d**) shows a bony spicule (*arrow*) traversing the thoracic spinal canal separating two thecal sacs.



■ Diagnosis

Diastematomyelia

■ Discussion and Differential Diagnosis

Diastematomyelia means split spinal cord; two hemicords are thought to result from developmental splitting of the notochord. Diastematomyelia has a female predominance, and over half the patients have a skin lesion overlying the dysraphic abnormality. Many patients with meningocele have associated diastematomyelia. Spinal cord syrinx is frequently present above the split and may extend caudally into one or both hemicords.¹ Other anomalies are also common, including thickening of the filum terminale, dermal sinus, dermoid/epidermoid tumors, and dural adhesions.²

Prenatal ultrasound diagnosis is generally made in the second trimester with widening of the spinal canal in the coronal view and an additional echogenic focus in the posterior part of the spinal column in the axial view.³ The diagnosis can be con-

firmed by fetal MRI, which may also show additional spinal abnormalities.⁴ Plain radiographs of the spine are almost always abnormal and include widening of the spinal canal, hemivertebrae, or a bony septum. Screening spinal ultrasound can identify two hemicords in infants with diastematomyelia, particularly during the newborn period and in patients with posterior bony dysraphism.⁵ MRI is the preferred imaging modality for preoperative planning. MRI should include sagittal and axial T1-weighted images and axial and coronal T2-weighted images. Coronal imaging is optimal to identify the length of the split cord. Axial T2-weighted images most accurately identify or exclude a bony or fibrocartilaginous spicule dividing the thecal sac and possibly tethering the hemicords.

Pearl

- ◆ Any newborn with a midline cutaneous lesion overlying the spine should undergo screening spinal ultrasound to determine the level of the conus medullaris and identify underlying spinal pathology.

Pitfall

- ◆ An interlaminar bar or cap, which is often present in patients with diastematomyelia, may block the ultrasound beam and make complete sonographic evaluation of the spinal canal difficult.

References

- Schlesinger AE, Naidich TP, Quencer RM. Concurrent hydromyelia and diastematomyelia. *AJNR Am J Neuroradiol* 1986;7:473–477 [PubMed](#)
- Barkovich AJ. Congenital anomalies of the spine. In: *Pediatric Neuroimaging*, 2nd ed. New York: Raven Press; 1995:477–540
- Has R, Yuksel A, Buyukkurt S, Kalelioglu I, Tatli B. Prenatal diagnosis of diastematomyelia: presentation of eight cases and review of the literature. *Ultrasound Obstet Gynecol* 2007;30:845–849 [PubMed](#)
- von Koch CS, Glenn OA, Goldstein RB, Barkovich AJ. Fetal magnetic resonance imaging enhances detection of spinal cord anomalies in patients with sonographically detected bony anomalies of the spine. *J Ultrasound Med* 2005;24:781–789 [PubMed](#)
- Unsinn KM, Geley T, Freund MC, Gassner I. US of the spinal cord in newborns: spectrum of normal findings, variants, congenital anomalies, and acquired diseases. *Radiographics* 2000;20:923–938 [PubMed](#)

Case 41

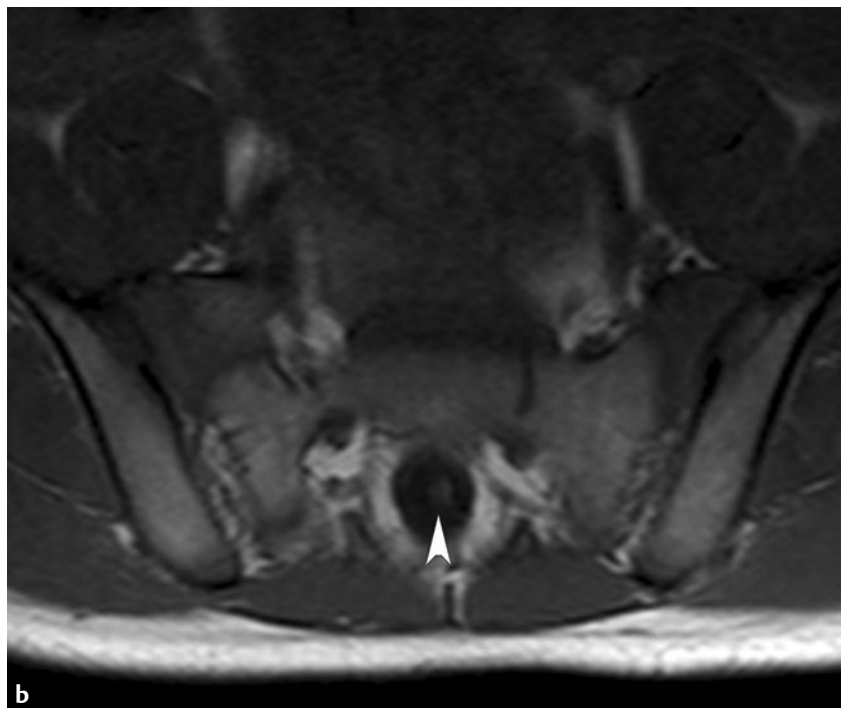
■ Clinical Presentation

A 9-year-old boy with encopresis.

■ Radiographic Studies

Sagittal T1-weighted MRI of the spine (**Fig. 41.1a**) shows a low-lying conus medullaris with thickened filum terminale (*arrow*) ending in a lipoma (*arrowhead*). Axial T1-weighted

MRI (**Fig. 41.1b**) shows a centrally located thickened filum terminale (*arrowhead*).



■ Diagnosis

Tethered Spinal Cord



■ Discussion and Differential Diagnosis

The tethered cord syndrome consists of a spectrum of neurologic and orthopedic abnormalities. Patients may present in infancy, childhood, or adulthood with clinical symptoms of bowel/bladder dysfunction, clubfoot, back pain, scoliosis, and various sensorimotor abnormalities in the lower extremities. Patients with tethered cord syndrome have an intraspinal lesion or lesions that are thought to prevent the normal movement of the spinal cord within the spinal canal as the vertebral column in the growing child elongates.¹ This tethering effect

results in traction on the spinal cord and roots with subsequent neurologic abnormalities.¹ These lesions include congenital dermal sinus, diastematomyelia, spinal lipoma, thickening of the filum terminale, and, most commonly, spinal dysraphism.¹

Imaging of the spine at birth consists of screening spinal ultrasound supplemented with MRI when abnormalities are detected with ultrasound.² CT can be useful for evaluation of osseous anomalies and surgical planning.

Pearls

- ◆ Any cutaneous abnormality (hemangioma, hair tuft, lipoma, sinus tract) over the midline of the spine may be associated with intraspinal pathology that results in tethered cord syndrome.
- ◆ The normal conus medullaris usually lies above the L2-L3 level.

Pitfall

- ◆ Although normal initial ultrasound can rule out most spinal pathology, MRI is necessary for preoperative evaluation.

References

1. Raghavan N, Barkovich AJ, Edwards M, Norman D. MR imaging in the tethered spinal cord syndrome. *AJR Am J Roentgenol* 1989;152:843–852 [PubMed](#)
2. Unsinn KM, Geley T, Freund MC, Gassner I. US of the spinal cord in newborns: spectrum of normal findings, variants, congenital anomalies, and acquired diseases. *Radiographics* 2000;20:923–938 [PubMed](#)

Case 42

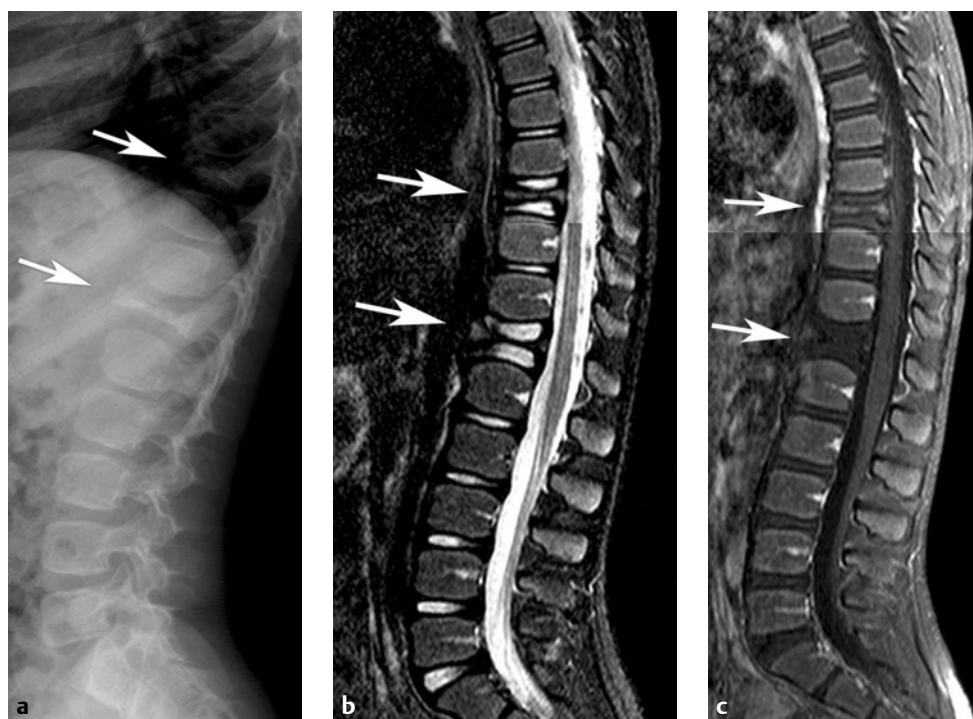
■ Clinical Presentation

An 8-year-old boy with back pain.

■ Radiographic Studies

Lateral thoracolumbar radiograph (**Fig. 42.1a**) demonstrates flattened T9 and T12 vertebral bodies (*arrows*) with preservation of adjacent disk spaces. Sagittal STIR MRI (**Fig. 42.1b**) shows flattened T9 and T12 vertebral bodies (*arrows*) with pre-

served adjacent disk spaces. Postcontrast sagittal T1-weighted MRI with fat saturation (**Fig. 42.1c**) shows no abnormal enhancement at sites of flattened vertebral bodies (*arrows*).



■ Diagnosis

Vertebra Plana

■ Discussion and Differential Diagnosis

Spinal involvement is found commonly in children with Langerhans cell histiocytosis. Most common involvement is seen in the thoracic and lumbar spine.¹ Focal destructive lesions are seen in the vertebral bodies that may result in the characteristic vertebra plana.¹ The posterior elements are less commonly involved than the vertebral bodies.¹ MRI may show vertebral body involvement in the absence of plain film changes. Typical findings on MRI in histiocytosis include lesions that are hypointense on T1-weighted sequences and hyperintense on T2-weighted sequences. Following contrast administration, focal soft tissue enhancement adjacent to the involved vertebral

body may be seen.² CT shows focal destructive changes with or without obvious soft tissue involvement.^{1,2} One or multiple vertebral bodies may be involved. There may be dramatic reconstitution of height of the flattened vertebral bodies without specific therapy.³

Differential diagnosis of destructive vertebral body lesions in children includes leukemia, hemangioma, metastatic neuroblastoma, tuberculosis, and steroid therapy.^{1,2} Biopsy may be necessary for precise diagnosis. Radiographic skeletal survey is helpful to search for other sites of involvement and to delineate potential biopsy sites.

Pearl

- ◆ Complete destruction with collapse of a vertebral body into a thin flat plate with preservation of disk spaces is characteristic of Langerhans cell histiocytosis.

Pitfall

- ◆ Platyspondyly is a radiographic finding that refers to multiple contiguous flattened vertebral bodies that can be seen in skeletal dysplasias such as Morquio syndrome, osteogenesis imperfecta, and thanatophoric dysplasia. This is in contrast to the flattening in vertebra plana that involves one or a few vertebral bodies.

References

1. Kilborn TN, Teh J, Goodman TR. Paediatric manifestations of Langerhans cell histiocytosis: a review of the clinical and radiological findings. *Clin Radiol* 2003;58:269–278 [PubMed](#)
2. Rodriguez DP, Poussaint TY. Imaging of back pain in children. *AJNR Am J Neuroradiol* 2010;31:787–802 [PubMed](#)
3. Greenlee JD, Fenoy AJ, Donovan KA, Menezes AH. Eosinophilic granuloma in the pediatric spine. *Pediatr Neurosurg* 2007;43:285–292 [PubMed](#)

Case 43

■ Clinical Presentation

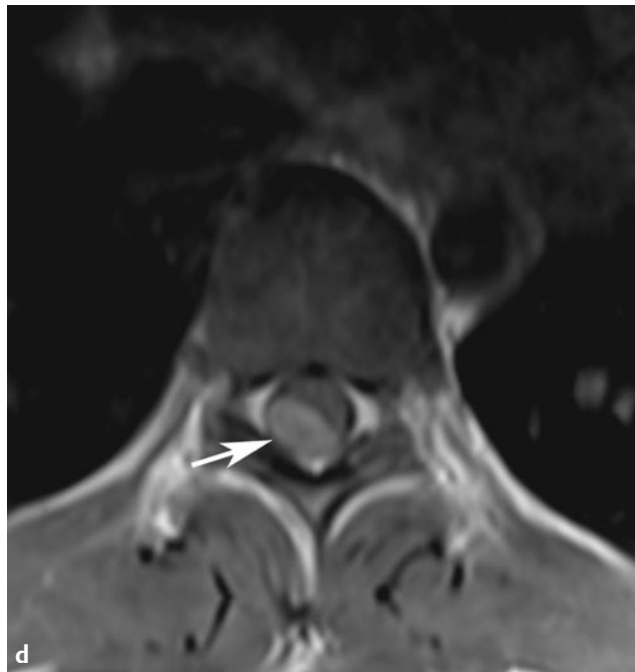
A 10-year-old girl with bilateral sensorineural hearing loss and progressive muscle weakness.

■ Radiographic Findings

Sagittal postcontrast T1-weighted MRI of the spine with fat saturation (**Fig. 43.1a**) shows an enhancing intramedullary cervical cord lesion (*arrow*) suggesting ependymoma and multiple extramedullary intradural lesions (*arrowheads*) in the lumbosacral canal suggesting schwannomas. Axial post-contrast T1-weighted MRI with fat saturation (**Fig. 43.1b**) shows small enhancing masses in the internal auditory canal

region bilaterally (*arrowheads*) compatible with acoustic schwannomas. A large lobular right Meckel's cave mass (*arrow*) is consistent with right trigeminal nerve schwannoma. Axial postcontrast T1-weighted MRI of the orbits with fat saturation (**Fig. 43.1c**) shows an enhancing mass along the right optic nerve sheath consistent with meningioma.





■ Diagnosis

Neurofibromatosis Type 2

■ Discussion and Differential Diagnosis

Neurofibromatosis type 2 (NF2) is an autosomal dominant disease characterized by the presence of bilateral vestibular schwannomas in nearly all affected individuals.¹ Characteristic spinal manifestations of NF2 include multiple nerve sheath schwannomas, meningiomas, and spinal cord tumors.^{1–3} The imaging modality of choice is contrast-enhanced MRI. The most common intramedullary tumor is ependymoma, but other tumor types such as astrocytoma and intramedullary schwan-

noma have been reported.² Intramedullary tumors in patients with NF2 have a more indolent course and are rarely treated, in contrast to these tumors in patients without NF2.^{2,4} The extramedullary tumors (**Fig. 43.1d, arrow**) are more frequently resected especially when there is increasing cord compression.² Differential diagnosis of multiple enhancing spinal intradural lesions in a child should include drop metastasis and multifocal hemangioblastomas.

Pearls

- ◆ Patients with NF2 do not have characteristic skin lesions.
- ◆ The presence of spinal meningioma or schwannomas in the pediatric age group should prompt a genetic workup and contrast-enhanced MRI of the brain.

Pitfall

- ◆ Differential diagnosis of multiple enhancing spinal intradural lesions in a child should include drop metastasis and multifocal hemangioblastomas.

References

1. Vezina G, Barkovich AJ. The phakomatoses. In: Barkovich AJ, Raybaud C, eds. *Pediatric Neuroimaging*. Philadelphia: Lippincott Williams & Wilkins; 2012:588–590
2. Patronas NJ, Courcousakis N, Bromley CM, Katzman GL, MacCollin M, Parry DM. Intramedullary and spinal canal tumors in patients with neurofibromatosis 2: MR imaging findings and correlation with genotype. *Radiology* 2001;218:434–442 [PubMed](#)
3. Egelhoff JC, Bates DJ, Ross JS, Rothner AD, Cohen BH. Spinal MR findings in neurofibromatosis types 1 and 2. *AJNR Am J Neuroradiol* 1992;13:1071–1077 [PubMed](#)
4. Jones RM, MacCollin M. The natural history of ependymoma in patients with neurofibromatosis 2. *Neurology* 1997;48:A35

Case 44

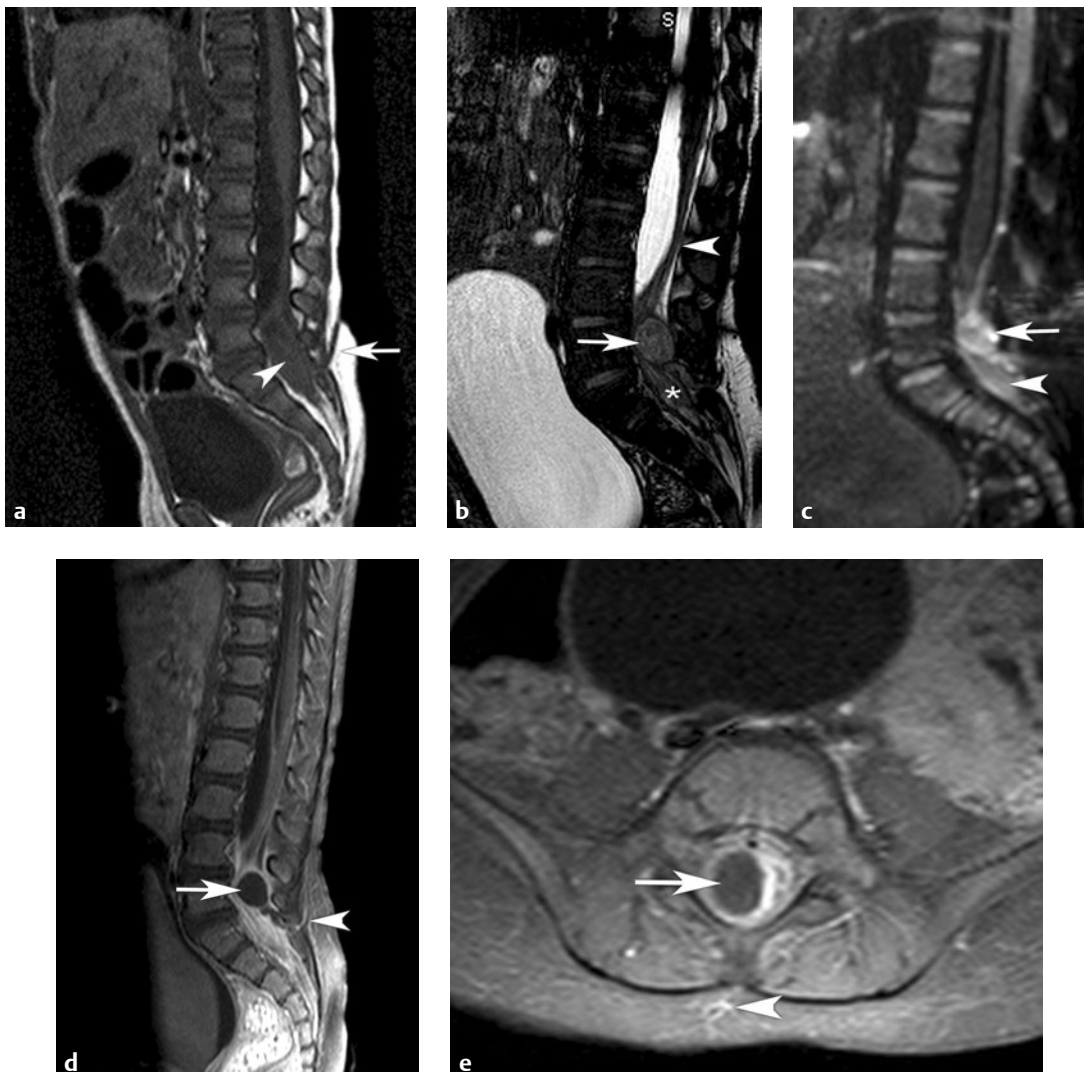
■ Clinical Presentation

A 16-month-old with skin dimple and intermittent fevers.

■ Radiographic Studies

Sagittal T1-weighted MRI (**Fig. 44.1a**) shows a low signal tubular channel (*arrow*) extending to the sacral spinal canal; heterogeneous signal is seen in the sacral thecal sac (*arrowhead*). Sagittal high-resolution T2-weighted MRI (**Fig. 44.1b**) shows a heterogeneous nodular mass (*arrow*) in the spinal canal at the L5 level and heterogeneous contents (*asterisk*) seen distally in the sacral canal. There is loculated fluid with clumped cauda equine nerve roots (*arrowhead*) in the lumbar canal. Sagittal diffusion-weighted MRI (**Fig. 44.1c**) shows re-

stricted diffusion in the round lower lumbar intraspinal mass (*arrow*) and also in the sacral thecal sac (*arrowhead*). Postcontrast sagittal T1-weighted MRI with fat saturation (**Fig. 44.1d**) shows an oval nonenhancing lesion in the lower lumbar canal (*arrow*). There is adjacent sacral thecal sac enhancement and an enhancing tract seen at the L5/S1 level (*arrowhead*). Postcontrast axial T1-weighted MRI with fat saturation (**Fig. 44.1e**) shows an oval nonenhancing intraspinal lesion (*arrow*) and an enhancing extraspinal soft tissue tract (*arrowhead*).



■ Diagnosis

Dermal Sinus with Intraspinal Epidermoid/Infection

■ Discussion and Differential Diagnosis

A dermal sinus tract is an epithelial-lined tube that extends from the skin to the CNS or its covering. It is most common in the lumbosacral region.¹ It occurs due to failure of separation of the cutaneous and neural ectoderm. Frequently there is a midline or paramidline dimple or tiny opening associated with a hairy nevus, capillary angioma, or hyperpigmented patch of skin.

Half to two thirds of dorsal dermal sinuses can extend into the spinal canal, reaching the dura or passing through it.² If they pass through the dura, they can empty into the subarachnoid space near the conus medullaris/filum terminale, or near an associated intrathecal lipoma, dermoid, or epidermoid. Patients may be asymptomatic or may present with meningitis,

intrathecal or epidural abscess, CSF leak, or cord compression from the intraspinal mass.

Magnetic resonance imaging is the diagnostic modality of choice. As the sinus tract is very thin and has a variable course, thin contiguous images should be obtained at the level of the external orifice. T1-weighted images best show the tract in the subcutaneous and epidural region relative to hyperintense fat. The intrathecal portion of the tract is best visualized on T2-weighted images. If continuity of the sinus tract with the thecal sac is established or an associated mass is seen, then it is important to obtain postcontrast fat-saturated images for further evaluation. Diffusion-weighted MRI can be helpful in confirming abscess and dermoids/epidermoids.

Pearl

- ◆ Intravenous contrast should be administered if the dermal sinus tract enters the thecal sac.

Pitfall

- ◆ Both abscess and dermoid show restricted diffusion.

References

1. Wright RL. Congenital dermal sinuses. *Prog Neurol Surg* 1971;4:175–191
2. Schwartz ES, Barkovich AJ. Congenital anomalies of the spine. In: Barkovich AJ, Raybaud C, eds. *Pediatric Neuroimaging*, 5th ed. Philadelphia: Lippincott Williams & Wilkins, 2012:870–874

Case 45

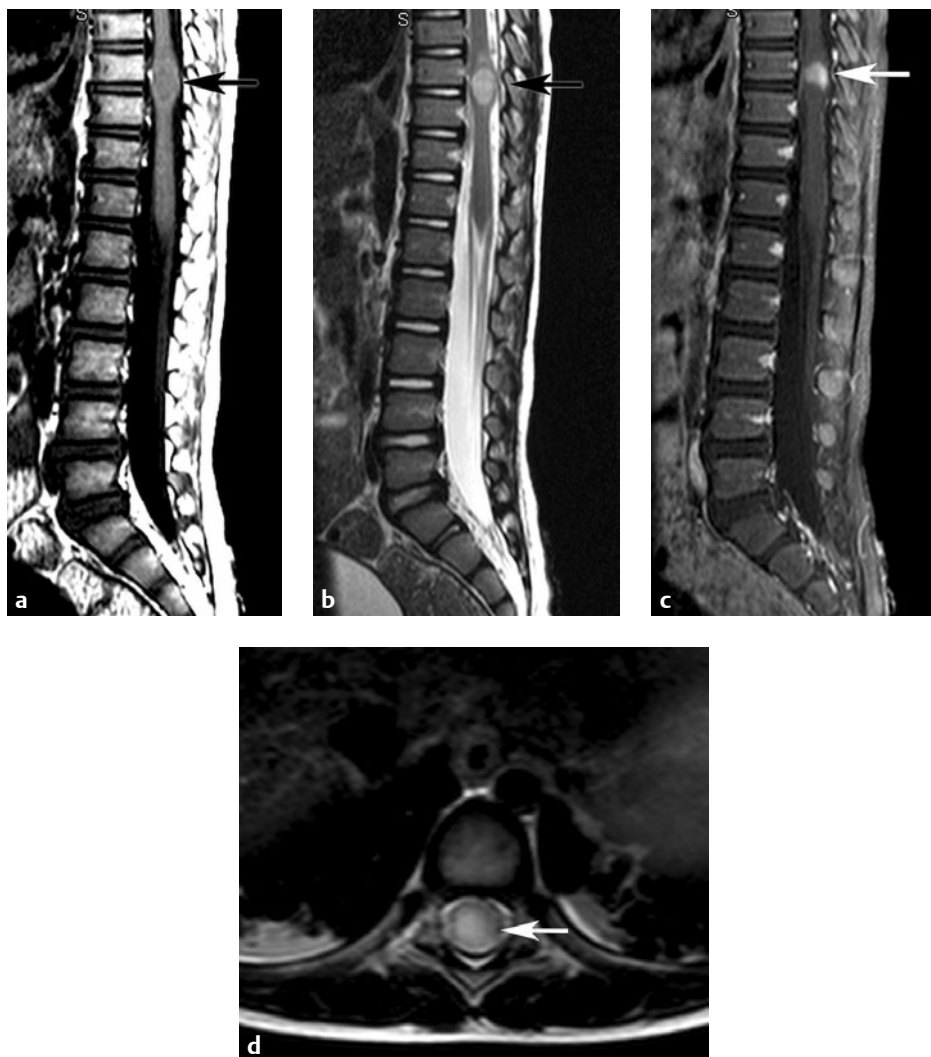
■ Clinical Presentation

A 10-year-old with diffuse back pain, accentuated at night.

■ Radiographic Studies

Sagittal T1-weighted MRI (**Fig. 45.1a**) shows hypointense, expansile lesion (*arrow*) in the lower thoracic spinal cord. Sagittal T2-weighted MRI (**Fig. 45.1b**) shows heterogeneous high signal (*arrow*) within the expanded thoracic cord. Postcon-

trast sagittal T1-weighted image with fat saturation (**Fig. 45.1c**) shows patchy enhancement (*arrow*) in the solid superior aspect of the lesion. Axial T2-weighted image (**Fig. 45.1d**) shows a hyperintense lesion expanding the spinal cord (*arrow*).



■ Diagnosis

Spinal Cord Tumor: Astrocytoma

■ Discussion and Differential Diagnosis

Spinal cord tumors are uncommon in children.¹ Astrocytomas and ependymomas account for > 90% of spinal cord tumors.² Intramedullary tumors cause cord signal abnormality, expansion of the spinal cord, and a decrease in the surrounding subarachnoid space. Cord expansion is the hallmark of intramedullary tumors.³ Cord signal abnormality in the absence of cord expansion, can be due to demyelination, infection, infarction, or trauma. Spinal cord tumors are usually slow growing and may cause remodeling of the bony spinal canal.

Astrocytomas arise from the cord parenchyma and are therefore eccentrically located. Most astrocytomas are of the pilocytic or fibrillary type. Pilocytic astrocytomas have well-defined margins, whereas the margins of the fibrillary type are diffuse.³ On MRI astrocytomas are T1 hypointense, T2 hyperintense, and show variable patchy enhancement (**Fig. 45.1a–d**). Hemorrhage is uncommon. Intratumoral and peritumoral cysts are frequent.

Pearl

- ◆ Cord expansion is the hallmark of spinal cord tumor.

Ependymomas arise centrally in the spinal cord. They displace rather than invade the cord parenchyma; as a result, a clear plane can be seen between the tumor and cord parenchyma. On MRI, ependymomas are heterogeneous/hypointense on T1-weighted sequences and hyperintense on T2-weighted sequences. They frequently show hemorrhage, and some of the tumors are associated with hemorrhage at the cranial or caudal end of the tumors. When such cap hemorrhages are seen, diagnosis of ependymoma can be made with a high degree of certainty. There may be nontumoral cysts at the tumor poles. When associated with NF2, they are usually multifocal, and have a more benign course.

Myxopapillary ependymoma is an ependymoma variant that typically occurs at the tip of conus medullaris or in the filum terminale. Other uncommon spinal cord tumors include gangliogliomas, hemangioblastomas, primitive neuroectodermal tumors (PNETs), and atypical teratohaboid tumors (ATRTs).

Pitfall

- ◆ When dealing with spinal cord tumor, it is important to distinguish between enhancing intratumoral cysts formed by tumor necrosis from nonenhancing, nontumoral cysts at the cranial and caudal end of tumor. Intratumoral cysts require resection because the wall may contain tumor cells while nontumoral cysts usually resolve after tumor resection.

References

1. Koeller KK, Rosenblum RS, Morrison AL. Neoplasms of the spinal cord and filum terminale: radiologic-pathologic correlation. *Radiographics* 2000;20:1721–1749 [PubMed](#)
2. Huisman TA. Pediatric tumors of the spine. *Cancer Imaging* 2009;9(Spec. No. A):S45–S48 [PubMed](#)
3. Smith AB, Soderlund KA, Rushing EJ, Smirniotopolous JG. Radiologic-pathologic correlation of pediatric and adolescent spinal neoplasms: Part 1, Intramedullary spinal neoplasms. *AJR Am J Roentgenol* 2012;198:34–43 [PubMed](#)



Head and Neck

Section Editors

Leah E. Braswell and Charles M. Glasier

Author

Ruba Khasawneh



Case 46

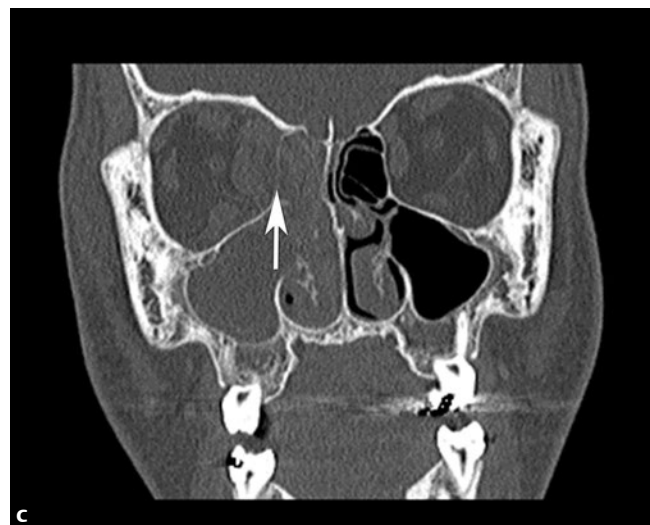
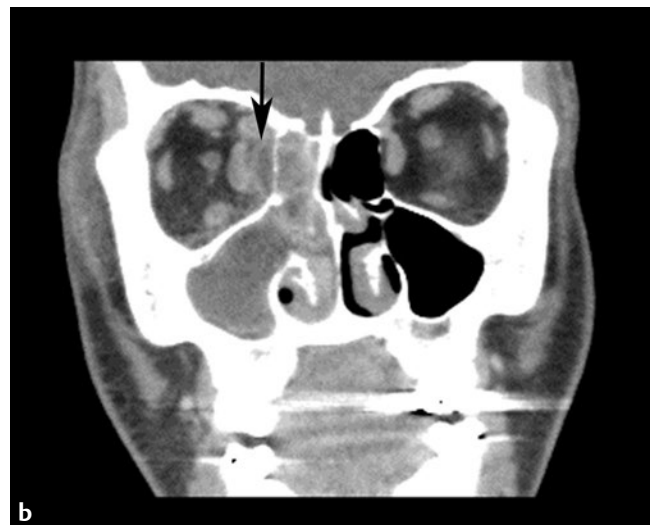
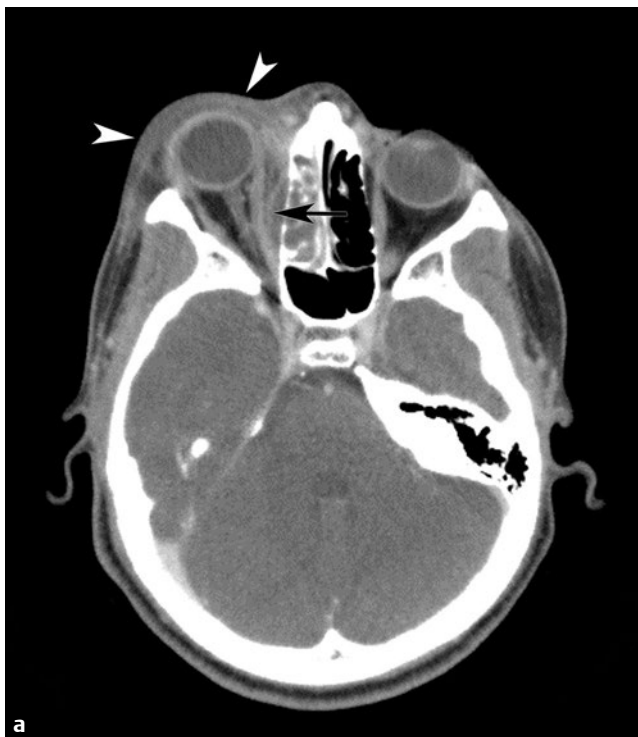
■ Clinical Presentation

A 10-year-old with periorbital swelling and nasal congestion.

■ Radiographic Studies

Postcontrast axial and coronal CT images of the orbit (**Figs. 46.1a,b**) show right preseptal soft tissue thickening (*arrow-heads*) with a rim-enhancing fluid collection (*arrow*) along the medial orbital wall displacing the medial rectus muscle. Coro-

nal reformatted CT bone window images of the orbits (**Fig. 46.1c**) shows the adjacent right maxillary and ethmoid sinusitis and the thinning and demineralization of the right lamina papyracea (*arrow*).



■ Diagnosis

Orbital Cellulitis

■ Discussion and Differential Diagnosis

Orbital infection is common, constituting more than 50% of primary orbital pathologies.¹ Orbital infection is classified as preseptal (periorbital) or postseptal (orbital) based on the location of the orbital septum.¹ Postseptal orbital cellulitis is most commonly caused by perivascular spread of adjacent paranasal sinusitis and is treated aggressively to prevent major complications such as meningitis, epidural/subdural empyema, and cavernous sinus thrombosis.¹ Subperiosteal orbital abscess is usually located in the postseptal portion of the medial orbit with bone destruction of the lamina papyracea. Other causes of orbital abscess include foreign body, trauma, skin infection, and bacteremia. Antibiotics have significantly lowered the morbidity and mortality of orbital cellulitis and its complications.

Enhanced CT is the procedure of choice for evaluating orbital cellulitis. Coronal and sagittal reconstructions and bone algorithm images are necessary. In preseptal cellulitis CT demonstrates diffuse enhancing soft tissue thickening anterior to the orbital septum.¹ Any spread of infection beyond the orbital septum including thickening of periorbital muscles or stranding of retro-orbital fat is diagnostic of postseptal (orbital) cellulitis. In postseptal cellulitis it is of prime importance to distinguish edema or phlegmon from a rim-enhancing abscess. Abscesses are surgically drained in addition to antibiotic administration. MRI is not usually performed in the acute diagnosis of orbital infections. Orbital abscess is differentiated from phlegmon or edema by the presence of restricted diffusion.²

Pearls

- ◆ Most orbital subperiosteal abscesses are caused by adjacent ethmoid sinusitis. If sinus disease is not present, look closely for a foreign body and ask about a history of trauma.
- ◆ Always check for cavernous sinus thrombosis and superior ophthalmic vein thrombosis in cases of orbital cellulitis.

Pitfall

- ◆ Congenital dermoid/epidermoid and dacryocystocele should be in the differential diagnosis of orbital abscess.

References

1. LeBedis CA, Sakai O. Nontraumatic orbital conditions: diagnosis with CT and MR imaging in the emergent setting. *Radiographics* 2008;28:1741–1753. [PubMed](#)
2. Sepahdari AR, Aakalu VK, Kapur R, et al. MRI of orbital cellulitis and orbital abscess: the role of diffusion-weighted imaging. *AJR Am J Roentgenol* 2009; 193:W244–50. [PubMed](#)

Case 47

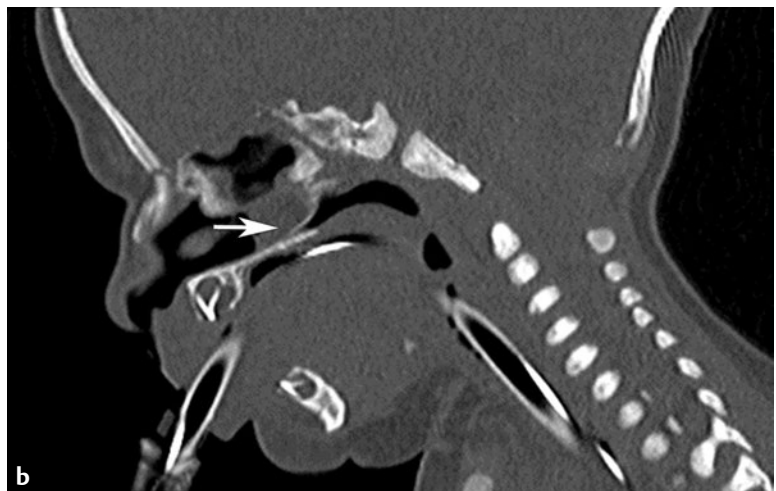
■ Clinical Presentation

A newborn with respiratory distress relieved by crying.

■ Radiographic Studies

Axial CT image (**Fig. 47.1a**) shows bilateral bony septa (*arrow-heads*), which are obstructing the narrowed posterior choanae. Note the thickened vomer and the secretions in the left nasal

cavity. Sagittal reformatted CT image (**Fig. 47.1b**) shows nasal secretions anterior to the obstructing bone septum (*arrow*).



■ Diagnosis

Choanal Atresia

■ Discussion and Differential Diagnosis

Choanal atresia is the most common congenital nasal anomaly. It occurs in 1 in 5,000 births and is often associated with other congenital anomalies.¹ The most common association is with the CHARGE syndrome (coloboma, *heart*, atresia of the choanae, retardation, genital anomalies, and ear anomalies).^{1,2} Choanal atresia can be bony, membranous, or mixed.^{1,2} Recent studies have shown that the mixed form is the most common, accounting for 70% of cases.¹ Obstruction can be unilateral (most commonly) or bilateral.^{1,2} In bilateral atresia, the infant has respiratory distress at birth, as infants are obligate nose breathers.^{1,2} The distress worsens with attempted feeding and is relieved by crying.^{1,2} The clinical diagnosis can be made by unsuccessful attempts to pass a catheter through the nasal cavity.² Noncontrast CT is the imaging procedure of choice to confirm the diagnosis.^{1,2} Findings include narrowing of the pos-

terior nasal cavity to < 3.4 mm, obliteration of the posterior choanae by bony septum or soft tissue density, thickening of the vomer, and medial bowing of the posterior maxilla.^{1,2} An atretic plate is attached to the vomer medially and the perpendicular plate of the palatine bone laterally. Treatment options include endoscopic perforation or surgical reconstruction.²

With unilateral obstruction, the diagnosis is typically made later in life. Patients present with chronic unilateral rhinitis associated with respiratory distress.¹ Respiratory distress in a newborn with a normal tracheobronchial airway and lungs should suggest the diagnosis of choanal atresia. Other causes of nasal obstruction in the newborn are nasopharyngeal dermoid cysts/teratomas, nasal cephaloceles, and complex craniofacial anomalies.

Pearls

- ◆ Choanal atresia coexists with additional congenital anomalies in more than 50% of cases. Associations include CHARGE syndrome, Treacher Collins syndrome, Crouzon syndrome, and Apert syndrome.
- ◆ Bony inlet stenosis can also cause symptoms of nasal obstruction.

Pitfall

- ◆ Mucus in the posterior nasal cavity can simulate a membrane. Nasal suctioning and decongestant spray should be performed before CT imaging.

References

1. Adil E, Huntley C, Choudhary A, Carr M. Congenital nasal obstruction: clinical and radiologic review. *Eur J Pediatr* 2012;171:641–650. [PubMed](#)
2. Baxter DJ, Shroff MM. Developmental maxillofacial anomalies. *Semin Ultrasound CT MR* 2011;32:555–568. [PubMed](#)

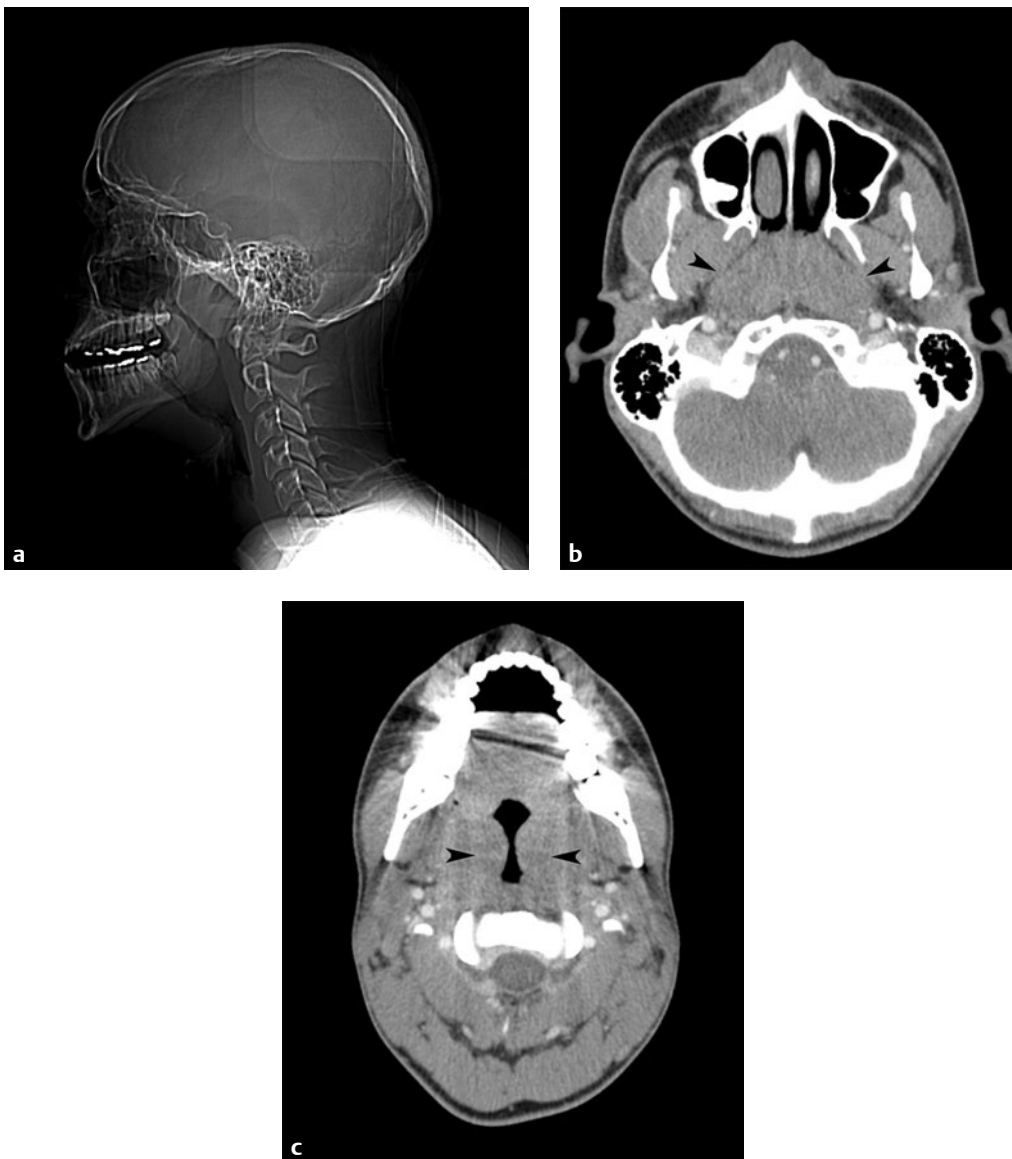
Case 48

■ Clinical presentation

A 16-year-old girl with fever and sore throat.

■ Radiographic studies

Lateral radiograph of the neck (**Fig. 48.1a**) reveals marked enlargement of the adenoids and palatine tonsils with upper airway narrowing. Postcontrast CT images (**Fig. 48.1b,c**) show marked enlargement of the adenoids and palatine tonsils (*arrowheads*) with narrowing of the nasopharynx and oropharynx.



■ Diagnosis

Infectious Mononucleosis

■ Discussion and Differential Diagnosis

Infectious mononucleosis is an acute systemic self-limiting disease of children and young adults (aged 15 to 25 years) caused by the Epstein-Barr virus (EBV). Characteristic findings include fever, pharyngitis, and lymphadenopathy.¹ Skin rash, splenomegaly and liver dysfunction can also be seen.¹ Diagnosis is made with laboratory data, which show lymphocytosis with atypical lymphocyte and persistent EBV antibody response.¹

Contrast CT of the neck is performed to rule out complications of the disease, including peritonsillar abscess and airway obstruction, seen in only 1.1% of cases of infectious mononucleosis.¹ The tonsils are enlarged and heterogeneous with interspersed streaky areas of low attenuation.¹ This finding, however, is not pathognomonic for infectious mononucleosis

and can be seen in severe streptococcal pharyngitis. The neck lymphadenopathy in infectious mononucleosis is most commonly found in the posterior cervical chain; generalized lymphadenopathy with involvement of the anterior cervical chain can be seen.¹ Splenomegaly is present in greater than 50% of patients with infectious mononucleosis and hepatomegaly in 10%. The lungs can be involved with a perihilar interstitial infiltrate. Pleural effusion is rare. Treatment of infectious mononucleosis is symptomatic, and recovery is seen in 3 to 4 weeks.¹ The differential diagnosis includes other viral exanthems and malignant diseases such as lymphoma, rhabdomyosarcoma, and lymphoepithelioma. With rhabdomyosarcoma, bone destruction is usually present.

Pearl

- ◆ Infectious mononucleosis should be suspected in teenagers with rapid marked enlargement of the tonsils and adenoids.

Pitfall

- ◆ Splenic rupture and secondary infection may complicate the course of infectious mononucleosis.

Reference

1. Kutuya N, Kurosaki Y, Suzuki K, Takata K, Shiraihshi A. Pharyngitis of infectious mononucleosis: computed tomography findings. *Radiat Med* 2008;26:248–251 [PubMed](#)

Case 49

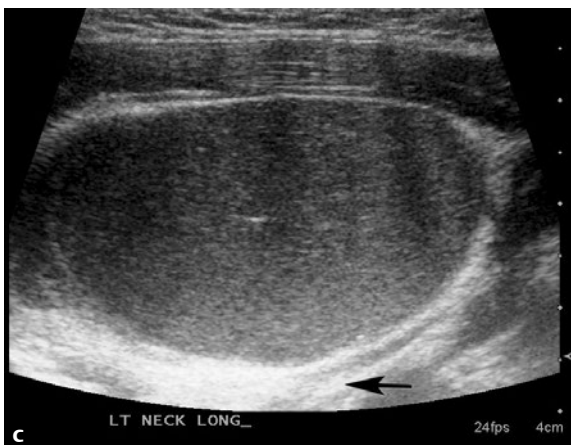
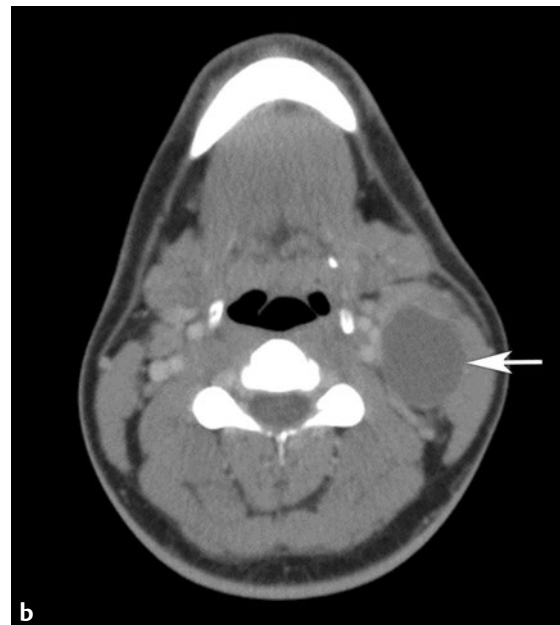
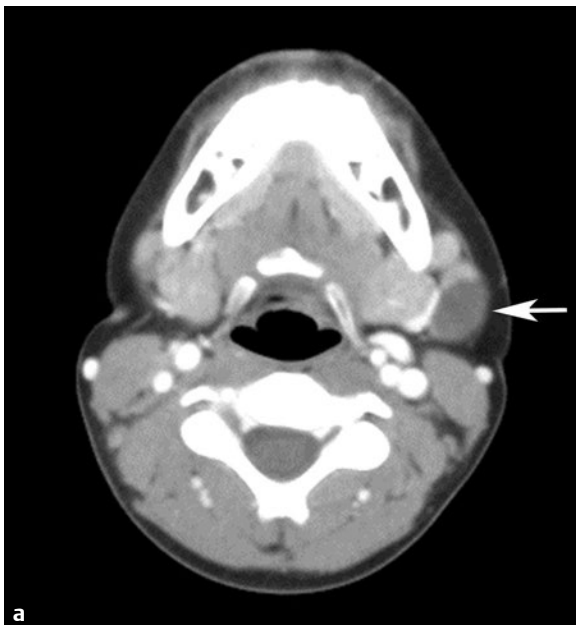
■ Clinical Presentation

A 12-year-old boy with palpable nontender neck mass.

■ Radiographic Studies

Postcontrast neck CT image (**Fig. 49.1a**) shows a well-demarcated oval low-attenuation lesion (*arrow*) near the mandibular angle and anterior to the left sternocleidomastoid muscle. Postcontrast neck CT image in another patient (**Fig. 49.1b**) shows a thin-walled oval low attenuation lesion (*arrow*) deep

to the sternocleidomastoid muscle, lateral to the carotid space, and posterior to the submandibular gland. An ultrasound image in this patient (**Fig. 49.1c**) shows moderate internal echoes and increased through transmission (*arrow*) consistent with cystic lesion.



■ Diagnosis

Branchial Cleft Cyst Type II

■ Discussion and Differential Diagnosis

Branchial cleft cyst (BCC) is a congenital neck cyst that can arise anywhere from the tonsillar fossa to the supraclavicular region of the neck. Many BCCs present in young adulthood as a slowly enlarging mass at the mandibular angle. Enlargement of the lesion is sometimes precipitated by an upper respiratory infection. Branchial cleft cysts can be classified into four types based on location; type II branchial cleft cysts constitute 95% of branchial cleft anomalies.¹ These cysts are classically located at the region of the mandibular angle, anterior to the sternocleidomastoid muscle, lateral to the carotid space, and posterior to the submandibular gland.¹

Ultrasound can be performed as a first-line investigation to confirm the cystic nature of the lesion.² CT is helpful for evaluation of the relationships of these cysts with surrounding

structures.² On CT the cysts are thin-walled and fluid-filled in the absence of inflammation.²

Magnetic resonance imaging is useful in assessing the deep tissue extent of these cysts and aiding presurgical planning.² BCCs have variable signal intensity on T1-weighted images and are hyperintense on T2-weighted images.² Minimal wall enhancement of the cysts is seen unless complicated by infection.² In the presence of infection, peripheral enhancement, wall thickening, and inflammatory changes in the surrounding soft tissues may be seen.^{1,2} Postcontrast neck CT (**Fig. 49.1d**) shows thick rim enhancement of a cystic neck lesion (*arrowheads*) with surrounding inflammation in a patient with clinical findings of superimposed infection.

Pearl

- ◆ Location is key to the diagnosis of second branchial cleft cysts. They most often present as cystic lesions at the angle of the mandible.

Pitfall

- ◆ Lymphatic malformations should be considered in the differential diagnosis of BCCs. Lobulated margins and the presence of internal septations are clues for the correct diagnosis of lymphatic malformation.

References

1. Koch BL. Cystic malformations of the neck in children. *Pediatr Radiol* 2005; 35:463–477. [PubMed](#)
2. Koeller KK, Alamo L, Adair CF, Smirniotopoulos JG. Congenital cystic masses of the neck: radiologic-pathologic correlation. *Radiographics* 1999;19:121–146, quiz 152–153. [PubMed](#)

Case 50

■ Clinical Presentation

A 5-year-old with hearing loss and hypoplastic pinna.

■ Radiographic Studies

High-resolution coronal CT images of the temporal bone (**Fig. 50.1a,b**) show complete bony atresia of the external auditory canal. Notice the deformed pinna (**Fig. 50.1a, arrow**) and the

deformed ossicles, which are fused to each other and to the atretic plate (**Fig. 50.1b, arrow**).



■ Diagnosis

External Auditory Canal Atresia

■ Discussion and Differential Diagnosis

External auditory canal atresia is uncommon, with a reported incidence of 1 in 10,000 to 1 in 20,000.¹⁻³ It results from defects of the first and second branchial arches and the first branchial cleft during embryogenesis.^{1,2} It can be membranous, bony, or mixed, and complete or incomplete.² Most cases are unilateral. Bilateral atresia, seen in one third of patients, is typically associated with congenital abnormalities such as Treacher Collins and Goldenhar syndromes.^{1,3} Patients present with conductive hearing loss, and microtia or hypoplastic pinna is commonly associated.² Anomalies of the external ear are invariably associated with middle ear and mastoid abnormalities due to their common embryological development.²

The external canal can be stenotic or atretic. In congenital bony external canal atresia, a bony plate (atresia plate) re-

places the tympanic membrane and forms the lateral wall of the middle ear.¹ The ossicles are usually deformed and fused to each other and to the atresia plate.² Fusion of the malleus and incus is the most common associated ossicular chain anomaly.² The inner ear is usually normal, but abnormalities of the oval and round windows may occur.^{2,3}

Management includes the use of bone-anchoring hearing aids (BAHA) or surgical reconstruction in some cases.^{1,2} Preoperative CT is performed to assess the thickness of the atresia plate, the presence of ossicular abnormalities, the degree of pneumatization and the development of the middle ear cavity/mastoid antrum, the status of the inner ear, and the course of the facial nerve. CT is also performed to search for vascular variants such as dehiscent jugular bulb.²

Pearl

- ◆ Look for middle ear anomalies with external canal atresia or stenosis. The presence and integrity of the stapes is crucial to predict surgical outcome.¹⁻³

Pitfalls

- ◆ The external auditory canal is curved and may appear narrow on single slices. Look at the entire exam.
- ◆ High-resolution CT of the temporal bone for presurgical planning should be performed around the age of 4 to 5 years for accurate assessment of the atresia plate. Imaging at an earlier age may be inadequate due to incomplete ossification of the structures.¹⁻³

References

1. White RD, Ananthakrishnan G, McKean SA, Brunton JN, Hussain SS, Sudarshan TA. Masses and disease entities of the external auditory canal: radiological and clinical correlation. *Clin Radiol* 2012;67:172-181. [PubMed](#)
2. Yuen HY, Ahuja AT, Wong KT, Yue V, van Hasselt AC. Computed tomography of common congenital lesions of the temporal bone. *Clin Radiol* 2003;58: 687-693. [PubMed](#)
3. Gassner EM, Mallouhi A, Jaschke WR. Preoperative evaluation of external auditory canal atresia on high-resolution CT. *AJR Am J Roentgenol* 2004; 182:1305-1312. [PubMed](#)

Case 51

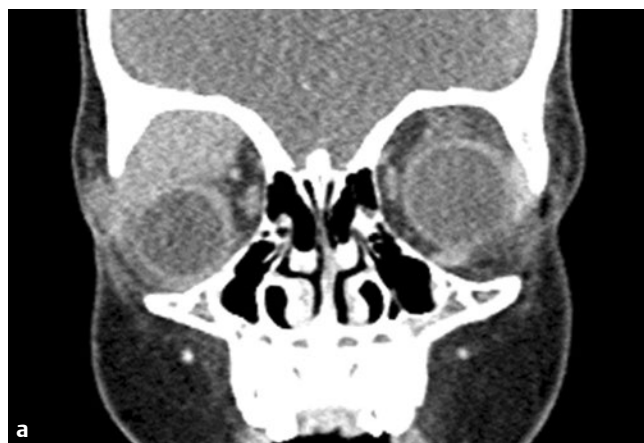
■ Clinical Presentation

An 8-year-old with right eye proptosis.

■ Radiographic Studies

Postcontrast coronal reformatted CT of the orbits (**Fig. 51.1a**) reveals a homogeneously enhancing soft tissue mass lesion at the superolateral aspect of the right orbit. Abnormal sclerosis of adjacent bone is seen with a bone window (**Fig. 51.1b**,

arrow). On axial postcontrast T1-weighted MRI with fat saturation (**Fig. 51.1c**), homogeneous enhancement of the right orbit lesion is seen with associated proptosis.



■ Diagnosis

Orbital Metastasis: Leukemia

■ Discussion and Differential Diagnosis

Leukemia is the most common malignancy in children, with acute myelogenous leukemia (AML) representing 15 to 20% of cases.¹ Granulocytic sarcomas are uncommon solid tumors of primitive granulocyte precursors that can develop in patients with AML,¹ with a reported incidence of 2.5 to 9.1%.² Those tumors were previously called chloromas in reference to the green color of the lesions, secondary to the presence of high levels of myeloperoxidase enzyme.^{1,3} The peak age of incidence is 7 to 8 years, and 75% of cases present before the age of 10 years.¹ Proptosis is the most common presenting symptom, and other symptoms include swelling, cellulitis, or mass in the eyelid or lacrimal gland.¹ Granulocytic sarcomas are unilateral in 90% of cases.³ Of note, 35% of these tumors may precede the diagnosis of AML by months or years.² They can also present during the course of the disease or as a sign of relapse.¹⁻³ The most common location for those tumors is the subperiosteal region of the lateral orbital wall.^{1,3} They can also involve the intra- or extraocular spaces or the lacrimal gland.¹

On CT, lesions appear as homogeneously enhancing mass lesions that tend to encase rather than invade the lacrimal gland or extraocular muscles.^{1,3} Typically, there is no calcification.¹ Bone destruction of the medial orbital wall with extension of the mass into the adjacent paranasal sinuses may be seen.^{1,2} On T1-weighted MRI, granulocytic sarcomas replace the normal high signal intensity of fatty marrow and appear isointense to low signal intensity compared with muscle or gray matter.¹ On T2-weighted MRI, the tumors are heterogeneously isointense to slightly hyperintense. Homogeneous enhancement is present with contrast administration.¹

The differential diagnosis for granulocytic sarcoma (in the absence of a known history of leukemia) includes neuroblastoma metastasis, Langerhans cell histiocytosis, rhabdomyosarcoma, or orbital inflammatory pseudotumor.¹

Pearls

- ◆ In children, orbital metastases arise in the extraocular soft tissues or osseous structures and almost never arise from the ocular structures. In adults, orbital metastases often arise in the ocular choroid.¹
- ◆ Always check for abnormal bone marrow signal intensity on MRI whenever an orbital mass is seen.

Pitfalls

- ◆ In children, leukemia is much more likely than lymphoma to involve the orbit.¹
- ◆ The differential diagnosis for granulocytic sarcoma in a child with a history of leukemia includes complications of the disease such as abscess, hematoma, or secondary malignancy.¹ Early diagnosis and differentiation is important to treat the patient accordingly.

References

1. Chung EM, Murphey MD, Specht CS, Cube R, Smirniotopoulos JG. From the Archives of the AFIP. Pediatric orbit tumors and tumorlike lesions: osseous lesions of the orbit. *Radiographics* 2008;28:1193–1214 [PubMed](#)
2. Guermazi A, Feger C, Rousselot P, et al. Granulocytic sarcoma (chloroma): imaging findings in adults and children. *AJR Am J Roentgenol* 2002;178:319–325 [PubMed](#)
3. Rao AA, Naheedy JH, Chen JY, Robbins SL, Ramkumar HL. A clinical update and radiologic review of pediatric orbital and ocular tumors. *J Oncol* 2013; 2013:975908 [PubMed](#)

Case 52

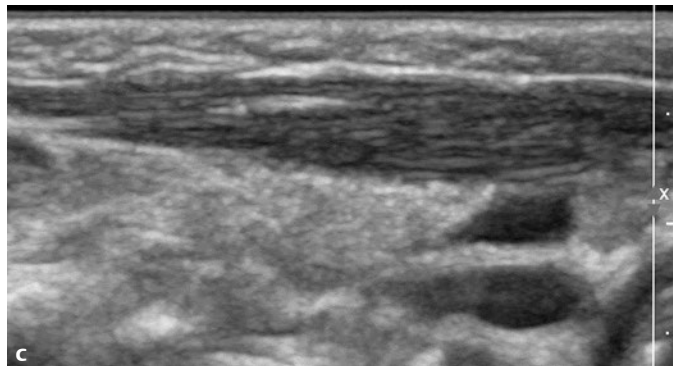
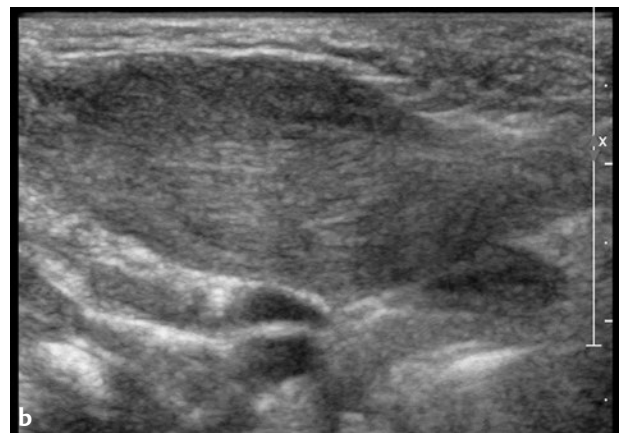
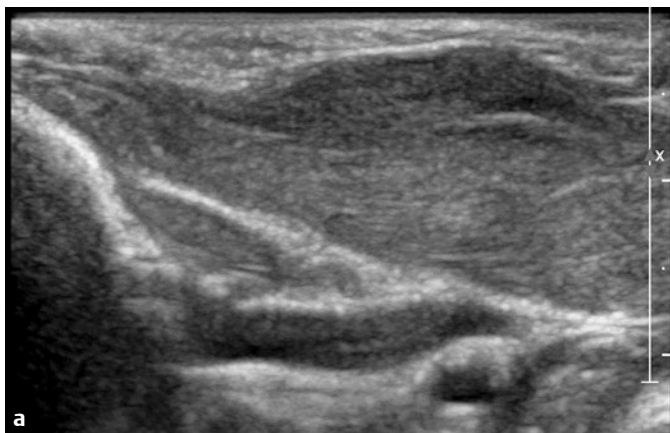
■ Clinical Presentation

A 1-month-old with right neck lump.

■ Radiographic Studies

Longitudinal ultrasound images of the upper and lower right neck (**Fig. 52.1a,b**) show fusiform enlargement of the right sternocleidomastoid (SCM) muscle. This enlarged muscle has increased echogenicity, especially in the middle and posterior

aspects. Ultrasound image of the left neck (**Fig. 52.1c**) shows normal size of the left SCM muscle with normal linear muscle striations.



■ Diagnosis

Fibromatosis Colli



■ Discussion and Differential Diagnosis

Fibromatosis colli (congenital muscular torticollis) is a benign fusiform mass arising in the SCM muscle of neonates and young infants.^{1,2} The condition is usually not present at birth but presents at 2 weeks of age.^{1,2} The natural course is rapid enlargement over a period of 2 to 4 weeks with spontaneous resolution by 4 to 8 months of age.^{1,2} Although the exact etiology is unknown, fibromatosis colli could represent an injury to the SCM muscle in utero or during birth. The head is tilted toward the side of the abnormal SCM muscle. Facial and skull asymmetry may be present.¹

Ultrasound is the procedure of choice, revealing the classic fusiform enlargement of the SCM muscle on longitudinal imaging.^{1,2} The echogenicity is variable, ranging from homogeneous to heterogeneous; internal calcifications may be present.^{1,2} A hypoechoic rim of muscle has been described that represents

normal muscle fibers at the periphery.^{1,2} The mass moves synchronously with the muscle on real-time images.^{1,2} CT and MRI are typically not performed. CT demonstrates isodense enlargement of the muscle; MRI shows heterogeneous signal intensity.^{1,2} The surrounding fatty planes are normal in both CT and MRI with no significant mass effect or encasement of surrounding structures.^{1,2}

Treatment is conservative, with stretching exercises and clinical observation.¹ Although rarely necessary, tenotomy, or (more recently) botulinum toxin injections may be used in refractory cases.¹ Other causes of torticollis in the first year of life include Sprengel's deformity and Klippel-Feil syndrome. These can be excluded with scapula and cervical spine radiographs.

Pearl

- ◆ Ultrasound is the examination of choice for an infant with torticollis and a neck mass.

Pitfall

- ◆ It is important to recognize fibromatosis colli as a benign condition to avoid unnecessary imaging and intervention.

References

1. Murphey MD, Ruble CM, Tyszkowski SM, Zbojnicki AM, Potter BK, Miettinen M. From the archives of the AFIP: musculoskeletal fibromatoses: radiologic-pathologic correlation. *Radiographics* 2009;29:2143–2173. [PubMed](#)
2. Ablin DS, Jain K, Howell L, West DC. Ultrasound and MR imaging of fibromatosis colli (sternomastoid tumor of infancy). *Pediatr Radiol* 1998; 28:230–233. [PubMed](#)

Case 53

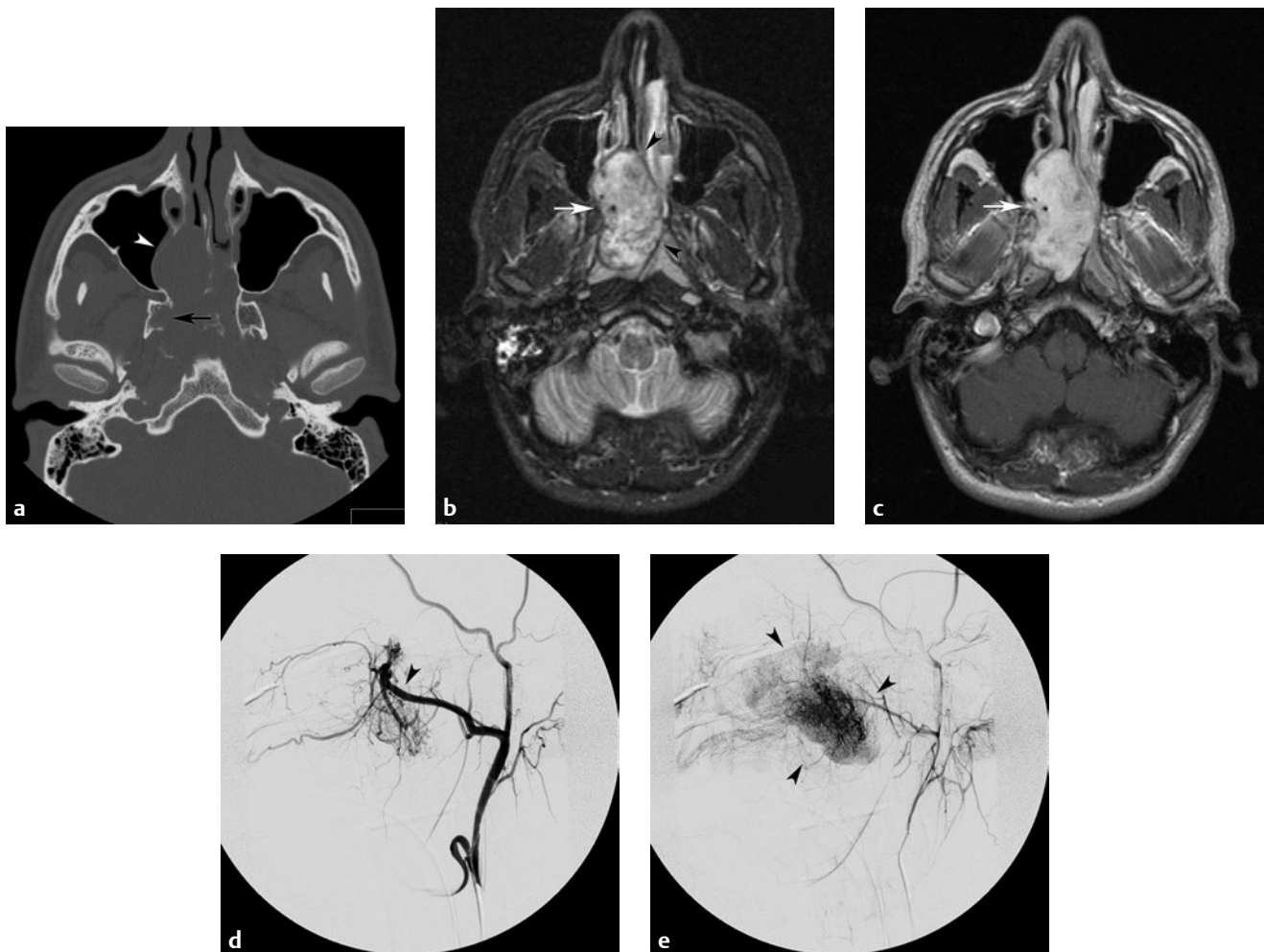
■ Clinical Presentation

Male teenager with nasal obstruction and epistaxis.

■ Radiographic Studies

Computed tomography bone window image (**Fig. 53.1a**) shows displacement of the medial wall maxillary sinus (*arrowhead*) and destruction of the medial pterygoid plate (*arrow*). T2-weighted MRI (**Fig. 53.1b**) shows heterogeneous signal mass (*arrowheads*) with internal flow void (*arrow*). On postcontrast T1-weighted image (**Fig. 53.1c**), the mass has diffuse enhance-

ment except for an internal flow void (*arrow*). Lateral external carotid angiogram (**Fig. 53.1d**) shows a dominant distal internal maxillary artery feeding branch (*arrowhead*) to the vascular mass. Later angiogram image (**Fig. 53.1e**) shows contrast blush of the vascular mass (*arrowheads*).



■ **Diagnosis**

Juvenile Nasopharyngeal Angiofibroma

■ **Discussion and Differential Diagnosis**

Juvenile nasopharyngeal angiofibroma (JNA) is an uncommon benign locally aggressive vascular tumor presenting in adolescent boys. The typical presentation includes epistaxis, nasal obstruction, or sinusitis.¹ Larger JNA lesions extend beyond the infratemporal fossa/nasal cavity and may present with cheek swelling, facial numbness, proptosis, visual changes, or cranial nerve palsy.^{1,2} CT imaging shows an avidly enhancing soft tissue mass in a characteristic sphenopalatine fossa location; extension of the vascular mass into the nasal cavity is common. Bowing of the posterior wall maxillary sinus, widening of the pterygopalatine fossa, and osseous erosion of the pterygoid plates/hard palate/nasal cavity are frequent on CT.³ MRI better displays soft tissue infiltration at the skull base and any intracranial extent. JNA is low signal on T1-weighted images and heterogeneous on T2-weighted images. The vascular mass has avid enhancement except for internal flow voids.³

Preoperative angiography is performed to delineate dominant external carotid artery (ECA) feeders to the mass and to perform selective distal ECA branch embolization to decrease surgical blood loss. Distal internal maxillary artery supply is most common in JNA. Identifying the ophthalmic artery origin from the internal carotid artery (ICA) and delineating any feeding artery branches from the ICA are important before ECA branch embolization.² Localized JNA lesions may be resected with a maxillofacial approach or a nasal endoscopic approach.⁴ Postsurgical recurrence rates ranging from 12 to 26% are reported.^{2,4-6} Larger JNA lesions may require a transcranial neurosurgical approach and/or radiation treatment for lesion control.⁵ With skull base involvement, residual disease in 40% of patients is reported on contrast-enhanced CT imaging performed days after surgical resection.⁷

Pearl

- ◆ Surgical blood loss and tumor recurrence with JNA increase if there are contralateral ECA feeders and an ipsilateral ICA blood supply.^{2,6}

Pitfall

- ◆ The interval between first symptoms and diagnosis may be over 1 year.⁵

References

1. Hodges JM, McDevitt AS, El-Sayed Ali AI, Sebelik ME. Juvenile nasopharyngeal angiofibroma: current treatment modalities and future considerations. *Indian J Otolaryngol Head Neck Surg* 2010;62:236–247. [PubMed](#)
2. Ballah D, Rabinowitz D, Vossough A, et al. Preoperative angiography and external carotid artery embolization of juvenile nasopharyngeal angiofibromas in a tertiary referral paediatric centre. *Clin Radiol* 2013;68:1097–1106. [PubMed](#)
3. Ludwig BJ, Foster BR, Saito N, Nadgir RN, Castro-Aragon I, Sakai O. Diagnostic imaging in nontraumatic pediatric head and neck emergencies. *Radiographics* 2010;30:781–799. [PubMed](#)
4. Midilli R, Karci B, Akyildiz S. Juvenile nasopharyngeal angiofibroma: analysis of 42 cases and important aspects of endoscopic approach. *Int J Pediatr Otorhinolaryngol* 2009;73:401–408. [PubMed](#)
5. Roche PH, Paris J, Régis J, et al. Management of invasive juvenile nasopharyngeal angiofibromas: the role of a multimodality approach. *Neurosurgery* 2007;61:768–777, discussion 777. [PubMed](#)
6. Chan KH, Gao D, Fernandez PG, Kingdom TT, Kumpe DA. Juvenile nasopharyngeal angiofibroma: vascular determinates for operative complications and tumor recurrence. *Laryngoscope* 2014;124:672–677. [PubMed](#)
7. Kania RE, Sauvaget E, Guichard J-P, Chapot R, Huy PTB, Herman P. Early postoperative CT scanning for juvenile nasopharyngeal angiofibroma: detection of residual disease. *AJNR Am J Neuroradiol* 2005;26:82–88. [PubMed](#)

Case 54

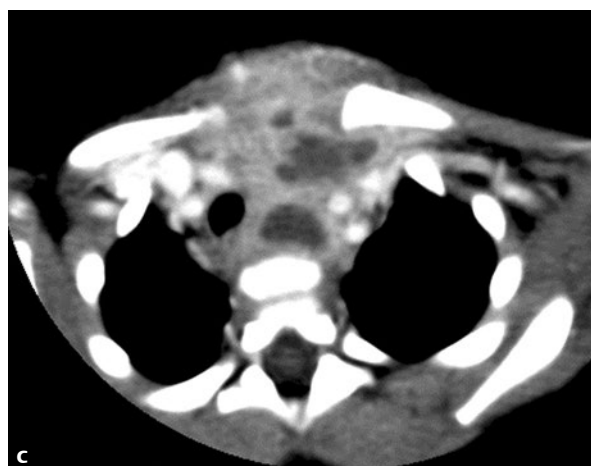
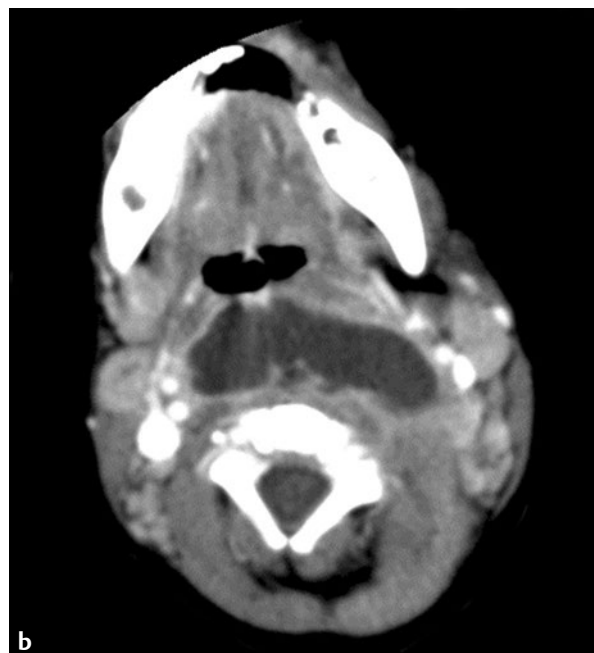
■ Clinical Presentation

A 2-year-old child with fever, neck pain, muffled voice, and drooling.

■ Radiographic Studies

Lateral soft tissue neck radiograph (**Fig. 54.1a**) reveals extensive prevertebral soft tissue swelling and thickening of the retropharyngeal soft tissues with mass effect on the airway and obliteration of the nasopharynx. Postcontrast CT image of the

neck (**Fig. 54.1b**) shows a large rim-enhancing fluid collection in the retropharyngeal space. Lower CT image (**Fig. 54.1c**) shows extension of the fluid collection into the superior mediastinum and the displacement of the trachea.



■ Diagnosis

Retropharyngeal Abscess

■ Discussion and Differential Diagnosis

The retropharyngeal space is a potential space that is located posterior to the pharynx and esophagus and that extends from the skull base to the upper mediastinum.^{1–3} Acute infections of the ear, nose, and throat in children spread to lymph nodes in the retropharyngeal space with resultant lymphadenitis, suppuration, and abscess formation.^{1–4} The majority of retropharyngeal abscesses are seen in children under the age of 6 years.⁴

The lateral soft tissue neck radiograph is obtained first in the radiographic evaluation of a child with a possible retropharyngeal abscess and will depict widening of the retropharyngeal soft tissues.^{2,4,5} The X-ray should be obtained in full inspiration with the neck in extension to avoid the false thickened appearance to the retropharyngeal soft tissues during the different phases of respiration. The average thickness of the

normal retropharyngeal soft tissue at the level of C2 is 5 mm.⁶ Fluoroscopy may be helpful by better visualizing the retropharyngeal soft tissue during different phases of respiration and neck position. Contrast-enhanced CT is the study of choice for detecting retropharyngeal edema, phlegmon, or abscess; for delineating potential mediastinal extent; and for identifying potential complications of retropharyngeal abscess.^{1–4} Retropharyngeal edema/phlegmon appears as ill-defined fluid or stranding of the fatty planes of the retropharyngeal space with no mass effect; retropharyngeal abscess has an enhancing wall.^{1–5} MRI can be used to assess intracranial and bony extension.² Ultrasound is helpful in demonstrating the presence of drainable fluid collection and is also useful in intraoperative/interventional drainage of the abscess.^{2,5}

Pearl

- ◆ Always check for potential complications of retropharyngeal abscess. These include airway obstruction, mediastinitis, septic embolization, dural sinus thrombosis, and intracranial abscess.^{2,3}

Pitfall

- ◆ Proper technique (inspiratory film with neck extension) is essential when evaluating soft tissue lateral neck radiographs for possible retropharyngeal abscess.

References

1. Hegde SV, Armstrong LK, Ramakrishnaiah RH, Shah CC. A space-based approach to pediatric face and neck infections. *Neurographics*. 2014;4:43–52.
2. Maroldi R, Farina D, Ravanelli M, Lombardi D, Nicolai P. Emergency imaging assessment of deep neck space infections. *Semin Ultrasound CT MR* 2012; 33:432–442. [PubMed](#)
3. Hoang JK, Branstetter BF IV, Eastwood JD, Glastonbury CM. Multiplanar CT and MRI of collections in the retropharyngeal space: is it an abscess? *AJR Am J Roentgenol* 2011;196:W426–32. [PubMed](#)
4. Capps EF, Kinsella JJ, Gupta M, Bhatki AM, Opatowsky MJ. Emergency imaging assessment of acute, nontraumatic conditions of the head and neck. *Radiographics* 2010;30:1335–1352. [PubMed](#)
5. Hegde AN, Mohan S, Pandya A, Shah GV. Imaging in infections of the head and neck. *Neuroimaging Clin N Am* 2012;22:727–754. [PubMed](#)
6. Vermess D, Rojas CA, Shaheen F, Roy P, Martinez CR. Normal pediatric prevertebral soft-tissue thickness on MDCT. *AJR Am J Roentgenol* 2012; 199:W130–3. [PubMed](#)

Case 55

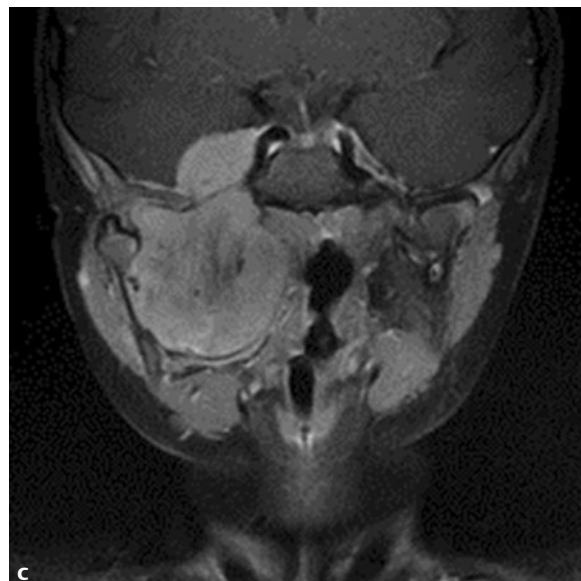
■ Clinical Presentation

A 15-year-old boy with headache, right facial pain, and weight loss.

■ Radiographic Studies

Coronal contrast-enhanced CT image of the maxillofacial region (**Fig. 55.1a**) shows a large heterogeneously enhancing soft tissue mass in the right masticator space and the right parapharyngeal space extending through an expanded foramen ovale (*arrowhead*) into the right cavernous sinus. Note the fat plane obliteration superficial and deep to the right mandib-

ular ramus. Coronal reformatted bone algorithm CT image (**Fig. 55.1b**) shows destruction of the floor of the right middle cranial fossa (*arrowheads*). Postcontrast coronal T1-weighted MRI with fat saturation (**Fig. 55.1c**) shows homogeneous enhancement of the mass.



■ Diagnosis

Rhabdomyosarcoma

■ Discussion and Differential Diagnosis

Rhabdomyosarcoma is the most common soft tissue sarcoma in children.^{1,2} Most cases occur in children younger than 10 years of age.¹⁻³ The most common area of origin is the head and neck region, accounting for 40% of cases.^{1,3} The next two most common areas are the genitourinary region and the extremities. Rhabdomyosarcoma is classified histologically into three types: embryonal (most common), alveolar, and pleomorphic.^{1,3} Head and neck rhabdomyosarcoma is classified based on location into three types: parameningeal (50%, in which the tumor is in direct or close contact with the skull base), nonparameningeal (25%), and orbital (25%).¹ Alveolar and parameningeal rhabdomyosarcoma have the worst prognosis.¹

On imaging, rhabdomyosarcoma appears as a heterogeneous, relatively well-circumscribed soft tissue mass.^{1,2} MRI is the

modality of choice for assessing rhabdomyosarcoma given its inherent superior soft tissue resolution.¹ The lesion has variable signal on T1- and T2-weighted images and shows moderate homogeneous enhancement.¹⁻³ Coronal images are particularly useful for assessment of intracranial extension.^{1,3} Perineural spread of head and neck rhabdomyosarcoma is most commonly seen along cranial nerves V and VII and appears as abnormal enhancement along the nerves.¹ CT is performed to assess bone destruction and to look for lung metastasis.¹

The differential diagnosis of head and neck rhabdomyosarcoma includes lymphoma, nasopharyngeal carcinoma, and juvenile nasal angiofibroma.^{1,2} Treatment is with a combination of surgery, chemotherapy, and radiation.¹⁻³

Pearls

- ◆ Of the three head and neck subtypes, orbital rhabdomyosarcoma has the best prognosis; intracranial extension and associated bone destruction are rare.¹
- ◆ There is no pathognomonic MRI appearance for rhabdomyosarcoma. Imaging is performed to assess local extent of the mass, for staging, and to assess response to therapy.¹

Pitfalls

- ◆ Tumor extension into adjacent compartments can be subtle. Always look for obliteration of fat planes, abnormal enhancement, and asymmetry compared with the contralateral side.¹
- ◆ Bilateral lymphadenopathy is not commonly seen in rhabdomyosarcoma, but is more commonly seen with nasopharyngeal carcinoma.¹

References

1. Freling NJ, Merks JH, Saeed P, et al. Imaging findings in craniofacial childhood rhabdomyosarcoma. *Pediatr Radiol* 2010;40:1723-1738, quiz 1855 [PubMed](#)
2. Robson CD. Imaging of head and neck neoplasms in children. *Pediatr Radiol* 2010;40:499-509 [PubMed](#)
3. Lloyd C, McHugh K. The role of radiology in head and neck tumours in children. *Cancer Imaging* 2010;10:49-61 [PubMed](#)

Case 56

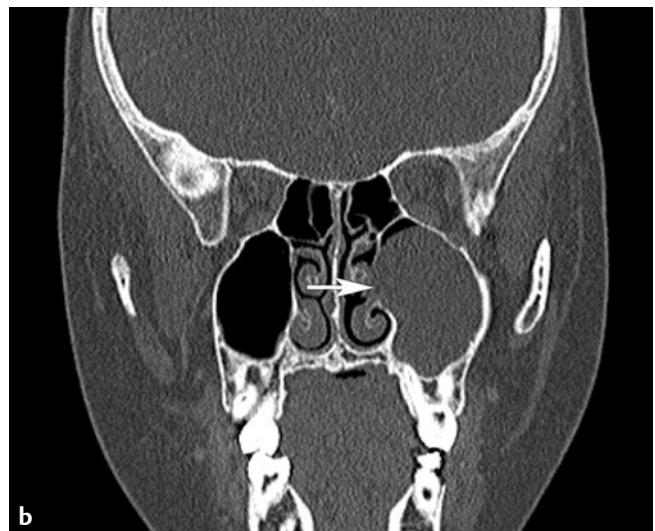
■ Clinical Presentation

A 15-year-old with nasal obstruction.

■ Radiographic Studies

Axial and coronal CT images of the sinuses (**Fig. 56.1a,b**) show soft tissue opacification of the left maxillary sinus. Note expansion of the maxillary sinus, lack of bone destruction, and the prolapse of the mass lesion into the left nasal cavity

through an expanded sinus ostium (**Fig. 56.1b, arrow**). Sagittal reformatted CT image shows the lobular mass (**Fig. 56.1c, arrowheads**) obstructing the nasal cavity.



■ Diagnosis

Antrochoanal Polyp

■ Discussion and Differential Diagnosis

The antrochoanal polyp is a benign, solitary, slow-growing lesion that arises in the maxillary sinus and prolapses into the nasal cavity.¹ On CT it appears as a dumbbell-shaped soft tissue mass lesion that fills and expands the maxillary antrum, passes through and widens the sinus ostium (or more commonly an accessory ostium), and extends into the nasal cavity without causing bone destruction.^{1,2} Teenagers and young adults are most commonly affected.² The imaging appearance of the antrochoanal polyp is pathognomonic and should not be confused with a more aggressive or malignant process. A crescent rim of air above the polyp (**Fig. 56.b**) is a differentiating feature from other antral masses.¹ Contrast-enhanced CT, although not required for the diagnosis, demonstrates peripheral enhancement of the lesion.

The differential diagnosis of antrochoanal polyp includes mucus retention cyst, which is a common incidental finding caused by obstruction of mucosal gland ducts.^{1,3} Another differential diagnosis is mucocele, in which the sinus itself and not the ostium is expanded.¹ Chronic sinusitis can also cause sinus opacification with bone remodeling, but not the expansion of the ostium and extension into the nasopharynx seen with antrochoanal polyp.³ Nasal polyps from chronic infections or allergies are usually multiple and have an inhomogeneous appearance on CT, with high-attenuation secretions trapped between the polyps.³

Treatment of antrochoanal polyp is complete surgical resection.¹

Pearl

- ◆ A mass in the nasopharynx with maxillary sinus opacification and an enlarged ostium is a benign antrochoanal polyp.

Pitfall

- ◆ Always look in the nasopharynx and at the maxillary sinus ostium when you see maxillary sinus opacification.

References

1. Pruna X, Ibañez JM, Serres X, Garriga V, Barber I, Vera J. Antrochoanal polyps in children: CT findings and differential diagnosis. *Eur Radiol* 2000;10:849–851 [PubMed](#)
2. Chung SK, Chang BC, Dhong HJ. Surgical, radiologic, and histologic findings of the antrochoanal polyp. *Am J Rhinol* 2002;16:71–76 [PubMed](#)
3. Madani G, Beale TJ. Sinonasal inflammatory disease. *Semin Ultrasound CT MR* 2009;30:17–24 [PubMed](#)

Case 57

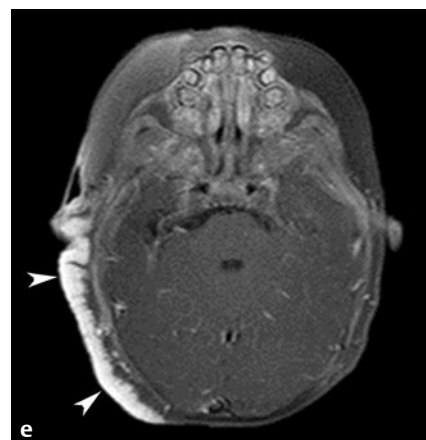
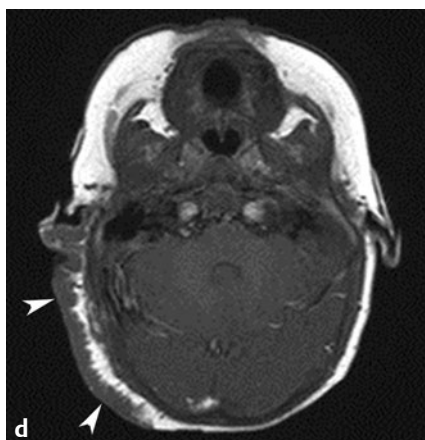
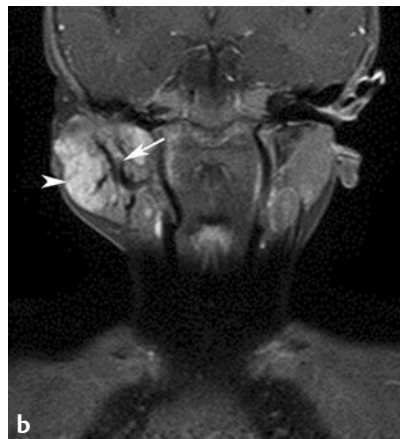
■ Clinical Presentation

A 2-month-old girl has right preauricular soft tissue mass with overlying reddish skin discoloration.

■ Radiographic Studies

Coronal T2-weighted MRI (**Fig. 57.1a**) shows a lobulated high signal soft tissue mass lesion (*arrowhead*) in the right parotid gland. Associated flow void enlargement (*arrow*) is seen. Postcontrast coronal and axial T1-weighted images with fat saturation (**Fig. 57.1b,c**) show enhancing soft tissue lobules (*arrowheads*) and associated flow void enlargement (*arrows*), indicating high flow. Axial T1-weighted MRI in another pa-

tient, a 5-month-old infant with extensive reddish skin lesion (**Fig. 57.1d**), shows a broad-based moderate signal mass infiltrating the subcutaneous tissue and skin of the right scalp (*arrowheads*), extending anteriorly into the right ear. Postcontrast T1-weighted image with fat saturation (**Fig. 57.1e**) shows intense enhancement (*arrowheads*) throughout this infiltrative subcutaneous mass with skin and ear involvement.



■ Diagnosis

Hemangioma

■ Discussion and Differential Diagnosis

Hemangiomas are the most common vascular tumors of infancy and the most common childhood tumor in the head and neck.^{1,2} Characteristic locations of hemangiomas include the skin/subcutaneous tissues and characteristic sites of deep involvement including the parotid gland, orbit, and subglottic airway. Hemangiomas of infancy are endothelial cell neoplasms that appear soon after birth and demonstrate a unique proliferative growth phase greatest in the first year of life followed by a variable involution phase throughout the first decade of life.³ Though many hemangiomas can be followed conservatively over time, treatment may be required in lesions with massive growth, ulceration, function impairment, and disfigurement. Propranolol treatment has been used with success in symptomatic lesions; treatment may be prolonged, as in the setting of vascular anomalies that are treated by a multidisciplinary team.^{3,4}

Ultrasound delineates superficial hemangiomas as well-demarcated solid lobular masses of variable echogenicity and high vascularity on color flow Doppler images.^{1,2} MRI may be needed to fully delineate the deep extent of hemangiomas and the relationship to other structures. A localized or infiltrating mass is seen with high T2-weighted signal intensity and intense lobular parenchymal enhancement on fat-saturated postcontrast T1-weighted images.^{1,2} Signs of high flow on MRI

include flow voids within or near the mass and prominent flow-related enhancement on gradient echo or time-of-flight images.^{1,2} On CT imaging, hemangiomas have attenuation similar to muscle, and intense contrast enhancement is noted.¹

Differential diagnosis of proliferating hemangiomas include the rare vascular tumor kaposiform hemangioendothelioma (KHE), the rare congenital hemangiomas, and vascular malformations.⁵ KHE is an infiltrative vascular tumor that often invades deep muscular compartments and may have characteristic low platelets (Kasabach-Merritt syndrome), not seen in proliferating hemangiomas. Unlike hemangiomas of infancy, congenital hemangiomas are fully formed at birth. Arteriovenous malformations (AVMs) have arterial and venous enlargement seen in bulky proliferating hemangiomas, but typically lack an intervening enhancing soft tissue mass characteristic of hemangioma.^{1,2} At angiography, AVM has characteristic arteriovenous shunting not seen in high-flow hemangiomas. Though bluish/reddish skin discoloration may be present in venous and lymphatic malformations, these low-flow malformations lack arterial enlargement seen in high-flow hemangiomas. In addition, calcified phleboliths of venous malformation or multiseptated macrocysts with dependent fluid-fluid levels of lymphatic malformation will not be seen in a proliferating hemangioma mass.^{1,2}

Pearls

- ◆ Glucose transporter 1 (GLUT1) immunoreactivity is a highly selective marker for hemangiomas and helps distinguish hemangiomas from vascular malformations.⁶
- ◆ PHACES syndrome (posterior fossa malformations, hemangioma, arterial anomalies, coarctation of the aorta and other cardiac defects, eye abnormalities, sternal clefts or supraumbilical raphe) is associated with hemangiomas.¹

Pitfall

- ◆ Some hemangiomas respond poorly to propranolol and may require laser therapy, steroids, or occasionally surgical resection.³

References

1. Baer AH, Parmar HA, DiPietro MA, Kasten SJ, Mukherji SK. Hemangiomas and vascular malformations of the head and neck: a simplified approach. *Neuroimaging Clin N Am* 2011;21:641–658. [PubMed](#)
2. Lowe LH, Marchant TC, Rivard DC, Scherbel AJ. Vascular malformations: classification and terminology the radiologist needs to know. *Semin Roentgenol* 2012;47:106–117. [PubMed](#)
3. Buckmiller LM, Munson PD, Dyamenahalli U, Dai Y, Richter GT. Propranolol for infantile hemangiomas: early experience at a tertiary vascular anomalies center. *Laryngoscope* 2010;120:676–681. [PubMed](#)
4. Parikh SR, Darrow DH, Grimmer JF, Manning SC, Richter GT, Perkins JA. Propranolol use for infantile hemangiomas: American Society of Pediatric Otolaryngology Vascular Anomalies Task Force practice patterns. *JAMA Otolaryngol Head Neck Surg* 2013;139:153–156. [PubMed](#)
5. Garcia-Monaco R, Giachetti A, Peralta O, et al. Kaposiform hemangioendothelioma with Kasabach-Merritt phenomenon: successful treatment with embolization and vincristine in two newborns. *J Vasc Interv Radiol* 2012;23:417–422. [PubMed](#)
6. North PE, Waner M, Mizeracki A, Mihm MC Jr. GLUT1: a newly discovered immunohistochemical marker for juvenile hemangiomas. *Hum Pathol* 2000;31:11–22. [PubMed](#)

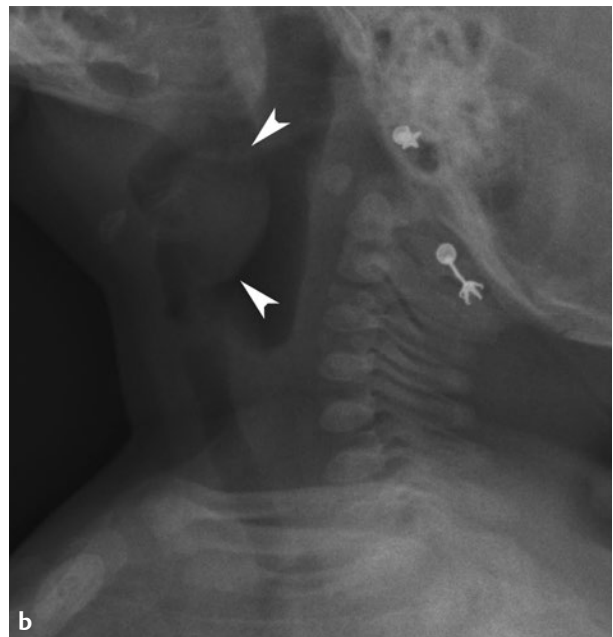
Case 58

■ Clinical Presentation

A 3-year-old with sore throat, drooling, and muffled speech.

■ Radiographic Studies

Lateral soft tissue neck radiograph (**Fig. 58.1a**) shows thickening of the epiglottis (*arrow*) and aryepiglottic folds (*arrowhead*).



■ Diagnosis

Epiglottitis

■ Discussion and Differential Diagnosis

Acute bacterial epiglottitis is a life-threatening condition characterized by infection and edema of the epiglottic and aryepiglottic folds. Children classically present with abrupt onset of fever, dysphagia, and respiratory distress.^{1,2} The highest incidence occurs between 2 and 8 years of age.² *Haemophilus influenzae* type B (Hib) is the etiologic agent in most cases.^{1,2} Since the introduction of the Hib vaccine in the late 1980s, a marked decrease in the incidence of epiglottitis has occurred.^{1,2} However, a recent increase in the number of cases caused by other viral and bacterial etiologies is being encountered, particularly in adults.¹

The diagnosis of acute epiglottitis is typically made clinically.¹ A portable lateral erect soft tissue radiograph of the neck should be obtained in the emergency department or operating room if the diagnosis is uncertain. Radiographs can exclude other conditions such as foreign body, retropharyngeal abscess, and croup.² A physician skilled in endotracheal intubation or emergency tracheostomy should be present, as these patients can experience a completely obstructed air-

way at any time.² Erect positioning is important because of the increased incidence of obstruction while the patient is recumbent.² Radiographs reveal an enlarged, thick and round epiglottis (thumb sign), indistinct aryepiglottic folds with inflammation throughout the supraglottic region, loss of vallecular air space, and loss of cervical lordosis.^{2,3} Subglottic edema can be present in 25% of cases. The hypopharynx is distended in inspiration because of supraglottic obstruction.

If an enlarged epiglottis is noted in the absence of a classic clinical presentation, differential considerations are an omega-shaped epiglottis (a normal prominent epiglottis), hemophilia, angioneurotic edema, chronic epiglottitis, Stevens-Johnson syndrome, aryepiglottic or epiglottic cyst, foreign body trauma, caustic or chemical ingestion, thermal injury, and irradiation. Lateral soft tissue neck radiograph in another 2-month-old girl with stridor (**Fig. 58.1b**) shows oval soft tissue density (*arrowheads*) at the epiglottis/aryepiglottic fold region. Post-contrast sagittal T1-weighted MRI in this infant (**Fig. 58.1c**) shows a rim-enhancing aryepiglottic cyst (*arrow*).

Pearls

- ◆ The Hib vaccine has markedly decreased the incidence of epiglottitis.¹
- ◆ Maintaining the airway is the cornerstone in managing epiglottitis.

Pitfall

- ◆ Leave the child in the emergency department if epiglottitis is suspected. Perform a portable lateral neck radiograph.

References

1. Capps EF, Kinsella JJ, Gupta M, Bhatki AM, Opatowsky MJ. Emergency imaging assessment of acute, nontraumatic conditions of the head and neck. *Radiographics* 2010;30:1335–1352 [PubMed](#)
2. Rotta AT, Wiryawan B. Respiratory emergencies in children. *Respir Care* 2003; 48:248–258, discussion 258–260 [PubMed](#)
3. Virk JS, Pang J, Okhovat S, Lingam RK, Singh A. Analysing lateral soft tissue neck radiographs. *Emerg Radiol* 2012;19:255–260 [PubMed](#)

Case 59

■ Clinical Presentation

A 10-year-old with recurrent otitis media and chronically draining ear.

■ Radiographic Studies

Coronal CT image (**Fig. 59.1a**) shows tissue in the epitympanum (*arrow*) with blunting of the scutum. Axial CT image (**Fig.**

59.1b) shows soft tissue filling the mastoid and epitympanum with associated ossicular erosion (*arrow*).



■ Diagnosis

Middle Ear Cholesteatoma

■ Discussion and Differential Diagnosis

Cholesteatoma is accumulation of keratinizing squamous epithelium in the middle ear cavity. Associated bone erosion is the hallmark of the disease.¹ Lesions can be congenital (2%) or acquired (98%). Congenital cholesteatomas are epithelial rests that can occur anywhere in or adjacent to the temporal bone.² Acquired cholesteatomas are uniquely located in the middle ear.² High-resolution CT is the imaging modality of choice in evaluating bony changes associated with cholesteatoma and potential intracranial complications.²

Characteristic CT findings include an expansile soft tissue mass in the epitympanic recess with extension into the mastoid antrum; tympanic membrane retraction; and erosion of the ossicles, scutum, and tegmen tympani.² Other possible areas of bone erosion include the sigmoid sinus plate, the posterior superior external auditory canal, the lateral semicircular canal, the labyrinth, and the facial nerve canal.³ On MRI, cholesteatoma has nonspecific low signal intensity on T1-

weighted sequences and high signal intensity on T2-weighted sequences. No enhancement is seen after contrast administration.² Cholesteatomas display internal restricted diffusion.²

Computed tomography has low specificity in characterizing soft tissue masses in the temporal bone, such as cholesterol granulomas, granulation tissue, secretions, and neoplasms.^{2,3} The CT diagnosis of a cholesteatoma is made by the characteristic bone erosion.¹⁻³ Opacification of the middle ear cavity and mastoid air cells with absent bone erosion suggests the alternative diagnosis of otomastoiditis without cholesteatoma formation.² MRI is helpful in differentiating postsurgical granulation tissue from cholesteatoma.^{2,3} Postsurgical granulation tissue may show delayed enhancement (30 to 45 minutes after contrast administration) and will not have restricted diffusion, as opposed to the absent enhancement and increased diffusivity seen with cholesteatoma.^{2,3}

Pearl

- ◆ Bone erosion is characteristic of cholesteatoma and is the cause of associated complications, including labyrinthine fistula (most common), facial nerve paralysis, conductive or sensorineural hearing loss, intracranial extension with intracranial abscess formation, recurrent bacterial meningitis, and sigmoid sinus thrombosis.³

Pitfall

- ◆ Absent bone erosion does not exclude the diagnosis of cholesteatoma in small lesions.²

References

1. Yates PD, Flood LM, Banerjee A, Clifford K. CT scanning of middle ear cholesteatoma: what does the surgeon want to know? *Br J Radiol* 2002; 75:847–852 [PubMed](#)
2. Baráth K, Huber AM, Stämpfli P, Varga Z, Kollias S. Neuroradiology of cholesteatomas. *AJNR Am J Neuroradiol* 2011;32:221–229 [PubMed](#)
3. Schwartz KM, Lane JI, Bolster BD Jr, Neff BA. The utility of diffusion-weighted imaging for cholesteatoma evaluation. *AJNR Am J Neuroradiol* 2011;32: 430–436 [PubMed](#)

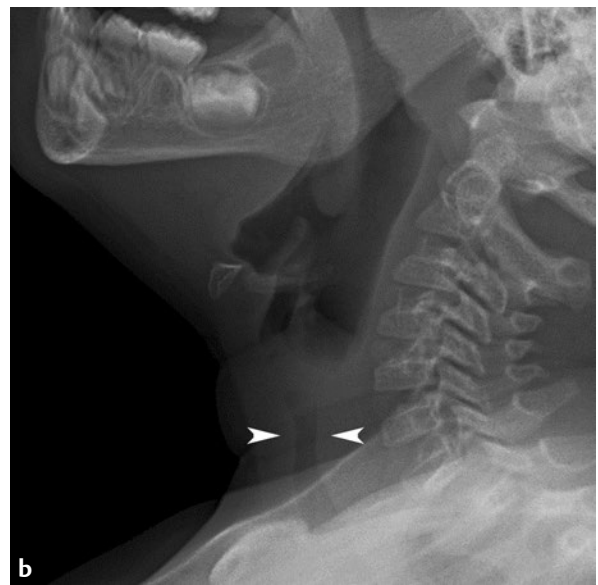
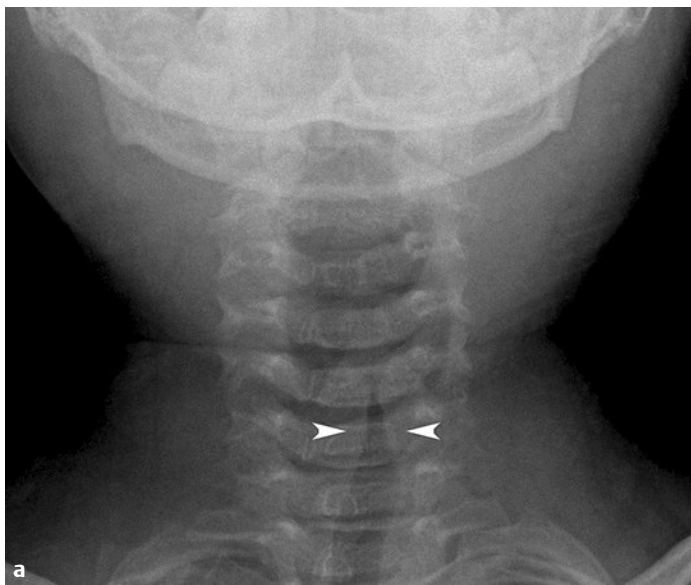
Case 60

■ Clinical Presentation

A 1-year-old presents with inspiratory stridor and cough.

■ Radiographic Studies

Frontal soft tissue neck radiograph (**Fig. 60.1a**) demonstrates symmetric subglottic tracheal narrowing (*arrowheads*). Lateral soft tissue neck radiograph (**Fig. 60.1b**) shows subglottic tracheal narrowing in the anteroposterior dimension (*arrowheads*). Associated hypopharyngeal distention is seen and a normal epiglottis is confirmed.



■ Diagnosis

Croup

■ Discussion and Differential Diagnosis

Croup, or laryngotracheobronchitis, is the most common infectious cause of acute stridor in children. Incidence is highest between the ages of 6 months and 4 years.¹ Croup is most commonly caused by parainfluenza virus or respiratory syncytial virus.¹ The classic presentation is fever, a “brassy” cough, and acute inspiratory stridor. Croup is a clinical diagnosis and usually a self-limited condition that resolves with conservative management.

Radiography is performed to rule out other causes of stridor such as foreign body, epiglottitis, congenital subglottic stenosis, retropharyngeal abscess, or hemangioma.¹ The AP radiograph reveals the classic “steep sign” of the symmetric subglottic tracheal narrowing (inverted-V configuration).² Ra-

diographic findings are caused by circumferential edema of the trachea, resulting in elevation of the mucosa (which is loosely attached at this level) and loss of the normal lateral convexities (shouldering) of the tracheal air column.² In addition, the lateral radiograph demonstrates hypopharyngeal distention with normal epiglottis and aryepiglottic folds.³

Membranous croup is an uncommon severe purulent infection of the upper airways.⁴ It is life threatening and typically affects older children.⁴ Diagnostic clues include tracheal irregularities and plaques on the lateral neck radiograph with subglottic narrowing in a toxic child.⁴ Pneumomediastinum is a rare complication.⁴

Pearl

- ◆ Negative radiographs do not exclude the diagnosis of croup. Radiographs are performed to exclude other causes of stridor in children.

Pitfall

- ◆ Do not forget to search for an enlarged epiglottis (“thumb sign”) on the lateral radiograph. The incidence of epiglottitis has reduced drastically since the introduction of the *Haemophilus influenzae* type B vaccine, but this life-threatening infection still occurs.¹

References

1. Rotta AT, Wiryawan B. Respiratory emergencies in children. *Respir Care* 2003;48:248–258, discussion 258–260 [PubMed](#)
2. Salour M. The steep sign. *Radiology* 2000;216:428–429 [PubMed](#)
3. Virk JS, Pang J, Okhovat S, Lingam RK, Singh A. Analysing lateral soft tissue neck radiographs. *Emerg Radiol* 2012;19:255–260 [PubMed](#)
4. Sammer M, Pruthi S. Membranous croup (exudative tracheitis or membranous laryngotracheobronchitis). *Pediatr Radiol* 2010;40:781 [PubMed](#)

Case 61

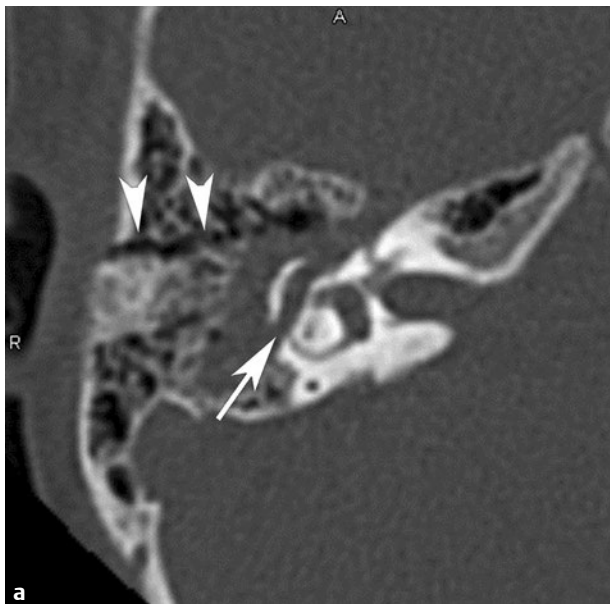
■ Clinical Presentation

A 12-year-old with loss of consciousness and hemotympanum after a fall from a height.

■ Radiographic Studies

Axial CT image (**Fig. 61.1a**) shows transverse fracture through the anterior mastoid (*arrowheads*). There is a displaced fracture fragment disrupting the lateral semicircular canal (*arrow*). Follow-up axial CT image following resolution of acute hemor-

rhage (**Fig. 61.1b**) shows malleo-incudal subluxation (*arrow*). The stapes (*arrowhead*) is widely separated from the malleus and incus secondary to incudostapedial dislocation.



■ Diagnosis

Temporal Bone Fracture

■ Discussion and Differential Diagnosis

Temporal bone injury results from high-energy blunt head trauma and is seen in 14 to 22% of patients with skull fractures.¹ Traditionally, temporal bone fractures were classified into longitudinal and transverse fractures in reference to whether the fracture line is oriented parallel or perpendicular to the long axis of the petrous bone.^{1–3} Most temporal bone fractures, however, are complex, and poor clinical correlation with imaging findings was found based on the traditional classification.¹

Computed tomography is essential to identify injury to critical structures.¹ Extension of the fracture line to the external auditory canal should be documented.¹ The axial plane is best for evaluating ossicular chain continuity. The ossicles can be fractured or (more commonly) subluxed in temporal bone injury.^{1,3} Incudostapedial joint separation is the most common traumatic ossicular subluxation.¹ Ossicular fractures most commonly involve the incus due to its lack of anatomic support compared with other ossicles.^{1,3} Fracture extension into the internal carotid canal should be assessed in the axial plane, and reformatted sagittal and coronal images and CTA should be performed.¹ In one series, vascular complications (e.g., dis-

section, pseudoaneurysm, transection, fistula) were seen in 11% of patients with fractures of the carotid canal.¹ Facial nerve injury is seen in 7% of cases of temporal bone fractures. Most injuries are seen in the region of the geniculate ganglion.^{1,3} Associated findings include fracture extending along the course of the facial nerve on CT and abnormal enhancement of the facial nerve or compressing hematoma on MR.³ Disruption of the cochlea, vestibule, and semicircular canals should be identified.¹

The most common complication of temporal bone fracture is hearing loss, either conductive or sensorineural.^{1,3} Associated imaging findings in conductive hearing loss include ossicular fracture or subluxation, blood filling the external auditory canal and middle ear cavity, rupture of the tympanic membrane (with or without fracture), and external auditory canal stenosis due to external auditory canal fracture.³ Most cases of posttraumatic sensorineural hearing loss have no associated imaging findings.³ Other complications of temporal bone fractures include dizziness and balance dysfunction, CSF leak, venous sinus thrombosis, and perilymphatic fistula.^{1,3}

Pearls

- ◆ Imaging findings on head CT suggestive of temporal bone fracture include opacification of the external auditory canal, middle ear cavity and mastoid air cells, pneumocephalus adjacent to the temporal bone, air–fluid level in the sphenoid sinus, and air in the glenoid fossa of the temporomandibular joint.¹ Dedicated CT scan of the temporal bone should be obtained in these cases.¹
- ◆ Identifying injury to the critical structures of the temporal bone is more important in determining patient outcome and directing management than is classifying fractures into a general category.^{1,3}

Pitfall

- ◆ Knowledge of the complex anatomy of the temporal bone is required to avoid confusing normal fissures and canals with true fracture.³

References

1. Zayas JO, Feliciano YZ, Hadley CR, Gomez AA, Vidal JA. Temporal bone trauma and the role of multidetector CT in the emergency department. *Radiographics* 2011;31:1741–1755 [PubMed](#)
2. Phillips GS, LoGerfo SE, Richardson ML, Anzai Y. Interactive Web-based learning module on CT of the temporal bone: anatomy and pathology. *Radiographics* 2012;32:E85–E105 [PubMed](#)
3. Collins JM, Krishnamoorthy AK, Kubal WS, Johnson MH, Poon CS. Multidetector CT of temporal bone fractures. *Semin Ultrasound CT MR* 2012;33:418–431 [PubMed](#)

Case 62

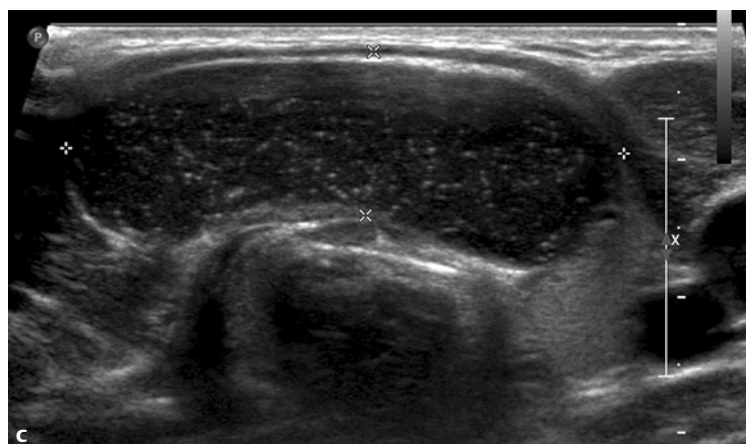
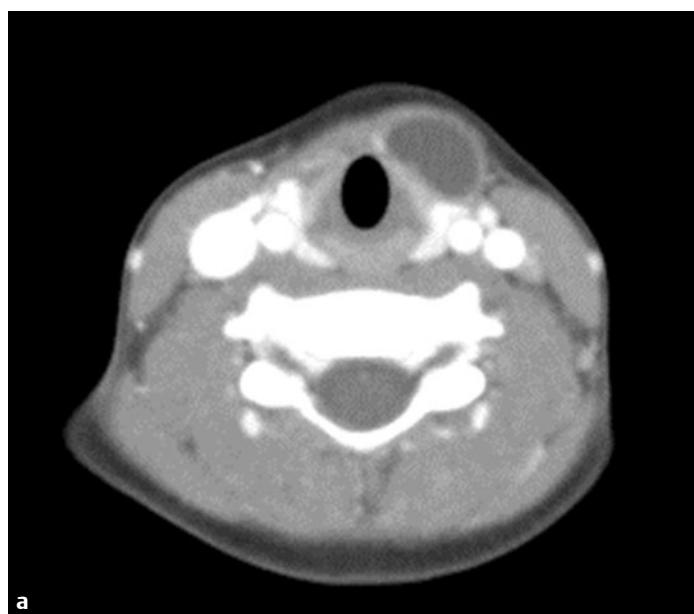
■ Clinical Presentation

An afebrile 7-year-old with anterior neck mass.

■ Radiographic Studies

Postcontrast axial and sagittal reformatted CT images (**Fig. 62.1a,b**) show an oval low attenuation rim-enhancing lesion anterior to the left lobe of the thyroid. Ultrasound image in

another patient with anterior neck mass (**Fig. 62.1c**) shows a well-demarcated oval lesion anterior to the trachea and abutting the left lobe of the thyroid with moderate internal echoes.



■ Diagnosis

Thyroglossal Duct Cyst

■ Discussion and Differential Diagnosis

Thyroglossal duct cysts account for 70% of all congenital neck masses. The usual presentation is a mass in the anterior midline neck that moves with swallowing or tongue protrusion.¹ The cysts commonly become symptomatic with inflammation and infection during childhood. During development, the thyroid primordium forms an epithelial-lined duct in the midline from the foramen cecum to the lower neck through which the thyroid gland descends to reach its final destination anterior to the trachea. Migration can be arrested anywhere along the duct, resulting in ectopic thyroid tissue. Failure of secretory epithelium involution results in cyst formation.² A majority of thyroglossal duct cysts are at or below the level of the hyoid bone; the remainder (20–25%) occur above the hyoid bone.²

Ultrasound is frequently performed first in the evaluation of neck masses in children. If a cystic mass is seen in the midline below the level of the hyoid bone, the diagnosis of a thyroglossal duct cyst is fairly certain. However, the classic simple cystic appearance is seen in fewer than 42% of cases. Thyroglossal duct cysts may appear homogeneously hypoechoic or heterogeneous (with fine to coarse internal echoes) even if there is no evidence of superimposed infection.¹ The location of the

thyroid gland should be assessed when evaluating a patient with a possible thyroglossal duct cyst. Ectopic thyroid tissue can be present along the duct rather than in the normal position. This most commonly occurs at the base of the tongue (lingual thyroid) and can be inadvertently removed at surgery. CT and MRI may also be useful. CT shows a fluid-attenuation midline mass that is usually unilocular; septations and rim enhancement may be seen. MRI shows a fluid-signal cyst that may be heterogeneous in signal intensity in the setting of infection or hemorrhage. Thyroglossal duct cyst may be an incidental finding, as is the case in this 1-month-old with torticollis (**Fig. 62.1d**). Sagittal T2-weighted MRI shows an oval high-signal thyroglossal duct cyst in the base of the tongue.

The Sistrunk procedure is the preferred surgical treatment of thyroglossal duct cysts. It entails excision of the cyst, the entire tract, and the central portion of the hyoid bone.² Fewer than 1% of these cysts may harbor thyroid carcinoma (mostly papillary carcinoma that presents in adulthood).¹ Differential diagnosis of a midline cystic neck mass in a child includes dermoid cyst and liquefied submental or anterior cervical lymph node.

Pearl

- ◆ Most thyroglossal duct cysts are cystic lesions in the midline of the anterior neck near the hyoid bone.

Pitfalls

- ◆ Do not mistake internal echoes in the cyst for a solid mass with ultrasound. Look for increased through-transmission deep to the lesion.
- ◆ The presence of thick walls and internal echoes does not always imply infection.

References

1. Koeller KK, Alamo L, Adair CF, Smirniotopoulos JG. Congenital cystic masses of the neck: radiologic-pathologic correlation. *Radiographics* 1999;19:121–146, quiz 152–153 [PubMed](#)
2. Koch BL. Cystic malformations of the neck in children. *Pediatr Radiol* 2005; 35:463–477 [PubMed](#)

IV

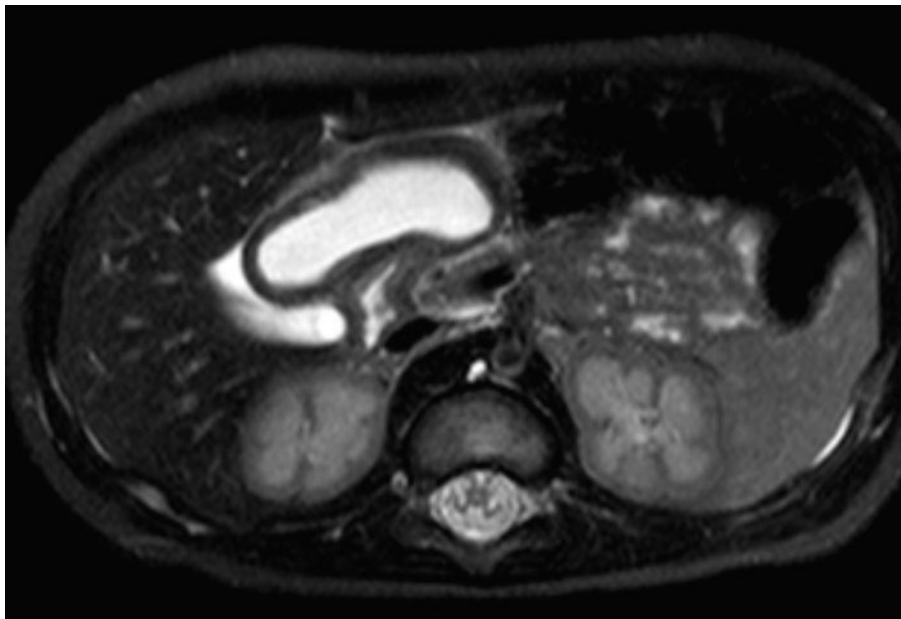
Gastrointestinal

Section Editors

Joanna J. Seibert and S. Bruce Greenberg

Authors

Scott A. Lile and Ananth Ravi



Case 63

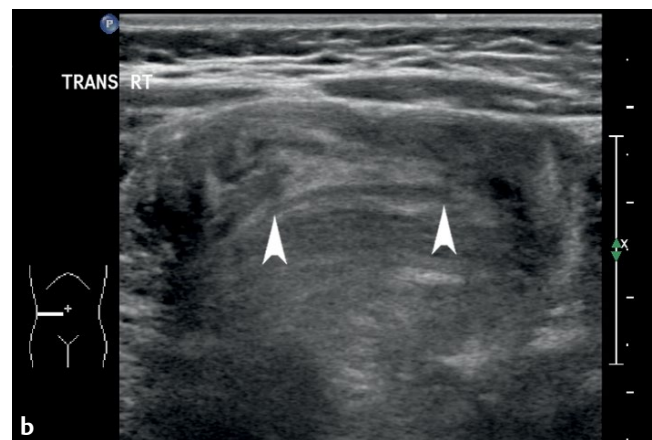
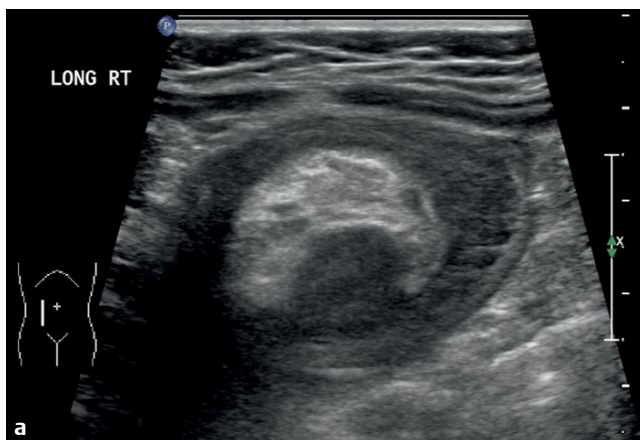
Clinical Presentation

An 11-month-old brought to the emergency department with irritability, vomiting, and mottled skin.

Radiographic Studies

Right abdomen ultrasound image (**Fig. 63.1a**) reveals a rounded mass with a hypoechoic outer layer and a crescent of central echogenicity (“crescent-in-donut” sign). Tangential ultrasound image (**Fig. 63.1b**) shows a linear lumen (*arrowheads*) within this thickened bowel lesion. Fluoroscopic air

enema (**Fig. 63.1c**) shows an oval obstructing intraluminal mass (*arrow*) within the cecum. Subsequent fluoroscopic image (**Fig. 63.1d**) shows reduction of the mass and air reflux into the small bowel (*arrowhead*).



■ Diagnosis

Intussusception



■ Discussion and Differential Diagnosis

Intussusception is the most common intestinal obstruction in the first 2 years of life and a common abdominal emergency in infants and children.¹ Early diagnosis and treatment are important in preventing bowel ischemia and perforation. Although intussusception can occur at any age, most cases present in infants between the ages of 5 and 9 months, with an incidence of 56/100,000 children/year.² The four classic symptoms—abdominal pain, vomiting, abdominal mass, and blood in the stool—are present in fewer than half of patients.¹ Most intussusceptions are ileocolic (93%) and are found in the transverse colon or hepatic flexure (88%). The majority of cases are classified as “idiopathic” because no lead point is identified, but an association with recent viral infection, especially adenovirus, has been identified.² A lead point is identified in 5% of patients with intussusception and may require further management.³ Lead points are more common in neonates (< 30 days) and in older children (> 5 years old).^{4,5} Possible lead points include polyps, Meckel diverticulum, gastrointestinal duplication, and Schönlein-Henoch purpura.

Conventional radiography sensitivity is only 45%. The best conventional radiography signs are the presence of a soft tissue mass within the colon and absence of gas within the ascending colon.² Ultrasound has become the primary diagnostic imaging modality with excellent sensitivity (98–100%) and specificity (88–100%).² The ultrasound appearance of intussusception in the transverse view shows alternating concentric hypoechoic and echogenic layers referred to as “target sign” or “donut sign.”⁵ At the intussusceptum base, the amount of enclosed mesentery is maximal, resulting in an outer hypoechoic ring with a hyperechoic crescentic center (“crescent-

in-donut sign”).⁶ In the longitudinal view a bowel-within-bowel appearance of the intussusception is seen; if the intussusception is curved or imaged obliquely, a “pseudokidney” sign may result.⁵ In addition to demonstrating the intussusception, ultrasound quantitates peritoneal fluid, identifies underlying lead points, or suggests alternate diagnoses.

Air reduction of intussusception is currently the preferred therapeutic reduction option in North America. Air reduction enables continuous monitoring of intracolonic pressure by the use of a blood pressure valve. The procedure is cleaner and faster than fluoroscopic-guided liquid contrast enemas and entails less radiation exposure. Perforation is a less serious complication. When liquid contrast agents are used, water-soluble contrast is preferred over barium. Successful reduction occurs in 74% with either contrast agent.² More recently, reduction has been performed using ultrasound guidance and liquid media (tap water, normal saline, or Ringer lactate) to provide hydrostatic pressure. Reduction rates with sonographic guidance are similar to the more traditional methods, and radiation exposure is avoided.⁷ Reduction rates are lower in cases of ileoileal or ileoileocolic intussusception, rectal bleeding, long duration (> 2 days), small bowel obstruction (35% reduced), and age younger than 6 months. Lack of detectable color flow bowel vascularity may indicate vascular compromise and correlates with unsuccessful enema reduction.⁵ Neither sedation nor medications increase the success rate. Delayed attempts after reduction failure have proved helpful, but are not indicated if the patient is unstable or the initial attempt did not produce a partial reduction. The perforation rate is 0.8%.² A recurrence rate of 10% generally occurs within 48 hours.⁸

Pearls

- ◆ Absolute contraindications to any enema include shock, peritonitis, and free air.
- ◆ Lead points are more difficult to identify with air than with positive contrast. In suspicious cases, water-soluble contrast may be helpful.

Pitfalls

- ◆ Spontaneous reductions may occur after failed enema reduction.
- ◆ Infectious/inflammatory bowel thickening may produce a “target” appearance similar to intussusception.⁵

■ Controversy

- Use of sonography in intussusception reduction has been widely recognized in Europe and Asia for over 3 decades;

98% of pediatric radiologists in North America still prefer fluoroscopic-guided reduction.⁷

References

1. Mendez D, Caviness AC, Ma L, Macias CC. The diagnostic accuracy of an abdominal radiograph with signs and symptoms of intussusception. *Am J Emerg Med* 2012;30:426–431 [PubMed](#)
2. Applegate KE. Intussusception in children: evidence-based diagnosis and treatment. *Pediatr Radiol* 2009;39(Suppl 2):S140–S143 [PubMed](#)
3. Ko HS, Schenk JP, Tröger J, Rohrschneider WK. Current radiological management of intussusception in children. *Eur Radiol* 2007;17:2411–2421 [PubMed](#)
4. Takeuchi M, Osamura T, Yasunaga H, Horiguchi H, Hashimoto H, Matsuda S. Intussusception among Japanese children: an epidemiologic study using an administrative database. *BMC Pediatr* 2012;12:36 [PubMed](#)

5. Cogley JR, O'Connor SC, Houshyar R, Al Dulaimy K. Emergent pediatric US: what every radiologist should know. *Radiographics* 2012;32:651–665. [PubMed](#)
6. del-Pozo G, Albillos JC, Tejedor D, et al. Intussusception in children: current concepts in diagnosis and enema reduction. *Radiographics* 1999;19:299–319. [PubMed](#)
7. Sanchez TR, Potnick A, Graf JL, Abramson LP, Patel CV. Sonographically guided enema for intussusception reduction: a safer alternative to fluoroscopy. *J Ultrasound Med* 2012;31:1505–1508. [PubMed](#)
8. Bajaj L, Roback MG. Postreduction management of intussusception in a children's hospital emergency department. *Pediatrics* 2003;112(6 Pt 1):1302–1307. [PubMed](#)

Case 64

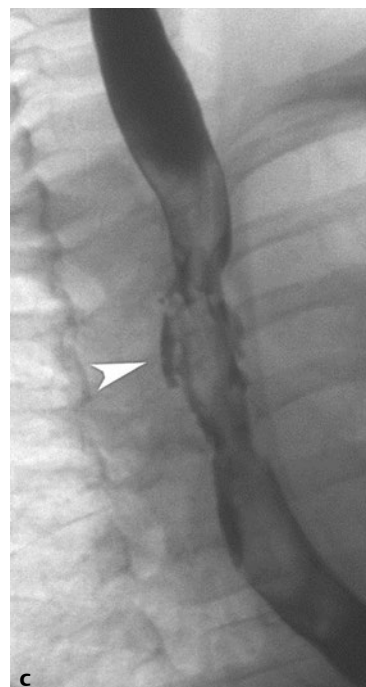
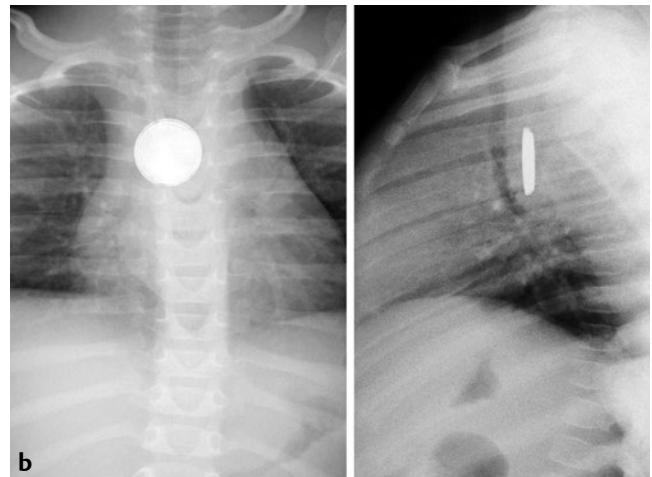
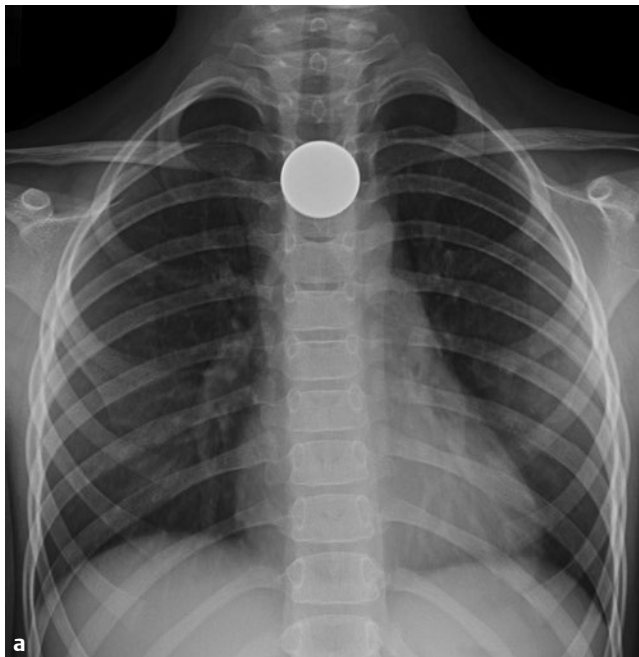
■ Clinical Presentation

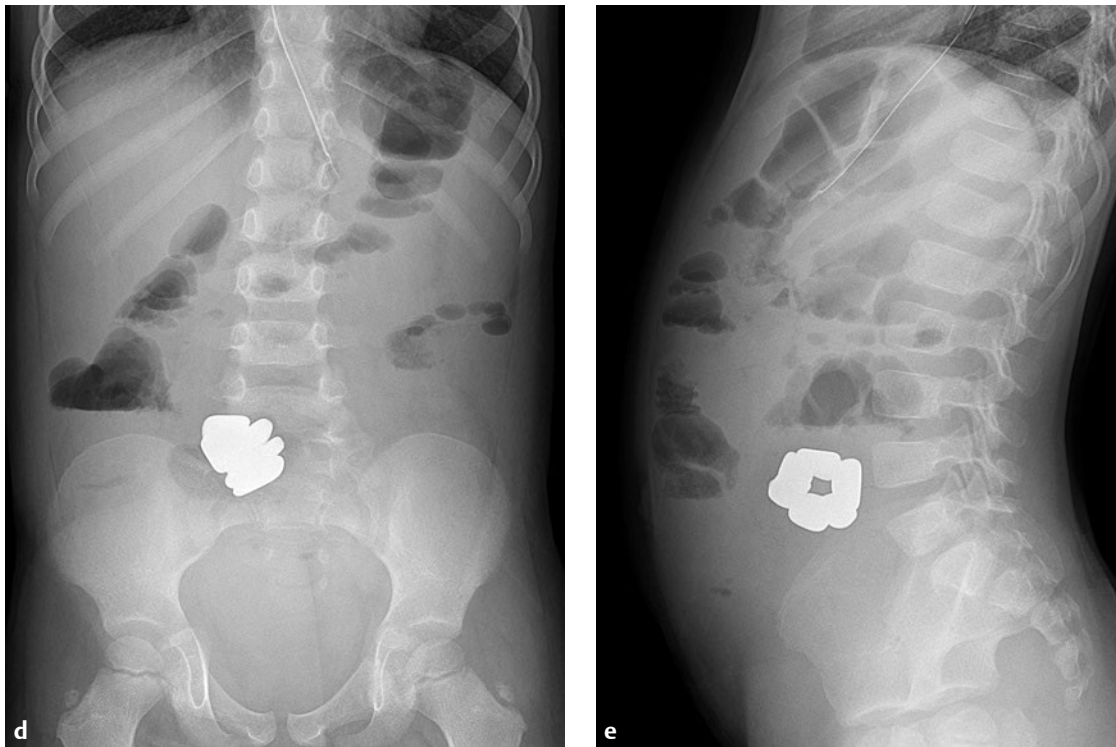
A 3-year-old with a history of ingested foreign body.

■ Radiographic Studies

Chest radiograph (**Fig. 64.1a**) shows a swallowed coin in the upper thoracic esophagus at the aortic arch level. The coin was removed by endoscopy. AP/lateral chest radiographs (**Fig. 64.1b**) in another 16-month-old infant with fever and dysphagia for 1 week demonstrate a circular density with a beveled

edge in the midthoracic esophagus. Note the swelling between the esophageal foreign body and the adjacent trachea. Esophagram with water-soluble contrast (**Fig. 64.1c**) performed after endoscopic disk battery removal shows contrast extravasation (*arrowhead*) secondary to esophageal erosion and perforation.





■ Diagnosis

Foreign Body Ingestion

■ Discussion and Differential Diagnosis

Swallowed foreign bodies, particularly coins and smooth blunt objects, are common in children. The common locations for esophageal foreign body are at the cervicothoracic junction, aortic arch, left main stem bronchus, and gastroesophageal junction. Esophageal foreign body ingestion symptoms include pain, gagging, poor feeding, cough, drooling, and respiratory symptoms. Initial radiographic evaluation should include radiographs of the neck, chest, and abdomen because the location and number of radiopaque foreign bodies need to be determined. Coins in the esophagus are viewed en face on frontal radiographs. The lateral radiograph helps delineate multiple overlapping coins and faintly radiopaque objects like bones and aluminum. Disk batteries usually demonstrate a characteristic double rim or halo effect on the AP radiograph and characteristic step-off on the lateral view. Fluoroscopic contrast studies may be necessary if a nonradiopaque foreign body such as food is present or if an underlying stricture is suspected. Non-ionic water-soluble contrast should be used if perforation is suspected. CT examination is helpful if a gastric or intestinal bezoar is suspected.¹

Initially, watchful waiting with repeat radiographs can be performed for many foreign bodies such as coins to see if they will pass into the stomach. Most foreign bodies at the time of clinical presentation are found beyond the esophagus, and a majority of them are passed per rectum without intervention. Endoscopic retrieval of foreign bodies within the esophagus is

the treatment of choice if the foreign body fails to advance.² Prompt removal of sharp foreign bodies is recommended by some authorities.³

Disk batteries in the esophagus need to be removed immediately, with expectant management once they pass into the stomach.⁴ Known complications from disk battery ingestion include esophageal perforation, tracheoesophageal fistula, aorto-esophageal fistula, mediastinitis, and stricture formation.⁵ Generation of hydroxide at the battery anode is the most important reason for battery-induced tissue irritation and necrosis. Lithium-containing batteries have higher capacitance and voltage, and produce more current and hydroxide; hence, the potential for damage with these batteries is greater than with other batteries. The 20-mm lithium cells, which are especially dangerous given their size, can be identified by their imprint codes (e.g., CR2032).⁵

Known complications from multiple magnet ingestion include intestinal necrosis, perforation, intussusception, obstruction, fistula, and volvulus. Magnets attract each other across adjacent bowel loops leading to tissue necrosis and perforation. AP and lateral radiographs are recommended for magnet ingestion, to evaluate the presence of multiple overlapping magnets, distended loops, air-fluid levels, and free air.⁶ Abdominal radiographs in a 4-year-old boy (Fig. 64.1d,e) show multiple adjacent magnets and associated small bowel air-fluid levels; this patient developed an ileal-ileal fistula requiring surgical repair.

Pearls

- ◆ Gastrointestinal foreign bodies with atypical alignment or stuck at unexpected locations should raise suspicion for an underlying abnormality (stricture, web, vascular ring, cartilaginous rings).
- ◆ Tooth picks and bones are the most common sharp objects that require retrieval. Prolonged presence of these objects can lead to intestinal perforation.⁷
- ◆ Narrowing of the trachea adjacent to an esophageal foreign body indicates that the foreign body has been there for some time.

Pitfall

- ◆ Be sure the density you see is a foreign body inside the patient. Electrocardiogram (ECG) leads, snaps, and batteries in pockets can simulate ingested foreign body.

References

1. Ripollés T, García-Aguayo J, Martínez MJ, Gil P. Gastrointestinal bezoars: sonographic and CT characteristics. *AJR Am J Roentgenol* 2001;177:65–69. [PubMed](#)
2. Smith MT, Wong RK. Esophageal foreign bodies: types and techniques for removal. *Curr Treat Options Gastroenterol* 2006;9:75–84. [PubMed](#)
3. Chen MK, Beierle EA. Gastrointestinal foreign bodies. *Pediatr Ann* 2001;30:736–742. [PubMed](#)
4. Kost KM, Shapiro RS. Button battery ingestion: a case report and review of the literature. *J Otolaryngol* 1987;16:252–257. [PubMed](#)
5. Litovitz T, Whitaker N, Clark L. Preventing battery ingestions: an analysis of 8648 cases. *Pediatrics* 2010;125:1178–1183. [PubMed](#)
6. Oestreich AE. Worldwide survey of damage from swallowing multiple magnets. *Pediatr Radiol* 2009;39:142–147. [PubMed](#)
7. Lelli JL Jr. Foreign bodies. In: Holcomb GW III, Murphy JP, eds. *Ashcraft's Pediatric Surgery*, 5th ed. Philadelphia: WB Saunders; 2010:135–143

Case 65

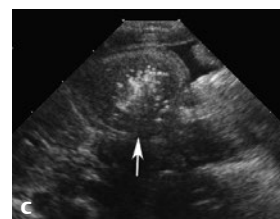
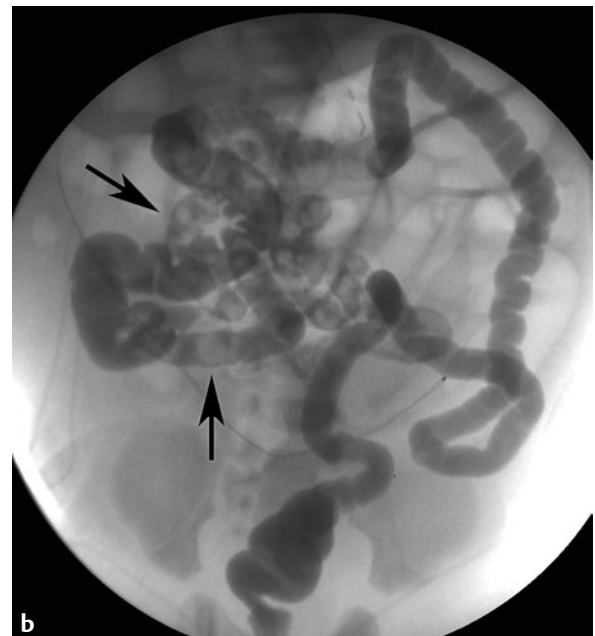
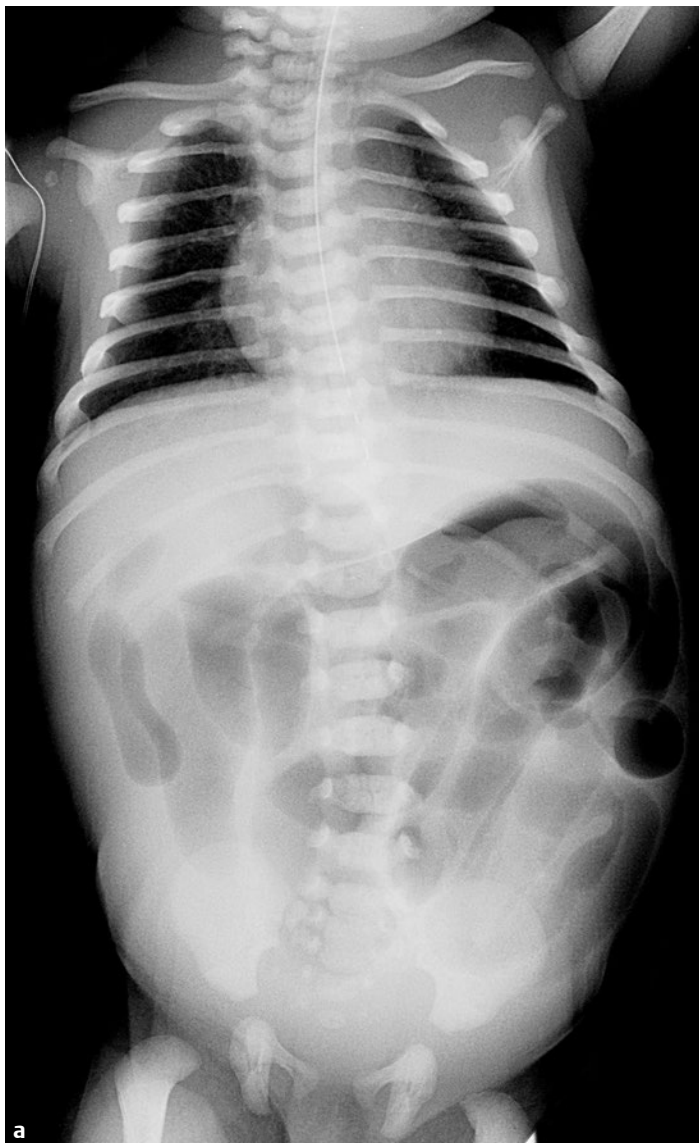
■ Clinical presentation

A newborn with abdominal distention.

■ Radiographic Studies

Radiograph of the chest/abdomen (**Fig. 65.1a**) shows multiple distended bowel loops throughout the abdomen in a pattern suggesting distal bowel obstruction. Contrast enema (**Fig. 65.1b**) reveals a microcolon with relatively normal rectal caliber. Reflux of contrast into the distal ileum shows multiple

filling defects (**Fig. 65.1b, arrows**). Transverse and longitudinal ultrasound images in the same patient (**Fig. 65.1c,d**) show a dilated bowel loop filled with thick echogenic intraluminal material (**arrows**). An adjacent normal fluid-filled bowel loop (**Fig. 65.1d, asterisk**) provides comparison.



■ Diagnosis

Meconium Ileus

■ Discussion and Differential Diagnosis

Meconium ileus is the cause of 10 to 25% of cases of bowel obstruction in newborns and is secondary to cystic fibrosis in most instances. Meconium ileus occurs in up to 20% of children with cystic fibrosis, and there may be a family history.^{1,2} Bowel obstruction results from abnormally viscous meconium in the distal ileal lumen. About half of cases are uncomplicated obstruction. The remaining patients have complications such as meconium peritonitis (with or without cyst formation), volvulus, atresia, and intestinal gangrene.²

Meconium ileus is the most common cause of neonatal bowel obstruction that presents at birth as abdominal distention. Abdominal radiographs may show a frothy or ground-glass appearance within a distended bowel, with absence of air–fluid levels. The differential diagnosis includes Hirschsprung's disease, ileal atresia/stenosis, meconium plug syndrome, and small left colon syndrome. The most common differential is between meconium ileus and ileal atresia. Both conditions present as bowel obstruction and reveal a microcolon on contrast enema. Ileal atresia is associated with air–fluid levels. Ultrasound may be helpful in demonstrating dilated

bowel loops filled with thick echogenic material in meconium ileus. In ileal atresia, the dilated loops at ultrasound are filled with air and fluid.

Contrast enema shows an unused small-caliber microcolon. Contrast refluxed in the distal ileum outlines inspissated meconium intraluminal filling defects. A therapeutic enema may be performed in uncomplicated cases using slightly hypertonic water-soluble contrast. The goal is to reflux contrast under fluoroscopy into the ileum to outline meconium and fill dilated small bowel loops. The slightly hypertonic contrast loosens the meconium, aiding subsequent passage. Relief of obstruction is obtained in 24 to 48 hours in 36 to 39% of cases.² Serial radiographs and repeat enemas may be necessary. Perforation rate from enemas is reported to be in the range of 5 to 11%.³

Meconium ileus equivalent or distal intestinal obstruction syndrome occurs in older children with cystic fibrosis who develop intestinal obstruction secondary to inspissation of bowel contents in the distal ileum.

Pearl

- ◆ Multiple enemas over several days may be required for complete treatment.

Pitfall

- ◆ Use diluted water-soluble contrast to avoid hypertonic dehydration; ensure that the patient is kept well hydrated after the therapeutic enema.

References

1. Munck A, Gérardin M, Alberti C, et al. Clinical outcome of cystic fibrosis presenting with or without meconium ileus: a matched cohort study. *J Pediatr Surg* 2006;41:1556–1560 [PubMed](#)
2. Carlyle BE, Borowitz DS, Glick PL. A review of pathophysiology and management of fetuses and neonates with meconium ileus for the pediatric surgeon. *J Pediatr Surg* 2012;47:772–781 [PubMed](#)
3. Rescorla FJ, Grosfeld JL. Contemporary management of meconium ileus. *World J Surg* 1993;17:318–325 [PubMed](#)

Case 66

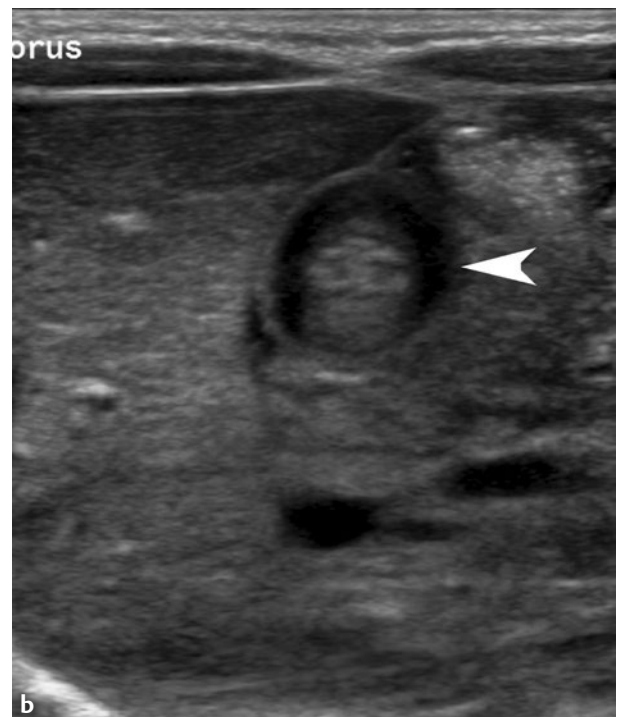
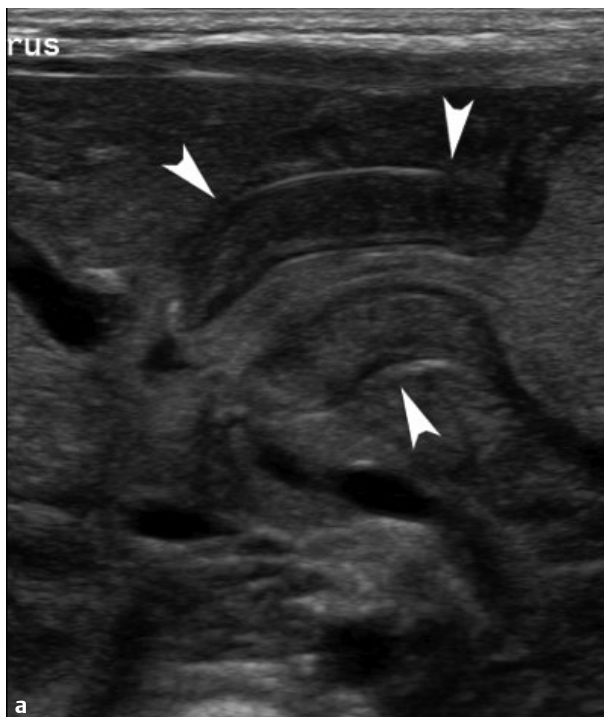
■ Clinical Presentation

A 1-month-old boy presents with projectile vomiting.

■ Radiographic Studies

Longitudinal ultrasound image of the pylorus (**Fig. 66.1a**) shows significant pyloric muscle thickening (*arrowheads*), which measured 5 mm, and pyloric channel elongation. No gastric contents were visualized to empty through the pylorus during

this ultrasound exam. Transverse ultrasound image (**Fig. 66.1b**) confirms hypoechoic pyloric muscle thickening (*arrowhead*) surrounding redundant echogenic mucosa.



■ Diagnosis

Pyloric Stenosis



■ Discussion and Differential Diagnosis

Pyloric stenosis is narrowing of the pyloric canal caused by pyloric muscle hypertrophy. Infants present with intermittent nonbilious vomiting that increases in frequency as the pyloric muscle thickening progresses. Persistent vomiting may lead to weight loss, dehydration, and electrolyte disturbances.¹ Infants typically present between 3 and 12 weeks of age with a peak incidence at 4 weeks. Pyloric stenosis is more common in boys than in girls.² The classic physical examination finding is a small palpable mass in the epigastrium that is caused by the hypertrophied muscle known as the olive.

Diagnostic imaging is based on ultrasound visualization of pyloric muscle thickening, which delays emptying of gastric contents.¹ Pyloric muscle thickening has a hypoechoic “target”

or “doughnut” appearance on transverse images. Pyloric muscle wall thickening > 3 mm is diagnostic of pyloric stenosis and the most important measurement criteria.³ The measurement of a pyloric channel elongation > 12 mm is less reliable. Use of gravity-aided patient positions may eliminate the need for additional oral fluid administration; absent or minimal opening of the pylorus is seen during real-time observation.¹ On fluoroscopic upper gastrointestinal (GI) examination, delayed gastric emptying, elongation of the pyloric channel, and mass effect are seen. The differential diagnosis includes pyloric spasm, which can cause delayed gastric emptying and pyloric channel elongation.

Pearls

- ◆ Ultrasound imaging is the primary diagnostic tool and may precede “olive” mass palpation on physical exam.
- ◆ Borderline measurements in preterm neonates favor the diagnosis of pyloric stenosis.

Pitfall

- ◆ Gastric distention may cause posterior displacement of the pylorus and lead to a false-negative result.³

References

1. Hernanz-Schulman M. Infantile hypertrophic pyloric stenosis. *Radiology* 2003;227:319–331 [PubMed](#)
2. Cogley JR, O'Connor SC, Houshyar R, Al Dulaimy K. Emergent pediatric US: what every radiologist should know. *Radiographics* 2012;32:651–665. [PubMed](#)
3. Costa Dias S, Swinson S, Torrão H, et al. Hypertrophic pyloric stenosis: tips and tricks for ultrasound diagnosis. *Insights Imaging* 2012;3:247–250. [PubMed](#)

Case 67

■ Clinical Presentation

A 2-day-old infant with vomiting and abdominal distention.

■ Radiographic Studies

Frontal radiograph (**Fig. 67.1a**) demonstrates multiple dilated bowel loops with no rectal gas. Lateral radiograph (**Fig. 67.1b**) demonstrates multiple air–fluid levels. Contrast enema (**Fig.**

67.1c) demonstrates microcolon beyond the air distended bowel loops.



■ Diagnosis

Small Bowel Atresia

■ Discussion and Differential Diagnosis

Small bowel atresias are fairly evenly distributed in bowel between the ligament of Treitz and the ileocecal junction.¹ In some cases the diagnosis may be made on prenatal ultrasound with detection of dilated bowel loops, polyhydramnios, or meconium peritonitis. However, in most instances the diagnosis is not made prenatally. Most patients present in the first few days of life with bilious emesis. On plain radiographs, patients with jejunal atresia have only a few air-distended proximal small bowel loops with air-fluid levels. Ileal atresia usually presents with a greater number of air-distended bowel loops and air-fluid levels. The most dilated loop is usually just proximal to the site of atresia.² In addition to distended bowel loops, plain radiographs may show calcification in cases with associated meconium peritonitis, indicating intrauterine bowel perforation and probably atresia at that site. Contrast enema shows a microcolon in cases of distal jejunal atresias, ileal atresia, and multiple small bowel atresias. Normal-caliber colon on contrast enema may be seen in proximal jejunal atresia. Upper GI exam is useful in patients with bilious emesis to rule out malrotation/volvulus if a small bowel atresia is not

obvious on contrast enema or abnormal cecum location is found. Treatment of small bowel atresia is surgical with favorable prognosis expected in most cases.³

The cause of intestinal atresia distal to the duodenum is thought to relate to vascular occlusion. Possible mechanisms include vascular emboli, vascular compression (volvulus or herniation through an abdominal wall defect), or vascular resorption. Bowel atresia classification includes intraluminal diaphragm, cord-like segment separating blind loops, mesenteric defect with complete separation of blind loops, large mesenteric defect, or multiple atresias.⁴

A gas pattern similar to that with ileal atresia can be seen in meconium ileus, meconium plug syndrome, small left colon syndrome, colonic atresia, and total colonic aganglionosis. Patients with meconium ileus usually demonstrate a ground-glass appearance secondary to inspissated meconium; air-fluid levels may be absent.⁵ Contrast enema in meconium ileus shows a microcolon. If reflux into distal small bowel is possible, there will be intraluminal filling defects. Colonic atresia may have one large dilated bowel loop proximal to the microcolon.

Pearls

- ◆ High jejunal atresia may have normal passage of meconium.^{1,2}
- ◆ Multiple bowel atresias may be familial.⁶
- ◆ Ileal atresia is more likely to be single, whereas jejunal atresias are more likely to be multiple.⁷
- ◆ Meconium peritonitis is almost always related to ileal atresia and uncommon in jejunal atresia.⁷

Pitfalls

- ◆ Radiographs of a normal neonate in the first few hours of life may show air filling of small bowel loops and paucity of colonic gas simulating small bowel atresia.
- ◆ Long-standing cases of ileal atresia with fluid-filled distal bowel may have only a few air-fluid levels and look like jejunal atresia.²

References

1. Touloukian RJ. Diagnosis and treatment of jejunoileal atresia. *World J Surg* 1993;17:310–317 [PubMed](#)
2. Carty H, Brereton RJ. The distended neonate. *Clin Radiol* 1983;34:367–380. [PubMed](#)
3. Dalla Vecchia LK, Grosfeld JL, West KW, Rescorla FJ, Scherer LR, Engum SA. Intestinal atresia and stenosis: a 25-year experience with 277 cases. *Arch Surg* 1998;133:490–496, discussion 496–497 [PubMed](#)
4. Grosfeld JL. Jejunoileal atresia and stenosis, section 3: the small intestine. In: Ravitch MM, Welch KJ, Benson CD, eds. *Pediatric Surgery*. Chicago: Year Book Medical; 1986:838
5. Berrocal T, Lamas M, Gutierrez J, Torres I, Prieto C, del Hoyo ML. Congenital anomalies of the small intestine, colon, and rectum. *Radiographics* 1999;19:1219–1236 [PubMed](#)
6. Cragan JD, Martin ML, Moore CA, Khoury MJ. Descriptive epidemiology of small intestinal atresia, Atlanta, Georgia. *Teratology* 1993;48:441–450. [PubMed](#)
7. Heij HA, Moorman-Voestermans CG, Vos A. Atresia of jejunum and ileum: is it the same disease? *J Pediatr Surg* 1990;25:635–637 [PubMed](#)

Case 68

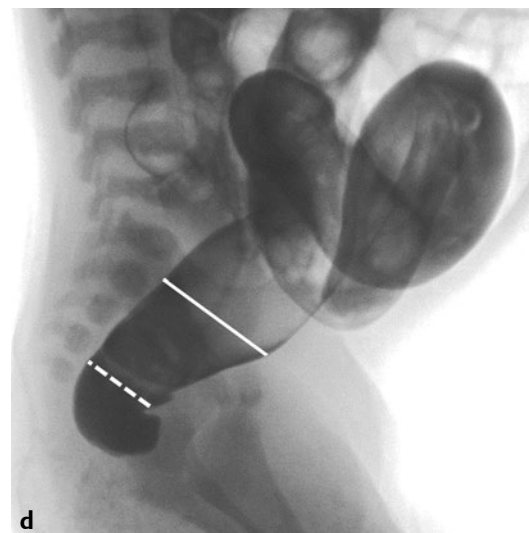
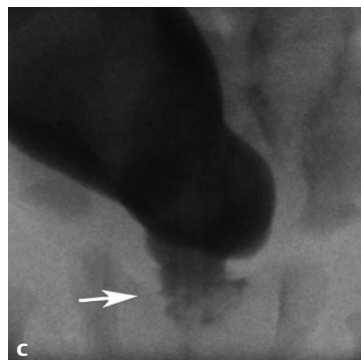
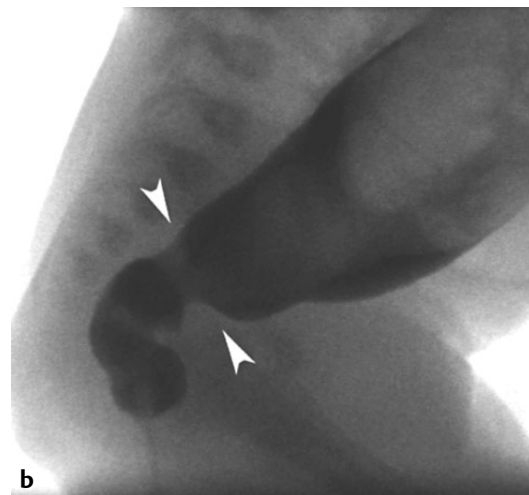
■ Clinical Presentation

A 22-day-old with abdominal distention and low stool output.

■ Radiographic Studies

Anteroposterior radiograph (**Fig. 68.1a**) shows bowel distention and moderate retained stool. Lateral fluoroscopic image (**Fig. 68.1b**) shows a rectal transition zone of caliber narrowing (*arrowheads*). AP fluoroscopic image (**Fig. 68.1c**) shows a sawtooth appearance (*arrow*) below the transition zone. Lat-

eral fluoroscopic image in another patient (**Fig. 68.1d**) shows the rectum (*lower dashed line*) to be smaller in caliber than the sigmoid colon (*upper line*), representing a reversed rectosigmoid ratio.



■ Diagnosis

Hirschsprung Disease

■ Discussion and Differential Diagnosis

Hirschsprung disease is a disorder of the distal GI tract characterized by the absence of ganglion cells in the myenteric plexus and submucosal plexus. Involved segments always include the internal anal sphincter and extend proximally for varying distances, rarely involving the entire intestinal tract.¹ More commonly, involvement is limited to the rectal, rectosigmoid, or sigmoid colon.² This disorder is thought to be the result of failure of migration of ganglion cells from the neural crest to the hindgut during weeks 5 to 12 of gestation.³ The aganglionic segment of colon demonstrates abnormal peristalsis, and acts as an obstruction to the passage of meconium or stool. Presenting signs and symptoms include failure to pass meconium in the first 24 to 48 hours of life, abdominal distention, bilious vomiting, and bowel obstruction. Complications of Hirschsprung disease include enterocolitis and bowel perforation.

Fluoroscopic contrast enema is the radiographic study of choice. The contrast enema helps distinguish other causes of distal bowel obstruction and guides suction biopsy in those with findings suspicious for Hirschsprung disease. Contrast

enema findings of Hirschsprung disease typically include a rectal diameter smaller than the sigmoid (reversed rectosigmoid ratio) and a transition zone of bowel narrowing; a saw-tooth appearance to the involved region (spasm) may be seen. The radiographic transition zone correlates well with the histological transition zone in short segment disease, but with long segment disease, the accuracy is diminished, and the contrast enema can underestimate the length of involved bowel.⁴ A shortened, question mark-shaped microcolon may be seen with total colonic involvement in Hirschsprung disease.

Confirmation of Hirschsprung disease is made by suction biopsy or rectal manometry. The differential diagnosis of Hirschsprung disease includes various causes of distal bowel obstruction, including small left colon syndrome, meconium ileus, colonic atresia, and ileal atresia. Treatment of Hirschsprung disease consists of surgical resection of the affected bowel segment. For short segment disease, a transanal pull-through can be performed; for longer segments of involvement, laparoscopic techniques or laparotomy must be performed.⁵

Pearls

- ◆ Hirschsprung disease is uncommon in premature infants and increased comorbidities may delay the diagnosis.⁶
- ◆ Hirschsprung disease is more common in patients with trisomy 21.

Pitfall

- ◆ With short-segment low rectal involvement, the colon can appear normal or nearly normal.

References

1. Reding R, de Ville de Goyet J, Gosseye S, et al. Hirschsprung's disease: a 20-year experience. *J Pediatr Surg* 1997;32:1221–1225. [PubMed](#)
2. Stranzinger E, DiPietro MA, Teitelbaum DH, Strouse PJ. Imaging of total colonic Hirschsprung disease. *Pediatr Radiol* 2008;38:1162–1170. [PubMed](#)
3. Kim HJ, Kim AY, Lee CW, et al. Hirschsprung disease and hypoganglionosis in adults: radiologic findings and differentiation. *Radiology* 2008;247:428–434. [PubMed](#)
4. Jamieson DH, Dundas SE, Belushi SA, Cooper M, Blair GK. Does the transition zone reliably delineate aganglionic bowel in Hirschsprung's disease? *Pediatr Radiol* 2004;34:811–815. [PubMed](#)
5. Teeraratkul S. Transanal one-stage endorectal pull-through for Hirschsprung's disease in infants and children. *J Pediatr Surg* 2003;38:184–187. [PubMed](#)
6. Baxter KJ, Bhatia AM. Hirschsprung's disease in the preterm infant: implications for diagnosis and outcome. *Am Surg* 2013;79:734–738. [PubMed](#)

Case 69

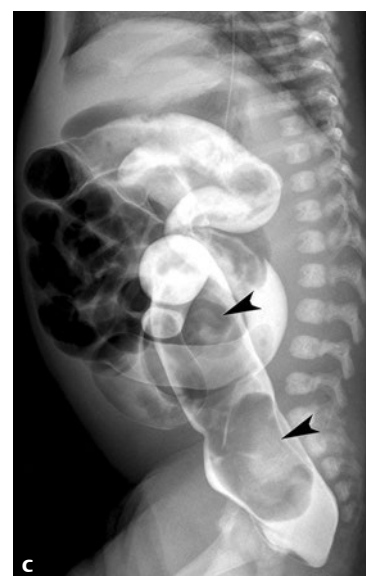
■ Clinical Presentation

A 1-day-old girl presents with vomiting, abdominal distention, and failure to pass meconium.

■ Radiographic Studies

Abdomen radiograph (**Fig. 69.1a**) demonstrates multiple distended bowel loops throughout the abdomen with paucity of gas in the rectum. AP and lateral contrast enema images (**Fig.**

69.1b,c) show large filling defects (*arrowheads*) within normal-caliber sigmoid colon and the rectum.



■ Diagnosis

Meconium Plug Syndrome

■ Discussion and Differential Diagnosis

Meconium plug syndrome is a relatively common cause of functional obstruction of the colon, occurring in 1 in 500 to 1 in 1,000 births.¹ The cause is functional immaturity and dysmotility of the colon with failure to pass meconium. An obstructive plug of thick and firm meconium forms that is often long.² Clinical presentation is a failure to pass normal amounts of meconium in the first days of life, abdominal distention, and vomiting (often bilious). Examination may reveal palpable tense bowel loops. The thick meconium will often pass following digital rectal stimulation.

Plain radiographs usually show dilated bowel with all loops of similar caliber; air–fluid levels and bubbly meconium may be present.³ Contrast enema is done to confirm the suspected diagnosis and is often therapeutic. Water-soluble contrast outlines a usually continuous or multiple meconium filling defects in a normal-caliber colon. Frequently, the stimulation of the enema will cause passage of a “plug” (up to 10 to 20 cm in length), and the symptoms will be relieved. Meconium plug syndrome is usually self-limited, but patients may have associated cystic fibrosis or Hirschsprung disease. The literature over the past 40 years has reported cystic fibrosis in as many

as 43% and Hirschsprung disease in as many as 38% of patients with meconium plug syndrome.⁴ A review found that when meconium plug syndrome was identified as small pellets in the colon, cystic fibrosis was rare and the incidence of Hirschsprung disease was around 13%.⁴

Small left colon syndrome is a similar condition, with retained meconium and decreased caliber of the splenic flexure and the distal colon (**Fig. 69.1d, arrowhead**). This condition is also associated with functional immaturity and dysmotility of the colon. Unlike patients with Hirschsprung disease, patients with meconium plug syndrome and small left colon syndrome have a normal-caliber rectum.

Other conditions relating to meconium plug syndrome include hypothyroidism, narcotic addiction, neuronal intestinal dysplasia, and maternal diabetes.² Serum thyroid-stimulating hormone (TSH) levels may be obtained to exclude hypothyroidism. If symptoms are not relieved within 24 to 48 hours after a contrast enema, a rectal biopsy may be considered to rule out Hirschsprung disease. Patients with meconium plug are usually tested for cystic fibrosis.⁵

Pearl

- ◆ Meconium plug syndrome may be secondary to hypermagnesemia caused by maternal treatment with magnesium sulfate for eclampsia.

Pitfall

- ◆ Air–fluid levels may develop and bowel perforation may occur after failure to diagnose and treat meconium plug syndrome.³

References

1. Hen J Jr, Dolan TF Jr, Touloukian RJ. Meconium plug syndrome associated with cystic fibrosis and Hirschsprung's disease. *Pediatrics* 1980;66:466–468 [PubMed](#)
2. Caty MG, Escobar MA. Meconium disease. In: Holcomb GW III, Murphy JP, eds. *Ashcraft's Pediatric Surgery*, 5th ed. Philadelphia: WB Saunders; 2010:425–438
3. Hussain SM, Meradji M, Robben SG, Hop WC. Plain film diagnosis in meconium plug syndrome, meconium ileus and neonatal Hirschsprung's disease. A scoring system. *Pediatr Radiol* 1991;21:556–559 [PubMed](#)
4. Keckler SJ, St Peter SD, Spilde TL, et al. Current significance of meconium plug syndrome. *J Pediatr Surg* 2008;43:896–898 [PubMed](#)
5. Messina M, Molinaro F. Meconium plug syndrome. In: Buonocore G, Bracci R, Weindling M, eds. *Neonatology*. New York: Springer; 2012:704–707

Case 70

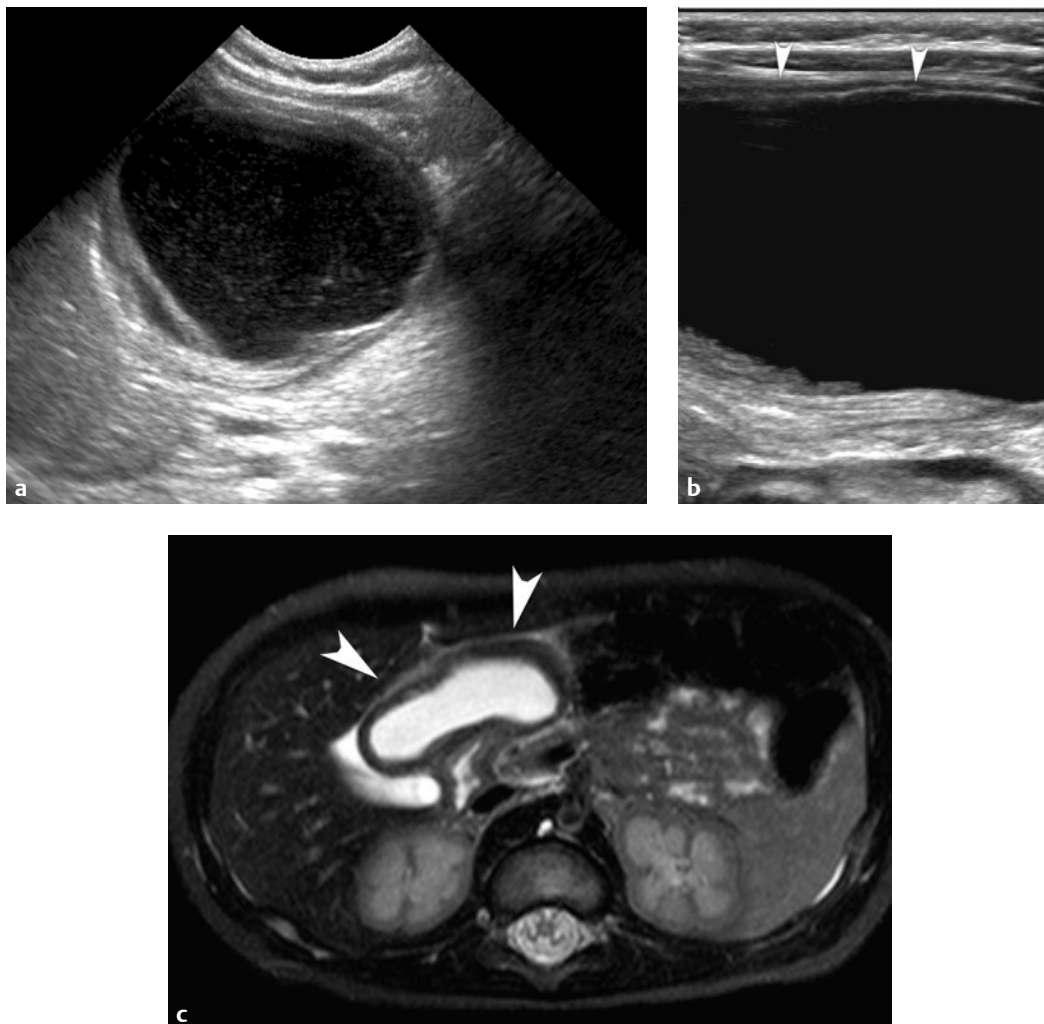
■ Clinical Presentation

A 1-year-old boy presents with abdominal pain and emesis.

■ Radiographic Studies

Ultrasound exam (**Fig. 70.1a**) shows a cystic lesion in the upper abdomen with internal echogenic debris. Linear transducer image (**Fig. 70.1b**) shows better detail of the thickened cyst wall with internal echogenic lining (*arrowheads*). T2-

weighted MRI (**Fig. 70.1c**) demonstrates an oval, high-signal, cystic lesion with mass effect at the gastric outlet. Thickened bowel lining of the cyst is seen (*arrowheads*).



■ Diagnosis

Duplication Cyst

■ Discussion and Differential Diagnosis

Duplication cysts of the gastrointestinal tract can occur anywhere from the base of the tongue to the anus. The ileum is the most frequent location.¹ These developmental cysts are rare, and clinical diagnosis may be difficult. Common presentations by location include the following:

1. Esophagus (respiratory distress or dysphagia)
2. Stomach (vomiting or bleeding)
3. Small bowel (bleeding, obstruction, or intussusception)

Duplication cysts may be round, oval, or tubular cystic lesions on imaging, often with complicated internal fluid.² Ultrasound demonstrates a “gut signature” with the cyst wall containing an internal echogenic mucosal lining and an adjacent hypoechoic muscle layer.³ Esophageal duplications can present as a posterior mediastinal mass and can be associated with vertebral anomalies in patients with neuroenteric cysts.⁴

Gastric duplications can have a mass effect on the stomach. Fluoroscopic contrast examinations show mass effect on adjacent bowel and may show contrast communication with the gut, especially with tubular lesions.⁵ Small-bowel duplications may contain pancreatic and gastric tissue; nuclear medicine pertechnetate scans can detect gastric mucosa. In many GI tract locations, CT and MRI are required to fully characterize duplications.

Differential diagnosis of esophageal duplications includes other mediastinal masses. Differential diagnosis of duplication cysts below the diaphragm includes other cystic masses such as mesenteric cyst, macrocystic lymphatic malformation, Meckel's diverticulum, ovarian cyst, anterior meningocele, and cystic sacrococcygeal teratoma. In contradistinction to Meckel's diverticulum, small bowel duplications are located on the mesenteric border.⁴

Pearls

- ◆ Duplication cysts can be multiple.⁴
- ◆ Colonic duplications are associated with genitourinary and vertebral anomalies.⁴

Pitfall

- ◆ Gastric mucosa in duplication cysts can cause a false-positive Meckel's scan.

References

1. Tong SC, Pitman M, Anupindi SA. Best cases from the AFIP. Ileocecal enteric duplication cyst: radiologic-pathologic correlation. *Radiographics* 2002;22:1217–1222. [PubMed](#)
2. Wootton-Gorges SL, Thomas KB, Harned RK, Wu SR, Stein-Wexler R, Strain JD. Giant cystic abdominal masses in children. *Pediatr Radiol* 2005;35:1277–1288. [PubMed](#)
3. Sutcliffe J, Munden M. Sonographic diagnosis of multiple gastric duplication cysts causing gastric outlet obstruction in a pediatric patient. *J Ultrasound Med* 2006;25:1223–1226. [PubMed](#)
4. Hur J, Yoon CS, Kim MJ, Kim OH. Imaging features of gastrointestinal tract duplications in infants and children: from oesophagus to rectum. *Pediatr Radiol* 2007;37:691–699. [PubMed](#)
5. Kume K, Sakata H, Otsuki M. Education and imaging. Gastrointestinal: tubular duplication of the descending colon. *J Gastroenterol Hepatol* 2007;22:1553. [PubMed](#)

Case 71

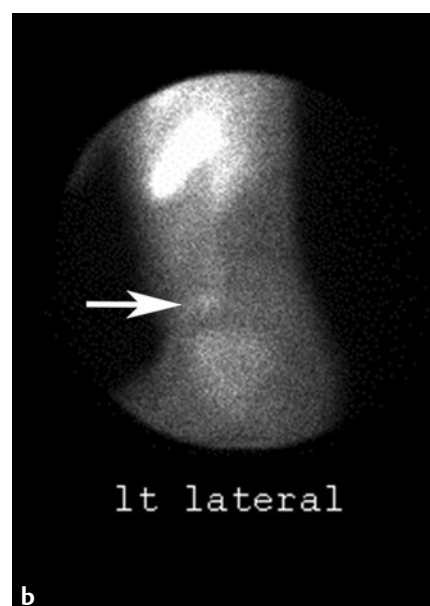
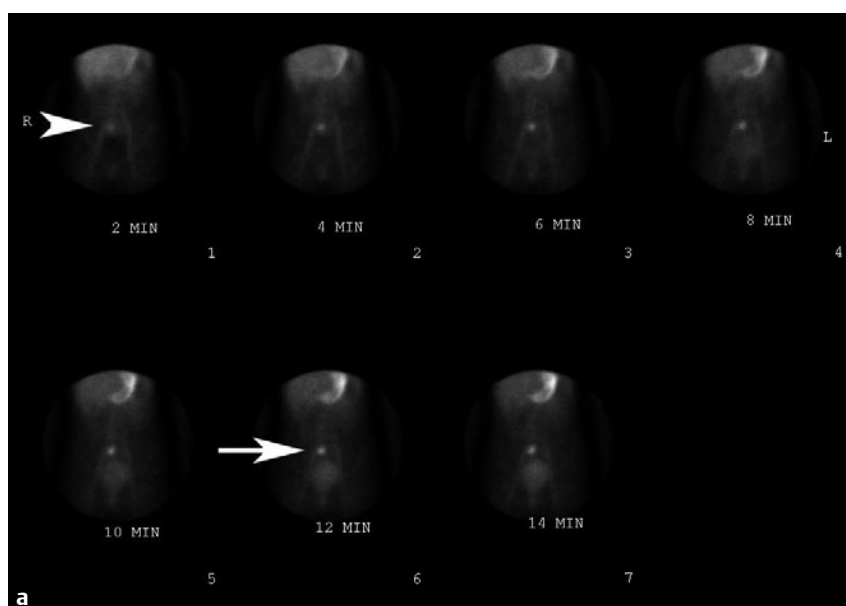
■ Clinical Presentation

A 10-year-old girl with lower gastrointestinal bleeding.

■ Radiographic Studies

Sequential frontal nuclear medicine images (**Fig. 71.1a**) show focal oval activity in the periumbilical region appearing on the initial 2-minute image (*arrowhead*), similar in timing to gastric mucosa and prior to the appearance of bladder activity.

Activity within the lesion increases on the 12-minute image (**Fig. 71.1a, arrow**) similar to gastric mucosa. Subsequent lateral scintigraphic image (**Fig. 71.1b**) confirms oval lower abdominal lesion (*arrow*), cephalad to the bladder.



■ Diagnosis

Meckel's Diverticulum

■ Discussion and Differential Diagnosis

Meckel's diverticulum is a true diverticulum of the antimesenteric border of the small bowel and is the most common congenital anomaly of the GI tract. Meckel's diverticulum is formed by incomplete regression of the proximal portion of the omphalomesenteric (or vitellointestinal) duct, which connects the embryo to the yolk sac in the third to fifth week of gestation. After that time, the placenta takes over nutritional needs and the duct atrophies. Other abnormalities of regression can result in formation of a cyst, a fistula, or fibrosis band to the umbilicus. Ectopic mucosa can be found within a Meckel's diverticulum, including gastric, colonic, or pancreatic. Although it occurs in 2% of the population, most cases remain asymptomatic. When symptoms do develop, 60% occur before age 10, and the remainder throughout childhood and into adulthood. Common complications include bleeding, obstruction (due to volvulus, intussusception, or internal hernia), inflammation, and perforation.^{1,2}

In children, hemorrhage due to ulceration in ectopic gastric mucosa within the diverticulum is also an important clinical

presentation. Patients most often present with painless rectal bleeding that is sometimes significant enough to require transfusion. In other cases, bleeding is occult but causes iron deficiency anemia. In children, technetium-99m pertechnetate scintigraphy is 80 to 90% accurate in identifying Meckel's diverticulum containing ectopic gastric mucosa; in adults, accuracy is only 46%. Other imaging techniques have been tried but are not helpful in most cases. In the absence of GI bleeding, laparoscopy may be the procedure of choice to identify a Meckel's diverticulum.³

Based on clinical findings alone, differential diagnosis includes other causes of bleeding (anal fissure, polyps, inflammatory bowel disease), obstruction (volvulus, intussusception, hernia, adhesions), or inflammation (appendicitis, inflammatory bowel disease, diverticular disease).⁴ Technetium scanning will almost always confirm or eliminate Meckel's diverticulum as the source of bleeding. In cases of obstruction, diagnosis is made at the time of surgery.

Pearls

- ◆ The rule of 2's in Meckel's diverticulum: occurs in 2% of the population, located within 2 feet of the ileocecal valve, and symptoms most commonly symptomatic before 2 years age.¹
- ◆ In difficult cases, the accuracy of technetium scans can be enhanced by using pentagastrin (enhances localization), cimetidine (inhibits release of technetium into the lumen), or glucagon (slows peristalsis).⁵

Pitfalls

- ◆ False-positive technetium scans can be caused by GI duplications containing gastric mucosa, foci of inflammation, vascular tumor, or an ectopic kidney.⁶
- ◆ False-negative scans can result from only a small amount of gastric mucosa in the diverticulum, low hematocrit, rapid peristalsis, or a distended bladder or stomach (they should be emptied before scanning).⁶
- ◆ Abdominal pain without bleeding should not be an indication for a technetium Meckel's scan.

■ Controversy

- Opinions differ over whether an incidentally discovered Meckel's diverticulum should be removed.

References

1. Kotecha M, Bellah R, Pena AH, Jaimes C, Mattei P. Multimodality imaging manifestations of the Meckel diverticulum in children. *Pediatr Radiol* 2012; 42:95–103. [PubMed](#)
2. Sinha CK, Fishman J, Clarke SA. Neonatal Meckel's diverticulum: spectrum of presentation. *Pediatr Emerg Care* 2009;25:348–349. [PubMed](#)
3. Shalaby RY, Soliman SM, Fawzy M, Samaha A. Laparoscopic management of Meckel's diverticulum in children. *J Pediatr Surg* 2005;40:562–567. [PubMed](#)
4. Feller AA, Movson J, Shah SA. Meckel diverticulum: a geriatric disease masquerading as common gastrointestinal tract disorders. *Arch Intern Med* 2003;163:2093–2096. [PubMed](#)
5. American College of Radiology, Society of Nuclear Medicine, and Society for Pediatric Radiology Practice Guideline for the Performance of Gastrointestinal Scintigraphy. <http://www.acr.org/Quality-Safety/Standards-Guidelines>. Revised 201.
6. Menezes M, Tareen F, Saeed A, Khan N, Puri P. Symptomatic Meckel's diverticulum in children: a 16-year review. *Pediatr Surg Int* 2008;24:575–577. [PubMed](#)

Case 72

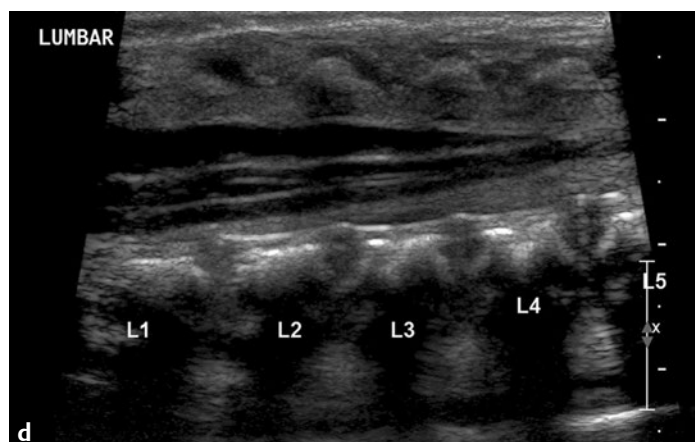
■ Clinical Presentation

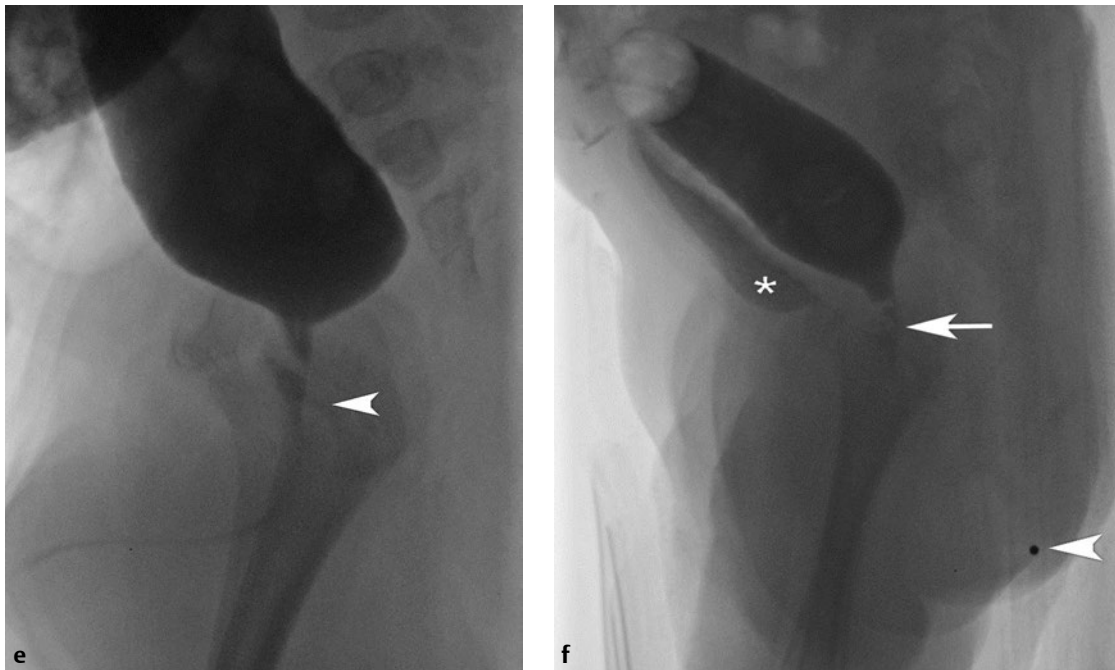
A 1-day-old boy has abdominal distention and absent meconium.

■ Radiographic Studies

Frontal and lateral abdominal radiographs (**Fig. 72.1a,b**) demonstrate diffuse bowel distention with paucity of rectal gas. Sacral hypoplasia is noted (**Fig. 72.1b**, *arrowhead*). Transverse pelvic ultrasound image (**Fig. 72.1c**) shows a dilated debris-filled rectum (*arrow*), posterior to the bladder. Longitudinal spine ultrasound image (**Fig. 72.1d**) shows a low conus level in

the same patient. Antegrade postoperative colostogram (**Fig. 72.1e**) shows a fistula between the rectum and the urethra (*arrowhead*). Fluoroscopic image in a different patient (**Fig. 72.1f**) demonstrates fistula between the rectum and the posterior urethra (*arrow*) and bladder (*asterisk*). Note the distance from the atresia level to the skin marker (*arrowhead*).





■ Diagnosis

Imperforate Anus

■ Discussion and Differential Diagnosis

Imperforate anus (anorectal atresia) occurs in 1 in 5,000 births.¹ It may be an isolated malformation, but more often (72%) is part of a syndrome involving multiple organ systems. These include the VACTERL syndrome (vertebral, anal, cardiovascular, tracheoesophageal, renal, limb), Currarino's triad, or caudal regression syndrome, with a high incidence of associated spinal anomalies.²

Oligohydramnios, hydronephrosis, distended bladder, cystic masses, and dilated bowel loops represent some of the prenatal sonographic and fetal MRI findings in imperforate anus. The Wingspread classification of anorectal anomalies is based on the location of the rectal pouch in relation to the levator sling dividing the imperforate anus into low, intermediate, and high types. The Krickenberg classification is based on the location and type of fistula and the position of the rectal pouch. The rectal fistula may extend externally to the perineum or may communicate internally with the vagina, bladder, prostate, or urethra.² Cloacal malformations, anorectal atresia without fistula, and anal stenosis are uncommon variants.² Recto-urethral fistula is the most common fistula in boys, and rectovaginal fistula (rectovestibular fistula) is the most common fistula in girls. Intermediate types have fistulae that insert lower on the urethra than do high types.

Evaluation for rectal malformations begins with physical examination. One perineal opening in a female or a smooth perineum in a male without corrugations is a sign of a high lesion. Perineal fistula and perineal pearls are external signs of

a low lesion. Males with external signs of a low lesion but with a fistula into the membranous or bulbous urethra are the intermediate type. If a perineal or vestibular fistula is identified on physical exam, primary repair through the perineal approach is possible. If no meconium is visualized at 24 hours, a prone cross-table lateral radiograph is performed. If the gas is below the coccyx, primary perineal repair is attempted at many institutions with or without a protective colostomy. If the rectal gas is very close to the skin, there may be a short perineal fistula. If the gas is 1 to 2 cm above the skin, it can represent an imperforate anus without fistula, especially in patients with Down syndrome.³ Calcified intraluminal meconium may be seen on prenatal or postnatal ultrasound and plain radiographs, and implies a fistula resulting in mixing of urine and meconium.

If the rectal gas is above the coccyx, meconium is not present in the urine, or if significant sacral abnormalities are noted, colostomy followed by secondary repair at 1 to 3 months is performed. A distal colostogram is mandatory in these cases to delineate the anatomy. When performing a distal ostomy contrast enema to define anatomy prior to a pull-through procedure, a Foley balloon may be used to allow full distention of the colon so that a small fistula will fill. Pelvic MRI can be helpful to delineate the position of the rectal pouch and the location of the fistula, and to evaluate the levator ani and sphincter musculature.⁴ Low atresias are associated with genital abnormalities and normal sphincter and levator muscula-

ture. Rectourethral and rectovesical fistulae are associated with abnormal, underdeveloped musculature except for the rectourethrobulbar type.³

Anomalies involving the cardiovascular system, genitourinary system, esophagus, sacrum, and spinal cord must be excluded within the first 24 hours and are more common in the

higher lesions.⁵ Sacral abnormalities including missing vertebra and hemisacrum are extremely common. Evaluation for tethered cord is particularly important in patients with high defects, abnormal sacrum, and spina bifida. In addition to hydronephrosis, hydrocolpos should be excluded in patients with cloacal malformations.³

Pearls

- ◆ Imperforate anus is 15 times more frequent in patients with Down syndrome than in the general population.⁶
- ◆ If there is a sacral hypoplasia and rectal stenosis, search for a presacral mass (anterior meningocele or sacrococcygeal teratoma) of Currarino's triad.
- ◆ A female with imperforate anus with an abdominal mass most probably has hydrometrocolpos or hydronephrosis.

Pitfall

- ◆ All patients with imperforate anus should be examined for spinal deformities with ultrasound. Missed spine anomalies may explain incontinence or constipation later in life.

References

1. Levitt MA, Peña A. Anorectal malformations. *Orphanet J Rare Dis* 2007;2:33. [PubMed](#)
2. Alamo L, Meyrat BJ, Meuwly JY, Meuli RA, Gudinchet F. Anorectal malformations: Finding the pathway out of the labyrinth. *Radiographics* 2013;33:491–512. [PubMed](#)
3. Levitt MA, Pena A. Imperforate anus and cloacal malformations. In: Holcomb GW III, Murphy JP, eds. *Ashcraft's Pediatric Surgery*, 5th ed. Philadelphia: WB Saunders; 2010:468–490
4. Berrocal T, Lamas M, Gutieérrez J, Torres I, Prieto C, del Hoyo ML. Congenital anomalies of the small intestine, colon, and rectum. *Radiographics* 1999;19:1219–1236. [PubMed](#)
5. Nieuvelstein RA, Vos A, Valk J. MR imaging of anorectal malformations and associated anomalies. *Eur Radiol* 1998;8:573–581. [PubMed](#)
6. Black CT, Sherman JO. The association of low imperforate anus and Down's syndrome. *J Pediatr Surg* 1989;24:92–94, Discussion 94. [PubMed](#)

Case 73

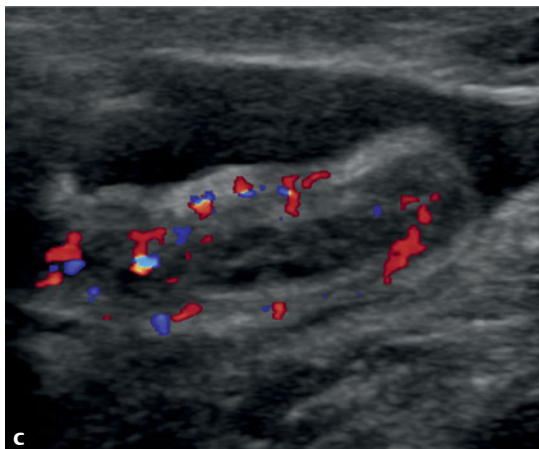
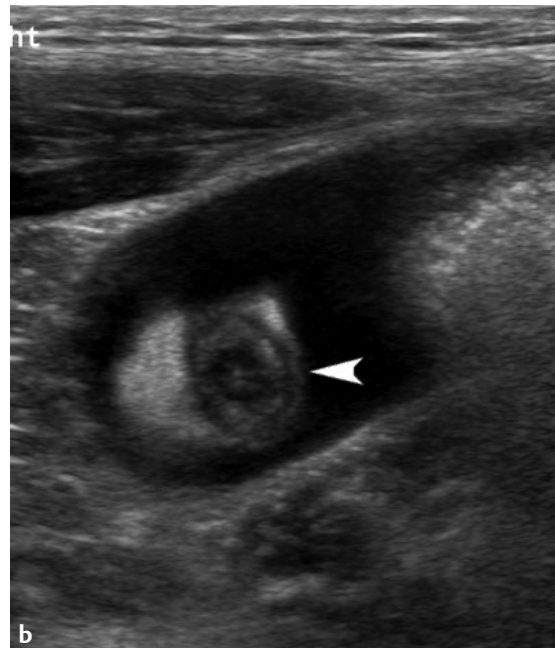
■ Clinical Presentation

An 8-year-old boy presents with vomiting and right lower quadrant abdominal pain.

■ Radiographic Studies

Ultrasound image (**Fig. 73.1a**) shows thickened appendix (*arrowheads*), which measured 8 mm, and periappendiceal fluid (*asterisk*). Transverse ultrasound image (**Fig. 73.1b**) confirmed dilated, noncompressible appendix (*arrowhead*) with surround-

ing echogenic fat and peritoneal fluid. Doppler evaluation (**Fig. 73.1c**) demonstrates diffuse hyperemia involving the appendix. CT image (**Fig. 73.1d**) shows a thickened appendix with prominent enhancement (*arrowhead*).



■ Diagnosis

Appendicitis



■ Discussion and Differential Diagnosis

Acute appendicitis is secondary to luminal obstruction from a variety of causes including appendicoliths. The peak age of incidence for appendicitis is the second decade of life. Perforation occurs in 16 to 39% of cases, and appendectomy is one of the most common urgent abdominal surgical procedures in children.^{1,2} The appendix originates from the cecum 3 cm from the ileocecal valve and usually remains within the right lower quadrant of the abdomen. In some instances, the appendix can extend to unusual locations within the abdomen or pelvis. Ultrasound and CT evaluation have significantly decreased the false-negative appendectomy rate in recent decades.

Typical radiographic findings radiographs are nonspecific and include paucity of right lower quadrant bowel gas, splinting of the lumbar spine, obscuration of the properitoneal fat stripe, and signs of small bowel obstruction. A calcified fecalith is seen in a minority of patients; extraluminal gas with perforation is rare. Ultrasound is considered the primary imaging modality because it does not use ionizing radiation.³ Ultrasound has a reported sensitivity and specificity of 88 and 94%.⁴ The entire appendix should be identified throughout its course and evaluated for diameter, wall thickness, compressibility, and blind-ending morphology. A diameter of ≥ 6 mm has sensitivity, specificity, negative predictive value, and posi-

tive predictive value of 98%; lack of compressibility has accuracy values close to 96%.⁵ Appendiceal luminal fluid and hyperemia are highly specific but have low sensitivity.⁵ Peritoneal fluid, echogenic fat, fecalith, and enlarged lymph nodes are additional nonspecific findings. The ultrasound exam may be limited as obesity and abdominal wall rigidity can hinder ultrasound compression. An appendix in the retrocecal location or pelvis can be difficult to find with ultrasound. Despite these limitations, ultrasound is helpful in patient management. Patients with diffuse fluid or small abscesses usually undergo immediate surgery. Patients with a large phlegmon or dominant abscesses may be treated with antibiotics and percutaneous drainage followed by delayed appendectomy. CT is more sensitive than ultrasound in identifying the appendix. Findings of an enlarged appendix with an enhancing wall, inflammatory fat stranding, and free peritoneal fluid are similar to those seen on ultrasound. CT is better at defining the extent of intra-abdominal abscesses prior to drainage.

Other causes of abdominal pain such as cholelithiasis, gynecologic abnormalities, urinary obstruction, inflammatory bowel disease, Burkitt's lymphoma, and intussusception can be detected in patients undergoing ultrasound for suspected appendicitis.

Pearls

- ◆ Ultrasound measurements of the appendix are the same in infants and children as in adults.
- ◆ Appendiceal perforation is more common in children than adults.

Pitfalls

- ◆ The terminal ileum can mimic the appendix but is not blind ending.
- ◆ A perforated appendix is more difficult to diagnose on ultrasound than an intact inflamed appendix.

References

1. Birnbaum BA, Wilson SR. Appendicitis at the millennium. *Radiology* 2000; 215:337–348 [PubMed](#)
2. Oyetunji TA, Ong'uti SK, Bolorunduro OB, Cornwell EE III, Nwomeh BC. Pediatric negative appendectomy rate: trend, predictors, and differentials. *J Surg Res* 2012;173:16–20 [PubMed](#)
3. Linam LE, Munden M. Sonography as the first line of evaluation in children with suspected acute appendicitis. *J Ultrasound Med* 2012;31:1153–1157 [PubMed](#)
4. Doria AS, Moineddin R, Kellenberger CJ, et al. US or CT for Diagnosis of Appendicitis in Children and Adults? A Meta-Analysis. *Radiology* 2006; 241:83–94 [PubMed](#)
5. Kessler N, Cyteval C, Gallix B, et al. Appendicitis: evaluation of sensitivity, specificity, and predictive values of US, Doppler US, and laboratory findings. *Radiology* 2004;230:472–478 [PubMed](#)

Case 74

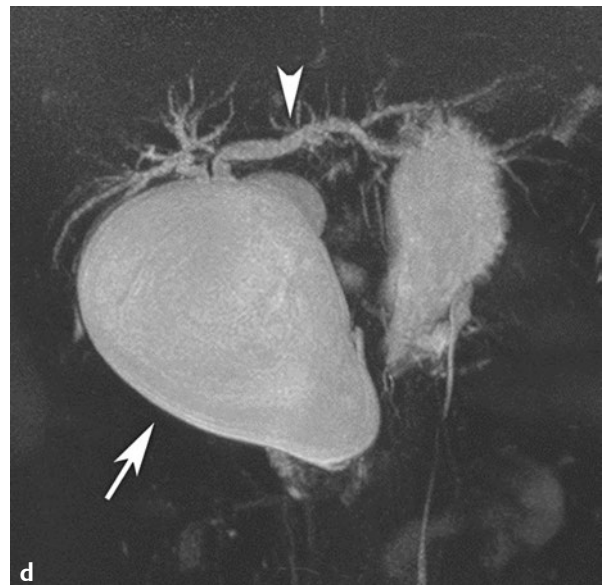
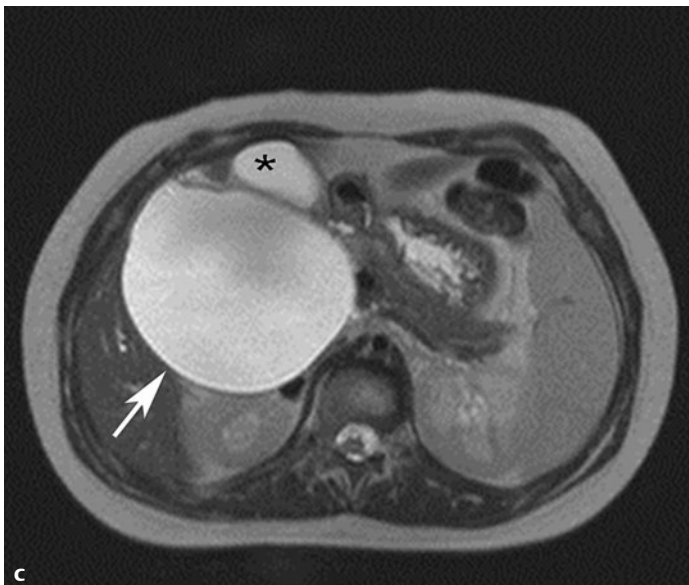
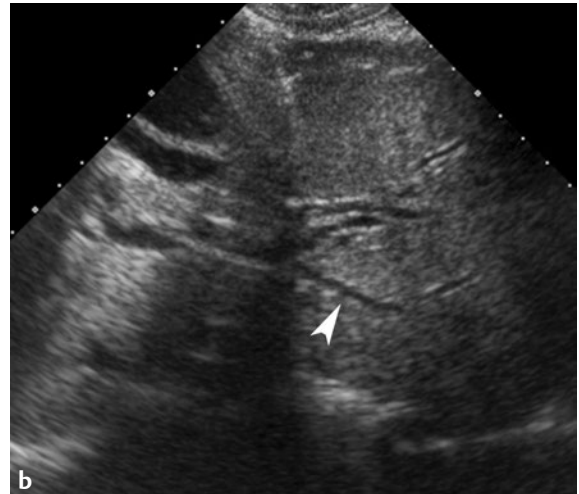
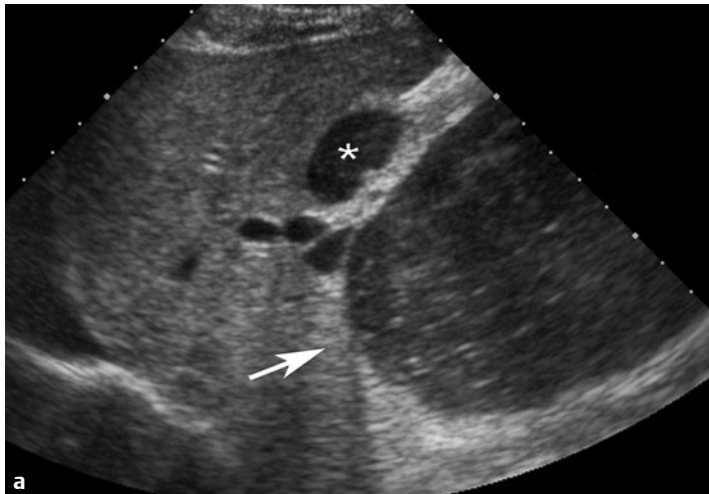
■ Clinical Presentation

A 12-year-old girl with right upper quadrant pain.

■ Radiographic Studies

Ultrasound image (**Fig. 74.1a**) reveals a large cystic lesion with internal echogenic debris in the right upper quadrant (*arrow*). Note the presence of a normal gallbladder (*asterisk*). Another ultrasound image shows dilated bile ducts in the left lobe of the liver (**Fig. 74.1b**, *arrowhead*). Magnetic resonance cholangio-

pancreatography (MRCP) images (**Fig. 74.1c,d**) confirm the cystic lesion (*arrow*), as well as its connection to the biliary tree. Again seen is a normal gallbladder (**Fig. 74.1c**, *asterisk*) and dilation of the left hepatic lobe biliary tree (**Fig. 74.1d**, *arrowhead*).



■ Diagnosis

Choledochal Cyst

■ Discussion and Differential Diagnosis

The Todani classification divides biliary ductal cysts into five types¹:

- Type I: cystic or fusiform dilatation of the common bile duct, known as choledochal cyst (50–90%)
- Type II: diverticulum off the common bile duct (2%)
- Type III: intraduodenal choledochoceles (1–4%)
- Type IV: multiple extrahepatic and intrahepatic cysts (15–35%)
- Type V: Caroli disease, single or multiple intrahepatic cysts (20%)

Approximately 80% of choledochal cysts present before 10 years of age.² The classic triad of symptoms (jaundice, pain, and palpable abdominal mass) presents in fewer than 20% of patients. However, nearly two thirds of patients present with two of the three. Patients are divided into neonatal (< 1 year of age) and “adult” (≥ 1 year of age) groups. The neonatal group tends to present with obstructive jaundice and abdominal mass. The adult group presents with pain, fever, nausea, jaundice, and vomiting.² Choledochal cysts are three to four times more common in females and more common in Asians. Choledochal cysts are congenital in one third of cases. In the remainder, patients are predisposed to cyst formation owing to the junction of the pancreatic duct with the bile duct, which is more proximal and at a more acute angle than normal. Be-

cause the sphincter of Oddi lies distal to the junction and the pressure in the pancreatic duct is higher than in the biliary tree, pancreatic enzymes reflux into the biliary tree. The resulting inflammation causes fibrosis, dilatation, and stricture of the biliary tree.¹

Ultrasound is usually performed as a screening exam for right upper quadrant pain or jaundice. When a choledochal cyst is identified the intrahepatic and extrahepatic anatomy of the cyst must be completely mapped. CT and MRCP are useful to show the extent of intrahepatic involvement.^{3,4} The differential diagnosis includes other cystic masses such as duplication cysts, as well as mesenteric, ovarian, renal, adrenal, and pancreatic cysts. In these cases, a nuclear medicine hepatobiliary scan confirms that the bile duct cyst connects to the biliary tree. If the biliary tree is still not completely visualized, percutaneous transhepatic cholangiography, endoscopic retrograde cholangiopancreatography (ERCP), or intraoperative cholangiography may be necessary for surgical planning.¹

Surgical treatment consists of excision of as much of the cyst as possible to prevent cholangitis and the 10 to 15% risk of cholangiocarcinoma. Preoperative percutaneous biliary drainage and stent placement may be indicated in some patients.⁵ Following cyst resection, Roux-en-Y hepaticojejunostomy is usually performed.

Pearls

- ◆ The classic triad of abdominal pain, jaundice, and right upper quadrant mass is seen in fewer than 20% of patients.²
- ◆ Especially in infants, cysts may rupture and present with bile peritonitis. Delayed scintigraphic images may show tracer leak.²
- ◆ Search carefully for choledocholithiasis, which is present in 8% of patients.
- ◆ The older a patient is at diagnosis, the greater the risk of malignancy.
- ◆ Biliary atresia in neonates can be concurrent and must be excluded.⁴

Pitfall

- ◆ Delayed treatment of choledochal cyst and biliary atresia can result in cirrhosis, portal hypertension, and pancreatitis.

■ Controversy

- Some authors believe that type II, type III, and type V (Caroli disease) cysts are entirely different entities and

should not be included in the classification of choledochal cysts.

References

1. Singham J, Yoshida EM, Scudamore CH. Choledochal cysts: part 1 of 3: classification and pathogenesis. *Can J Surg* 2009;52:434–440. [PubMed](#)
2. Singham J, Yoshida EM, Scudamore CH. Choledochal cysts: part 2 of 3: Diagnosis. *Can J Surg* 2009;52:506–511. [PubMed](#)
3. Chavhan GB, Babyn PS, Manson D, Vidarsson L. Pediatric MR cholangiopancreatography: principles, technique, and clinical applications. *Radiographics* 2008;28:1951–1962. [PubMed](#)
4. Rozel C, Garel L, Rypens F, et al. Imaging of biliary disorders in children. *Pediatr Radiol* 2011;41:208–220. [PubMed](#)
5. Singham J, Yoshida EM, Scudamore CH. Choledochal cysts. Part 3 of 3: management. *Can J Surg* 2010;53:51–56. [PubMed](#)

Case 75

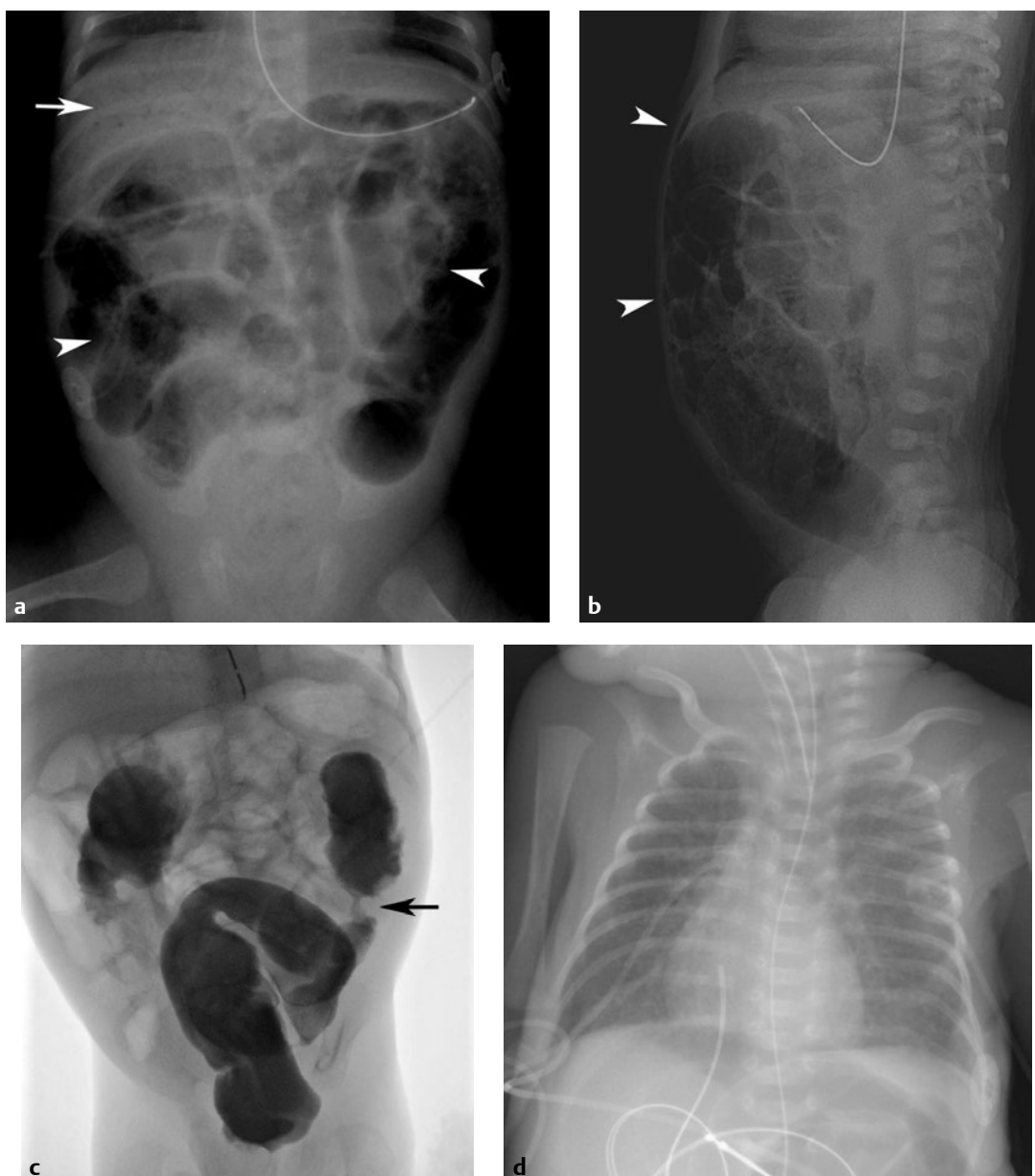
■ Clinical Presentation

A newborn with abdominal distention, increased residuals, and blood in the stool.

■ Radiographic Studies

Anteroposterior radiograph (**Fig. 75.1a**) demonstrates diffuse mottled appearance with linear lucencies (*arrowheads*) along the bowel wall. Multiple branching lucencies (*arrow*) are seen

within the liver. Cross-table lateral radiograph (**Fig. 75.1b**) demonstrates diffuse oval and linear lucencies and anterior abdominal free air (*arrowheads*).



■ Diagnosis

Necrotizing Enterocolitis

■ Discussion and Differential Diagnosis

Necrotizing enterocolitis (NEC) is the most common GI emergency in the neonatal intensive care unit (NICU). The major risk factors are prematurity and low birth weight. Most patients are under 2 weeks of age and are receiving enteral feeds. Clinically, the condition presents as abdominal distention, feeding residuals, peritoneal signs, blood in the stools, palpable abdominal mass, cardiorespiratory symptoms and, in fulminant cases, rapid deterioration and shock. The exact etiology of NEC is unknown. Currently, most experts agree that NEC is a final common pathway for several different insults to the bowel (hypoxia, hyperosmolar feeds, stress, infection, etc.) in a susceptible host with decreased barrier function of the enteric mucosa (impaired immunity, reduced secretory function, decreased blood flow regulation, and antioxidant function).¹ Necrotizing enterocolitis occasionally occurs in term babies. Forty percent have predisposing risk factors such as hypoxia, hypoglycemia, and respiratory distress.² In this group, the disease usually involves the colon, occurs earlier (first 4 days), has fewer systemic symptoms, and has a higher survival rate (90%).²

The most common but nonspecific radiographic finding is diffuse or localized gaseous bowel distention, which may appear unchanged or “fixed” over several radiographs. Bowel loops wider than one vertebral body width should be considered to be dilated. Air in the bowel wall, pneumatosis intestinalis, is a more specific finding. Submucosal pneumatosis is

cystic/bubbly and can be confused with stool or meconium.³ Subserosal gas is linear in configuration and is more definitive, although a later finding. Another important radiographic finding is portal venous gas, seen as branching lucencies in the liver. It is important to evaluate the supine neonate with decubitus or cross-table lateral films for evidence of peritoneal air, which can often be subtle on supine radiographs.⁴ The lateral radiograph may also increase conspicuity of pneumatosis or portal vein air. Ultrasound is more sensitive than radiographs for portal venous air, and it can be used for confirmation in questionable cases.³ Ultrasound is helpful in confirming, localizing, and characterizing ascites fluid; a fluid–debris level may be seen.⁵

Pneumoperitoneum and stool/bile in ascites fluid are the only major accepted indications for surgery.⁶ Management choices include laparotomy with ostomy placement versus peritoneal drainage. Randomized trials in the recent past show no significant difference in mortality between these two treatment choices, and management usually varies from case to case and based on surgeon preference.⁷ Contrast enema is usually performed after NEC recovery, before ostomy takedown, to identify any strictures in the colon (**Fig. 75.1c**, *arrow*). Most strictures are single; mild strictures may resolve without resection. The splenic flexure is a watershed area and is the most common site for NEC stricture.³

Pearls

- ◆ If NEC occurs in the first 24 hours in a premature newborn, look for hypoplastic left heart syndrome.³
- ◆ Ultrasound can be useful for detecting an abscess at the site of perforation in neonates with a drain and not responding to medical management.⁸
- ◆ Look at the abdomen on every NICU chest radiograph. Free air (**Fig. 75.1d**) or pneumatosis may be seen.

Pitfalls

- ◆ Although NEC is the most common cause of pneumoperitoneum in premature infants, other causes include enteric tube perforations, barotrauma, or maternal cocaine exposure.³
- ◆ Some cases of NEC with perforation have radiographic signs of ascites without peritoneal air.

References

1. Faix RG, Adams JT. Neonatal necrotizing enterocolitis: current concepts and controversies. In: *Advances in Pediatric Infectious Diseases*. St. Louis: Mosby-Year Book; 1994:1–36
2. Andrews DA, Sawin RS, Ledbetter DJ, Schaller RT, Hatch EI. Necrotizing enterocolitis in term neonates. *Am J Surg* 1990;159:507–509 [PubMed](#)
3. Morrison SC, Jacobson JM. The radiology of necrotizing enterocolitis. *Clin Perinatol* 1994;21:347–363 [PubMed](#)
4. Seibert JJ, Parvey LS. The telltale triangle: use of the supine cross table lateral radiograph of the abdomen in early detection of pneumoperitoneum. *Pediatr Radiol* 1977;5:209–210 [PubMed](#)
5. Miller SF, Seibert JJ, Kinder DL, Wilson AR. Use of ultrasound in the detection of occult bowel perforation in neonates. *J Ultrasound Med* 1993;12:531–535 [PubMed](#)
6. Raval MV, Moss RL. Current concepts in the surgical approach to necrotizing enterocolitis. *Pathophysiology* 2014;21:105–110 [PubMed](#)
7. Moss RL, Dimmitt RA, Barnhart DC, et al. Laparotomy versus peritoneal drainage for necrotizing enterocolitis and perforation. *N Engl J Med* 2006;354:2225–2234 [PubMed](#)
8. Silva CT, Daneman A, Navarro OM, et al. Correlation of sonographic findings and outcome in necrotizing enterocolitis. *Pediatr Radiol* 2007;37:274–282 [PubMed](#)

Case 76

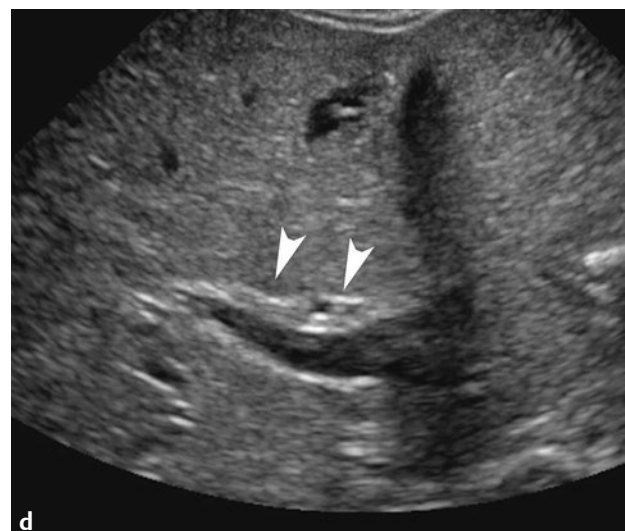
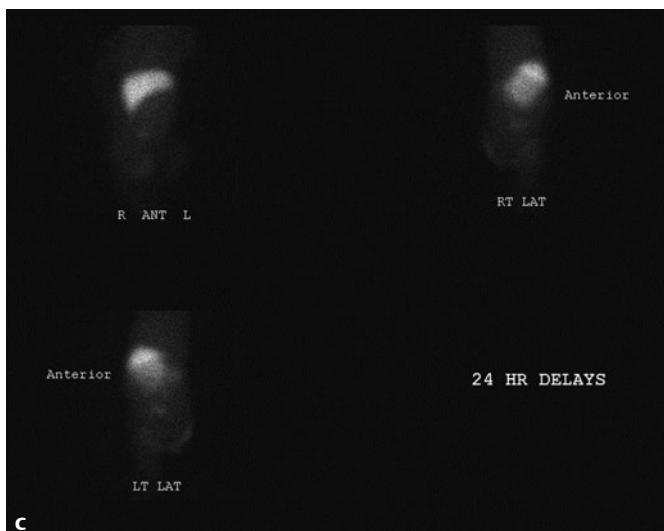
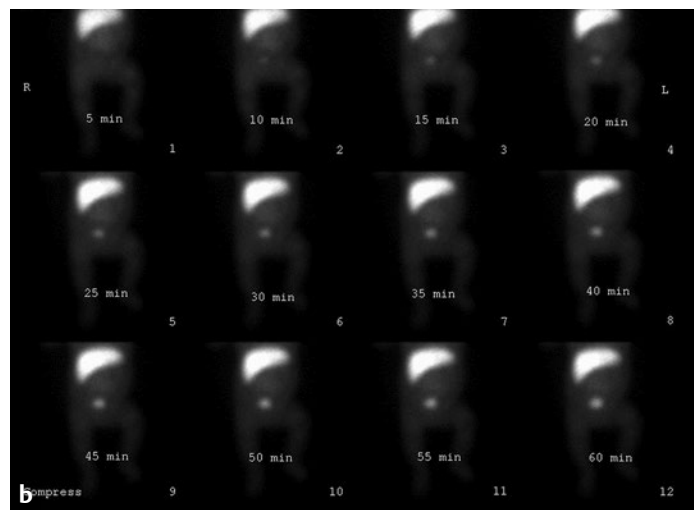
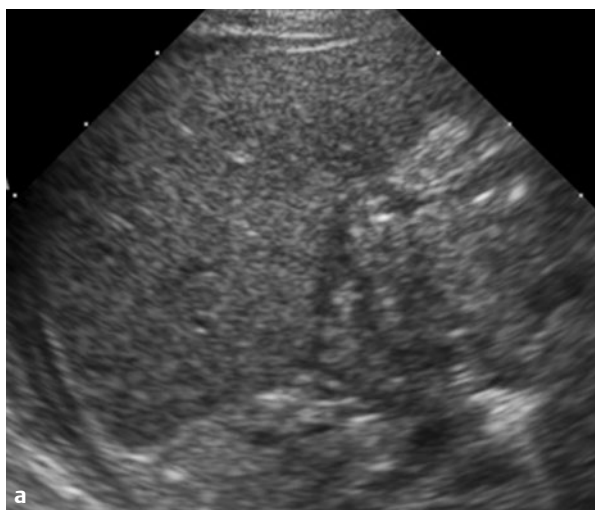
Clinical Presentation

A 1-month-old with jaundice.

Radiographic Studies

Absent gallbladder was noted on abdomen ultrasound image of the liver (**Fig. 76.1a**). Sequential nuclear medicine hepatobiliary images over 1 hour (**Fig. 76.1b**) show normal uptake of

radiopharmaceutical into the liver, but no excretion into the bowel. Subsequent 24-hour delay images (**Fig. 76.1c**) show lack of tracer excretion into the bowel.



■ Diagnosis

Biliary Atresia

■ Discussion and Differential Diagnosis

Biliary atresia is a progressive disease of the extrahepatic biliary tree. Its etiology is unknown, and it occurs with an incidence of 1 in 15,000 births. In a minority of cases, the atresia can be associated with additional congenital abnormalities, including polysplenia and cardiac abnormalities, but the majority of cases are isolated or perinatal in occurrence. Left untreated, the disease is uniformly fatal by age 2.¹ Infants present with persistent jaundice; light-colored stools and dark urine may develop. Splenomegaly is a late finding, indicating portal hypertension.¹

Imaging is used to distinguish biliary atresia from other sources of jaundice, including physiological jaundice, neonatal hepatitis, bile plug syndrome, and choledochal cyst. Sonography is usually in the initial imaging study; the liver may appear enlarged with inhomogeneous parenchyma. The gallbladder, if present, may appear small (gallbladder length < 19 mm), lack a smooth complete echogenic mucosal lining, and have an irregular or lobular contour (gallbladder ghost triad).² The triangular cord sign is a triangular or tubular echogenic cord of fibrous tissue seen in the porta hepatis on ultrasonography and is relatively specific in the diagnosis of biliary atresia. It is

defined as echogenic anterior wall thickness of the right portal vein (EARPV) > 4 mm measured on a longitudinal ultrasound scan (**Fig. 76.1d**, *arrowheads*).³ The common bile duct is not visualized in most cases of biliary atresia; increased hepatic artery diameter may be seen.⁴ A nuclear medicine hepatobiliary scan is performed after pretreatment with oral phenobarbital for 5 days or ursodeoxycholic acid for 2 to 3 days. This study should demonstrate no excretion of radiopharmaceutical into the small bowel, indicating an extrahepatic obstruction.

The definitive treatment for biliary atresia is surgical; a Kasai portoenterostomy is best performed when the patient is younger than 2 months of age. Many patients subsequently require liver transplantation later in life. Those with a native liver show increased incidence of portal hypertension, sclerosing cholangitis, bacterial cholangitis, and biliary cirrhosis.⁵ Patients with biliary atresia are also at increased risk for hepatic tumors (8%). The majority of tumors are benign, including focal nodular hyperplasia, adenomas, and regeneration nodules. Malignant tumors include hepatocellular carcinoma, cholangiocarcinoma, and hepatoblastoma.⁶

Pearl

- ◆ The reported sensitivity of hepatobiliary scintigraphy is high (100%). The specificity is variable.

Pitfall

- ◆ Patients should not have had barium studies within the 48 hours preceding hepatobiliary scintigraphy.

References

1. Kelly DA, Davenport M. Current management of biliary atresia. *Arch Dis Child* 2007;92:1132–1135 [PubMed](#)
2. Tan Kendrick AP, Phua KB, Ooi BC, Tan CE. Biliary atresia: making the diagnosis by the gallbladder ghost triad. *Pediatr Radiol* 2003;33:311–315. [PubMed](#)
3. Lee HJ, Lee SM, Park WH, Choi SO. Objective criteria of triangular cord sign in biliary atresia on US scans. *Radiology* 2003;229:395–400 [PubMed](#)
4. Humphrey TM, Stringer MD. Biliary atresia: US diagnosis. *Radiology* 2007; 244:845–851 [PubMed](#)
5. Kumagi T, Drenth JP, Guttman O, et al. Biliary atresia and survival into adulthood without transplantation: a collaborative multicentre clinic review. *Liver Int* 2012;32:510–518 [PubMed](#)
6. Yoon HJ, Jeon TY, Yoo SY, et al. Hepatic tumours in children with biliary atresia: single-centre experience in 13 cases and review of the literature. *Clin Radiol* 2014;69:e113–e119 [PubMed](#)

Case 77

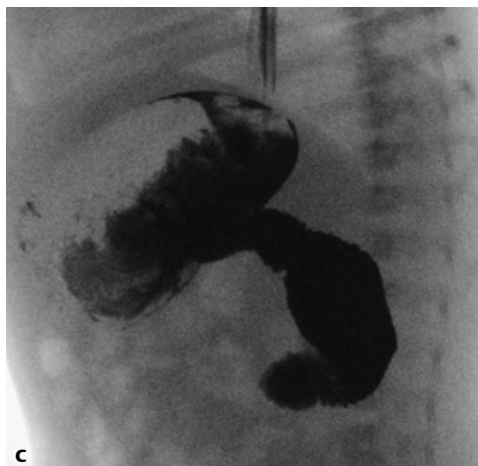
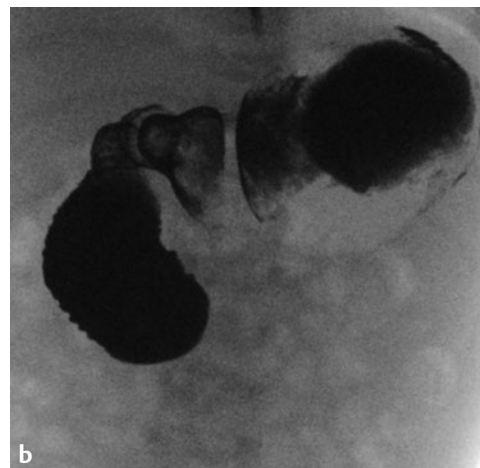
■ Clinical Presentation

A 1-day-old boy presents with bilious vomiting.

■ Radiographic Studies

Frontal radiograph (**Fig. 77.1a**) demonstrates dilated stomach and duodenal bulb with no distal gas. Frontal and lateral fluo-

roscopy images (**Fig. 77.1b,c**) demonstrate dilated stomach and proximal duodenum with complete duodenal obstruction.



■ Diagnosis

Duodenal Atresia

■ Discussion and Differential Diagnosis

Failure in recanalization of the solid portion of the gastrointestinal tract leads to duodenal atresia, stenosis or webs. Duodenal atresia is seen in 1 in 6,000 births and is located between the first and second portions of the duodenum.¹ Atretic bowel segments may be separated by a gap, or may remain connected with a fibrous cord or intraluminal diaphragm. These proximal duodenal anomalies are extremely common in patients with trisomy 21 syndrome.¹

Prenatal evaluation may show polyhydramnios in conjunction with a double-bubble sign from distention of the stomach and the first portion of the duodenum. Postnatally, neonates present with emesis after the first feed, bilious in most cases. A scaphoid abdomen and stable vital signs are typical. Radiographs usually demonstrate the double-bubble sign with a dilated stomach and proximal duodenum. Gastric and first duodenal distention and complete duodenal obstruction are noted on fluoroscopic imaging. The rest of the abdomen is usually gasless except for the rare patient with a bifid common

bile duct (CBD) termination.² Nonemergent duodenoduodenostomy is the surgical treatment of choice in duodenal atresia.³

Patients with duodenum stenosis and web present with partial obstruction on radiographs (**Fig. 77.1d**). On fluoroscopy, duodenal stenosis demonstrates partial luminal narrowing with distal passage of contrast; the third and fourth duodenum may be involved. Duodenal web patients show a transverse or curvilinear intraluminal contrast-filling defect. In more chronic cases, a wind-sock appearance may be seen from gradual stretching of the intraluminal membrane. Patients with annular pancreas can have both intrinsic stenosis and extrinsic compression of the second portion of the duodenum. Patients with malrotation can present with proximal bowel distention on radiographs, and must be distinguished from duodenal obstruction from other causes. The tortuous (corkscrew) alignment of the duodenum in malrotation and volvulus (when present) are distinguishing findings.

Pearls

- ◆ Radiographic and upper GI examination in malrotation/volvulus with obstructing bands can mimic duodenal atresia.⁴
- ◆ The degree of proximal duodenal distention is usually more prominent in patients with duodenal atresia than with malrotation/volvulus.⁵

Pitfalls

- ◆ Vomiting or an indwelling orogastric or nasogastric tube can decompress the double-bubble sign.
- ◆ Duplication cysts with extrinsic compression can mimic other causes of duodenal obstruction.

References

1. Kuenzler KA, Rothenberg SS. Duodenal atresia. In: Mattei P, ed. *Fundamentals of Pediatric Surgery*. New York: Springer; 2011:353–358
2. Panuel M, Bourliere-Najean B, Delarue A, Viard L, Faure F, Devred P. [Duodenal atresia with bifid termination of the common bile duct]. *Arch Fr Pediatr* 1992; 49:365–367 [PubMed](#)
3. Kay S, Yoder S, Rothenberg S. Laparoscopic duodenoduodenostomy in the neonate. *J Pediatr Surg* 200 9;44:906–908 [PubMed](#)
4. Gilbertson-Dahdal DL, Dutta S, Varich LJ, Barth RA. Neonatal malrotation with midgut volvulus mimicking duodenal atresia. *AJR Am J Roentgenol* 2009;192: 1269–1271 [PubMed](#)
5. Traubici J. The double bubble sign. *Radiology* 2001;220:463–464 [PubMed](#)

Case 78

■ Clinical Presentation

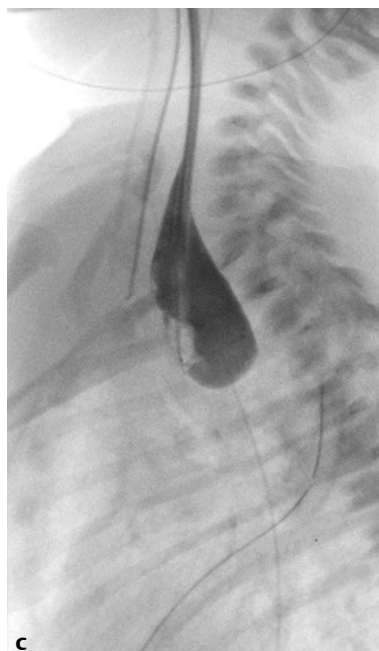
A 36-week-old premature newborn presents on the first day of life with respiratory distress and stridor. The neonatal team

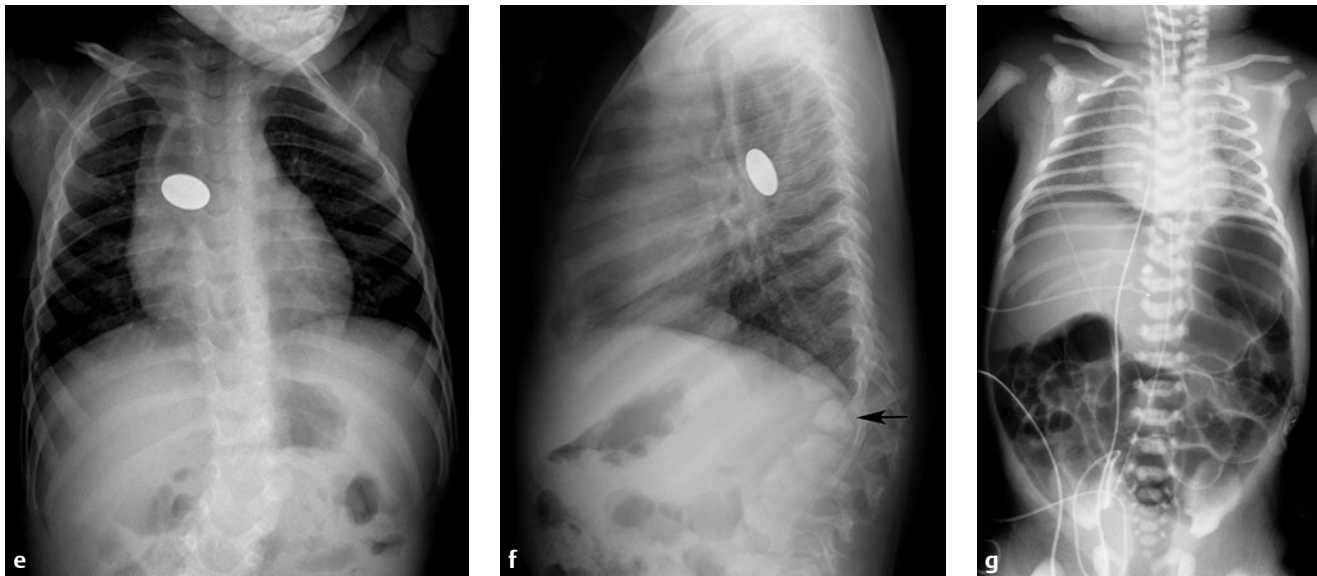
was unable to pass an enteric tube into the stomach at the bedside.

■ Radiographic Studies

Frontal chest radiograph (**Fig. 78.1a**) reveals a curvature in the enteric tube, with the tip at the level of the upper thoracic esophagus. Lateral chest radiograph (**Fig. 78.1b**) shows the enteric tube tip (*arrowhead*) above an air-distended esophageal pouch (*arrow*). Note the presence of air throughout the ab-

dominal bowel loops. Fluoroscopic contrast study 5 days after surgical treatment (**Fig. 78.1c**) shows no contrast flow beyond the thoracic esophagus repair site. Five days later, postoperative edema has decreased and contrast flows through the surgical repair site (**Fig. 78.1d**).





■ Diagnosis

Esophageal Atresia with Tracheoesophageal Fistula

■ Discussion and Differential Diagnosis

Esophageal atresia (EA), with or without tracheoesophageal fistula (TEF), is the most common congenital abnormality of the esophagus, occurring in 1 in 2,500 to 1 in 4,500 births.¹ EA and TEF result from abnormal separation of the primitive foregut into trachea and tubular esophagus; 88.5% of EA cases have a fistula between the distal esophagus and the distal trachea, and 8% of EA cases have no fistula. These two most common forms of the anomaly can be differentiated by the presence of air in abdominal bowel loops. Rarely, there is a fistula between the blind upper esophagus pouch and the trachea (0.8%) or between the proximal and distal ends of a discontinuous esophagus and trachea (1.4%). In the H-type fistula, the esophagus is a continuous tube, but there is a fistula between its ventral wall and the posterior wall of the trachea (4%).² Given the oblique orientation of this fistula, it is also referred to as an N-type fistula.³

Approximately 25% of these patients have additional congenital anomalies and may be part of the VACTERL association (vertebral, anal, cardiovascular, tracheoesophageal, renal, and limb), the CHARGE syndrome (coloboma, heart defect, atresia choanae, retarded growth and development, genital abnormality, and ear abnormality), Down syndrome, Di George syndrome, or Pierre Robin sequence. Anomalies not recognized at birth are detected later in life in up to 50% of patients, including vertebral anomalies, scoliosis, and radial ray abnormalities.^{2,4}

In the most common forms, the newborn presents with excessive oral secretions, failure of an enteric tube to pass, or regurgitation of the initial feed. The atresia is usually at the level of the junction of the proximal one third and distal two thirds of the esophagus. Because the proximal pouch is inter-

mittently dilated in utero, it may be visualized on prenatal ultrasound, but esophageal atresia is rarely diagnosed prenatally. It may be suspected in the fetus with polyhydramnios and a small stomach; confirmation with MRI is recommended.⁵ The dilated proximal pouch often compresses the developing fetal trachea, causing tracheomalacia.

The diagnosis of esophageal atresia can be made on plain radiographs and is usually confirmed with the visualization of a feeding tube tip coiled at the distal end of the pouch. Air may be injected for confirmation. The presence of air in abdominal bowel loops confirms a distal fistula.⁶ The injection of contrast into the pouch can cause aspiration with secondary respiratory compromise.

In the very rare cases of EA without TEF and duodenal atresia, the distal esophagus, stomach, and proximal duodenum are dilated and form a C-shaped fluid collection in the fetal abdomen and a fluid collection behind the heart on prenatal ultrasound. Postnatal radiographs demonstrate an air-filled proximal esophageal pouch, a distended gasless abdomen, and a retrocardiac density.

Patients with a fistula from the upper esophagus to the trachea may present with severe respiratory distress and pulmonary infiltrates secondary to aspiration of saliva and feeds. An H-type (also called N-type) fistula may have more subtle clinical signs and present later as coughing while the infant is feeding. Contrast must usually be used for diagnosis of these fistulae, which are most commonly at or above the T1 vertebral level.³ Repeat exams or pull-back tube esophagram may be required to identify a small fistula.³

Postoperative complications and sequelae of EA repair are common and include tracheomalacia, anastomotic leak, recur-

rent fistula, anastomotic stricture (frequently presenting with foreign body impaction), gastroesophageal reflux, and esophageal dysmotility. Problems seen later in life include persistent cough, asthma, hiatal hernia, and a slightly increased incidence of eosinophilic esophagitis.⁷ Frontal and lateral radiographs in a patient with past repair of esophageal atresia (**Fig. 78.1e,f**)

show a foreign body coin lodged in an air distended esophageal pouch. Note vertebral anomaly on the lateral view (**Fig. 78.1f, arrow**), and secondary upper lumbar scoliosis on the frontal view (**Fig. 78.1e**). In addition, right posterior rib changes are seen relating to past right thoracotomy in this patient with left aortic arch.

Pearl

- ◆ Note the location of the aortic arch, as the surgical approach to correct the atresia will be from the side opposite the aorta.

Pitfalls

- ◆ Aspiration and significant respiratory distress may occur during contrast exams evaluating for an H-type (N-type) fistula; be prepared for airway suctioning.³
- ◆ When esophageal atresia with tracheoesophageal fistula occurs in premature newborns with surfactant deficiency, positive pressure ventilation barotrauma may result in gastric perforation. **Figure 78.1g** shows the enteric tube at the thoracic inlet level (above esophageal atresia), lower thoracic vertebral anomalies, low lung volume/lung granularity (surfactant deficiency), and large pneumoperitoneum from gastric perforation.

References

1. Pinheiro PF, Simões e Silva AC, Pereira RM. Current knowledge on esophageal atresia. *World J Gastroenterol* 2012;18:3662–3672 [PubMed](#)
2. Kovesi T, Rubin S. Long-term complications of congenital esophageal atresia and/or tracheoesophageal fistula. *Chest* 2004;126:915–925 [PubMed](#)
3. Laffan EE, Daneman A, Ein SH, Kerrigan D, Manson DE. Tracheoesophageal fistula without esophageal atresia: are pull-back tube esophagograms needed for diagnosis? *Pediatr Radiol* 2006;36:1141–1147 [PubMed](#)
4. Sistonen SJ, Pakarinen MP, Rintala RJ. Long-term results of esophageal atresia: Helsinki experience and review of literature. *Pediatr Surg Int* 2011;27:1141–1149 [PubMed](#)
5. Langer JC, Hussain H, Khan A, et al. Prenatal diagnosis of esophageal atresia using sonography and magnetic resonance imaging. *J Pediatr Surg* 2001;36:804–807 [PubMed](#)
6. Berrocal T, Torres I, Gutiérrez J, Prieto C, del Hoyo ML, Lamas M. Congenital anomalies of the upper gastrointestinal tract. *Radiographics* 1999;19:855–872 [PubMed](#)
7. Gorter RR, Heij HA, van der Voorn JP, Kneepkens CM. Eosinophilic esophagitis after esophageal atresia: is there an association? Case presentation and literature review. *J Pediatr Surg* 2012;47:e9–e13 [PubMed](#)

Case 79

Clinical Presentation

A 2-year-old boy with abdominal pain, vomiting, and vague history of trauma.

Radiographic Studies

Abdominal radiograph (**Fig. 79.1a**) shows gastric air–fluid level and inferior displacement of the transverse colon. CT image (**Fig. 79.1b**) shows gastric distention with an air–fluid level, proximal second duodenal distention (*arrowhead*), and fluid within the gastrohepatic space (*arrow*). CT image (**Fig. 79.1c**)

shows an eccentric duodenal hematoma within the medial wall of the distal second portion of the duodenum (*arrowhead*). At 10-day follow-up, fluoroscopy images show residual duodenal fold thickening (**Fig. 79.1d**, *arrowhead*) and duodenal luminal narrowing (**Fig. 79.1e**, *arrowheads*).



■ Diagnosis

Duodenal Hematoma

■ Discussion and Differential Diagnosis

Duodenal hematoma is caused by the rapid compression of the duodenum against the spine; a bicycle handlebar injury is a classic mechanism. If an appropriate clinical history of blunt abdominal injury is absent, child abuse should be suspected, especially if the child is younger than 2 years of age.¹ Mortality and morbidity following duodenal trauma depends on associated solid organ injuries, vascular injuries, or bowel perforation. An important consideration, especially in children with physical symptoms of acute abdomen, is duodenal perforation. Early surgical management in these cases is critical to reduce morbidity and mortality.²

Computed tomography in duodenal hematoma usually demonstrates distention of the stomach and duodenum proximal to the hematoma. A > 3 mm eccentric wall thickening or

a hyperdense mass is seen, usually involving the second or third portions of the duodenum. Findings of thickened duodenal wall, intraperitoneal fluid, fluid in the right pararenal space, as well as solid viscera injury may be seen in both duodenal hematoma and duodenal rupture.³ Intraperitoneal air and contrast extravasation are specific but rare signs for rupture. Ultrasound demonstrates focal duodenal thickening or a duodenal mass with variable echogenicity. The hematoma becomes more hypoechoic or cystic at follow-up ultrasound examination.⁴ Plain radiographs may show gastric distention. On fluoroscopy, findings include fold thickening, intramural mass, coiled spring appearance, or high-grade duodenal obstruction.⁵ Duodenal hematoma usually resolves without sequelae in 2 weeks.⁶

Pearl

- ◆ Delayed presentation of more than 2 days following injury is common with abuse. Delay may result from fear of discovery or lack of recognition of injury severity.¹

Pitfalls

- ◆ Intraperitoneal air in duodenal perforation may be caused by rupture of the intraperitoneal portion of the duodenum or traumatic disruption of the peritoneal membrane with escape of gas from the retroperitoneum.³
- ◆ An intussusception may have a similar appearance to duodenal hematoma on ultrasound, but the location of a hematoma and lack of alternating echogenic and lucent bands should help to differentiate the two.⁷

References

1. Sowrey L, Lawson KA, Garcia-Filion P, et al. Duodenal injuries in the very young: child abuse? *J Trauma Acute Care Surg* 2013;74:136–141, discussion 141–142 [PubMed](#)
2. Desai KM, Dorward IG, Minkes RK, Dillon PA. Blunt duodenal injuries in children. *J Trauma* 2003;54:640–645, discussion 645–646 [PubMed](#)
3. Kunin JR, Korobkin M, Ellis JH, Francis IR, Kane NM, Siegel SE. Duodenal injuries caused by blunt abdominal trauma: value of CT in differentiating perforation from hematoma. *AJR Am J Roentgenol* 1993;160:1221–1223. [PubMed](#)
4. Megremis S, Segkos N, Andrianaki A, et al. Sonographic diagnosis and monitoring of an obstructing duodenal hematoma after blunt trauma: correlation with computed tomographic and surgical findings. *J Ultrasound Med* 2004;23:1679–1683 [PubMed](#)
5. Sidhu MK, Weinberger E, Healey P. Intramural duodenal hematoma after blunt abdominal trauma. *AJR Am J Roentgenol* 1998;170:38 [PubMed](#)
6. Clendenon JN, Meyers RL, Nance ML, Scaife ER. Management of duodenal injuries in children. *J Pediatr Surg* 2004;39:964–968 [PubMed](#)
7. Orel SG, Nussbaum AR, Sheth S, Yale-Loehr A, Sanders RC. Duodenal hematoma in child abuse: sonographic detection. *AJR Am J Roentgenol* 1988;151:147–149 [PubMed](#)

Case 80

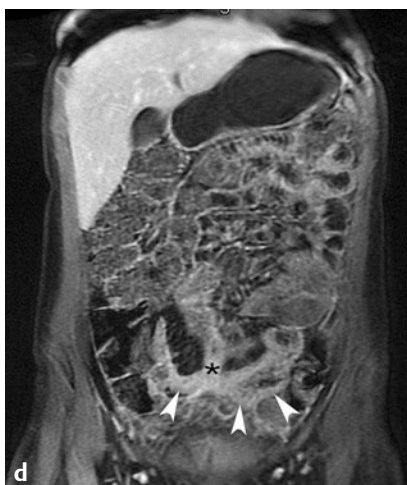
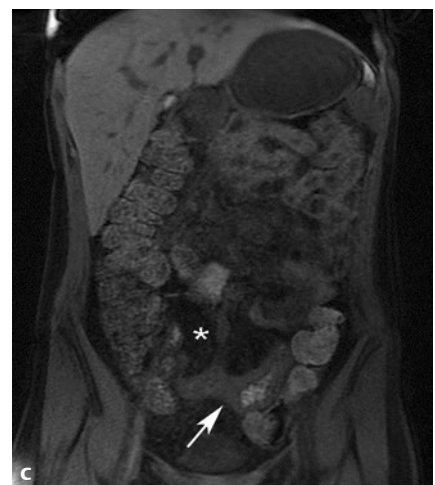
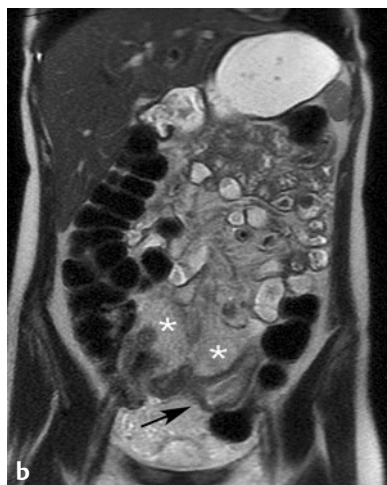
Clinical Presentation

A 13-year-old girl with a history of abdominal pain, diarrhea, and weight loss.

Radiographic Studies

Postcontrast coronal reformatted CT image (**Fig. 80.1a**) shows diffuse thickening of ileal loops (*asterisk*) and thickened terminal ileum (*arrow*). Coronal T2-weighted MRI without fat suppression in the same patient (**Fig. 80.1b**) shows diffuse fibrofatty proliferation of the mesentery (*asterisks*) and bowel wall thickening of the ileum (*arrow*). Precontrast coronal T1-weighted image with fat saturation (**Fig. 80.1c**) shows bowel wall thickening (*arrow*) with adjacent low signal fatty promi-

nence (*asterisk*). Postcontrast T1-weighted image with fat saturation image (**Fig. 80.1d**) shows abnormal bowel wall enhancement (*arrowheads*) and an enhancing enteroenteric fistula (*asterisk*) between adjacent small bowel loops. Post-contrast coronal T1-weighted MRI with fat saturation in another patient (**Fig. 80.1e**) shows an enhancing perianal fissure (*arrow*).



■ Diagnosis

Crohn's Disease

■ Discussion

Crohn's disease is a chronic inflammatory disease of the gastrointestinal tract characterized by transmural bowel wall inflammation. The terminal ileum is involved in most cases, but lesions can be found anywhere in the gastrointestinal tract. Skip lesions with intervening normal bowel are a common and important differentiating feature compared with other forms of inflammatory bowel disease. Crohn's disease is most commonly diagnosed in young adults, but 20% present before the age of 18 years.¹ Presenting symptoms include abdominal pain, diarrhea, rectal bleeding, and fever. Bowel wall biopsy reveals noncaseating granulomas.

Imaging is important for evaluation of small bowel between the ligament of Treitz and the ileocecal valve that is not adequately evaluated by endoscopy.² Traditional small bowel follow-through examinations can detect mucosal abnormalities such as aphthoid ulcers, cobblestone mucosa, pseudopolyps, skip lesions, and stenosis, but are largely being replaced by cross-sectional imaging that is more sensitive to transmural and extramural disease.

Computed tomography enterography (CTE) and magnetic resonance enterography (MRE) are better than traditional small bowel follow-through examinations because they enable evaluation of the entire bowel wall, mesentery, and extraintestinal complications such as abscess or fistula.³ Negative intraluminal contrast agents (water for CTE and barium sulfate for MRE)

enable separation of intravenous contrast enhancement of mucosa from the bowel lumen. Intravenous glucagon reduces bowel peristalsis, improving MRE image quality.

Acutely inflamed bowel has a trilaminar appearance on postcontrast CTE and MRE with enhancement of the mucosa and serosa and fluid density in the submucosa. Submucosal fat deposition leads to mural stratification prior to transmural fibrosis.² CTE shows decreased attenuation, and MRE shows signal loss on fat-suppressed images with submucosal fat deposition. Fibrotic bowel has homogeneous enhancement and hypointense signal on T2-weighted images. Small bowel feces sign may be seen in cases of strictures.

Extraluminal findings include engorgement of the vasa recta, inflammation of perienteric or pericolonic fat, increased pericolonic fat, prominent lymph nodes, abscesses, fistula, and bowel perforation. Engorged vasa recta produce the comb sign or multiple enhancing dots on CTE and MRE.¹ CTE and MRE study images should also be evaluated for gallstones, sclerosing cholangitis, pancreatitis, sacroiliitis, and ankylosing spondylitis that can be associated with Crohn's disease.

Ulcerative colitis is the most important differential diagnosis. Ulcerative colitis has continuous involvement of bowel rather than skip lesions. Ulcerative colitis is a mucosal abnormality and does not show strictures or transmural inflammation.

Pearls

- ◆ Magnetic resonance enterography is performed with the patient in the prone position to decrease the motion artifact from respiration and bowel peristalsis. The prone position also helps with lumen distention.
- ◆ Diffusion-weighted images with background body suppression distinctly demonstrates inflamed bowel.

Pitfall

- ◆ Multiple lymph nodes larger than 1 cm in short axis diameter or matted lymph nodes should raise suspicion for lymphoma, as various medications for Crohn's disease increase the risk of non-Hodgkin's lymphoma and other lymphoproliferative disorders.

■ Controversy

- Computed tomography enterography may be better for initial screening and diagnosis.⁴ MRE may be better for follow-up.

References

1. Casciani E, De Vincentiis C, Poletini E, et al. Imaging of the small bowel: Crohn's disease in paediatric patients. *World J Radiol* 2014;6:313–328. [PubMed](#)
2. Gee MS, Harisinghani MG. MRI in patients with inflammatory bowel disease. *J Magn Reson Imaging* 2011;33:527–534. [PubMed](#)
3. Towbin AJ, Sullivan J, Denson LA, Wallihan DB, Podberesky DJCT. CT and MR enterography in children and adolescents with inflammatory bowel disease. *Radiographics* 2013;33:1843–1860. [PubMed](#)
4. Duigenan S, Gee MS. Imaging of pediatric patients with inflammatory bowel disease. *AJR Am J Roentgenol* 2012;199:907–915. [PubMed](#)

Case 81

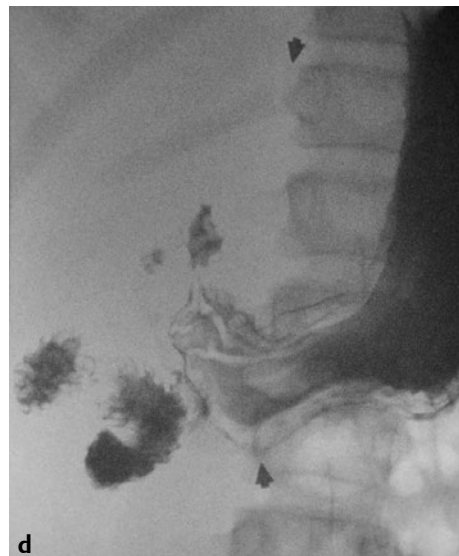
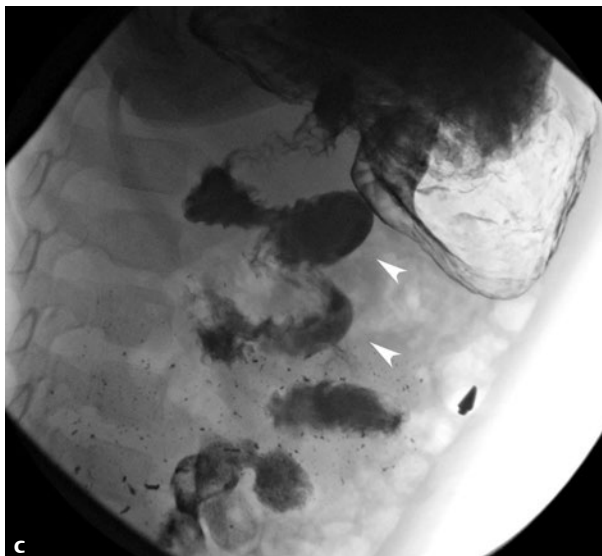
■ Clinical Presentation

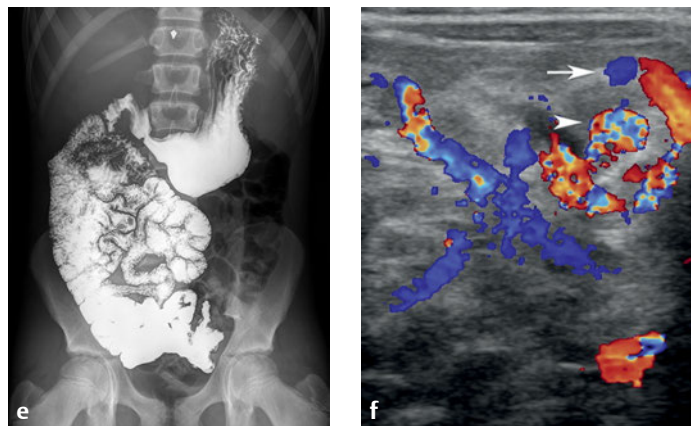
A 1-month-old infant with bilious vomiting.

■ Radiographic Studies

Anteroposterior fluoroscopy image (**Fig. 81.1a**) shows a distended stomach, distended proximal duodenum, and low alignment of the duodenal-jejunal junction. Subsequent AP and lateral fluoroscopic images (**Fig. 81.1b,c**) show corkscrew alignment (*arrowheads*) of the distal duodenum/proximal jejunum consistent with midgut volvulus. This patient had urgent sur-

gical treatment. AP fluoroscopy image in a teenage patient with vomiting (**Fig. 81.1d**) demonstrates the duodenal-jejunal junction to the right of midline, much lower than the duodenal bulb. Subsequent AP fluoroscopic image in this teenager (**Fig. 81.1e**) shows the small bowel loops abnormally aligned within the right abdomen. Elective surgery was planned for this patient.





■ Diagnosis

Malrotation with Midgut Volvulus

■ Discussion and Differential Diagnosis

No other pediatric disease has caused more distress or controversy in the pediatric radiology community than malrotation. Malrotation represents a spectrum of abnormalities involving the midgut, ranging from nonrotation to incomplete rotation with associated malfixation. Embryologically the midgut undergoes a series of counterclockwise rotations up to 270 degrees both outside and then within the abdominal cavity. Arrest of rotation can occur at any point in this sequence, with anatomic and radiographic manifestations representing a continuum ranging from right-sided duodenum and left-sided cecum to normal position of the duodenal-jejunal junction with obstructing duodenal bands.¹ Ladd's bands transfixing the cecum to the right-sided abdominal wall and obstructing the second portion of the duodenum may be seen. In addition, a short mesenteric base predisposes these patients to midgut volvulus.¹ Malrotations may be isolated to the colon with normal duodenal appearance.

Malrotation is invariably present in patients with diaphragmatic hernia, gastroschisis, and omphalocele, and is commonly seen in patients with heterotaxy syndrome.² In heterotaxy patients, the duodenal-jejunal junction is mirror image to that in normal patients and is on the right side. Most malrotations present in the first month of life, with the remaining usually presenting in the first year of life. Common symptoms include vomiting (usually bilious), diarrhea, and hematochezia in some cases. Patients can present with chronic abdominal pain, vomiting, and failure to thrive into adolescence and adulthood.

On radiographs, the bowel pattern is usually normal. Small bowel gas in the right upper abdomen in older children should raise suspicion for malrotation. Distention of the duodenum can be seen, especially in cases with complete obstruction, and mimics duodenal atresia in the neonate. In older infants with bilious vomiting, isolated dilation of the stomach and proximal duodenum with decreased distal gas warrants further evaluation to rule out volvulus. Distal small bowel obstruction pattern can be seen in delayed presentations and may indicate bowel ischemia with poor prognosis.¹

On upper GI exams, the duodenal-jejunal junction should be located to the left of the pedicles or overlying the pedicles, at or slightly below the level of the duodenal bulb on a straight AP view. Obtaining a lateral view to confirm the retroperitoneal position of the third portion of the duodenum is mandatory.³ An anteriorly directed second portion of the duodenum on the lateral view usually indicates malrotation.³ In equivocal cases, abnormal dilation of the duodenum, if present, can sway the diagnosis toward malrotation. Jejunum within the right side of the abdomen and cecum on the left side or midline may be seen in asymptomatic patients. Changing positions of bowel loops on repeat exams can indicate a narrow mesenteric base, a predisposing factor for volvulus. An excessively redundant duodenum should be viewed with suspicion, whereas a single redundant loop can be within normal limits. A low threshold for repeating a normal or equivocal upper GI exam should be maintained, as findings may change on a repeat exam.³

Corkscrew duodenal alignment can be seen with midgut volvulus or malrotation with Ladd's bands. Complete obstruction secondary to Ladd's bands can present with complete duodenal obstruction mimicking duodenal atresia; in addition, these conditions can coexist.

Ultrasound exam can show an inverted relationship between the superior mesenteric artery (SMA) and superior mesenteric vein (SMV) and the whirlpool sign in patients with volvulus. The whirlpool sign (**Fig. 81.1f**) depicts the SMV (*arrow*) and mesentery encircling around the SMA (*arrowhead*), indicating volvulus.⁴ Evaluation of the third portion of the duodenum between the SMA and the aorta has been recently proposed as a useful sonographic finding to exclude malrotation, although this finding has been deemed controversial.⁵⁻⁷

Surgical correction of malrotation in symptomatic and asymptomatic patients, regardless of age, is recommended. Ladd's procedure involves, untwisting of the volvulus, surgical excision of the Ladd's bands, and widening of the mesentery. Surgical handling of the bowel loops creates adhesions and diminishes the likelihood of recurrent volvulus.

Pearls

- ◆ Malrotation with midgut volvulus may not present with signs of acute abdomen until late in the clinical course. Attention to symptoms including bilious emesis and patient age are crucial to prevent catastrophic bowel ischemia.¹
- ◆ Chylous ascites, mesenteric lymphoceles, and melena can be seen in patients with malrotation and chronic intermittent volvulus.¹

Pitfalls

- ◆ An anterior intraperitoneal location of the third portion of the duodenum is diagnostic for malrotation. However, retroperitoneal duodenum can be seen in both normal patients and those with partial nonrotation (between 180 and 270 degrees). Most centers, therefore, prefer fluoroscopy over ultrasound to confirm normal duodenal-jejunal junction alignment among other findings.

References

1. Strouse PJ. Disorders of intestinal rotation and fixation ("malrotation"). *Pediatr Radiol* 2004;34:837–851 [PubMed](#)
2. Applegate KE. Evidence-based diagnosis of malrotation and volvulus. *Pediatr Radiol* 2009;39(Suppl 2):S161–S163 [PubMed](#)
3. Tang V, Daneman A, Navarro OM, Gerstle JT. Disorders of midgut rotation: making the correct diagnosis on UGI series in difficult cases. *Pediatr Radiol* 2013;43:1093–1102 [PubMed](#)
4. Rokade ML, Yamgar S, Tawri D. Ultrasound "Whirlpool Sign" for midgut volvulus. *J Med Ultrasound* 2011;19:24–26
5. Yousefzadeh DK. The position of the duodenojejunal junction: the wrong horse to bet on in diagnosing or excluding malrotation. *Pediatr Radiol* 2009;39(Suppl 2):S172–S177 [PubMed](#)
6. Karmazyn B. Duodenum between the aorta and the SMA does not exclude malrotation. *Pediatr Radiol* 2013;43:121–122 [PubMed](#)
7. Menten R, Reding R, Godding V, Dumitriu D, Clapuyt P. Sonographic assessment of the retroperitoneal position of the third portion of the duodenum: an indicator of normal intestinal rotation. *Pediatr Radiol* 2012;42:941–945 [PubMed](#)

Case 82

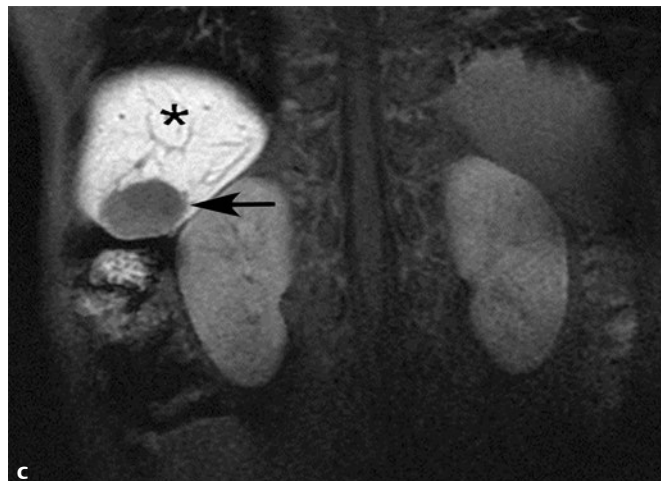
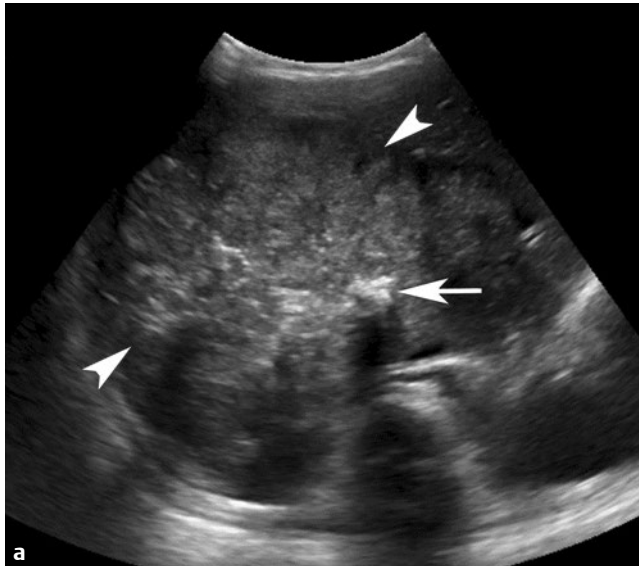
■ Clinical Presentation

A 1-year-old with abdominal protuberance.

■ Radiographic Studies

Abdomen ultrasound (**Fig. 82.1a**) shows a large heterogeneous mass (*arrowheads*) replacing most of the liver; echogenic calcification (*arrow*) with posterior acoustic shadowing is seen. Postcontrast coronal reformatted CT image (**Fig. 82.1b**) shows

the large liver tumor with chunky calcifications (*arrow*). Significant mass effect on the mesenteric vessels is seen (*arrowhead*).



■ Diagnosis

Hepatoblastoma

■ Discussion and Differential Diagnosis

Hepatoblastoma is the most common primary liver malignancy in children, with 90% presenting before 5 years of age.^{1,2} The cells resemble embryonic liver and histologically are broadly classified into two types: epithelial type and the mixed epithelial and mesenchymal type.² Abdominal distention is the most common presentation, with anorexia and weight loss being less common.² Alpha-fetoprotein (AFP) is abnormally elevated in almost 90% of cases and also can be reliably used in monitoring recurrence.^{2,3} Hepatoblastomas present as large solitary masses in 80% of cases and as multifocal masses in the remaining 20%.¹ These circumscribed masses are lobular and vary in size. The liver may be markedly enlarged, with most of the liver parenchyma replaced by tumor.¹ Calcification is present in more than half of hepatoblastomas.² Hepatoblastoma most commonly metastasizes to lungs. Less common organs of involvement include bone, brain, lymph nodes, eye, and ovary.² A survival rate of 80% can be achieved with preoperative chemotherapy followed by surgical excision.⁴ However inoperable cases may need total hepatectomy and liver transplantation.¹

The echogenicity of hepatoblastoma on ultrasound is variable. Hyperechoic regions with posterior acoustic shadowing indicative of calcification or bone can be present within the tumor.¹ Hepatoblastoma is characterized by low attenuation

and with peripheral and septal enhancement on CT, with associated calcifications and ossifications easily demonstrated.¹ Hepatoblastoma is predominantly T1 hypointense and T2 hyperintense with septal and peripheral enhancement on MRI.² Hepatobiliary MRI contrast agents are useful for demonstrating small satellite and recurrent lesions as well as delineating the relation of the tumor with the portal and hepatic veins.¹ **Fig. 82.1c** shows an abdomen MRI with hepatobiliary contrast administration in a 9-year-old boy with rising AFP following right hepatectomy for hepatoblastoma. There is enhancement of normal liver (*asterisk*), and a nonenhancement of recurrent hepatoblastoma (*arrow*).

Differential diagnosis of hepatoblastoma includes vascular lesions (hemangioendothelioma, infantile hepatic hemangioma), mesenchymal hamartoma, and hepatocellular carcinoma. Contrast pattern may be helpful in favoring vascular tumors over hepatoblastoma; dominant or infiltrating hepatic hemangiomas may have clinically evident skin lesions and signs of increased hepatic arterial flow. Mesenchymal hamartoma presents in children less than 2 years of age, but the cystic nature of the lesions and normal levels of AFP help differentiate it from hepatoblastoma. Hepatocellular carcinoma occurs in children older than 5 years of age, and usually there is a history of chronic liver disease.²

Pearls

- ◆ Hepatoblastomas occur with increased frequency in former premature newborns and very low birth weight infants.²
- ◆ Syndromes associated with hepatoblastoma include Beckwith-Wiedemann syndrome, familial adenomatous polyposis syndrome, Gardner syndrome, type 1 glycogen storage disease, and trisomy 18.^{1,2}

Pitfall

- ◆ Physiological AFP elevation is expected for several months after birth.

References

1. Hegde SV, Dillman JR, Lopez MJ, Strouse PJ. Imaging of multifocal liver lesions in children and adolescents. *Cancer Imaging* 2013;12:516–529 [PubMed](#)
2. Chung EM, Lattin GE Jr, Cube R, et al. From the archives of the AFIP: Pediatric liver masses: radiologic-pathologic correlation. Part 2. Malignant tumors. *Radiographics* 2011;31:483–507 [PubMed](#)
3. Rojas Y, Guillermin RP, Zhang W, Vasudevan SA, Nuchtern JG, Thompson PA. Relapse surveillance in AFP-positive hepatoblastoma: re-evaluating the role of imaging. *Pediatr Radiol* 2014;44:1275–1280 [PubMed](#)
4. Davies JQ, de la Hall PM, Kaschula ROC, et al. Hepatoblastoma—evolution of management and outcome and significance of histology of the resected tumor. A 31-year experience with 40 cases. *J Pediatr Surg* 2004;39:1321–1327 [PubMed](#)



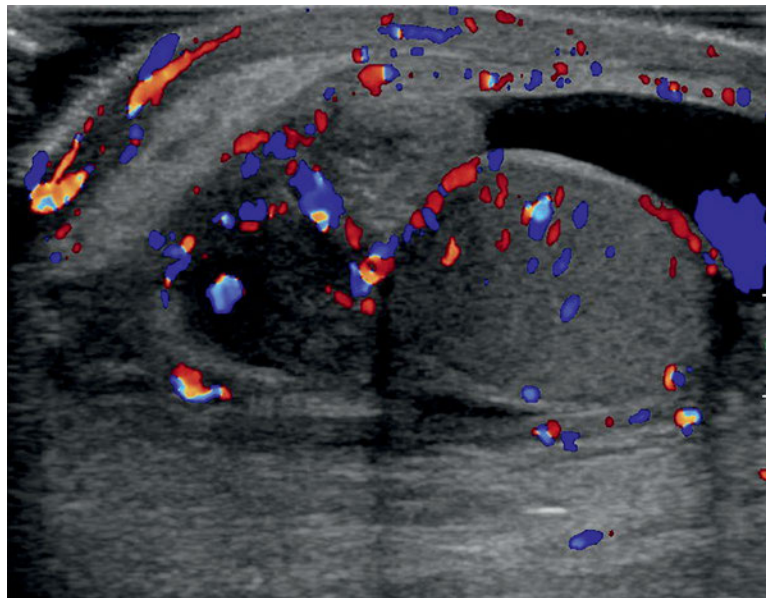
Genitourinary

Section Editors

Joanna J. Seibert and Leah E. Braswell

Authors

Leann E. Linam and Nadir Khan



Case 83

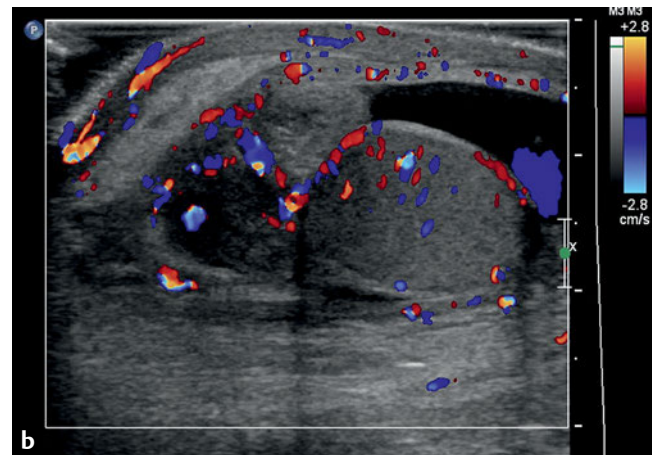
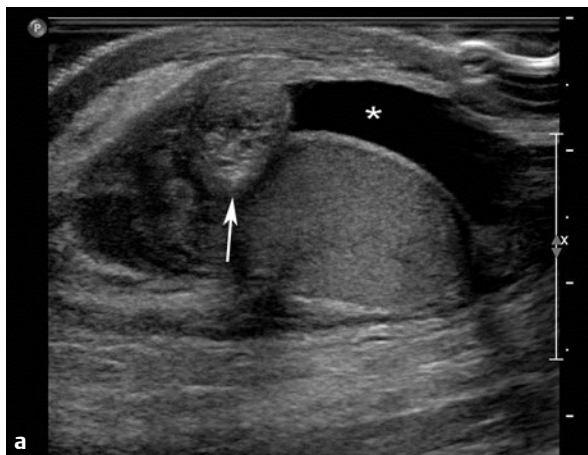
■ Clinical Presentation

A 13-year-old boy with acute right scrotal pain.

■ Radiographic Studies

Longitudinal gray-scale ultrasound image of the right testis (**Fig. 83.1a**) shows an enlarged, echogenic nodule located in the groove between the epididymis and the testis (*arrow*). There is a simple hydrocele (*asterisk*). Color flow ultrasound

image (**Fig. 83.1b**) shows that there is no flow to this nodule. Gray-scale ultrasound image of the same patient several days later (**Fig. 83.1c**) shows interval increase in echogenicity of the nodule (*arrow*) and increasing complexity of the hydrocele.



■ Diagnosis

Torsion of the Appendix Testis

■ Discussion and Differential Diagnosis

Torsion of the appendix testis is the most common cause of an acute scrotum in children,^{1,2} with a prevalence of 30 to 60%.^{1,3} The appendix testis is a remnant of the müllerian duct and is present in 80% of males.²⁻⁴ It is normally located in the groove between the head of the epididymis and the superior pole of the testis.^{3,4} The appendix epididymis is a wolffian duct remnant and is present in 25% of males.²⁻⁴ Patients typically present before puberty with acute onset of scrotal pain, usually less than 12 hours in duration. On physical exam, tenderness is usually localized to the superior pole of the testis, and the testis should be normal to palpation.⁴ The “blue dot” sign is due to the torsed appendix seen through the scrotal skin. This is specific for a torsed appendix, but only seen in the minority of patients.¹ Torsion of a testicular or epididymal appendage is self-limited; treatment is conservative, and symptoms gradually resolve in about a week.^{2,4}

Sonographically, a normal appendix testis is an oval structure, isoechoic to the epididymis, located between the testis and the head of the epididymis.³ The normal appendix epididymis is also isoechoic to the epididymis, and projects from the head of the epididymis.³ A torsed appendix testis enlarges to

> 5 mm and can be echogenic or heterogeneous with punctate areas of hyperechogenicity.¹⁻⁵ Lack of flow within the appendix is not specific, as flow can be hard to detect in a normal appendix.^{3,5} The adjacent epididymis, and occasionally the testis, can also be enlarged and hyperemic. A reactive hydrocele is not uncommon.

The differential diagnosis for acute scrotum in the absence of trauma in a child includes testicular torsion and epididymitis/epididymo-orchitis. Testicular torsion can be easily differentiated sonographically due to decreased testicular blood flow. Epididymitis/epididymo-orchitis presents more commonly after puberty and generally has a longer duration of symptoms, ranging from 24 to 72 hours.⁴ On ultrasound, the epididymis is enlarged and heterogeneous, most markedly at the head. There may be a reactive hydrocele and scrotal wall thickening. With color flow ultrasound imaging, the epididymis is hyperemic. Epididymitis may have bacterial, viral, or postinflammatory etiology. In a young child, it can be associated with congenital genitourinary anomalies. Ultrasound evaluation of the kidneys and bladder should be performed.¹

Pearls

- ◆ An echogenic nodule ≥ 5 mm in the groove between the epididymal head and the testis is highly specific for a torsed appendix testis.⁵
- ◆ The “blue-dot” sign is a specific clinical finding, but only seen 20% of the time.¹

Pitfall

- ◆ Sonographically, torsion of the appendix testis is very difficult to differentiate from epididymitis/epididymo-orchitis. Both have enlargement and hyperemia of the epididymis and/or testis. Patient age, duration of symptoms, and identification of the enlarged appendix testis is key to diagnosing a torsed appendix testis.

References

1. Baldisserotto M. Scrotal emergencies. *Pediatr Radiol* 2009;39:516–521. [PubMed](#)
2. Park SJ, Kim HL, Yi BH. Sonography of intrascrotal appendage torsion: varying echogenicity of the torsed appendage according to the time from onset. *J Ultrasound Med* 2011;30:1391–1396. [PubMed](#)
3. Baldisserotto M, de Souza JCK, Pertence AP, Dora MD. Color Doppler sonography of normal and torsed testicular appendages in children. *AJR Am J Roentgenol* 2005;184:1287–1292. [PubMed](#)
4. Munden MM, Trautwein LM. Scrotal pathology in pediatrics with sonographic imaging. *Curr Probl Diagn Radiol* 2000;29:185–205. [PubMed](#)
5. Yang DM, Lim JW, Kim JE, Kim JH, Cho H. Torsed appendix testis: gray scale and color Doppler sonographic findings compared with normal appendix testis. *J Ultrasound Med* 2005;24:87–91. [PubMed](#)

Case 84

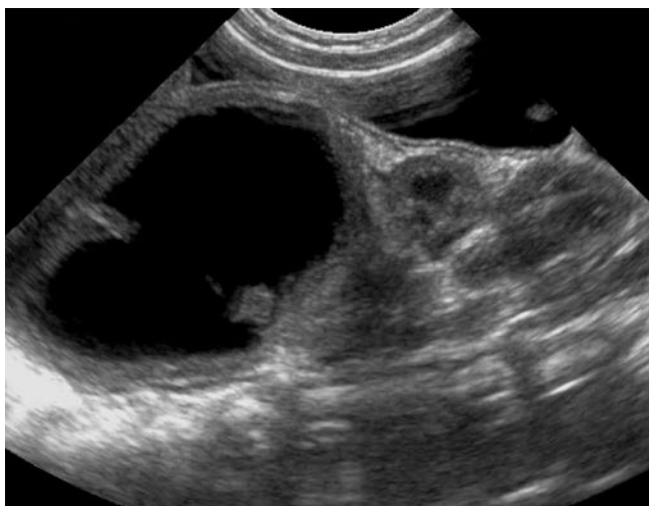
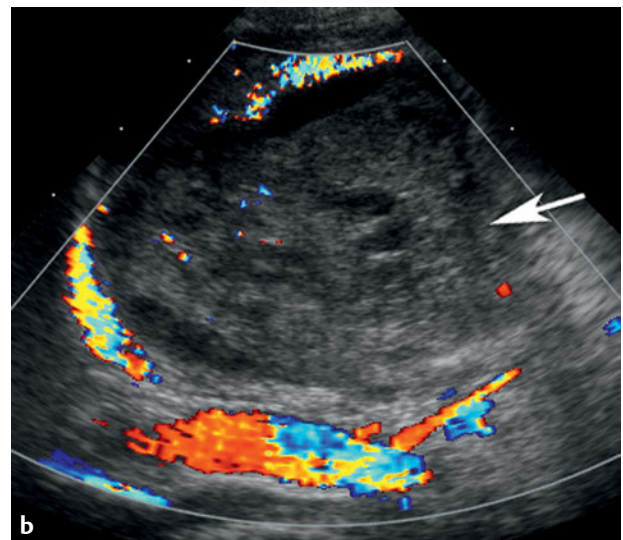
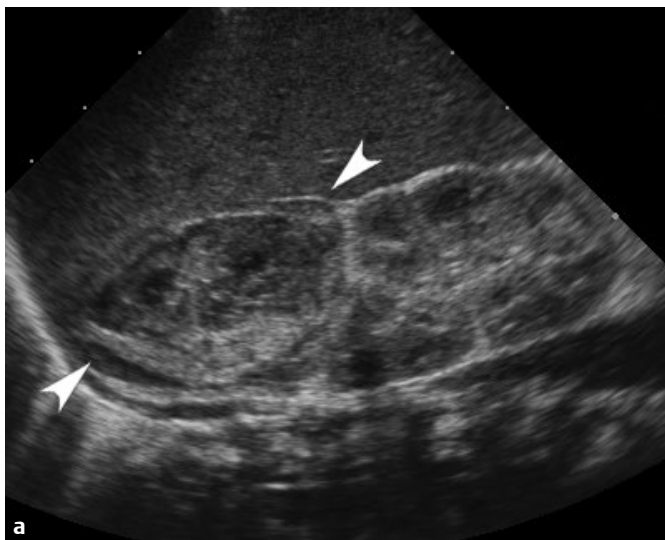
■ Clinical Presentation

A term newborn with emesis, abdominal distention, and anemia.

■ Radiographic Studies

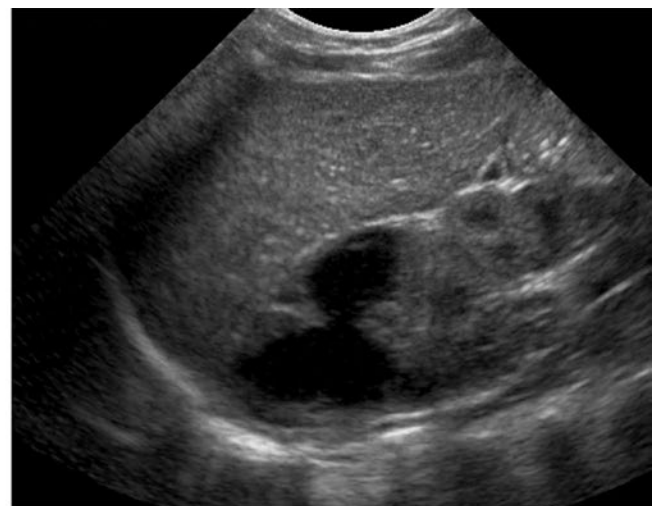
Longitudinal ultrasound image (**Fig. 84.1a**) shows a heterogeneous oval echogenic lesion superior to the right kidney (**arrowheads**). A similar echogenic oval lesion is seen superior to the left kidney (**Fig. 84.1b, arrow**) with no significant internal color flow vascularity. Serial ultrasound images of another

patient show decreasing size of a complex right suprarenal cystic lesion (**Fig. 84.1c**). A similar left suprarenal cystic lesion was noted in this patient; follow-up ultrasound at 6 weeks showed resolution of these bilateral suprarenal lesions.



c

Initial



1 week follow-up

■ Diagnosis

Adrenal Hemorrhage

■ Discussion and Differential Diagnosis

Adrenal hemorrhage can occur in the neonatal period and in older age groups. Incidence of neonatal adrenal hemorrhage ranges from 1.6 to 2.1 per 1,000 births and occurs more commonly in term infants and in male neonates.¹⁻³ Bilateral hemorrhage occurs in 10 to 15% of cases.^{1,2} Neonatal adrenal hemorrhage occurs in birth trauma, large-for-gestational-age infants, infants of diabetic mothers, prolonged labor, perinatal asphyxia, sepsis, hemorrhagic disorder, extracorporeal membrane oxygenation, and renal vein thrombosis.¹ Neonates with adrenal hemorrhage may be asymptomatic, with the lesion detected incidentally at sonography.^{3,4} Alternatively, a neonate may present acutely with fever, vomiting, jaundice, hypotension, anemia, and a palpable flank mass.^{3,4}

Adrenal hemorrhage occurs more frequently in the right adrenal gland, which is thought to be more vulnerable, as it is compressed between the liver, kidney, and the spine. The increased frequency may also be due to the fact that the right venous drainage is directly into the inferior vena cava (IVC), which when compressed causes a rise in the intra-adrenal venous pressure.⁴ Adrenal hemorrhage may be secondary to renal vein thrombosis, particularly on the left side.³ This association relates to the left adrenal vein anatomy, which drains into the left renal vein.⁵

Traumatic adrenal hemorrhage is observed in older children after blunt abdominal injury.³ Many mechanisms have been postulated to explain adrenal hemorrhage in trauma, including direct trauma and compression of the gland between the spine and liver, shearing of small vessels that perforate the adrenal capsule because of deceleration forces, and a short-term rise in intra-adrenal venous pressure due to compression of the IVC.⁶

Ultrasound is the preferred modality for initial detection and follow-up of adrenal hemorrhage because it is portable, rapid, sensitive, and lacks ionizing radiation. Initially the hemorrhage appears as a solid echogenic mass superior to the kidney; the lesion decreases in size and echogenicity over time. The primary differential diagnosis of an echogenic adrenal mass in a neonate is neuroblastoma, which will have branching color flow vascularity within the mass on Doppler. Eventually an adrenal hemorrhage will liquefy and become cystic and multiloculated; the lesion completely resolves within 4 to 16 weeks.¹ Peripheral calcifications can develop and may be seen incidentally on plain abdominal radiographs and CT.^{1,3}

Computed tomography shows an oval or triangular adrenal hematoma that is of moderate to high attenuation on noncontrast CT and relatively lower in attenuation compared with the enhancing liver and spleen on postcontrast CT.⁴ Associated CT findings include periadrenal fat stranding and thickening of the ipsilateral diaphragmatic crus.⁴ Adrenal hemorrhage is reported in 3% of children following blunt abdominal trauma and is associated with a high frequency of ipsilateral intra-abdominal and intrathoracic injuries.⁶ Adrenal hemorrhage in nonaccidental injury indicates the use of a severe force to injure the child and has been reported to occur in 10% of deaths.⁷

Magnetic resonance imaging is particularly useful to distinguish between adrenal hemorrhage and other causes of a cystic adrenal mass on ultrasound. Most importantly, MRI helps differentiate adrenal hemorrhage from cystic neuroblastoma in a neonate. Other differential diagnoses of adrenal hemorrhage include adrenal abscess, cortical renal cyst, obstructed calyceal diverticulum, and an obstructed upper moiety collecting system in a duplicated kidney.¹

Pearls

- ◆ Serial ultrasound is an acceptable method to differentiate neuroblastoma from adrenal hemorrhage. Hemorrhage will decrease in size, whereas neuroblastoma will remain stable or increase in size.
- ◆ Adrenal hemorrhage occurs more commonly in the right adrenal gland.
- ◆ With right adrenal hemorrhage, always look carefully for a clot in the adjacent IVC. With left adrenal hemorrhage, look carefully for left renal vein thrombosis.

Pitfall

- ◆ Hemorrhage into a congenital neuroblastoma may make differentiation between adrenal hemorrhage and neuroblastoma very difficult. Metaiodobenzylguanidine (MIBG) scintigraphy and urinary catecholamines may help distinguish these two entities but may be equivocal in the newborn.

References

1. Mutlu M, Karag zel G, Aslan Y, Cansu A, Okten A. Adrenal hemorrhage in newborns: a retrospective study. *World J Pediatr* 2011;7:355-357 [PubMed](#)
2. Demirel N, Bař AY, Zenciroglu A, Tařci-Yildiz Y. Adrenal bleeding in neonates: report of 37 cases. *Turk J Pediatr* 2011;53:43-47 [PubMed](#)
3. Westra SJ, Zaninovic AC, Hall TR, Kangaroo H, Boechat MI. Imaging of the adrenal gland in children. *Radiographics* 1994;14:1323-1340 [PubMed](#)
4. Paterson A. Adrenal pathology in childhood: a spectrum of disease. *Eur Radiol* 2002;12:2491-2508 [PubMed](#)
5. Orazi C, Fariello G, Malena S, Schingo P, Ferro F, Bagolan P. Renal vein thrombosis and adrenal hemorrhage in the newborn: ultrasound evaluation of 4 cases. *J Clin Ultrasound* 1993;21:163-169 [PubMed](#)
6. Sivit CJ, Ingram JD, Taylor GA, Bulas DI, Kushner DC, Eichelberger MR. Posttraumatic adrenal hemorrhage in children: CT findings in 34 patients. *AJR Am J Roentgenol* 1992;158:1299-1302 [PubMed](#)
7. deRoux SJ, Prendergast NC. Adrenal lacerations in child abuse: a marker of severe trauma. *Pediatr Surg Int* 2000;16:121-123 [PubMed](#)

Case 85

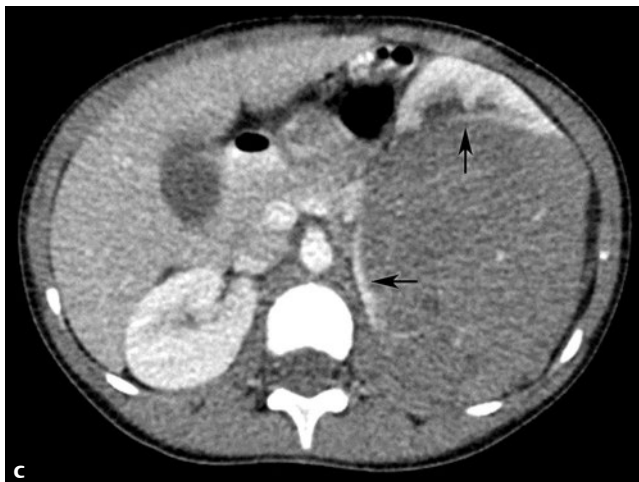
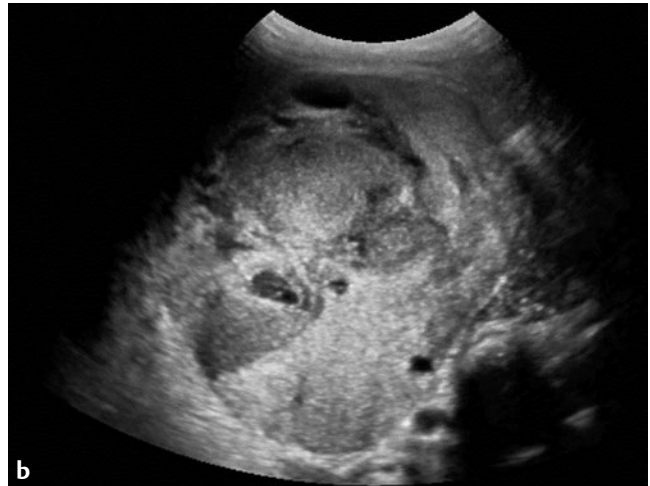
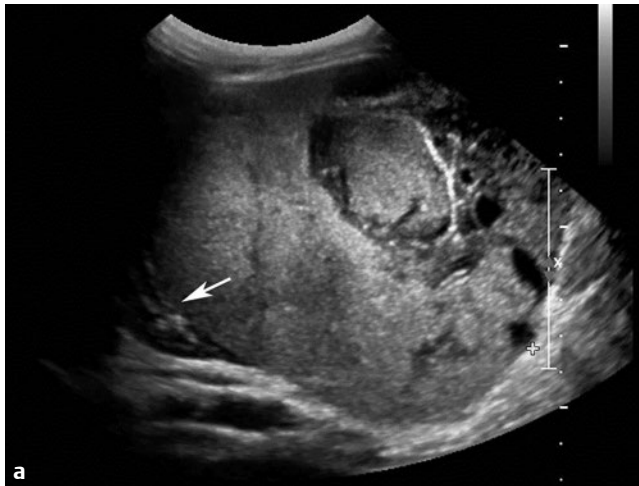
■ Clinical Presentation

A 2-year-old with abdominal mass.

■ Radiographic Studies

Longitudinal and transverse ultrasound images (**Fig. 85.1a,b**) show a large, heterogeneous, predominantly echogenic mass infiltrating much of the kidney. Echogenic renal fat and normal-appearing kidney can be seen draped over the renal mass (**Fig. 85.1a**, arrow). Postcontrast CT image (**Fig. 85.1c**) shows a

well-demarcated mass of renal origin, with functioning renal parenchyma displaced medially and anteriorly (arrows, “claw sign”). Postcontrast coronal reformatted CT image (**Fig. 85.1d**) shows significant low density within the mass (asterisk) related to necrosis or hemorrhage.



■ Diagnosis

Wilms' Tumor

■ Discussion and Differential Diagnosis

Wilms' tumor is the most common pediatric malignant renal tumor and represents 8% of all childhood malignancies. The most common presentation is an asymptomatic abdominal mass. Peak incidence occurs at 3 to 4 years of age, and 4 to 13% are bilateral. Associated anomalies include aniridia, hemihypertrophy, cryptorchidism, and hypospadias.¹

Ultrasound is the screening modality of choice showing a heterogeneous intrarenal echogenic mass displacing or splaying the collecting system. Doppler sonography is very useful in demonstrating tumor extension into the renal vein and inferior vena cava. CT is useful for defining the organ of origin, detecting nodal metastases, and identifying tumor thrombus. Tumor thrombus may extend into the renal vein, the inferior vena cava, and the right atrium, occasionally causing inferior vena caval obstruction and pulmonary tumor emboli.²

Search for bilateral Wilms' tumor and consideration of nephroblastomatosis is imperative. Nephroblastomatosis in-

cludes rests of nephrogenic tissue or renal blastoma that resemble Wilms' tumor microscopically but lack mitosis.³ Nephroblastomatosis complex usually presents as a solid oval lesion, generally in a subcapsular location. Follow-up imaging is required because nephroblastomatosis is a precursor of Wilms' tumor.

Wilms' tumor must be distinguished from neuroblastoma, an extrarenal tumor, which involves adjacent lymph nodes, encases vascular structures, and may extend across the midline.³ Mesoblastic nephroma, a neonatal renal mass, is distinguished by earlier clinical presentation but is indistinguishable from Wilms' tumor on ultrasound and CT. Renal cell carcinoma is a nonspecific solid renal mass indistinguishable on ultrasound from Wilms' tumor, but usually occurs in older patients. Multilocular cystic nephroma, a complex cystic lesion, is difficult to distinguish from the atypical cystic Wilms' except by pathological exam.

Pearls

- ◆ Familial Wilms' tumor accounts for 1% of cases; genetic association is seen in Wilms' tumor occurring with syndromes such as Beckwith-Wiedemann or the WAGR syndrome (Wilms' tumor, aniridia, genitourinary anomalies, and mental retardation).²
- ◆ Left renal vein tumor thrombus may obstruct the left gonadal vein, causing a varicocele, a rare initial presentation of Wilms' tumor.⁴
- ◆ If a right atrial tumor thrombus is identified, cardiopulmonary bypass may be necessary at the time of tumor resection.⁴

Pitfall

- ◆ The combination of renal mass with brain lesion favors rhabdoid tumor over Wilms' tumor.

References

1. Green DM, D'Angio GJ, Beckwith JB, et al. Wilms tumor. *CA Cancer J Clin* 1996;46:46–63 [PubMed](#)
2. Lowe LH, Isuani BH, Heller RM, et al. Pediatric renal masses: Wilms tumor and beyond. *Radiographics* 2000;20:1585–1603 [PubMed](#)
3. White KS, Grossman H. Wilms' and associated renal tumors of childhood. *Pediatr Radiol* 1991;21:81–88 [PubMed](#)
4. Swinson S, McHugh K. Urogenital tumours in childhood. *Cancer Imaging* 2011;11(Spec. No. A):S48–S64 [PubMed](#)

Case 86

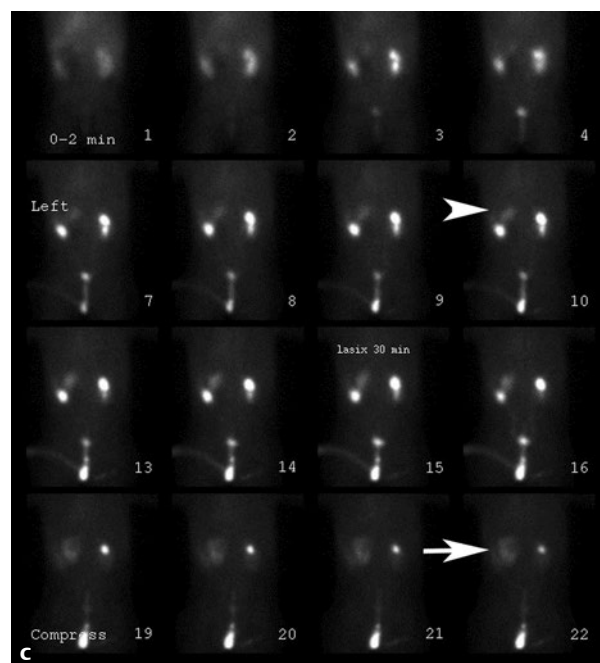
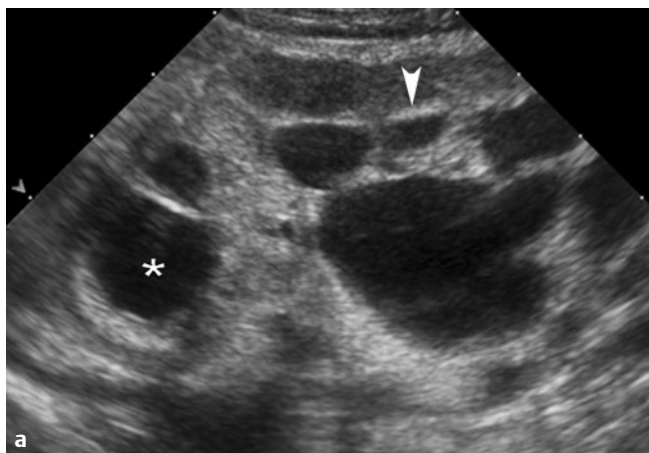
Clinical Presentation

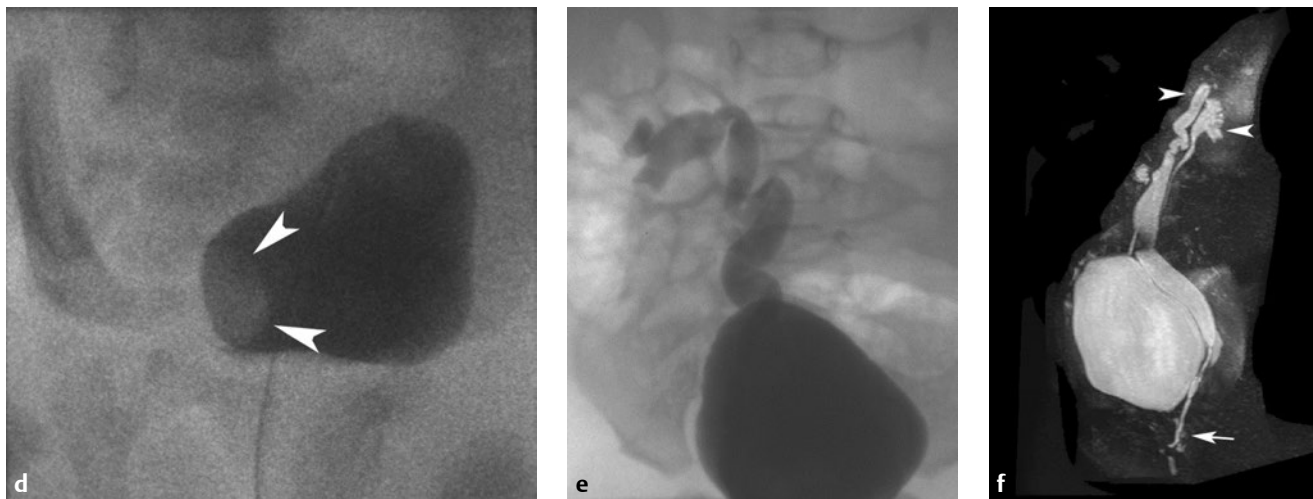
A 5-month-old infant with vomiting, fever, and urinary tract infection.

Radiographic Studies

Longitudinal ultrasound image of the right kidney (**Fig. 86.1a**) shows dilated pelvicaliceal systems separated by renal parenchyma into lower pole (*arrowhead*) and upper pole (*asterisk*) moieties. Increased echogenicity of the upper pole moiety renal parenchyma is noted. Longitudinal pelvic ultrasound image (**Fig. 86.1b**) shows a dilated upper pole moiety ureter (*arrowheads*) terminating in a cystic ureterocele in the bladder

(*arrow*). A dilated lower pole moiety ureter is also seen (*asterisk*). Nuclear medicine renogram in a different patient, a 1-year-old girl with left hydronephrosis (**Fig. 86.1c**), shows delayed excretion from the left upper pole moiety collecting system (*arrowhead*) with subsequent delayed Lasix washout of tracer (*arrow*) compatible with upper pole moiety obstruction.





■ Diagnosis

Collecting System Duplication/Ectopic Ureter/Ureterocele

■ Discussion and Differential Diagnosis

A duplicated urinary collecting system is the most common anomaly of the urinary tract.¹ With incomplete duplication, the two pelvicaliceal systems may join at the level of renal pelvis (bifid pelvis) or may drain into separate ureters that will join at any level before draining into the urinary bladder.^{1,2} With complete duplication, the two pelvicaliceal systems drain into separate ureters that do not join at any level; each enters the urinary bladder separately.^{1,2} The lower pole moiety ureter joins the urinary bladder at the normal position on the trigone.² The ureter arising from the upper pole moiety drains into an abnormal location more inferiorly and is referred to as ectopic ureter.² Sometimes this ectopic insertion is into the prostatic urethra in males or vagina in females. These patients present with urinary dribbling. Girls are affected about twice as often as boys.¹

Collecting system duplication may go undiagnosed into adulthood. Clinical significance arises when it is complicated by ureteral ectopia, vesicoureteral reflux (VUR), urinary tract infection, or ureteropelvic junction (UPJ) obstruction. VUR is the most commonly detected association, and it is more common with complete than incomplete duplication.² The incidence of ectopic ureterocele is 20%.¹ Ureterocele is dilatation of the intravesical component of the upper pole ureter. It is usually associated with obstructive dilatation of the associated ureter/calices.

Ultrasound demonstrates a prominent segment of renal cortex between the two duplicated intrarenal collecting systems.² The upper pole moiety and its ureter may be dilated and tor-

tuous on ultrasound secondary to obstruction at the insertion into the bladder. The lower pole moiety may also be dilated secondary to vesicoureteral reflux or UPJ obstruction.^{2,3} Ureterocele on ultrasound appears as a round intraluminal fluid-filled structure.² Ureterocele on voiding cystourethrogram (VCUG) appears as a round filling defect in the expected location of the ureteral orifice (**Fig. 86.1d**, *arrowheads*). VCUG is performed to document the presence and severity of reflux. Higher grades of reflux correspond with higher rates of urinary tract infection.² The classic VCUG appearance of reflux is the inferior displacement of a contrast-filled lower pole calyx by an obstructed and enlarged upper pole moiety, the so-called drooping lily sign (**Fig. 86.1e**).

More recent advances have made CT urography and magnetic resonance (MR) urography useful in children.³ The excretory phase of a CT urogram protocol can be performed to answer a specific question when a congenital anomaly is suspected.³ MR urography is superior to CT in that it provides better tissue contrast resolution and does not utilize ionizing radiation. This is especially favored in children, particularly those who may need repeated examinations.³ Both anatomic and functional information about the urinary tract can be obtained in a single examination, potentially eliminating the need for nuclear scintigraphy.³ **Fig. 86.1f** is an oblique MR urography image in a 5-year-old girl with constant wetting and shows duplicated collecting systems (*arrowheads*) and ectopic insertion of the upper pole moiety ureter (*arrow*) into the vagina.

Pearls

- ◆ Weigert-Meyer rule: In complete duplication, the upper pole moiety ureter almost always inserts in an ectopic location into the bladder medially and inferiorly to the lower pole moiety ureter (which inserts in the normal location in the trigone of bladder).
- ◆ The ectopic upper pole moiety ureter is more prone to obstruction; the lower pole moiety ureter is more prone to vesicoureteral reflux.

Pitfall

- ◆ Voiding cystourethrogram should be performed with small amounts of dilute contrast to search for ureterocele early in the filling phase of the exam. Dense contrast or a completely filled bladder may completely obscure the ureterocele.

References

1. Siomou E, Papadopoulou F, Kollios KD, et al. Duplex collecting system diagnosed during the first 6 years of life after a first urinary tract infection: a study of 63 children. *J Urol* 2006;175:678–681, discussion 681–682. [PubMed](#)
2. Fernbach SK, Feinstein KA, Spencer K, Lindstrom CA. Ureteral duplication and its complications. *Radiographics* 1997;17:109–127. [PubMed](#)
3. Silverman SG, Leyendecker JR, Amis ES Jr. What is the current role of CT urography and MR urography in the evaluation of the urinary tract? *Radiology* 2009;250:309–323. [PubMed](#)

Case 87

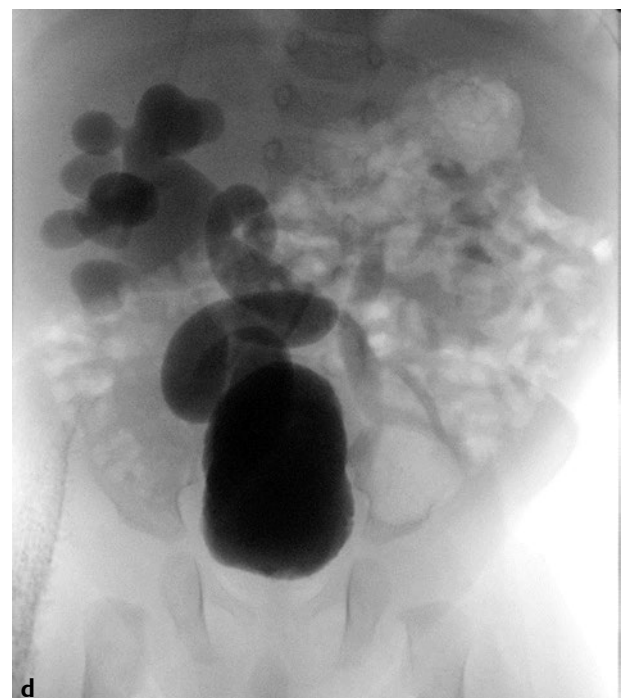
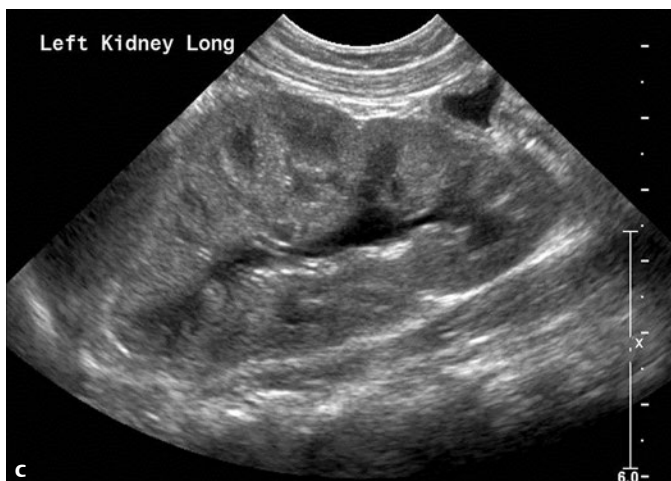
■ Clinical Presentation

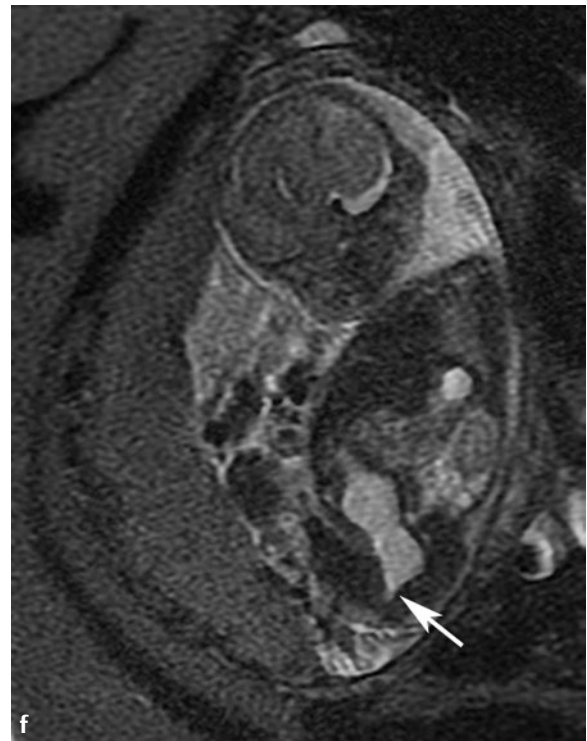
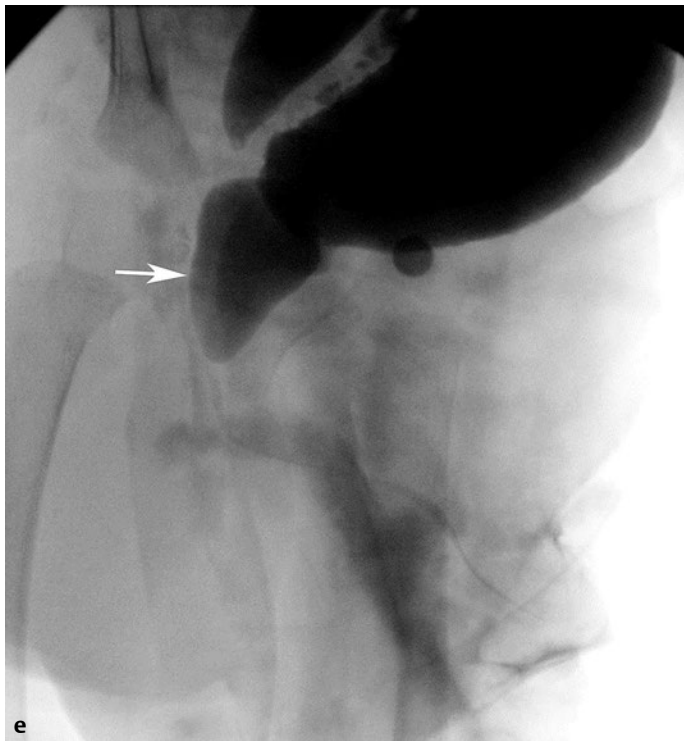
Male neonate with obstructive urinary symptoms.

■ Radiographic Studies

Ultrasound image of the bladder (**Fig. 87.1a**) shows mild bladder wall thickening and a distended bladder. Dilated ureter is seen posterior to the bladder (*arrow*). Longitudinal ultrasound images of the kidneys (**Fig. 87.1b,c**) show mildly echogenic kidneys bilaterally (right worse than left). There is grade 4 hydronephrosis on the right and grade 1 hydronephrosis on the

left. AP image from a VCUG (**Fig. 87.1d**) shows bilateral vesico-ureteral reflux, right grade 4 and left grade 2. Oblique voiding image from VCUG (**Fig. 87.1e**) shows a dilated posterior urethra (*arrow*) with a nondilated anterior urethra. Sagittal prenatal MRI in another patient (**Fig. 87.1f**) shows a thick-walled distended bladder. The posterior urethra is dilated (*arrow*).





■ Diagnosis

Posterior Urethral Valves

■ Discussion and Differential Diagnosis

Posterior urethral valves (PUVs) are the most common cause of lower urinary tract obstruction in males. Despite the rarity, PUVs are an important cause of end-stage renal disease, accounting for almost 17% of children with renal failure.¹ The most common clinical presentation of PUV is detection of hydronephrosis on routine prenatal sonography.¹ Concurrent ultrasound findings of dilated bladder, dilated posterior urethra, and oligohydramnios in a male fetus confirm the diagnosis. If not prenatally detected, a neonate with PUV may present with abdominal mass (due to hydronephrosis or distended bladder), urinary ascites, or respiratory distress. An older child may present with urinary tract infections, failure to thrive, or urinary insufficiency.^{1,2} PUVs cause urine outflow obstruction with secondary bladder wall hypertrophy and trabeculation. Massive hydronephrosis is common, secondary to either vesicoureteral reflux or obstruction. In either case, renal dysplasia is common with chronic renal failure and end-stage renal disease. Even after ablation of the valves, hydronephrosis may persist secondary to a hypertrophied noncompliant bladder.³ Persistent reflux after valve ablation can be due to ureteral dysplasia, peristaltic failure from ureteral fibrosis, or decreased peristaltic force in a dilated tortuous ureter.⁴

Definitive postnatal diagnosis of PUVs is usually made with a voiding cystourethrogram, which delineates the urethral obstruction and searches for vesicoureteral reflux. Findings

suggesting good prognosis are unilateral high-grade reflux, perinephric urinomas, and urinary ascites; these are believed to represent a pressure “pop-off,” helping to preserve renal function.² Renal ultrasound may demonstrate hydronephrosis and hydroureter from obstruction or reflux, a thickened bladder wall, and a dilated posterior urethra (keyhole appearance). Rarely one can see a linear echogenic structure within it, representing the posterior urethral valve membrane.^{2,5} Transperineal ultrasound delineating the linear echogenic structure representing the valves within the urethra helps differentiate patients with PUVs from patients with urethral strictures.⁵ Other findings are echogenic kidneys and renal cysts, indicating renal dysplasia.² Nuclear medicine studies may be useful in assessing renal function and the degree of residual obstruction after valve ablation.

The differential diagnosis includes bilateral ureteropelvic junction obstruction or bilateral ureterovesical obstruction; these patients usually have a normal bladder. There are many normal variants to the appearance of the male urethra, and nonobstructed urethral ectasia or kinking should not be confused with PUVs.³ Prune-belly syndrome is indistinguishable from PUVs in utero, but, at birth, the deficiency of abdominal musculature confirms the diagnosis of prune-belly syndrome. The urethra in prune-belly syndrome may be dilated but is not elongated.

Pearls

- ◆ Transient hydronephrosis of the newborn may be a normal variant seen on prenatal ultrasound and may resolve spontaneously.³
- ◆ Of patients with PUVs, 50% have vesicoureteral reflux at presentation; 50% of these patients have bilateral reflux.
- ◆ A male newborn who presents with isolated ascites most likely has PUVs.

Pitfall

- ◆ Urethral strictures can be confused with PUVs, but strictures are usually irregular in outline and in a different location. Urethral strictures are inflammatory, congenital, traumatic, or iatrogenic in origin.³

■ Controversies

- In older children, primary valve ablation through a trans-urethral approach is usually the treatment of choice. If hydronephrosis persists and renal function worsens, upper tract diversion may be necessary.¹ Many of these patients go on to renal transplant.
- If the urethra is too small to accommodate the urethroscope/cystoscope, temporary urinary diversion with vesicostomy

may be necessary until the urethra grows larger and the patient is more stable.¹

- Selected cases may undergo antenatal treatment to prevent pulmonary hypoplasia and preserve renal function. Vesicoamniotic shunts and fetal cystoscopic valve ablation have been reported.⁶

References

1. Hodges SJ, Patel B, McLorie G, Atala A. Posterior urethral valves. *Scientific WorldJournal* 2009;9:1119–1126 [PubMed](#)
2. Perks AE, MacNeily AE, Blair GK. Posterior urethral valves. *J Pediatr Surg* 2002;37:1105–1107 [PubMed](#)
3. Macpherson RI, Leithiser RE, Gordon L, Turner WR. Posterior urethral valves: an update and review. *Radiographics* 1986;6:753–791 [PubMed](#)
4. Lal R, Bhatnagar V, Mitra DK. Upper-tract changes after treatment of posterior urethral valves. *Pediatr Surg Int* 1998;13:396–399 [PubMed](#)
5. Cohen HL, Zinn HL, Patel A, Zinn DL, Haller JO. Prenatal sonographic diagnosis of posterior urethral valves: identification of valves and thickening of the posterior urethral wall. *J Clin Ultrasound* 1998;26:366–370 [PubMed](#)
6. Chauvin NA, Epelman M, Victoria T, Johnson AM. Complex genitourinary abnormalities on fetal MRI: imaging findings and approach to diagnosis. *AJR Am J Roentgenol* 2012;199:W222–31 [PubMed](#)

Case 88

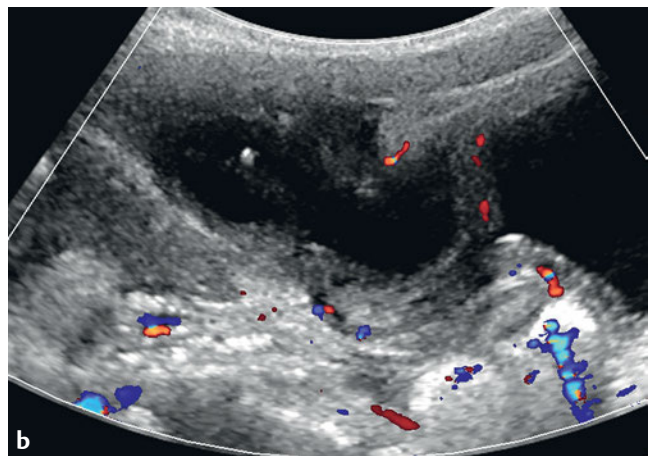
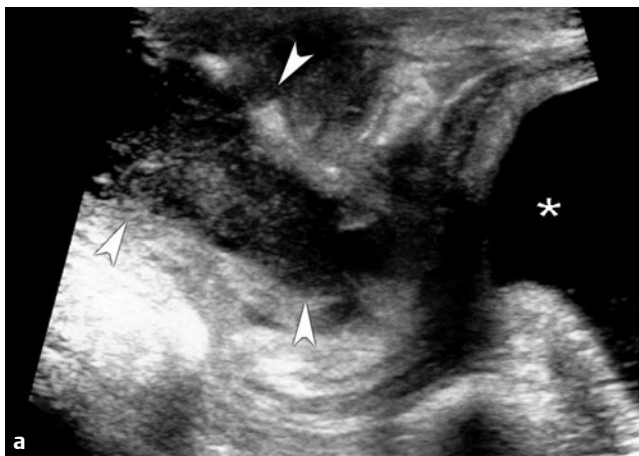
■ Clinical Presentation

A 4-year-old boy with fever, abdominal pain, midline hypogastric mass, and urinary frequency.

■ Radiographic Studies

Longitudinal pelvic ultrasound image (**Fig. 88.1a**) shows a complex oval lesion (*arrowheads*) with mixed internal echogenic debris. The lesion abuts the bladder dome (*asterisk*). The

thickened cyst wall is hyperemic on color flow imaging (**Fig. 88.1b**). An associated tract extending to the umbilicus is seen (**Fig. 88.1c, arrowheads**).



■ Diagnosis

Urachal Anomalies

■ Discussion and Differential Diagnosis

The urachus is the embryonic remnant of the allantois and the cloaca that lies in the midline between the transverse fascia and the peritoneum.^{1,2} In the fetus, the urachus joins the bladder dome to the umbilicus, but the lumen obliterates at between 4 and 5 months of gestation as the bladder descends into the pelvis.¹⁻⁴ The fibrous remnant forms the median umbilical ligament.

Urachal anomalies are classified into four subgroups. A completely patent urachus is secondary to failure of obliteration of the urachal channel in the fetus and represents 16% of urachal anomalies.³ A patent urachus frequently presents in the newborn with urine leakage at the umbilicus.² About one third of these patients have an associated bladder outlet obstruction such as posterior urethral valves or urethral atresia.² Diagnosis can be made with umbilical orifice contrast injection to show communication to the bladder.^{1,2} Ultrasound often demonstrates a fluid-containing channel between the dome of the bladder and the umbilicus. Voiding cystourethrography (VCUG) shows contrast filling of the patent channel with drainage at the umbilicus.

The second subgroup of urachal anomalies includes patients with a blind-ending urachal sinus tract that opens into the umbilicus and comprises 37% of urachal anomalies. Symptoms may occur at any age and are usually secondary to infected discharge from the sinus.² The diagnosis is usually made by contrast injection into the sinus orifice at the umbilicus.¹ Ultrasound may show a thickened tubular structure below the umbilicus in the midline.²

The third subgroup of urachal anomalies includes patients with the rare urachal diverticulum, which is a cystic structure

connecting with the anterior-superior aspect of the bladder.² Diverticula are usually detected incidentally on ultrasound or CT for unrelated reasons.² They can be associated with or complicated by infection, stone formation, or increased risk of carcinoma in teenage.

The most common subgroup of urachal anomalies is the urachal cyst, which accounts for 45% of reported urachal anomalies.^{3,4} The cysts form within the isolated urachal channel, and the lumen enlarges over time secondary to desquamated or degenerative tissue.² Urachal cysts are usually asymptomatic, but can become symptomatic when they enlarge or become infected. If direct communication with the bladder occurs, infection is common. Complications include rupture of the infected cysts into the preperitoneal tissues and rupture into the intraperitoneal tissues with secondary peritonitis.² On ultrasound or CT imaging, the urachal cyst is seen as a fluid-filled structure in the midline below the umbilicus, just deep to the rectus muscle. When infected, complicated fluid, cyst wall thickening, and surrounding inflammatory changes are seen.²

Urachal neoplasms, such as fibromas, fibroadenomas, fibromyomas, and hamartomas, are extremely rare in children and are usually benign.² Urachal carcinoma usually occurs in patients 40 to 70 years of age and is predominantly adenocarcinoma.²

The differential diagnosis of urachal cyst includes ovarian cyst and mesenteric cyst. Differentiation can usually be made based on location/configuration of the anomaly combined with imaging. The differential diagnosis for symptomatic urachal anomalies includes appendicitis, omphalitis, and inflamed umbilical stump.³

Pearls

- ◆ A patent urachal anomaly should be suspected if there is a history of umbilical cord cyst, edematous umbilical cord, delayed sloughing of the umbilical cord, or umbilical soft tissue protrusion.⁵
- ◆ Analysis of the umbilical drainage fluid for blood urea nitrogen (BUN) and creatinine may confirm the diagnosis of a patent urachal anomaly.

Pitfall

- ◆ An ovarian cyst on a long stalk may mimic an urachal cyst, and final diagnosis may depend on surgical pathology.

■ Controversy

- Traditional thought has held that urachal remnants should uniformly be surgically resected due to the risk of recurrent infection and the small risk of urachal carcinoma. However, recent studies have shown that asymptomatic urachal remnants often spontaneously resolve in children younger than 1 year of age.⁶ Infected urachal remnants may be

treated with drainage and antibiotics and followed with clinical examination and serial ultrasound for resolution.⁴ If the urachal remnant does not resolve after 6 months of age or if symptoms persist, then operative management should be considered.⁴

References

1. Cappele O, Sibert L, Descargues J, Delmas V, Grise P. A study of the anatomic features of the duct of the urachus. *Surg Radiol Anat* 2001;23:229–235. [PubMed](#)
2. Yu J-S, Kim KW, Lee H-J, Lee Y-J, Yoon C-S, Kim M-J. Urachal remnant diseases: spectrum of CT and US findings. *Radiographics* 2001;21:451–461. [PubMed](#)
3. Yiee JH, Garcia N, Baker LA, Barber R, Snodgrass WT, Wilcox DT. A diagnostic algorithm for urachal anomalies. *J Pediatr Urol* 2007;3:500–504. [PubMed](#)
4. Galati V, Donovan B, Ramji F, Campbell J, Kropp BP, Frimberger D. Management of urachal remnants in early childhood. *J Urol* 2008;180(4, Suppl): 1824–1826, discussion 1827. [PubMed](#)
5. Frazier HA, Guerrieri JP, Thomas RL, Christenson PJ. The detection of a patent urachus and allantoic cyst of the umbilical cord on prenatal ultrasonography. *J Ultrasound Med* 1992;11:117–120. [PubMed](#)
6. Ueno T, Hashimoto H, Yokoyama H, Ito M, Kouda K, Kanamaru H. Urachal anomalies: ultrasonography and management. *J Pediatr Surg* 2003;38: 1203–1207. [PubMed](#)

Case 89

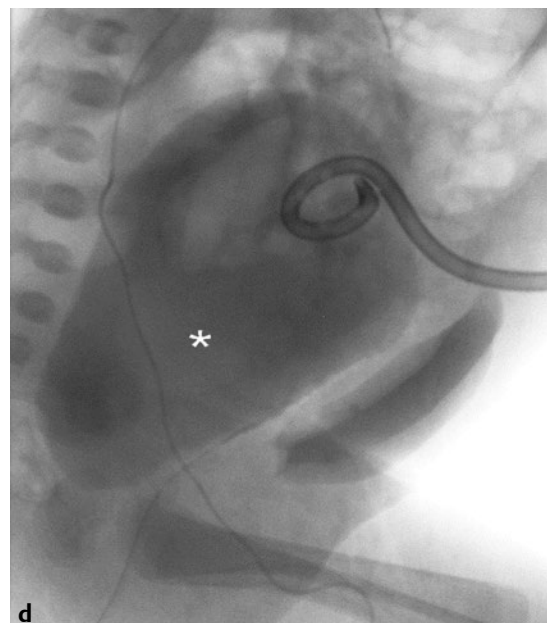
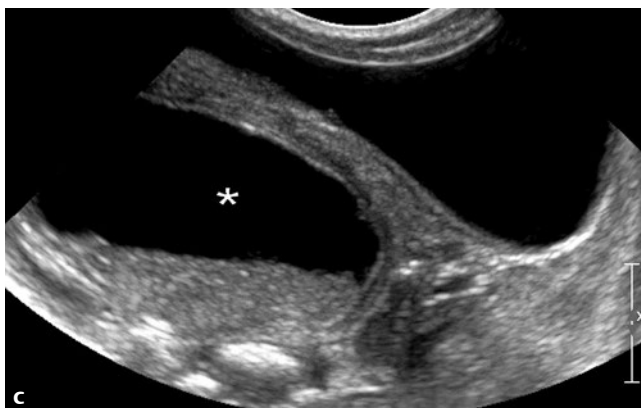
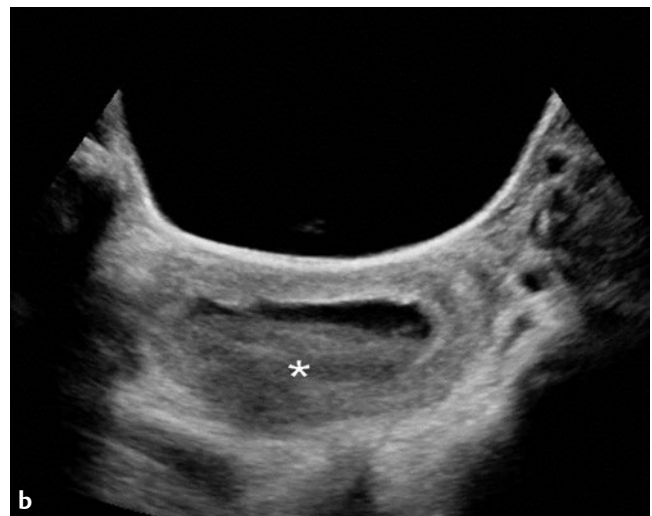
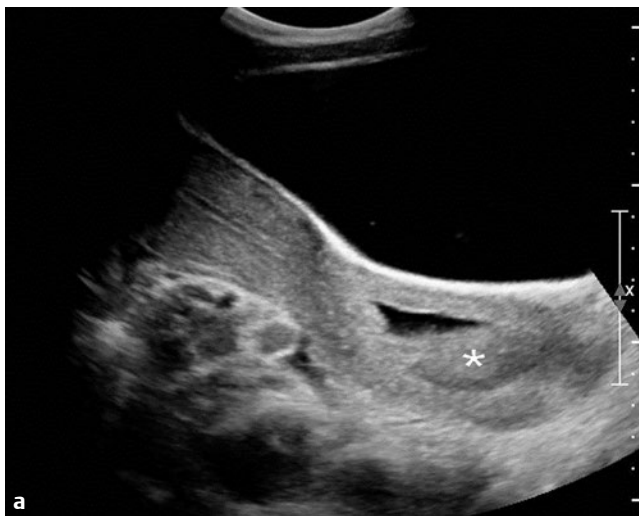
■ Clinical Presentation

A 16-year-old girl with crampy abdominal pain and delayed onset of menses.

■ Radiographic Studies

Longitudinal and transverse ultrasound images of the pelvis (**Fig. 89.1a,b**) show fluid and echogenic debris within the vagina (*asterisk*). Ultrasound image from a different patient, a newborn (**Fig. 89.1c**), shows an oval cystic pelvic structure (*asterisk*) with layering internal debris. Mass effect on the pos-

terior aspect of the bladder is noted. Fluoroscopic contrast study (**Fig. 89.1d**) demonstrates communication between the dilated vagina (*asterisk*) and bladder in the same patient as in **Fig. 89.1c**. This newborn patient had cloacal malformation.



■ Diagnosis

Hydrocolpos

■ Discussion and Differential Diagnosis

Hydrocolpos is the term for a dilated, fluid-filled vagina, typically resulting from a congenital vaginal obstruction.¹ Hydrometrocolpos is present if there is dilatation of the uterus as well as the vagina. In most cases, the obstruction is secondary to an imperforate hymen, and simple lysis of the hymen provides resolution of the problem.^{2,3} In more complex forms, vaginal atresia or stenosis is the cause of the obstruction. These patients may have other complicated congenital anomalies, including anorectal malformation, cloacal anomalies, a common urogenital sinus, duplicated/septated uterus or vagina, rectovaginal fistula, and renal anomalies with hydronephrosis.^{4–6} These conditions are obviously more complicated, and correction of hydrocolpos or hydrometrocolpos must be coordinated with correction of the other complex anomalies. At the time of diagnosis, it is important to evaluate the upper urinary tract for obstruction. Hydronephrosis and hydroureter may be present due to compression of the distal ureters and subsequent obstruction by the large pelvic mass.⁵

The typical patient is a female newborn with a palpable pelvic/abdominal mass. Diagnosis of more complex anomalies is often made prenatally. With simple imperforate hymen, diagnosis may be delayed, and the patient may present at puberty, when there is an increased accumulation of menstrual blood and secretions causing uterine and vaginal distention.³ The differential diagnosis includes ovarian cysts, mesenteric cysts, duplication cysts, anterior meningoceles, and sacrococcygeal teratomas.^{3,6} In patients with ovarian cysts and mesenteric cysts, the uterus and vagina are usually identified by ultrasound but may be difficult to visualize because of severe compression or displacement. Ultrasound of patients with anterior meningocele and sacrococcygeal teratomas usually shows that the masses are related to the sacrum or distal neural canal. In patients whose diagnosis is uncertain, or if further delineation of adjacent structures is necessary, an MRI of the pelvis may prove helpful.

Pearls

- ◆ In isolated vaginal outlet obstruction, fluid in the vagina is usually simple, but can contain small amounts of echogenic debris due to mucus or debris.^{1,6} If there are associated complex anomalies, the fluid is more likely to be inhomogeneous, with clumps of echogenic debris and septations. Multiple cystic structures can be seen with cloacal anomalies.¹
- ◆ In patients with associated congenital anomalies, the vagina and uterus may be septated/duplicated.¹
- ◆ A female with an imperforate anus with a single perineal orifice has a cloacal anomaly. If there is an associated abdominal mass, it is most likely hydrocolpos.⁷

Pitfalls

- ◆ If the bladder is completely empty, or markedly compressed against the anterior abdominal wall, it may not be identified on ultrasound. In these patients, the dilated vagina/uterus may be confused with dilated bladder.⁶
- ◆ Errors in diagnosis can result in unnecessary laparotomy or hysterectomy, which have reported mortality up to 50%.⁸

References

1. Dhombres F, Jouannic JM, Brodaty G, Bessiere B, Daffos F, Bénifla JL. Contribution of prenatal imaging to the anatomical assessment of fetal hydrocolpos. *Ultrasound Obstet Gynecol* 2007;30:101–104. [PubMed](#)
2. Elsayes KM, Narra VR, Dillman JR, et al. Vaginal masses: magnetic resonance imaging features with pathologic correlation. *Acta Radiol* 2007;48:921–933. [PubMed](#)
3. Yildirim G, Gungorduk K, Aslan H, Sudolmus S, Ark C, Saygin S. Prenatal diagnosis of imperforate hymen with hydrometrocolpos. *Arch Gynecol Obstet* 2008;278:483–485. [PubMed](#)
4. Subramanian S, Sharma R, Gamanagatti S, Agarwala S, Gupta P, Kumar S. Antenatal MR diagnosis of urinary hydrometrocolpos due to urogenital sinus. *Pediatr Radiol* 2006;36:1086–1089. [PubMed](#)
5. Breech L. Gynecologic concerns in patients with anorectal malformations. *Semin Pediatr Surg* 2010;19:139–145. [PubMed](#)
6. Picone O, Laperelle J, Sonigo P, Levailant JM, Frydman R, Senat MV. Fetal magnetic resonance imaging in the antenatal diagnosis and management of hydrocolpos. *Ultrasound Obstet Gynecol* 2007;30:105–109. [PubMed](#)
7. Levitt MA, Peña A. Anorectal malformations. *Orphanet J Rare Dis* 2007;2:33. [PubMed](#)
8. Nazir Z, Rizvi RM, Qureshi RN, Khan ZS, Khan Z. Congenital vaginal obstructions: varied presentation and outcome. *Pediatr Surg Int* 2006;22:749–753. [PubMed](#)

Case 90

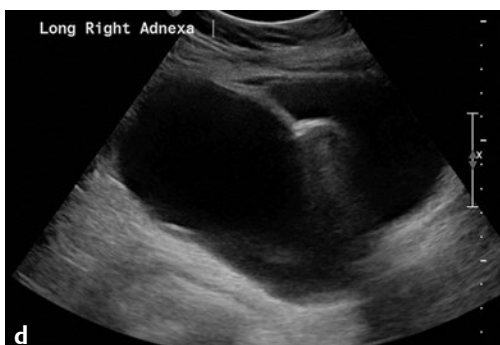
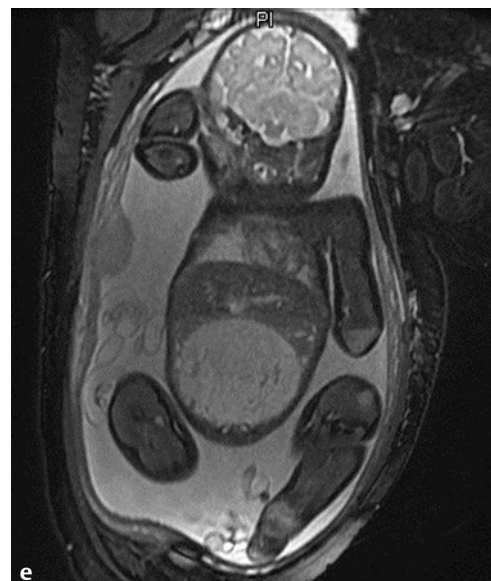
■ Clinical Presentation

A 15-year-old girl with right lower quadrant pain.

■ Radiographic Studies

A CT exam was performed to evaluate the patient for appendicitis. Axial CT image (**Fig. 90.1a**) and coronal reformatted CT image (**Fig. 90.1b**) show a large oval fluid attenuation lesion in the abdomen and upper pelvis. Subsequent ultrasound images (**Fig. 90.1c,d**) show a large oval cystic lesion with mass effect

on the bladder. The right ovary was not identified separate from this cyst. Coronal T2-weighted prenatal MRI (**Fig. 90.1e**) in another patient shows a large oval fluid signal lesion arising from the pelvis.



■ Diagnosis

Ovarian Cyst

■ Discussion and Differential Diagnosis

In the female neonate, ovarian cysts are the most common cystic abdominal mass.¹ On ultrasound, the cysts are identified as thin-walled cystic lesions, usually unilateral, and measure up to 3 cm in diameter with prominent through-transmission deep to the lesion.² These small cysts are generally asymptomatic and usually resolve spontaneously in the weeks following birth.³

In the fetus, follicular cysts develop under the influence of maternal estrogen, placental human chorionic gonadotropin (HCG), and fetal gonadotropins.^{1,4} There is an increased incidence of large ovarian cysts in infants of diabetic mothers, maternal toxemia, or maternal isoimmunization.¹ Occasionally, these cysts can become large; potential complications include pulmonary hypoplasia, cyst rupture, visceral compression, and polyhydramnios.^{1,2} These large cysts may be identified prenatally and have a variable ultrasound appearance. Simple cysts are generally follicular in origin, but more complex cysts may be the result of torsion or hemorrhage.³ Shortly after birth, the diagnosis of a large ovarian cyst is usually made with ultrasound, which identifies a unilocular or septated cyst, with or without internal echoes. The differential diagnosis of large cystic abdominal masses includes hydronephrosis, gastrointestinal duplication cysts, mesenteric duplication cysts, macrocystic lymphatic malformation, choledochal cysts, ante-

rior myelomeningocele, hydrocolpos, megacystis, and urachal cysts.^{1,3,4} Diagnostic criteria for the sonographic diagnosis of an ovarian cyst include female sex, a regular cystic structure off midline in location, identification of normal urinary tract anatomy, and identification of normal gastrointestinal structures.¹

Ovarian cysts are less common in early childhood, once the neonatal period has passed, due to low levels of gonadotropin and estradiol.^{1,2} Small cysts usually result from failure of the follicle to involute.¹ Occasionally, cyst formation can be associated with precocious puberty, and larger cysts require an extensive endocrine evaluation.^{1,2}

In the adolescent, ovarian cysts may be follicular in origin or the result of persistence of the corpus luteum. Follicular cysts are generally 2 to 3 cm in diameter and simple in appearance; however, if ovulation does not occur, these cysts can continue to grow and become very large.¹ Corpus luteum cysts can also grow up to 6 cm in size and are more likely to rupture, causing hemorrhage.¹ Resolution of both these cysts occurs spontaneously in over 90% of cases.¹ The differential diagnosis for an ovarian cyst in an adolescent includes a hemorrhagic/torsed ovary, an ectopic pregnancy, pelvic inflammatory disease, or endometriosis.^{1,2}

Pearls

- ◆ Unilocular anechoic cysts are benign, regardless of the patient's age or size.
- ◆ Most cysts smaller than 5 cm resolve spontaneously.
- ◆ Ovarian malignancies are extremely rare in the neonate.²

Pitfall

- ◆ A complicated cyst can be difficult to distinguish by imaging alone from ovarian torsion; both entities have enlarged, echogenic ovaries.

■ Controversy

- Some authors advocate prenatal ovarian cyst aspiration for large fetal ovarian cysts.^{1,2} Cyst aspiration is thought to prevent complications such as pulmonary hypoplasia,

torsion, and rupture.² However, cyst reaccumulation is common, and there is a risk of hemorrhage into the cyst or aspirating a cyst of nonovarian origin.¹

References

1. Brandt ML, Helmrich MA. Ovarian cysts in infants and children. *Semin Pediatr Surg* 2005;14:78–85 [PubMed](#)
2. Strickland JL. Ovarian cysts in neonates, children and adolescents. *Curr Opin Obstet Gynecol* 2002;14:459–465 [PubMed](#)
3. Akin MA, Akin L, Özbek S, et al. Fetal-neonatal ovarian cysts—their monitoring and management: retrospective evaluation of 20 cases and review of the literature. *J Clin Res Pediatr Endocrinol* 2010;2:28–33 [PubMed](#)
4. Helmrich MA, Shin CE, Warner BW. Ovarian cysts in the pediatric population. *Semin Pediatr Surg* 1998;7:19–28 [PubMed](#)

Case 91

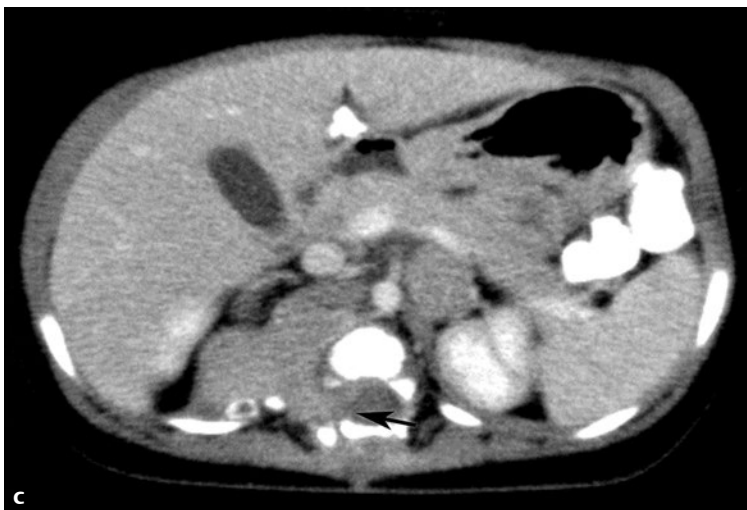
■ Clinical Presentation

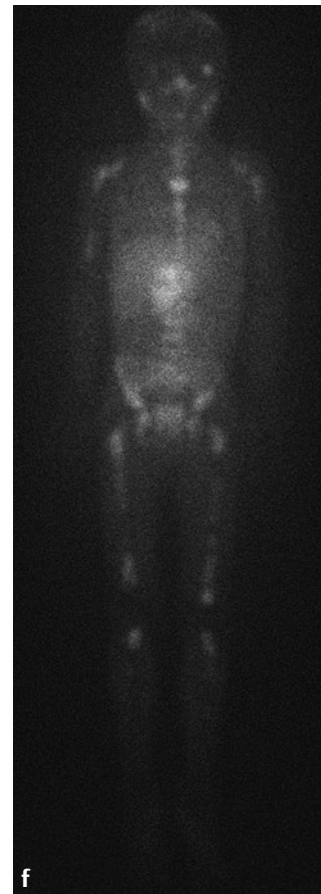
A 3-year-old boy with weight loss and irritability.

■ Radiographic Studies

Longitudinal ultrasound image (**Fig. 91.1a**) shows a heterogeneous solid mass (*arrowheads*) between the kidney and the liver. Postcontrast coronal reformatted CT image (**Fig. 91.1b**) shows lateral displacement of the right kidney by the paraspinal mass; internal stippled calcifications are noted (*arrow*). Postcontrast CT image (**Fig. 91.1c**) shows mild enhancement of the mass, which invades the spinal canal (*arrow*). Axial T2-weighted MRI (**Fig. 91.1d**) depicts spinal canal extent and

thecal sac displacement (*arrow*) more clearly. Postcontrast CT image in another patient (**Fig. 91.1e**) shows a large heterogeneously enhancing retroperitoneal mass that encases the vessels, crosses the midline, and displaces the aorta and IVC from the spine. On whole-body nuclear medicine metaiodobenzylguanidine (MIBG) imaging (**Fig. 91.1f**), there is increased uptake in the abdominal paraspinal mass and scattered throughout the skeleton.





■ Diagnosis

Neuroblastoma

■ Discussion and Differential Diagnosis

Neuroblastoma is the most common extracranial solid malignancy in children, accounting for 8 to 10% of all childhood cancers.¹ Neuroblastoma is a small round blue cell tumor arising from the neural crest cells of the adrenal medulla and the sympathetic chain ganglia. Two thirds of neuroblastomas arise in the abdomen, and of those, two thirds are adrenal in origin.² Adrenal origin is more common in children than in infants.¹ Patients usually present with abdominal pain, distention, or palpable mass.² On imaging, neuroblastoma presents as a large, often ill-defined, abdominal mass that usually displaces the kidney inferiorly and frequently crosses the midline. The tumor mass may displace or invade adjacent abdominal organs and often encases vessels in the central abdomen. Extensive lymphadenopathy is frequently identified. The tumor may arise anywhere along the sympathetic chain in the neck, thorax, and abdomen including the organ of Zuckerkandl.¹⁻³ Some 50 to 70% of children have metastatic disease at the time of diagnosis.^{1,4} Ninety-five percent of tumors have elevated urinary metabolites of catecholamine production.^{1,2}

Initial imaging is usually performed with ultrasound. The mass is usually a heterogeneous solid lesion with echogenic

calcifications. The aorta may be displaced anteriorly, and mesenteric vessels may be encased. Vessel invasion is rare, but Doppler ultrasound (US) should be performed to assess patency.³ Staging of neuroblastoma is performed most commonly with CT, but can also be accomplished with MRI. On CT, 80% of neuroblastomas have calcification; on routine radiographs of the abdomen, at least 30% have visible calcifications.² Neuroblastoma is frequently disseminated at presentation and may involve skin, lymph nodes, liver, bone marrow, or cortical bone. Metastatic involvement may be identified with CT, MRI, or nuclear medicine imaging. MRI is superior for identifying bone marrow involvement as well as for identifying the organ of origin.² MRI should be performed in any patient with a paraspinal tumor to evaluate intraspinal involvement.²

The differential diagnosis includes Wilms' tumor, rhabdomyosarcoma, teratoma, and lymphoma. Ganglioneuroma is the mature benign variant of neuroblastoma, which may produce local invasion. Ganglioneuroblastoma is the intermediate form of the tumor, between the benign ganglioneuroma and the malignant neuroblastoma.²

Pearls

- ◆ Neuroblastoma is sometimes detected prenatally. Treatment may be conservative, as these lesions often regress, and surgical resection is usually curative.³
- ◆ An unusual paraneoplastic syndrome is opsoclonus-myoclonus, which entails rapid eye movements, ataxia, and myoclonia, and is seen in 2 to 4% of patients.¹
- ◆ A young child with widening of the paravertebral stripe on chest radiograph should be investigated for neuroblastoma. Associated findings may include scoliosis and calcifications.

Pitfall

- ◆ Metaiodobenzylguanidine (MIBG) is a very useful nuclear imaging agent for detection of local or distant metastases. However, 30% of neuroblastomas do not take up MIBG; therefore, a normal MIBG does not exclude the diagnosis.²

References

1. Kaste SC, McCarville MB. Imaging pediatric abdominal tumors. *Semin Roentgenol* 2008;43:50–59 [PubMed](#)
2. Loneragan GJ, Schwab CM, Suarez ES, Carlson CL. Neuroblastoma, ganglioblastoma, and ganglioneuroma: radiologic-pathologic correlation. *Radiographics* 2002;22:911–934 [PubMed](#)
3. McHugh K. Renal and adrenal tumours in children. *Cancer Imaging* 2007; 7:41–51 [PubMed](#)
4. McCarville MB. Imaging neuroblastoma: what the radiologist needs to know. *Cancer Imaging* 2011;11(Spec. No. A):S44–S47 [PubMed](#)

Case 92

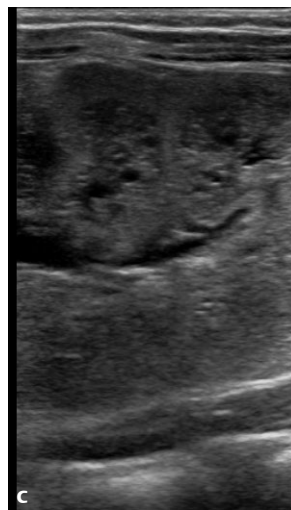
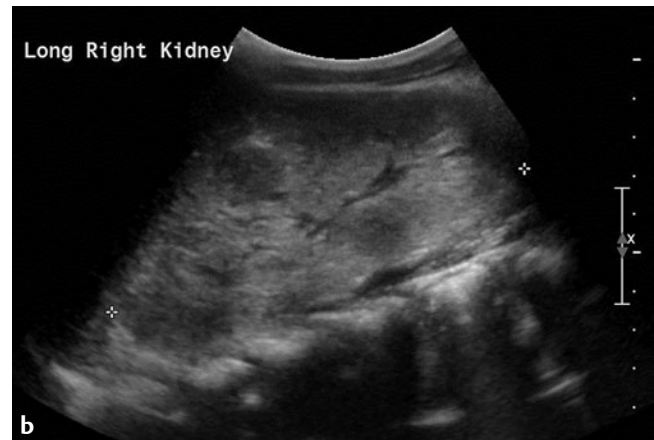
■ Clinical Presentation

A newborn with enlarged abdomen and respiratory distress.

■ Radiographic Studies

Longitudinal ultrasound images of both kidneys (**Fig. 92.1a,b**) show enlarged, echogenic kidneys with loss of corticomedul-

lary differentiation. High-resolution linear ultrasound imaging of the left kidney (**Fig. 92.1c**) shows multiple tiny cysts.



■ Diagnosis

Autosomal Recessive Polycystic Kidney Disease

■ Discussion and Differential Diagnosis

Autosomal recessive polycystic kidney disease (ARPKD) is a ciliopathy that presents in utero or in early childhood, affecting 1 in 20,000 live births.^{1,2} Patients with ARPKD may present in utero during the third trimester of pregnancy with ultrasound findings including oligohydramnios and bilateral large echogenic kidneys. The large kidneys can cause abdominal distention, causing pulmonary hypoplasia.¹ The typical patient presents as a newborn with an enlarged abdomen secondary to bilateral flank masses. Associated respiratory problems include pulmonary hypoplasia, pneumothoraces, and respiratory insufficiency, which may lead to death.^{3–5}

Autosomal recessive polycystic kidney disease is always associated with a ductal plate malformation of the liver.¹ This leads to congenital hepatic fibrosis with variable degrees of portal hypertension as the children age.^{1,3} ARPKD can be associated with Caroli's disease.⁴ Liver disease and kidney disease seem to have an inverse relationship, in that severe kidney disease has a milder form of liver disease, and vice versa.¹ Children who survive the neonatal period have a 60% chance of surviving to age 15.⁶ These children develop portal hypertension and chronic renal failure as they age; systemic hypertension is present in 75 to 80% of patients.^{1,3}

Ultrasound of ARPKD shows markedly enlarged, echogenic kidneys; increased echogenicity is secondary to the dilated collecting ducts. As patients age, the dilated tubules lose communication with nephrons and become macroscopic cysts.³ There may be a surrounding rim of relatively normal or hypoechoic renal cortex, but there is uniform loss of the corticomedullary differentiation throughout the kidneys. There may be multiple non-shadowing echogenic foci throughout the kidneys, thought to be due to stagnant urine with calcium deposition.^{1,3} There are varying degrees of congenital hepatic fibrosis, which manifests by an echogenic liver, splenomegaly, and biliary ductal dilatation or cysts.³ CT scan shows massively enlarged kidneys, with low attenuation due to the high renal parenchymal water content.³ After contrast administration, there is radial streaking of contrast in the dilated tubules.^{1,3} On MRI, the kidneys are enlarged with decreased T1 and increased T2 signal, due to the high water content.³ The differential diagnosis of bilateral renal enlargement includes bilateral hydronephrosis, which is usually easily excluded at ultrasound. The uniform echogenicity of ARPKD excludes bilateral multicystic dysplastic kidneys and bilateral mesoblastic nephromas.

Pearls

- ◆ Neonates with severe disease have a high mortality rate (25–30%) due to respiratory failure from pulmonary hypoplasia.^{1,2}
- ◆ Patients who present in childhood usually have fewer symptoms of renal failure, but more liver involvement (portal hypertension, varices, and hepatic fibrosis).¹

Pitfall

- ◆ Imaging differentiation between ARPKD and autosomal dominant polycystic kidney disease (ADPKD) may be difficult in older children; the presence of hepatic fibrosis can help differentiate them.⁴ Genetic testing may be necessary for diagnosis.

References

1. Epelman M, Victoria T, Meyers KE, Chauvin N, Servaes S, Darge K. Postnatal imaging of neonates with prenatally diagnosed genitourinary abnormalities: a practical approach. *Pediatr Radiol* 2012;42(Suppl 1):S124–S141 [PubMed](#)
2. Gunay-Aygun M. Liver and kidney disease in ciliopathies. *Am J Med Genet C Semin Med Genet* 2009;151C:296–306 [PubMed](#)
3. Turkbey B, Ocak I, Daryanani K, et al. Autosomal recessive polycystic kidney disease and congenital hepatic fibrosis (ARPKD/CHF). *Pediatr Radiol* 2009;39:100–111 [PubMed](#)
4. Sessa A, Meroni M, Righetti M, Battini G, Maglio A, Puricelli SL. Autosomal recessive polycystic kidney disease. *Contrib Nephrol* 2001;136:50–56 [PubMed](#)
5. Tahvanainen E, Tahvanainen P, Kääriäinen H, Höckerstedt K. Polycystic liver and kidney diseases. *Ann Med* 2005;37:546–555 [PubMed](#)
6. Vanderheyden T, Kumar S, Fisk NM. Fetal renal impairment. *Semin Neonatol* 2003;8:279–289 [PubMed](#)

Case 93

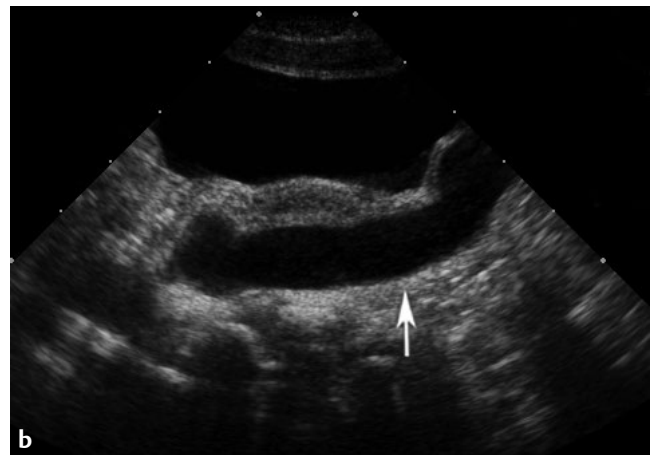
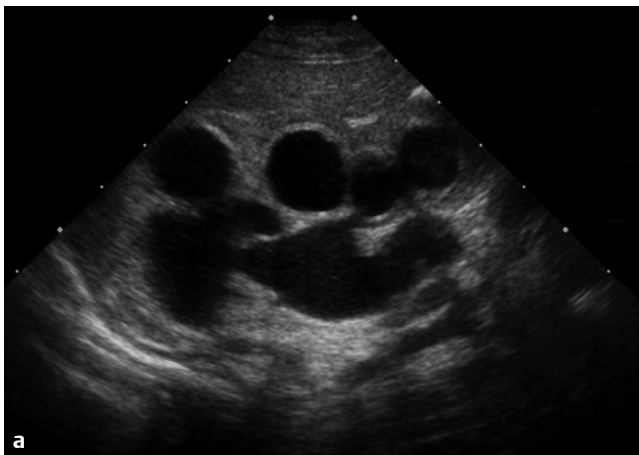
■ Clinical Presentation

A 4-year-old girl with dysuria, frequency, and urinary tract infection.

■ Radiographic Studies

Longitudinal ultrasound (**Fig. 93.1a**) of the right kidney shows marked hydronephrosis with parenchymal thinning or compression. Longitudinal ultrasound (**Fig. 93.1b**) of the right pelvis shows a dilated ureter (*arrow*) posterior to the bladder. After completion of urinary tract infection (UTI) treatment,

a voiding cystourethrogram (VCUG) was performed. Fluoroscopic image of the abdomen (**Fig. 93.1c**) shows a catheter and contrast in the bladder. Contrast opacifies a dilated/tortuous right ureter and fills dilated renal pelvis/calices with absent papillary impressions.



■ Diagnosis

Vesicoureteral Reflux

■ Discussion and Differential Diagnosis

Vesicoureteral reflux, the retrograde flow of urine from the bladder into the ureter, is an anatomic or functional disorder.¹ Normally when the bladder fills with urine, the intramural ureter is compressed, preventing retrograde flow of urine. This function is not effective when the intramural ureter is short.² The prevalence of VUR is 1% and most commonly is associated with UTI and pyelonephritis. VUR may resolve with time, but can result in renal scarring, hypertension, and renal failure. Increasing severity of VUR correlates with increasing frequency of pyelonephritis. Boys are more likely to have VUR than girls and tend to have higher grades of VUR diagnosed at younger ages.¹⁻³

Vesicoureteral reflux can be evaluated by VCUG and radionuclide cystography (RC). Both studies involve urethral catheterization and retrograde filling of the bladder. VCUG is performed by infusing radiographic contrast into the bladder, intermittent fluoroscopic monitoring for reflux, and evaluation of the urethra during voiding. In RC, a radioisotope mixed with saline is instilled into the bladder. The major advantage of VCUG over RC is the ability to visualize anatomic details that can be missed on RC. The advantages of RC over VCUG are higher sensitivity to detect VUR with continuous imaging during bladder filling/voiding, no effect of overlying gas/stool, and lower gonadal radiation dose.² However, despite the concerns about ionizing radiation, conventional VCUG still remains the gold standard for the presence and severity of VUR and is the initial test in most practices.² Radionuclide cystography is performed after treatment to determine if VUR persists.² If there is delay in diagnosis and reflux is not treated appropriately, it can result in permanent renal damage with loss of parenchyma and scarring.² Renal cortical scintigraphy with technetium-99m dimercaptosuccinic acid (DMSA) is the imaging technique of choice to detect renal scarring because of its high sensitivity.²

Imaging is usually delayed until antibiotic therapy has been complete and the urine is sterile to decrease bladder irritability and underfilling of the bladder, thereby avoiding false-negative examinations. In addition, high-pressure reflux to the kidney with infected urine has been reported to increase damage to the kidney.⁴ In 1985, the International Reflux Study Committee introduced a uniform system for the classification of VUR.¹ Vesicoureteral reflux is graded as follows:

- Grade I: Ureter only
- Grade II: Nondilated ureter, pelvis, and calyces
- Grade III: Mild or moderate dilatation of the ureter and renal pelvis (no or slight calyceal forniceal blunting)
- Grade IV: Moderate dilatation/tortuosity of the ureter and moderate dilatation of the renal pelvis/calyces (papillary impressions remain in majority of calyces)
- Grade V: Gross dilatation/tortuosity of the ureter, renal pelvis, and calyces (most papillary impressions no longer visible)

The latest American Academy of Pediatrics guidelines recommend ultrasound (US) after the initial febrile UTI in children between 2 and 24 months of age.⁵ VCUG is reserved for recurrent febrile UTI and if the US reveals hydronephrosis, scarring, or findings indicating high-grade VUR or obstructive uropathy.⁵ The European Association of Urology (EAU) continues to recommend VCUG after the first febrile UTI in children aged 0 to 2 years and cortical scintigraphy if VUR is diagnosed.⁵ Current American Urological Association (AUA) guidelines recommend proceeding with VCUG in cases of grade III and IV hydronephrosis, abnormal bladder wall findings, or in those who develop a UTI while on observation.⁵

The main objective of VUR management is to prevent UTI. There are two main treatment approaches: conservative and surgical. The conservative approach involves continuous antibiotic prophylaxis. Regardless of the grade of reflux or presence of renal scars, all patients diagnosed in the first year of life should be treated initially with continuous antibiotic prophylaxis.¹ Surgical treatment should be considered for patients with febrile breakthrough infections while on continuous antibiotic prophylaxis and for patients with persistent high-grade reflux (grades IV/V).¹

Endoscopic injection of periureteral bulking agents has been used for the management of VUR.⁵ The procedure is performed cystoscopically by a submucosal injection of a bulking agent beneath the intravesical portion of the ureter. The procedure elevates and narrows the distal ureteroureteral orifice, preventing retrograde passage of urine, while still allowing antegrade flow.⁵ Various surgical techniques to prevent VUR have been described. All share the principle of lengthening the intramural ureter.¹

Pearls

- ◆ Some 25 to 50% of children who have UTI are found to have VUR.^{1,2}
- ◆ Prenatal hydronephrosis should be first followed by US several days after birth due to the relative oliguria seen in the neonate. Postnatal evaluation affords the opportunity to diagnose and manage VUR before secondary injury is sustained.⁵

Pitfall

- ◆ Acute pyelonephritis in the absence of vesicoureteral reflux is common.

■ Controversy

- The literature suggests that antibiotic prophylaxis does not significantly decrease the risk of recurrent UTI and does not reduce the overall incidence of pyelonephritis/renal scarring.²

References

1. Tekgul S, Riedmiller H, Gerharz E, et al. Vesicoureteric reflux (VUR). In: Guidelines on Paediatric Urology. Arnhem, The Netherlands: European Association of Urology, European Society for Paediatric Urology; 2009:44–49
2. Lim R. Vesicoureteral reflux and urinary tract infection: evolving practices and current controversies in pediatric imaging. *AJR Am J Roentgenol* 2009; 192:1197–1208 Review [PubMed](#)
3. Lebowitz RL, Olbing H, Parkkulainen KV, Smellie JM, Tamminen-Möbius TE; International Reflux Study in Children. International system of radiographic grading of vesicoureteric reflux. *Pediatr Radiol* 1985;15:105–109 [PubMed](#)
4. Strife JL, Bisset GS III, Kirks DR, et al. Nuclear cystography and renal sonography: findings in girls with urinary tract infection. *AJR Am J Roentgenol* 1989;153:115–119 [PubMed](#)
5. Weinberg AE, Hsieh MH. Current management of vesicoureteral reflux in pediatric patients: a review. *Pediatr Health Med Therap*. 2013;4:1–12

Case 94

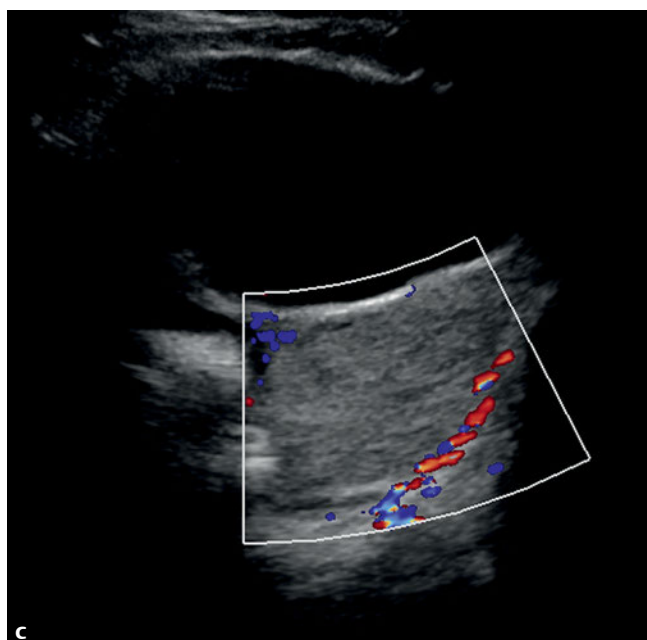
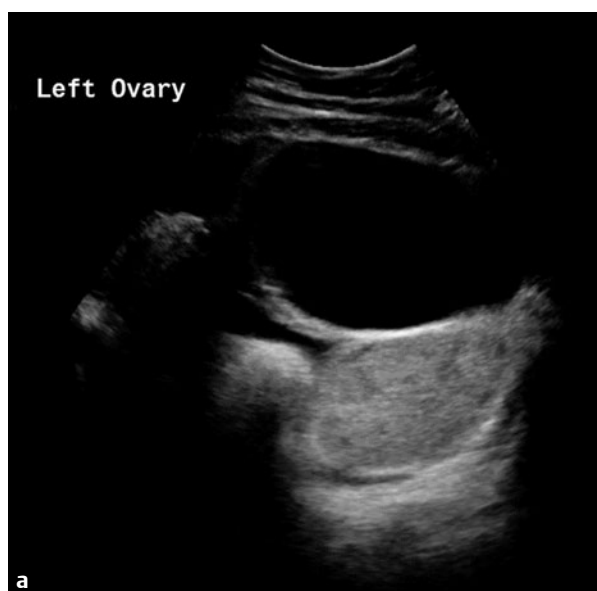
■ Clinical Presentation

A 14-year-old girl with 2 weeks of intermittent abdominal pain.

■ Radiographic Studies

Ultrasound image of the left pelvis (**Fig. 94.1a**) shows an enlarged, echogenic ovary with multiple small peripheral follicles. Left ovarian volume was increased at 120 mL. Image of the con-

tralateral pelvis (**Fig. 94.1b**) shows a normal right ovary with volume of 17.5 mL. Moderate hypoechoic pelvic fluid is present. There is no flow on Doppler of the left ovary (**Fig. 94.1c**).



■ Diagnosis

Ovarian Torsion

■ Discussion and Differential Diagnosis

Ovarian torsion (adnexal torsion) is an uncommon but important cause of acute abdominal pain in the pediatric and adolescent female. It is reported to be the fifth most common gynecologic emergency.^{1,2} Adnexal torsion is also concerning because it occurs most commonly during the first three decades of life, which is before or during reproductive age.^{1,2}

Adnexal torsion occurs with partial or complete twisting of the ovarian pedicle. This disrupts venous and lymphatic flow, and can eventually lead to disruption of arterial flow as well.² Torsion more commonly occurs in an adnexa with underlying pathology. However, in the pediatric population, torsion of a normal ovary is more frequent due to relatively long fallopian tubes and therefore mobile ovaries.^{1,3} Adnexal pathology predisposing to torsion is most commonly benign, and includes ovarian cyst, teratomas, and serous or mucinous cystadenomas.^{1,4} Malignant lesions are uncommon in children, occurring in less than 0.5% in one population study.⁵

The diagnosis of adnexal torsion can be difficult, because the symptoms and clinical signs are similar to other causes of acute abdominal pain. The most common presenting symptom is unilateral abdominal pain. Multiple studies have found that the right side is more frequently affected.^{1,4} Nausea and vomiting is common (70–80%); fever can be present, and occasionally there may be a palpable mass on physical exam.¹

The most common sonographic finding in adnexal torsion is an enlarged ovary or adnexal mass.^{1,4,6} The classic finding is

an enlarged ovary with multiple peripheral cysts, and no flow on Doppler. However, the peripheral cysts are seen in 75% of cases of torsion,⁴ and Doppler flow can be present in up to 64% of cases of torsion.^{4,6} The volume ratio (comparing the volume of the affected side to the volume of the normal side) is also a useful indicator of torsion; an adnexal volume ratio of 15 to 20 is a predictor of torsion.^{4,6}

The most worrisome alternative diagnosis for acute right-sided abdominal pain in a girl or female adolescent is acute appendicitis. Other causes of pain originating from the adnexa include hemorrhagic cyst and ruptured cyst. These can be difficult to distinguish from ovarian torsion, both by clinical symptoms and by sonography. If clinical and sonographic findings are suspicious for torsion, exploration is warranted.

In the past, oophorectomy was the standard treatment for ovarian torsion. This was the result of concern about ovarian malignancy and the potential of thromboembolism from ovarian vein thrombosis. In children, there is minimal potential for malignancy, and there are no reports of thromboembolism following detorsion.^{1,5} Currently, a conservative approach has been accepted, with detorsion of the adnexa and cystectomy if a cyst is present.¹ Follow-up ultrasound 6 weeks after detorsion should be performed to search for viable ovarian tissue.

Pearl

- ◆ An adnexal volume > 75 mL and marked adnexal asymmetry (ratio > 15 to 20) should increase suspicion for ovarian torsion.⁶

Pitfall

- ◆ Presence of Doppler flow does not exclude ovarian torsion.

References

1. Breech LL, Hillard PJ. Adnexal torsion in pediatric and adolescent girls. *Curr Opin Obstet Gynecol* 2005;17:483–489 [PubMed](#)
2. Gittleman AM, Price AP, Goffner L, Katz DS. Ovarian torsion: CT findings in a child. *J Pediatr Surg* 2004;39:1270–1272 [PubMed](#)
3. Garel L, Dubois J, Grignon A, Filiatrault D, Van Vliet G. US of the pediatric female pelvis: a clinical perspective. *Radiographics* 2001;21:1393–1407 [PubMed](#)
4. Servaes S, Zurakowski D, Laufer MR, Feins N, Chow JS. Sonographic findings of ovarian torsion in children. *Pediatr Radiol* 2007;37:446–451 [PubMed](#)
5. Guthrie BD, Adler MD, Powell EC. Incidence and trends of pediatric ovarian torsion hospitalizations in the United States, 2000–2006. *Pediatrics* 2010; 125:532–538 [PubMed](#)
6. Linam LE, Darolia R, Naffaa LN, et al. US findings of adnexal torsion in children and adolescents: size really does matter. *Pediatr Radiol* 2007;37:1013–1019 [PubMed](#)

Case 95

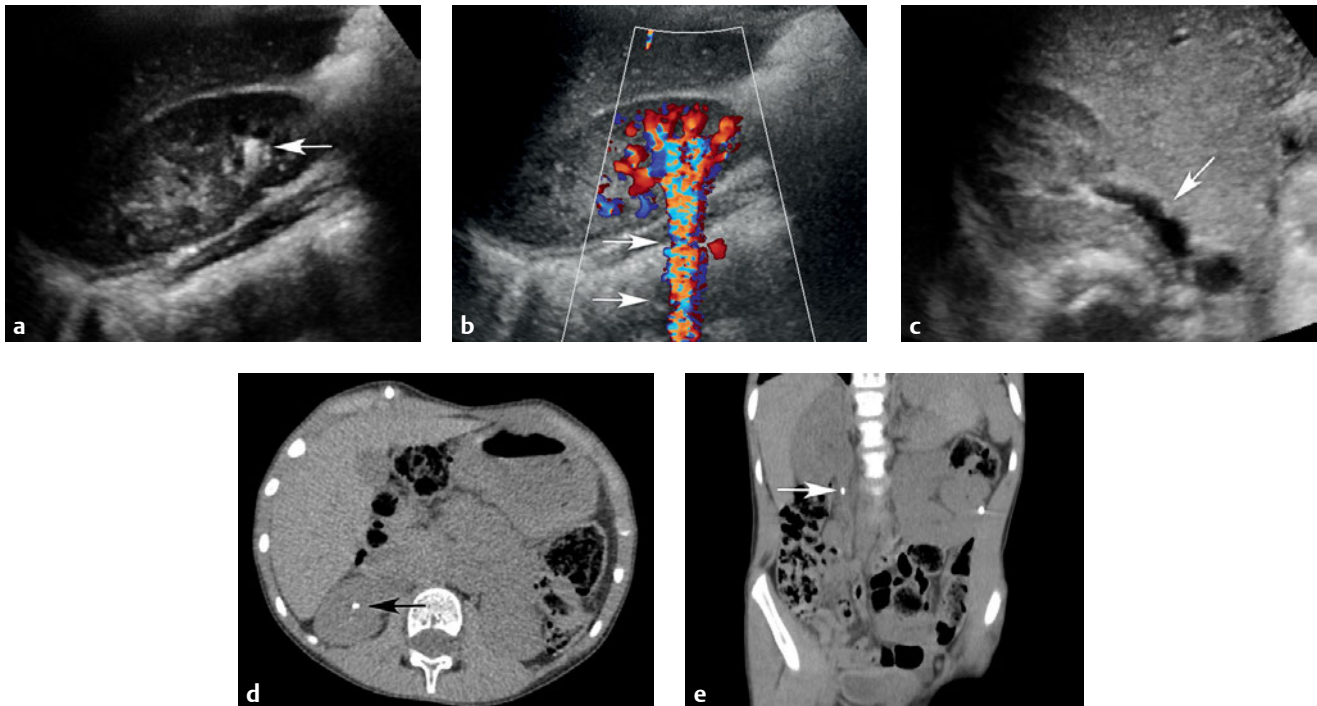
■ Clinical Presentation

A 5-year-old girl with acute right flank pain and gross hematuria.

■ Radiographic Studies

Longitudinal ultrasound image of right kidney (**Fig. 95.1a**) shows an echogenic density (*arrow*) in a lower pole calyx without any posterior acoustic shadowing or calyceal dilatation. Doppler ultrasound image (**Fig. 95.1b**) shows intense “twinkle” artifact (*arrows*) compatible with calculus. Transverse ultrasound image (**Fig. 95.1c**) shows mild dilation of a

right extrarenal pelvis (*arrow*). Noncontrast axial CT image (**Fig. 95.1d**) shows a nonobstructing stone in the right kidney (*arrow*). Noncontrast coronal reformatted CT image (**Fig. 95.1e**) shows a second calculus in the proximal right ureter (*arrow*) causing proximal hydroureter.



■ Diagnosis

Urolithiasis

■ Discussion and Differential Diagnosis

Urolithiasis occurs less frequently in infants and children than in adults.¹ The most common clinical presentation is flank pain, and less commonly suprapubic pain.¹ Other symptoms include urinary frequency, nausea/vomiting, gross hematuria, and fever; 30% of pediatric urolithiasis is found incidentally.¹ Factors that affect the propensity of stone formation include substance concentration/solubility and the presence of crystal aggregation promoters or inhibitors.¹ Pediatric urinary tract calculi are most commonly calcium oxalate/calcium phosphate (75–80%), followed by magnesium ammonium phosphate/calcium carbonate/calcium phosphate (10–15%), and less commonly uric acid (< 5%). Cysteine and xanthine stones are rare in children.¹ Stasis of urine is significantly associated with a higher incidence of urolithiasis. The most common causes of stasis in children are neurogenic bladder and congenital urinary tract anomalies such as ureteropelvic junction (UPJ) and ureterovesical junction (UVJ) obstruction.¹ Hypercalciuria is the most common biochemical abnormality in children with urolithiasis, resulting in the formation of calcium oxalate stones. Causes of hypercalciuria include hyperparathyroidism, type 1 renal tubular acidosis, hypervitaminosis, and immobilization.^{1,2} In many patients the serum calcium is normal. The vast majority (98%) of pediatric urolithiasis, however, occurs in the presence of normal urinary calcium.¹ Additional associations with urolithiasis include medications (e.g., Lasix), cystic fibrosis, and ketogenic diet.²

Infants and young children are often imaged radiographically owing to their nonspecific clinical presentation and ab-

sence of classic renal colic.² Although 90% of renal stones are radiopaque, stone smaller than 5 mm are not well seen on radiographs, particularly when the overlying bowel gas obscures detail.^{2,3} If hematuria is present, an ultrasound is usually the first imaging obtained. Ultrasound can image small stones (< 5 mm) and radiolucent stones, as it is not dependent on stone composition.^{2,3} Ultrasound may also demonstrate findings of hydronephrosis, nephrocalcinosis, associated infection, and scarring.^{2,3} One useful finding that can increase ultrasound's sensitivity for calculi detection is the "twinkle" artifact. Color flow ultrasound often demonstrates a strip of turbulent color signal deep to the renal calculus.³ In addition, color flow ultrasound demonstration of a ureteral jet in the bladder lumen may help exclude ureteral obstruction on the respective side.⁴ Relative disadvantages of ultrasound include difficulty in the visualization of distal ureteral calculi due to intervening structures deep in the pelvis.^{2,3}

Noncontrast CT offers a high sensitivity and specificity (96% to 98% in adult studies) for urolithiasis, even when stones are small.² CT can measure stone attenuation, evaluate secondary effects of obstruction, delineate surgically relevant anatomy, and detect other potential sources of pain or pathological abnormality.^{2,3} More recently, low-dose protocols, tube current modulation, and noise reduction technologies have been developed with little loss in sensitivity in the detection of urinary and nonurinary diseases.²

Pearls

- ◆ Distal ureteral stones are better visualized on ultrasound when the bladder is distended.
- ◆ Urinary infection with urea-splitting organisms such as *Proteus mirabilis* can also increase the formation of stones containing magnesium ammonium phosphate.

Pitfall

- ◆ Overlying bowel gas, obesity, ectopic kidneys, or medially located kidneys (common in patients with spinal dysraphism) may limit visualization of stones on radiographs.

References

1. Shore R. Scurvy. In: Slovis T, ed. Caffey's Pediatric Diagnostic Imaging, 11th ed. Philadelphia: Mosby Elsevier; 2007:2739–2743
2. Gillespie RS, Stapleton FB. Nephrolithiasis in children. *Pediatr Rev* 2004;25:131–139 Review [PubMed](#)
3. Cheng PM, Moin P, Dunn MD, Boswell WD, Duddalwar VA. What the radiologist needs to know about urolithiasis: part 1—pathogenesis, types, assessment, and variant anatomy. *AJR Am J Roentgenol* 2012;198:W540–7 Review [PubMed](#)
4. Palmer JS, Donaher ER, O'Riordan MA, Dell KM. Diagnosis of pediatric urolithiasis: role of ultrasound and computerized tomography. *J Urol* 2005;174(4 Pt 1):1413–1416 [PubMed](#)

Case 96

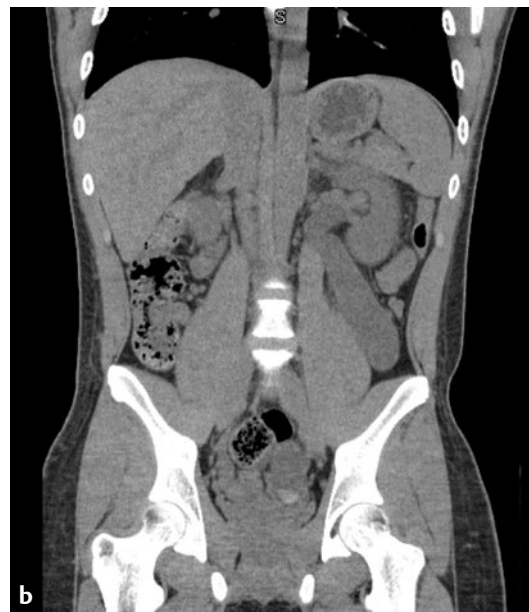
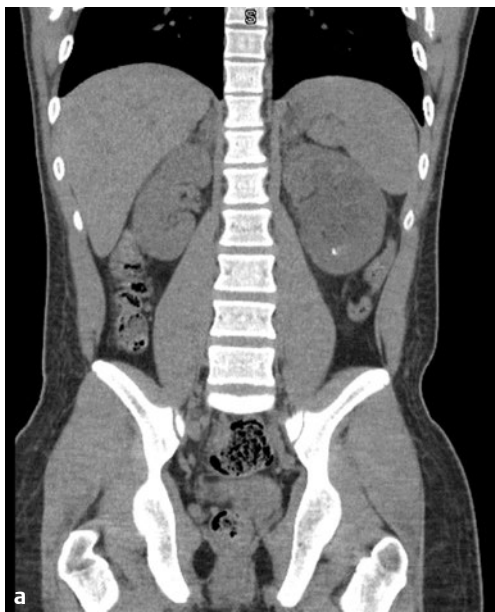
■ Clinical Presentation

A 15-year-old with left flank pain and hematuria.

■ Radiographic Studies

Noncontrast CT of the abdomen (**Fig. 96.1a–c**) shows markedly dilated, tortuous ureter with a stone in the renal collecting system, but no ureteral stone. Pelvis ultrasound image in

another patient (**Fig. 96.1d**) shows transition to a normal-caliber ureter just above the ureterovesical junction (*arrow*). Echogenic debris or hemorrhage is noted in the bladder lumen.



■ Diagnosis

Megaureter

■ Discussion and Differential Diagnosis

Megaureter is a general term used to describe ureteral dilatation greater than 5 to 7 mm in diameter, with variable degrees of dilatation of the collecting system.^{1,2} The term is not defined as a distinct entity and, in fact, incorporates ureteral dilatation with multiple causes and diverse pathology.³ Megaureter can either be primary or secondary. Causes of secondary megaureter include infection, external obstruction, posterior urethral valves, neurogenic bladder, and diabetes insipidus.¹ Primary megaureter can be divided into obstructed primary megaureter, refluxing primary megaureter, and nonrefluxing nonobstructed primary megaureter.^{1,2}

The cause of obstructed primary megaureter is unclear, but in most cases there is not a true narrowing at the ureterovesical junction (UVJ); rather, there is a functional obstruction arising from a short (0.5–4 cm) aperistaltic segment just above the UVJ.^{1–3} This aperistaltic ureter segment causes dilation above it because urine does not pass into the bladder at a fast enough rate.^{1–3} This condition may resolve spontaneously within the first 2 years of life.³

Refluxing primary megaureter is caused by derangement of the UVJ.^{2,3} In these cases, the megaureter is caused by the increased volume of urine refluxing into the ureter.

Nonrefluxing nonobstructed primary megaureters occur in 23% of neonates who have prenatal dilation of the urinary tract.^{1,3} Most neonates with primary megaureter belong to this category.^{2,3} The cause of nonrefluxing nonobstructed megaureter is poorly understood. The most widely accepted hypothesis is that the UVJ may be transiently delayed in maturation,¹ causing a delay in peristalsis. Most of these patients normalize in the first 2 years of life.¹

Primary megaureter may present with UTI, fever, abdominal pain, or hematuria.¹ Ultrasound identifies a dilated ureter that can be traced from renal pelvis to bladder; antiperistaltic waves, and the transition to the thin, aperistaltic segment, can frequently be seen.¹ Pelvocaliectasis is frequently present, but the degree of ureteral dilation is usually greater in comparison.¹

Renal parenchymal thinning may be seen. Contrast-voiding cystourethrography is necessary to search for bladder outlet obstruction, neurogenic bladder, or vesicoureteral reflux.^{1–3} Once reflux has been excluded, nuclear medicine diuretic renography is indicated to search for obstruction.^{1,2}

If these examinations define primary megaureter with no evidence of obstruction, and no secondary cause of megaureter, then surgery is not indicated. However, regular follow-up including diuretic renography is necessary because these patients may later develop obstruction.⁴ If the megaureter is symptomatic (colicky pain, hematuria, recurrent infection), then surgery is indicated.¹ If obstruction is identified at the UVJ from the primary megaureter, resection of the abnormal terminal ureter and reimplantation are indicated, before development of obstructive renal damage.

Patients with prune belly syndrome may also have dilated ureters caused by reflux or UVJ obstruction, or may have nonrefluxing, nonobstructed ureteral dilation.³ Congenital megacystis/megaureter syndrome is a different entity, usually detected in utero or just after birth, in which the ureters, urinary bladder, and upper collecting systems are grossly dilated, secondary to massive reflux during voiding.³

Pearls

- ◆ Primary megaureter is more common in males than in females, more common on the left than on the right, bilateral in 20% of patients, and associated with contralateral renal agenesis in 9% of cases.^{1–3}
- ◆ The diagnosis of megaureter may be made prenatally when a tubular anechoic structure is identified behind the bladder with varying degrees of renal pelvis dilatation. Renal dysplastic changes may be present.^{1,3}

Pitfall

- ◆ Primary megaureter can be difficult to differentiate from secondary megaureter. It is important to exclude treatable causes.

References

1. Merlini E, Spina P. Primary non-refluxing megaureters. *J Pediatr Urol* 2005; 1:409–417 [PubMed](#)
2. Berrocal T, López-Pereira P, Arjonilla A, Gutiérrez J. Anomalies of the distal ureter, bladder, and urethra in children: embryologic, radiologic, and pathologic features. *Radiographics* 2002;22:1139–1164 [PubMed](#)
3. Shokeir AA, Nijman RJM. Primary megaureter: current trends in diagnosis and treatment. *BJU Int* 2000;86:861–868 [PubMed](#)
4. Di Renzo D, Aguiar L, Cascini V, et al. Long-term followup of primary nonrefluxing megaureter. *J Urol* 2013;190:1021–1026 [PubMed](#)

Case 97

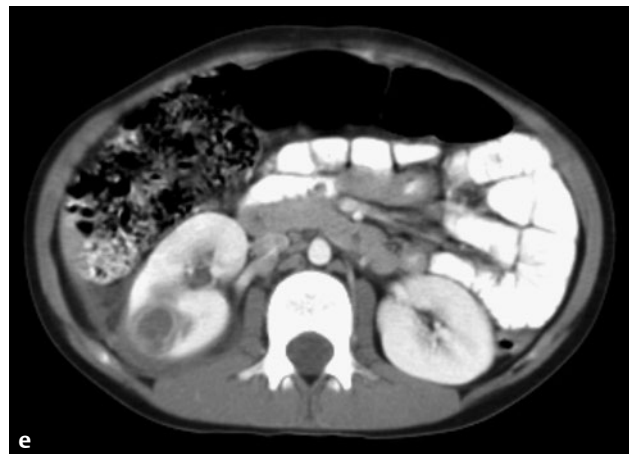
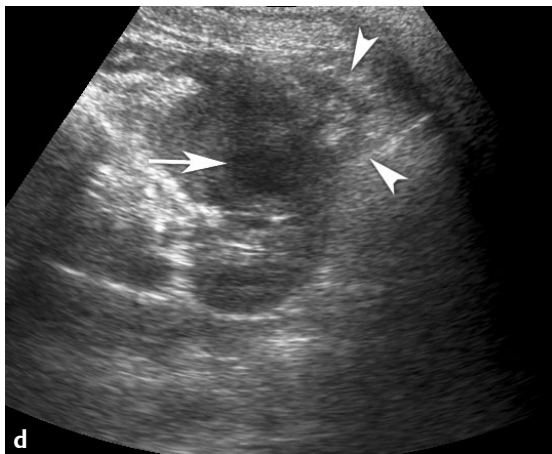
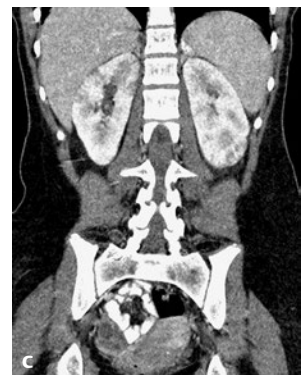
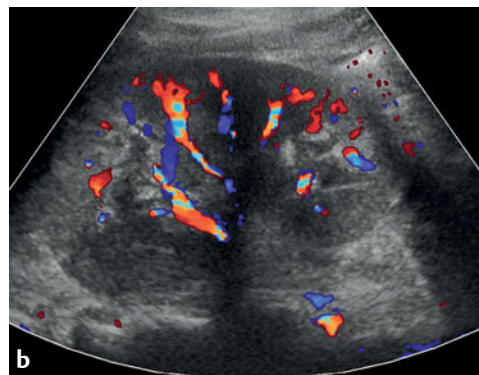
■ Clinical Presentation

A 14-year-old girl with 3 days of fever and left abdomen pain.

■ Radiographic Studies

Ultrasound image of the kidney (**Fig. 97.1a**) shows a wedge-shaped hyperechoic lesion in the upper pole of a swollen kidney. Doppler image reveals associated segmental loss in vascularity (**Fig. 97.1b**). Postcontrast coronal CT reconstruction image in another patient (**Fig. 97.1c**) shows patchy non-enhancing lesions scattered throughout both kidneys, greatest in the cortices. Transverse ultrasound image of the right kid-

ney in a third patient (**Fig. 97.1d**) shows poorly defined thickening of the cortex with a central hypoechoic region (*arrow*). Adjacent hyperechoic perinephric changes (*arrowheads*) suggest perinephric fat inflammation. Postcontrast CT image (**Fig. 97.1e**) shows an oval low attenuation rim enhancing lesion in the posterior cortex of the right kidney consistent with a renal abscess.



■ Diagnosis

Acute Pyelonephritis



■ Discussion and Differential Diagnosis

Acute pyelonephritis is infection of the renal pelvis and parenchyma and generally presents with fever, chills, flank pain, and tenderness.^{1–3} Acute pyelonephritis is a cause of major morbidity in children, as it may lead to irreversible renal scarring with subsequent renal growth retardation, hypertension, and chronic renal failure.³ Early diagnosis and treatment are of critical importance in preventing the development of renal scars.³ The diagnosis of pyelonephritis in infants and young children can be difficult, as they may present with nonspecific signs such as irritability, poor appetite, lethargy, vomiting, diarrhea, or failure to thrive.^{2,3} Clinical and laboratory data may be inadequate to diagnose acute pyelonephritis. Vesicoureteral reflux may be associated with acute pyelonephritis, but acute pyelonephritis in the absence of reflux is also common.³

Specific signs of pyelonephritis on ultrasound include poorly margined, wedge-shaped, hypoechoic parenchymal lesions representing interstitial edema.⁴ Sometimes the area of infection may be hyperechoic, which may be related to hemorrhage.⁴ Renal enlargement, loss of corticomedullary differentiation, and compression of renal sinus fat may also be observed. The use of Doppler greatly improves sensitivity in detecting renal parenchymal abnormalities, as most pyelonephritic lesions have relative ischemia.⁴ Therefore, pyelonephritis appears as

wedge-shaped areas of decreased perfusion.⁴ Power Doppler is superior to color Doppler in defining the extent of hypoperfusion. Abscess cavities typically appear as rounded hypoechoic lesions that may demonstrate increased through-transmission and lack internal vascularity on color flow Doppler images.¹

Nuclear medicine renal scintigraphy with technetium-99m dimercaptosuccinic acid (DMSA) offers visualization of the renal cortex and may show areas of peripheral decreased uptake related to acute pyelonephritis or scar formation. Up to 90% of children with a febrile urinary tract infection (UTI) have positive scintigraphic findings, including focal or global areas of diminished radiotracer uptake.¹ Unlike the adult population, CT is not routinely performed in children with suspected pyelonephritis due to the relatively higher radiation dose and the necessity for intravenous contrast. Acute pyelonephritis on CT presents as an ill-defined, wedge-shaped area of decreased attenuation radiating from the medulla to the cortical surface.⁴ These wedge-shaped areas probably represent areas of poorly functioning parenchyma due to vasospasm, tubular obstruction, or interstitial edema.⁴ MRI is as sensitive as renal cortical scintigraphy in detecting abnormal parenchymal changes, and it eliminates radiation; higher cost has restricted its clinical use for this purpose.⁴

Pearls

- ◆ Clinical and laboratory data are inadequate in differentiating acute pyelonephritis from simple lower UTI.
- ◆ Most episodes of acute parenchymal inflammatory changes are reversible and do not lead to scarring.

Pitfall

- ◆ It is difficult to distinguish acute pyelonephritis from renal scars with nuclear medicine.

■ Controversy

- The effectiveness of antimicrobial prophylaxis for patients who have vesicoureteral reflux has been challenged in the past decade. If antibiotic prophylaxis is not beneficial and

vesicoureteral reflux is not required for the development of pyelonephritis, then the rationale for performing VCUG routinely after an initial febrile UTI must be questioned.

References

1. Craig WD, Wagner BJ, Travis MD. Pyelonephritis: radiologic-pathologic review. *Radiographics* 2008;28:255–277, quiz 327–328. Review [PubMed](#)
2. Newman TB. The new American Academy of Pediatrics urinary tract infection guideline. *Pediatrics* 2011;128:572–575. [PubMed](#)
3. Andrich MP, Majd M. Diagnostic imaging in the evaluation of the first urinary tract infection in infants and young children. *Pediatrics* 1992;90:436–441. [PubMed](#)
4. Stunell H, Buckley O, Feeney J, Geoghegan T, Browne RF, Torreggiani WC. Imaging of acute pyelonephritis in the adult. *Eur Radiol* 2007;17:1820–1828. [PubMed](#)

Case 98

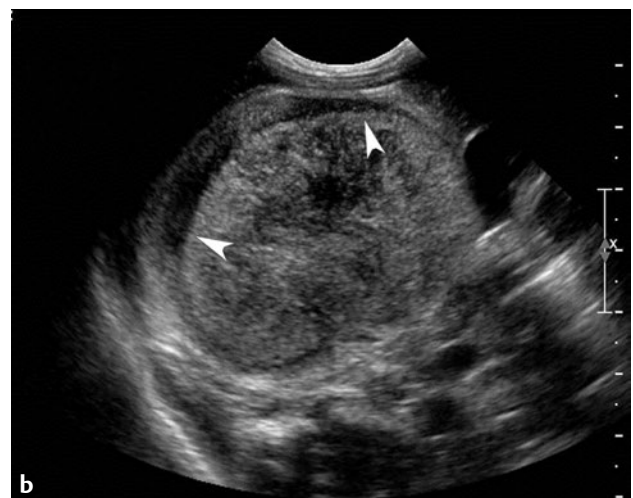
■ Clinical Presentation

A term newborn with right upper abdominal mass.

■ Radiographic Studies

Longitudinal ultrasound image (**Fig. 98.1a**) shows a heterogeneous solid mass infiltrating the right kidney. Transverse ultrasound image (**Fig. 98.1b**) shows the intrarenal mass compressing adjacent normal renal parenchyma (*arrowheads*).

Postcontrast coronal reformatted CT image (**Fig. 98.1c**) shows the solid mass centrally in the kidney with some normally enhancing renal parenchyma superior and inferior.



■ Diagnosis

Mesoblastic Nephroma

■ Discussion and Differential Diagnosis

Mesoblastic nephroma, also known as fetal renal hamartoma, is the most common solid renal tumor in the newborn. Mean age at diagnosis is 3 months. This variable-sized mass is predominantly solid, unilateral, and usually benign.¹ Mesoblastic nephroma may be associated with polyhydramnios, often leading to prematurity delivery.^{2,3} Mesoblastic nephroma is a hamartomatous lesion, consisting of interlacing spindle cells in a collagen background.^{4–6} The cut surface has a whorled appearance that resembles a uterine fibroid.⁴ The margins of the tumor interlace with the normal renal parenchyma.⁶ Imaging studies usually define a heterogeneous solid renal mass that rarely calcifies. On ultrasound, the mass is predominantly solid but may have some cystic components.⁷ There is often a peripheral hypoechoic rim, and color Doppler may show a rim of

peripheral increased flow.⁷ CT shows a nonspecific solid renal mass of variable attenuation that does not invade the renal vein and does not extend into the renal pelvis.^{5,6} Functioning nephrons are frequently trapped within the mass, and therefore variable concentrations of contrast may accumulate within the mass on CT imaging.⁶ Differential diagnosis includes other solid renal tumors. Wilms' tumor is the primary consideration, and the two cannot be distinguished based on imaging.^{1,7} Nephroblastomatosis is easily distinguishable from mesoblastic nephroma by the presence of multifocal solid masses subcapsular in location.⁶ Multilocular cystic renal tumor can be difficult to distinguish from a cystic mesoblastic nephroma.⁶ Other renal lesions such as hydronephrosis and multicystic dysplastic kidney are readily distinguishable at ultrasound.¹

Pearls

- ◆ In the first 3 months of life, a solid renal tumor favors mesoblastic nephroma. Wilms' tumor is rare in the first year of life.⁷
- ◆ Nephrectomy is usually curative, but wide surgical margins are necessary to prevent local recurrence.⁵

Pitfall

- ◆ The "cellular" subtype of mesoblastic nephroma is more aggressive with abundant mitotic activity and rare local recurrence; pulmonary metastases have been described.^{5,7}

References

1. White KS, Grossman H. Wilms' and associated renal tumors of childhood. *Pediatr Radiol* 1991;21:81–88 [PubMed](#)
2. Blank E, Neerhout RC, Burry KA. Congenital mesoblastic nephroma and polyhydramnios. *JAMA* 1978;240:1504–1505 [PubMed](#)
3. Bolande RP. Congenital mesoblastic nephroma of infancy. *Perspect Pediatr Pathol* 1973;1:227–250 [PubMed](#)
4. Hartman DS, Lesar MS, Madewell JE, Lichtenstein JE, Davis CJ Jr. Mesoblastic nephroma: radiologic-pathologic correlation of 20 cases. *AJR Am J Roentgenol* 1981;136:69–74 [PubMed](#)
5. Lowe LH, Isuani BH, Heller RM, et al. Pediatric renal masses: Wilms tumor and beyond. *Radiographics* 2000;20:1585–1603 [PubMed](#)
6. Chaudry G, Perez-Atayde AR, Ngan BY, Gundogan M, Daneman A. Imaging of congenital mesoblastic nephroma with pathological correlation. *Pediatr Radiol* 2009;39:1080–1086 [PubMed](#)
7. Linam LE, Yu X, Calvo-Garcia MA, et al. Contribution of magnetic resonance imaging to prenatal differential diagnosis of renal tumors: report of two cases and review of the literature. *Fetal Diagn Ther* 2010;28:100–108 [PubMed](#)

Case 99

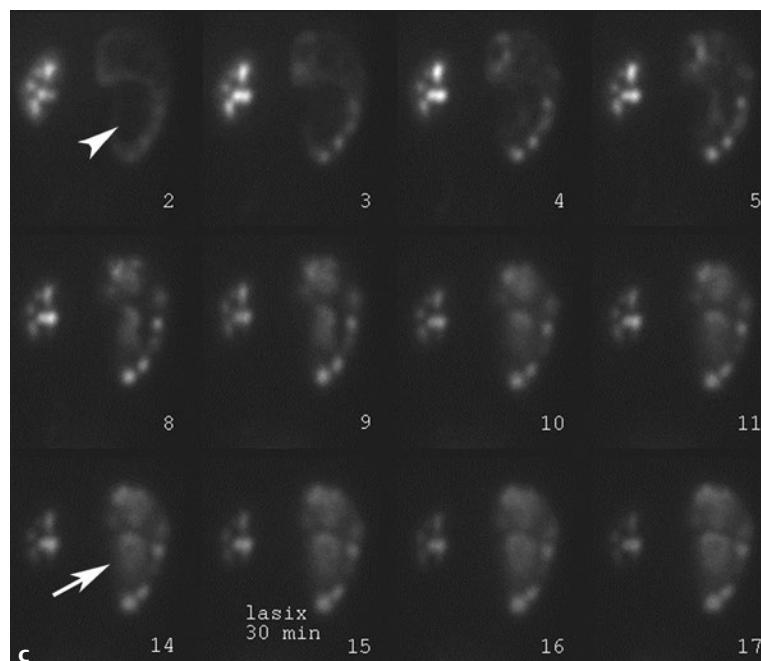
Clinical Presentation

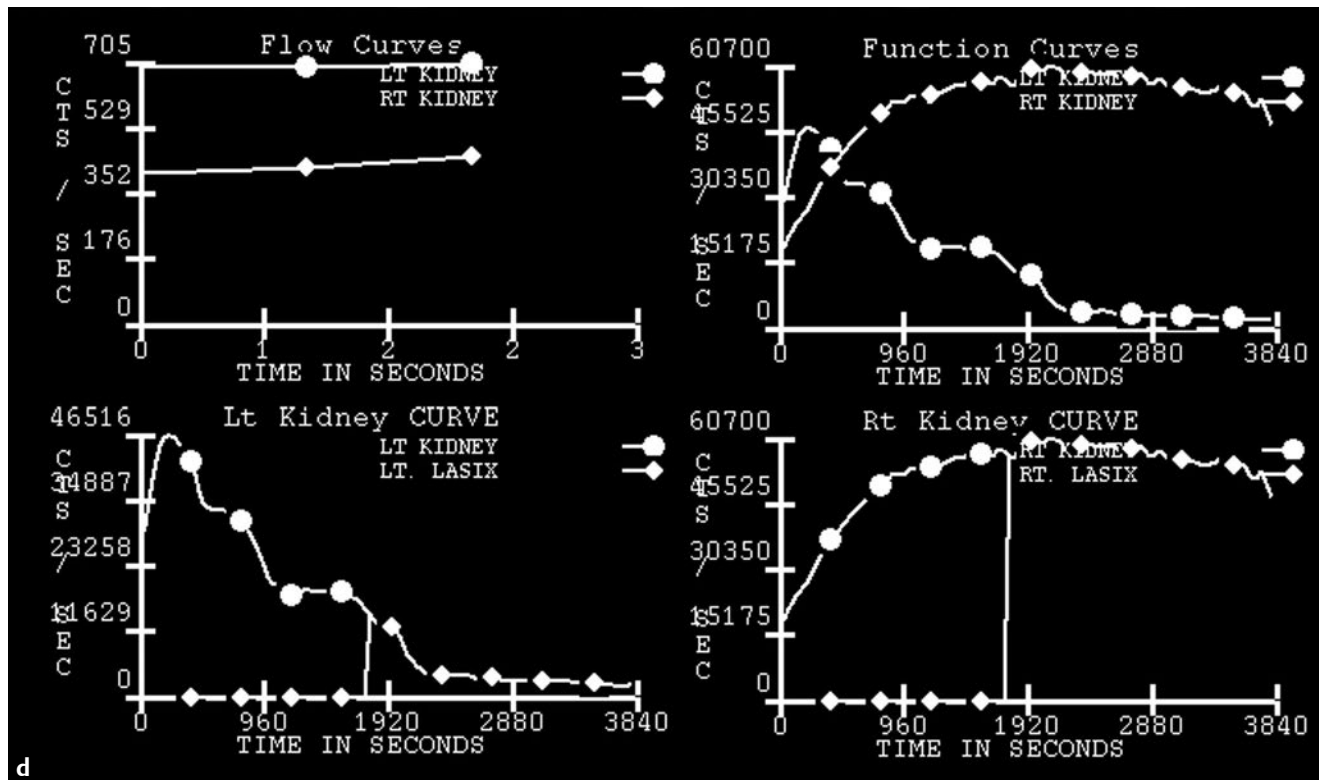
A 14-year-old boy with intermittent abdomen pain.

Radiographic Studies

Axial postcontrast CT image (**Fig. 99.1a**) shows marked right hydronephrosis with parenchymal thinning and delayed contrast excretion (*arrowhead*). The left kidney is normal. Longitudinal ultrasound image of the right kidney (**Fig. 99.1b**) shows severe hydronephrosis with parenchymal thinning. No dilated right ureter is seen. Posterior images from a nuclear

medicine Lasix renogram (**Fig. 99.1c**) show central photopenia of the right collecting system at 2 minutes (*arrowhead*) and delayed excretion of tracer into the right collecting system at 14 minutes (*arrow*). The renogram time activity curve (**Fig. 99.1d**) shows delayed tracer washout from the obstructed right collecting system. The left kidney tracer washout is normal.





■ Diagnosis

Ureteropelvic Junction Obstruction

■ Discussion and Differential Diagnosis

Ureteropelvic junction obstruction (UPJO) is the most common cause of prenatal and neonatal hydronephrosis¹⁻³; its incidence is 1 in 1,500, with a male and left-sided predominance.^{2,3} Up to 40% of cases are bilateral; this occurs more frequently in those diagnosed younger than 6 months of age.³ Associated anomalies are seen in up to 50% of cases and include contralateral multicystic dysplastic kidney, vesicoureteral reflux, VATER (vertebral, anal, tracheal, esophageal, and renal) anomalies, congenital heart disease, duplex collecting system, and rotation and fusion anomalies.³ Intrinsic anomalies of the ureteropelvic junction are the most common cause, and include ureteric stenosis and adynamic ureteric segment secondary to muscle discontinuity.^{1,2} Extrinsic compression of the ureteropelvic junction is less common and is usually secondary to ureteral kinking, fibrous bands, or vascular compression; this is more commonly seen in older children.^{1,2}

Ureteropelvic junction obstructions are frequently diagnosed prenatally. Renal pelvis diameter of 5 mm or less in the second or third trimester is normal; renal pelvis dilatation greater than 10 to 12 mm is definitely abnormal and requires evaluation after birth. The investigation includes an initial ultrasound to confirm the abnormality; if the initial neonatal ultrasound is abnormal, a repeat study should be performed at

4 weeks.⁴ Ultrasound shows dilatation of the central renal pelvis communicating with dilated calyces at the lateral margins of the kidney. The ureter is not dilated. Changes of dysplasia due to longstanding obstruction may be seen, and include increased echogenicity of the renal parenchyma, cortical cysts, and parenchymal thinning.¹ Voiding cystourethrography should be performed to differentiate dilatation secondary to UPJO from dilatation secondary to vesicoureteral reflux. Functional evaluation is performed with diuretic nuclear renography to evaluate the degree of obstruction; in the newborn, it is best to wait 3 to 4 weeks after birth, for complete renal function to develop. If the time for drainage of half of the radioisotope from the upper collecting system is greater than 20 minutes after the administration of furosemide (Lasix), then the patient has obstruction, and surgical treatment is indicated. Additional criteria for surgical treatment include decreased split renal function of the affected kidney (< 30%), ongoing pain, recurrent UTI, hypertension, or hematuria.⁵ The standard surgical procedure is open or laparoscopic pyeloplasty. In infants or in cases of acute obstruction or infection, placement of a diverting percutaneous nephrostomy may be useful to decompress the collecting system as a bridge to definitive surgical treatment.⁶

The differential diagnosis of UPJO includes ureterovesical junction obstruction (UVJO), multicystic dysplastic kidney, and dilated nonobstructed collecting system. Ureterovesical junction obstruction shows similar findings, but a dilated ureter is identified behind the bladder at ultrasound. On ultrasound, the cystic structures of multicystic dysplastic kidneys do not

communicate with one another or with a large central renal pelvis.⁷ Patients with reflux may show dilated upper collecting systems, but voiding cystourethrography delineates these patients. Dilated nonobstructed collecting systems are differentiated from UPJO by nuclear diuretic renography or duplex Doppler ultrasound.

Pearls

- ◆ Ultrasound is the primary observation tool after initial evaluation, with diuretic renogram used only in the case of worsening hydronephrosis or symptoms.⁵
- ◆ Technetium-99m mercaptoacetyltriglycine (MAG3), the tracer that relies on tubular extraction, is the preferred tracer in infants with possible obstruction, rather than the standard Tc-99m diethylenetriaminepentaacetate (DTPA), which depends on glomerular filtration.⁸

Pitfall

- ◆ In rare cases, renal stone with stricture, atypical valve, or intraluminal polyp/masses may cause secondary ureteropelvic junction obstruction.⁹

References

1. Mercado-Deane MG, Beeson JE, John SD. US of renal insufficiency in neonates. *Radiographics* 2002;22:1429–1438. [PubMed](#)
2. Epelman M, Victoria T, Meyers KE, Chauvin N, Servaes S, Darge K. Postnatal imaging of neonates with prenatally diagnosed genitourinary abnormalities: a practical approach. *Pediatr Radiol* 2012;42(Suppl 1):S124–S141. [PubMed](#)
3. Karnak I, Woo LL, Shah SN, Sirajuddin A, Kay R, Ross JH. Prenatally detected ureteropelvic junction obstruction: clinical features and associated urologic abnormalities. *Pediatr Surg Int* 2008;24:395–402. [PubMed](#)
4. Kitchens DM, Herndon CD. Antenatal hydronephrosis. *Curr Urol Rep* 2009;10:126–133. [PubMed](#)
5. Heinlen JE, Manatt CS, Bright BC, Kropp BP, Campbell JB, Frimberger D. Operative versus nonoperative management of ureteropelvic junction obstruction in children. *Urology* 2009;73:521–525, discussion 525. [PubMed](#)
6. Linscott L. Pediatric urologic interventional radiology. *Semin Intervent Radiol* 2011;28:407–414. [PubMed](#)
7. Fryer K, Nield LS, Muchant DG. Resident Rounds. Multicystic dysplastic kidney. *Clin Pediatr* 2007;46:365–367
8. Gordon I, Piepsz A, Sixt R; Auspices of Paediatric Committee of European Association of Nuclear Medicine. Guidelines for standard and diuretic renogram in children. *Eur J Nucl Med Mol Imaging* 2011;38:1175–1188. [PubMed](#)
9. Wang XM, Jia LQ, Wang Y, Wang N. Utilizing ultrasonography in the diagnosis of pediatric fibroepithelial polyps causing ureteropelvic junction obstruction. *Pediatr Radiol* 2012;42:1107–1111. [PubMed](#)

Case 100

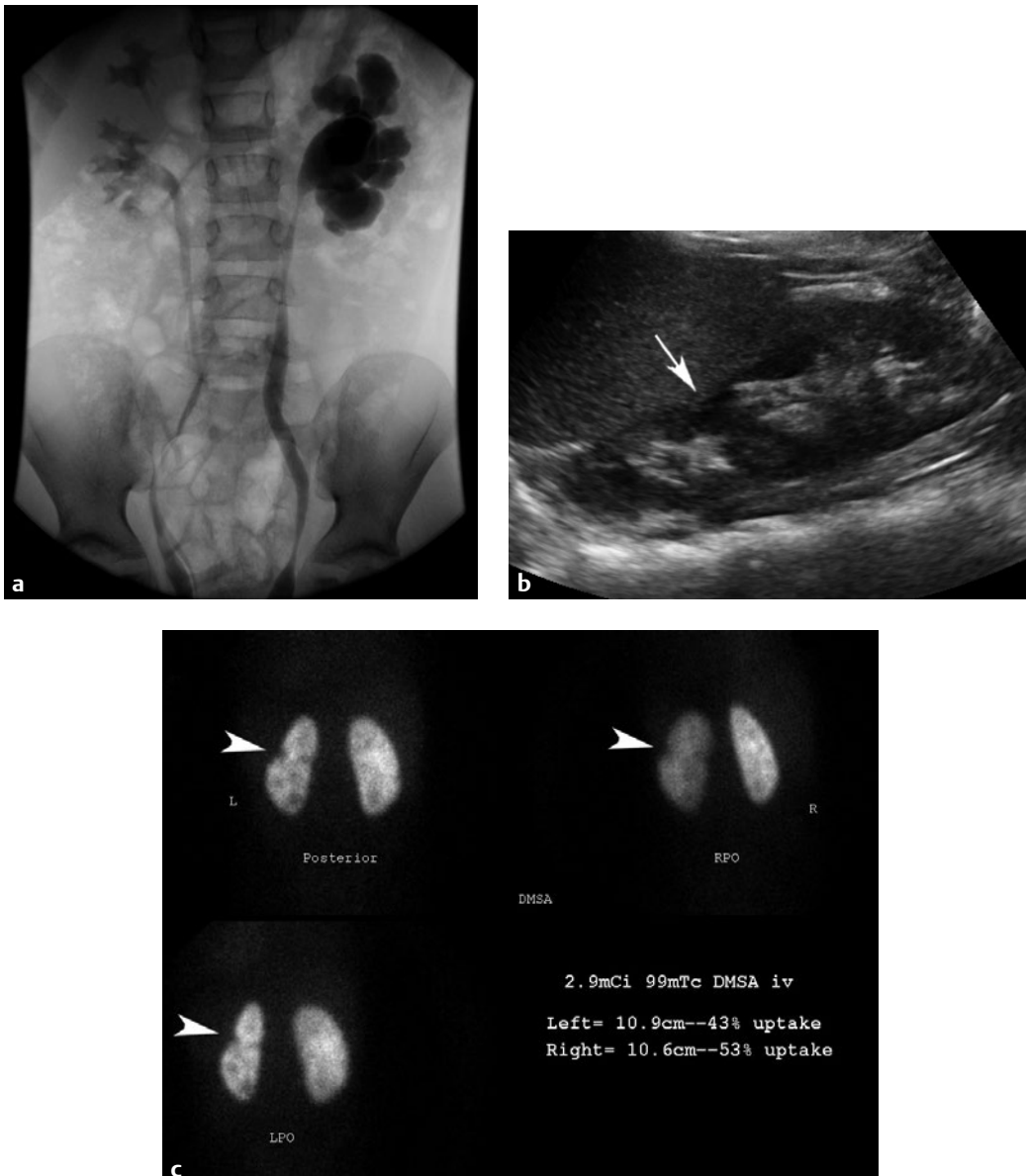
■ Clinical Presentation

A 7-year-old girl with recurrent urinary tract infections.

■ Radiographic Studies

Radiograph during voiding cystourethrogram (VCUG) exam (**Fig. 100.1a**) shows bilateral vesicoureteral reflux with duplicated right renal collecting system and ureter. Longitudinal ultrasound of the left kidney (**Fig. 100.1b**) shows focal cortical thinning in the midpole of the left kidney (arrow). Subsequent

technetium-99m dimercaptosuccinic acid (DMSA) nuclear scintigraphy (**Fig. 100.1c**) shows a focal wedge-shaped defect in the midpole of the left kidney (*arrowheads*) corresponding to the ultrasound finding. Asymmetric decreased left renal tracer uptake compared with the right kidney is noted.



■ Diagnosis

Cortical Scarring

■ Discussion and Differential Diagnosis

Urinary tract infection (UTI) can lead to renal scarring, and children with scarred kidneys are predisposed to hypertension and chronic renal failure.¹ Imaging studies focus on identifying the potential underlying cause of UTI and potential complications.² Although renal scarring from UTI can occur in the absence of vesicoureteral reflux, VCUG is commonly performed in patients with UTI to identify the presence and severity of reflux.² If scarring does occur, ultrasound may demonstrate a hyperechoic wedge-shaped region with the base toward the renal capsule and the apex toward the calyx.³ Other ultrasound features are irregularity or indentation of the cortical outline, decreased or asymmetrical cortical thickness, and flattening of papillae.³ There may be focal retraction of the renal surface and dilatation or clubbing of the underlying calyx.³ If multiple areas of scarring are present, the kidney is usually small, heterogeneous, and lobulated.³ Doppler

ultrasound shows reduced peripheral vascularity at the site of scarring.¹

Nuclear scintigraphy using the cortical agent technetium-99m DMSA is considered the gold standard for the detection of renal scarring.² DMSA has a high affinity for the renal cortex because of its concentration in tubular cells and gives sufficient detail to evaluate basic renal morphology.² Use of single photon emission computed tomography (SPECT) increases the sensitivity of DMSA to changes of renal scarring.² Although not the initial study of choice, CT shows wedge-shaped areas of cortical nonenhancement with associated cortical thinning.⁴

The primary differential diagnosis for cortical scarring is fetal lobulation of the kidney. With fetal lobulation, parenchymal thickness is normal, and contour indentations between renal pyramids are smooth. Scarring, on the other hand, causes contour indentations that overlie the renal pyramids.⁴

Pearls

- ◆ There is a positive relationship between severity of reflux and formation of scarring.
- ◆ There is evidence that scarring occurs due to reflux from infected urine rather than sterile urine.⁴
- ◆ On ultrasound at the site of a scar the pyramid may be gone and there is a dilated calyx as well as an indentation in the cortex.⁵

Pitfall

- ◆ Ultrasound may not detect small focal scars that are better seen with DMSA.

References

1. Moorthy I, Wheat D, Gordon I. Ultrasonography in the evaluation of renal scarring using DMSA scan as the gold standard. *Pediatr Nephrol* 2004;19: 153–156 [PubMed](#)
2. Siomou E, Giapros V, Fotopoulos A, et al. Implications of 99mTc-DMSA scintigraphy performed during urinary tract infection in neonates. *Pediatrics* 2009;124:881–887 [PubMed](#)
3. Barry BP, Hall N, Cornford E, Broderick NJ, Somers JM, Rose DH. Improved ultrasound detection of renal scarring in children following urinary tract infection. *Clin Radiol* 1998;53:747–751 [PubMed](#)
4. Shore R. Scurvy. In: Slovis T, ed. *Caffey's Pediatric Diagnostic Imaging*, 11th ed. Philadelphia: Mosby Elsevier; 2007:2347–2349
5. Calado AA, Barroso U Jr, Barroso VA, Souza AS, Filho MZ. Ultrasound evaluation of renal scarring in children with vesicoureteral reflux. *Br J Urol* 2002;28:250–253

Case 101

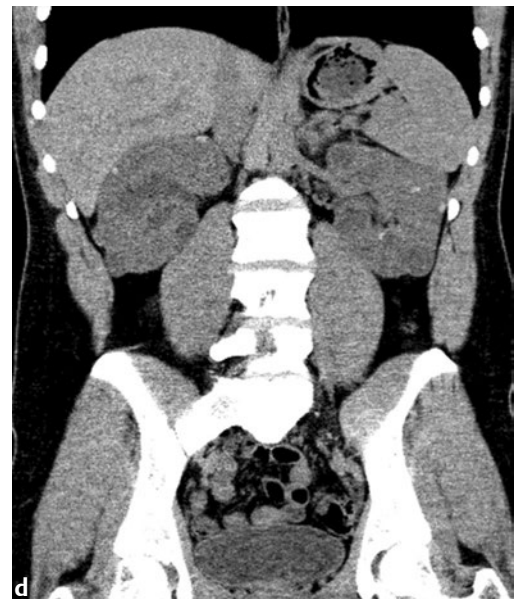
■ Clinical Presentation

A 10-year-old with hematuria and right flank pain.

■ Radiographic Studies

Longitudinal scans of both kidneys (**Fig. 101.1a,b**) show multiple variable-sized renal cysts involving the cortex and the medulla, separated by areas of normal parenchyma. No hydronephrosis, hydroureter, or renal calculi are identified. Transverse ultrasound image in a different 17-year-old patient (**Fig.**

101.1c) shows multiple variable-sized oval cysts in renal cortex and medulla. This same patient presented 1 year later with acute flank pain and noncontrast coronal reformatted CT image (**Fig. 101.1d**) shows bilateral renal cysts with lobular renal contour and scattered sites of focal high attenuation hemorrhage.



■ Diagnosis

Autosomal Dominant Polycystic Kidney Disease

■ Discussion and Differential Diagnosis

Autosomal dominant polycystic kidney disease (ADPKD) usually presents in the third or fourth decade of life as hypertension, hematuria, or slowly progressive renal failure.¹ Some patients may present early in life, even as early as in utero. In ADPKD, cysts arise from the nephron, lose their connection to the tubules, enlarge, and eventually replace normal renal tissue.² It is now known that ADPKD is a ciliopathy (a disorder of cilia), and cysts can occur in the pancreas, liver, arachnoid membrane, and seminal vesicles.³ Other extrarenal manifestations include intracranial aneurysms (6–21%), mitral valve prolapse (25%), colonic diverticula, dilation of the aortic root, and thoracic aorta dissection.^{1–3} Most ADPKD patients are born with normal kidneys; cysts develop and increase in size over time.³ ADPKD may also present in early childhood with a flank mass, hematuria, or flank pain. In the neonatal period, patients can have multiple small renal cysts that may be difficult to differentiate from autosomal recessive polycystic kidney disease (ARPKD).¹ Differentiation can be made by the presence

of pancreatic cysts in ADPKD and the absence of portal fibrosis or bile duct proliferation (although liver cysts may be seen). In children with a family history, a single cyst in both kidneys is adequate to make the diagnosis of ADPKD.

Two genes have been identified for ADPKD: *PKD-1* and *PKD-2*. *PKD-1* defects usually cause earlier presentation and more severe disease.² Approximately 85% of affected individuals have a mutation of *PKD-1*. In patients with suspected ADPKD, ultrasound is the initial imaging modality. Findings at ultrasound include asymmetric bilateral renal enlargement with multiple renal cysts of varying sizes, involving the cortex and the medulla.^{1,3} The cysts enlarge over time and often distort the collecting system and renal pelvis.³ The cysts are usually macroscopic with normal appearance of intervening parenchyma.⁴ MRI may be performed for further evaluation, especially if there are extrarenal manifestations.¹ The differential diagnosis includes tuberous sclerosis and ARPKD.

Pearls

- ◆ ADPKD is occasionally unilateral.³
- ◆ Cysts in ADPKD may be complicated by hemorrhage or infection⁵

Pitfall

- ◆ In the neonate, ADPKD may be difficult to differentiate from ARPKD, but with increasing age, the cysts in ADPKD become more discrete, larger, and more easily isolated on ultrasound from areas of normal renal parenchyma.^{2–4}

References

1. Rizk D, Chapman AB. Cystic and inherited kidney diseases. *Am J Kidney Dis* 2003;42:1305–1317 [PubMed](#)
2. Tahvanainen E, Tahvanainen P, Kääriäinen H, Höckerstedt K. Polycystic liver and kidney diseases. *Ann Med* 2005;37:546–555 [PubMed](#)
3. Gunay-Aygun M. Liver and kidney disease in ciliopathies. *Am J Med Genet C Semin Med Genet* 2009;151C:296–306 [PubMed](#)
4. Epelman M, Victoria T, Meyers KE, Chauvin N, Servaes S, Darge K. Postnatal imaging of neonates with prenatally diagnosed genitourinary abnormalities: a practical approach. *Pediatr Radiol* 2012;42(Suppl 1):S124–S141 [PubMed](#)
5. Turkbey B, Ocak I, Daryanani K, et al. Autosomal recessive polycystic kidney disease and congenital hepatic fibrosis (ARPKD/CHF). *Pediatr Radiol* 2009;39:100–111 [PubMed](#)

Case 102

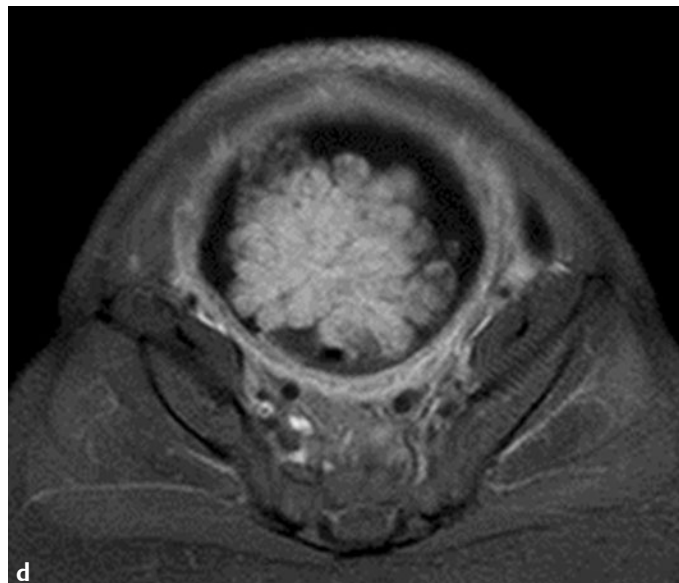
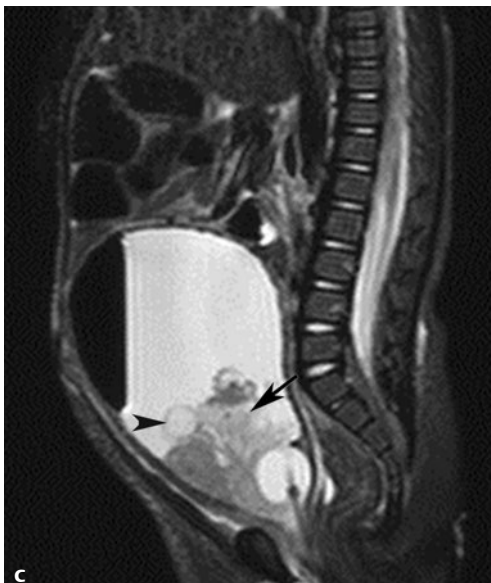
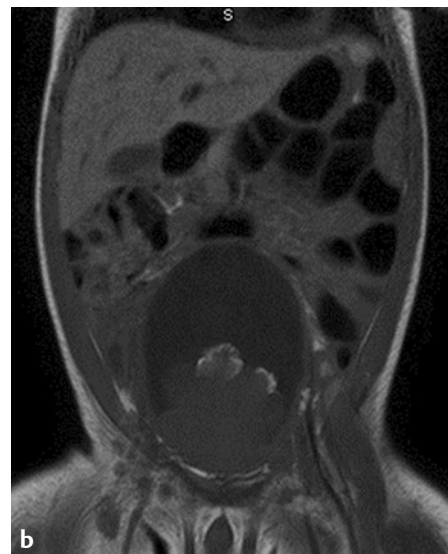
■ Clinical Presentation

A 3-year-old boy with dysuria and hematuria.

■ Radiographic Studies

Longitudinal ultrasound image of the bladder (Fig. 102.1a) shows a lobular intraluminal mass of mixed echogenicity arising from the bladder base. Coronal T1-weighted MRI (Fig. 102.1b) shows a lobulated mass, isointense to muscle, arising from the bladder base. There is a rim of increased signal superiorly that may represent hemorrhage. Sagittal T2-weighted

MRI (Fig. 102.1c) shows that most of the mass is intermediate in signal intensity (*arrow*) with some cystic components noted (*arrowhead*). Axial T1-weighted postcontrast MRI with fat saturation (Fig. 102.1d) shows intense enhancement of the lobular mass.



■ Diagnosis

Rhabdomyosarcoma

■ Discussion and Differential Diagnosis

Rhabdomyosarcoma is the most common pediatric soft tissue sarcoma, and accounts for 5% of all childhood cancers.^{1–4} It occurs most frequently in young children, with a peak incidence between 2 and 5 years; there is a smaller peak in early to mid-adolescence.¹ Rhabdomyosarcoma can occur at virtually any site in the body; the most frequent location is the head and neck (40%), followed by the genitourinary tract.^{3,4} Histologically, rhabdomyosarcoma arises from primitive mesenchymal cells committed to differentiate into skeletal muscle cells.^{1,3} There are two main histological subtypes: embryonal and alveolar. Embryonal rhabdomyosarcoma is the more common (60%) and usually occurs in the head and neck, retroperitoneum, and genitourinary tract.⁴ The embryonal subtype includes botryoid rhabdomyosarcoma, which usually invades hollow visceral organs such as the bladder and vagina in young children and the nasopharynx of older children.¹ Alveolar and pleomorphic/undifferentiated histological types are less common, and usually involve the limbs and trunk.^{3,4}

Presentation varies according to the site. In the lower urinary tract, patients usually present with hematuria, palpable abdominal mass, or obstructive symptoms.^{1,3} Vaginal masses are almost exclusively found in girls younger than 2 years of age³; they typically present as polypoid grape-like masses protruding through the introitus. Cervical/uterine rhabdomyosarcoma is more common in older girls.¹ Both vaginal and cervical/uterine rhabdomyosarcoma may present with urinary symptoms (resulting from invasion of the bladder) or with bloody vaginal discharge.² Paratesticular tumors may present as painless, unilateral scrotal enlargement.¹

Some 10 to 20% of cases are metastatic at diagnosis,⁴ most commonly to the lung, bone marrow, and bone.³ Regional lymph node involvement is seen in 20% of bladder and prostate tumors.² Rhabdomyosarcoma invades adjacent organs in the pelvis, and it may be difficult to differentiate tumor arising from the bladder base, the vagina, or the prostate. In all patients with bladder wall masses, cystoscopy and biopsy is important in diagnosis.⁵

The differential diagnosis of pelvic rhabdomyosarcoma includes neurofibroma, vascular tumor or malformation, or lymphoma.⁴ Infiltration and inflammation of the bladder wall from eosinophilic cystitis may cause asymmetric bladder wall thickening (pseudotumor cystitis), trigone and ureteral wall invasion with obstruction, and bladder outlet obstruction; this diagnosis is difficult to differentiate from rhabdomyosarcoma.

Ultrasound is usually the initial imaging modality for bladder and pelvic lesions. It is typically a lobulated, hypoechoic, solid mass than can have increased flow.^{2,3} CT is generally performed for further characterization of the mass, to define extension into adjacent soft tissues, and to search for pulmonary metastases.^{2,3} On MRI, the tumor is high signal on T2-weighted images and variable signal on T1-weighted images, and it intensely enhances.^{3,4} MRI may be preferable to CT for bladder and prostate origin rhabdomyosarcoma, especially for post-treatment follow-up. Bladder-wall thickening is difficult to see on CT (especially with a partially distended bladder), but T2-weighted MRI enables distinguishing the bladder wall from fluid-filled bladder.⁴ Nuclear medicine bone imaging is usually performed to search for bone metastases.^{2,3}

Pearl

- ◆ Paratesticular, vaginal, and uterine rhabdomyosarcoma lesions have a favorable prognosis.⁴

Pitfall

- ◆ Intravesical rhabdomyosarcoma may be confused with intravesical blood clot at ultrasound. Blood clot is typically non-adherent and lacks internal Doppler flow.

References

1. Park K, van Rijn R, McHugh K. The role of radiology in paediatric soft tissue sarcomas. *Cancer Imaging* 2008;8:102–115 [PubMed](#)
2. Swinson S, McHugh K. Urogenital tumours in childhood. *Cancer Imaging* 2011;11 Spec No A:S48–S64 [PubMed](#)
3. Kaste SC, McCarville MB. Imaging pediatric abdominal tumors. *Semin Roentgenol* 2008;43:50–59 [PubMed](#)
4. Stein-Wexler R. MR imaging of soft tissue masses in children. *Magn Reson Imaging Clin N Am* 2009;17:489–507, vi [PubMed](#)
5. McLean TW, Buckley KS. Pediatric genitourinary tumors. *Curr Opin Oncol* 2010;22:268–273 [PubMed](#)

Case 103

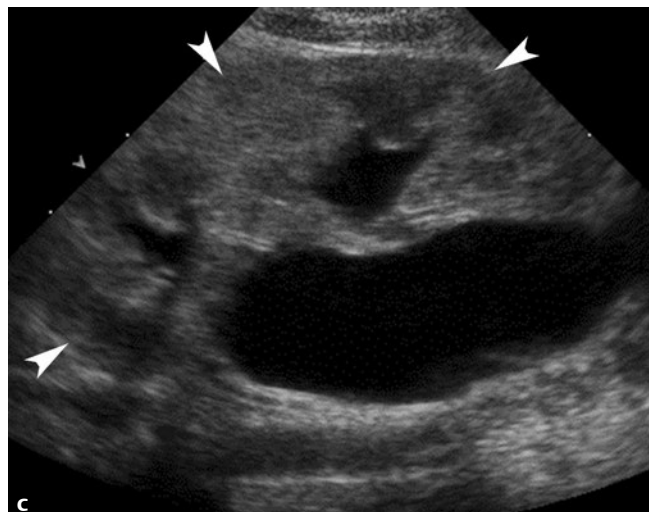
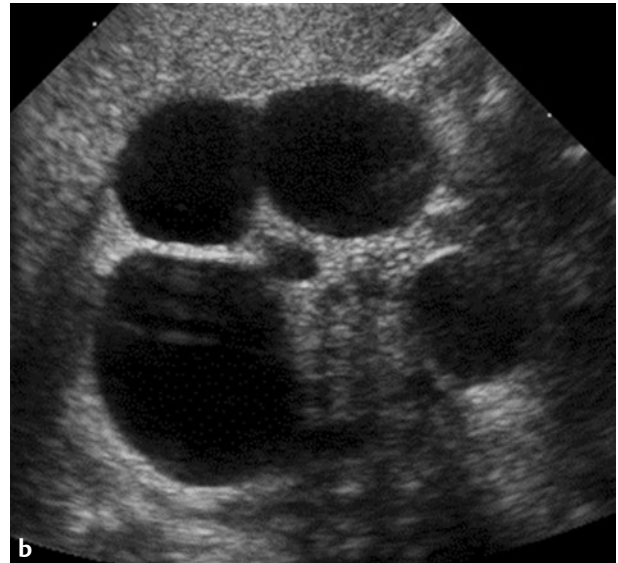
■ Clinical Presentation

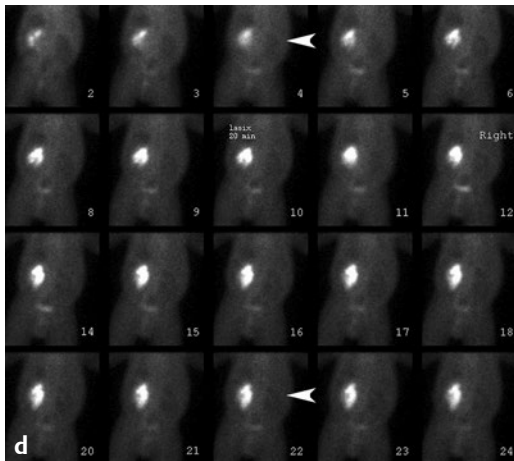
A 2-month-old boy with renal cystic lesions seen on prenatal imaging.

■ Radiographic Studies

Longitudinal and transverse ultrasound images of the right kidney (**Fig. 103.1a,b**) show noncommunicating cysts of variable size and the absence of normal right renal parenchyma; no collecting system or proximal ureter is seen. Longitudinal ultrasound of the contralateral left kidney (**Fig. 103.1c**) shows normal renal parenchymal thickness (*arrowheads*) and dilated calyces extending toward a dilated central renal pelvis. Nuclear

medicine Lasix renogram (**Fig. 103.1d**) shows no tracer uptake in the right kidney (*arrowheads*). The contralateral left collecting system is dilated with delayed tracer washout post-Lasix consistent with ureteropelvic junction obstruction. Prone longitudinal ultrasound image of the right kidney 8 years later (**Fig. 103.1e**) shows interval decrease size of the right kidney and associated cysts.





■ Diagnosis

Multicystic Dysplastic Kidney

■ Discussion and Differential Diagnosis

Multicystic dysplastic kidney (MCDK) is one of the most frequent urinary tract abnormalities identified prenatally.¹ It is a common cause of an abdominal or flank mass in an infant and the most common cystic renal disease.² MCDK is a type of renal dysplasia characterized by abnormal metanephric differentiation; multiple noncommunicating cysts are separated by dysplastic parenchyma.^{1,3} The cause is not completely clear, but may be related to abnormal formation of the ureteric bud or abnormal interactions between the ureteric bud and metanephric mesenchyme.^{1,2} MCDK is usually sporadic, but may in rare cases be familial.^{2,3} Some studies have implicated teratogens such as in utero viral infections.¹ Other cystic renal diseases are included in the differential and can have similar ultrasound appearances: cystic Wilms' tumor, multilocular cyst, and cystic mesoblastic nephroma.²

At sonography, MCDK appears as multiple noncommunicating cysts of varying sizes with little or no renal parenchyma, and no identification of a dominant central cyst.² If renal tissue is present, it is abnormally echogenic. Hydronephrosis, the primary differential diagnosis, typically consists of a dilated central renal pelvis with radiating, communicating, relatively uniformly dilated calyces. With nuclear medicine imaging, multicystic dysplastic kidney usually shows no function at 4 hours. By distinction, hydronephrosis is identified by crescents of functioning renal tissue, with eventual presence of radioisotope in the central renal pelvis. The contralateral kidney is abnormal in up to 30% of cases of MCDK (Fig. 103.1c,d).

Pearls

- ◆ The most common contralateral abnormality in MCDK is vesicoureteral reflux, and a voiding cystourethrogram (VCUG) is recommended on all MCDK patients.^{1,4,5} Other contralateral anomalies include ureteropelvic junction obstruction (7 to 15% of patients with MCDK), ureterovesical junction obstruction, and horseshoe kidney.^{1,2}
- ◆ Involution of the multicystic dysplastic kidney may occur before or after birth. Different studies report different rates of involution, but 74% involute by age 10.¹
- ◆ There is a small risk of hypertension developing, so blood pressure examinations should be a routine part of the clinical follow-up.¹

Pitfall

- ◆ In 5 to 10% of the cases, a "hydronephrotic" type of MCDK is identified. At ultrasound, a dilated renal pelvis or central cyst is seen, making differentiation of MCDK from hydronephrosis difficult. In these cases, a diuretic renogram should be performed to differentiate MCDK from severe hydronephrosis.¹

■ Controversy

- Management is usually conservative, with serial ultrasound examinations documenting involution of the MCDK. Some authors have reported rare malignant degeneration, but large studies have found the incidence of malignancy in MCDK to be only slightly higher than in the general population.

References

1. Hains DS, Bates CM, Ingraham S, Schwaderer AL. Management and etiology of the unilateral multicystic dysplastic kidney: a review. *Pediatr Nephrol* 2009; 24:233–241 [PubMed](#)
2. Fryer K, Nield LS, Muchant DG. Resident Rounds. Multicystic dysplastic kidney. *Clin Pediatr*. 2007;46:365–367
3. Bisceglia M, Galliani CA, Senger C, Stallone C, Sessa A. Renal cystic diseases: a review. *Adv Anat Pathol* 2006;13:26–56 [PubMed](#)
4. Hayes WN, Watson AR; Trent & Anglia MCDK Study Group. Unilateral multicystic dysplastic kidney: does initial size matter? *Pediatr Nephrol* 2012;27:1335–1340 [PubMed](#)
5. Hollowell JG, Kogan BA. How much imaging is necessary in patients with multicystic dysplastic kidneys? *J Urol* 2011;186:785–786 [PubMed](#)

Case 104

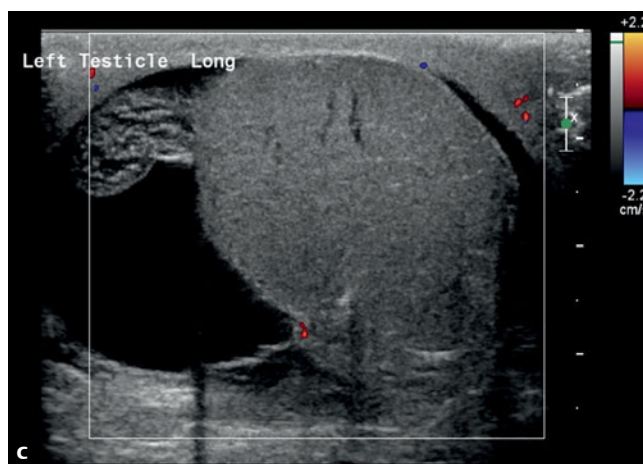
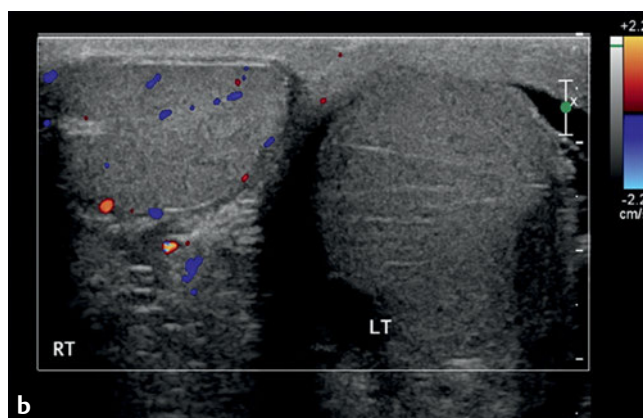
■ Clinical Presentation

A 12-year-old with acute onset of left scrotal pain.

■ Radiographic Studies

Transverse midline image of the scrotum (**Fig. 104.1a**) shows an enlarged left testis that is hypoechoic compared with the right testis; there is also a hydrocele. Transverse midline image with Doppler (**Fig. 104.1b**) shows no flow in the left testis.

Longitudinal Doppler image of the left testis (**Fig. 104.1c**) shows the enlarged, mildly heterogeneous left testis with no color flow in the testis or epididymis.



■ Diagnosis

Testicular Torsion



■ Discussion and Differential Diagnosis

Although not the most common cause of an acute scrotum in children (around 25%), testicular torsion is certainly the most important.¹ Patients typically present with acute onset of severe scrotal pain, often with nausea and vomiting. The pain is constant and is not relieved with scrotal elevation.² On physical exam, the testis is extremely tender, high-riding, and has a transverse lie.³ Scrotal swelling, erythema, and loss of the cremasteric reflex may also be present.²⁻⁴

There is a 90% testicular salvage rate if the spermatic cord is untwisted within 6 hours from the onset of symptoms, and a 75% salvage rate within 12 hours.^{2,3} After 24 hours, the testis will generally not regain blood flow.² Salvage rate also depends on the degree of twist: blood flow changes are minimal after torsion of 360 degrees or less, and significantly reduced in 720 degrees.^{1,3} Salvage rate is higher for normally located testes than undescended testes.¹

Testicular torsion has a bimodal age distribution. Approximately two thirds of cases occur in the adolescent age group, and are intravaginal torsions. In these patients, the tunica vaginalis completely surrounds the testis and epididymis (bell-clapper deformity), preventing their fixation to the scrotal wall and allowing rotation of the spermatic cord.^{3,4} This anatomic abnormality is bilateral in up to 80% of patients.³

The other common type of torsion occurs perinatally. This is caused by the absence of normal fixation of the tunica vaginalis and gubernaculum to the scrotal wall, resulting in

abnormal mobility and torsion of the tunica vaginalis as well as testis and epididymis.¹⁻³ This is infrequently bilateral, and often presents as chronic torsion.

Gray-scale sonography can be normal in the early phase of testicular torsion^{1,2}; however, blood flow will be decreased or absent even early.³ Within 4 to 6 hours, the testis and epididymis enlarge and become hypoechoic, with persistent decrease or absent flow on Doppler.²⁻⁴ Several studies have reported identification of the site of spermatic cord torsion, which appears as a mass or swirl of vessels cranial to the affected testis ("whirlpool" or "cord knot" sign).^{1,4} Once the testis has been torsed for longer than 24 hours ("late" or "missed" torsion), the testis returns to normal echogenicity, and eventually becomes atrophic.²

The differential diagnosis for acute scrotum in the absence of trauma in a child includes torsion of the appendix testis and epididymitis/epididymo-orchitis. Testicular torsion can be easily differentiated sonographically due to decreased testicular blood flow. Torsion of the appendix testis can be differentiated from testicular torsion by increased blood flow to the epididymis and testis. Epididymitis/epididymo-orchitis generally has a longer duration of symptoms prior to presentation, ranging from 24 to 72 hours.³ Sonographically, the epididymis is enlarged and heterogeneous, most markedly at the head; on Doppler, the epididymis is hyperemic.

Pearls

- ◆ An enlarged hypoechoic testis with decreased flow is testicular torsion until proven otherwise.
- ◆ Given the 90% salvage rate within the first 6 hours from onset of symptoms, time is of the essence.

Pitfalls

- ◆ Severe epididymitis can cause edema significant enough to occlude blood flow to the testicle, causing infarction.³
- ◆ Spontaneous detorsion (also called "torsion/detorsion") may have increased blood flow with enlarged, hypoechoic testis and epididymis, mimicking epididymo-orchitis. A history of spontaneous clinical improvement prior to ultrasound indicates this diagnosis.⁴

References

1. Drlik M, Kočvara R. Torsion of spermatic cord in children: a review. *J Pediatr Urol* 2013;9:259-266 [PubMed](#)
2. Hörmann M, Balassy C, Philipp MO, Pumberger W. Imaging of the scrotum in children. *Eur Radiol* 2004;14:974-983 [PubMed](#)
3. Munden MM, Trautwein LM. Scrotal pathology in pediatrics with sonographic imaging. *Curr Probl Diagn Radiol* 2000;29:185-205 [PubMed](#)
4. Baldisserotto M. Scrotal emergencies. *Pediatr Radiol* 2009;39:516-521 [PubMed](#)

VI

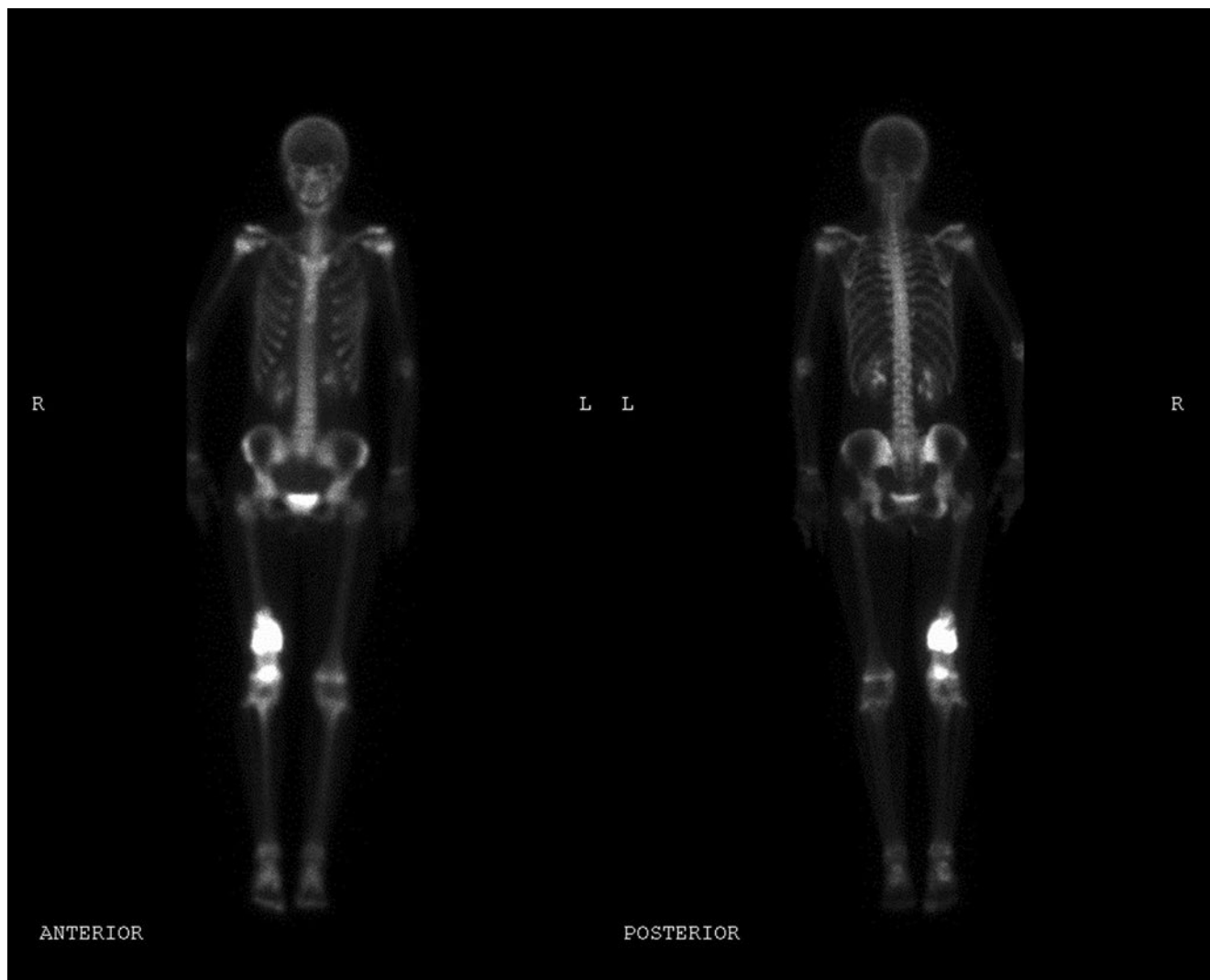
Bone

Section Editor

Charles A. James

Authors

Robert F. Buchmann and Mary B. Moore



Case 105

■ Clinical Presentation

A 3-year-old boy with arm pain after a fall.

■ Radiographic Studies

Anteroposterior and lateral radiographs of the elbow (**Fig. 105.1a,b**) show a nondisplaced supracondylar elbow fracture (type 1) and small posterior fat pad (*arrowhead*). Lateral elbow radiograph in another patient (**Fig. 105.1c**) shows a supracon-

dylar elbow fracture with marked displacement (type 3). AP radiograph in another child (**Fig. 105.1d**) shows a lateral condyle elbow fracture (arrowheads) with overlying soft tissue swelling.



■ Diagnosis

Elbow Fracture

■ Discussion and Differential Diagnosis

Elbow fractures are extremely common in children, comprising 15% of all pediatric fractures.¹ A majority of pediatric elbow fractures (85%) involve the distal humerus; olecranon and proximal radius fractures are less common.² Supracondylar fractures of the distal humerus are the most common pediatric elbow injury (50–70% of all pediatric elbow fractures) and occur predominantly in children aged 3 to 10 years.¹ These fractures are best seen on lateral radiograph; the distal fracture fragment is often displaced and angulated posteriorly. These fractures have a 10 to 15% association with neurologic injury. Nondisplaced fractures (type 1) are treated conservatively with splint or cast immobilization. Displaced fractures (types 2 and 3) require reduction and percutaneous pinning.³ Lateral condyle fractures are the second most common pediatric elbow injury (10–15% of all pediatric elbow fractures) and occur predominantly in children aged 6 to 10 years.² This

Salter-Harris type 2 injury involves the distal lateral metaphysis with oblique extension to the physis. Most fractures are displaced and often require open reduction and percutaneous pinning. The risk of neurovascular injury with lateral condyle fractures is much lower than that of a supracondylar fractures. Medial epicondyle fractures account for 10% of all pediatric elbow fractures and typically affect children and adolescents aged 7 to 15 years.⁴ The injury occurs from valgus stress on the elbow, resulting in avulsion of the medial epicondyle. Approximately 50 to 60% of these injuries are associated with posterior elbow dislocation.^{1,4} Treatment depends on the position and severity of displacement of the medial epicondyle fragment. Conservative management and splinting is performed with mild displacement. Surgical fixation is generally performed for fractures with > 5 mm displacement or entrapped fragments with elbow dislocation.⁴

Pearls

- ◆ The six centers of secondary ossification in the elbow appear in a predictable fashion, and knowledge of their appearance is essential for accurate interpretation of pediatric elbow fractures.^{1,2}
- ◆ Fat pad displacement indicates elbow joint effusion, occurs in the setting of trauma, and is useful for diagnosing occult or nondisplaced elbow fractures.^{1,2}

Pitfall

- ◆ Nondisplaced lateral condyle fractures are notoriously difficult to diagnose. Displaced lateral condyle fractures may be misdiagnosed as supracondylar fractures.¹

References

1. Shrader MW. Pediatric supracondylar fractures and pediatric physeal elbow fractures. *Orthop Clin North Am* 2008;39:163–171
2. Iyer RS, Thapa MM, Khanna PC, Chew FS. Pediatric bone imaging: imaging elbow trauma in children—a review of acute and chronic injuries. *AJR Am J Roentgenol* 2012;198:1053–1068 [PubMed](#)
3. Herzog MA, Oliver SM, Ringler JR, Jones CB, Sietsema DL. Mid-America Orthopaedic Association Physician in Training Award: Surgical technique: Pediatric supracondylar humerus fractures: a technique to aid closed reduction. *Clin Orthop Relat Res* 2013;471:1419–1426 [PubMed](#)
4. Gottschalk HP, Eisner E, Hosalkar HS. Medial epicondyle fractures in the pediatric population. *J Am Acad Orthop Surg* 2012;20:223–232 [PubMed](#)

Case 106

■ Clinical Presentation

A 3-year-old boy with left arm pain.

■ Radiographic Studies

Radiograph of the left humerus (**Fig. 106.1a**) shows an aggressive lesion in the mid-diaphysis with permeative osteolysis and laminated periosteal reaction. Sagittal STIR MRI (**Fig. 106.1b**) shows high signal intensity within the lesion, extensive mar-

row edema, and overlying soft tissue signal abnormality. Coronal fat-suppressed postcontrast T1-weighted MRI (**Fig. 106.1c**) shows intense enhancement of the lesion, bone marrow, and surrounding soft tissues.



■ Diagnosis

Langerhans Cell Histiocytosis

■ Discussion and Differential Diagnosis

Langerhans cell histiocytosis (LCH) refers to a group of disorders in three different forms, all demonstrating a proliferation of pathologic Langerhans cell histiocytes. Bone is the most common single organ to be involved in childhood LCH, but involvement of lung, lymph nodes, thymus, liver, central nervous system, and skin may occur.¹ Peak childhood incidence is between 1 and 4 years of age. Eosinophilic granuloma (EG) is the most common form of LCH with isolated lung or bone involvement and an excellent prognosis. Hand-Schüller-Christian disease is a chronic form of systemic LCH, and most of these patients have bone involvement. Letterer-Siwe disease is the least frequent form of LCH and occurs in children younger than 1 year of age. This form represents an acute disseminated life-threatening disease; bone involvement may be absent.

Children with LCH bone involvement typically present with pain and swelling. Any bone can be involved, but more than 50% of cases involve the skull, spine, pelvis, ribs, and mandible. Long bones are frequently affected, most commonly the diaphysis of the femur.² Imaging evaluation of LCH should begin with a skeletal survey. The radiographic appearance depends on the phase of disease. In the acute or early stages of disease,

lesions typically have an aggressive pattern of permeative osteolysis, are ill-defined, and demonstrate laminated periosteal reaction. The differential diagnosis of LCH includes osteomyelitis, Ewing sarcoma, leukemia, and lymphoma. In later stages of disease the lesions regress and become better defined with surrounding sclerosis and mature or absent periosteal reaction. Classic radiographic findings include “punched-out” lytic lesions in the skull (**Fig. 106.1d, arrowheads**), “vertebra plana” in the spine, and “floating teeth” in the mandible. CT (**Fig. 106.1e**) is useful for assessing osseous destruction and cortical disruption. MRI is superior for assessing the extent of marrow and soft tissue involvement.³ Imaging findings of LCH are non-specific. Diagnosis is based on clinical findings and histological/immunohistochemical criteria. Definitive diagnosis requires the presence of Birbeck granules seen on electron microscopy.^{1,2} Patients with single organ system LCH have a high incidence of spontaneous remission and favorable outcome, with treatment options including surgery, steroids, low-dose radiation, and systemic chemotherapy. Treatment of multisystem LCH is variable, given patients with a wide range of disease extent and severity.⁴

Pearls

- ◆ Langerhans cell histiocytosis is a common benign condition that can mimic aggressive bone tumors such as Ewing sarcoma.
- ◆ Beveled-edge appearance of a lytic lesion is characteristic of LCH (**Fig. 106.1e**).

Pitfall

- ◆ MRI may overestimate a lesion's aggressiveness and should always be viewed in conjunction with plain radiographs.

References

1. McCarville MB. The child with bone pain: malignancies and mimickers. *Cancer Imaging* 2009;9(Spec. No. A):S115–S121 [PubMed](#)
2. Kilborn TN, Teh J, Goodman TR. Paediatric manifestations of Langerhans cell histiocytosis: a review of the clinical and radiological findings. *Clin Radiol* 2003;58:269–278 [PubMed](#)
3. Azouz EM, Saigal G, Rodriguez MM, Podda A. Langerhans' cell histiocytosis: pathology, imaging and treatment of skeletal involvement. *Pediatr Radiol* 2005;35:103–115 [PubMed](#)
4. Abla O, Egeler RM, Weitzman S. Langerhans cell histiocytosis: Current concepts and treatments. *Cancer Treat Rev* 2010;36:354–359 [PubMed](#)

Case 107

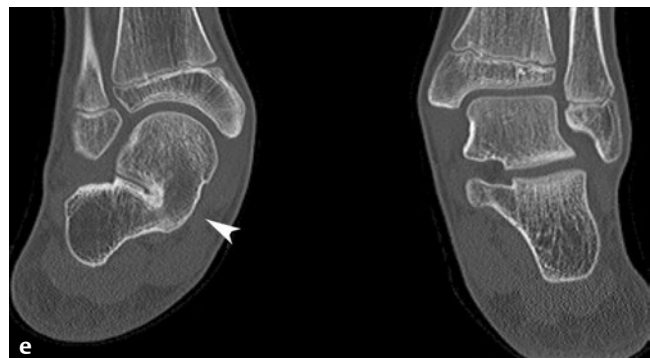
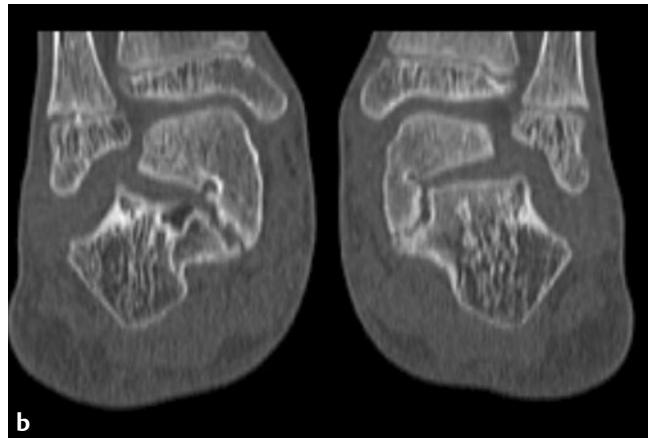
■ Clinical Presentation

A 7-year-old girl with bilateral foot pain.

■ Radiographic Studies

Standing lateral radiograph of the right foot (**Fig. 107.1a**) shows the lack of a plantar arch (pes planus) and narrowing of the subtalar joint. Lateral left foot radiograph showed similar findings. Coronal CT image of the feet in this patient (**Fig. 107.1b**) shows joint space narrowing, articular surface irreg-

ularity, and subchondral sclerosis at the sustentaculum tali of both feet. Oblique radiograph of the right foot in another patient with foot pain (**Fig. 107.1c**) shows narrowing, irregularity, and sclerosis of the calcaneonavicular joint.



■ Diagnosis

Tarsal Coalition

■ Discussion and Differential Diagnosis

Tarsal coalition is a congenital fusion between one or more tarsal bones. The fusion may be fibrous, cartilaginous, or osseous. Approximately 90% of tarsal coalitions involve the calcaneonavicular and talocalcaneal (subtalar) joints. Other sites, such as the talonavicular, calcaneocuboid, and cubonavicular joints, are much less common. Tarsal coalition occurs in 1 to 2% of the population, with a slight male predominance; 50% of affected individuals have bilateral disease.¹ Symptoms typically manifest in the second decade of life and include flat foot, pain, decreased hindfoot range of motion, and peroneal muscle spasm.² Calcaneonavicular coalition ossifies earlier and therefore presents earlier (8–12 years) than talocalcaneal coalition (12–16 years).¹ Suspected tarsal coalition is initially evaluated with three-view radiographs of the foot. Calcaneonavicular coalition is well-depicted on a 45-degree oblique X-ray. The “anteater” sign is classic (**Fig. 107.1d**, *arrowheads*) and represents elongation of the anterior process of the calcaneus, which abuts the lateral margin of the navicular bone.³ Talocalcaneal coalition most commonly involves the middle subtalar facet at the level of the sustentaculum tali. Subtalar

coalition is more difficult to visualize on radiographs, with secondary findings including joint space narrowing, subchondral sclerosis, and the C-sign on the lateral view. The C-sign is formed by the close apposition of the inferomedial border of the talus with the sustentaculum tali. A talar beak may occur with either calcaneonavicular or subtalar coalition.

Computed tomography and MRI are the most reliable methods for diagnosing subtalar coalition, particularly when the coalition is nonosseous in nature.^{1,3} The coronal plane best displays the fusion between the middle facet of the talus and the sustentaculum tali process of the calcaneus. Coronal CT image of the feet (**Fig. 107.1e**) shows unilateral right bony talocalcaneal coalition (*arrowhead*). For nonosseous fusion, joint space narrowing and articular surface irregularity are seen. On MRI, cartilaginous coalition demonstrates increased T2 signal at the articulation, whereas fibrous coalition demonstrates intermediate to low signal on all sequences. Initial treatment is conservative, such as casting. If nonoperative management fails, surgical resection of the coalition or arthrodesis is performed.⁴

Pearls

- ◆ Most subtalar coalitions involve the middle facet.
- ◆ Tarsal coalition may be found incidentally in asymptomatic patients.

Pitfalls

- ◆ Imaging of only one extremity may miss bilateral tarsal coalitions.
- ◆ A talar beak should not be confused with a talar osteophyte or talar ridge.³

References

1. Newman JS, Newberg AH. Congenital tarsal coalition: multimodality evaluation with emphasis on CT and MR imaging. *Radiographics* 2000; 20:321–332, quiz 526–527, 532 [PubMed](#)
2. Iyer RS, Thapa MM. MR imaging of the paediatric foot and ankle. *Pediatr Radiol* 2013;43(Suppl 1):S107–S119 [PubMed](#)
3. Crim J. Imaging of tarsal coalition. *Radiol Clin North Am* 2008;46:1017–1026, vi [PubMed](#)
4. Mosca VS, Bevan WP. Talocalcaneal tarsal coalitions and the calcaneal lengthening osteotomy: the role of deformity correction. *J Bone Joint Surg Am* 2012;94:1584–1594 [PubMed](#)

Case 108

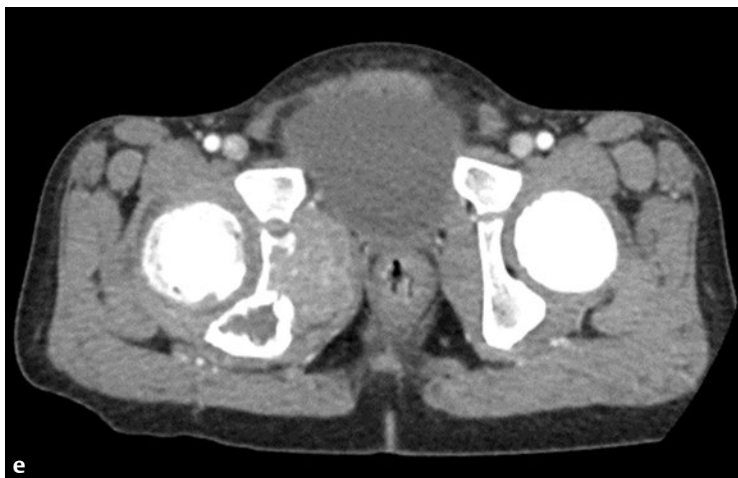
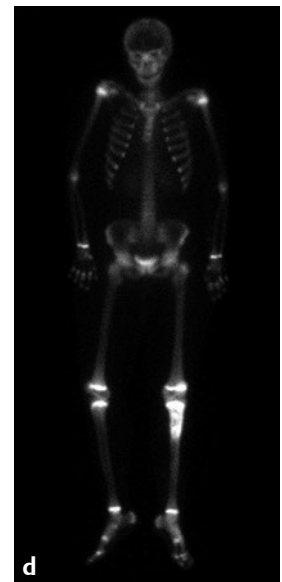
Clinical Presentation

A 12-year-old-girl with left leg pain for 3 months.

Radiographic Studies

Frontal radiograph (**Fig. 108.1a**) shows a poorly marginated lytic lesion (*arrow*) in the proximal tibia metadiaphysis with associated periosteal reaction (*arrowheads*). Sagittal STIR MRI (**Fig. 108.1b**) shows abnormal heterogeneous signal within the bone lesion, surrounding marrow edema, and soft tissue mass (*arrowheads*) anterior and posterior to the proximal tibia. Post-

contrast coronal T1-weighted MRI with fat saturation (**Fig. 108.1c**) shows heterogeneous enhancement of the intramedullary lesion and overlying enhancing soft tissue mass. Delayed image from a technetium-99m methylene diphosphonate (MDP) bone scan (**Fig. 108.1d**) shows intense tracer uptake in the proximal left tibial lesion but no bone metastases.



■ Diagnosis

Ewing Sarcoma

■ Discussion and Differential Diagnosis

Ewing sarcoma is the second most common malignant bone tumor in children and adolescents after osteosarcoma.^{1–3} “Classic” intraosseous Ewing sarcoma is included in the Ewing sarcoma family of tumors, which includes extraosseous Ewing sarcoma and primitive neuroectodermal tumor (PNET).^{2,4} Ewing sarcoma is an aggressive cancer with peak age at 15 years.² Histologically, the tumor is composed of small, blue, round cells that may originate in neural crest cells or mesenchymal stem cell origin.^{1,3,5} Patients usually present with localized pain, swelling, and constitutional symptoms. An elevated white blood cell count and erythrocyte sedimentation rate may be seen.³ The pelvis is the most common site of involvement of bony Ewing sarcoma followed by the metadiaphysis of the long bones.^{3,4} Diaphyseal origin of Ewing sarcoma occurs more commonly than in osteosarcoma.³

The classic radiographic appearance of Ewing sarcoma is a poorly marginated lytic intramedullary lesion. Other radiographic appearances include a well-defined lytic lesion, a mixed lytic/sclerotic pattern, a permeative honeycomb appearance of the bone, and a lesion with dense sclerosis.^{2–4} These varied appearances may make it difficult to distinguish some cases of Ewing sarcoma from osteosarcoma or osteomyelitis, especially in the pelvis and spine. Aggressive periosteal reaction may be onion skin (lamellated), spiculated, or solid in appearance. An associated large soft tissue mass is present in most cases.^{2,3} CT

is sensitive for detecting subtle bone lesions, identifying cortical breakthrough/pathological fractures, delineating soft tissue mass extent (**Fig. 108.1e**), and detecting lung metastases (**Fig. 108.1f**).^{1,5} MRI has superb contrast resolution, displays osseous/soft tissue extent of the lesion, and delineates the relationship with the neurovascular bundle, which is important for planning limb salvage surgery.¹ At some centers, dynamic enhanced MR and FDG-PET are used in the workup and follow-up of Ewing sarcoma.¹

Metastatic disease spreads hematogenously and is present in at least one fourth of patients at presentation.⁴ As metastases most commonly involves the lungs, cortical bone, and bone marrow, a chest CT, whole body bone scan, and bilateral bone marrow sampling are usually performed.⁵ Recent evidence suggests that FDG-PET may be superior to bone scan in detection of Ewing sarcoma bony metastatic disease.^{1,5} Treatment generally consists of chemotherapy plus local control of the tumor via surgery and/or radiation therapy. Targeted therapies are being investigated, especially for those with relapsed or refractory disease.^{4,5} Poorer prognosis is expected with metastases at presentation, larger tumor volume, pelvic location of the primary lesion, and high lactate dehydrogenase (LDH) levels at time of diagnosis.⁵ Decreased prognosis is also seen with poor tumor response to therapy and disease recurrence.^{1,5}

Pearl

- ◆ Extraosseous Ewing sarcoma is indistinguishable pathologically from intraosseous Ewing sarcoma and presents as a noncalcified soft tissue mass.⁴

Pitfall

- ◆ Clinical presentation and radiographic findings may simulate osteomyelitis.

References

1. Kaste SC. Imaging pediatric bone sarcomas. *Radiol Clin North Am* 2011;49:749–765, vi–vii [PubMed](#)
2. McCarville MB. The child with bone pain: malignancies and mimickers. *Cancer Imaging* 2009;9(Spec. No. A):S115–S121 [PubMed](#)
3. Wootton-Gorges SL. MR imaging of primary bone tumors and tumor-like conditions in children. *Magn Reson Imaging Clin N Am* 2009;17:469–487, vi [PubMed](#)
4. American Cancer Society. Ewing family of tumors. <http://www.cancer.org/cancer/ewingfamilyoftumors/detailedguide/index>. Published 2013. Accessed May 27, 2014
5. Rainusso N, Wang LL, Yustein JT. The adolescent and young adult with cancer: state of the art—bone tumors. *Curr Oncol Rep* 2013;15:296–307 [PubMed](#)

Case 109

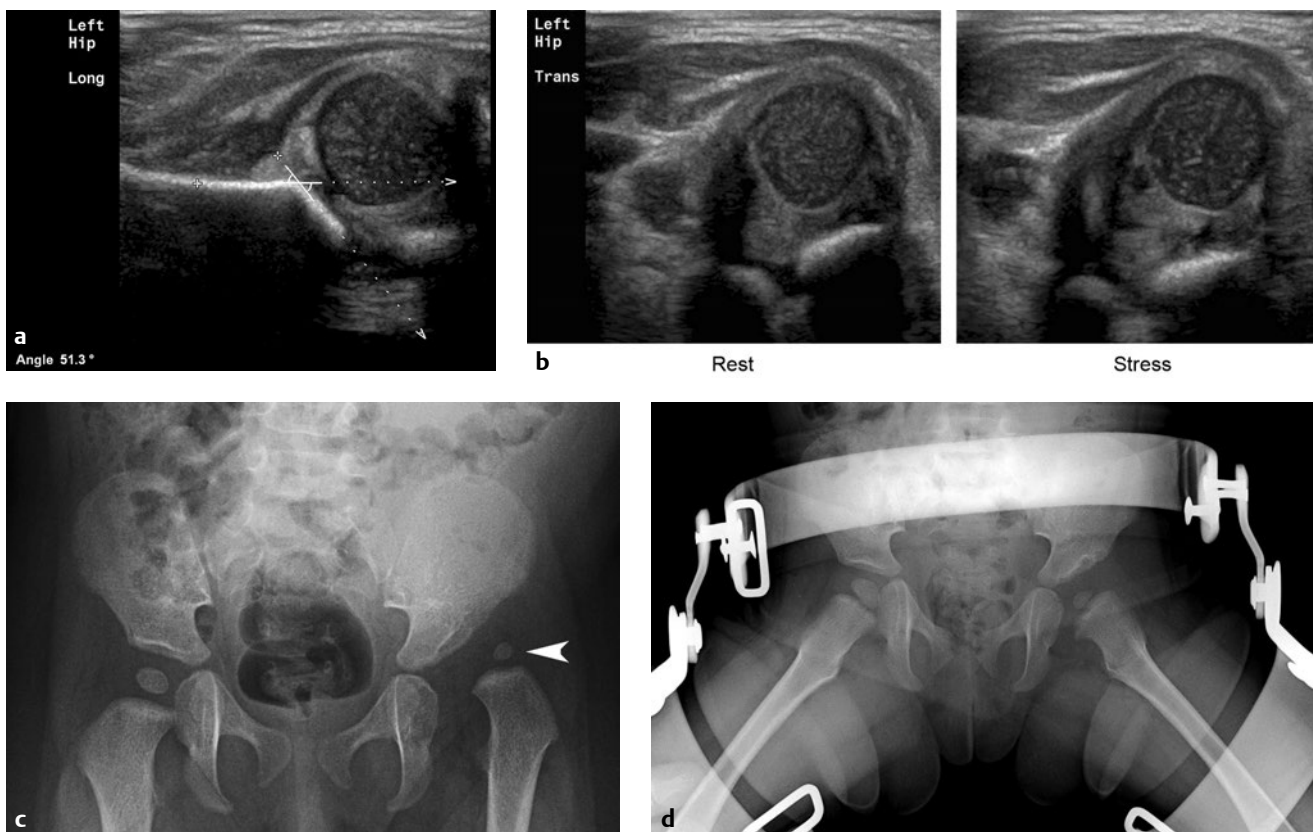
Clinical Presentation

An 8-day-old girl from a breech delivery has a left hip click.

Radiographic Studies

Longitudinal ultrasound image of the left hip (**Fig. 109.1a**) shows superolateral hip subluxation, decreased femoral head coverage, and decreased α angle measuring 51 degrees. Transverse ultrasound images of the left hip at rest and with stress application (**Fig. 109.1b**) show marked posterolateral hip subluxation at rest, which increases with stress. AP radiograph of the pelvis (**Fig. 109.1c**) in a different patient, an 11-month-old,

shows superolateral left hip dislocation relative to a shallow and dysplastic left acetabulum. The ossified component of the proximal left femoral epiphysis (*arrowhead*) is smaller compared with the right proximal femoral epiphysis. AP radiograph of the pelvis with the same patient in an abduction brace (**Fig. 109.1d**) shows good reduction of the left hip.



■ Diagnosis

Developmental Dysplasia of the Hip



■ Discussion and Differential Diagnosis

Developmental dysplasia of the hip (DDH) refers to an abnormal position of the femoral head relative to the acetabulum, resulting in abnormal growth and morphology as well as instability or subluxation/dislocation of the affected hip. DDH is much more common in females than males and more common in Caucasians than African-American newborns. Possible risk factors include abnormal ligamentous laxity, breech delivery, oligohydramnios, and family history.¹ Routine physical examination includes both the Barlow maneuver to determine if a hip is dislocatable and the Ortolani maneuver to reduce a dislocated hip. If physical exam is abnormal and other risk factors are present, hip ultrasound should be performed.

Ultrasound is the modality of choice for evaluating infants up to 4 to 5 months of age, while the femoral head is largely cartilaginous.² The static hip ultrasound developed by Graf is a morphological assessment of the femoral head and acetabulum. On coronal imaging the femoral head should rest within the concavity of the bony acetabulum. A subluxed or dislocated hip will displace in lateral, superior, and posterior directions. The α angle is measured between the straight edge of the iliac

bone and the bony acetabulum and should normally measure ≥ 60 degrees (Graf type 1). Femoral head coverage and α angle measurements decrease as the severity of dysplasia increases (Graf types 2, 3, and 4).² Dynamic hip ultrasound is also performed to assess stability by stressing the hip with a modified Barlow maneuver. If the hip is already dislocated, is being treated, or has been treated, stress imaging is optional. As the femoral head begins to ossify, ultrasound evaluation becomes limited, and plain film radiographs of the pelvis replace ultrasound. Typical imaging findings of DDH on plain films include increased acetabular angle, superolateral displacement of proximal femur, and delayed ossification of the capital femoral epiphysis (**Fig. 109.1c**).

Treatment is aimed at achieving and maintaining a normal relationship between the acetabulum and femoral head (**Fig. 109.1d**). The Pavlik harness is the current gold standard for treatment of DDH.¹ Other treatment options include splinting, casting, or open surgical reduction. Surgical reconstruction, including femoral and/or pelvic osteotomy, is reserved for patients who have failed other treatment methods.

Pearl

- ◆ Developmental dysplasia of the hip has an excellent prognosis when diagnosed and treated early. Delayed diagnosis or treatment can result in long-term disability, limb shortening, decreased range of motion, degenerative changes, and avascular necrosis.

Pitfall

- ◆ Improper hip ultrasound technique is common and can lead to significant error in diagnosis and management of DDH.³

References

1. Gulati V, Eseonu K, Sayani J, et al. Developmental dysplasia of the hip in the newborn: A systematic review. *World J Orthod* 2013;4:32–41 [PubMed](#)
2. Sewell MD, Eastwood DM. Screening and treatment in developmental dysplasia of the hip—where do we go from here? *Int Orthop* 2011;35:1359–1367 [PubMed](#)
3. Graf R, Mohajer M, Plattner F. Hip sonography update. Quality-management, catastrophes—tips and tricks. *Med Ultrasound* 2013;15:299–303 [PubMed](#)

Case 110

■ Clinical Presentation

A 3-year-old girl refuses to bear weight after a fall.

■ Radiographic Studies

Anteroposterior radiograph of the right tibia and fibula (**Fig. 110.1a**) shows a subtle nondisplaced oblique fracture in the distal tibial diaphysis, which is easier seen with edge enhancement (**Fig. 110.1b**, *arrowheads*).



d Initial



1 month

■ Diagnosis

Toddler Fracture

■ Discussion and Differential Diagnosis

Toddler fracture is a well-known cause of limping or leg pain in infants and young children. The classic toddler fracture originally referred to a nondisplaced oblique fracture of the distal tibial shaft.¹ The fracture lucency can be extremely subtle, and additional oblique views of the tibia may be required to establish a diagnosis. In rare cases, the fracture is completely occult, but adjacent soft tissue swelling may help localize the tibial injury. If initial radiographs are indeterminate, follow-up radiographs are helpful to confirm fracture-line sclerosis or adjacent periosteal reaction. Other fractures in a limping infant or young child that should be considered toddler fractures include fractures of the metatarsals, talus, cuboid, calcaneus, and upper tibial metaphysis.² Oblique radiograph

of the right foot (**Fig. 110.1c**) in a 19-month-old with limp demonstrates transverse sclerosis in a healing nondisplaced cuboid fracture (*arrowhead*). Initial and 1-month follow-up lateral radiographs of the tibia/fibula (**Fig. 110.1d**) in another patient show an acute fracture of the proximal tibial metaphysis with characteristic anterior cortical buckling on the initial radiograph (*arrowhead*) and subsequent healing medullary sclerosis (*arrow*) at 1 month. Treatment of toddler fracture consists of a few weeks of immobilization, and uneventful healing is expected. When a fracture is not demonstrated on radiographs in a limping infant or young child, the differential diagnosis includes osteomyelitis. Bone scan is helpful in establishing the correct diagnosis.³

Pearl

- ◆ Additional radiographic views or follow-up radiographs may be required.

Pitfall

- ◆ Do not overlook toddler fractures in the foot or proximal tibia.

References

1. Dunbar JS, Owen HF, Nogrady MB, McLeese R. Obscure tibial fracture of infants—the toddler's fracture. *J Can Assoc Radiol* 1964;15:136–144. [PubMed](#)
2. Swischuk LE, John SD, Tschoepe EJ. Upper tibial hyperextension fractures in infants: another occult toddler's fracture. *Pediatr Radiol* 1999;29:6–9. [PubMed](#)
3. Miller JH, Sanderson RA. Scintigraphy of toddler's fracture. *J Nucl Med* 1988;29:2001–2003. [PubMed](#)

Case 111

■ Clinical Presentation

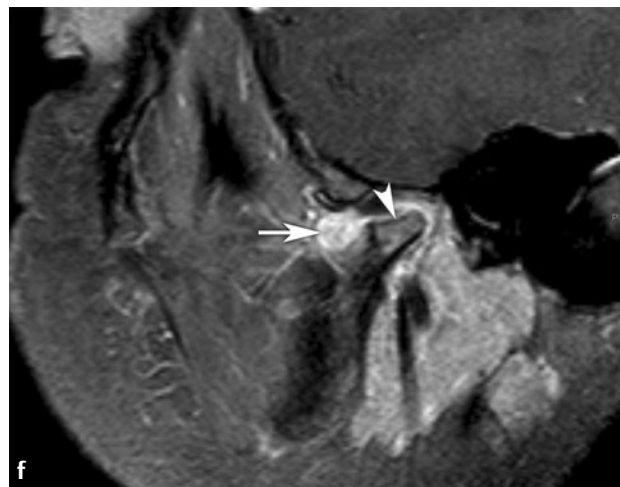
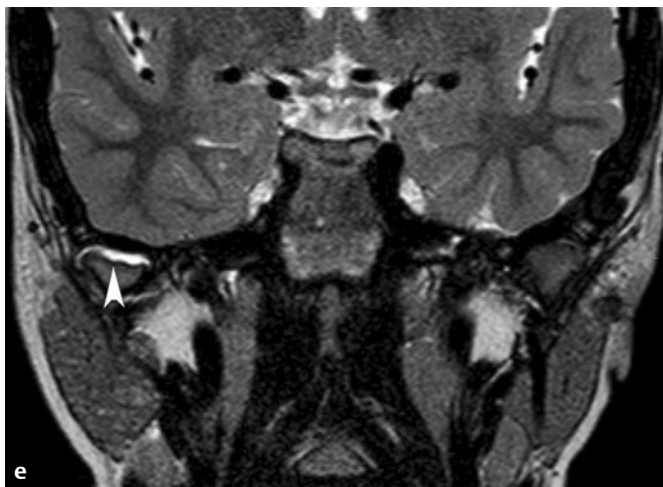
A 13-year old boy with pain and swelling of the hand and wrist.

■ Radiographic Studies

An AP radiograph of the hand (**Fig. 111.1a**) shows diffuse periarticular osteopenia, diffuse joint space narrowing, and periarticular erosion of the thumb proximal phalanx (*arrowhead*). Sagittal T2-weighted and postcontrast fat-saturated T1-weighted MRI of the knee in another patient (**Fig. 111.1b,c**)

show a large knee joint effusion and thick, irregular synovial proliferation. Sagittal proton density MRI (**Fig. 111.1d**) shows attenuation of menisci (*arrowheads*) and thinning of articular cartilage (*arrow*).





■ Diagnosis

Juvenile Idiopathic Arthritis



■ Discussion and Differential Diagnosis

Juvenile arthritis is the most common chronic arthropathy of childhood, with prevalence varying considerably throughout the world, ranging from 8 to 400 per 100,000.¹ Historically, the term *juvenile rheumatoid arthritis* (JRA) was frequently used in the United States, whereas in Europe and internationally the terms *juvenile chronic arthritis* (JCA) and *juvenile idiopathic arthritis* (JIA), respectively, were used.² More recently, JIA has become the preferred term. JIA is a systemic disease, represents a diagnosis of exclusion, and persists for ≥ 6 weeks before the age of 16 years. The majority of children (85%) with JIA are seronegative for rheumatoid factor. Oligoarticular disease (four or fewer joints) affects 40 to 50% of children with JIA and most typically affects large joints such as the knee, elbow, or ankle. Polyarticular disease affects 25% of children with JIA, and is usually symmetric. Polyarticular rheumatoid factor positive JIA is uncommon (5–15%) and resembles adult rheumatoid arthritis with polyarticular distribution involving, in order of decreasing frequency, the hands, wrists, feet, knees, and hips.

Imaging in JIA is crucial for determining the diagnosis, assessing the severity/prognosis, monitoring the disease progression and treatment response, and evaluating complications associated with the disease or associated therapy. Imaging focuses on synovium-based changes.^{2,3} Early findings include synovitis, joint effusion, periarticular soft tissue swelling, and osteopenia. Periostitis can occur within weeks after the onset of symptoms. Prolonged disease with synovial proliferation and

pannus formation can lead to bony erosion, cartilage damage, joint space narrowing, and growth disturbances. Such growth disturbances include epiphyseal overgrowth, advanced skeletal maturation, early physeal fusion, bony ankylosis, shortened tubular bones, and decreased diaphyseal diameter. Radiographs provide the rheumatologist with an important baseline investigation and help exclude other disorders, such as fractures, tumors, or skeletal dysplasias. However, radiographs are insensitive to early disease and the detection of synovitis.^{2,3} Ultrasound lacks radiation and is more sensitive than clinical examination or radiography in the detection of effusions and synovitis. However, ultrasound has a limited field of view, and not all joints are accessible.⁴ MRI is the most sensitive imaging modality in detecting early changes of JIA.^{2,3} It clearly depicts joint effusions, synovitis, bone marrow edema, bone erosion, cartilage damage, tenosynovitis, and enthesitis. Coronal T2-weighted and postcontrast fat-saturated sagittal T1-weighted MRI of the temporomandibular joint (**Fig. 111.1e,f**) show severe flattening deformity of the right mandibular condyle (*arrowhead*), effusion, and prominent thickened enhancing synovium (*arrow*). Clinical applications of MRI include detecting subclinical synovitis, excluding differential diagnoses, assessing disease activity, identifying children most likely to develop joint damage, aiding treatment selection, and monitoring treatment efficacy. Image-guided steroid joint injection may be beneficial in selected patients.⁵

Pearls

- ◆ Some 10 to 20% of children with JIA present with systemic arthritis, which includes arthritis in one or more joints with or preceded by fever and one or more of the following: rash, hepatosplenomegaly, lymphadenopathy, and serositis.
- ◆ In JIA, cervical spine ankylosis and atlantoaxial subluxation are frequent.

Pitfall

- ◆ Radiographs are insensitive to early disease and the detection of synovitis.

References

1. Cassidy JT, Petty RE, Laxer RM, Lindsley C, eds. Textbook of Pediatric Rheumatology, 6th ed. Philadelphia: WB Saunders; 2011
2. Buchmann RF, Jaramillo D. Imaging of articular disorders in children. Radiol Clin North Am 2004;42:151–168, vii [PubMed](#)
3. Damasio MB, Malattia C, Martini A, Tomà P. Synovial and inflammatory diseases in childhood: role of new imaging modalities in the assessment of patients with juvenile idiopathic arthritis. Pediatr Radiol 2010;40:985–998. [PubMed](#)
4. Johnson K. Imaging of juvenile idiopathic arthritis. Pediatr Radiol 2006;36:743–758 [PubMed](#)
5. Collado P, Jousse-Joulin S, Alcalde M, Naredo E, D'Agostino MA. Is ultrasound a validated imaging tool for the diagnosis and management of synovitis in juvenile idiopathic arthritis? A systematic literature review. Arthritis Care Res (Hoboken) 2012;64:1011–1019 [PubMed](#)

Case 112

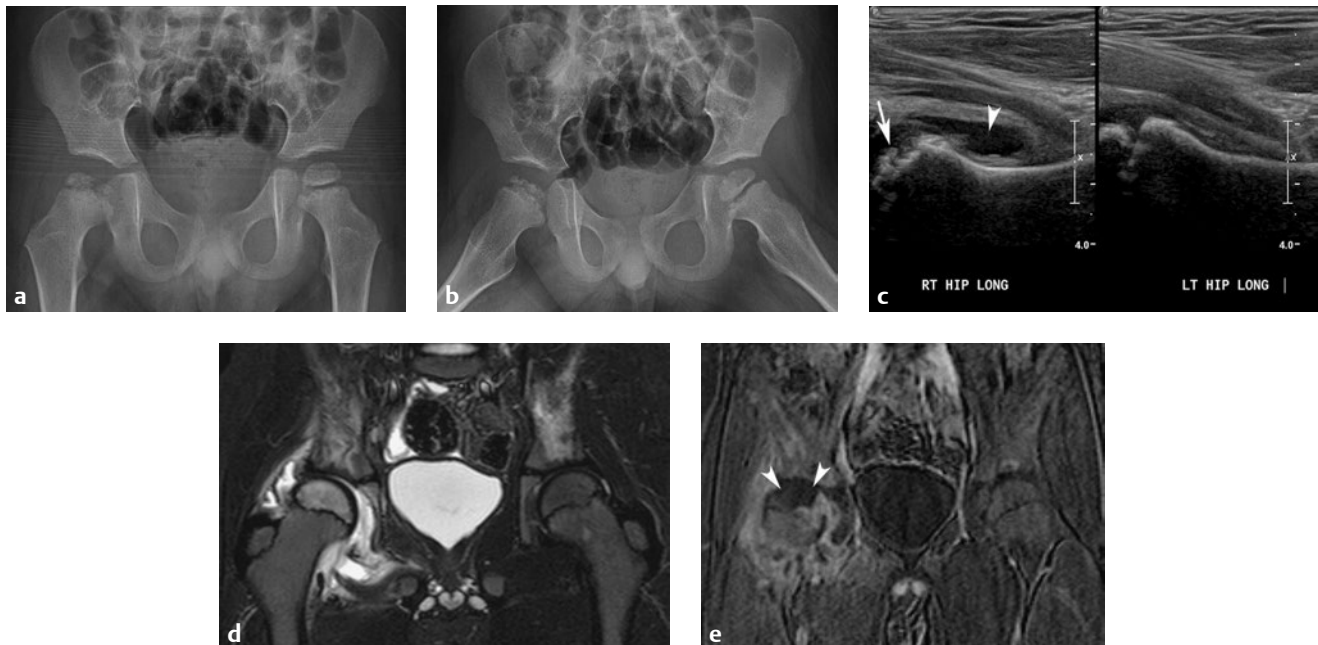
■ Clinical Presentation

A 4-year-old boy with right hip pain.

■ Radiographic Studies

Anteroposterior and frog-leg lateral radiographs of the pelvis (**Fig. 112.1a,b**) demonstrate sclerosis, fragmentation, and loss of height of the right proximal femoral epiphysis. Widening of the right femoral neck is present. Ultrasound image of both hips (**Fig. 112.1c**) shows asymmetric irregularity and flattening of the right proximal femoral epiphysis (*arrow*) and a reactive right hip joint effusion (*arrowhead*). Coronal STIR MRI of the pelvis (**Fig. 112.1d**) in another patient with suspected but

radiographically occult avascular necrosis of the right hip shows marrow edema in the right proximal femoral epiphysis and a reactive right hip effusion. Coronal T1-weighted, post-contrast, subtracted MRI of the pelvis (**Fig. 112.1e**) shows nonenhancement of the central and lateral aspects of the right proximal femoral epiphysis (*arrowheads*), confirming the presence of avascular necrosis.



■ Diagnosis

Legg-Calvé-Perthes Disease

■ Discussion and Differential Diagnosis

Legg-Calvé-Perthes disease (Perthes disease) is an idiopathic avascular necrosis of the proximal femoral epiphysis. It is a rare condition that affects 5 to 15 in 100,000 children. It is typically diagnosed between 2 and 14 years of age, with a peak incidence at 5 to 6 years of age. Boys are affected five times more commonly than girls. The disease is typically unilateral but can occur in both hips in 15% of patients. When bilateral, the femoral heads are affected in an asymmetric fashion.¹ Evaluation begins with anteroposterior and frog-leg lateral radiographs of the pelvis. Initial radiographs may be normal or demonstrate localized epiphyseal demineralization, sclerosis, or a discrete subchondral fracture line. In more advanced cases, fragmentation and loss of height of the femoral epiphysis occurs, widening of the femoral neck is evident, and secondary metaphyseal changes are present.² Subsequent radiographs show reossification and remodeling of the fragmented femoral epiphysis. In mild cases, a nearly spherical femoral head contained within a normal acetabulum results. A flattened and deformed femoral head results in more severe cases. Restricted hip joint motion and joint pain can be expected when lateral subluxation of the femoral head and adaptive changes in the acetabulum alter congruity of the cartilage space of the hip

joint.² A better prognosis is expected when the extent of femoral epiphysis is more localized at diagnosis, when the lateral pillar of the femoral epiphysis is spared, and in those patients who are younger at presentation.^{2,3} MRI can play an important role in diagnosing early disease by detecting changes of ischemia prior to radiographic changes. MRI is better than plain films in providing accurate staging, helping predict outcomes, and delineating the extent of epiphyseal involvement.^{1,4,5}

Treatment of Perthes disease is focused on preventing premature hip arthritis. Various treatment methods exist and aim to increase containment of the femoral head within the acetabulum, thereby maintaining hip motion and articular surface sphericity.^{6,7} Conservative measures include casting or abduction braces (containment method), and operative procedures include femoral varus osteotomy or shelf acetabuloplasty. Currently there is a lack of agreement as to the most appropriate form of treatment and the patient groups to whom it should be applied.⁸ Differential diagnostic considerations include known causes of avascular necrosis such as Gaucher's disease, sickle cell disease, steroid therapy, hypothyroidism, trauma, and osteomyelitis.

Pearl

- ◆ Postcontrast MRI may define sites of hypervascular regenerative tissue prior to radiographic reossification.⁴

Pitfall

- ◆ When disease is bilateral, it should not be at the same stage. If symmetrical changes are present, consider the diagnosis of epiphyseal dysplasia, trichorhinophalangeal syndrome, or Meyer dysplasia.

References

1. Milla SS, Coley BD, Karmazyn B, et al. ACR Appropriateness Criteria® limping child—ages 0 to 5 years. *J Am Coll Radiol* 2012;9:545–553 [PubMed](#)
2. Catterall A. The natural history of Perthes' disease. *J Bone Joint Surg Br* 1971;53:37–53 [PubMed](#)
3. Farsetti P, Tudisco C, Caterini R, Potenza V, Ippolito E. The Herring lateral pillar classification for prognosis in Perthes disease. Late results in 49 patients treated conservatively. *J Bone Joint Surg Br* 1995;77:739–742 [PubMed](#)
4. Dillman JR, Hernandez RJ. MRI of Legg-Calvé-Perthes disease. *AJR Am J Roentgenol* 2009;193:1394–1407 [PubMed](#)
5. Kim HK, Kaste S, Dempsey M, Wilkes D. A comparison of non-contrast and contrast-enhanced MRI in the initial stage of Legg-Calvé-Perthes disease. *Pediatr Radiol* 2013;43:1166–1173 [PubMed](#)
6. Shah H, Siddesh ND, Pai H, Tercier S, Joseph B. Quantitative measures for evaluating the radiographic outcome of Legg-Calvé-Perthes disease. *J Bone Joint Surg Am* 2013;95:354–361 [PubMed](#)
7. Hosalkar HS, Mulpuri K. Legg-Calvé-Perthes disease: where do we stand after 100 years? Editorial comment. *Clin Orthop Relat Res* 2012;470:2345–2346 [PubMed](#)
8. Karimi MT, McGarry T. A comparison of the effectiveness of surgical and nonsurgical treatment of legg-calve-perthes disease: a review of the literature. *Adv Orthop* 2012;2012:490806 [PubMed](#)

Case 113

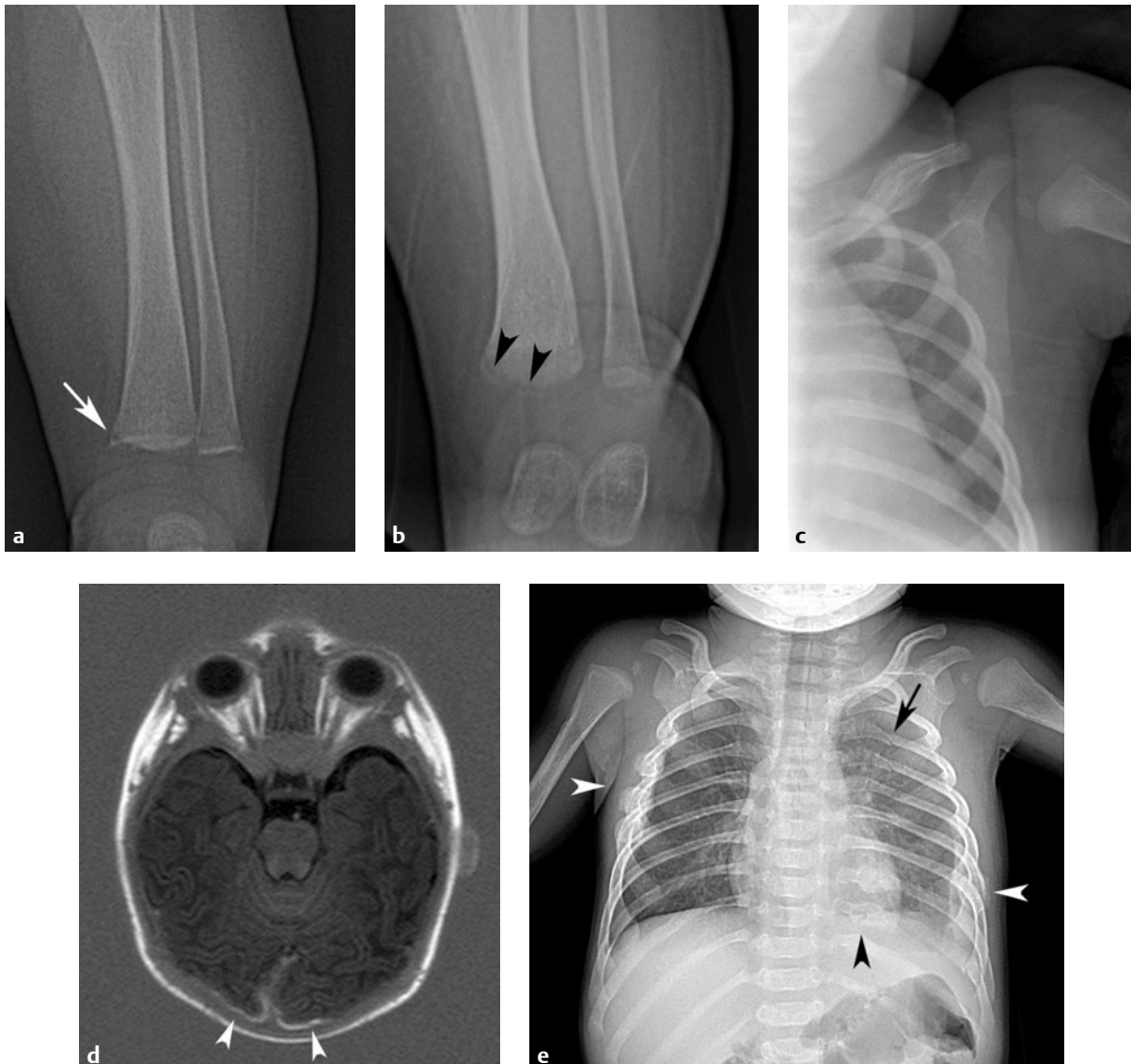
■ Clinical Presentation

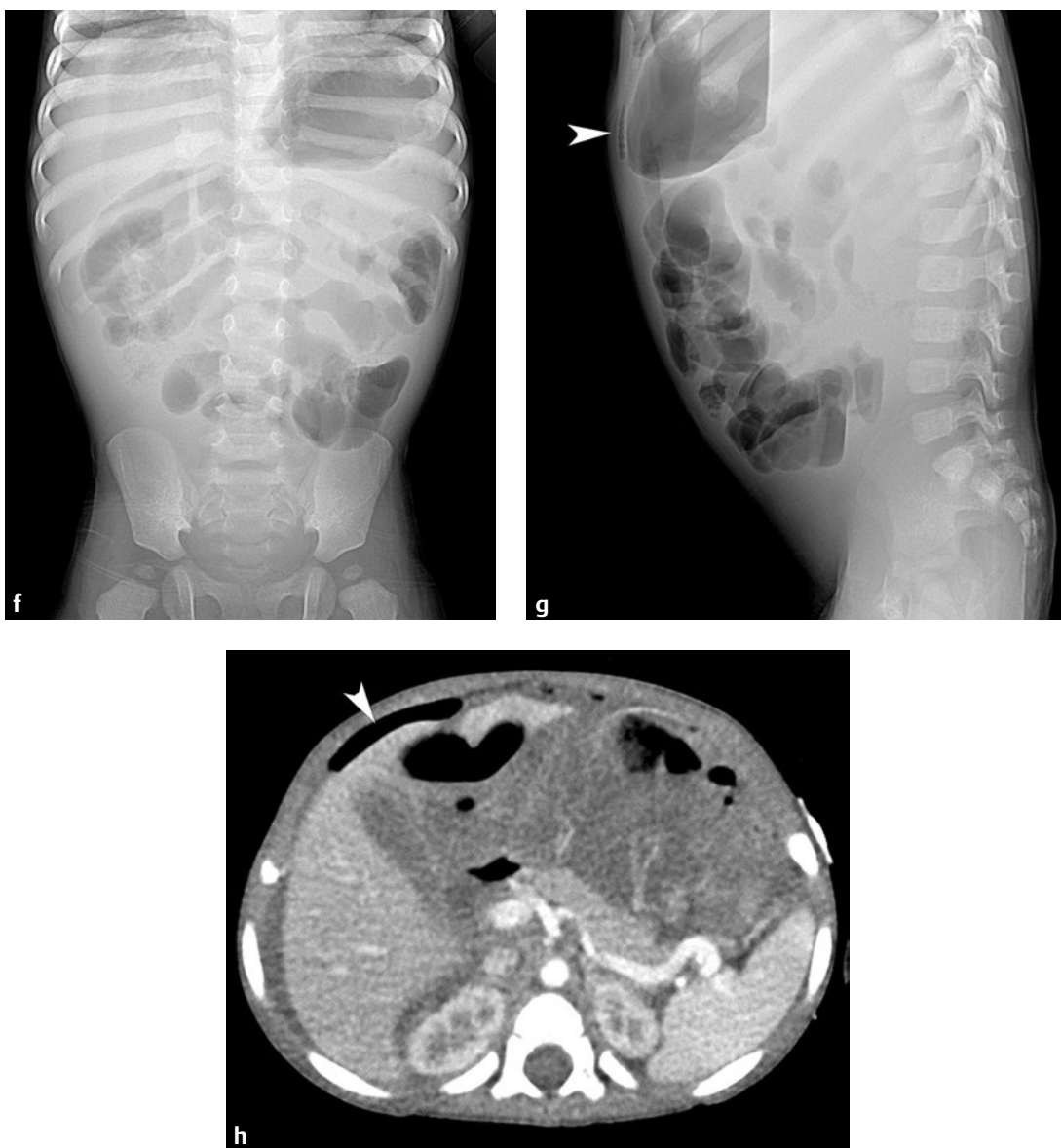
A 9-week-old girl with apnea and retinal hemorrhages.

■ Radiographic Studies

Radiograph of the left lower leg (**Fig. 113.1a**) shows oblique lucency of the distal tibial metaphysis (*arrow*)—a “corner” fracture. Additional radiograph in a slightly different projection (**Fig. 113.1b**) shows the transverse nature of this acute distal tibial metaphyseal “bucket handle” fracture (*arrowheads*). Shoulder radiograph in the same patient (**Fig. 113.1c**) shows a healing left clavicle fracture.

MRI (**Fig. 113.1d**) shows small posterior subdural hemorrhages overlying the occipital cortex bilaterally (*arrowheads*). Chest radiograph from a skeletal survey in another patient (**Fig. 113.1e**) shows a left pleural effusion, numerous bilateral healing rib fractures in posteromedial and lateral locations (*arrowheads*), and several acute left upper posteromedial rib fractures (*arrow*).





■ Diagnosis

Child Abuse

■ Discussion and Differential Diagnosis

Skin lesions such as bruises and contusions are the most common findings in physical child abuse (nonaccidental injury, child maltreatment syndrome); fractures are the second most common findings. In suspected physical abuse, the radiographic skeletal survey is the cornerstone radiological exam.¹ The American College of Radiology and Society for Pediatric Radiology (ACR-SPR) provide online practice guidelines for skeletal surveys in children with known or suspected child abuse.² Use of these guidelines in joint collaboration with pediatricians or the use of the American Academy of Pediatrics

and Society for Pediatric Radiology (AAP-SPR) joint abuse guidelines is encouraged.³ A single radiograph of an infant is insufficient. Each extremity should be radiographed in at least the frontal view, and the axial skeleton should be radiographed in two projections. Oblique views of the rib cage should also be obtained and have been shown to increase the diagnostic yield for child abuse.¹ Equivocal fractures may require additional projections. Characteristic radiographic findings in abuse include metaphyseal fractures, posteromedial rib fractures, and fractures at various stages of healing. Pediatric radiologists

play an important role in documenting the type, location, and distribution of bone injuries and to search for underlying bone conditions that may predispose to fracture.³

Depending on the projection, a classic metaphyseal lesion (CML) may appear as either a “corner” fracture or a “bucket-handle” lesion.^{4,5} A follow-up skeletal survey in 14 days (excluding skull images because the skull does not form callus) can be very useful to increase the sensitivity and specificity for child abuse, especially if there were questionable findings on the original survey. Bone scintigraphy has higher sensitivity for rib fractures but has lower sensitivity for classic metaphyseal lesions and for skull fractures than skeletal survey.¹

Specificity of fracture locations for child abuse is categorized as follows¹:

- High specificity: CMLs, rib fractures (especially posteromedial), scapula, spinous process, and sternum
- Moderate specificity: multiple fractures (especially if bilateral), fractures at different ages, epiphyseal separations, vertebral body fractures/subluxations, digital fractures, and complex skull fractures

- Low specificity: subperiosteal new bone formation, clavicle fractures, long-bone shaft fractures, and linear skull fractures

Skeletal survey radiographs of the axial skeleton may show findings suspicious for blunt abdominal injury. **Figure 113.1f** shows a healing right posteromedial right ninth rib fracture, irregularity of several left lower anterior ribs, gaseous distention of multiple bowel loops, and lucency overlying the liver. Lateral abdomen radiograph (**Fig. 113.1g**) shows gaseous bowel loop distention/air–fluid levels, and paucity of rectal gas; a small amount of free air is seen (*arrowhead*). Postcontrast abdomen CT image (**Fig. 113.1h**) shows a large amount of upper abdomen ascites and free air anterior to the liver (*arrowhead*) in this 17-month-old boy with jejunal perforation at surgical exploration. Abused children have a significantly increased relative risk of hollow viscus bowel injury than do children following accidental injuries such as a motor vehicle accident or fall; the parents’ delay in seeking care is predictive of an inflicted injury.^{6,7}

Pearls

- ◆ The radiologist may be the first to suggest child abuse, and must distinguish abuse from other pathologies and normal variants.
- ◆ The presence of rib fractures in infants is highly specific for abuse. Mechanisms for rib injury are compressions of the chest (especially anterior-posterior) and blunt impact.
- ◆ Classic metaphyseal lesions are most common in the distal tibia and are most conspicuous along its the medial aspect. Proximal humeral CMLs are usually lateral corner fractures and are less common and more subtle.^{4,5}
- ◆ Mechanisms for CML injury include torsional and tractional shear strains across the metaphysis as the infant extremity is twisted or pulled. Another CML cause is due to acceleration forces when an infant is shaken by the torso.⁴
- ◆ Normal physiological diaphyseal periosteal reaction is less than 2 mm and only occurs in infants younger than 4 months of age.⁸

Pitfalls

- ◆ Rib fractures may also be present in metabolic bone diseases (including prematurity), skeletal dysplasias (osteogenesis imperfecta), following vaginal delivery, and rarely after cardiopulmonary resuscitation (CPR) with hands encircling the chest.¹
- ◆ Many CMLs heal without subperiosteal new bone formation and most become inconspicuous at 4 weeks.⁴
- ◆ Differential diagnosis for CMLs: rickets, obstetric injury, skeletal dysplasias (osteogenesis imperfecta), developmental variants, and iatrogenic causes (physical therapy, orthopedic manipulation).⁴

References

1. Offiah A, van Rijn RR, Perez-Rossello JM, Kleinman PK. Skeletal imaging of child abuse (non-accidental injury). *Pediatr Radiol* 2009;39:461–470 [PubMed](#)
2. American College of Radiology and Society for Pediatric Radiology Practice Parameter for Skeletal Surveys in Children. Resolution 39. Amended 2014. http://www.acr.org/~media/ACR/Documents/PGTS/guidelines/Skeletal_Surveys.pdf. Accessed January 10, 2014
3. Perez-Rossello JM. The AAP and the SPR Child Abuse Committee issue a clinical report on “Evaluating Children with Fractures for Child Physical Abuse.” *Pediatr Radiol* 2014;44:243 [PubMed](#)
4. Kleinman PK. Problems in the diagnosis of metaphyseal fractures. *Pediatr Radiol* 2008;38(Suppl 3):S388–S394 [PubMed](#)
5. Tsai A, McDonald AG, Rosenberg AE, Gupta R, Kleinman PK. High-resolution CT with histopathological correlates of the classic metaphyseal lesion of infant abuse. *Pediatr Radiol* 2014;44:124–140 [PubMed](#)
6. Barnes PM, Norton CM, Dunstan FD, Kemp AM, Yates DW, Sibert JR. Abdominal injury due to child abuse. *Lancet* 2005;366:234–235 [PubMed](#)
7. Wood J, Rubin DM, Nance ML, Christian CW. Distinguishing inflicted versus accidental abdominal injuries in young children. *J Trauma* 2005;59:1203–1208 [PubMed](#)
8. Quigley AJ, Stafrace S. Skeletal survey normal variants, artefacts and commonly misinterpreted findings not to be confused with non-accidental injury. *Pediatr Radiol* 2014;44:82–93, quiz 79–81 [PubMed](#)

Case 114

Clinical Presentation

A 10-year-old girl with left anterior knee swelling.

Radiographic Studies

Anteroposterior radiograph of the left knee (**Fig. 114.1a**) shows oval lytic lesion of the proximal left tibial epiphysis with a narrow zone of transition (*arrowheads*). Lateral radiograph (**Fig. 114.1b**) shows the epiphyseal lytic lesion, adjacent apophyseal involvement, cortical breakthrough (*arrowhead*), and adjacent extraosseous soft tissue thickening. CT image (**Fig. 114.1c**) shows the epiphyseal lytic lesion with thinning of the anterior cortex and cortical breakthrough (*arrowhead*). Sagittal STIR MRI (**Fig. 114.1d**) shows a heterogeneous high-

signal epiphyseal lesion with a low-signal rim (*arrowhead*), apophyseal extent, and high-signal soft tissue thickening anteriorly (*arrow*). High signal in the adjacent bone marrow and anterior cruciate ligament is also seen. Postcontrast sagittal T1-weighted MRI with fat saturation (**Fig. 114.1e**) shows heterogeneous enhancement of the epiphyseal lesion and intense enhancement of the associated anterior soft tissue mass (*arrow*). Reactive bone marrow and anterior cruciate ligament enhancement is also seen.



■ Diagnosis

Chondroblastoma

■ Discussion and Differential Diagnosis

Chondroblastoma is a rare benign chondral tumor usually located in the epiphysis or apophysis of long bones. Other locations include the foot (especially talus and calcaneus) or flat bones.¹ Age at presentation is generally under 20 years, usually in middle to late adolescence.^{1,2} Presenting symptoms include pain, swelling, tenderness, and limping; joint effusion is less common.² The most common sites of long bone involvement include the proximal tibia, distal femur, proximal humerus, and proximal femur.² Within a long tubular bone, chondroblastoma is located within the epiphysis or apophysis 90% of the time; extension to the adjacent metaphysis is fairly common after closure of the growth plate.² The classic radiographic presentation is an eccentric oval or round lytic lesion with a thin sclerotic margin.^{1,2} Matrix mineralization is present in 30% of lesions.² A thick solid periosteal reaction is seen

in over 60% of long bone chondroblastomas, and it is located in the metaphysis adjacent to the epiphyseal lesion.² Pathological fracture (**Fig. 114.1f, arrow**) and muscle wasting are seen in some cases.¹

Computed tomography may improve detection of matrix calcification, cortical fractures/destruction, and anatomic extent of the lesion.^{1,2} MRI is superior at demonstrating extraosseous soft tissue extent, bone marrow edema, periostitis, joint effusion, and synovitis.² The differential diagnosis of chondroblastoma includes osteomyelitis, subchondral bone cyst, histiocytosis, aneurysmal bone cyst, and giant cell tumor (after physeal closure).³ Treatment generally consists of surgical curettage and bone grafting. Adjuvant therapies including electrocautery, cryosurgery, and radiofrequency ablation.¹

Pearls

- ◆ Purely metaphyseal or diaphyseal location of chondroblastoma is very rare.²
- ◆ Associated aneurysmal bone cyst within chondroblastoma occurs in 15 to 32% of cases and may manifest on MRI with internal fluid or fluid–fluid levels.^{1,2}
- ◆ Postoperative recurrence of chondroblastoma is significant, but declining due to meticulous and advanced surgical techniques and novel interventional radiology treatments.¹

Pitfalls

- ◆ Because periosteal reaction is often distant from the primary lesion, it can be overlooked.
- ◆ Chondroblastoma may have a more aggressive appearance in small bones or flat bones.¹

References

1. De Mattos CB, Angsanuntsukh C, Arkader A, Dormans JP. Chondroblastoma and chondromyxoid fibroma. *J Am Acad Orthop Surg* 2013;21:225–233. [PubMed](#)
2. Douis H, Saifuddin A. The imaging of cartilaginous bone tumours. I. Benign lesions. *Skeletal Radiol* 2012;41:1195–1212. [PubMed](#)
3. Helms CA. Benign lytic lesions. In: Helms CA, ed. *Fundamentals of Skeletal Radiology*, 4th ed. Philadelphia: Elsevier; 2014:7–31

Case 115

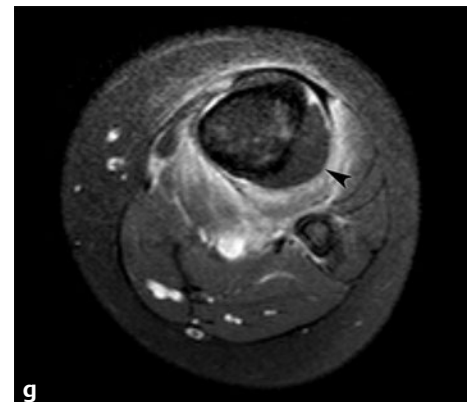
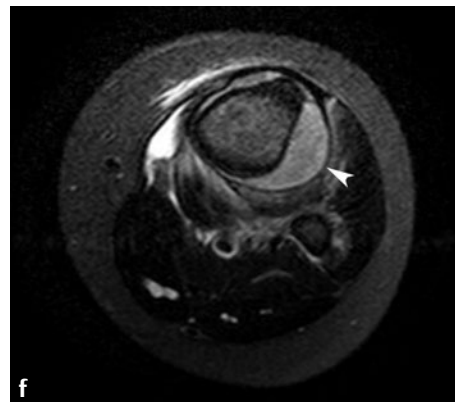
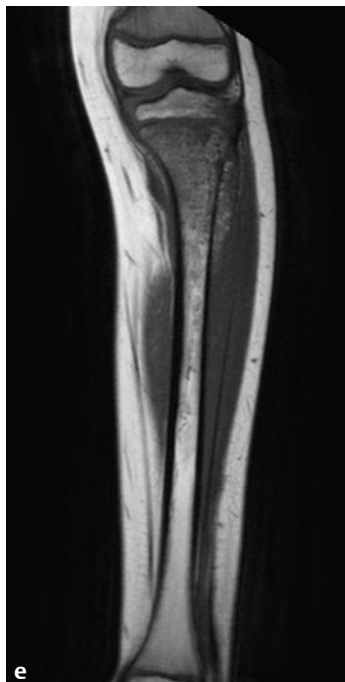
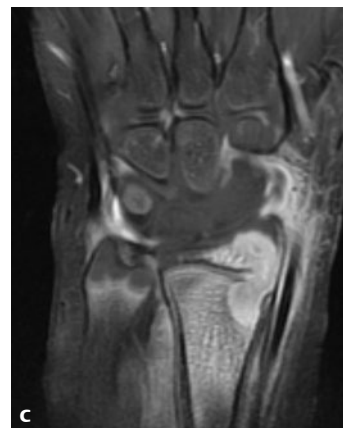
■ Clinical Presentation

A 5-year-old boy with wrist pain and swelling.

■ Radiographic Studies

An AP radiograph of the wrist (**Fig. 115.1a**) shows lytic bone destruction of the distal radial metaphysis and epiphysis with surrounding soft tissue swelling. Coronal T1-weighted and post-contrast T1-weighted MRI of the wrist (**Fig. 115.1b,c**) confirm marrow edema, and osseous and extraosseous enhancement with transphyseal spread of disease. Follow-up radiograph of the wrist 3 years later (**Fig. 115.1d**) shows growth arrest of the

distal radial physis (*arrowhead*) and large metaphyseal lytic defect. Coronal T1-weighted MRI of the tibia (**Fig. 115.1e**) in another patient with suspected osteomyelitis and normal radiographs shows abnormal marrow infiltration of the proximal tibia metaphysis. Axial T2-weighted and postcontrast T1-weighted MRI of the proximal tibia (**Fig. 115.1f,g**) show a large subperiosteal abscess (*arrowhead*) and surrounding myositis.



■ Diagnosis

Osteomyelitis

■ Discussion and Differential Diagnosis

Osteomyelitis in children is most commonly hematogenous in origin and most commonly affects the highly vascularized metaphyses of long bones such as the distal femur, proximal tibia, proximal humerus, and distal radius. The pelvis and spine are also frequently involved in children. In addition to hematogenous spread, osteomyelitis in children can also occur from adjacent soft tissue or joint infection or by direct implantation from trauma, surgery, or foreign body. The clinical findings of acute bone infection include fever, localized bone tenderness, leukocytosis, and elevated erythrocyte sedimentation rate (ESR). When the disease is more advanced, swelling, erythema, and decreased range of motion at an adjacent joint may be found. The diagnosis is established by identifying the causative organism in blood or tissue cultures. Common organisms isolated include *Staphylococcus aureus* in all children, and group B *Streptococcus* and *Escherichia coli* in neonates.^{1,2} In neonates, localizing clinical findings are often absent, multifocal lesions are common, and epiphyseal involvement may occur.

Plain films and CT are of limited clinical value in acute osteomyelitis and are more useful in advanced or chronic disease. Radiographic lytic bone destruction and periosteal new bone formation are typically not seen until the second week of

disease.³ Bone scintigraphy is more sensitive for detection of acute osteomyelitis, can demonstrate multifocal lesions, and provides screening for the entire skeleton when the suspected site of disease is not clinically evident.⁴ MRI has great sensitivity for detection of early disease and demonstrates superior resolution of the involved bone marrow and adjacent soft tissues. Postcontrast MR sequences are particularly useful for demonstrating noncontiguous sites of active inflammation and the intramedullary extent of disease, and for detecting the presence and extent of physeal involvement.³ If patients are appropriately treated with antibiotics, morbidity is low; if inadequately treated, development of Brodie's abscess and subperiosteal and adjacent soft tissue abscesses may occur. Transphyseal spread of disease and growth disturbances may result. Associated septic arthritis may ensue, particularly when osteomyelitis occurs near the hip or shoulder joint. Given the ischemia and thrombosis associated with the inflammatory process, a sequestrum of dead bone may result and provide a source of prolonged or recurrent infection. In such instances, imaging with CT or MRI may be necessary to demonstrate soft tissue or subperiosteal fluid collections to be drained or sequestra to be resected.

Pearls

- ◆ Pelvic osteomyelitis may be difficult to detect radiographically and may clinically simulate hip joint disease, abdominal pathology, or discitis.
- ◆ Specific indications for MRI include suspected osteomyelitis of the spine or pelvis, disease involving the growth plate, and infection that fails to respond to therapy.

Pitfalls

- ◆ Without high-resolution imaging equipment and magnification views, distinction of metaphyseal osteomyelitis from the active physis on bone scintigraphy may be difficult.⁴
- ◆ Septic arthritis, prior antibiotic treatment, and cold defects from ischemia can obscure osteomyelitis on bone scan imaging.

References

1. Schmit P, Glorion C. Osteomyelitis in infants and children. *Eur Radiol* 2004; 14(Suppl 4):L44–L54. [PubMed](#)
2. Dodwell ER. Osteomyelitis and septic arthritis in children: current concepts. *Curr Opin Pediatr* 2013;25:58–63. [PubMed](#)
3. van Schuppen J, van Doorn MM, van Rijn RR. Childhood osteomyelitis: imaging characteristics. *Insights Imaging* 2012;3:519–533. [PubMed](#)
4. DiPoce J, Jbara ME, Brenner AI. Pediatric osteomyelitis: a scintigraphic case-based review. *Radiographics* 2012;32:865–878. [PubMed](#)

Case 116

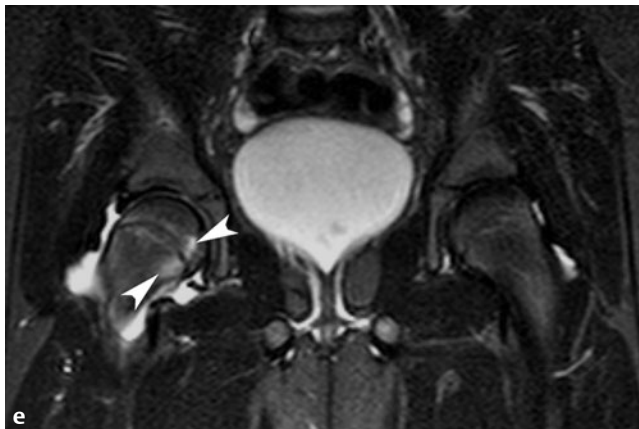
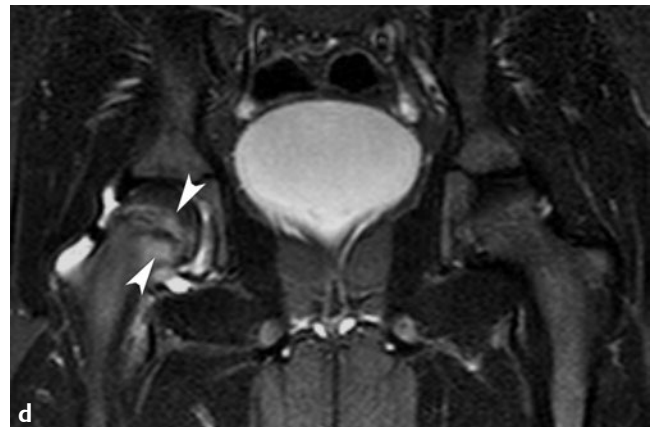
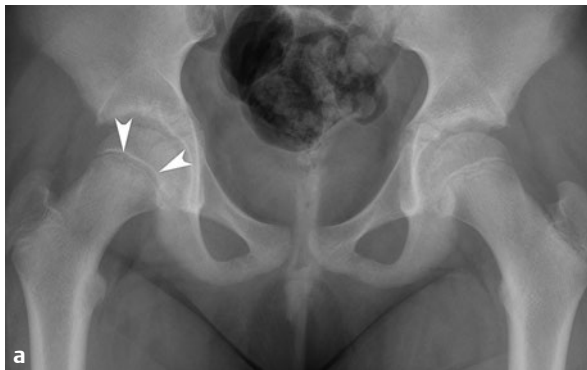
■ Clinical Presentation

An 11-year-old girl with right hip pain.

■ Radiographic Studies

Anteroposterior radiograph of the pelvis (**Fig. 116.1a**) shows subtle physeal widening of the right hip (*arrowheads*) and obvious slippage of the right proximal femoral epiphysis on the frog-leg lateral view (**Fig. 116.1b**). Patient underwent surgical pinning of the right hip (**Fig. 116.1c**). Coronal STIR MRI of

the pelvis (**Fig. 116.1d,e**) in another patient with suspected but radiographically occult slipped capital femoral epiphysis of the right hip shows marrow edema surrounding the right proximal femoral physis (*arrowheads*) and reactive right hip effusion.



■ Diagnosis

Slipped Capital Femoral Epiphysis

■ Discussion and Differential Diagnosis

Slipped capital femoral epiphysis (SCFE) involves posterior and inferior slippage of the proximal femoral epiphysis on the metaphysis through the growth plate. The disorder usually occurs during puberty, has a higher prevalence in obese patients, and is associated with certain endocrine disorders such as hypothyroidism and growth hormone deficiency.¹ Though hip pain, limp, and decreased internal rotation on physical exam constitute the typical presentation, a significant number of cases have vague findings clinically (thigh or knee pain), resulting in a delay in diagnosis.² SCFE has traditionally been classified as acute, chronic (more than 3 weeks of symptoms, 85% of all SCFE cases), and acute-on-chronic. An alternative classification of SCFE categorizes it as stable (able to ambulate with or without crutches) and unstable (unable to ambulate with or without crutches).³ Initial radiographic assessment includes AP and frog-leg lateral views of the pelvis to detect

physeal widening, epiphyseal displacement, and alteration of the femoral head-shaft angle. Inspection of the opposite hip is imperative, given a high incidence (18–50%) of bilateral SCFE,² particularly in patients with underlying endocrine or metabolic disease.¹ MRI is useful in evaluating “pre-slip” or impending SCFE and can help distinguish SCFE from other radiographically occult causes of hip pain, including early avascular necrosis, synovitis, traumatic injury, and neoplasm.⁴ Treatment options include preoperative traction, maneuvers attempting reduction of the displaced epiphysis, and surgical fixating procedures (pins or cannulated screws). Follow-up radiographs are useful for displaying posttreatment reduction of the epiphysis, adjacent bony remodeling, and alignment of orthopedic hardware, and for monitoring the known complications of avascular necrosis and chondrolysis.⁵

Pearl

- ◆ Slipped capital femoral epiphysis relating to endocrine disease presents in a wider age range, and most commonly is caused by hypothyroidism or growth hormone deficiency.¹

Pitfall

- ◆ Delayed diagnosis is more common when hip pain is absent or when thigh or knee pain is found on exam.²

■ Controversy

- A minority of opinion favors prophylactic fixation of the contralateral hip.⁵

References

1. Loder RT, Wittenberg B, DeSilva G. Slipped capital femoral epiphysis associated with endocrine disorders. *J Pediatr Orthop* 1995;15:349–356. [PubMed](#)
2. Peck D. Slipped capital femoral epiphysis: diagnosis and management. *Am Fam Physician* 2010;82:258–262. [PubMed](#)
3. Loder RT, Dietz FR. What is the best evidence for the treatment of slipped capital femoral epiphysis? *J Pediatr Orthop* 2012;32(Suppl 2):S158–S165. [PubMed](#)
4. Lalaji A, Umans H, Schneider R, Mintz D, Liebling MS, Haramati N. MRI features of confirmed “pre-slip” capital femoral epiphysis: a report of two cases. *Skeletal Radiol* 2002;31:362–365. [PubMed](#)
5. Hansson G, Nathorst-Westfelt J. Management of the contralateral hip in patients with unilateral slipped upper femoral epiphysis: to fix or not to fix—consequences of two strategies. *J Bone Joint Surg Br* 2012;94:596–602. [PubMed](#)

Case 117

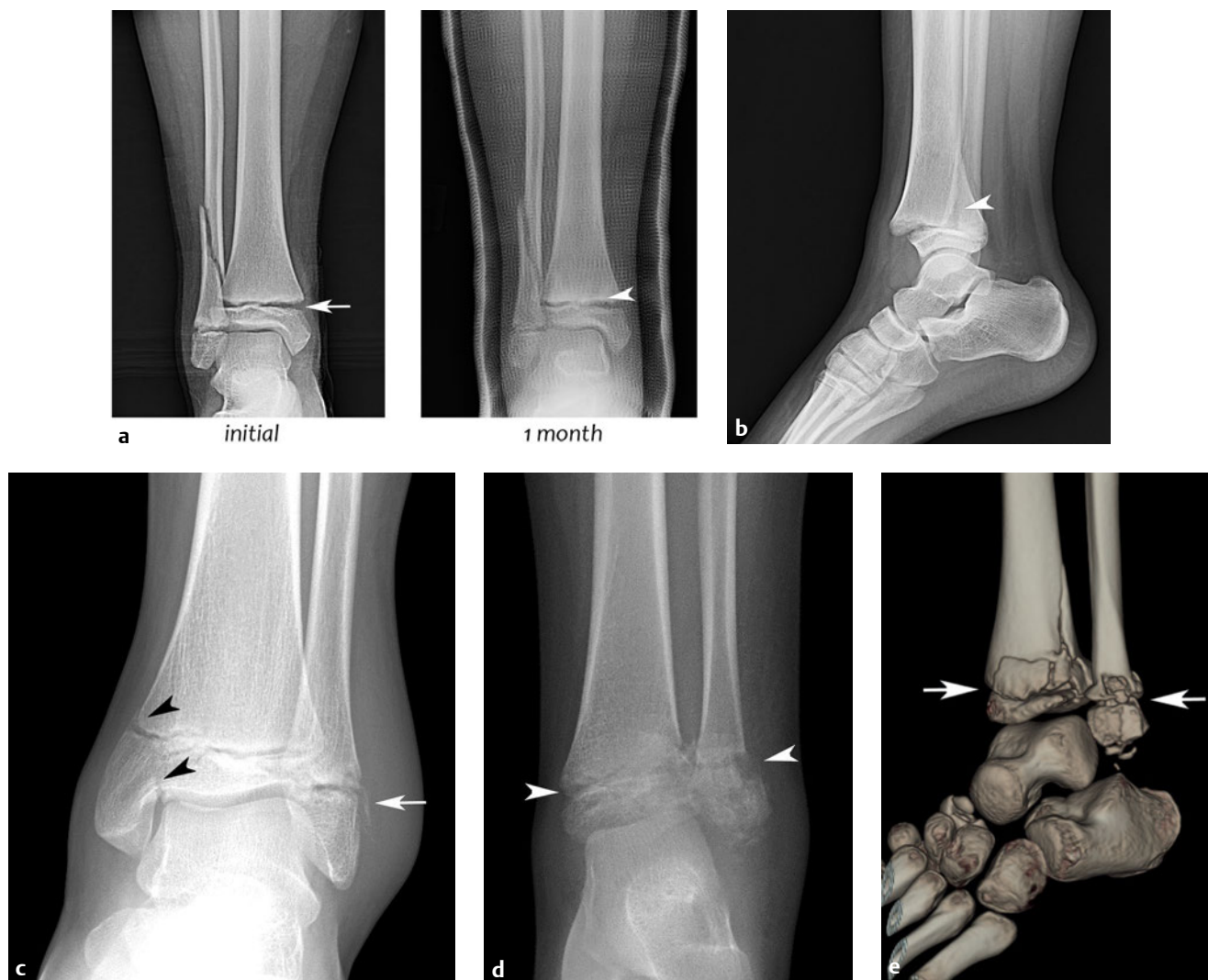
Clinical Presentation

A 9-year-old girl with ankle pain after fall playing softball.

Radiographic Studies

Serial AP ankle radiographs (**Fig. 117.1a**) show distal tibial physeal widening (*arrow*) at initial injury; distal tibial metaphyseal sclerosis (*arrowhead*) is noted at 1 month follow-up. Oblique fracture of the distal fibula is also present. Lateral ankle radiograph in a different patient, a 10-year-old (**Fig. 117.1b**), shows an oblique metaphyseal fracture (*arrowhead*) extending into the physis. No epiphyseal fracture component is seen. AP ankle radiograph in another patient, a 14-year-old (**Fig. 117.1c**), shows a distal fibular epiphyseal fracture extend-

ing to the physis (*arrow*), and an oblique distal tibial fracture (*arrowheads*) extending from the epiphysis and crossing the physis into the metaphysis. AP ankle radiograph in another patient, a 6-year-old boy with ankle pain after a tree fell on his leg (**Fig. 117.1d**), shows complex fractures (*arrowheads*) crossing the distal tibial and fibular physes. A 3D volume-rendered CT image in this same patient (**Fig. 117.1e**) shows comminuted fractures (*arrows*) crossing the distal tibial and fibular physes.



■ Diagnosis

Physeal Fractures

■ Discussion and Differential Diagnosis

Physeal fractures are unique to pediatrics because the unfused growth plate is weak and prone to fracture. These fractures account for 15 to 20% of major long-bone fractures and 34% of hand fractures in childhood.¹ The Salter-Harris classification categorizes these growth plate fractures with regard to the physis, metaphysis, and epiphysis, which is important because the classification may determine the treatment.² There are five basic Salter-Harris fractures (types I to V) outlined below.^{1,2} Following the acute injury, CT is helpful in selected patients to delineate additional fracture components not seen on initial plain radiographs and more accurately display fracture line diastasis and articular surface offset useful in surgical planning.³

Most physeal fractures heal without any growth impairment, especially types I and II.¹ However, some physeal fractures (especially Salter types III to V) may disrupt the epiphyseal circulation and result in formation of a bony bridge across the growth plate (physeal bar).^{1,4} This may lead to clinically important limb shortening and angulation. MRI may be useful

during fracture healing to display physeal injury and delineate location and extent of physeal osseous bar formation.⁴ Intra-articular fractures with fracture fragment diastasis may lead to posttraumatic arthritis.⁵

The Salter-Harris classification is as follows:

- Type I fractures are through the physis, usually resulting in physeal widening.
- Type II fractures are through the physis and a portion of the metaphysis. They are the most common type of Salter-Harris fracture.
- Type III fractures are through the physis and epiphysis and are intra-articular.
- Type IV fractures are through the metaphysis, physis, and epiphysis, and are intraarticular.
- Type V fractures are physeal crush injuries caused by severe axial loading. These have the greatest likelihood of growth plate arrest and are often diagnosed retrospectively.

Pearl

- ◆ Physeal bars can be classified as peripheral or central; common locations include the distal tibia, proximal tibia, and distal femur.⁴

Pitfall

- ◆ Triplane fractures of the distal tibia are classified separately from the Salter-Harris classification.^{3,5}

References

1. Wheelless CR. Salter Harris Classification of growth plate fractures. In: Wheelless's Textbook of Orthopaedics. http://www.wheellessonline.com/ortho/salter_harris_classification_of_growth_plate_fractures. Updated May 31, 2012. Accessed January 11, 2014
2. Moore W. Salter-Harris fracture imaging. Medscape. <http://emedicine.medscape.com/article/412956-overview#a01/>. Updated March 14, 2014. Accessed January 12, 2014
3. Lemburg SP, Lilienthal E, Heyer CM. Growth plate fractures of the distal tibia: is CT imaging necessary? *Arch Orthop Trauma Surg* 2010;130:1411–1417. [PubMed](#)
4. Lurie B, Koff MF, Shah P, et al. Three-dimensional magnetic resonance imaging of physeal injury: reliability and clinical utility. *J Pediatr Orthop* 2014;34:239–245. [PubMed](#)
5. Crawford AH. Triplane and Tillaux fractures: is a 2 mm residual gap acceptable? *J Pediatr Orthop* 2012;32(Suppl 1):S69–S73. [PubMed](#)

Case 118

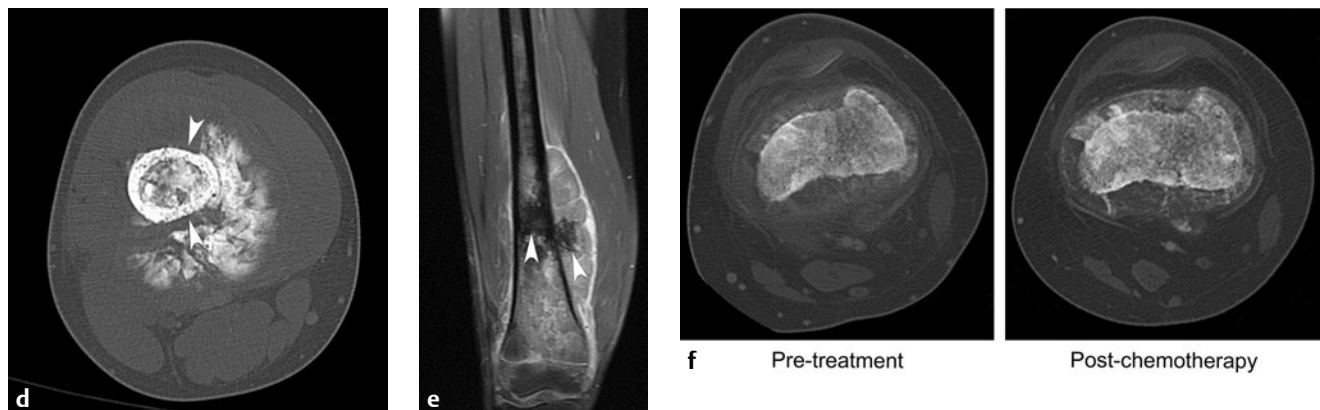
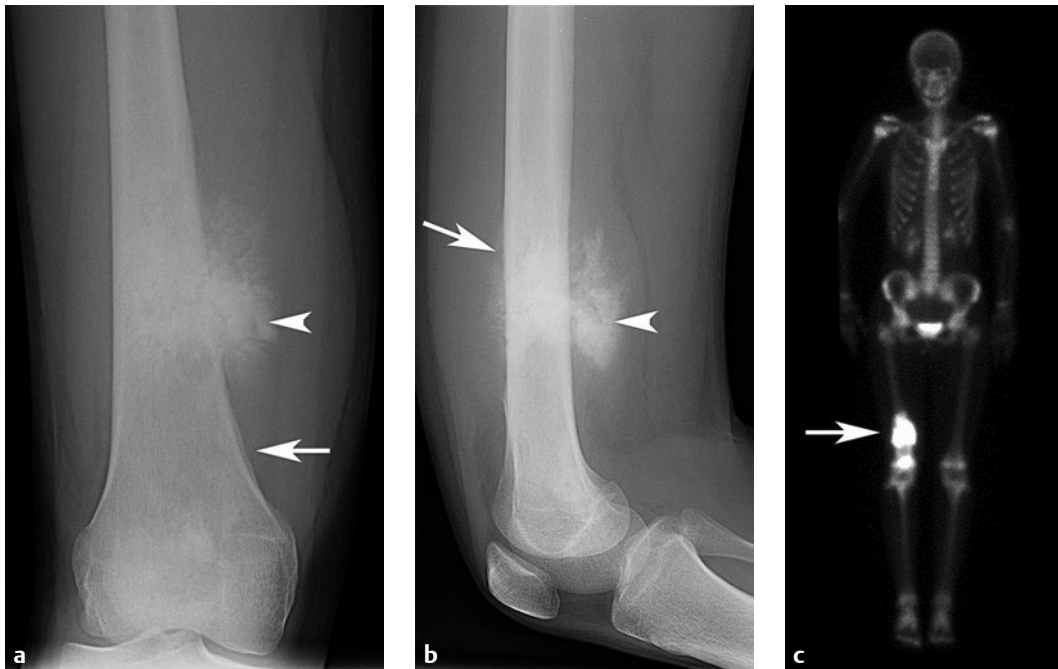
■ Clinical Presentation

A 14-year-old girl with right thigh mass and pain.

■ Radiographic Studies

Frontal and lateral radiographs (**Fig. 118.1a,b**) show a mixed lytic and sclerotic lesion of the distal femoral metadiaphysis with multifocal periosteal reaction (*arrows*) and calcification within the associated soft tissue mass (*arrowheads*). Delayed image from a technetium-99m bone scan (**Fig. 118.1c**) shows intense tracer uptake in the right distal femur lesion (*arrow*) but no bone metastases. CT bone window image (**Fig. 118.1d**) shows the mixed lytic and sclerotic intraosseous lesion with

cortical irregularity (*arrowheads*) and a large adjacent soft tissue mass containing calcified osteoid. Postcontrast coronal T1-weighted MRI with fat saturation (**Fig. 118.1e**) shows extensive heterogeneous marrow signal abnormality and a heterogeneously enhancing soft tissue mass. Low signal intensity components are seen with the marrow and the soft tissue mass (*arrowheads*) corresponding to sites of calcified osteoid.



■ Diagnosis

Osteosarcoma

■ Discussion and Differential Diagnosis

Osteosarcoma is the most common primary bone malignancy of childhood.^{1–4} Most lesions present during the adolescent growth spurt with localized pain and usually with an associated soft tissue mass. The tumor tends to develop at the metaphysis of rapidly growing bones; the distal femur, proximal tibia, and proximal humerus are the most common sites.^{3,4} Conventional osteosarcoma (80% of cases) has an intramedullary origin, has three subtypes (osteoblastic, chondroblastic, and fibroblastic), and is high-grade.⁴ Nonconventional osteosarcoma subtypes include intramedullary (telangiectatic, low-grade central, and small cell), surface (parosteal, periosteal, and high-grade), and secondary osteosarcoma.

On plain radiographs, conventional “classic” intramedullary osteosarcoma appears as a mixed lytic and sclerotic metaphyseal lesion with ill-defined borders and cortical destruction. An associated soft tissue mass is usually present and may contain calcification in a cloud-like osteoid matrix. Periosteal reaction types include the more specific sunburst spiculated type or the less specific Codman’s triangle (also seen in Ewing sarcoma or osteomyelitis).^{3,4} A rare presentation of osteosarcoma is osteosarcomatosis, in which multiple tumors are detected.⁵ Approximately 20% of patients with osteosarcoma have metastatic disease at diagnosis, most frequently involving the lungs (61%), skeleton (16%), or both.¹ MRI is most accurate in

demonstrating the lesion extent (intraosseous, extraosseous, intra-articular) and relationship to adjacent neurovascular structures. Discontinuous osteosarcoma metastases (skip lesions) are best seen on MRI.² Dynamic enhanced MRI is an emerging modality for osteosarcoma in some centers.² Nuclear Medicine bone scan is used to detect bone metastases.^{1,2} CT helps detect pulmonary metastases.^{1,2}

The treatment approach to osteosarcoma is neoadjuvant chemotherapy preceding local tumor control (usually surgery), followed by adjuvant chemotherapy. A high percentage of tumor necrosis (> 90%) at histology following neoadjuvant chemotherapy correlates with improved long-term survival.¹ Radiographic indicators of a good response to chemotherapy include increased tumor ossification and improved demarcation of the soft tissue component.² **Fig. 118.1f** shows another patient with distal femoral osteosarcoma and favorable response to 3 months of chemotherapy. If limb salvage surgery is not feasible, surgical amputation of the primary tumor may be required.

The most important prognostic factor in osteosarcoma is the presence of metastatic disease.¹ The ability to completely resect all bulky disease is also an important prognostic factor.¹ Survival rate is 30% among children with metastatic osteosarcoma, even with aggressive surgical resection of lung metastases in the absence of other metastatic disease.⁶

Pearls

- ◆ Spontaneous pneumothorax can occur in osteosarcoma patients, especially with lung metastases and chemotherapy treatment.⁷
- ◆ Pathological fracture is an uncommon presentation and has a worse survival rate.⁸
- ◆ Due to dense osteoid, osteosarcoma may decrease little in size during therapy.²

Pitfalls

- ◆ Lung parenchymal and lymph node metastases may ossify and must be distinguished from calcified granulomatous disease.
- ◆ Less commonly, osteosarcoma can be either purely lytic or purely blastic.⁴

■ Controversy

- Recent literature considers osteosarcomatosis to be the aggressive metastatic spread of disease rather than representing multifocal primary sites of osteosarcoma,

because there is usually a dominant metaphyseal tumor site as well as multiple smaller sclerotic osseous lesions.⁵

References

1. Rainusso N, Wang LL, Yustein JT. The adolescent and young adult with cancer: state of the art — bone tumors. *Curr Oncol Rep* 2013;15:296–307 [PubMed](#)
2. Kaste SC. Imaging pediatric bone sarcomas. *Radiol Clin North Am* 2011;49:749–765, vi–vii [PubMed](#)
3. McCarville MB. The child with bone pain: malignancies and mimickers. *Cancer Imaging* 2009;9 Spec No A:S115–S121 [PubMed](#)
4. Wootton-Gorges SL. MR imaging of primary bone tumors and tumor-like conditions in children. *Radiol Clin North Am* 2009;47:957–975 [PubMed](#)
5. Currall VA, Dixon JH. Synchronous multifocal osteosarcoma: case report and literature review. *Sarcoma* 2006;2006:53901 [PubMed](#)
6. Harting MT, Blakely ML. Management of osteosarcoma pulmonary metastases. *Semin Pediatr Surg* 2006;15:25–29 [PubMed](#)
7. Fayda M, Kebudi R, Dizdar Y, et al. Spontaneous pneumothorax in children with osteosarcoma: report of three cases and review of the literature. *Acta Chir Belg* 2012;112:378–381 [PubMed](#)
8. Lee RK, Chu WC, Leung JH, Cheng FW, Li CK. Pathological fracture as the presenting feature in pediatric osteosarcoma. *Pediatr Blood Cancer* 2013;60:1118–1121 [PubMed](#)

VII

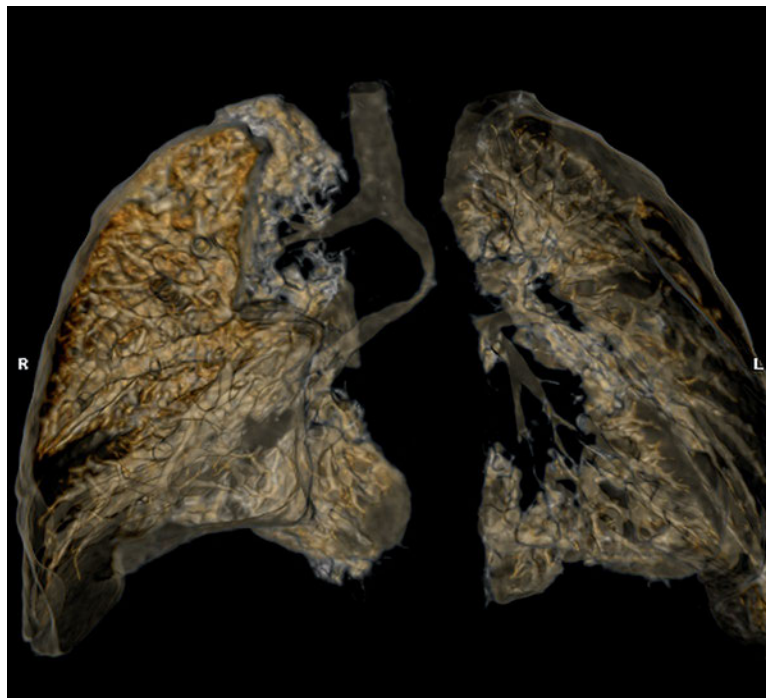
Chest

Section Editor

S. Bruce Greenberg

Authors

Shilpa V. Hegde and Chetan C. Shah



Case 119

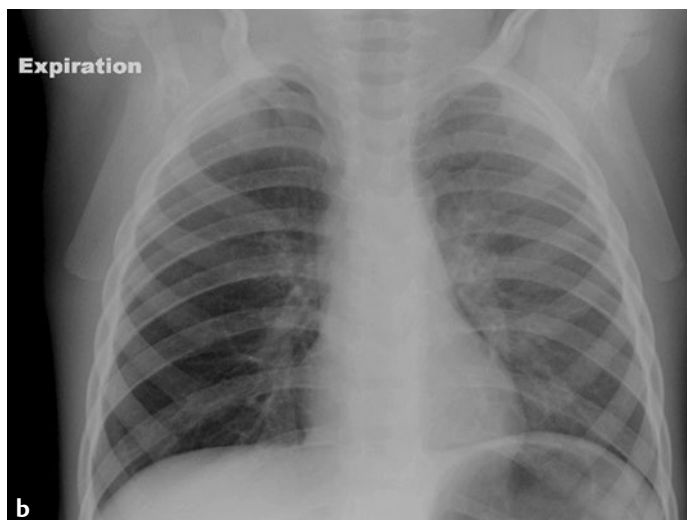
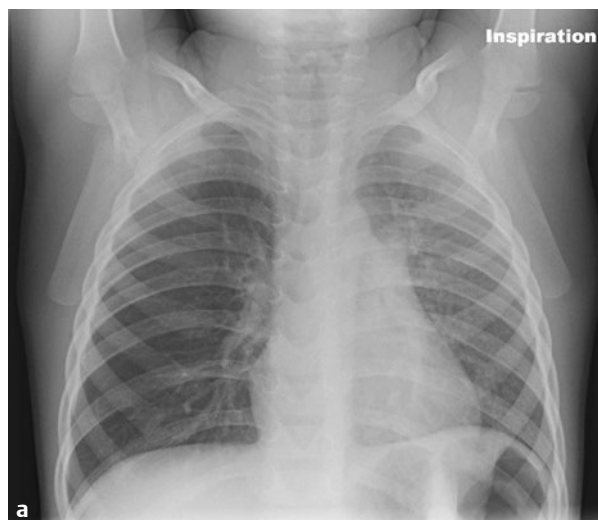
■ Clinical Presentation

A 2-year-old boy with a history of choking and respiratory distress.

■ Radiographic Studies

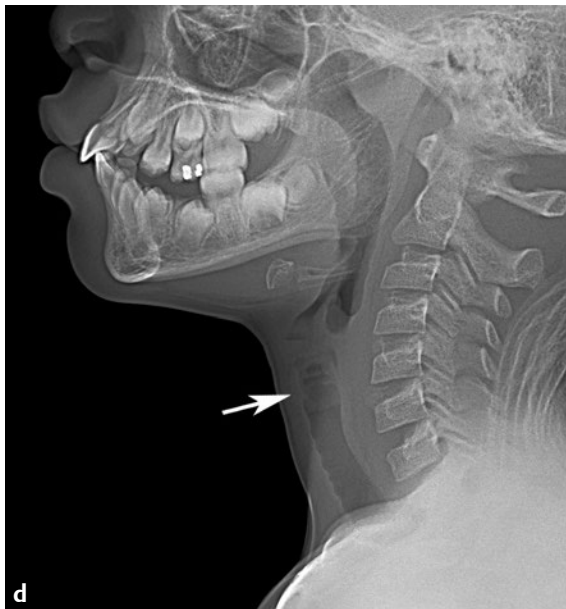
Frontal chest radiograph in inspiration (**Fig. 119.1a**) shows asymmetric hyperinflation of the right lung. Frontal chest radiograph in expiration (**Fig. 119.1b**) shows persistent asymmetric hyperinflation of the right lung consistent with air

trapping. Bilateral decubitus radiographs (**Fig. 119.1c**) show persistent hyperinflation of the dependent right lung (right decubitus), consistent with air trapping; normal collapse of the dependent left lung is noted (left decubitus).



c Right decubitus

Left decubitus



■ Diagnosis

Foreign Body Aspiration

■ Discussion and Differential Diagnosis

Foreign body aspiration is a common pediatric emergency and is the sixth most common cause of accidental deaths in children.¹ Foreign bodies can cause complete airway obstruction and sudden death. Sharp objects can directly injure the airway. However, the symptoms of tracheobronchial foreign body aspiration are usually nonspecific and include cough, wheeze, dyspnea, fever, and pneumonia.¹

Plain radiographs are frequently used as the first-line imaging modality. Radiographs are sensitive in identifying radiopaque foreign bodies such as glass and metals.² Unfortunately, 90% of foreign bodies are not opaque and are not directly detected on radiographic examinations. Indirect signs of air trapping, atelectasis, and consolidation may be absent.³ A normal radiograph does not exclude the presence of a foreign body. Lateral decubitus and expiratory radiographs help detect air trapping. Organic foreign bodies include nuts, seeds, meat, and fruits such as apples and carrots are nonopaque. Peanuts are the most commonly aspirated foreign bodies reported in the English-language literature.⁴ The rate of compli-

cations is higher in cases of organic foreign body inhalation, which could be partly related to a delayed diagnosis in these cases.⁴ Fish bones, plastic, and wood are nonopaque.²

Computed tomography is performed on patients with ongoing symptoms in whom radiographs were noncontributory. CT is superior to radiographs in demonstrating less dense foreign bodies such as plastic and aluminum and is also superior in demonstrating air trapping, atelectasis, consolidation, and bronchiectasis.⁵ CT scout image (**Fig. 119.1d**) and sagittal reconstructed CT neck image (**Fig. 119.1e**) show a plastic foreign body (arrows) lodged in the subglottic trachea in a 9-year-old neurologically normal boy with respiratory distress after playing with toys. Rigid bronchoscopy is considered as the standard for retrieving airway foreign bodies in children.⁵

Mucous plugs can mimic tracheobronchial foreign bodies, and imaging cannot always distinguish between the two. Endobronchial tumors, extrinsic airway compression, and tracheobronchial stenosis can mimic an airway foreign body.

Pearl

- ◆ The symptoms of tracheobronchial foreign body aspiration are nonspecific and can mimic asthma or pneumonia.

Pitfalls

- ◆ Ninety percent of foreign bodies are not opaque, and the indirect signs of air trapping, atelectasis, and consolidation can be absent. A normal chest radiograph does not exclude foreign body aspiration.
- ◆ Aluminum is less opaque than other metals, and careful review of radiographs is required for detection.²

References

1. Sahin A, Meteroglu F, Eren S, Celik Y. Inhalation of foreign bodies in children: experience of 22 years. *J Trauma Acute Care Surg* 2013;74:658–663 [PubMed](#)
2. Hunter TB, Taljanovic MS. Foreign bodies. *Radiographics* 2003;23:731–757. [PubMed](#)
3. Hong SJ, Goo HW, Roh JL. Utility of spiral and cine CT scans in pediatric patients suspected of aspirating radiolucent foreign bodies. *Otolaryngol Head Neck Surg* 2008;138:576–580 [PubMed](#)
4. Karakoç F, Karadağ B, Akbenlioğlu C, et al. Foreign body aspiration: what is the outcome? *Pediatr Pulmonol* 2002;34:30–36 [PubMed](#)
5. Hitter A, Hullo E, Durand C, Righini CA. Diagnostic value of various investigations in children with suspected foreign body aspiration: review. *Eur Ann Otorhinolaryngol Head Neck Dis* 2011;128:248–252 [PubMed](#)

Case 120

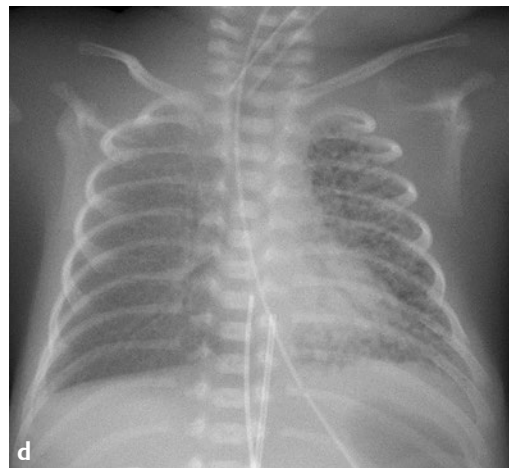
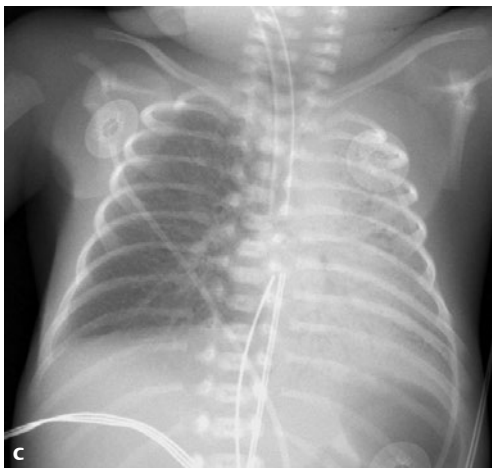
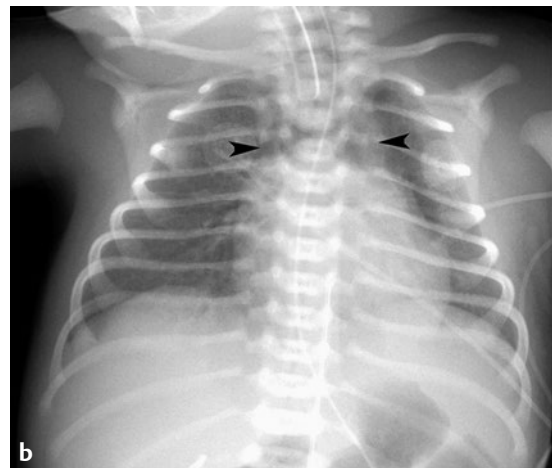
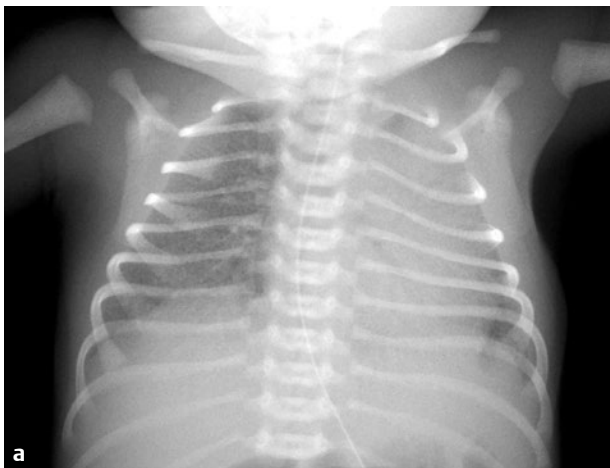
Clinical Presentation

A 25-week-gestation premature newborn presents with tachypnea and intercostal retractions immediately after birth.

Radiographic Studies

Chest radiograph (**Fig. 120.1a**) shows low lung volumes with a bilateral symmetric granular lung pattern. Follow-up radiograph on day 2 of life (**Fig. 120.1b**) shows improved aeration following intubation and surfactant therapy. Mediastinal lucency is present (*arrowheads*), consistent with pneumomediastinum. Another premature newborn (**Fig. 120.1c,d**) had cesarean section due to premature rupture of membranes and placental abruption; bradycardia required resuscitation. Chest

radiograph following surfactant administration per endotracheal tube (**Fig. 120.1c**) shows the endotracheal tube extending to the right bronchus, diffuse granularity of the right lung, and volume loss of the left lung. Follow-up radiograph on day 2 of life (**Fig. 120.1d**) shows improved lung aeration, diffuse granularity of the right lung, and interval development of left lung pulmonary interstitial emphysema.



■ Diagnosis

Respiratory Distress Syndrome

■ Discussion and Differential Diagnosis

Respiratory distress syndrome (RDS) is also known as hyaline membrane disease or surfactant deficiency disease. It is most common in infants born before 28 weeks' gestation; one third of infants born at 28 to 34 weeks are affected.¹ Surfactant deficiency increases alveolar surface tension, resulting in diffuse alveolar atelectasis. Symptoms of respiratory distress begin within the first 6 hours of life and peak during the first 2 days of life. If uncomplicated, respiratory symptoms improve by the third day of life. Antenatal steroid administration decreases the incidence and severity of RDS. Postnatal surfactant therapy decreases the severity of disease. Use of continuous positive airway pressure immediately after birth with selective surfactant administration is an alternative to routine intubation with early surfactant administration.² Persistence of symptoms and radiographic findings beyond day 3 of life is suspicious for an additional process such as neonatal pneumonia or pulmonary edema associated with a patent ductus arteriosus.

Chest radiography is characterized by low lung volumes, a ground-glass appearance, and air bronchograms. Pleural effusion is not a feature of RDS. Surfactant therapy ameliorates the chest radiograph findings. Asymmetric surfactant distribution can result in a unilateral ground-glass distribution. Following surfactant therapy, multifocal areas of opacity may mimic pneumonia or meconium aspiration syndrome, and localized overaeration may mimic pulmonary interstitial emphysema. Pulmonary hemorrhage is a complication of surfactant therapy and is manifested by dense airspace opacification on radiographs.³

Complications of respiratory therapy of premature lungs include barotrauma, such as pulmonary interstitial emphysema, as well as pneumomediastinum, pneumothorax, and bronchopulmonary dysplasia. Bronchopulmonary dysplasia or chronic lung disease of infancy occurs in conditions that require prolonged ventilation and is an important consequence of surfactant deficiency.¹

Pearl

- ◆ Infants of diabetic mothers are predisposed to RDS. Genetic surfactant deficiency should be considered when a term infant presents with a clinical and radiographic picture of RDS.⁴

Pitfalls

- ◆ Group B streptococcal infection mimics the clinical and radiographic findings of RDS. The presence of pleural effusions may be a distinguishing feature.
- ◆ Administration of surfactant may result in asymmetric clearing. The residual areas of opacity may resemble changes of pneumonia.

References

1. Hermansen CL, Lorah KN. Respiratory distress in the newborn. *Am Fam Physician* 2007;76:987–994. [PubMed](#)
2. Committee on Fetus and Newborn; American Academy of Pediatrics. Respiratory support in preterm infants at birth. *Pediatrics* 2014;133:171–174. [PubMed](#)
3. Agrons GA, Courtney SE, Stocker JT, Markowitz RI. From the archives of the AFIP: Lung disease in premature neonates: radiologic-pathologic correlation. *Radiographics* 2005;25:1047–1073. [PubMed](#)
4. Newman B, Kuhn JP, Kramer SS, Carcillo JA. Congenital surfactant protein B deficiency—emphasis on imaging. *Pediatr Radiol* 2001;31:327–331. [PubMed](#)

Case 121

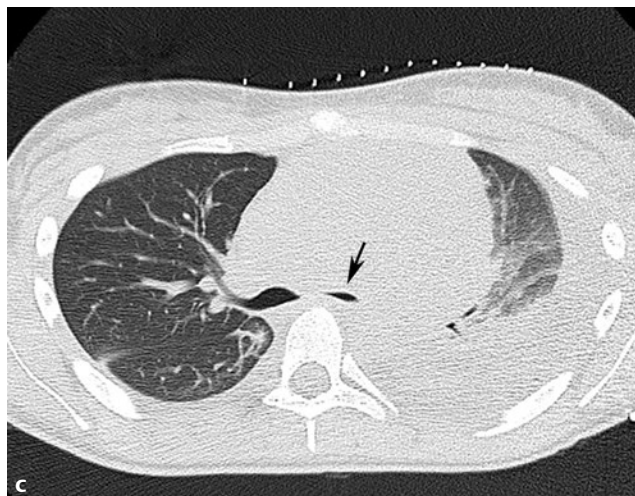
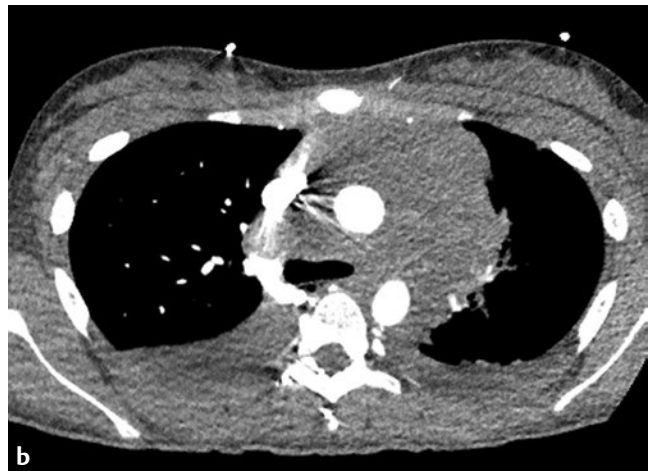
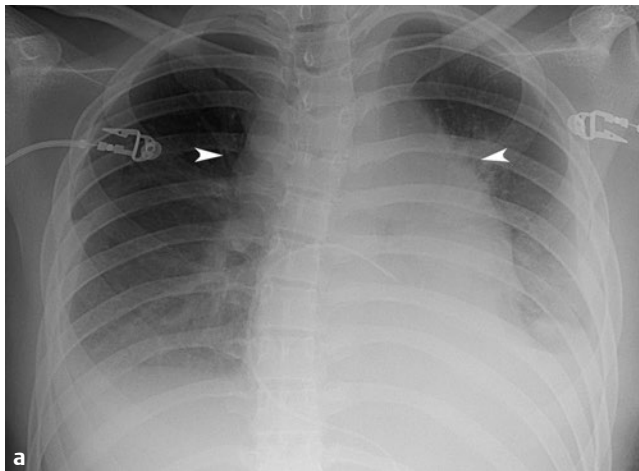
■ Clinical Presentation

A 15-year-old girl with respiratory distress and loss of appetite.

■ Radiographic Studies

Frontal chest radiograph (**Fig. 121.1a**) shows mediastinal widening (*arrowheads*) and bilateral pleural effusions. A pericardial effusion drain overlies the middle/right heart. Axial postcontrast CT image (**Fig. 121.1b**) shows a lobular anterior mediastinal mass extending into the middle mediastinum and

encasing the ascending and descending thoracic aorta. Bilateral pleural effusions are present. CT image during subsequent percutaneous biopsy procedure (**Fig. 121.1c**) shows bilateral pleural effusions and significant compression of the left bronchus (*arrow*) from the bulky mediastinal mass.



■ Diagnosis

Lymphoma

■ Discussion and Differential Diagnosis

The mediastinum is the most common location of childhood chest masses, with lymphoma the most common malignancy. Lymphoma most frequently is located in the anterior and middle mediastinum in children.¹ Non-Hodgkin's lymphoma accounts for two thirds of childhood mediastinal lymphomas.^{1,2} Epstein-Barr virus and immunosuppression are associated with lymphoma.² Children usually present with local symptoms such as cough, stridor, respiratory distress, and superior vena cava syndrome. Systemic symptoms such as fever, weight loss, and night sweats are often present. Cervical lymphadenopathy can be present. Pleural effusions are more often associated with non-Hodgkin's lymphoma.²

Radiography commonly shows an anterior mediastinal mass that is characterized by anterior mediastinal widening. The trachea may be displaced or compressed. CT with intravenous

contrast usually identifies a bland mass without calcification prior to treatment. Lymph node necrosis may be present. Pulmonary nodules, lung consolidation, pleural effusion, and pericardial effusion may be present.²

Differential diagnosis for an anterior mediastinal mass in children includes teratoma and other germ cell tumors, thymic masses such as thymoma and thymic cyst, and retrosternal extension of the thyroid gland. Fat and calcification are characteristic of teratoma. The normal thymus can be large, simulating an anterior mediastinal mass, but, unlike lymphoma, lacks mass effect on adjacent structures. Mediastinal lymphadenopathy can be associated with nonmalignant etiologies such tuberculosis, histoplasmosis, sarcoidosis, and Castleman disease.

Pearl

- ◆ Lymphoma is the most common cause of a mediastinal mass in childhood, representing about half of all mediastinal masses. Calcification on pretreatment imaging is rare for lymphoma.

Pitfall

- ◆ It is important to differentiate a normal thymus from an anterior mediastinal mass, especially in a younger child. An important feature of a normal thymus is the absence of mass effect on adjacent structures.

References

1. Jaggars J, Balsara K. Mediastinal masses in children. *Semin Thorac Cardiovasc Surg* 2004;16:201–208. [PubMed](#)
2. Guillerman RP, Voss SD, Parker BR. Leukemia and lymphoma. *Radiol Clin North Am* 2011;49:767–797, vii. [PubMed](#)

Case 122

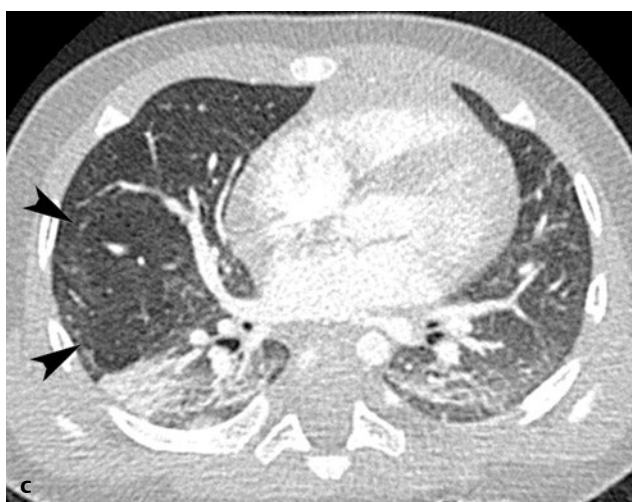
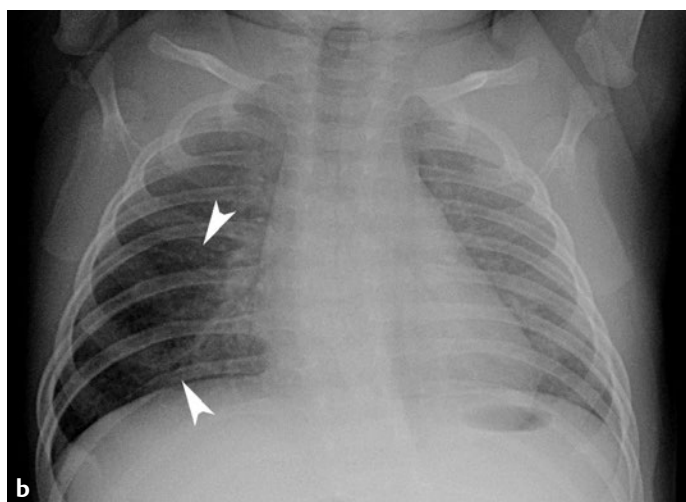
■ Clinical Presentation

An 11-day-old with right lung mass.

■ Imaging Studies

Axial CT image (**Fig. 122.1a**) demonstrates oval right lung mass with small internal cysts (*arrowhead*). Follow-up chest radiograph at 2 months of age (**Fig. 122.1b**) shows an oval lucent right lung lesion (*arrowheads*). Post-contrast CT image (**Fig.**

122.1c) shows interval lucent aeration of the oval lesion (*arrowheads*). Note the mass effect with anterior displacement of the adjacent pulmonary vein and compressive atelectasis posterior to the cystic lesion.



■ Diagnosis

Congenital Pulmonary Airway Malformation

■ Discussion and Differential Diagnosis

Congenital pulmonary airway malformations (CPAMs) include both cystic and noncystic lung anomalies. Bronchiole proliferation with abnormal communication to the central airways during early development results in maldevelopment.^{1,2} CPAM has replaced the older term *congenital cystic adenomatoid malformation* because the anomalies may be neither cystic or adenomatoid.¹ CPAM are usually solitary without lobar predilection.³

The CPAM classification is as follows:

- Type 0: Acinar dysgenesis or dysplasia with a tracheal or bronchial origin
- Type 1: Large cyst (2 to 10 cm in diameter) with a bronchial or bronchiolar origin
- Type 2: Small cysts (0.5 to 2 cm diameter) with bronchiolar origin
- Type 3: Adenomatoid anomaly of bronchiolar-alveolar duct origin
- Type 4: Unlined cysts of distal acinar origin.

Types 1 and 4 are characterized by macrocysts. Type 4 may mimic pleuropulmonary blastoma. Most CPAMs are supplied

by pulmonary artery branches and drained by pulmonary veins; however, hybrid lesions that include a sequestration can have a systemic arterial supply.¹

Antenatal CPAM diagnosis is made by prenatal ultrasound or fetal MRI. Larger anomalies are usually anechoic on ultrasound; smaller cysts can have increased echogenicity. Hyperintense signal on T2-weighted MRI of unilocular or multilocular cysts is typical. Postnatal contrast-enhanced CT can assess both the lung parenchyma and vascularity. Large cysts are usually air filled, whereas small cysts usually have increased attenuation.¹ Patients who are not detected prenatally usually present during infancy either due to respiratory distress or recurrent infections. Some CPAM lesions are incidentally detected in older children.²

Surgical resection is the treatment of choice in symptomatic patients. Surgical resection in asymptomatic patients is advocated due to the risk of infection and the increased risk of malignant degeneration.²

Pearl

- ◆ Congenital pulmonary airway malformations can be cystic and noncystic on imaging and should be detected in utero.

Pitfall

- ◆ Hybrid lesions with features of CPAM and pulmonary sequestration can occur and demonstrate systemic arterial blood supply.

References

1. Biyyam DR, Chapman T, Ferguson MR, Deutsch G, Dighe MK. Congenital lung abnormalities: embryologic features, prenatal diagnosis, and postnatal radiologic-pathologic correlation. *Radiographics* 2010;30:1721–1738. [PubMed](#)
2. Lee EY, Boiselle PM, Cleveland RH. Multidetector CT evaluation of congenital lung anomalies. *Radiology* 2008;247:632–648. [PubMed](#)
3. Daltro P, Fricke BL, Kuroki I, Domingues R, Donnelly LF. CT of congenital lung lesions in pediatric patients. *AJR Am J Roentgenol* 2004;183:1497–1506. [PubMed](#)

Case 123

■ Clinical Presentation

A 2-year-old boy with fever.

■ Radiographic Studies

An AP chest radiograph (**Fig. 123.1a**) shows a round opacity in the right perihilar region. The opacity is poorly visualized on the lateral view (**Fig. 123.1b**). Follow-up chest radiograph

2 weeks later (**Fig. 123.1c**) shows resolution of the right perihilar opacity.



■ Diagnosis

Round Pneumonia

■ Discussion and Differential Diagnosis

Round pneumonia is usually a disease of children with a mean age of 5 years. Some 90% of the cases occur in children younger than 12 years of age.¹ Children typically present with fever, cough, and malaise, and occasionally with abdominal pain. The pores of Kohn and channels of Lambert allow collateral air circulation within the lung lobes. Infection spreads through these passages to adjacent alveoli and throughout a lobe. Underdevelopment of the pores of Kohn and canals of Lambert impede the spread of pneumonia in children with community-acquired pneumonia.² Pneumonia spreads concentrically rather than to lobe fissures, resulting in a spherical shaped pneumonia.² Round pneumonia is most often caused by *Streptococcus pneumoniae*.¹

Chest radiography is characterized by a round, sharply margined, soft tissue density mimicking a pulmonary mass. The margins of the opacity may be irregular, and air bronchograms can be seen in up to 20% of cases, indicating lung parenchymal location.¹ Round pneumonia responds rapidly to antibiotics and becomes ill-defined during early resolution.² In a study

of 109 children, round pneumonias were solitary in 98%, posteriorly located in 83%, and occurred more frequently in the lower lobes.²

The history and physical findings usually enable an accurate diagnosis of round pneumonia in a young child with a pulmonary mass. Differential considerations include congenital anomalies (pulmonary sequestration, congenital pulmonary airway malformation, bronchogenic cysts, diaphragmatic hernia), plasma cell granuloma (postinflammatory pseudotumor), and neoplasms. Neuroblastoma can be the main differential diagnosis due to the frequent posterior location of round pneumonia. Aspergilloma and other fungal lesions can mimic round pneumonia.¹ The diagnosis of round pneumonia can usually be confidently made on the chest radiograph alone with the associated clinical symptoms. Cross-sectional imaging should be considered only if the clinical symptoms are not typical of pneumonia, the opacity persists despite appropriate antibiotic therapy, or the chest radiograph findings suggest an extrapulmonary lesion.¹

Pearl

- ◆ A child with typical signs and symptoms of pneumonia and a rounded opacity on a chest radiograph is most consistent with round pneumonia.

Pitfall

- ◆ Lower lobe round pneumonia may be missed on underpenetrated frontal chest radiographs and may be better seen on a well-penetrated abdominal radiograph.

References

1. Restrepo R, Palani R, Matapathi UM, Wu YY. Imaging of round pneumonia and mimics in children. *Pediatr Radiol* 2010;40:1931–1940 [PubMed](#)
2. Kim YW, Donnelly LF. Round pneumonia: imaging findings in a large series of children. *Pediatr Radiol* 2007;37:1235–1240 [PubMed](#)

Case 124

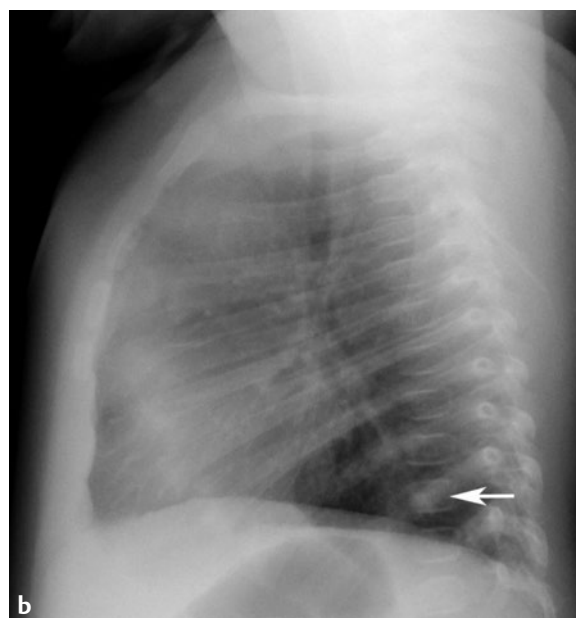
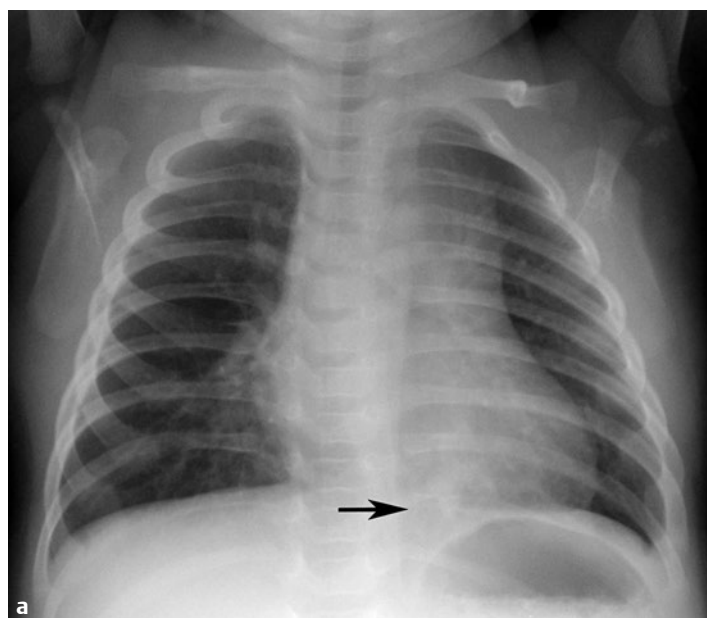
■ Clinical Presentation

A 9-week-old girl with lung abnormality on prenatal ultrasound.

■ Radiographic Studies

Frontal chest radiograph (**Fig. 124.1a**) shows an irregular opacity in the medial left lower lobe (*arrow*). Lateral chest radiograph (**Fig. 124.1b**) shows focal lower lobe opacity (*arrow*).

Postcontrast coronal reformatted CT image (**Fig. 124.1c**) shows left lower lobe lesion supplied by a systemic arterial branch from the descending thoracic aorta (*arrow*).



■ Diagnosis

Pulmonary Sequestration

■ Discussion and Differential Diagnosis

Pulmonary sequestration is a congenital malformation composed of nonfunctioning pulmonary tissue without a normal tracheobronchial tree connection.¹ Sequestration is the second most common antenatally detected pulmonary anomaly following congenital pulmonary airway malformation. Sequestration is categorized as intralobar or extralobar. Intralobar sequestrations usually result from chronic infection and account for 75% of cases. By contrast, extralobar sequestrations are true congenital anomalies and account for the remaining 25% of cases. Unlike intralobar sequestration, extralobar sequestration is invested in its own pleura. Both types are supplied by systemic arteries. Intralobar sequestration usually drains into an inferior pulmonary vein, whereas extralobar sequestration drains into a systemic vein, typically the azygous vein.¹ Extralobar sequestration is associated with other congenital anomalies such as cardiac defects and diaphragmatic anomalies in up to 60% of the cases. Extralobar seques-

tration frequently presents in utero or infancy due to the additional congenital anomalies. Intralobar sequestration presents early in childhood with respiratory distress, pneumonia, and/or cyanosis.

Chest radiographs show focal basilar lung opacity in up to 98% of children with intralobar sequestration, more frequently on the left.¹ CTA is valuable in demonstrating the arterial supply and the venous drainage necessary for surgical planning. Extralobar sequestration appears as a hyperechoic mass on prenatal ultrasound and as a T2 hyperintense mass on fetal MRI.²

Surgical resection is the treatment of choice for symptomatic patients. Elective surgical resection is often recommended even in asymptomatic children, as the procedure gets complicated if the sequestration becomes infected.¹ Pulmonary sequestration can spontaneously involute.

Pearls

- ◆ Pulmonary sequestrations include nonfunctioning pulmonary tissue supplied by systemic arteries, but venous drainage may be either pulmonary or systemic.
- ◆ Sequestration can be associated with congenital pulmonary airway malformation in hybrid lesions.

Pitfall

- ◆ An extralobar sequestration can be located below the diaphragm and mimic neuroblastoma or adrenal hemorrhage.

References

1. Lee EY, Boiselle PM, Cleveland RH. Multidetector CT evaluation of congenital lung anomalies. *Radiology* 2008;247:632–648 [PubMed](#)
2. Biyyam DR, Chapman T, Ferguson MR, Deutsch G, Dighe MK. Congenital lung abnormalities: embryologic features, prenatal diagnosis, and postnatal radiologic-pathologic correlation. *Radiographics* 2010;30:1721–1738. [PubMed](#)

Case 125

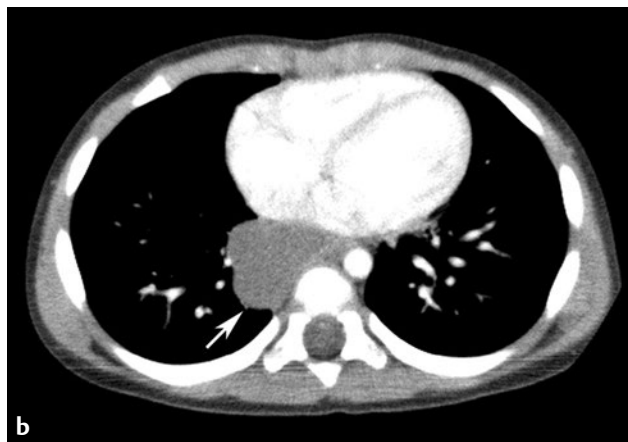
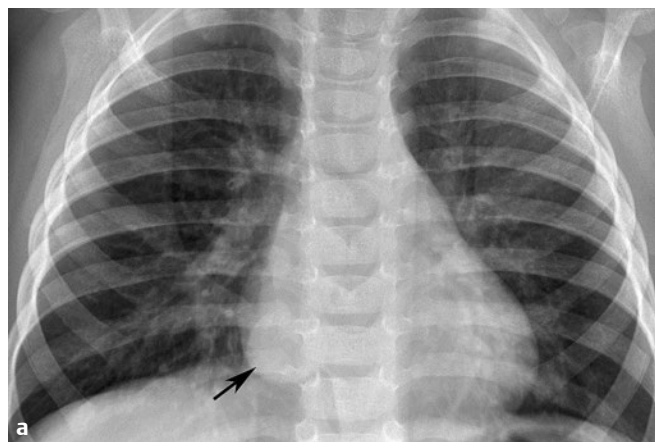
■ Clinical Presentation

A 19-month-old boy with vomiting and cough.

■ Radiographic Studies

Frontal chest radiograph (**Fig. 125.1a**) shows a well-demarcated oval density (*arrow*) posterior to the right heart border. Post-contrast chest CT (**Fig. 125.1b**) shows a well-demarcated oval right paraspinal lesion (*arrow*) with imperceptible wall enhancement. Attenuation values within the lesion ranged from

25 to 45 Hounsfield units. Coronal reformatted CT image (**Fig. 125.1c**) shows the extent of the oval lesion into the subcarinal location with minimal mass effect on the right mainstem bronchus (*arrow*).



■ Diagnosis

Bronchogenic Cyst

■ Discussion and Differential Diagnosis

Bronchogenic cysts are foregut malformations that result from abnormal budding of the ventral foregut during the 4th to 5th week of intrauterine life.^{1,2} Bronchogenic cysts account for 40 to 50% of all congenital intrathoracic cysts.¹ Two thirds of the cysts are mediastinal, and one third occur within the lungs.¹ Most lesions are within the middle mediastinum adjacent to the trachea, but hilar and pulmonary locations also occur. Rare locations include the diaphragm, retroperitoneum, neck, and the base of the tongue.² Intrapulmonary cysts are usually located in the lower lobes.¹ Bronchogenic cysts can be associated with sequestration, congenital lobar overinflation, and congenital diaphragmatic hernia.³ The cyst wall is lined by respiratory epithelium containing mucous glands, cartilage, and smooth muscle. The cyst content is usually a mixture of serous fluid and proteinaceous mucus.³ Calcium in the cyst wall and milk of calcium with fluid–fluid levels are rare.³ Mediastinal bronchogenic cysts usually do not communicate with the tracheobronchial tree, and the presence of gas in them is secondary to infection or instrumentation.¹

Two thirds are symptomatic, and the symptoms usually are related to the tracheobronchial compression.¹ Most patients present within the first few decades of life; chest pain is the most common presenting symptom.³ Infection occurs in 20% of the pulmonary lesions, secondary to communication with the tracheobronchial tree.

A bronchogenic cyst appears as a solitary, rounded mass with homogeneous density on chest radiographs, often located just inferior to the carina.⁴ CT shows a round or elliptical cyst with attenuation varying from near-water to high attenuation.^{3,4} High attenuation is present if proteinaceous fluid, calcium, or blood products are within the cyst.³ The cyst wall is imperceptible on CT imaging. Cyst wall thickening or enhancement suggests that the bronchogenic cyst is complicated by infection or that alternate diagnoses should be considered. T1-weighted MRI shows variable signal, which depends on the presence of protein, calcium, and hemorrhage, but high signal is always present with T2-weighted and STIR MRI.⁴ Bronchogenic cysts are rarely diagnosed at fetal imaging. They are usually seen as a unilocular cyst in the middle or posterior mediastinum.

Differential diagnosis for a mediastinal bronchogenic cyst includes esophageal duplication cyst and neurenteric cyst. Occasionally, a bronchogenic cyst may appear solid and mimic mediastinal masses such as teratoma and lymphoma. The differential diagnosis of an intrapulmonary bronchogenic cyst includes congenital pulmonary airway malformation, lung abscess, and round pneumonia.²

Treatment of the bronchogenic cyst is by surgical removal. Surgery is recommended for symptomatic individuals.³

Pearl

- ◆ Bronchogenic cysts commonly present as a nonenhancing, solitary, round or elliptical mass inferior to the carina. CT attenuation varies due to different possible cyst contents, but high signal is always present on T2-weighted MRI sequences.

Pitfall

- ◆ Cyst wall thickening is not characteristic of an uncomplicated bronchogenic cyst and should raise suspicion for infection complicating a bronchogenic cyst or a neoplasm.

References

1. Berrocal T, Madrid C, Novo S, Gutiérrez J, Arjonilla A, Gómez-León N. Congenital anomalies of the tracheobronchial tree, lung, and mediastinum: embryology, radiology, and pathology. *Radiographics* 2004;24:e17 [PubMed](#)
2. Kocaoglu M, Frush DP, Uğurel MS, Somuncu I. Bronchopulmonary foregut malformations presenting as mass lesions in children: spectrum of imaging findings. *Diagn Interv Radiol* 2010;16:153–161 [PubMed](#)
3. McAdams HP, Kirejczyk WM, Rosado-de-Christenson ML, Matsumoto S. Bronchogenic cyst: imaging features with clinical and histopathologic correlation. *Radiology* 2000;217:441–446 [PubMed](#)
4. Jeung MY, Gasser B, Gangi A, et al. Imaging of cystic masses of the mediastinum. *Radiographics* 2002;22(Spec. No.):S79–S93 [PubMed](#)

Case 126

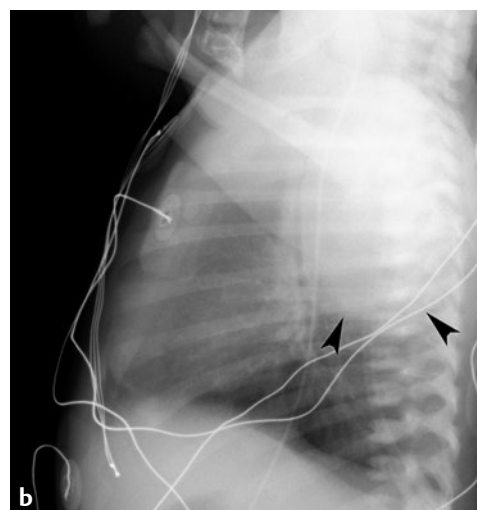
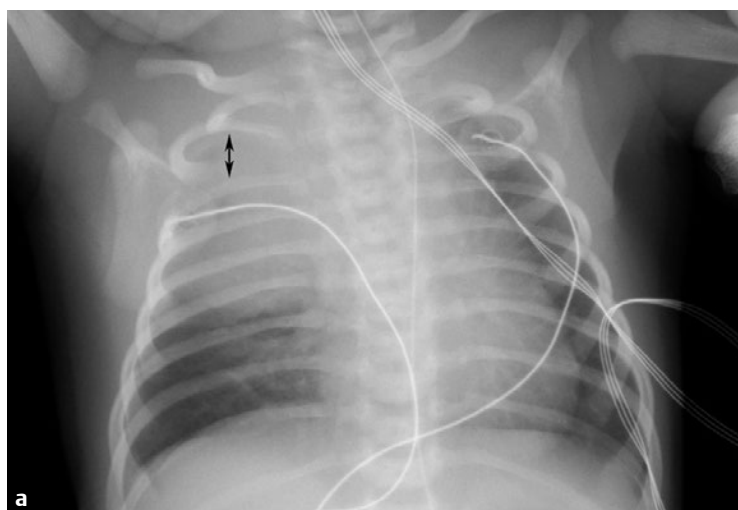
■ Clinical Presentation

A 2-day-old term infant with respiratory distress.

■ Radiographic Studies

Frontal chest radiograph (**Fig. 126.1a**) shows round opacity right/upper hemithorax with widening of several right upper intercostal spaces (*double arrow*). Lateral chest radiograph (**Fig. 126.1b**) shows an oval posterior mediastinal mass (*arrow-*

heads) with anterior displacement of trachea. Postcontrast CT image (**Fig. 126.1c**) shows the enhancing posterior mediastinum mass, which crosses the midline, displaces mediastinal structures to the left, and extends into the spinal canal (*arrow*).



■ Diagnosis

Posterior Mediastinal Mass: Neuroblastoma

■ Discussion and Differential Diagnosis

The posterior mediastinum is located posterior to the heart and trachea and extends to the thoracic vertebral margin and includes the paravertebral gutters.¹ The posterior mediastinum contents include the descending thoracic aorta, azygous vein, thoracic duct, autonomic ganglia, lymph nodes, and fat.¹ Some 30 to 40% of mediastinal tumors are located in the posterior mediastinum, of which 85 to 90% are neurogenic in origin.¹ Neuroblastoma, ganglioneuroblastoma, and ganglioneuroma are the most common neurogenic tumors in children. After the abdomen, the thorax is the second most common location of neuroblastoma.¹ Other posterior mediastinal lesions include foregut duplication cysts, neurenteric cysts, lymphoma, Bochdalek diaphragmatic hernia, hemangioma, and lymphatic malformation.²

The median age of presentation for neuroblastoma is younger than 2 years, and more than 95% of cases are diagnosed by 10 years of age.¹ Patients with thoracic neuroblastoma can be asymptomatic and may be found incidentally on chest or abdominal radiographs. Symptoms may be due to local mass effect on adjacent structures such as the airway or spinal cord. Metastatic disease can present with constitutional symptoms such as bone pain, fever, and weight loss.¹

Radiographs show a paraspinal soft tissue mass that may cause rib spreading or erosion; calcification is seen in up to 30% of cases.³ Round pneumonia can mimic a posterior mediastinal mass on radiographs, but will not be associated with rib abnormalities. CT detects calcification within the mass in 80 to 90% of thoracic neuroblastomas and displays tumor extent, vascular encasement, adenopathy, and metastases. Areas of necrosis and hemorrhage are frequently seen within the mass. MRI better displays intraspinal extension, marrow changes, and hepatic metastases. Scintigraphic evaluation with MIBG helps identify the primary tumor and monitor metastases.³

Low-risk tumors are treated with surgery, combined with chemotherapy if necessary. High-risk tumors are treated with surgery and chemotherapy. Bone marrow transplantation is necessary in some cases. Children younger than 1 year of age have a better prognosis relating to better differentiated tumor histology. Children older than 1 year at the time of diagnosis with stage 3 or 4 disease have a worse prognosis.

Pearls

- ◆ The most common posterior mediastinal mass in children is neuroblastoma.
- ◆ Urinary catecholamines are elevated in most patients with thoracic neuroblastoma.³

Pitfall

- ◆ Round pneumonia can mimic a posterior mediastinal mass on a chest radiograph.

References

1. Franco A, Mody NS, Meza MP. Imaging evaluation of pediatric mediastinal masses. *Radiol Clin North Am* 2005;43:325–353 [PubMed](#)
2. Frush DP. Imaging of paediatric mediastinal masses. *Ann Acad Med Singapore* 2003;32:525–535 [PubMed](#)
3. Lonergan GJ, Schwab CM, Suarez ES, Carlson CL. Neuroblastoma, ganglioneuroblastoma, and ganglioneuroma: radiologic-pathologic correlation. *Radiographics* 2002;22:911–934 [PubMed](#)

Case 127

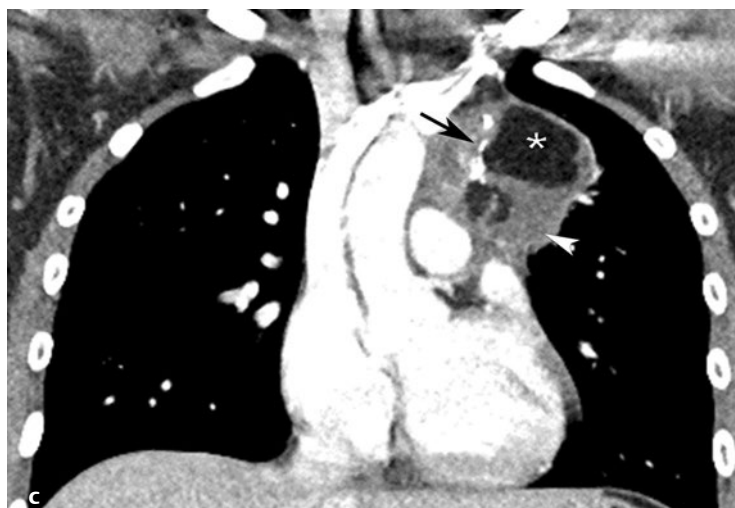
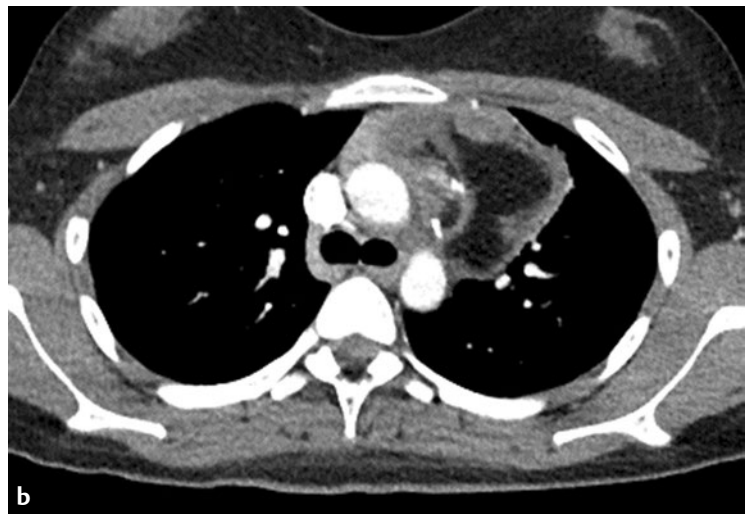
■ Clinical Presentation

A 13-year-old girl with incidental mass on spine radiograph.

■ Radiographic Studies

Frontal chest radiograph (**Fig. 127.1a**) shows a lobulated left mediastinal mass. Postcontrast CT image (**Fig. 127.1b**) shows the heterogeneous mass arising from the left lobe of thymus.

Coronal reformatted CT image (**Fig. 127.1c**) demonstrates soft tissue components (*arrowhead*), fat components (*asterisk*), and calcifications (*arrow*) within the mass.



■ Diagnosis

Teratoma

■ Discussion and Differential Diagnosis

Mediastinal germ cell tumors account for 25% of anterior mediastinal tumors in children.¹ The mediastinum is the second most common extragonadal site for germ cell tumors but accounts for only 1 to 3% of all germ cell tumors.^{2,3} Normal primordial germ cells arise in the yolk sac and migrate along the mesentery into the gonadal ridge to form gonads. Incomplete differentiation or aberrant migration gives rise to gonadal or extragonadal germ cell tumors.³ Teratomas are the most common mediastinal germ cell tumors.² Most teratomas occur in the anterior mediastinum, with a few cases occurring in the posterior mediastinum. Teratomas can be benign or malignant; most pediatric teratomas are benign.³ Mature teratomas contain tissue from all three germinal cell layers.⁴ Most contain ectodermal elements such as cutaneous and neuroglial tissue. Other tissues that can be found include bone, cartilage, fat, smooth muscle, and endocrine tissue.⁴ Nonteratomatous germ cell tumors include seminoma, yolk sac tumor, embryonal carcinoma, choriocarcinoma, and mixed types.² Most patients present as infants or young adults.⁴ Presenting signs relate to local mass effect or invasion and include cough, dyspnea, hoarseness, and chest pain.⁴

Teratomas present as a large rounded or lobulated mass on chest radiographs. Calcifications can be identified by radiography on up to 26% of cases.² Contrast-enhanced CT is the best imaging modality to demonstrate the extent of disease, show different tissue components, and identify associated complications. The presence of fluid, soft tissue, calcification, and fat in an anterior mediastinal mass is highly specific for teratoma.² Surgical resection is the mainstay of treatment. Mature teratomas have an excellent prognosis following complete resection. The presence of immature or premalignant elements influences treatment and long-term prognosis.³

The differential diagnosis includes other anterior mediastinal masses. Lymphoma is the most common anterior mediastinal mass in children but rarely calcifies. Thymoma is usually seen in older individuals over 40 years of age. Thymolipoma has predominantly fat and is rarely seen in children. Vascular malformations may have fluid attenuation and may contain calcium, but not fat.⁵

Pearl

- ◆ The typical mature mediastinal teratoma is prevascular, extends to one side of the mediastinum, and demonstrates fat, fluid, and calcified components.

Pitfall

- ◆ A small number of mature teratomas may have a nonspecific cystic appearance without identifiable fat or calcium.

References

1. Takahashi K, Al-Janabi NJ. Computed tomography and magnetic resonance imaging of mediastinal tumors. *J Magn Reson Imaging* 2010;32:1325–1339. [PubMed](#)
2. Franco A, Mody NS, Meza MP. Imaging evaluation of pediatric mediastinal masses. *Radiol Clin North Am* 2005;43:325–353. [PubMed](#)
3. Barksdale EM Jr, Obokhare I. Teratomas in infants and children. *Curr Opin Pediatr* 2009;21:344–349. [PubMed](#)
4. Jagers J, Balsara K. Mediastinal masses in children. *Semin Thorac Cardiovasc Surg* 2004;16:201–208. [PubMed](#)
5. Frush DP. Imaging of paediatric mediastinal masses. *Ann Acad Med Singapore* 2003;32:525–535. [PubMed](#)

Case 128

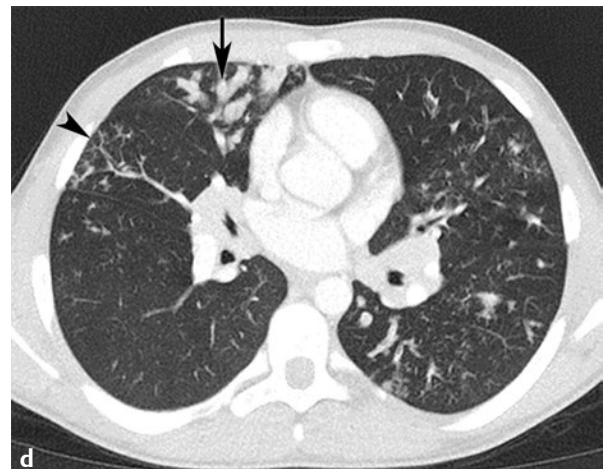
■ Clinical Presentation

An 18-year-old with recurrent pulmonary infections.

■ Radiographic Studies

Frontal and lateral chest radiographs (**Fig. 128.1a,b**) show peribronchial thickening, bronchiectatic changes in the upper lobes bilaterally, and scattered areas of mucus plugging. Axial slice from postcontrast CT of the chest at the level of trachea (**Fig. 128.1c**) shows bronchiectasis in both upper lobes. The

dilated bronchi are larger than the adjacent vessel (*arrows*). Another axial slice at a lower level (**Fig. 128.1d**) shows a tree-in-bud appearance (*arrowhead*) in the lateral middle right lung and bronchiectasis with mucus plugging more medially in the right middle lobe (*arrow*).



■ Diagnosis

Cystic Fibrosis

■ Discussion

Cystic fibrosis (CF) is an autosomal recessive disease caused by gene abnormality on the long arm of chromosome 7. CF is most commonly found in Caucasians. Abnormal chloride transport leads to thick, tenacious, viscous mucus difficult to expectorate that frequently becomes secondarily infected. Repeated pulmonary infections lead to destruction of smaller airways, causing air trapping and bronchiectasis. Abnormal chloride transport also results in pancreatic enzyme insufficiency.

The chest radiograph in infants and young children may initially be normal or show nonspecific interstitial disease. Hyperinflation with mucus plugging and bronchiectasis are characteristic in older children and teenagers. Bronchiectasis in CF predominantly involves the upper lobes. Small airway destruction from repeated infection leads to air trapping and pulmonary hyperinflation. Bronchial mucus plugs may lead to atelectasis. Mucus impaction of small airways appears as poorly defined opacities in the peripheral lungs. Children with CF are at risk for recurrent pneumonias, pneumothorax, and allergic bronchopulmonary aspergillosis. *Pseudomonas*, *Staph-*

yllococcus, and *Haemophilus* are common organisms in recurrent pneumonias.

High-resolution computed tomography (HRCT) detects dilated bronchi with adjacent smaller pulmonary artery branch (signet ring sign, **Fig. 128.1c**). Bronchiectasis is progressive, irreversible, and the most reliable change seen on CT that can be scored.¹ Secretions and mucus plugging within the centrilobular bronchioles can give “tree-in-bud” opacities. CT scoring is more sensitive than pulmonary function tests for the detection of relevant disease progression in CF.²

Differential diagnosis for bronchiectasis in children includes CF, immotile cilia syndrome, and recurrent aspirations. Bronchiectasis is predominantly seen in lower lobes in immotile cilia syndrome and in recurrent aspirations, whereas bronchiectasis is seen predominantly in the upper lobes in CF. Extrapulmonary features of CF include chronic sinusitis, nasal polyposis, meconium peritonitis, meconium ileus, cholelithiasis, pancreatic dysfunction, and malabsorption.

Pearls

- ◆ Chest radiography may initially be normal or nonspecific.
- ◆ Extrapulmonary manifestations such as meconium ileus may present prior to pulmonary symptoms.

Pitfall

- ◆ Bronchiectasis can also be seen with immotile cilia syndrome and recurrent aspirations.

■ Controversy

- High-resolution computed tomography is of limited value in infants with CF because late manifestations such as bronchiectasis and mucus plugs are frequently absent.³

References

1. Tepper LA, Caudri D, Utens EM, van der Wiel EC, Quittner AL, Tiddens HA. Tracking CF disease progression with CT and respiratory symptoms in a cohort of children aged 6–19 years. *Pediatr Pulmonol* 2014;49:1182–1189 [epub ahead of print] [PubMed](#)
2. Tiddens HA, de Jong PA. Imaging and clinical trials in cystic fibrosis. *Proc Am Thorac Soc* 2007;4:343–346 [PubMed](#)
3. Thia LP, Calder A, Stocks J, et al; London Cystic Fibrosis Collaboration. Is chest CT useful in newborn screened infants with cystic fibrosis at 1 year of age? *Thorax* 2014;69:320–327 [PubMed](#)

Case 129

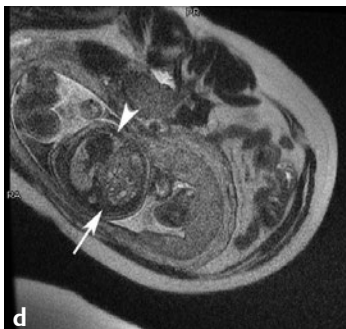
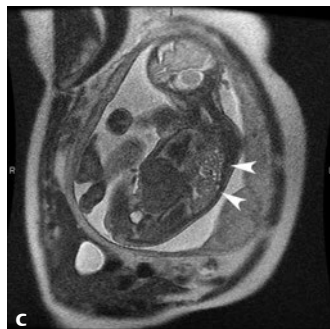
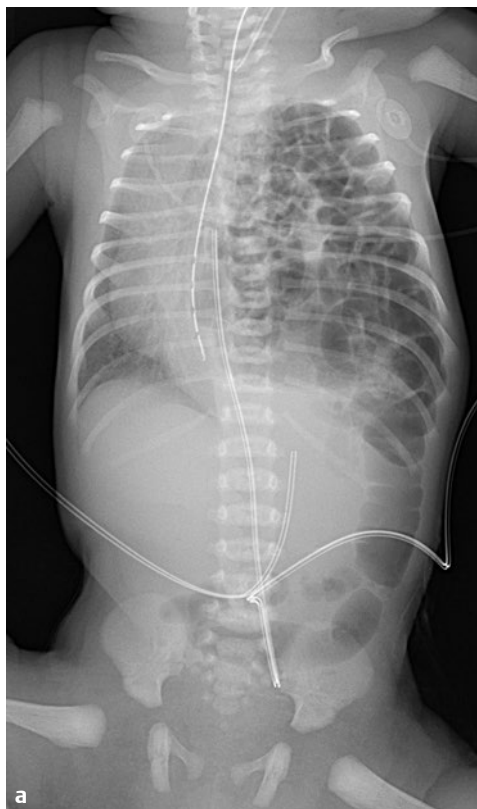
■ Clinical Presentation

A newborn with respiratory distress.

■ Radiographic Studies

An AP chest/abdomen radiograph (**Fig. 129.1a**) shows aerated bowel loops filling the left hemithorax and shift of mediastinal structures to the right. Note the bowel loop continuity across the left hemidiaphragm and atypical umbilical venous catheter alignment in the left upper abdomen. Lateral chest/abdomen radiograph (**Fig. 129.1b**) shows a majority of aerated bowel

loops within the chest. Coronal T2-weighted MRI of the same fetus (**Fig. 129.1c**) shows herniation of bowel loops into the left chest (**arrowheads**). Axial T2-weighted MRI of the same fetus (**Fig. 129.1d**) shows bowel loops filling the left hemithorax (**arrow**) and displacement of the heart into the right hemithorax (**arrowhead**).



■ Diagnosis

Congenital Diaphragmatic Hernia

■ Discussion and Differential Diagnosis

Congenital defects in the diaphragm lead to herniation of abdominal contents into the thoracic cavity. The foramina of Bochdalek are located in the posterior lateral diaphragm, and the foramina of Morgagni are anterior and medial defects in the diaphragm.¹ Left-sided Bochdalek hernias account for 90% of diaphragmatic hernias. The herniated contents cause ipsilateral lung hypoplasia and shift of the mediastinum to the contralateral side. Congenital diaphragmatic hernia (CDH) is associated with other congenital anomalies involving the central nervous system, heart, and kidneys.² Karyotyping is performed to identify associated chromosomal anomalies, particularly trisomies.

The diaphragmatic hernia is an echogenic chest mass on fetal ultrasound. The differential diagnosis includes congenital pulmonary airway malformation and pulmonary sequestra-

tion. Pulmonary sequestration can be differentiated by demonstrating arterial supply from the aorta. Fetal MRI shows hyperintense T2 signal in the lower chest from herniated bowel. A lung-to-head ratio < 1.0 , as measured on prenatal ultrasound, has a poor prognosis, but a ratio > 1.4 has a favorable prognosis. Lung volume measured on fetal MRI can predict the need for postnatal extracorporeal membrane oxygenation (ECMO).³⁻⁵

Chest radiograph initially shows opacity in the lower thorax immediately after birth. Later, bubbly lucencies are characteristic as ingested air distends the bowel. If liver has herniated, it appears as opacity on radiographs. Isolated congenital diaphragmatic hernia has a good prognosis if the liver is not involved.

Pearl

- ◆ Children with associated liver herniation, lung head ratio < 1 , right-sided hernia, bilateral hernias, polyhydramnios, and multiple complex congenital anomalies have a poor prognosis.

Pitfall

- ◆ Congenital pulmonary airway malformation and pulmonary sequestration also appear as echogenic lesions in the chest on fetal ultrasound.

References

1. Merrell AJ, Kardon G. Development of the diaphragm—a skeletal muscle essential for mammalian respiration. *FEBS J* 2013;280:4026–4035 [PubMed](#)
2. Greer JJ. Current concepts on the pathogenesis and etiology of congenital diaphragmatic hernia. *Respir Physiol Neurobiol* 2013;189:232–240 [PubMed](#)
3. Hagelstein C, Weidner M, Kilian AK, et al. Repetitive MR measurements of lung volume in fetuses with congenital diaphragmatic hernia: individual development of pulmonary hypoplasia during pregnancy and calculation of weekly lung growth rates. *Eur Radiol* 2014;24:312–319 [PubMed](#)
4. Walleyo A, Debus A, Kehl S, et al. Periodic MRI lung volume assessment in fetuses with congenital diaphragmatic hernia: prediction of survival, need for ECMO, and development of chronic lung disease. *AJR Am J Roentgenol* 2013;201:419–426 [PubMed](#)
5. Odibo AO, Najaf T, Vachharajani A, Warner B, Mathur A, Warner BW. Predictors of the need for extracorporeal membrane oxygenation and survival in congenital diaphragmatic hernia: a center's 10-year experience. *Prenat Diagn* 2010;30:518–521 [PubMed](#)

Case 130

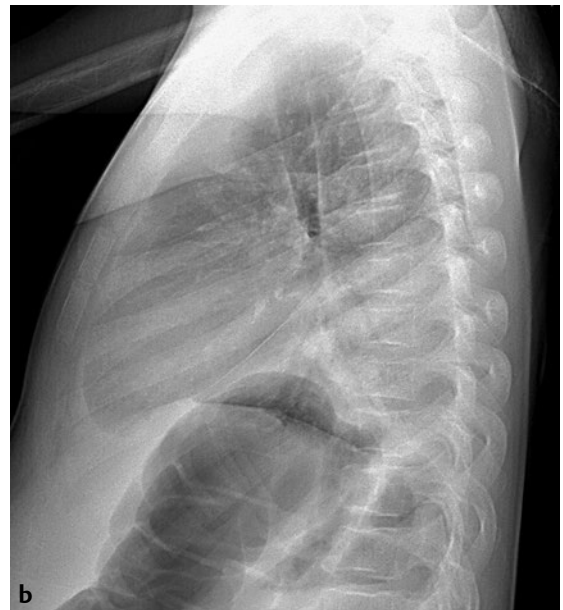
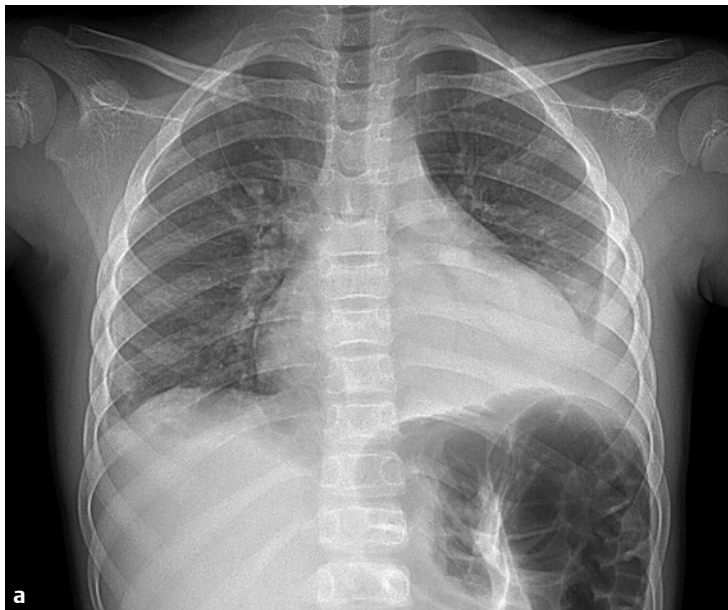
■ Clinical Presentation

A 7-year-old girl with increased work of breathing.

■ Radiographic Studies

Frontal chest radiograph (**Fig. 130.1a**) shows left lower lung alveolar infiltrate and moderate left pleural effusion. Lower thoracic vertebral end-plate depressions and paucity of splenic

tissue are noted. Lateral chest radiograph (**Fig. 130.1b**) shows the lower lung alveolar infiltrate and middle-lower thoracic vertebral end-plate depressions.



■ Diagnosis

Sickle Cell Disease: Acute Chest Syndrome

■ Discussion and Differential Diagnosis

In sickle cell disease hemoglobin deoxygenation events lead to red cell polymerization and sickling. Sickled red cells occlude small vessels, leading to ischemia, resulting in pulmonary ischemia, bone infarction, and autosplenectomy. Acute chest syndrome in sickle cell disease is defined as new lung opacity on chest radiograph with one of the following: fever, chest pain, respiratory distress, or new-onset hypoxemia.¹ Acute chest syndrome is a common cause of hospitalization in patients with sickle cell disease and may lead to premature death. Acute chest syndrome may be caused by pneumonia (30%), pulmonary infarction (18%), or pulmonary fat embolism from necrotic bone marrow (9%).² The specific inciting factor may be unidentified. Incidence of febrile acute chest syndrome in sickle cell disease has significantly decreased after the introduction of pneumococcal vaccine in 2000.³

Chest radiograph may be normal in 46% of the patients. New pulmonary opacity may be seen within 2 to 3 days after the

onset of symptom.⁴ Upper and middle lung involvement is more common in children younger than 10 years of age. Rib infarction causes splinting and pain leading to hypoventilation and atelectasis. Pleural effusions may be seen in more than 50% of the patients.⁵ Chlamydia, mycoplasma, and respiratory syncytial virus are commonly seen in pneumonia associated with acute chest syndrome.⁵ Other chest radiographic findings in sickle cell disease include cardiomegaly, vertebral end-plate depressions, small/absent spleen from autosplenectomy, and avascular necrosis of the humeral head. Management in acute chest syndrome involves supportive therapy with oxygen, bronchodilators, analgesia, and antibiotics. Hydroxyurea reduces sickling of red cells by increasing fetal hemoglobin level and decreases the incidence of acute chest syndrome. Stem cell transplant helps in recurrent acute chest syndrome refractory to hydroxyurea therapy.⁴

Pearl

- ◆ Chest radiograph may be normal for 2 to 3 days after the onset of symptoms.

Pitfall

- ◆ Isolated pneumonia and acute chest syndrome are difficult to differentiate as both have new lung opacity and fever.

■ Controversy

- Steroid use for treatment of acute chest syndrome is controversial and may predispose to fat emboli.⁴

References

1. Paul RN, Castro OL, Aggarwal A, Oneal PA. Acute chest syndrome: sickle cell disease. *Eur J Haematol* 2011;87:191–207 [PubMed](#)
2. Vichinsky EP, Neumayr LD, Earles AN, et al; National Acute Chest Syndrome Study Group. Causes and outcomes of the acute chest syndrome in sickle cell disease. *N Engl J Med* 2000;342:1855–1865 [PubMed](#)
3. Chang TP, Kriengsoontorkij W, Chan LS, Wang VJ. Clinical factors and incidence of acute chest syndrome or pneumonia among children with sickle cell disease presenting with a fever: a 17-year review. *Pediatr Emerg Care* 2013;29:781–786 [PubMed](#)
4. Abbas HA, Kahale M, Hosn MA, Inati A. A review of acute chest syndrome in pediatric sickle cell disease. *Pediatr Ann* 2013;42:115–120 [PubMed](#)
5. Donnelly LF, Merrow AC, Anton CG, et al. *Diagnostic Imaging: Pediatrics*, 2nd ed. Salt Lake City: Amirsys; 2011

Case 131

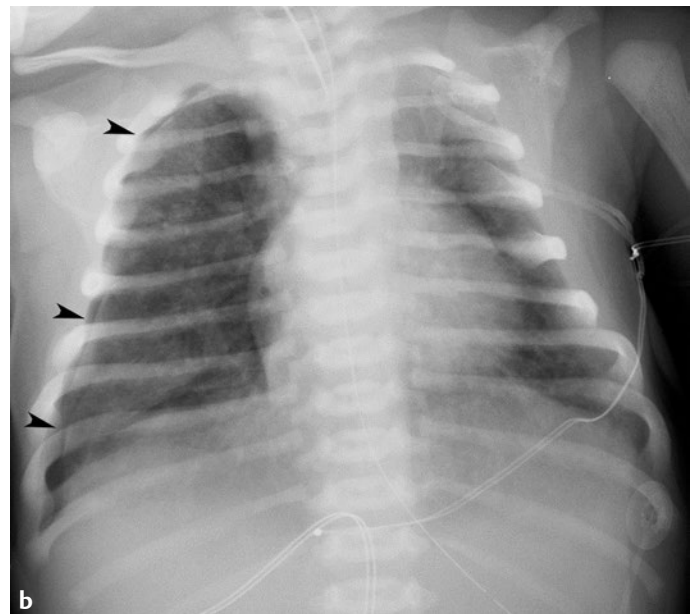
■ Clinical Presentation

A term newborn with respiratory distress.

■ Radiographic Studies

Frontal chest radiograph on the first day of life (**Fig. 131.1a**) shows coarse asymmetric interstitial infiltrates and malpositioned umbilical vascular catheters. Follow-up radiographs show developing interstitial air, small right lateral pneumo-

thorax (**Fig. 131.1b**, *arrowheads*), and then a tension left pneumothorax (**Fig. 131.1c**). On day 9 of life (**Fig. 131.1d**) coarse asymmetric interstitial infiltrates with interstitial air remain; ECMO vascular cannulas have been placed in the right neck.



■ Diagnosis

Meconium Aspiration

■ Discussion and Differential Diagnosis

Meconium aspiration syndrome is caused by aspiration of meconium and characterized by hypoxia, hypercapnia, and acidosis.¹ Fetal stress after 34 week of gestation can lead to in utero passage of meconium. Aspirated thick meconium migrates to the peripheral airway, causing obstruction. Postnatal air trapping in small airway obstruction may rupture, leading to pulmonary interstitial emphysema, pneumothorax, or pneumomediastinum. Enzymes and bile salts of the meconium cause airway irritation with release of cytokines, producing chemical pneumonitis. Meconium causes surfactant dysfunction, leading to atelectasis, and provides a medium for bacterial growth and secondary pneumonia. Meconium is cleared by macrophages that initiate inflammation of the lung parenchyma and causes pulmonary vasoconstriction. In addition, intrauterine hypoxia may lead to hypertrophy of pulmonary vasculature. Increased pulmonary resistance does not allow ductus arteriosus to close and results in persistent pulmonary hypertension of the newborn.²

Reduction in postterm delivery has decreased the incidence of meconium aspiration. Although meconium-stained amniotic fluid is observed in 10 to 15% of all live births, actual me-

conium aspiration occurs in fewer than 2% of newborns born after 37 weeks of gestation.³

Preventing intrauterine hypoxia, early airway suctioning, and management of complications like pulmonary hypertension and air leak are important in patient care. Surfactant replacement improves the outcome and reduces the need for ECMO. Ventilator support is required in 30% of cases. Nitric oxide therapy delivered through a ventilator helps selective vasodilatation of pulmonary vasculature. Steroids help by inhibiting inflammation and decreasing cytokine-induced pulmonary vasoconstriction.¹

Meconium aspiration is a clinical diagnosis. Meconium is recovered from the airway during endotracheal suctioning in the presence of characteristic symptoms. Radiographs are helpful to diagnose complications and monitor recovery. Bilateral patchy and linear pulmonary opacities in an asymmetric distribution are characteristic on chest radiographs. Both atelectasis and hyperinflation are common. Air leaks lead to pulmonary interstitial emphysema, pneumothorax, or pneumomediastinum. Differential diagnosis for asymmetric bilateral patchy opacities in lungs of the newborn includes neonatal pneumonia and pulmonary hemorrhage.

Pearl

- ◆ Typical meconium aspiration infants have ossified proximal humeral and/or coracoid epiphyses, indicating that the infant is at least term and could be postmature.

Pitfall

- ◆ Chest radiography can be normal.

■ Controversy

- Routine common practice of nasopharyngeal and oropharyngeal suction immediately after the delivery of head, but

before the delivery of chest, may not always prevent meconium aspiration syndrome.⁴

References

1. Yeh TF. Core concepts: meconium aspiration syndrome: pathogenesis and current management. *NeoReviews*. 2010;11:e503–e512
2. Storme L, Aubry E, Rakza T, et al; French Congenital Diaphragmatic Hernia Study Group. Pathophysiology of persistent pulmonary hypertension of the newborn: impact of the perinatal environment. *Arch Cardiovasc Dis* 2013; 106:169–177 [PubMed](#)
3. Yoder BA, Kirsch EA, Barth WH, Gordon MC. Changing obstetric practices associated with decreasing incidence of meconium aspiration syndrome. *Obstet Gynecol* 2002;99(5 Pt 1):731–739 [PubMed](#)
4. Vain NE, Szyld EG, Prudent LM, Wiswell TE, Aguilar AM, Vivas NI. Oropharyngeal and nasopharyngeal suctioning of meconium-stained neonates before delivery of their shoulders: multicentre, randomised controlled trial. *Lancet* 2004;364:597–602 [PubMed](#)

Case 132

■ Clinical Presentation

A 1-year-old girl with persistent respiratory distress and asymmetric lungs on chest radiograph.

■ Radiographic Studies

Frontal chest radiographs (**Fig. 132.1a**) obtained at 1 day of life and at 6 months of life show progressive asymmetric lucency of the left upper hemithorax. Coronal reformatted CT image (**Fig. 132.1b**) shows hyperlucent left upper lobe with attenu-

ated lung markings (*arrow*). A more anterior CT image (**Fig. 132.1c**) shows mediastinal shift to the right with a markedly deviated anterior junctional line (*arrowhead*).



a

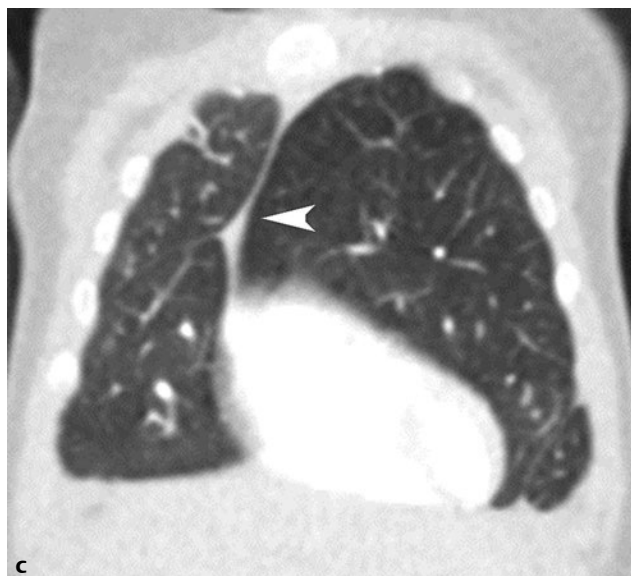
Day 1



6 months



b



c

■ Diagnosis

Congenital Lobar Overinflation



■ Discussion and Differential Diagnosis

Congenital lobar overinflation (CLO), previously known as congenital lobar emphysema, is overdistention of one or more lobes of a lung that is otherwise histologically normal.¹ *Congenital lobar overinflation* is the preferred term because the alveolar walls are intact despite lobar hyperinflation.² The left upper lobe is the most frequent site (42.2%), followed by the right middle lobe (35.3%) and right upper lobe (20.7%). Lower lobe, multilobar, and sublobar CLO are rare.^{2,3} Cardiovascular anomalies can be associated with CLO.² Congenital lobar overinflation is caused by either an intrinsic bronchocartilage abnormality or extrinsic airway compression, resulting in lobar bronchomalacia.⁴ The resultant deficient bronchial cartilage causes lobar bronchial collapse during expiration.⁴ The malacic airway acts as a one-way valve, leading to progressive air trapping. The majority of patients present before 6 months of age with respiratory distress.⁵

Prenatal detection of CLO can be performed by ultrasound or MRI. The affected fluid-filled lobe appears hyperechoic on ultrasound and exhibits T2 hyperintense signal on MRI.² Chest radiographs during the first day of life may show a segmental lung density. However, as fetal fluid is resorbed, the affected lobe becomes hyperlucent due to air trapping.⁵ Mass effect is created by the hyperexpanded lobe causing mediastinal shift away from the lobe and ipsilateral lung compression.² Patients with respiratory compromise are treated with surgical resection of the affected lobe.⁵ Patients with milder symptoms are conservatively managed.

Congenital lobar overinflation can be confused with pneumothorax, pulmonary cyst, or congenital pulmonary airway malformation. Unlike the other conditions, the affected lung preserves pulmonary architecture with normal though attenuated lung markings.²

Pearl

- ◆ In the neonatal period, congenital lobar overinflation demonstrates a transition from alveolar opacification to interstitial opacification to generalized hyperlucency as fetal fluid is absorbed.

Pitfall

- ◆ Congenital lobar overinflation can be confused with pneumothorax, lung cyst, or congenital pulmonary airway malformation.

References

1. Ulku R, Onat S, Özçelik C. Congenital lobar emphysema: differential diagnosis and therapeutic approach. *Pediatr Int* 2008;50:658–661 [PubMed](#)
2. Biyyam DR, Chapman T, Ferguson MR, Deutsch G, Dighe MK. Congenital lung abnormalities: embryologic features, prenatal diagnosis, and postnatal radiologic-pathologic correlation. *Radiographics* 2010;30:1721–1738. [PubMed](#)
3. Lee EY, Boiselle PM, Cleveland RH. Multidetector CT evaluation of congenital lung anomalies. *Radiology* 2008;247:632–648 [PubMed](#)
4. Özçelik U, Göçmen A, Kiper N, Doğru D, Dilber E, Yalçın EG. Congenital lobar emphysema: evaluation and long-term follow-up of thirty cases at a single center. *Pediatr Pulmonol* 2003;35:384–391 [PubMed](#)
5. Berrocal T, Madrid C, Novo S, Gutiérrez J, Arjonilla A, Gómez-León N. Congenital anomalies of the tracheobronchial tree, lung, and mediastinum: embryology, radiology, and pathology. *Radiographics* 2004;24:e17 [PubMed](#)

VIII

Cardiac

Section Editor

S. Bruce Greenberg

Author

Sadaf T. Bhutta



Case 133

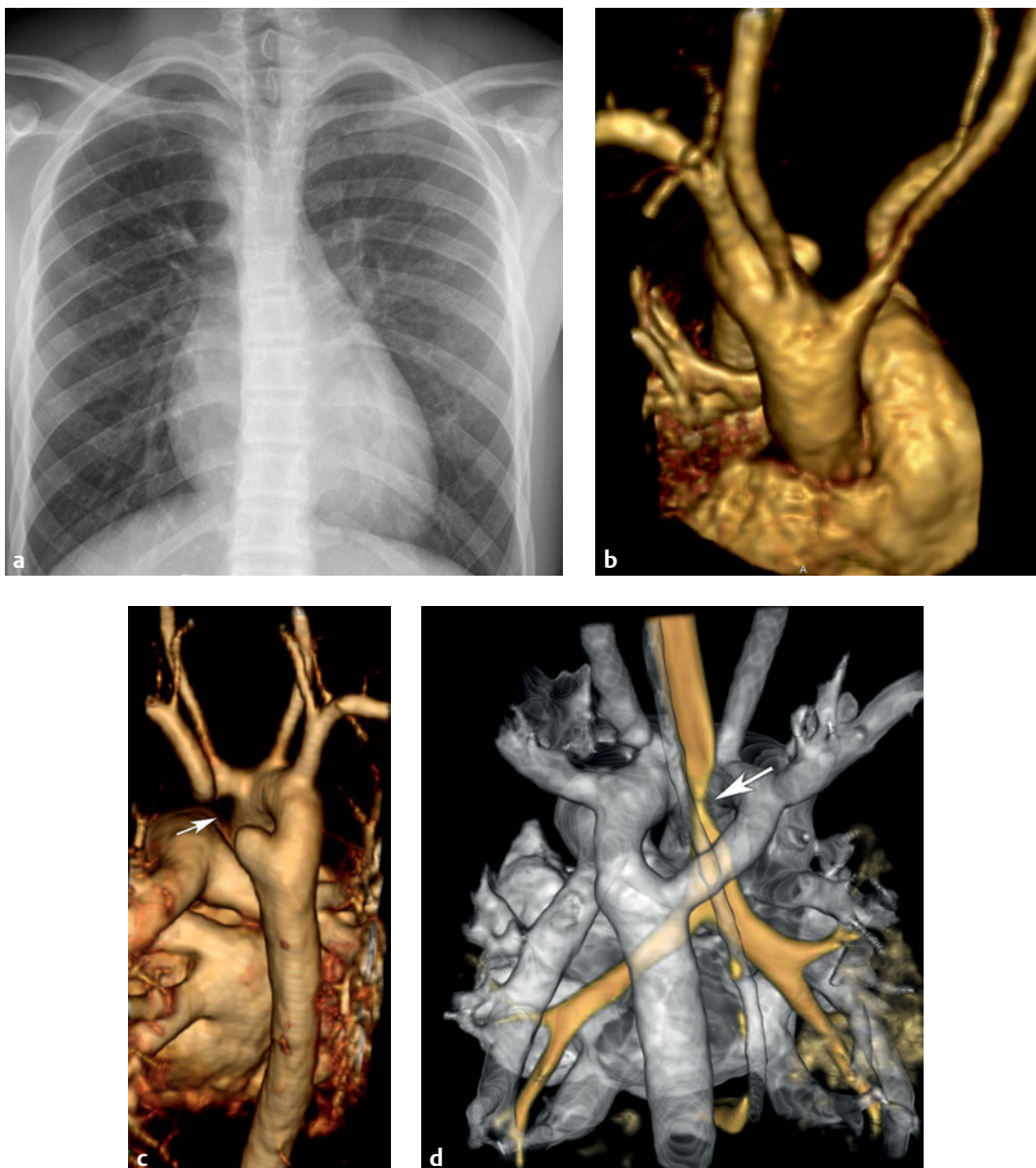
■ Clinical Presentation

A 15-year-old male with respiratory distress.

■ Radiographic Studies

A chest radiograph (**Fig. 133.1a**) shows a right aorta arch but a midline trachea. Frontal (**Fig. 133.1b**) and dorsal (**Fig. 133.1c**) view 3D MRA volume rendering shows a double aortic arch with an atretic segment (*arrow*) of the dorsal left arch. Posterior view of a 3D volume-rendered chest CTA with vessel

transparency filter in a different patient (**Fig. 133.1d**) shows a double aortic arch with the trachea and an esophageal enteric tube coursing through the vascular ring. Tracheal narrowing (*arrow*) is seen at the level of the vascular ring.



■ Diagnosis

Double Aortic Arch



■ Discussion and Differential Diagnosis

Double aortic arch is a congenital anomaly characterized by persistence of both right and left embryological arches, creating a complete vascular ring.¹ Stridor, wheezing, and dysphagia symptoms are proportional to the tightness of the vascular ring. Tracheomalacia can cause persistent respiratory symptoms leading to multiple hospitalizations. The right arch is usually the larger, higher, and more posterior of the two arches.^{2,3} Equal left or right arches or a dominant left aortic arch can be present. Atretic arch components are common.

Each aortic arch passes over the ipsilateral mainstem bronchus before fusing into the descending aorta, which is more commonly located on the left side of the spine.

Congenital aortic arch anomalies historically were evaluated using conventional radiographs, esophagography, echocardiography, and conventional angiography. CTA and MRA are the current gold standards for vascular ring evaluation.^{4–6} MRA is equal to CTA in for evaluating vascular ring anatomy but inferior for airway evaluation.⁷

Pearls

- ◆ Computed tomography angiography 3D image reconstructions are helpful to demonstrate the relationship between the aorta arch anatomy and the trachea.
- ◆ Look for the “four-artery” sign on axial images, which depicts the symmetric take-off of four arch branches—the two ventral carotids and the two dorsal subclavian arteries.

Pitfall

- ◆ Lumen patency is not required for a double aortic arch to be complete.

References

1. Kellenberger CJ. Aortic arch malformations. *Pediatr Radiol* 2010;40:876–884. [PubMed](#)
2. Türkvan A, Büyükbayraktar FG, Olçer T, Cumhuri T. Congenital anomalies of the aortic arch: evaluation with the use of multidetector computed tomography. *Korean J Radiol* 2009;10:176–184. [PubMed](#)
3. Paul JF, Serraf A. Images in cardiovascular medicine. Truncus arteriosus and double aortic arch. *Circulation* 2002;105:e170. [PubMed](#)
4. Goo HW, Park IS, Ko JK, Kim YH, Seo DM, Park JJ. Computed tomography for the diagnosis of congenital heart disease in pediatric and adult patients. *Int J Cardiovasc Imaging* 2005;21:347–365, discussion 367. [PubMed](#)
5. Goo HW. Cardiac MDCT in children: CT technology overview and interpretation. *Radiol Clin North Am* 2011;49:997–1010. [PubMed](#)
6. Greenberg SB. Dynamic pulmonary CT of children. *AJR Am J Roentgenol* 2012;199:435–440. [PubMed](#)
7. Donato R, Lentini S, Di Bella G. Magnetic resonance angiography for diagnosis of right aortic arch with vascular ring. *Arch Cardiovasc Dis* 2010;103:631–633. [PubMed](#)

Case 134

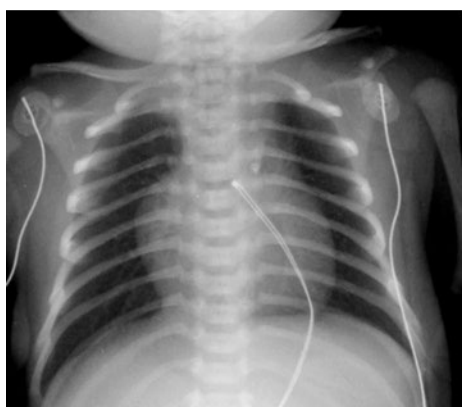
■ Clinical Presentation

A newborn with respiratory distress and heart murmur.

■ Radiographic Studies

Serial newborn chest radiographs (**Fig. 134.1a**) show normal heart size and pulmonary vascularity (day 1 of life) and then progressive enlargement of the heart and pulmonary vascularity (day 20 of life). This neonate remained acyanotic. AP and

lateral radiographs in another patient, a 3-month-old infant (**Fig. 134.1b,c**), show cardiomegaly with left heart prominence (*arrowhead*) and increased pulmonary vascularity.



a

Day 1



Day 20



b



c



■ Diagnosis

Ventricular Septal Defect

■ Discussion and Differential Diagnosis

Ventricular septal defect (VSD) accounts for 50% of all congenital heart disease and is the most common form of congenital heart disease. VSD can be an isolated abnormality or a part of a more complex form of congenital heart disease.¹ It can be perimembranous or muscular, and can be multiple. The hemodynamic significance of VSD depends on its size, right and left ventricular chamber pressure, and pulmonary resistance. At birth, pulmonary resistance is high, impeding left to right shunting. As pulmonary resistance drops during the first month of life, left to right shunting increases (**Fig. 134.1a**, Day 20 radiograph). In the absence of pulmonary hypertension or right ventricular obstruction, the left to right shunt causes pulmonary artery, left atrial, and left ventricular volume overload. Chest radiography shows cardiomegaly with left ventricle and left atrium enlargement as well as increased pulmonary vascularity (**Figs. 134.1b,c**).

Atrial septal defects (ASDs) are secundum or primum septum defects. Sinus venosum defects and unroofed coronary

sinus are not septal defects but function like atrial septal defects.² Like VSD, cardiomegaly and increased pulmonary vascularity are expected on chest radiographs of patients with ASD (**Figs. 134.1d,e**). However, ASD has characteristic right heart enlargement (**Fig. 134.1e**, arrowhead) not seen in patients with VSD.

The primary modality for septal defects is echocardiography. Cardiac MRI is a noninvasive modality to quantify shunt volume and functional evaluation of shunt severity. Monitoring the ratio of pulmonary and systemic flow ($Q_p:Q_s$) can aid in treatment planning.³ Current guidelines suggest percutaneous or surgical closure of left to right shunt if $Q_p:Q_s > 2$.⁴

The differential diagnosis with left to right shunt vascularity includes patent ductus arteriosus (PDA), which is seen in up to 30% of preterm infants.⁵ Admixture lesions frequently have increased pulmonary vascularity on chest radiographs, but unlike isolated septal defects will be cyanotic.

Pearls

- ◆ Eisenmenger syndrome results from fixed increased pulmonary resistance, which in turn results from long-standing left to right shunting, causing endothelial thickening and elevated pulmonary artery pressures. The pressure is irreversible and causes reversal in shunt, desaturation, cyanosis, and secondary erythrocytosis.
- ◆ Muscular VSDs usually undergo spontaneous closure due to muscular occlusion.

Pitfall

- ◆ Cardiomegaly and increased pulmonary vascularity can be absent in the newborn, but progress as pulmonary resistance drops in the neonate.

References

1. Minette MS, Sahn DJ. Ventricular septal defects. *Circulation* 2006;114:2190–2197 [PubMed](#)
2. Rojas CA, El-Sherief A, Medina HM, et al. Embryology and developmental defects of the interatrial septum. *AJR Am J Roentgenol* 2010;195:1100–1104. [PubMed](#)
3. Wang ZJ, Reddy GP, Gotway MB, Yeh BM, Higgins CB. Cardiovascular shunts: MR imaging evaluation. *Radiographics* 2003;23(Spec. No.):S181–S194. [PubMed](#)
4. Mongeon FP, Burkhardt HM, Ammash NM, et al. Indications and outcomes of surgical closure of ventricular septal defect in adults. *JACC Cardiovasc Interv* 2010;3:290–297 [PubMed](#)
5. Hoffman JL, Kaplan S. The incidence of congenital heart disease. *J Am Coll Cardiol* 2002;39:1890–1900 [PubMed](#)

Case 135

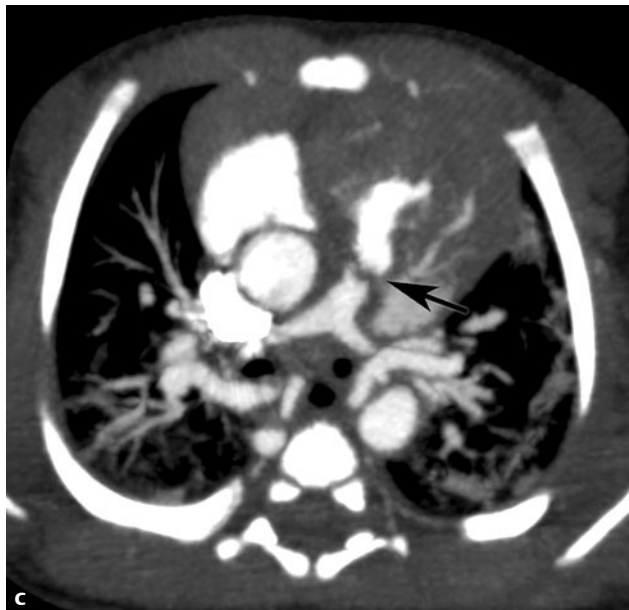
■ Clinical Presentation

A newborn presents with cyanosis.

■ Radiographic Studies

A sagittal oblique reformatted CTA image (**Fig. 135.1a**) shows that the ascending aorta overrides a ventricular septal defect (*arrow*). An axial oblique reformatted CTA image of the same patient (**Fig. 135.1b**) shows pulmonary artery and branch pulmonary artery stenoses; a right aortic arch is noted. Axial

oblique CTA image in another patient (**Fig. 135.1c**) shows pulmonary atresia (*arrow*). Posterior 3D volume-rendered chest CTA image (**Fig. 135.1d**) shows multiple major aortopulmonary collateral arteries originating from the descending thoracic aorta to supply the lungs.



■ Diagnosis

Tetralogy of Fallot

■ Discussion and Differential Diagnosis

Tetralogy of Fallot (TOF) is the most common cyanotic congenital heart disease and is equally prevalent in males and females. It is caused by anterior malalignment of the ventricular septum, which results in a ventricular septal defect, right ventricle outflow tract obstruction, an overriding ascending aorta, and right ventricle hypertrophy. The degree of malalignment determines the severity of right ventricular outflow tract obstruction and cyanosis. Obstruction is classically infundibular, but can also be valvar or supra-valvar. Pulmonary valve abnormalities are present in 90% of patients with TOF, including bicuspid or unicuspid valves with stenosis or complete absence of pulmonary valve.¹ If left untreated, TOF has a mortality of 33% in the first year of life, 50% by the third year of life, and 70% by age 10 years.^{2,3}

The classic boot-shaped configuration, or *Coeur en sabot* appearance, of the heart seen on conventional radiography, is uncommon. The cardiac size is normal, but right ventricle hypertrophy causes elevation of the cardiac apex. The pulmonary artery segment is concave and is inversely proportional to the size of the ascending aorta. The pulmonary vascularity is decreased. A right aortic arch is present in 25% of children with TOF.¹ CT and MRI complement echocardiography in delineating branch pulmonary artery anatomy and major aortopulmonary collateral arteries (MAPCAs) prior to surgical repair.

Surgical repair for TOF is performed in infancy and includes closing the ventricular septal defect and enlarging the right ventricular infundibulum and pulmonary valve annulus, usually with a patch. Definitive repair with placement of a pulmonary valve is deferred until the patient grows to adult size. Postsurgical complications include aneurysmal dilatation of the right ventricle outflow tract, chronic pulmonary valve regurgitation, and right ventricular dysfunction.⁴ Long-standing pulmonary valve regurgitation results in right ventricle dilatation and failure, increasing tricuspid regurgitation, impaired exercise performance, and arrhythmias.⁵ MRI enables complete morphological and functional evaluation and is considered the gold standard for evaluating right ventricle size. The right ventricle end diastolic volume index has become a key indicator for determining the timing for pulmonary valve replacement.⁶ Cardiac CT is used when MRI is contraindicated, and is particularly useful for the visualization of endovascular stents and stent-mounted valves.⁷

The differential diagnosis of TOF includes tricuspid atresia. Cyanotic admixture lesions such as D-transposition of the great arteries (D-TGA) and truncus arteriosus frequently have increased pulmonary vascularity and cardiomegaly. At birth, D-TGA may not have cardiomegaly until the pulmonary vascular resistance is reduced.

Pearl

- ◆ Tetralogy of Fallot is characterized by cyanosis and decreased pulmonary vascularity.

Pitfall

- ◆ Major aortopulmonary collateral arteries (MAPCAs) can compensate for decreased pulmonary artery flow so that peripheral pulmonary vascularity is initially normal or increased.

References

1. Bailliard F, Anderson RH. Tetralogy of Fallot. *Orphanet J Rare Dis* 2009;4:2. [PubMed](#)
2. Karl TR. Tetralogy of fallot: a surgical perspective. *Korean J Thorac Cardiovasc Surg* 2012;45:213–224. [PubMed](#)
3. Bédard E, Shore DF, Gatzoulis MA. Adult congenital heart disease: a 2008 overview. *Br Med Bull* 2008;85:151–180. [PubMed](#)
4. Quail MA, Frigiola A, Giardini A, et al. Impact of pulmonary valve replacement in tetralogy of Fallot with pulmonary regurgitation: a comparison of intervention and nonintervention. *Ann Thorac Surg* 2012;94:1619–1626. [PubMed](#)
5. Cheung MM, Konstantinov IE, Redington AN. Late complications of repair of tetralogy of Fallot and indications for pulmonary valve replacement. *Semin Thorac Cardiovasc Surg* 2005;17:155–159. [PubMed](#)
6. Geva T. Repaired tetralogy of Fallot: the roles of cardiovascular magnetic resonance in evaluating pathophysiology and for pulmonary valve replacement decision support. *J Cardiovasc Magn Reson* 2011;13:9. [PubMed](#)
7. Ahmed S, Johnson PT, Fishman EK, Zimmerman SL. Role of multidetector CT in assessment of repaired tetralogy of Fallot. *Radiographics* 2013;33:1023–1036. [PubMed](#)

Case 136

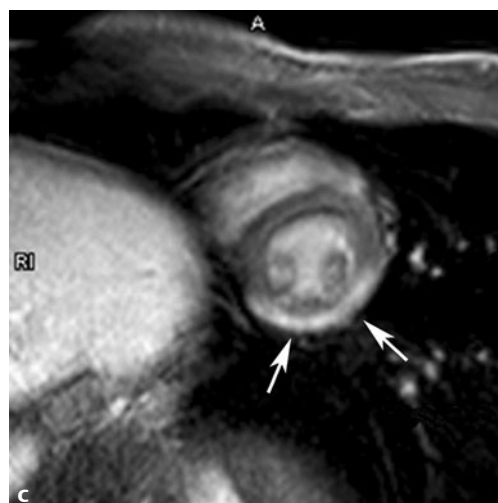
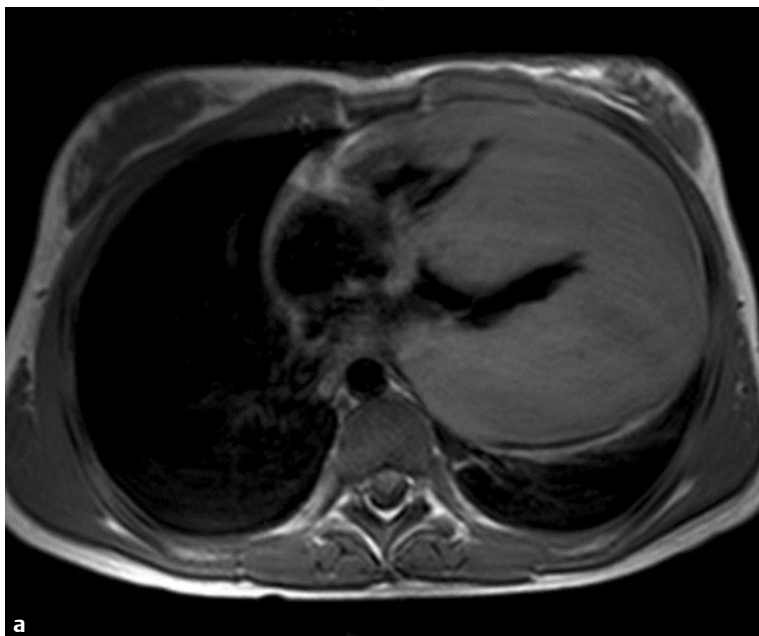
■ Clinical Presentation

An 18-year-old athlete with sudden loss of consciousness during football practice.

■ Radiographic Studies

Axial T1-weighted (black blood) MRI (**Fig. 136.1a**) shows global hypertrophy of the left ventricle, including the interventricular septum, and mild hypertrophy of the right ventricular free wall. Short-axis STIR MRI through the heart (**Fig. 136.1b**) shows patchy areas of increased signal in the myocardium

(*arrows*). Short-axis delayed postcontrast MRI (**Fig. 136.1c**) in a different patient with Duchenne muscular dystrophy shows enhancement in the subepicardial portion of the left ventricle free wall (*arrows*).



■ Diagnosis

Cardiomyopathy

■ Discussion and Differential Diagnosis

Cardiomyopathies are defined by the American Heart Association as a set of diseases of myocardium associated with mechanical and/or electrical dysfunction, either confined to the heart or part of a generalized systemic disorder. Cardiomyopathy was previously categorized as hypertrophic, dilated, restrictive, and arrhythmogenic right ventricular cardiomyopathies, but more recently are classified as primary or secondary.¹ Primary cardiomyopathies, whether genetic, acquired, or mixed, are confined to the myocardium. The secondary cardiomyopathies are part of systemic disorders such as amyloidosis, sarcoidosis, and siderotic cardiomyopathy.

Hypertrophic Cardiomyopathy

Hypertrophic cardiomyopathy (HCM) is the most common cause of sudden cardiac death in the young, including athletes. It is an autosomal dominant disease caused by a variety of mutations and is characterized by localized or global left ventricle and/or right ventricle myocardial hypertrophy in the absence of any obvious hypertrophic stimulus such as aortic obstruction or increased afterload. Cardiac MRI is superior to echocardiography in the diagnosis of HCM, with its high resolution, tissue characterization, and visualization of whole heart, revealing focal areas of hypertrophy that could be missed by an echocardiogram.² Quantification of myocardial mass, assessment of regional functional abnormalities such as systolic anterior motion of anterior mitral valve leaflet, and delayed enhancement imaging of myocardial scars indicating fibrosis are all performed using cardiac MRI.

Dilated Cardiomyopathy

Dilated cardiomyopathy (DCM) is characterized by ventricular chamber enlargement and systolic dysfunction with normal left ventricle wall thickness, leading to progressive heart failure, arrhythmias, thromboemboli, and sudden cardiac death. DCM is the most frequent indication for heart transplantation and is caused by primary and secondary etiologies including viral infections, autoimmune diseases, and neuromuscular disorders. Cardiac MRI quantifies left ventricle volume and mass more accurately than does two-dimensional (2D) echo and is accepted as the noninvasive gold standard for diagnosis and surveillance of DCM.³ Myocardial tagging studies can evaluate left ventricle fiber shortening in cardiomyopathies. Delayed enhancement is seen in subendocardial regions

similar to ischemic cardiomyopathy, as well as in midwall intramyocardium.

Myocarditis (Inflammatory Cardiomyopathy)

Myocarditis is an acute or chronic inflammatory condition of the myocardium caused by multiple etiologies such as infectious agents, systemic diseases, toxins, and drugs. Viral myocarditis may trigger an autoimmune response that causes dilated cardiomyopathy and heart failure. Cardiac MRI is useful to evaluate the activity, extent, and localization of inflammation within the myocardium. Focal abnormal myocardial enhancement is frequently seen in the epicardium of the left ventricle lateral wall.⁴

Cardiac MRI is useful in comparing myocarditis with acute myocardial infarction (AMI). In first-pass perfusion imaging, the vast majority of myocarditis patients show normal findings, whereas AMI patients have segmental subendocardial defects in vascular distribution.⁵

Arrhythmogenic Right Ventricular Dysplasia/Cardiomyopathy

Arrhythmogenic right ventricular dysplasia/cardiomyopathy (ARVC) is characterized by progressive loss of myocytes with segmental or diffuse fibrofatty replacement of the ventricular myocardium, predominantly right ventricle with concurrent or later left ventricle involvement. Patients experience tachyarrhythmias, abnormal right ventricle morphology, and right ventricle myocardial dysfunction that progresses to heart failure.⁶

Cardiac MRI is regarded as the most reproducible diagnostic imaging tool of choice because it provides better quantification of function and structural details of the right ventricle than do other imaging modalities. Delayed enhancement is present in almost all patients with biopsy proven ARVC.⁷

Muscular Dystrophies

Muscular dystrophies, such as Duchenne and Becker, are a group of diverse disorders primarily affecting skeletal muscles. Cardiac findings include arrhythmias, myocardial thickening, ventricular hypertrabeculation, cavitory thrombus, and heart failure. Cardiac MRI is an important tool for structural and functional assessment for diagnosis and surveillance.

Pearls

- ◆ Cardiac MRI can accurately diagnose noncompaction cardiomyopathy. A diastolic noncompact/compact ratio > 2.3 distinguishes pathological segments with high sensitivity and specificity.
- ◆ Restrictive cardiomyopathy and constrictive pericarditis have similar clinical characteristics and treatments. Cardiac MRI and cardiac CT are helpful in determining the presence of thickened pericardium (> 4 mm) in constrictive pericarditis. The remaining features of diastolic dysfunction, the dilation of the atria and systemic veins, are similar in both conditions.

Pitfall

- ◆ First-pass perfusion images and delayed enhancement patterns are crucial in differentiating ischemic from nonischemic cardiomyopathies.

References

1. Maron BJ, Towbin JA, Thiene G, et al; American Heart Association; Council on Clinical Cardiology, Heart Failure and Transplantation Committee; Quality of Care and Outcomes Research and Functional Genomics and Translational Biology Interdisciplinary Working Groups; Council on Epidemiology and Prevention. Contemporary definitions and classification of the cardiomyopathies: an American Heart Association Scientific Statement from the Council on Clinical Cardiology, Heart Failure and Transplantation Committee; Quality of Care and Outcomes Research and Functional Genomics and Translational Biology Interdisciplinary Working Groups; and Council on Epidemiology and Prevention. *Circulation* 2006;113:1807–1816 [PubMed](#)
2. Rickers C, Wilke NM, Jerosch-Herold M, et al. Utility of cardiac magnetic resonance imaging in the diagnosis of hypertrophic cardiomyopathy. *Circulation* 2005;112:855–861 [PubMed](#)
3. Strohm O, Schulz-Menger J, Pilz B, Osterziel KJ, Dietz R, Friedrich MG. Measurement of left ventricular dimensions and function in patients with dilated cardiomyopathy. *J Magn Reson Imaging* 2001;13:367–371 [PubMed](#)
4. Mahrholdt H, Goedecke C, Wagner A, et al. Cardiovascular magnetic resonance assessment of human myocarditis: a comparison to histology and molecular pathology. *Circulation* 2004;109:1250–1258 [PubMed](#)
5. Abdel-Aty H, Boyé P, Zagrosek A, et al. Diagnostic performance of cardiovascular magnetic resonance in patients with suspected acute myocarditis: comparison of different approaches. *J Am Coll Cardiol* 2005;45:1815–1822. [PubMed](#)
6. Gottlieb I, Macedo R, Bluemke DA, Lima JA. Magnetic resonance imaging in the evaluation of non-ischemic cardiomyopathies: current applications and future perspectives. *Heart Fail Rev* 2006;11:313–323 [PubMed](#)
7. Tandri H, Saranathan M, Rodriguez ER, et al. Noninvasive detection of myocardial fibrosis in arrhythmogenic right ventricular cardiomyopathy using delayed-enhancement magnetic resonance imaging. *J Am Coll Cardiol* 2005;45:98–103 [PubMed](#)

Case 137

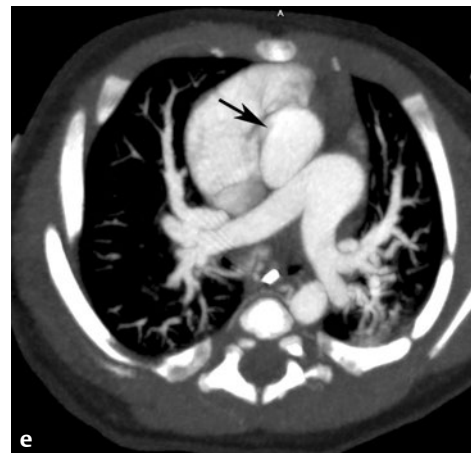
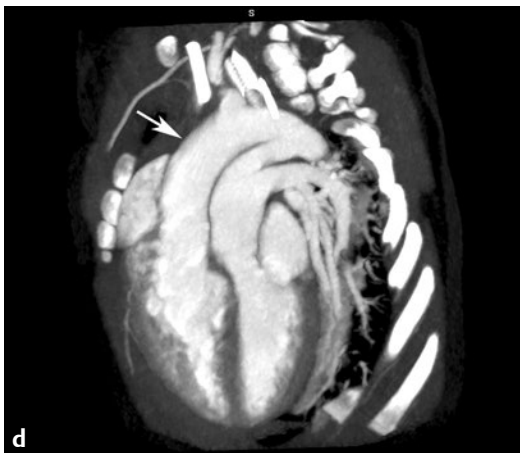
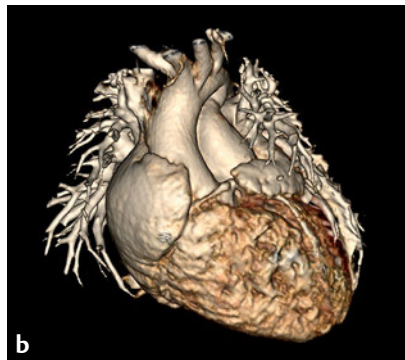
■ Clinical Presentation

A 4-week-old with cyanosis.

■ Radiographic Studies

Chest radiograph (**Fig. 137.1a**) shows cardiomegaly with increased pulmonary vascularity; the pulmonary artery is not apparent. Anterior 3D CTA image (**Fig. 137.1b**) shows that the aorta is anterior to the pulmonary artery and takes origin from the right ventricle. The lateral 3D CTA image (**Fig. 137.1c**) shows the pulmonary artery posterior to the ascending aorta. The position makes the pulmonary artery non-border form-

ing on the frontal radiograph. A patent ductus arteriosus (PDA) (*asterisk*) mixes oxygenated and deoxygenated blood. Para-sagittal oblique and axial oblique reconstructed CTA images (**Figs. 137.1d,e**) show that the aorta (*arrow*) originates from the right ventricle anterior to the pulmonary artery, which originates from the left ventricle.



■ Diagnosis

D-Transposition of Great Vessels

■ Discussion and Differential Diagnosis

D-transposition of the great vessels (d-TGV) is ventriculoarterial discordance with atrioventricular concordance in which the aorta arises from the morphological right ventricle and the pulmonary artery from the morphological left ventricle. The systemic and pulmonary circulations are in parallel instead of in series. Communications between the two circulations by septal defects or a patent ductus arteriosus creates an admixture lesion.

Fetal ultrasound can diagnose d-TGV in utero. If not diagnosed in utero, infants present with cyanosis soon after birth and are then diagnosed by echocardiography. Chest radiography in the newborn may be normal, but cardiomegaly and increased pulmonary vascularity will be present as pulmonary vascular resistance decreases. Cardiac MRI and CTA are usually unnecessary for preoperative planning but can be helpful for extracardiac anatomic evaluation in selected patients. Cardiac MRI and CTA are more useful for evaluation of complications

following surgical repair, such as coronary artery obstruction, branch pulmonary artery stenosis, and neo-aortic root aneurysm.^{1,2}

In neonates with insufficient oxygenation, initial palliation can be atrial septostomy to improve blood mixing.³ Prior to the development of bypass surgery, atrial baffles using either the Senning or Mustard procedures were performed to re-create flow in series. Many adult patients remain alive with these procedures. Long-term complications following the baffle surgeries include baffle obstruction, baffle leak, systemic (right) ventricular dysfunction, tricuspid valve incompetence, left ventricular outflow obstruction, arrhythmias, and sudden death.⁴ Currently, the arterial switch procedure is the corrective surgery choice for most patients with d-TGV. The arterial switch is performed in the neonatal period with an overall survival rate > 90% after 6 years.^{5,6}

Pearls

- ◆ Perfusion and delayed enhancement imaging can be utilized to identify myocardial scarring of left ventricle, secondary to ischemia from coronary translocation.
- ◆ Branch pulmonary artery stenosis can result from the Le Compte maneuver, which is part of the arterial switch procedure, and is best evaluated by either MRA or CTA.

Pitfall

- ◆ L-TGV is characterized by atrioventricular discordance as well as ventriculoarterial discordance and should not be confused with d-TGV. Segmental analysis of congenital heart disease will help avoid this pitfall. The three stages of segmental analysis include determination of viscerotransposition, the ventricular loop, and the position of the great vessels.⁷ The relationship between these segments is further assessed at the atrioventricular and ventriculoarterial levels.

References

1. Fogel MA, Crawford M. Cardiac magnetic resonance of the common arterial trunk and transposition of the great arteries. *Cardiol Young* 2012;22:677–686 [PubMed](#)
2. Han BK, Lesser JR. CT imaging in congenital heart disease: an approach to imaging and interpreting complex lesions after surgical intervention for tetralogy of Fallot, transposition of the great arteries, and single ventricle heart disease. *J Cardiovasc Comput Tomogr* 2013;7:338–353 [PubMed](#)
3. Squarcia U, Macchi C. Transposition of the great arteries. *Curr Opin Pediatr* 2011;23:518–522 [PubMed](#)
4. Hörer J, Herrmann F, Schreiber C, et al. How well are patients doing up to 30 years after a mustard operation? *Thorac Cardiovasc Surg* 2007;55:359–364. [PubMed](#)
5. Turon-Viñas A, Riverola-de Veciana A, Moreno-Hernando J, et al. Characteristics and outcomes of transposition of great arteries in the neonatal period. *Rev Esp Cardiol (Engl Ed)* 2014;67:114–119 [PubMed](#)
6. Cain MT, Cao Y, Ghanayem NS, et al. Transposition of the great arteries—outcomes and time interval of early neonatal repair. *World J Pediatr Congenit Heart Surg* 2014;5:241–247 [PubMed](#)
7. Lapiere C, Déry J, Guérin R, Viremouneix L, Dubois J, Garel L. Segmental approach to imaging of congenital heart disease. *Radiographics* 2010;30:397–411 [PubMed](#)

Case 138

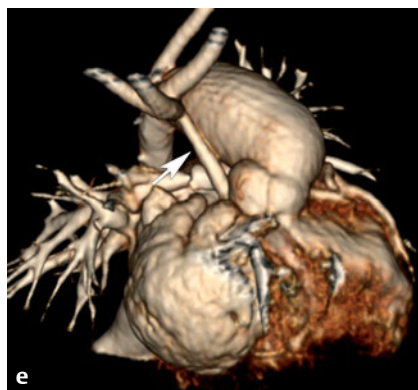
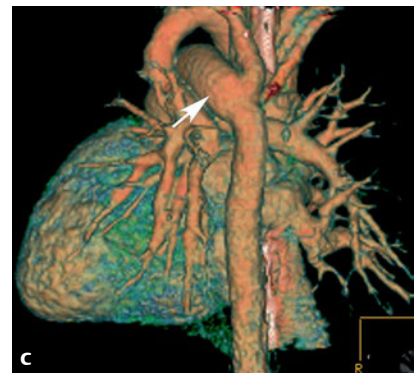
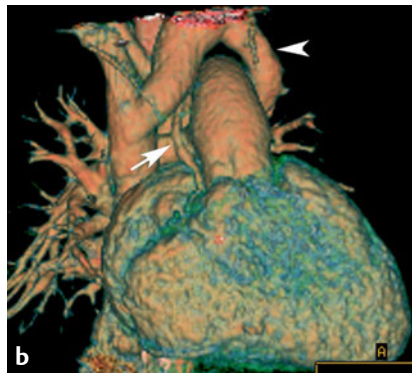
Clinical Presentation

A newborn with cardiomegaly and cyanosis.

Radiographic Studies

An axial oblique CTA image (**Fig. 138.1a**) shows a hypoplastic left ventricle (*arrow*) and an atrial septal defect (*asterisk*). An anterior 3D volume-rendered CTA image (**Fig. 138.1b**) shows the tiny ascending aorta (*arrow*) and an enlarged pulmonary artery. Anomalous venous return of the left pulmonary veins to the vertical vein is demonstrated (**Fig. 138.1b**, *arrowhead*). The dorsal oblique 3D CTA view shows a large patent ductus arteriosus (**Fig. 138.1c**, *arrow*) continuing as the descending

aorta. An axial oblique CTA image in another patient (**Fig. 138.1d**) shows a hypoplastic left ventricle that does not fill with contrast; an atrial septal defect is present (*arrowhead*). 3D volume-rendered CTA images (**Figs. 138.1e,f**) show the hypoplastic aorta (*arrow*) and massive pulmonary artery enlargement. A large patent ductus arteriosus (*arrowhead*) continues as the descending aorta.



■ Diagnosis

Hypoplastic Left Heart Syndrome

■ Discussion and Differential Diagnosis

Hypoplastic left heart syndrome (HLHS) is a spectrum of underdevelopment of the mitral valve, left ventricle, aortic valve, and aorta. Obstruction to blood flow from the left-sided heart results in systemic hypoperfusion with hypoxemia, acidosis, and shock, making this a duct-dependent lesion. Diagnosis is usually made by fetal echocardiography, and the differential diagnosis includes critical aortic stenosis, coarctation of the aorta, and interrupted aortic arch.¹ The prognosis of patients with HLHS has improved during the past three decades from nearly 100% fatality to almost 70% survival into adulthood, with even 90% survival seen in some centers.²

Palliative management is the three-stage Norwood procedure. The initial surgery is the creation of a neo-aorta by anastomosing the native aorta to the pulmonary root. The ductal tissue is removed and the neo-aorta anastomosed to the aortic arch. The distal pulmonary artery and branch pulmonary arteries are detached from the pulmonary artery root and classically supplied by a modified Blalock-Taussig shunt. The goal of the first stage is to relieve systemic outflow obstruction and provide restrictive pulmonary and nonrestrictive coronary flow. Alternatives to the Blalock-Taussig shunt are the central or Sano shunts. An alternative to the Norwood I is the hybrid procedure that includes a large PDA stent with branch pulmonary artery banding.

The Norwood II palliation includes take down of the systemic to pulmonary shunt and creation of a bidirectional Glenn or bilateral Glenn shunts. The second stage eliminates the high-flow arterial or ventricular pulmonary blood flow and connects the low-pressure superior vena cava to the pulmonary artery. The Norwood III entails creation of a Fontan palliation, allowing for complete return to flow in series. The third stage directs the remaining desaturated blood from the inferior vena cava to the branch pulmonary arteries.

Failure of Fontan surgery can result in the need for a cardiac transplant. Significant comorbidities of Norwood palliation include coagulopathy, thrombosis of shunts and conduits, right to left shunts such as venovenous collaterals and pulmonary arteriovenous malformations, renal dysfunction, cardiac cirrhosis, protein losing enteropathy, arrhythmias, and heart failure.³

Cardiac MRI and CTA are helpful for surgical planning and postoperative follow-up, specifically for Norwood II and III palliations.⁴ MRI evaluates preoperative ventricular size and function and assesses the right ventricular to pulmonary artery conduit, the Glenn and Fontan shunts, and extracardiac complications.

Pearl

- ◆ Pulmonary arteriovenous malformations (AVMs) can develop following Norwood II palliation of HLHS due to the lack of hepatic antiangiogenesis factor excreted by the liver. Once the Fontan circuit is established, the pulmonary AVMs regress if inferior vena caval and hepatic vein flow is balanced between the lungs.

Pitfall

- ◆ Contrast streaming can complicate post-Fontan CTA or MRA imaging. Dual injections or delayed imaging sequences may be required.

References

1. Hickey EJ, Caldarone CA, McCrindle BW. Left ventricular hypoplasia: a spectrum of disease involving the left ventricular outflow tract, aortic valve, and aorta. *J Am Coll Cardiol* 2012;59(1, Suppl):S43–S54 [PubMed](#)
2. Ohye RG, Sleeper LA, Mahony L, et al; Pediatric Heart Network Investigators. Comparison of shunt types in the Norwood procedure for single-ventricle lesions. *N Engl J Med* 2010;362:1980–1992 [PubMed](#)
3. Feinstein JA, Benson DW, Dubin AM, et al. Hypoplastic left heart syndrome: current considerations and expectations. *J Am Coll Cardiol* 2012;59(1, Suppl):S1–S42 [PubMed](#)
4. Fonseca BM. Perioperative imaging in hypoplastic left heart syndrome. *Semin Cardiothorac Vasc Anesth* 2013;17:117–127 [PubMed](#)

Case 139

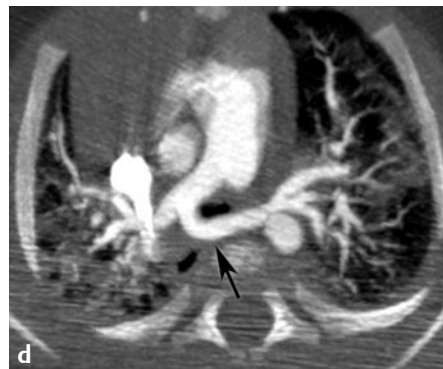
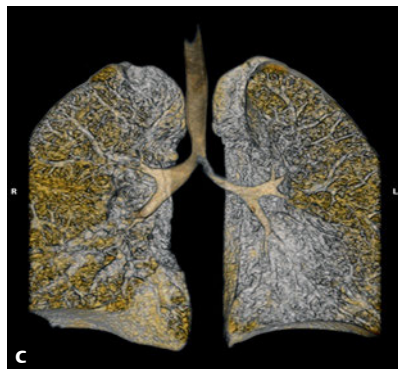
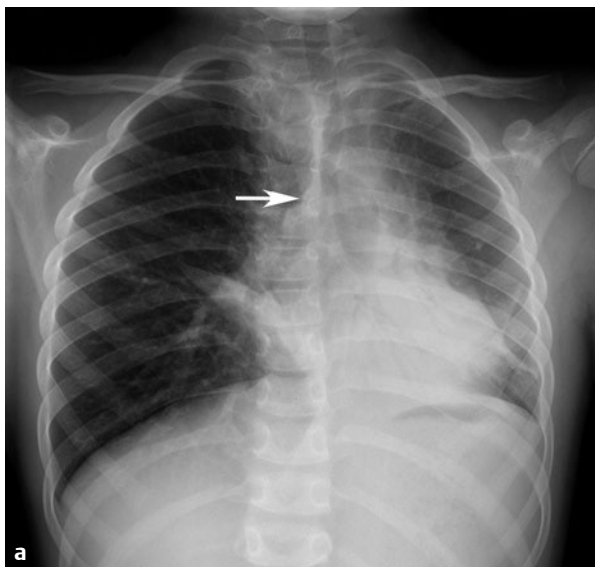
Clinical Presentation

A 10-year-old boy with cough, dysphagia, intermittent wheezing, and recurrent pneumonias.

Radiographic Studies

Frontal chest radiograph (**Fig. 139.1a**) shows leftward displacement and narrowing of the distal trachea by the pulmonary sling (*arrow*) and bilateral lower lung atelectasis. Axial CTA image (**Fig. 139.1b**) shows the left pulmonary artery (*arrow*) arising from the right pulmonary artery and coursing posterior to the carina. A dynamic pulmonary CT imaging study (**Fig. 139.1c**) shows moderate narrowing of the distal trachea and severe narrowing of the proximal left bronchus. Axial CTA

image in another patient, a 3-year-old with stridor and cough (**Fig. 139.1d**), shows an anomalous left pulmonary artery (*arrow*) coursing between the trachea and the gas-filled esophagus. Posterior view of 3D volume-rendered chest CTA (**Fig. 139.1e**) shows the anomalous left pulmonary artery (*arrow*) originating from the right pulmonary artery. It courses posterior to the distal trachea (*blue*). A small patent ductus arteriosus is also seen (*arrowhead*).



■ Diagnosis

Pulmonary Sling



■ Discussion and Differential Diagnosis

The left pulmonary artery sling is a rare vascular anomaly in which the left pulmonary artery arises from the posterior aspect of the right pulmonary artery and courses between the distal trachea and esophagus to reach the hilum of the left lung. In addition, the ligamentum arteriosum or a patent ductus may complete a vascular ring surrounding the trachea on its left side. Tracheobronchial and cardiovascular anomalies are commonly associated with the pulmonary sling. These include diffuse tracheal stenosis and cartilaginous rings (ring sling complex).^{1,2} Other associated anomalies include right tracheal bronchus, hypoplastic right lung, persistent left superior vena cava, and left patent ductus arteriosus.² The pulmonary sling is classified into two types: type I has a normal

carina with or without a right tracheal bronchus, and type II has a low, T-shaped carina with diffuse tracheal stenosis and complete cartilaginous rings.

Radiological diagnosis includes plain film evaluation, fluoroscopic esophageal swallow study, echocardiogram, and cross-sectional imaging including CTA, virtual bronchoscopy, dynamic pulmonary CTA, or MRI and MRA.^{3,4} Lateral chest radiography shows a soft tissue density between the trachea and esophagus. Unlike vascular rings that encircle the trachea and esophagus, the anomalous left pulmonary artery passes between the trachea and esophagus. An anterior indentation on the esophagus is present on an esophagram. Dynamic CTA is ideal for evaluating airway compression.⁴

Pearls

- ◆ Pulmonary sling is the only vascular abnormality associated with asymmetric lung inflation.
- ◆ Complete tracheal rings are round with a small internal diameter.

Pitfall

- ◆ Classification and demonstration of tracheal stenosis by CTA are important for surgical planning.

References

1. Newman B, Cho Ya. Left pulmonary artery sling—anatomy and imaging. *Semin Ultrasound CT MR* 2010;31:158–170 [PubMed](#)
2. Chen SJ, Lee WJ, Lin MT, et al. Left pulmonary artery sling complex: computed tomography and hypothesis of embryogenesis. *Ann Thorac Surg* 2007;84:1645–1650 [PubMed](#)
3. Heyer CM, Nuesslein TG, Jung D, et al. Tracheobronchial anomalies and stenoses: detection with low-dose multidetector CT with virtual tracheo-
- bronchoscopy—comparison with flexible tracheobronchoscopy. *Radiology* 2007;242:542–549 [PubMed](#)
4. Greenberg SB, Dyamenahalli U. Dynamic pulmonary computed tomography angiography: a new standard for evaluation of combined airway and vascular abnormalities in infants. *Int J Cardiovasc Imaging* 2014;30:407–414 [PubMed](#)

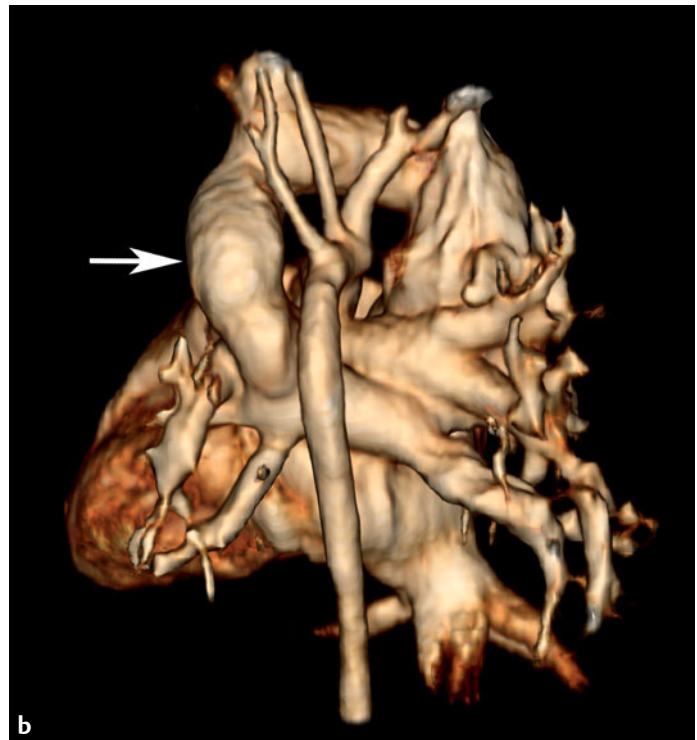
Case 140

■ Clinical Presentation

A newborn with cardiomegaly, heart failure, and cyanosis.

■ Radiographic Studies

Anterior (**Fig. 140.1a**) and posterior (**Fig. 140.1b**) views of a 3D volume-rendered CTA show a vertical vein (*arrows*) draining into the left innominate vein. The left innominate vein and superior vena cava are dilated.



■ Diagnosis

Total Anomalous Pulmonary Venous Return

■ Discussion and Differential Diagnosis

The common pulmonary vein grows from the superior aspect of the left atrium toward the lung buds. Once the connection with the pulmonary venous plexus is established, the common pulmonary vein connections with the splanchnic plexus regress. The common pulmonary vein then incorporates into the left atrial wall, with the four pulmonary veins separately entering the chamber.¹ Total anomalous pulmonary venous return (TAPVR) occurs if there is anomalous development of the atrial septum or if the common pulmonary vein fails to develop. Anomalous pulmonary venous drainage results in an extracardiac left to right shunt as the pulmonary venous blood flows directly into the right heart or via the systemic veins. Anomalous pulmonary venous return can be partial or total. The latter requires a right to left shunt requires a right to left shunt which is usually an atrial septal defect or patent foramen ovale.

Total anomalous pulmonary venous return is classified according to the site of pulmonary venous drainage: type I, supracardiac; type II, cardiac; type III, infracardiac; and type IV, mixed. In supracardiac TAPVR, anomalous return is through a vertical vein that courses along the left side of the mediastinum and drains into the left innominate vein. The cardiac type TAPVR has direct drainage of the common pulmonary vein into the coronary sinus. The infracardiac anomalous vein tra-

verses the diaphragm to drain into the hepatic veins or the inferior vena cava. Cardiac and supracardiac types are more commonly nonobstructed, whereas type III is invariably obstructed due to its long course through the diaphragm and hepatic parenchyma. Surgical repair of TAPVR is the definitive treatment.

Partial anomalous pulmonary venous return (PAPVR) is anomalous drainage of one to three pulmonary veins into the right-sided circulation. Scimitar syndrome is a specific type of PAPVR in which the right lung pulmonary vein drains into inferior vena cava, right atrium, coronary sinus, portal vein, or hepatic veins. Hypoplastic right lung/right pulmonary artery, right lower lobe sequestration, congenital heart disease, diaphragmatic hernia, and musculoskeletal anomalies are associated with scimitar syndrome. The most common location of PAPVR in children is the right upper lobe pulmonary vein, and it is associated with sinus venosus defect.²

Chest radiography in TAPVR demonstrates increased shunt vascularity and cardiomegaly, with enlargement of right atrium, right ventricle, and main pulmonary artery. CTA and MRA are ideal imaging modalities if echocardiography is not definitive.³ Shunt quantification can be performed by MR flow analysis of pulmonary artery, aorta, and the aberrant pulmonary vein.⁴

Pearls

- ◆ Pulmonary interstitial edema without cardiomegaly is associated with obstructive type III TAPVR.
- ◆ Patients with type II TAPVR and atrial septal defect (ASD) are not cyanotic.

Pitfall

- ◆ The classic “snowman” appearance of supracardiac TAPVR is not apparent in infants and may be obscured by the normal thymus silhouette.

References

1. Zylak CJ, Eyler WR, Spizarny DL, Stone CH. Developmental lung anomalies in the adult: radiologic-pathologic correlation. *Radiographics* 2002;22(Spec No.):S25–S43 Review [PubMed](#)
2. Fraser RS, Muller NL, Colman N, Pare PD. Developmental anomalies affecting the pulmonary vessels. In: Fraser RS, Muller NL, Colman N, Pare PD, eds. *Diagnosis of Diseases of the Chest*. Philadelphia: WB Saunders; 1999:637–675
3. Ho ML, Bhalla S, Bierhals A, Gutierrez F. MDCT of partial anomalous pulmonary venous return (PAPVR) in adults. *J Thorac Imaging* 2009;24:89–95. [PubMed](#)
4. Kramer U, Dörnberger V, Fenchel M, Stauder N, Claussen CD, Miller S. Scimitar syndrome: morphological diagnosis and assessment of hemodynamic significance by magnetic resonance imaging. *Eur Radiol* 2003;13(Suppl 4):L147–L150 [PubMed](#)

Case 141

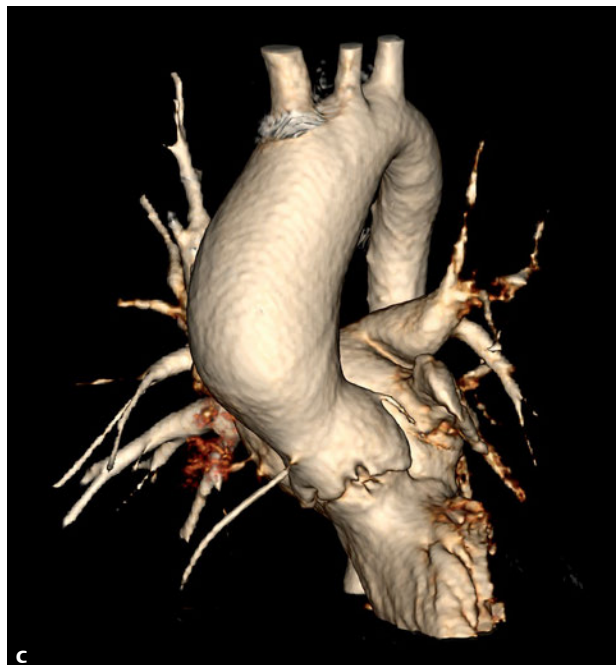
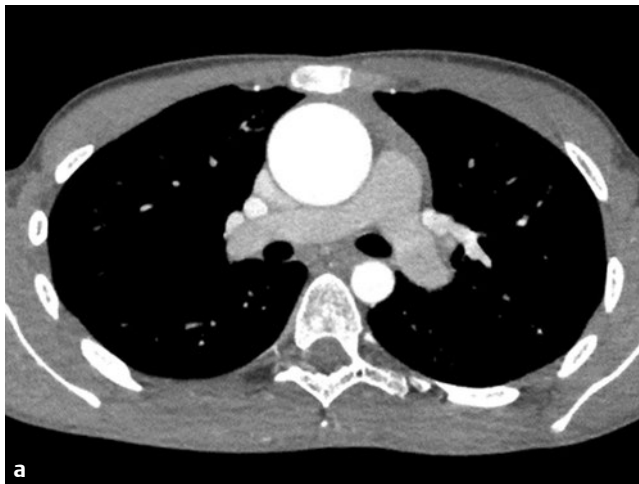
■ Clinical Presentation

A 13-year-old with systolic murmur since birth.

■ Radiographic Studies

An ECG-gated CTA of the aorta was performed. A double oblique reconstruction perpendicular to the ascending aorta (**Fig. 141.1a**) shows aneurysmal dilatation of the ascending aorta. A double oblique reconstruction through the sinus of Valsalva (**Fig. 141.1b**) shows two aortic valve leaflets (arrow-

heads) instead of three. A 3D volume-rendered image of the aorta in a sagittal oblique plane (**Fig. 141.1c**) shows aneurysmal dilatation of the ascending aorta and proximal aortic arch. The distal arch and descending aorta have a normal caliber.



■ Diagnosis

Bicuspid Aortic Valve

■ Discussion and Differential Diagnosis

Left-sided obstructive heart disease includes congenital aortic valve stenosis, bicuspid aortic valve, hypoplastic left heart syndrome, coarctation of aorta, and interrupted aortic arch. Obstructed or altered in utero blood flow results in hypoplasia or atresia of the cardiac valves, the left ventricle, and/or the aorta.¹ Epidemiological studies show a higher rate of these concordant diagnoses in families.²

The bicuspid aortic valve is the most common congenital heart anomaly and is reported in 1–2% of the general population. This anomaly is due to the failure of the cusps to separate, resulting in a cusp that is larger than the remaining normal cusp but smaller than the two cusps combined together.³ The vast majority of patients also have functional valve disturbances, most commonly aortic stenosis.⁴ Mixed aortic stenosis and regurgitation and pure aortic regurgitation

can also occur. Most patients are initially asymptomatic but stenosis is progressive and leads to an ascending aorta aneurysm requiring repair. The high incidence of associated coarctation of the aorta and aortic dilatation with bicuspid aortic valve is genetic.

Although the aortic valve anatomy and mean pressure gradient are assessed by echocardiography, CTA or cardiac MRI is routinely performed to assess increasing ascending aorta size. Altered systolic blood flow can be measured by MR phase-contrast flow analysis to evaluate the degree of stenosis and wall shear stress.^{5,6} In the absence of high-risk factors such as a family history of aortic dissection, rupture, or sudden death and an aortic growth rate > 5 mm per year, yearly CTA or cardiac MRI surveillance is recommended.⁷

Pearls

- ◆ Fusion between right and left coronary cusps has a high association with coarctation of aorta and other heart diseases.⁴
- ◆ Surgery is recommended for aortic root or ascending aorta aneurysms measuring ≥ 5 cm.

Pitfall

- ◆ Measuring flow velocity too close to the bicuspid aortic valve may yield aliasing artifact on MR phase-contrast flow analysis.

References

1. Clark EB. Pathogenetic mechanisms of congenital cardiovascular malformations revisited. *Semin Perinatol* 1996;20:465–472 [PubMed](#)
2. McBride KL, Marengo L, Canfield M, Langlois P, Fixler D, Belmont JW. Epidemiology of noncomplex left ventricular outflow tract obstruction malformations (aortic valve stenosis, coarctation of the aorta, hypoplastic left heart syndrome) in Texas, 1999–2001. *Birth Defects Res A Clin Mol Teratol* 2005;73:555–561 [PubMed](#)
3. Fedak PW, David TE, Borger M, Verma S, Butany J, Weisel RD. Bicuspid aortic valve disease: recent insights in pathophysiology and treatment. *Expert Rev Cardiovasc Ther* 2005;3:295–308 [PubMed](#)
4. Ciotti GR, Vlahos AP, Silverman NH. Morphology and function of the bicuspid aortic valve with and without coarctation of the aorta in the young. *Am J Cardiol* 2006;98:1096–1102 [PubMed](#)
5. Burris NS, Sigovan M, Knauer HA, Tseng EE, Saloner D, Hope MD. Systolic flow displacement correlates with future ascending aortic growth in patients with bicuspid aortic valves undergoing magnetic resonance surveillance. *Invest Radiol* 2014;49:635–639 [PubMed](#)
6. Hope MD, Sigovan M, Wrenn SJ, Saloner D, Dyverfeldt P. MRI hemodynamic markers of progressive bicuspid aortic valve-related aortic disease. *J Magn Reson Imaging* 2014;40:140–145 [PubMed](#)
7. Verma S, Siu SC. Aortic dilatation in patients with bicuspid aortic valve. *N Engl J Med* 2014;370:1920–1929 [PubMed](#)

Case 142

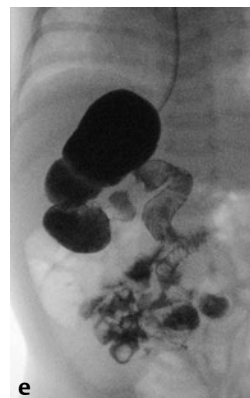
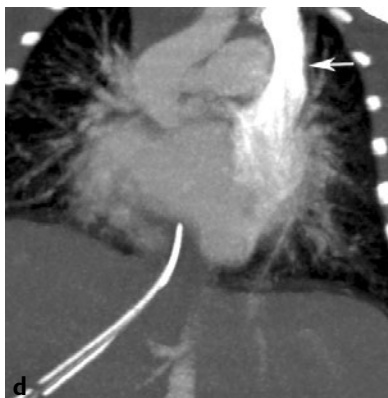
■ Clinical Presentation

Premature newborn with respiratory distress.

■ Radiographic Studies

Chest/abdomen radiograph post-line placement (**Fig. 142.1a**) shows umbilical venous catheter (UVC) to the left of the spine and orogastric tube in a right-sided stomach. Increased density of the left-sided pedicles indicates a left-sided aortic arch. Ultrasound images (**Fig. 142.1b,c**) show transverse liver alignment with inferior vena cava (IVC) confluence to the left of

the midline; multiple splenic lobules (*asterisks*) are seen in the right upper abdomen. CTA image (**Fig. 142.1d**) shows a left-sided superior vena cava (SVC) (*arrow*) and orogastric tube projecting in the right-sided stomach. Upper GI exam at 1 month of age (**Fig. 142.1e**) shows right-sided stomach and malrotation.



■ Diagnosis

Heterotaxy

■ Discussion and Differential Diagnosis

Situs is the site or position of an organ. Situs solitus is characterized by levocardia, a left aortic arch, a right trilobed lung and left bilobed lung, solitary or dominant spleen on the left side of the abdomen, and liver on the right side of the abdomen. Situs inversus is the reverse of situs solitus. Heterotaxy or situs ambiguous is neither situs solitus nor situs inversus. For example, bilateral right or left atrial appendages or bilateral bilobed or trilobed lungs may be present. Most heterotaxy is subclassified as either polysplenia or asplenia. Children with asplenia tend to have more complex congenital heart disease and a worse prognosis.¹

The large number of anomalies associated with heterotaxy requires careful segmental analysis.²⁻⁵ Cardiovascular segmental analysis includes the following:

1. Venoatrial (common abnormalities: interruption of IVC, total anomalous venous return)
2. Atrial appendages (bilateral triangular or tubular shape)

3. Atrioventricular connection (common abnormalities: atresia, atrioventricular septal defects, hypoplastic ventricle)
4. Septal defects (atrial or ventricular)
5. Ventricular-arterial connections (common anomalies: pulmonary atresia, transposition)

Extracardiac analysis includes evaluation of the location of the liver and spleen (or spleens). Bowel malrotation is common. Noncardiac abnormalities include renal anomalies, biliary atresia, duodenal atresia, and gastric volvulus. Bowel rotation is determined by an upper GI examination. Ultrasound, CT, and MRI provide detailed delineation of intra- and extracardiovascular anatomy and connections needed for preoperative surgical planning and postoperative follow-up.⁶ MRA image in a 19-year-old patient (**Fig. 142.1f**) shows interruption of the IVC with azygous continuation (*arrows*). The suprahepatic portion of the IVC drains to the functional right atrium (*arrowhead*).

Pearls

- ◆ Polysplenia is “bilateral left-sidedness” and is associated with bilateral bilobed lungs, multiple spleens, and interruption of the inferior vena cava with azygous continuation.
- ◆ Bilateral superior venae cavae are associated with both polysplenia and asplenia.

Pitfall

- ◆ If a careful segmental approach utilizing cross-sectional imaging is not employed, important anomalies are likely to be missed.

References

1. Jacobs JP, Anderson RH, Weinberg PM, et al. The nomenclature, definition and classification of cardiac structures in the setting of heterotaxy. *Cardiol Young* 2007;17(Suppl 2):1–28 [PubMed](#)
2. Van Praagh R. The segmental approach to diagnosis in congenital heart disease. In: Bergsma D, Blumenthal S, eds. *Birth Defects, Original Article Series: Vol. VIII, No. 1, Feb 1972, Congenital Cardiac Defects—Recent Advances*. Baltimore: Williams & Wilkins; 1972:4–23
3. Van Praagh R, Vlad P. Dextrocardia, mesocardia, and levocardia: the segmental approach in congenital heart disease. In: Keith JD, Rowe RD, Vlad P, eds. *Heart Disease in Infancy and Childhood*, 3rd ed. New York: Macmillan; 1978
4. Anderson RH, Becker AE, Freedom RM, et al. Sequential segmental analysis of congenital heart disease. *Pediatr Cardiol* 1984;5:281–287 [PubMed](#)
5. Anderson RH, Ho SY. Sequential segmental analysis—description and categorization for the millennium. *Cardiol Young* 1997;7:98–116
6. Geva T, Vick GW III, Wendt RE, Rokey R. Role of spin echo and cine magnetic resonance imaging in presurgical planning of heterotaxy syndrome. Comparison with echocardiography and catheterization. *Circulation* 1994;90:348–356 [PubMed](#)

Case 143

■ Clinical Presentation

A 6-year-old girl with hypertension.

■ Radiographic Studies

Sagittal oblique maximum intensity projection (MIP) post-gadolinium MRA image of the chest (**Fig. 143.1a**) shows a focal short segment coarctation in a periductal location of the descending aorta (*arrow*). Numerous collaterals are seen in soft tissues of the upper back (*arrowhead*). A 2D MRA multiplanar reformatted image in the same projection (**Fig. 143.1b**) shows

a linear dephasing post-stenotic flow jet (*arrow*) in the descending aorta. Sagittal oblique view of 3D volume-rendered chest MRA (**Fig. 143.1c**) shows the periductal coarctation (*arrow*), post-stenotic aortic dilation, and associated collaterals (*arrowheads*).



■ Diagnosis

Coarctation of the Aorta



■ Discussion and Differential Diagnosis

Aortic coarctation is a narrowing of the aorta that can be tubular hypoplasia or focal. Tubular hypoplasia results from decreased intrauterine flow and may be associated with forms of hypoplastic left heart syndrome. Focal coarctation of the aorta typically occurs at the insertion of the ductus arteriosus and is associated with excess ductal tissue during patent ductus arteriosus closure. A shelf-like ridge within the aortic lumen characterizes focal coarctation.

Infants frequently present with failure to thrive and heart failure. Absent or weak femoral pulses and upper extremity hypertension are present. Chest radiography may detect cardiomegaly and signs of heart failure. Rib notching and the “reverse-3” sign are unusual in infants and young children. Collateral circulation develops gradually during childhood and can result in rib notching. Bicuspid aortic valve is the most

common association and is present in 40% of children with coarctation.¹ Surgical repair is the first-line treatment for infants, but stent placement is an alternative for re-coarctation.

Echocardiography is the first-line imaging modality for evaluation of coarctation. If the proximal descending thoracic aorta is not adequately visualized, either CTA or MRA should be performed. Magnetic resonance can image both primary and postoperative coarctation, but also can evaluate pressure gradients and quantifies collateral flow.^{2–4} CTA is an alternative when MRI is contraindicated or unavailable, or when the vascular stents require evaluation. Re-coarctation and aneurysm formation are associated with coarctation repair. Current recommendations are that, following initial repair, patients with coarctation need to be imaged with CT or MR every 5 years.

Pearls

- ◆ A large collateral flow volume reduces the pressure gradient in the aorta at the coarctation and may lead to underestimation of coarctation severity.
- ◆ Pseudocoarctation has a similar morphological appearance as coarctation but no pressure gradient is present.

Pitfall

- ◆ Sonographic windows in the postoperative patient are frequently poor in the descending aorta, making echocardiography inadequate for long-term follow-up of coarctation.

References

1. Darabian S, Zeb I, Rezaeian P, Razipour A, Budoff M. Use of noninvasive imaging in the evaluation of coarctation of aorta. *J Comput Assist Tomogr* 2013;37:75–78 [PubMed](#)
2. van der Hulst AE, Roest AA, Westenberg JJ, Kroft LJ, de Roos A. Cardiac MRI in postoperative congenital heart disease patients. *J Magn Reson Imaging* 2012;36:511–528 [PubMed](#)
3. Hom JJ, Ordovas K, Reddy GP. Velocity-encoded cine MR imaging in aortic coarctation: functional assessment of hemodynamic events. *Radiographics* 2008;28:407–416 [PubMed](#)
4. Ralovich K, Itu L, Mihalef V, et al. Hemodynamic assessment of pre- and post-operative aortic coarctation from MRI. *Med Image Comput Comput Assist Interv* 2012;15(Pt 2):486–493

IX

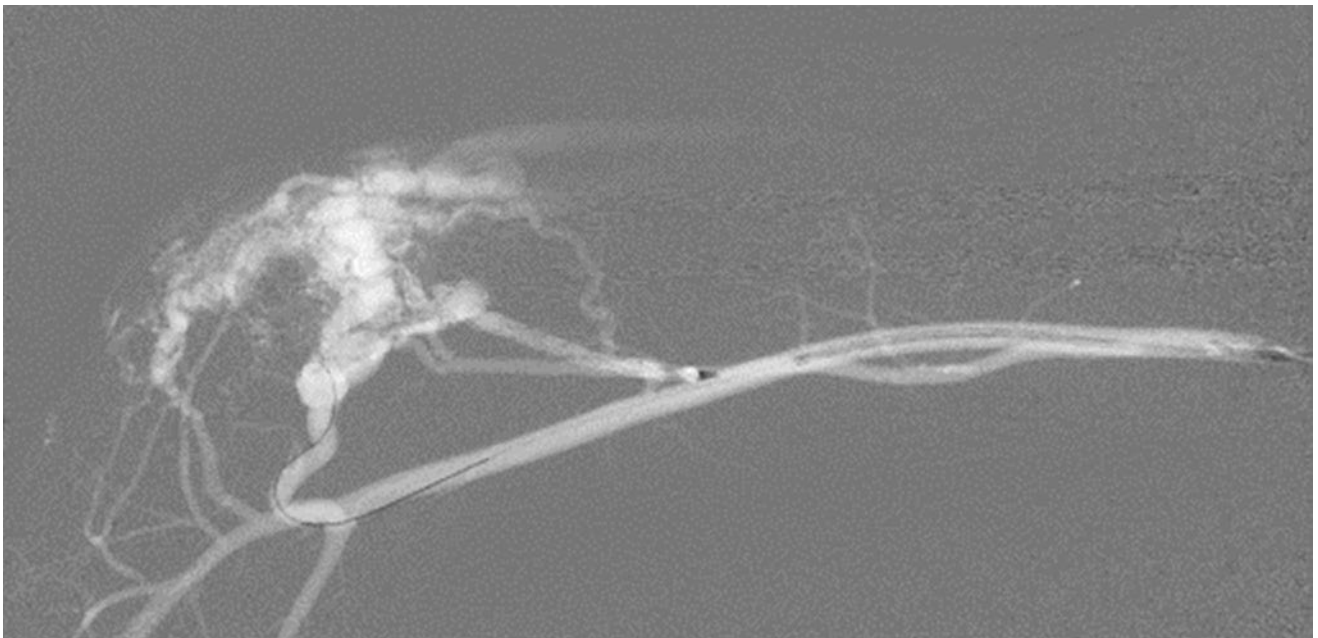
Interventional Radiology

Section Editor

Charles A. James

Author

Leah E. Braswell



Case 144

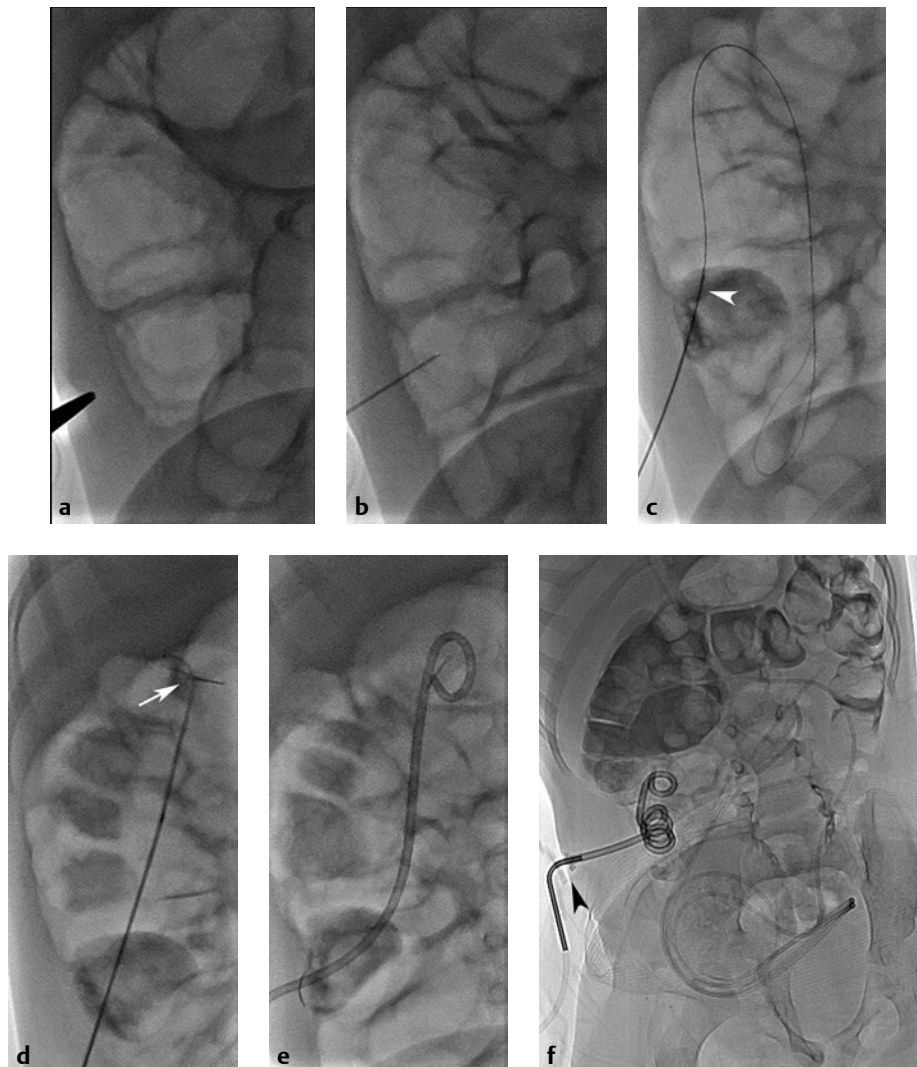
■ Clinical Presentation

A 10-year-old boy with spina bifida, fecal incontinence, and chronic constipation is referred to the interventional radiology service.

■ Radiographic Studies

A skin site is chosen after the cecum is distended with air via a rectal tube (**Fig. 144.1a**). After needle puncture of the colon (**Fig. 144.1b**), contrast injection confirms the intraluminal position. A guidewire is advanced into the colon, and exchange for a micropuncture dilator (**Fig. 144.1c**, arrowhead) is made. Two retention sutures are deployed via the one needle punc-

ture site (**Fig. 144.1d**, arrow). Serial fascial tract dilatation is performed, and then an 8-French (F) locking loop pigtail catheter is placed (**Fig. 144.1e**). After 2-month tract maturation in another patient with spina bifida, conversion to a 10F low-profile (**Fig. 144.1f**, arrowhead) cecostomy tube is performed to facilitate long-term use for antegrade enemas.



■ Diagnosis

Percutaneous Cecostomy



■ Discussion and Differential Diagnosis

Percutaneous cecostomy tube placement can be performed in children and adults to establish an antegrade enema bowel program. Patients with spina bifida, imperforate anus, and spinal cord injury often have associated fecal incontinence, leading to embarrassing accidents and restriction in daily activities.¹⁻³ Patients with chronic constipation or motility disorders may also benefit from antegrade colonic enema flushes via a cecostomy tube. When conservative behavioral and pharmaceutical measures fail to establish normal bowel habits, percutaneous cecostomy is indicated.

Patients are evaluated clinically for suitability of cecostomy placement. Imaging studies are reviewed for preprocedure planning. A bowel preparation is performed before the scheduled procedure. On hospital admission, intravenous hydration is initiated and antibiotic therapy begun. With the assistance of a sedation or anesthesia service, the procedure is performed in interventional radiology. An initial ultrasound confirms the absence of urinary bladder distention, ascites, or abdominal

mass in the cecum region.² A rectal tube is inserted to enable retrograde air distention of the colon. After intravenous glucagon is given to decrease bowel motility, the cecum is punctured and retention sutures placed. An 8F pigtail drain is positioned into the colon.¹⁻³

Following the procedure, inpatient intravenous (IV) fluid hydration, pain control, and antibiotic administration are provided. Potential complications include ileus, abdominal abscess, bowel leak, and ventriculoperitoneal shunt tube infection.¹⁻³ If no complications are encountered, antegrade colonic enema flushes via the cecostomy tube are begun 1 week after hospital discharge. A bowel program is established to reduce unexpected accidents and constipation. After 2 months of tract healing, conversion to a 10F low-profile cecostomy tube is performed over a guidewire under fluoroscopy.¹ Maintenance cecostomy tube exchanges every 12 to 18 months are expected in most patients.^{2,3}

Pearls

- ◆ Lateral decubitus patient positioning may be necessary to distend the cecum with air prior to initial puncture.
- ◆ Some centers favor a 21-gauge micropuncture needle puncture for the initial cecal puncture.

Pitfall

- ◆ Inadvertent ileal puncture may occur. It should be promptly detected and corrected during the initial procedure.

References

1. Chait PG, Shandling B, Richards HM, Connolly BL. Fecal incontinence in children: treatment with percutaneous cecostomy tube placement—a prospective study. *Radiology* 1997;203:621–624 [PubMed](#)
2. Chait PG, Shlomovitz E, Connolly BL, et al. Percutaneous cecostomy: updates in technique and patient care. *Radiology* 2003;227:246–250 [PubMed](#)
3. Sierre S, Lipsich J, Questa H, Bailez M, Solana J. Percutaneous cecostomy for management of fecal incontinence in pediatric patients. *J Vasc Interv Radiol* 2007;18:982–985 [PubMed](#)

Case 145

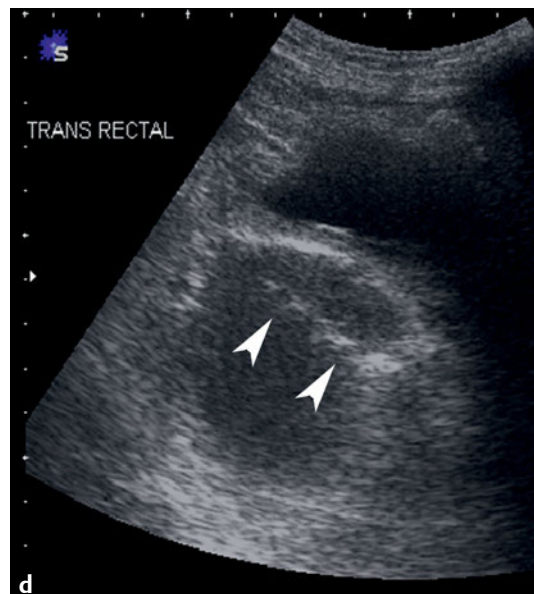
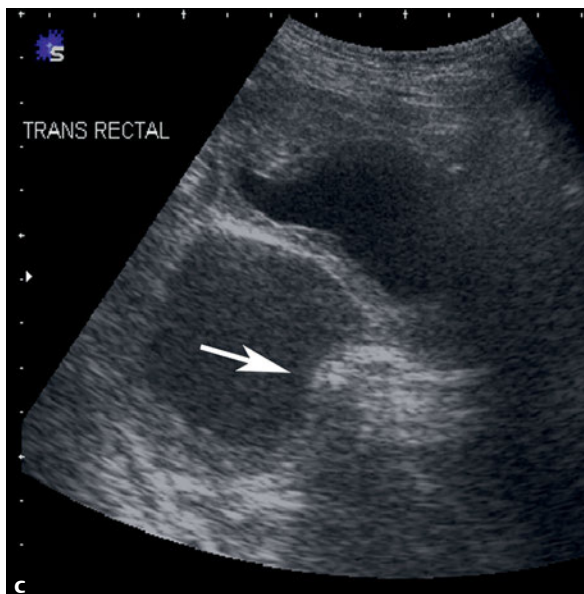
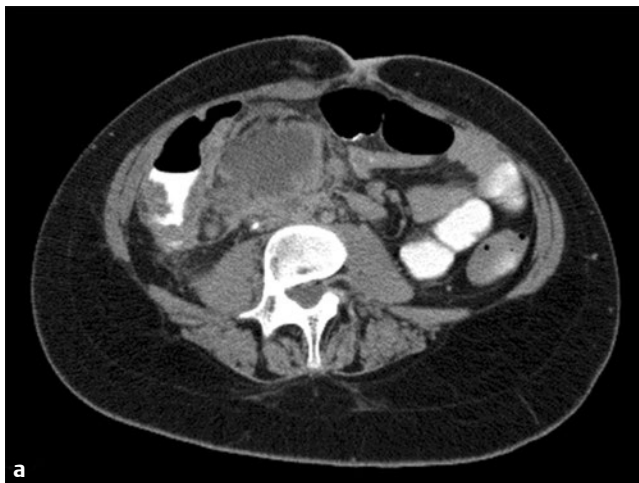
■ Clinical Presentation

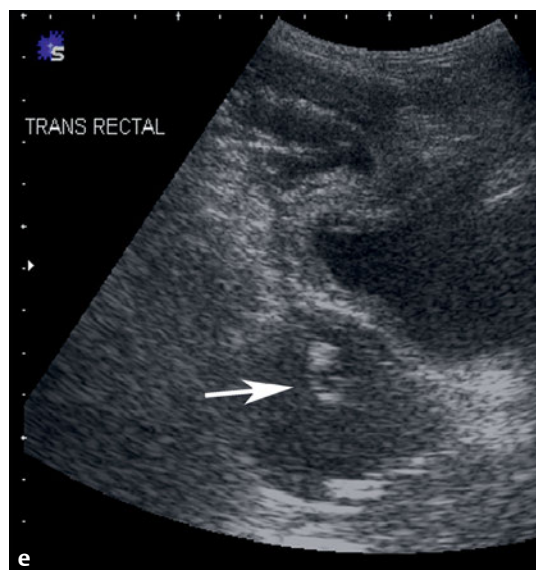
An 11-year-old with fever and abdominal pain 5 days after surgery for appendicitis.

■ Radiographic Studies

Abdomen CT image (**Fig. 145.1a**) shows a rim-enhancing right lower quadrant fluid collection. Advancement of a 0.035-inch guidewire through a 19-gauge sheathed needle was performed using CT guidance, and a pigtail drainage catheter was placed over the wire (**Fig. 145.1b**). A transrectal approach with lower abdominal ultrasound guidance was utilized in a different patient who had a deep pelvic abscess posterior to

the bladder (**Fig. 145.1c**). With the transducer on the anterior abdominal wall and using the bladder as an acoustic window, the rectal introducer indents the inferior wall of the abscess (**Fig. 145.1c, arrow**). Subsequent ultrasound images demonstrate trocar puncture into the cavity (**Fig. 145.1d, arrowheads**) and subsequent pigtail catheter in a good position within the abscess (**Fig. 145.1e, arrow**).





■ Diagnosis

Abscess Drainage



■ Discussion and Differential Diagnosis

A majority of pediatric abdominal abscesses arise after appendiceal perforation or following surgery for appendicitis. Other causes of abscess formation include Crohn's disease, prior bowel surgical procedures, and traumatic bowel injury. Indications for percutaneous abscess drainage continue to increase and include complicating features such as multilocular cavities, cavities with communications (fistulas), and cavities shielded by overlying structures.¹ Most pediatric abscess drainages can be performed with intravenous sedation, though general anesthesia may be needed in some instances. Imaging and drainage can be performed under ultrasound guidance in many cases, with advantages of lower cost, lack of ionizing radiation, and real-time visualization of procedural maneuvers. However, CT has advantages for demonstration of multiplicity of fluid collections and when intervening bowel loops must be delineated. Fluoroscopy is used as an adjunct to some drainage procedures and is particularly valuable in demonstrating fistulae and documenting cavity collapse.

Catheter diameter choice depends on the fluid character and location of the abscess. Typically, even in small children, an 8F or 10F drain is required to adequately drain viscous abscess fluid. Larger drains may be necessary. Dependent position of the drainage catheter, placement of multiple drainage catheters when necessary, and daily saline irrigation of the drainage catheter will decrease drainage duration.¹ A vast majority of pediatric abscess drainages are successful, although occasional incomplete drainage is encountered in cavities associated with fistulae, phlegmons, or underlying tumors.

Abscess cavities in the deep pelvis (**Fig. 145.1f**, arrow) are often more challenging because an anterior approach of the percutaneous drainage is precluded by overlying bladder, bowel, and neurovascular structures. Ultrasound-guided transrectal drainage is a safe and reliable method to treat these pelvic collections.² Alternatively, CT-guided transgluteal needle aspiration and drainage are sometimes preferable based on the location of the abscess.

Pearl

- ◆ Adequate fluid resuscitation, broad-spectrum antibiotics, and knowledge of coagulation status are imperative prior to the procedure.

Pitfall

- ◆ Injury to neurovascular structures in the greater sciatic foramen may occur during transgluteal drainage.¹

References

1. Gervais DA, Brown SD, Connolly SA, Brec SL, Harisinghani MG, Mueller PR. Percutaneous imaging-guided abdominal and pelvic abscess drainage in children. *Radiographics* 2004;24:737–754 [PubMed](#)
2. Sheyn DD, Racadio JM, Racadio JM, et al. Use of an Amplatz dilator to facilitate transrectal abscess drainage in children. *J Vasc Interv Radiol* 2011;22:687–690 [PubMed](#)

Case 146

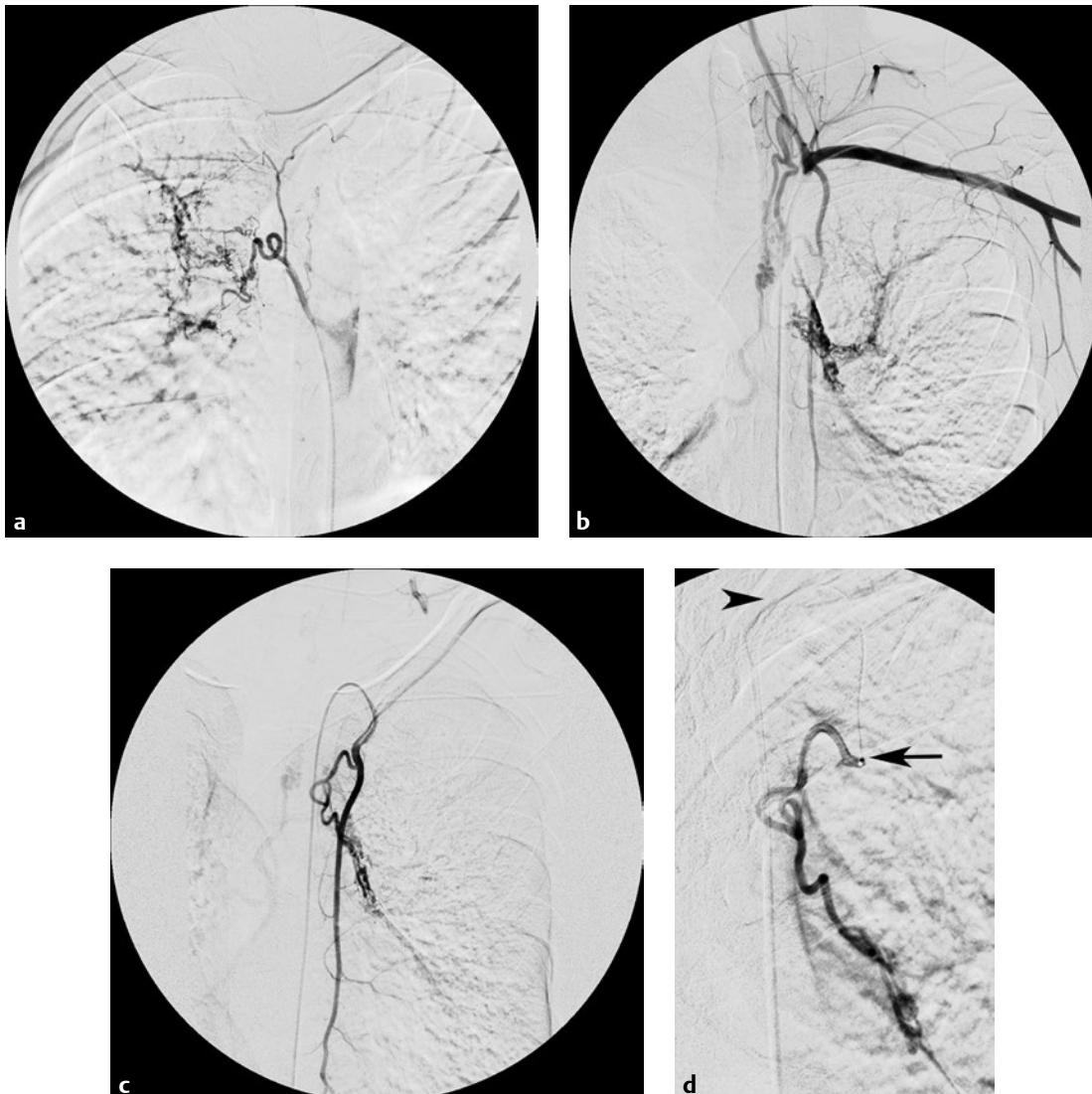
■ Clinical Presentation

An 18-year-old male with recurrent hemoptysis despite optimal medical management of cystic fibrosis exacerbation.

■ Radiographic Studies

Selective angiogram (**Fig. 146.1a**) of a right bronchial artery arising from the descending thoracic aorta shows enlargement of the artery with numerous distal tortuous vessels supplying the right lung. No contrast extravasation was present. Angiogram of the left subclavian artery in the same patient (**Fig. 146.1b**) shows abnormally enlarged subclavian branches with tortuous arterial supply to the left bronchus. Selective

internal mammary artery injection shows the bronchial hyperemia to greater detail (**Fig. 146.1c**). Selective embolization (**Fig. 146.1d**) was performed by advancing a 2.7F microcatheter (*arrow*) coaxially through the 4F angiographic access catheter (*arrowhead*); particle embolization was performed with subsequent reduction in abnormal flow.



■ Diagnosis

Embolization of Hemoptysis

■ Discussion and Differential Diagnosis

Hemoptysis in children and young adults in the developed world is most often caused by pulmonary inflammation related to underlying cystic fibrosis. Massive or life-threatening hemoptysis (>8 mL/kg in a 24-hour period) should prompt treatment focused on resuscitation, airway support, and cessation of bleeding.¹ In some centers, imaging evaluation (CT angiography) and bronchoscopy are performed to define the bleeding site.² When conservative measures fail to control bleeding, proceeding to bronchial artery embolization is indicated.

The bronchial arteries most commonly arise from the descending thoracic aorta between T5 and T6, but many anatomic variations in their origins and branching patterns exist. Knowledge of these patterns and of the nontarget supply is critical. Most notably, spinal arterial branches can arise from

common bronchial trunks; spinal cord ischemia is a known complication of embolization.³ A thoracic aortogram is often performed to identify bronchial anatomy and guide initial catheter placement into bronchial arteries. Contrast extravasation is a rare finding, but abnormal vessels can be identified by their enlargement and tortuous course. Aneurysms and shunting may be present.³ Distal selective microcatheter access is typically required to avoid embolizing normal branch vessels. Peripheral embolization with polyvinyl alcohol (PVA) particles and absorbable gelatin pledgets are used most commonly, and control of hemoptysis is achieved in up to 95% of cases.⁴ Routine occlusion with metallic coils can preclude future arterial access if hemoptysis recurs, but coils can be useful to occlude aneurysms, in emergent situations to control bleeding, and to preclude embolizing nontarget communication pathways.³

Pearl

- ◆ Not all pediatric hemoptysis is due to cystic fibrosis. Tuberculosis is the most common cause in endemic locations. Other etiologies include congenital heart disease, tumors, pulmonary AVMs, and iatrogenic causes.²

Pitfall

- ◆ Watch for shunting through the bronchial arteries to the pulmonary arterial or venous supply, as these shunts can be a route for nontarget embolization.

References

1. Batra PS, Holinger LD. Etiology and management of pediatric hemoptysis. *Arch Otolaryngol Head Neck Surg* 2001;127:377–382. [PubMed](#)
2. Roebuck DJ, Barnacle AM. Haemoptysis and bronchial artery embolization in children. *Paediatr Respir Rev* 2008;9:95–104. [PubMed](#)
3. Kalva SP. Bronchial artery embolization. *Tech Vasc Interv Radiol* 2009;12:130–138. [PubMed](#)
4. Barben J, Robertson D, Olinsky A, Ditchfield M. Bronchial artery embolization for hemoptysis in young patients with cystic fibrosis. *Radiology* 2002;224:124–130. [PubMed](#)

Case 147

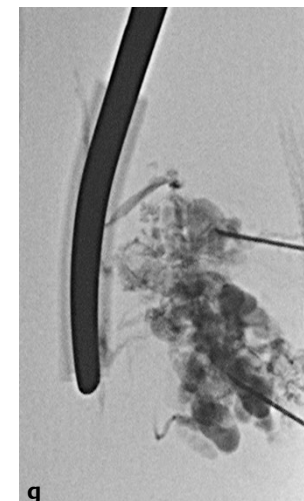
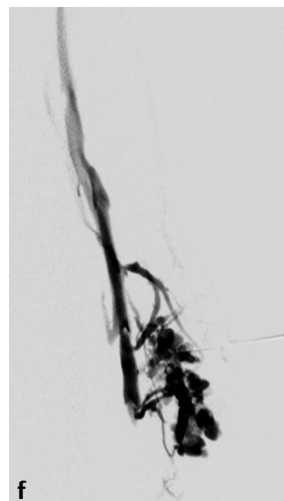
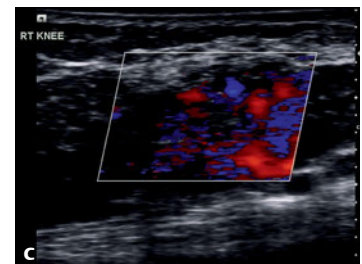
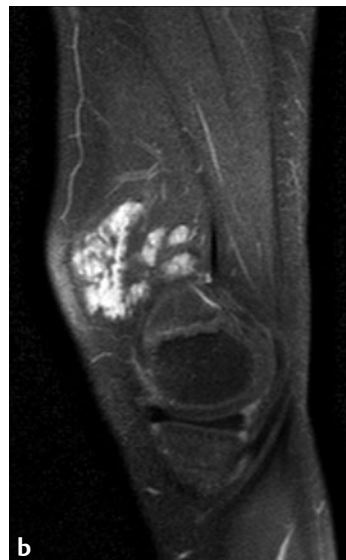
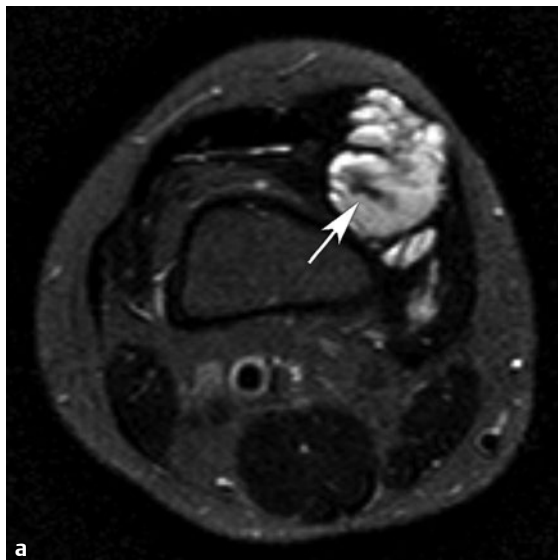
Clinical Presentation

A 7-year-old girl with distal thigh pain limiting knee function.

Radiographic Studies

Axial T2-weighted image (**Fig. 147.1a**) shows a high-signal intramuscular lesion with focal oval low-signal phlebolith (*arrow*). Sagittal T1-weighted fat-suppressed postcontrast image (**Fig. 147.1b**) shows that a majority of the lesion enhances. Color flow ultrasound image (**Fig. 147.1c**) shows dominant luminal component with augmented venous flow prior to sclerotherapy. Direct puncture venogram image (**Fig. 147.1d**) shows filling of an oval luminal component without venous

egress. Fluoroscopic image following sclerotherapy (**Fig. 147.1e**) shows contrast stasis within the oval venous malformation. Direct puncture venography in another patient (**Fig. 147.1f**) shows an oval venous malformation with multiple narrow venous channels communicating with the adjacent deep venous system. Extrinsic compression technique and inflow/outflow needle access (**Fig. 147.1g**) were used to decrease the risk of sclerosant outflow into the deep venous system.



■ Diagnosis

Sclerotherapy: Venous Malformation



■ Discussion and Differential Diagnosis

Venous malformations are developmental errors in vein formation that typically enlarge throughout life with growth of the patient.¹ A slow-flow venous malformation (VM) causes chronic soft tissue swelling, pain, disfigurement, and, in some cases, function limitation. On physical exam a compressible soft tissue lesion is noted that may have a palpable internal nodule (phlebolith) and, if superficial, associated blue skin discoloration. A compression garment for extremity lesions may provide symptomatic relief and slow further distention of the venous malformation over time. Treatment of venous malformation is indicated when lesion size and symptoms are not controlled with conservative measures.

Magnetic resonance imaging is preferred for pretreatment planning to characterize the venous malformation (VM) and delineate lesion extent. Venous sclerotherapy consists of instilling a liquid medication into a symptomatic VM component under image guidance. Ultrasound imaging is helpful to identify dominant VM components for sclerotherapy needle puncture. Direct puncture contrast venography shows the VM morphology, provides a volume estimate, and delineates po-

tential dangerous communications to the deep or central venous system. Sclerotherapy medications are instilled slowly while the patient's vital signs are carefully monitored. Sclerotherapy causes localized injury of the VM endothelium and a surrounding inflammatory response. On the sclerotherapy procedure day, intravenous fluid hydration, alkalization of the urine, or diuretic administration may be needed for hemoglobinuria or oliguria.² Soft tissue injury and nerve paresis may occur and may be temporary or permanent.³ Although post-sclerotherapy VM size reduction may take months, symptomatic improvement is realized in most patients. Lesion recanalization at long-term follow-up is frequent, and repeat venous sclerotherapy sessions may be needed for lesion control.

Differentiation on imaging from microcystic lymphatic malformation in superficial soft tissues can be difficult given significant septal contrast enhancement in microcystic lymphatic malformation. When imaging deeper extremity muscle lesions, fibroadipose vascular anomaly (FAVA) is a differential diagnostic consideration.⁴

Pearls

- ◆ Venous sclerotherapy agents include sodium tetradecyl sulfate (STS), ethanol, and bleomycin. Side-effect profiles differ, and agent use for sclerotherapy may be "off-label."
- ◆ Preoperative sclerotherapy of large venous malformations can decrease operative time and operative blood loss.⁵
- ◆ Fewer sclerotherapy procedural risks are expected in lesions that have nonvisualized venous egress (**Fig. 147.1d**) or narrow venous outflow channels (**Fig. 147.1f**) at direct puncture venography.⁶

Pitfalls

- ◆ A dose of 1 mL/kg of intralesional ethanol in the treatment of vascular malformations may be associated with raised serum ethanol levels.⁷
- ◆ Cardiopulmonary collapse is a rare reported complication of ethanol sclerotherapy.⁷
- ◆ Pulmonary fibrosis may be a late complication of bleomycin use.⁸

■ Controversy

- Ultrasound-guided interstitial laser therapy may control lesion size and symptoms in some patients.⁹

References

1. Mulliken JB, Glowacki J. Hemangiomas and vascular malformations in infants and children: a classification based on endothelial characteristics. *Plast Reconstr Surg* 1982;69:412–422. [PubMed](#)
2. Barranco-Pons R, Burrows PE, Landrigan-Ossar M, Trenor CC III, Alomari AI. Gross hemoglobinuria and oliguria are common transient complications of sclerotherapy for venous malformations: review of 475 procedures. *AJR Am J Roentgenol* 2012;199:691–694. [PubMed](#)
3. Berenguer B, Burrows P, Zurakowski D, Mulliken. Sclerotherapy of craniofacial venous malformations: Complications and results. *J Plastic and Reconstructive Surgery*. 1999;104:1–11
4. Alomari AI, Spencer SA, Arnold RW, et al. Fibro-adipose vascular anomaly: clinical-radiologic-pathologic features of a newly delineated disorder of the extremity. *J Pediatr Orthop* 2014;34:109–117. [PubMed](#)
5. James CA, Braswell LE, Wright LB, et al. Preoperative sclerotherapy of facial venous malformations: impact on surgical parameters and long-term follow-up. *J Vasc Interv Radiol* 2011;22:953–960. [PubMed](#)
6. Puig S, Aref H, Chigot V, Bonin B, Brunelle F. Classification of venous malformations in children and implications for sclerotherapy. *Pediatr Radiol* 2003;33:99–103. [PubMed](#)
7. Burrows PE, Mason KP. Percutaneous treatment of low flow vascular malformations. *J Vasc Interv Radiol* 2004;15:431–445. [PubMed](#)
8. Orford J, Barker A, Thonell S, King P, Murphy J. Bleomycin therapy for cystic hygroma. *J Pediatr Surg* 1995;30:1282–1287. [PubMed](#)
9. Sidhu MK, Perkins JA, Shaw DW, Bittles MA, Andrews RT. Ultrasound-guided endovenous diode laser in the treatment of congenital venous malformations: preliminary experience. *J Vasc Interv Radiol* 2005;16:879–884. [PubMed](#)

Case 148

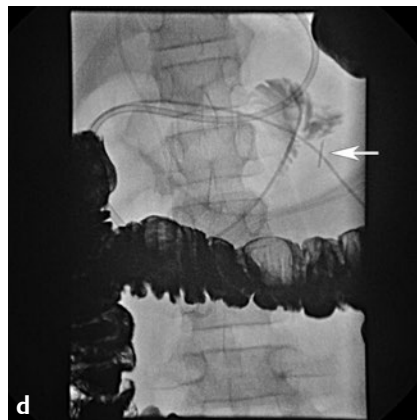
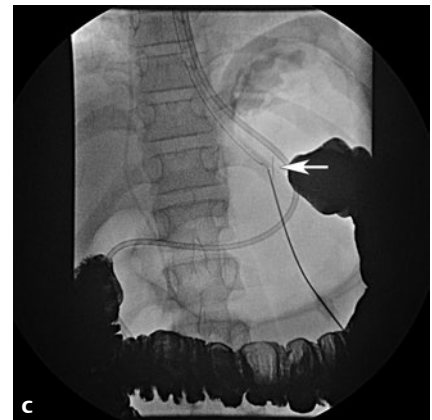
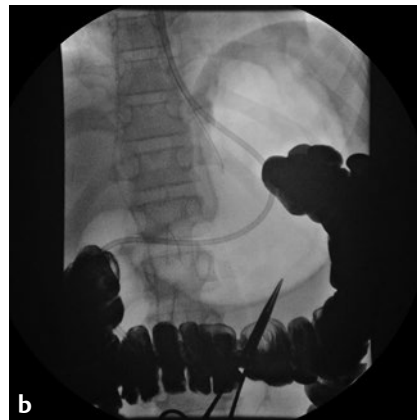
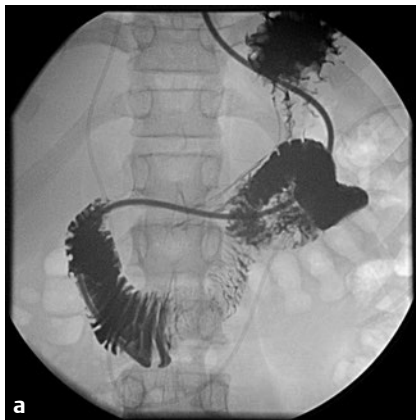
■ Clinical Presentation

A 13-year-old boy with brain tumor, weight loss, and vomiting on transpyloric tube feeds.

■ Radiographic Studies

Preprocedure fluoroscopic contrast image (**Fig. 148.1a**) shows findings of a superior mesenteric artery (SMA) duodenal obstruction. Procedural fluoroscopic image (**Fig. 148.1b**) shows air insufflation of the stomach and colonic barium for skin site selection for gastric puncture. Subsequent image (**Fig. 148.1c**) demonstrates contrast in the gastric fundus and deployed gas-

tric retention suture (*arrow*). The retention suture is retracted (*arrow*), and then guiding catheter access to the duodenal-jejunal junction is obtained (**Fig. 148.1d**). A gastrojejunostomy tube is advanced over a stiff guidewire and the distal tube pig-tail is positioned in the distal fourth duodenum (**Fig. 148.1e**).



■ Diagnosis

Gastrojejunostomy

■ Discussion and Differential Diagnosis

Percutaneous feeding in the pediatric population is performed for patients with inadequate oral nutrition. Indications include central nervous system (swallowing) impairment, failure to thrive, malignancy, chronic gastrointestinal disease, and anatomic anomalies of the craniofacial area or aerodigestive tract. Nutritional feeds may be delivered directly into the stomach with a gastrostomy tube or into the proximal small bowel with a gastrojejunostomy tube. Specific indications for the latter tube include gastroesophageal reflux unresponsive to medical management, intolerance to gastrostomy feeds for any other reason, and SMA duodenal obstruction.

Primary pediatric radiological gastrostomy and gastrojejunostomy placement have progressed as quick and safe procedures in infants and children of all sizes.¹ Both antegrade placement through the mouth and retrograde placement through the anterior abdominal wall have been described in pediatric patients. Advantages of the antegrade technique include fewer tube dislodgments and improved capability to drain the stomach with a larger caliber tube.² In rare cases, the antegrade technique is not feasible because of nasopharyngeal or esophageal obstruction. Regardless of approach, a majority

of pediatric interventionalists administer barium many hours prior to the procedure to opacify the transverse colon and image the left lobe of the liver with ultrasound immediately prior to gastric puncture. In the retrograde insertion technique, the stomach is distended with air via a nasogastric tube, and gastric motility is decreased with intravenous glucagon. Retention suture placement prevents displacement of the stomach from the anterior abdominal wall during tract dilatation and tube placement steps.² A gastrojejunostomy tube can be placed at the time of initial gastric puncture. This is achieved with a directional catheter-guidewire combination, which is advanced through the pylorus and into the proximal small bowel. Over the guidewire, the gastrojejunostomy tube is advanced and the distal tip of the tube positioned near the duodenal-jejunal junction. Major complications after percutaneous gastrostomy placement such as hemorrhage or peritonitis are decreased compared with surgical rates.³ Feeding begins after the return of bowel sounds and lack of complications are documented.² Similar guiding catheter/guidewire manipulations are employed when converting a mature gastrostomy tract to gastrojejunal feeding.

Pearls

- ◆ Exchange for a stiff guidewire prior to gastrojejunal tube advancement may be necessary to avoid undesirable guidewire loops in the stomach.
- ◆ Percutaneous feeding tubes can be maintained indefinitely, with patient caregivers and the radiology team working together closely to solve problems as they arise.

Pitfalls

- ◆ Small-bowel intussusception at the distal tip of a gastrojejunostomy tube should be recognized and treated, as it can lead to bowel necrosis and perforation.⁴
- ◆ Pneumoperitoneum at the time of tube placement is not problematic if the volume is small and decreasing. Moderate to large amounts of air can be aspirated to promote apposition of stomach to anterior abdominal wall.²

References

1. Chait PG, Weinberg J, Connolly BL, et al. Retrograde percutaneous gastrostomy and gastrojejunostomy in 505 children: a 4 1/2-year experience. *Radiology* 1996;201:691–695. [PubMed](#)
2. Connolly B, Krishnamurthy G, Amaral J. Upper gastrointestinal access in children: techniques and outcomes. *Tech Vasc Interv Radiol* 2010;13:222–228. [PubMed](#)
3. Friedman JN, Ahmed S, Connolly B, Chait P, Mahant S. Complications associated with image-guided gastrostomy and gastrojejunostomy tubes in children. *Pediatrics* 2004;114:458–461. [PubMed](#)
4. Hughes UM, Connolly BL, Chait PG, Muraca S. Further report of small-bowel intussusceptions related to gastrojejunostomy tubes. *Pediatr Radiol* 2000;30:614–617. [PubMed](#)

Case 149

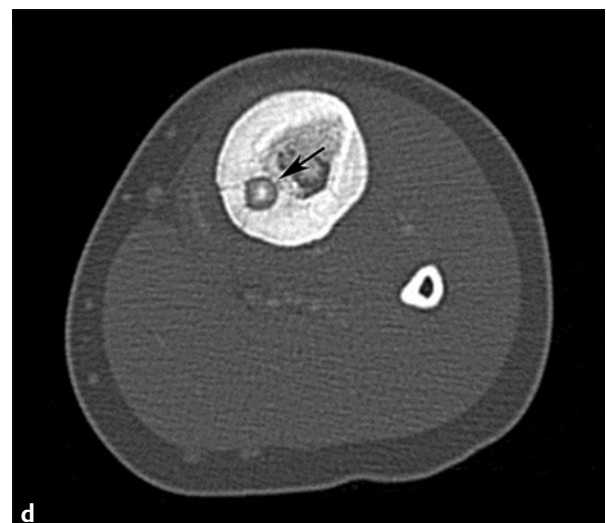
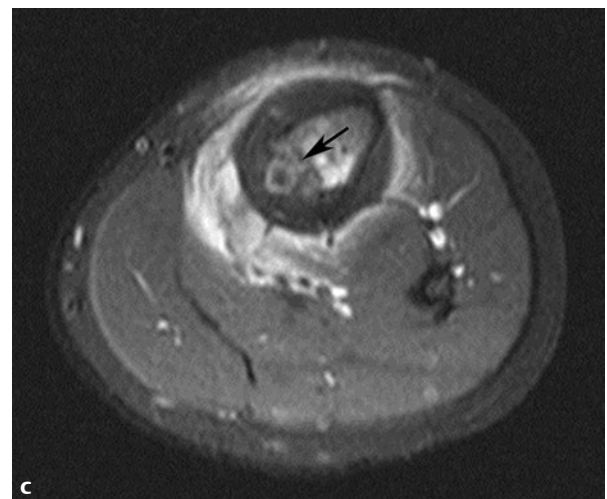
■ Clinical Presentation

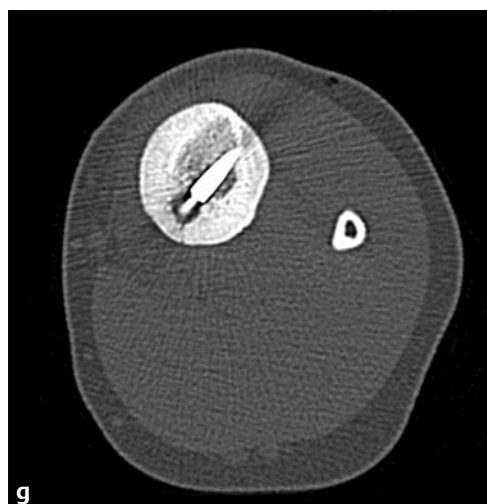
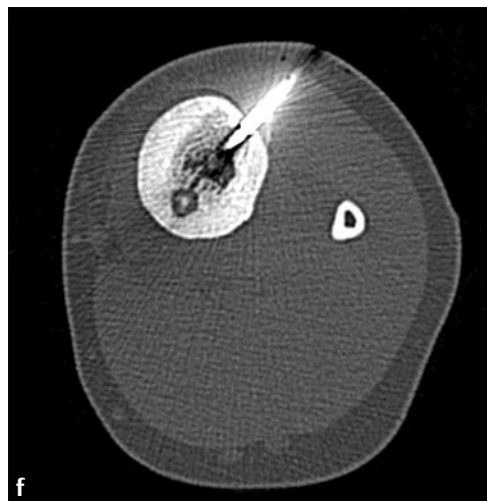
An 8-year-old boy with several months of leg pain and limping.

■ Radiographic Studies

An AP radiograph (**Fig. 149.1a**) shows medullary sclerosis of the proximal left tibia, an oval lucent lesion with central calcification (*arrow*), and associated cortical thickening (*arrow-head*). Bone scan image (**Fig. 149.1b**) shows a moderate increase in tracer uptake within the proximal left tibia with focal more intense tracer uptake adjacent to the medial cortex (*arrow-head*). Axial STIR MRI shows an oval lesion with high signal rim (**Fig. 149.1c**, *arrow*) with adjacent marrow and extraosseous soft tissue edema. CT image (**Fig. 149.1d**) shows the oval

lucent “nidus” with central calcification (*arrow*) and associated cortical thickening. Coronal reformatted CT image (**Fig. 149.1e**) displays the size and shape of the nidus for interventional radiology (IR) treatment planning. Axial CT image during an IR ablation procedure (**Fig. 149.1f**) guides the advancement of the coaxial needle toward the nidus. Subsequent procedure CT image (**Fig. 149.1g**) shows coaxial radiofrequency probe aligned within the nidus before ablation treatment.





■ Diagnosis

Osteoid Osteoma Ablation

■ Discussion and Differential Diagnosis

Osteoid osteoma is a benign neoplasm of bone. Most patients present between the ages of 5 and 24 years; there is a 2:1 to 3:1 male predominance.¹ The lesion causes a classic severe pain syndrome that is most pronounced at night and can be relieved with nonsteroidal anti-inflammatory medications.¹ The lesion can occur in any bone; long bones and spine locations are most common. Radiographs demonstrate a round or oval radiolucent nidus that by definition measures < 1.5 cm in diameter. A surrounding zone of sclerosis is common. If the lesion occurs in the spine, scoliosis can occur. Lesions near joints and intra-articular lesions may cause reactive synovitis, effusions, and cartilage loss.² The most useful modality for lesion characterization is CT, which demonstrates the pre-

cise location of the central nidus, thereby guiding treatment planning.

Preprocedure imaging is important to plan a safe access route and to avoid injury to adjacent nerves and blood vessels.¹ CT imaging is used to guide a needle cannula or drill through bone cortex and into the nidus. A radiofrequency electrode is then advanced coaxially through the cannula into the nidus, and several minutes of heat ablation is administered.³ Same-day discharge is expected, and postprocedure pain should abate within 1 week of treatment. When weight-bearing locations are treated, exertional sports limitations for a few months may be indicated.⁴ Larger lesions require more than one treatment location to effectively treat the entire nidus.⁴

Pearls

- ◆ Percutaneous ablation has been shown to treat the lesion with a clinical success rate comparable to that of surgery while requiring a shorter recovery period.³
- ◆ Knowledge of ablation equipment treatment volume is crucial for success.
- ◆ MR-guided focused ultrasound has shown early success in safely treating osteoid osteoma.⁵

Pitfall

- ◆ Recurrence rates of 6 to 9% are reported after percutaneous ablation, and the success rate for repeat ablation is variable for recurrent lesions (60–100%).^{2,4}

References

1. Towbin R, Kaye R, Meza MP, Pollock AN, Yaw K, Moreland M. Osteoid osteoma: percutaneous excision using a CT-guided coaxial technique. *AJR Am J Roentgenol* 1995;164:945–949 [PubMed](#)
2. Woertler K, Vestring T, Boettner F, Winkelmann W, Heindel W, Lindner N. Osteoid osteoma: CT-guided percutaneous radiofrequency ablation and follow-up in 47 patients. *J Vasc Interv Radiol* 2001;12:717–722 [PubMed](#)
3. Rosenthal DI, Hornicek FJ, Wolfe MW, Jennings LC, Gebhardt MC, Mankin HJ. Percutaneous radiofrequency coagulation of osteoid osteoma compared with operative treatment. *J Bone Joint Surg Am* 1998;80:815–821 [PubMed](#)
4. Rosenthal DI, Hornicek FJ, Torriani M, Gebhardt MC, Mankin HJ. Osteoid osteoma: percutaneous treatment with radiofrequency energy. *Radiology* 2003;229:171–175 [PubMed](#)
5. Napoli A, Mastantuono M, Cavallo Marincola B, et al. Osteoid osteoma: MR-guided focused ultrasound for entirely noninvasive treatment. *Radiology* 2013;267:514–521 [PubMed](#)

Case 150

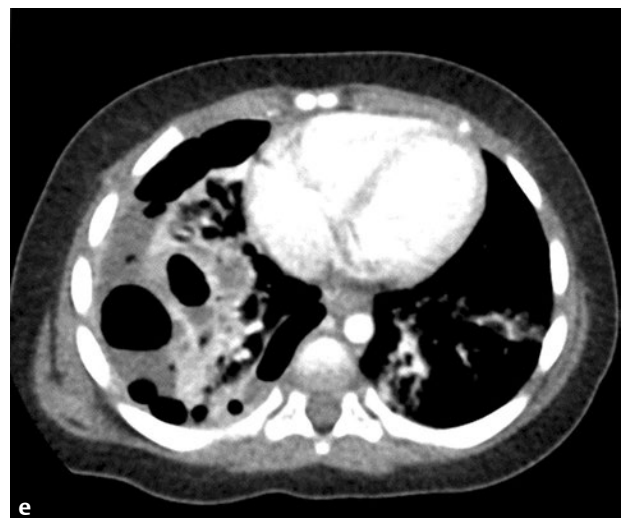
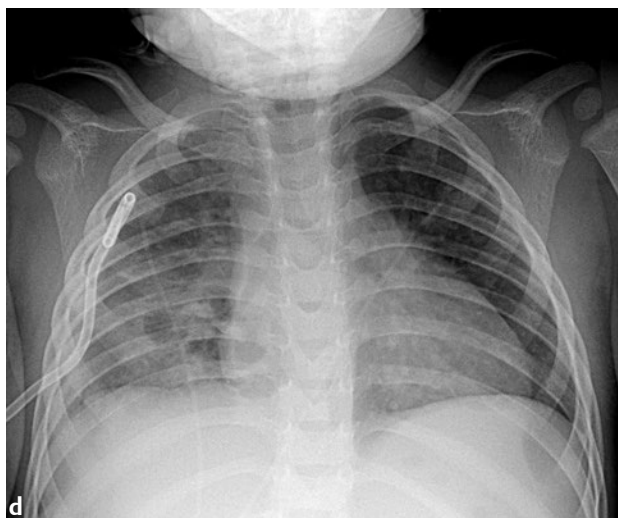
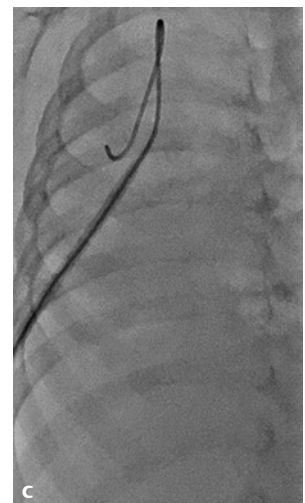
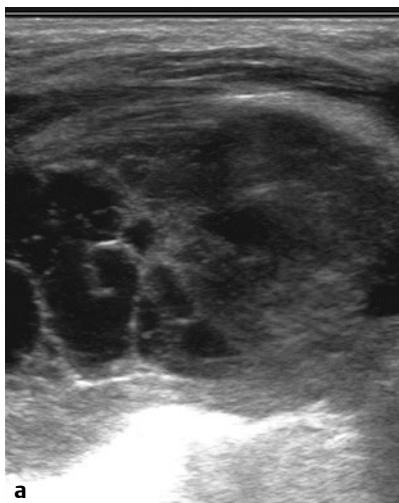
■ Clinical Presentation

A 1-year-old boy with fever and tachypnea.

■ Radiographic Studies

Diagnostic ultrasound of the chest (**Fig. 150.1a**) demonstrated a mixed echogenicity pleural fluid collection and underlying lung consolidation. Debris and septations were present within the complex parapneumonic effusion. Ultrasound and fluoroscopy were utilized for procedure image guidance. Initial sheath needle puncture was directed posteriorly toward the lung apex (**Fig. 150.1b**), and a locking loop pigtail catheter was advanced over a guidewire after sequential soft tissue tract dilatation (**Fig. 150.1c**). Through the catheter, fibrinolytic medication was given twice daily. Follow-up radiograph on day 2

of alteplase therapy demonstrated near resolution of pleural effusion with persistent patchy airspace opacities (**Fig. 150.1d**). The tube output tapered over several days, and the patient's oxygen requirement resolved before chest tube removal. CT image of another patient (**Fig. 150.1e**) shows lung parenchymal low-attenuation areas and air-fluid levels compatible with necrotizing pneumonia. Though treatment of pneumonia was prolonged, the complex pleural effusion in this patient resolved with 4 days of alteplase therapy per chest tube.



■ Diagnosis

Parapneumonic Pleural Effusion

■ Discussion and Differential Diagnosis

The incidence of childhood pneumonia requiring hospitalization has decreased in recent years, following the introduction of the pneumococcal vaccine in 2000.¹ Nevertheless, the rate of complex parapneumonic effusion associated with pneumonia seems to have increased.¹ Although it was historically considered mandatory that patients with complex effusions undergo surgical debridement, intrapleural fibrinolysis after small-bore chest tube placement has emerged as a safe and cost-effective alternative to invasive therapy.²

Initial chest tube placement is performed in interventional radiology with moderate sedation. Knowledge of resuscitation techniques and recognition of the possibility of periprocedural respiratory distress are essential. Coughing and initial respiratory depression are often encountered as the lung re-expands during effusion drainage. Ultrasound guides sheathed needle puncture into the pleural fluid, and a sample may be obtained for laboratory analysis and culture. Equipment is di-

rected posteriorly via a midaxillary line approach so that the tube is dependent within fluid. Over a guidewire, soft tissue tract dilatation and pigtail drain tube placement are performed using fluoroscopic guidance. Tube output is monitored regularly during suction drainage.³

After successful chest tube placement, initiation of fibrinolytic therapy can begin as per the interventional radiology service protocol; alteplase (tissue plasminogen activator [t-PA]) is the current standard agent.⁴ Instillation of t-PA directly into the chest tube is performed. By causing enzymatic debridement of the fibrin sheets that develop in the pleural space and breaking down loculations, t-PA facilitates fluid drainage into the tube.⁴ Sequential daily or twice-daily doses are given to completely treat the collection, and tube output and patient clinical course are monitored. When tube output diminishes below threshold, chest radiography is performed to document resolution of effusion, and the tube is removed.³

Pearls

- ◆ Clinical rounding is necessary to evaluate tube patency and function. Small-bore catheters can easily kink and occlude.³
- ◆ Daily follow-up chest radiographs are not necessary in children who have a chest tube, but they can be useful to confirm the end-of-therapy response and resolution. Parenchymal pneumonia takes longer to resolve than effusion.

Pitfalls

- ◆ Contraindications to intrapleural fibrinolytic therapy include active bleeding, coagulopathy, and recent surgery.
- ◆ Some patients may not improve with percutaneous drainage and fibrinolytic therapy. If treatment fails, video-assisted thoracic surgery (VATS) is necessary.³

References

1. Grijalva CG, Nuorti JP, Zhu Y, Griffin MR. Increasing incidence of empyema complicating childhood community-acquired pneumonia in the United States. *Clin Infect Dis* 2010;50:805–813 [PubMed](#)
2. St Peter SD, Tsao K, Spilde TL, et al. Thoracoscopic decortication vs tube thoracostomy with fibrinolysis for empyema in children: a prospective, randomized trial. *J Pediatr Surg* 2009;44:106–111, discussion 111 [PubMed](#)
3. Feola GP, Shaw LC, Coburn L. Management of complicated parapneumonic effusions in children. *Tech Vasc Interv Radiol* 2003;6:197–204 [PubMed](#)
4. Wells RG, Havens PL. Intrapleural fibrinolysis for parapneumonic effusion and empyema in children. *Radiology* 2003;228:370–378 [PubMed](#)

Case 151

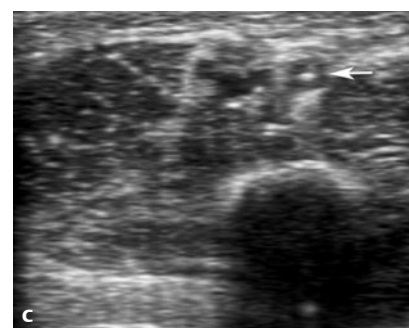
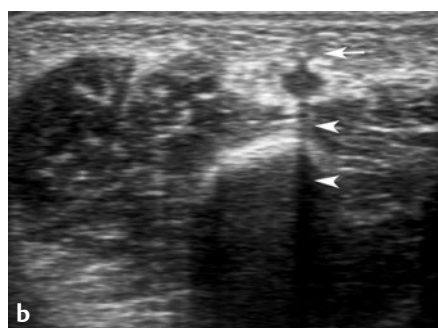
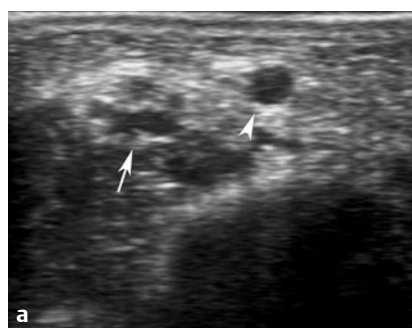
■ Clinical Presentation

A 10-month-old boy with psoas abscess needs stable venous access for antibiotics.

■ Radiographic Studies

Ultrasound image (**Fig. 151.1a**) delineates the right basilic vein (*arrowhead*) medial to the right brachial artery/brachial vein (*arrow*). Subsequent ultrasound image (**Fig. 151.1b**) shows the access needle tip centered on the basilic vein (*arrow*) with deep acoustic fall-off (*arrowheads*). Following vein puncture,

the access needle is centered within the basilic vein lumen (**Fig. 151.1c, arrow**). Fluoroscopic guidewire position (**Fig. 151.1d**) is used to measure the length of the venous catheter before peripherally inserted central catheter (PICC) placement (**Fig. 151.1e**) into the superior vena cava (SVC).



■ Diagnosis

Peripherally Inserted Central Catheter



■ Discussion and Differential Diagnosis

The peripherally inserted central catheter (PICC) is a commonly placed device in children who need stable central venous access for infusions of medications, fluids, or vesicant/irritant solutions such as total parenteral nutrition (TPN) or chemotherapy. In the pediatric population, blood sampling is often performed via this catheter to avoid repeat venipuncture. Advantages of the catheter include increased stability and durability relative to peripheral IV. The procedure itself is considered to be minimally invasive.¹

The PICC is typically placed without difficulty in the proximal arms or legs of infants and children. Although there are patients in whom bedside placement is straightforward, many patients are referred to the interventional radiology department for combined ultrasound and fluoroscopic guidance during placement. For most infants and children, the upper extremity is the initial choice for venipuncture, with basilic and cephalic veins preferable to the brachial vein due to its close proximity to the brachial artery and median nerve.² For infants with some types of congenital heart disease, specifically with single ventricle physiology (e.g., hypoplastic left heart syndrome), lower extremity access may be requested to protect the central veins in the chest from potential stenosis or injury.

In children, sedation and distraction are planned based on the patient's age and ability to cooperate with the procedure.² After sterile prepping of the extremity, ultrasound guides needle placement for venipuncture (**Fig. 151.1a–c**). A guidewire is advanced into the central venous system and measured under fluoroscopic guidance. The PICC is cut to measured length and advanced into place. Final tip position, ideally in the vena cava or at the cavoatrial junction, is confirmed with a final fluoroscopic image.² When central venous guidewire resistance is encountered, digital subtraction venography or roadmap fluoroscopic venography (**Fig. 151.1f**) is helpful to delineate venous occlusive disease and guide appropriate catheter placement.

Although the procedure is safe, immediate and long-term complications exist, particularly in children in whom multiple catheters are placed over time.³ These include infection, catheter malfunction/malposition, venous stenosis or thrombosis, bleeding, and inadvertent arterial puncture.¹ In low birth weight infants, cardiac tamponade related to catheter erosion into the myocardium is a rare complication.⁴

Pearl

- ◆ In a dehydrated infant, an IV bolus treatment may increase venipuncture success.²

Pitfall

- ◆ The PICC distal tip position may advance or retract with changing arm positions (abduction/adduction).

References

1. Gibson C, Connolly BL, Moineddin R, Mahant S, Filipescu D, Amaral JG. Peripherally inserted central catheters: use at a tertiary care pediatric center. *J Vasc Interv Radiol* 2013;24:1323–1331 [PubMed](#)
2. Braswell LE. Peripherally inserted central catheter placement in infants and children. *Tech Vasc Interv Radiol* 2011;14:204–211 [PubMed](#)
3. Yang RY, Moineddin R, Filipescu D, et al. Increased complexity and complications associated with multiple peripherally inserted central catheter insertions in children: the tip of the iceberg. *J Vasc Interv Radiol* 2012;23:351–357 [PubMed](#)
4. Pezzati M, Filippi L, Chiti G, et al. Central venous catheters and cardiac tamponade in preterm infants. *Intensive Care Med* 2004;30:2253–2256. [PubMed](#)

Case 152

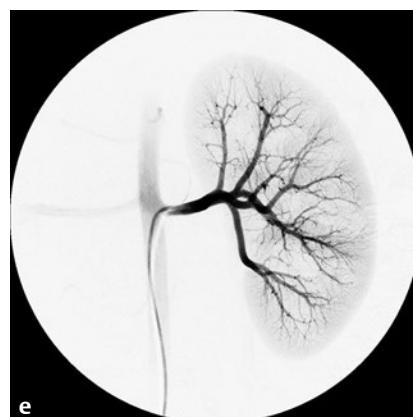
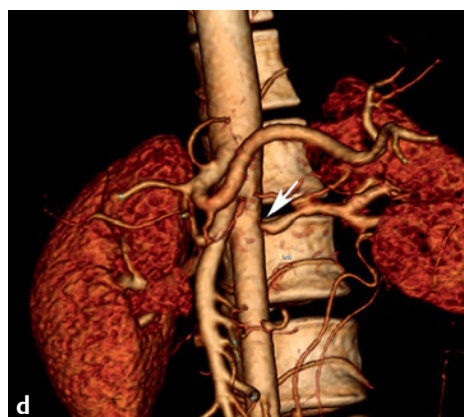
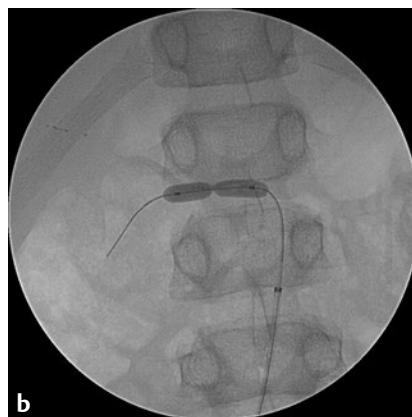
■ Clinical Presentation

A 12-year-old boy requiring three medications for hypertension control.

■ Radiographic Studies

Abdominal aortogram (**Fig. 152.1a**) shows focal high-grade stenosis of the right main renal artery with post-stenotic dilation. Note that the origin of the right main renal artery is smaller than the left main renal artery origin, and there is delayed parenchymal blush of the right kidney. After placement of a guiding sheath to the L2 level, an intravenous heparin bolus (2,000 units) was given, and exchange for a 0.018-inch guidewire across the right main renal artery stenosis was made. Inflation of a 4-mm angioplasty balloon showed the focal

waist of the angioplasty balloon (**Fig. 152.1b**). Several 4-mm balloon inflations were required to relieve the balloon waist; given multiple manipulations, two intra-arterial nitroglycerin doses were given into the right main renal artery. Postangioplasty angiogram showed mild decrease of the right main renal artery stenosis (**Fig. 152.1c**). This patient had only temporary modest blood pressure improvement following this procedure.



■ Diagnosis

Renovascular Hypertension

■ Discussion and Differential Diagnosis

Whereas adult renovascular hypertension is predominantly due to atherosclerosis, the many causes in children include fibromuscular dysplasia (FMD), syndromes (most commonly neurofibromatosis type 1 [NF1]), vasculitis, extrinsic compression by tumor, and others such as scarring, emboli (umbilical artery catheter), radiation, or trauma.¹ In children with severe hypertension, end-organ impairment (seizures, stroke, heart failure, renal dysfunction), a known syndrome or vasculitis, or inadequate control with two or more antihypertensive medications, a renovascular cause of the high blood pressure should be sought.¹ Noninvasive imaging modalities include ultrasound with Doppler waveform analysis, CTA, and MRA. Recent technical improvements in pediatric renal CTA with low radiation dose have been shown to be useful in identifying aortic and main renal arterial lesions.² A volume-rendered CTA image (**Fig. 152.1d**) shows high-grade stenosis (*arrow*) of the left main renal artery origin in a 16-year-old patient on two medications for hypertension.

The most accurate and detailed imaging study for localizing vascular lesions, however, is catheter angiography, particularly in light of the fact that a relatively high proportion of lesions occur in segmental renal artery branches.³ Abdominal

aortic hypoplasia and multifocal arterial disease is common in children with renovascular hypertension, particularly those with genetic disease (NF1, Williams syndrome).² After arterial sheath placement, aortography with a pigtail flush catheter is performed. It is important to evaluate the abdominal aorta caliber/contour, mesenteric artery origins, and bilateral renal arteries (including accessory renal artery branches).² Selective bilateral renal arteriograms are then performed with breath holding by anesthesia; multiple oblique projections may be required. Additional angiographic findings may include asymmetric kidney size/perfusion, aneurysms, and collateral blood flow.

If angioplasty is indicated, vascular surgical backup is arranged, and the patient is anticoagulated with systemic heparin.⁴ Arterial stenoses are crossed with a small-diameter flexible guidewire. The procedure is performed with conventional balloons initially; high-pressure or cutting balloons may be used in lesions that have a persistent waist.¹ In several reported series of patients with FMD and NT1, more than 50% of patients can be expected to have hypertension improvement or cure.⁴ In cases of refractory hypertension, surgical treatment is indicated.

Pearl

- ◆ High-quality selective renal artery angiograms with breath holding by anesthesia are necessary to adequately search for segmental, peripheral renal arterial stenoses. **Figure 152.1e** shows normal segmental left renal artery branches in a child with hypertension.

Pitfalls

- ◆ Complications of renal angioplasty include arterial spasm, dissection, perforation, and postprocedural blood pressure fluctuations.³
- ◆ Guidewire access across a lesion should be maintained during follow-up angiography so that the balloon can be reinflated or a stent can be placed. Vascular surgery availability is imperative.⁴

■ Controversy

- Renal vein renin sampling may be helpful in selected cases.

References

1. Tullus K, Brennan E, Hamilton G, et al. Renovascular hypertension in children. *Lancet* 2008;371:1453–1463 [PubMed](#)
2. Kurian J, Epelman M, Darge K, Meyers K, Nijs E, Hellinger JC. The role of CT angiography in the evaluation of pediatric renovascular hypertension. *Pediatr Radiol* 2013;43:490–501, quiz 487–489 [PubMed](#)
3. Roebuck DJ, McLaren CA. Noninvasive imaging in children with hypertension. *Pediatr Radiol* 2013;43:502–505 [PubMed](#)
4. Srinivasan A, Krishnamurthy G, Fontalvo-Herazo L, et al. Angioplasty for renal artery stenosis in pediatric patients: an 11-year retrospective experience. *J Vasc Interv Radiol* 2010;21:1672–1680 [PubMed](#)

Case 153

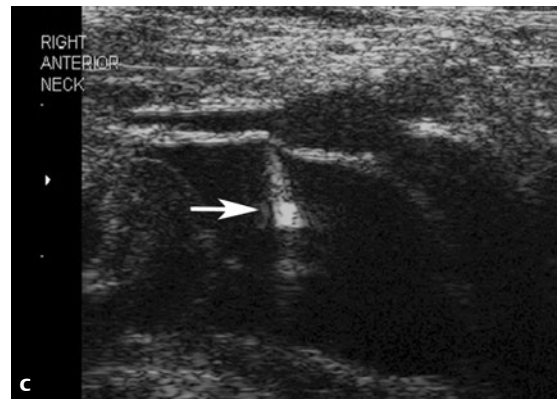
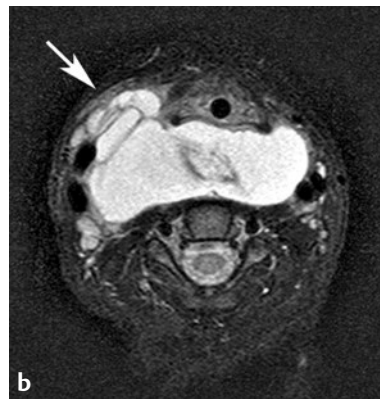
■ Clinical Presentation

A 2-year-old boy with snoring and right anterior neck redness.

■ Radiographic Studies

Neck CT image (**Fig. 153.1a**) shows a right anterior cervical drain within an infected prevertebral/retropharyngeal cystic lesion. Following temporary drain removal, the patient was subsequently hospitalized for increasing respiratory distress. MRI (**Fig. 153.1b**) shows the increased size of a multiseptated prevertebral cystic lesion. An access route (*arrow*) for cystic lesion drainage anterior and medial to the right carotid space

is planned. Ultrasound guides needle puncture (**Fig. 153.1c**, *arrow*) across a septation and into the dominant cyst component. Following 6F locking-loop drain placement, a frontal roadmap fluoroscopic image (**Fig. 153.1d**) confirms contrast flow within a large cyst and shows no contrast extravasation. Lateral fluoroscopic image (**Fig. 153.1e**) shows drain placement and injected contrast within a large prevertebral macrocyst.



■ Diagnosis

Sclerotherapy: Lymphatic Malformation

■ Discussion and Differential Diagnosis

Lymphatic malformations result from developmental errors in lymph channel formation and can be categorized as macrocystic, microcystic, or combined macrocystic-microcystic slow-flow vascular malformations. A majority of lymphatic malformations occur in the head and neck, followed by trunk and extremity locations.^{1,2} Though lymphatic malformations typically expand slowly with growth of the patient, rapid lesion expansion may occur with secondary infection or internal bleeding after local trauma. The presence of characteristic cutaneous skin vesicles and lack of response to Valsalva maneuvers may distinguish lymphatic malformations from slow-flow venous malformations.^{1,2} Treatment indications include pain, swelling, disfigurement, recurrent infection/bleeding, weeping skin vesicles, and recurrence following surgical resection.¹⁻³ Review of imaging studies prior to treatment delineates macrocystic from microcystic components, shows internal macrocyst fluid–fluid levels (from internal debris/hemorrhage), and displays lesion extent and relationship to critical structures (airway, major nerves). Images should also be assessed for features of a combined vascular malformation such as Klippel-Trenaunay syndrome (capillary-lymphatic-venous malformation) or CLOVES syndrome (congenital lipomatous overgrowth with vascular, epidermal, and skeletal anomalies).

Given pain with sclerotherapy agent injection, lymphatic sclerotherapy is most often performed under general anesthesia.^{1,2} Initial needle access of macrocystic components is performed under ultrasound guidance with needle or sheath

needle aspiration of lymphatic fluid. A small amount of contrast may be injected under fluoroscopy to confirm the location within the malformation and to exclude contrast extravasation from the lesion.¹⁻⁴ Multiple agents in liquid or foam solution have been used to treat lymphatic malformations including ethanol, sodium tetradecyl sulfate, OK-432, doxycycline, and bleomycin. Though sclerotherapy most commonly involves a single agent, the value of dual agent lymphatic macrocyst ablation has been reported.³ Drain placement for sclerotherapy of larger macrocysts may allow variable dwell time of the sclerosing agent during or beyond the sclerotherapy procedure; external drainage of sclerosed contents and repeat sclerotherapy sessions may be performed.²⁻⁴ Postprocedure complications are typically minor (pain, persistent swelling, skin blister, infection); infrequent major complications may occur (nerve injury, vision loss).^{1-3,5}

Reduction in lymphatic malformation size and favorable patient response to sclerotherapy is expected in the majority of patients; better results have been reported for macrocystic lesions.^{1-3,5} Complete procedural macrocyst aspiration and the presence of post-sclerotherapy inflammatory-type symptoms have been suggested as predictors of successful outcome following OK-432 sclerotherapy.⁵ Multiple repeat sclerotherapy sessions may be required for lesion control.¹ Cutaneous laser therapy and surgical treatment for lesion debulking or recurrence may be required.

Pearl

- ◆ Most procedures can be performed as outpatient procedures; extensive facial or deep cervical lymphatic malformations with microcystic components are more difficult to treat and may require airway protection.²

Pitfalls

- ◆ Sclerotherapy typically entails off-label use of sclerosing medications; OK-432 is not approved by the Food and Drug Administration (FDA).
- ◆ The risk of sclerotherapy complications is higher in certain locations (orbital compartment, adjacent major nerves).

■ Controversy

- Optimal duration of lymphatic malformation external drainage and specific indications for repeat lymphatic

malformation sclerotherapy sessions via a macrocyst drain are poorly defined.

References

1. Burrows PE, Mitri RK, Alomari A, et al. Percutaneous sclerotherapy of lymphatic malformations with doxycycline. *Lymphat Res Biol* 2008;6:209–216 [PubMed](#)
2. Alomari AI, Karian VE, Lord DJ, Padua HM, Burrows PE. Percutaneous sclerotherapy for lymphatic malformations: a retrospective analysis of patient-evaluated improvement. *J Vasc Interv Radiol* 2006;17:1639–1648 [PubMed](#)
3. Shiels WE II, Kenney BD, Caniano DA, Besner GE. Definitive percutaneous treatment of lymphatic malformations of the trunk and extremities. *J Pediatr Surg* 2008;43:136–139, discussion 140 [PubMed](#)
4. Chaudry G, Burrows PE, Padua HM, Dillon BJ, Fishman SJ, Alomari AI. Sclerotherapy of abdominal lymphatic malformations with doxycycline. *J Vasc Interv Radiol* 2011;22:1431–1435 [PubMed](#)
5. Kim DW. OK-432 sclerotherapy of lymphatic malformation in the head and neck: factors related to outcome. *Pediatr Radiol* 2014;44:857–862 [PubMed](#)

Case 154

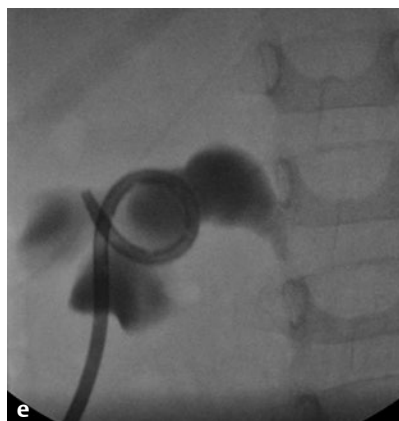
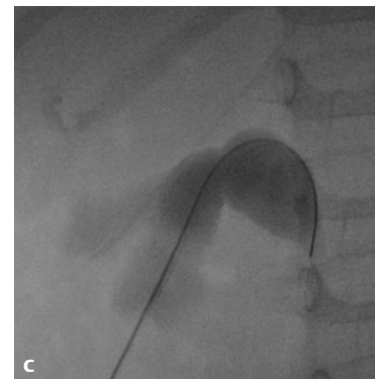
Clinical Presentation

A 3-year-old with hypertension, acute renal failure, and left hydronephrosis.

Radiographic Studies

Renal ultrasound demonstrated hydronephrosis of the left kidney with pelvic and calyceal involvement (**Fig. 154.1a**). No dilated ureter was present. Procedural ultrasound of the lower pole of the left kidney shows needle placement (*arrowheads*) within the dilated lower pole calyx (**Fig. 154.1b**). Contrast injection in the prone position confirms 21-gauge needle placement, and a 0.018-inch guidewire was advanced into the renal pelvis using fluoroscopic guidance (**Fig. 154.1c**). Conversion to a 0.035-inch guidewire was performed via a renal access puncture set (**Fig. 154.1d**), and an 8F locking loop nephros-

tomy catheter was placed (**Fig. 154.1e**). No contrast entered the ureter, compatible with obstruction at the level of the ureteropelvic junction, which was likely related to vasculitis (Henoch-Schönlein purpura). After lack of response to a trial of steroids, definitive pyeloplasty was required. In another patient, a 5-year-old, percutaneous access provided a route for antegrade nephroureteral stent placement (**Fig. 154.1f**) due to persistent post-pyeloplasty hydronephrosis. The obstruction could not be crossed from a retrograde cystoscopic approach.



■ Diagnosis

Percutaneous Nephrostomy

■ Discussion and Differential Diagnosis

Percutaneous nephrostomy can be performed safely in infants and children for a variety of congenital and acquired conditions. Most commonly, pediatric urinary tract drainage is performed to improve renal function prior to treatment of an obstructing lesion (e.g., uteropelvic junction obstruction, pelvic tumor) or to temporarily control infection. In other instances, such as urinary diversion for urine leak or antimicrobial irrigation for urinary tract infection, urinary drainage may provide definitive treatment.^{1,2} Increasingly, percutaneous nephrostomy tract establishment is performed to accommodate percutaneous urinary tract procedures such as lithotripsy or antegrade ureteric interventions.¹

Preprocedural review of anatomic and functional imaging studies is important to assess appropriateness of indications and for treatment planning. Review may reveal anomalies such as horseshoe kidney or crossed fused ectopic kidney, which require percutaneous access sites differing from the norm. Antibiotics and sedation appropriate for the patient's age and

duration of the procedure are administered.³ Unique challenges in infants and small children include mobility of the kidney; thinner, more elastic parenchymal tissues (less support during manipulation); need for smaller equipment; and the need for additional steps to preclude dislodgment.⁴

Most nephrostomy tube placement procedures can be performed through an easily accessible lower or midpole calyx. Complications are typically minor and self-limited (local bleeding, hematuria, asymptomatic urine leak, etc.).² One of the most serious complications of nephrostomy placement is sepsis, which can occur even in patients with asymptomatic infection. Extensive equipment manipulation and vigorous contrast injection should be avoided; prophylactic antibiotics are routine.^{2,3} Some percutaneous procedures require upper pole or specific caliceal entry. If an intercostal approach is necessary, more significant complications (pneumothorax, hemothorax) may occur.

Pearl

- ◆ Percutaneous collecting system access for ureteral perfusion test (Whitaker test) may be useful to discriminate obstructive from nonobstructive dilatation.

Pitfall

- ◆ Direct nephrostomy entry into the renal pelvis should be avoided given the proximity of major vessels and the lack of surrounding renal parenchyma.

References

1. Roebuck DJ. Genitourinary intervention in children. *Pediatr Radiol* 2011;41:17–26 [PubMed](#)
2. Linscott L. Pediatric urologic interventional radiology. *Semin Intervent Radiol* 2011;28:407–414 [PubMed](#)
3. Hogan MJ, Coley BD, Jayanthi VR, Shiels WE, Koff SA. Percutaneous nephrostomy in children and adolescents: outpatient management. *Radiology* 2001;218:207–210 [PubMed](#)
4. Koral K, Saker MC, Morello FP, Rigsby CK, Donaldson JS. Conventional versus modified technique for percutaneous nephrostomy in newborns and young infants. *J Vasc Interv Radiol* 2003;14:113–116 [PubMed](#)

Case 155

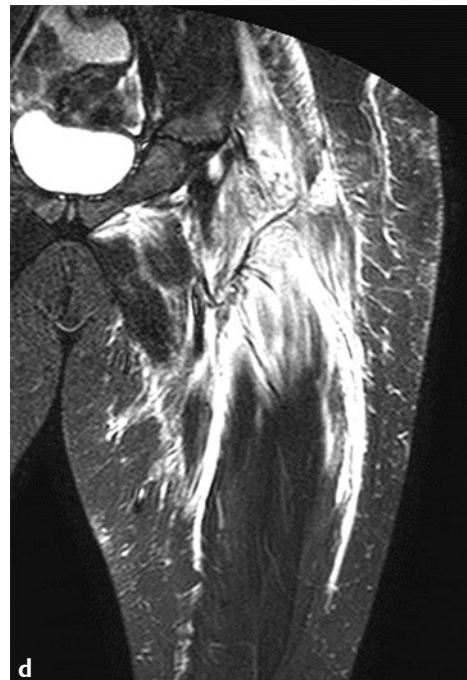
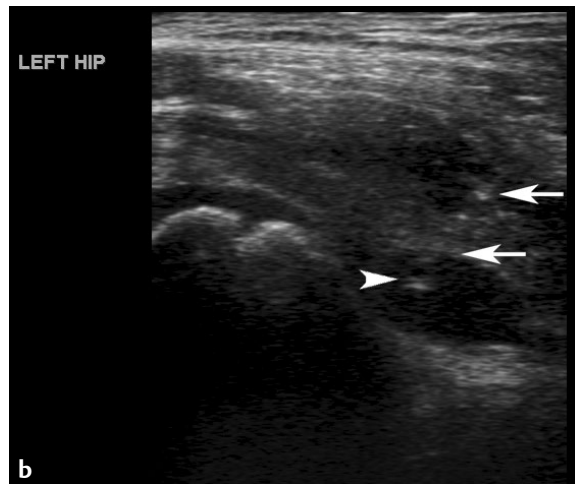
■ Clinical Presentation

A 6-year-old girl refusing to bear weight.

■ Radiographic Studies

Longitudinal ultrasound of the left hip (**Fig. 155.1a**) demonstrates capsular distention of the joint with anechoic fluid representing joint effusion. Ultrasound was utilized to guide spinal needle placement into the joint (**Fig. 155.1b**). The needle is seen throughout its course (*arrows*), with the tip in good

position in the fluid (*arrowhead*). Coronal STIR MRI in another patient with aspiration of purulent left hip joint effusion (**Fig. 155.1c,d**) shows increased marrow signal indicative of osteomyelitis and associated myositis in the thigh.



■ Diagnosis

Septic Arthritis

■ Discussion and Differential Diagnosis

During evaluation of the child with an irritable hip, prompt consideration and evaluation for septic arthritis is imperative to avoid long-term sequelae of suppurative infection of the hip joint. Children typically have acute presentation of hip pain, limp, and refusal to bear weight. The clinical signs which, when seen in combination, are highly predictive of septic arthritis include fever, elevated C-reactive protein, elevated erythrocyte sedimentation rate, and elevated serum white blood cell count (WBC).^{1,2} A plain radiograph of the pelvis is inspected for the presence of joint fluid and for obliteration of soft tissue planes about the hip joint. Radiographic findings of fracture, osteomyelitis, avascular necrosis, or juvenile arthritis are excluded. Accurate detection of hip joint effusion is provided by

ultrasound imaging of the hip using an anterior parasagittal approach. Anechoic or echogenic displacement of the hip joint capsule from the proximal femoral cortex is found in both septic arthritis and toxic synovitis as compared with the contralateral hip joint. Definitive diagnosis is achieved with needle aspiration of hip joint fluid. Joint fluid WBC $> 50,000/\text{mm}^3$ is diagnostic of septic arthritis.² Appropriate treatment of septic arthritis includes surgical drainage with antibiotic treatment, whereas toxic synovitis resolves with bed rest and analgesic therapy. Prompt treatment reduces the likelihood of cartilage destruction, growth arrest, and sepsis. Associated intramedullary or intramuscular infection may be present.

Pearls

- ◆ Though the hip is the most common site of pediatric septic arthritis, the knee joint is commonly involved in older children.
- ◆ Magnetic resonance imaging demonstrates the associated myositis and osteomyelitis that can accompany septic arthritis.
- ◆ Multiple joints are involved in 10% of children with septic arthritis.³

Pitfalls

- ◆ In neonatal patients, delay in diagnosis of septic arthritis is common because localizing clinical findings are subtle.³
- ◆ Hip joint capsular distention may cause referred pain to the groin, thigh, or knee.

References

1. Caird MS, Flynn JM, Leung YL, Millman JE, D'Italia JG, Dormans JP. Factors distinguishing septic arthritis from transient synovitis of the hip in children. A prospective study. *J Bone Joint Surg Am* 2006;88:1251–1257 [PubMed](#)
2. Kocher MS, Zurakowski D, Kasser JR. Differentiating between septic arthritis and transient synovitis of the hip in children: an evidence-based clinical prediction algorithm. *J Bone Joint Surg Am* 1999;81:1662–1670 [PubMed](#)
3. Nade S. Septic arthritis. *Best Pract Res Clin Rheumatol* 2003;17:183–200. [PubMed](#)



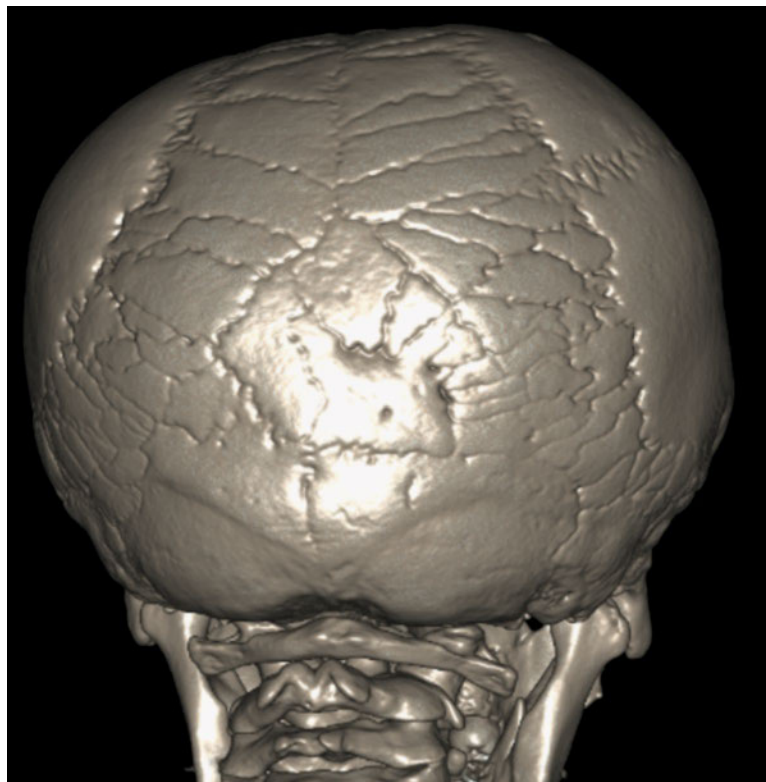
Syndromes

Section Editor

Charles A. James

Authors

Chinar Lath and Joanna J. Seibert



Case 156

■ Clinical Presentation

An infant with limb shortening and a large head.

■ Radiographic Studies

Upper extremity radiographs show rhizomelic shortening with disparate short humerus (**Fig. 156.1a**). The lower extremities (**Fig. 156.1b**) are short and thick with V-shaped growth plates. The iliac wings are squared, the sciatic notches are narrow,

and the acetabular roof is flat. Spine radiograph (**Fig. 156.1c**) demonstrates decrease in the interpediculate distance from upper to lower lumbar spine. The bones of the hands are short and thick (**Fig. 156.1d**).



■ Diagnosis

Achondroplasia

■ Discussion and Differential Diagnosis

Achondroplasia is the most common nonlethal skeletal dysplasia (1 in 26,000 live births).¹ It is the most common rhizomelic dwarfism, with greatest shortening in the humeri and femurs. The underlying abnormality is a defect in the maturation of the cartilage growth plate of long bones. Characteristic findings in the axial skeleton include decreased vertebral body height, decreased interpediculate distance, squared iliac wings (elephant ear), narrow sciatic notch, and flattening of the acetabular roof.

This autosomal dominant disorder is accompanied by a high incidence of neurologic complications. Cranial findings include megaloccephaly, hydrocephalus (usually communicating), and brainstem compression by a narrowed foramen magnum (**Fig.**

156.1e). Associated sleep apnea, sudden infant death, and hypotonia are reported.^{1–6} Spinal findings include cord compression (especially cervicomedullary) and nerve root impingement with associated paresthesias, deep tendon reflex changes, and progressive paraparesis/quadripareisis.^{1–6}

The major differential diagnosis is hypochondroplasia, in which the face and hands are normal.^{7–9} Medical complications common to achondroplasia (e.g., spinal stenosis, tibial bowing, obstructive apnea) occur less frequently in hypochondroplasia, but deficiency in mental capacity may be more prevalent.⁷ Hypochondroplastic patients are largely normal in appearance except for their disproportionately short limbs.

Pearl

- ◆ Patients with achondroplasia have normal intelligence.

Pitfalls

- ◆ The radiographic characteristics of homozygous achondroplasia lie between those of heterozygous achondroplasia and thanatophoric dwarfism.
- ◆ Heterozygous achondroplasia cannot be diagnosed until the third trimester, whereas homozygous achondroplasia can be easily diagnosed in the second trimester.¹⁰

■ Controversies

- Bilateral lower limb lengthening using the Ilizarov method has multiple potential complications and remains controversial.¹¹
- Although there has been some increase in growth rate reported with the use of growth hormone, long-term benefit is not established.⁶

References

1. Taybi H, Lachman RS. Radiology of Syndromes. Metabolic Disorder, and Skeletal Dysplasias, 5th ed. Philadelphia: Mosby; 2007:865–871
2. Gordon N. The neurological complications of achondroplasia. *Brain Dev* 2000;22:3–7 Review [PubMed](#)
3. Keiper GL Jr, Koch B, Crone KR. Achondroplasia and cervicomedullary compression: prospective evaluation and surgical treatment. *Pediatr Neurosurg* 1999;31:78–83 [PubMed](#)
4. Pauli RM. Achondroplasia. In: Pagon RA, Adam MP, Ardinger HH, et al, eds. *Gene Reviews* [online]. Seattle: University of Washington; 2012
5. Kao SC, Waziri MH, Smith WL, Sato Y, Yuh WT, Franken EA Jr. MR imaging of the craniovertebral junction, cranium, and brain in children with achondroplasia. *AJR Am J Roentgenol* 1989;153:565–569 [PubMed](#)
6. Horton WA, Hall JG, Hecht JT. Achondroplasia. *Lancet* 2007;370:162–172 Review [PubMed](#)
7. Bober MB, Bellus GA, Nikkel SM, Tiller GE. Hypochondroplasia. In: Pagon RA, Adam MP, Ardinger HH, et al, eds. *Gene Reviews* [online]. Seattle: University of Washington; 1999
8. Hall BD, Spranger J. Hypochondroplasia: clinical and radiological aspects in 39 cases. *Radiology* 1979;133:95–100 [PubMed](#)
9. Heselson NG, Cremin BJ, Beighton P. The radiographic manifestations of hypochondroplasia. *Clin Radiol* 1979;30:79–85 [PubMed](#)
10. Patel MD, Filly RA. Homozygous achondroplasia: US distinction between homozygous, heterozygous, and unaffected fetuses in the second trimester. *Radiology* 1995;196:541–545 [PubMed](#)
11. Kim SJ, Balce GC, Agashe MV, Song SH, Song HR. Is bilateral lower limb lengthening appropriate for achondroplasia?: midterm analysis of the complications and quality of life. *Clin Orthop Relat Res* 2012;470:616–621 [PubMed](#)

Case 157

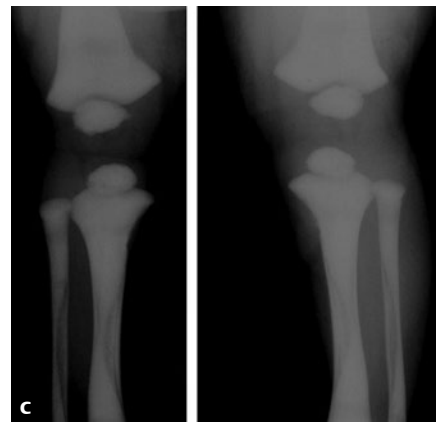
■ Clinical Presentation

A newborn with left arm swelling.

■ Radiographic Studies

Neonatal chest radiograph (**Fig. 157.1a**) shows a fracture of the left humerus with marked increased density in all the bones. Radiographs of the foot and lower extremities (**Fig. 157.1b,c**) show marked increased bone density with a “bone within a bone” appearance. Pelvic/femur radiograph (**Fig. 157.1d**)

shows obliteration of the corticomedullary junction. Lateral radiograph of the spine shows a “sandwich” appearance to the vertebral bodies due to this “bone within a bone” appearance (**Fig. 157.1e**).



■ Diagnosis

Osteopetrosis

■ Discussion and Differential Diagnosis

Osteopetrosis (marble bone disease, Albers-Schönberg disease) is a genetic disorder affecting osteoclast development/function and is characterized by generalized increased bone density.^{1,2} Characteristic features are irregular and inhomogeneous cortical thickening and sclerosis of the diaphyses of tubular bones. The medullary cavity is narrowed with endosteal involvement greater than periosteal involvement.³

The osteopetrotic conditions vary greatly in their presentation and severity. The disease can be inherited as autosomal recessive, autosomal dominant, or X-linked traits with the most severe forms being autosomal recessive. Classic autosomal re-

cessive osteopetrosis (infantile form) is characterized by fractures, short stature, compressive neuropathies, hypocalcemia with associated tetanic seizures, and life-threatening pancytopenia because of marrow encroachment. Onset of fractures and osteomyelitis is typically seen in late childhood/adolescence and is typical of the more common autosomal dominant osteopetrosis.² Though treatment for osteopetrosis is largely supportive, stem cell transplantation or gamma-interferon treatment may be options in selected patients with bone marrow failure.²

Pearls

- ◆ Increase in skull bone density is greatest at the skull base.
- ◆ At least 10 gene mutations have been identified in osteopetrosis.²

Pitfall

- ◆ Rickets may occur in patients with osteopetrosis, producing an intriguing radiograph of dense diaphyses with flared irregular demineralized metaphyses.^{4,5}

References

1. Taybi H, Lachman RS. Radiology of Syndromes. Metabolic Disorder, and Skeletal Dysplasias, 5th Ed. Philadelphia, PA: Mosby. 2007:1028–1034
2. Stark Z, Savarirayan R. Osteopetrosis. Orphanet J Rare Dis 2009;4:5 [PubMed](#)
3. McAlister WH. Current concepts: an approach to skeletal dysplasias. In: Seibert JJ, ed. A Categorical Course in Pediatric Radiology. Chicago: RSNA; 1994:115
4. Oliveira G, Boechat MI, Amaral SM, Young LW. Osteopetrosis and rickets: an intriguing association. Am J Dis Child 1986;140:377–378 [PubMed](#)
5. Donnelly LF, Johnson JF III, Benzing G. Infantile osteopetrosis complicated by rickets. AJR Am J Roentgenol 1995;164:968–970 [PubMed](#)

Case 158

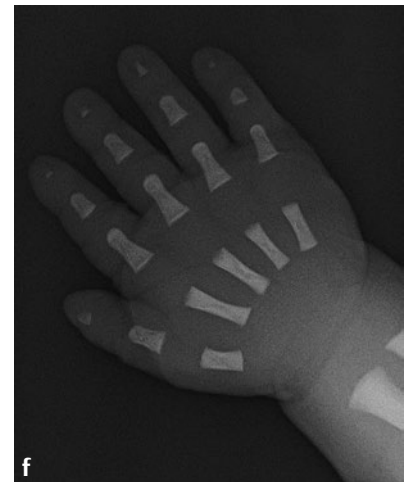
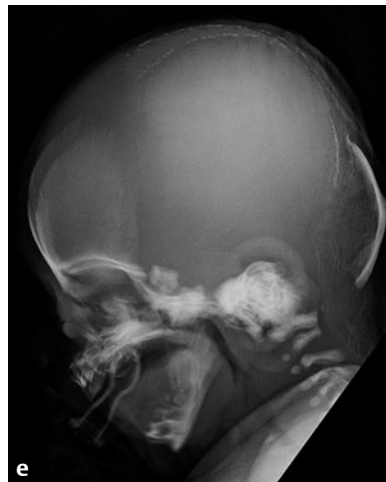
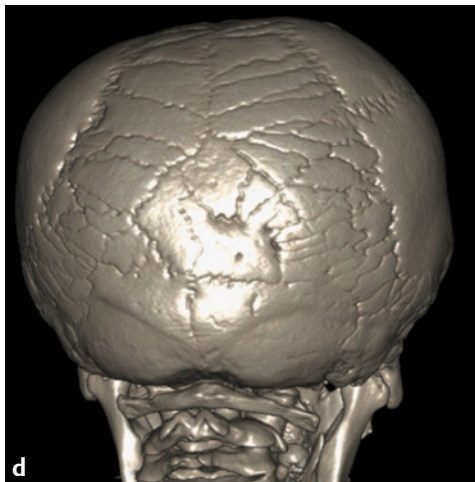
■ Clinical Presentation

A newborn with multiple congenital anomalies.

■ Radiographic Studies

Newborn chest radiograph (**Fig. 158.1a**) shows absent clavicles, small scapula, and short ribs. Pelvic radiographs at 8 months (**Fig. 158.1b**) show small iliac wings and delayed ossification of the pubic bones with a wide symphysis pubis. Coronal CT

(**Fig. 158.1c**) in a 25-year-old woman with droopy shoulders and conductive hearing loss shows an unerupted tooth (*arrow*) and multiple sutural wormian bones (*arrowhead*). A 3D CT image (**Fig. 158.1d**) shows the extent of the wormian bones.



■ Diagnosis

Cleidocranial Dysplasia

■ Discussion and Differential Diagnosis

Cleidocranial dysplasia is an autosomal dominant disorder characterized by ossification defects, especially in the midline. The anterior fontanelle may be prominent (**Fig. 158.1e**) and remain open into adulthood, and the mandible is often broad, with resulting prognathism. All or any portion of the clavicle may be missing, usually the middle third. The ossification of pubic bones is commonly delayed (wide symphysis pubis) but usually normalizes. Anomalies of the bones of the hands are typically present, including long second and fifth metacarpals,

short middle phalanges, tapered terminal phalanges (**Fig. 158.1f**), and delayed bone age.¹ Eustachian tube dysfunction, conductive hearing loss, and sensorineural hearing loss are common because of structural and functional changes of the temporal bone and palate.² There is slow appearance of the permanent teeth, and dental caries are frequent. Other conditions with ossification defects in the skull with open anterior fontanelle and wormian bones include pyknodysostosis, osteogenesis imperfecta, and hypophosphatasia.³

Pearls

- ◆ This condition was first described in Homer's *Iliad*.
- ◆ Intelligence is normal in individuals with classic cleidocranial dysplasia.⁴
- ◆ One third of cases are spontaneous mutations.

Pitfall

- ◆ There is considerable interfamilial variability.

References

1. Jarvis JL, Keats TE. Cleidocranial dysostosis. A review of 40 new cases. *Am J Roentgenol Radium Ther Nucl Med* 1974;121:5–16 [PubMed](#)
2. Visoski AM, et al. Otolaryngological manifestations of CCD. *Laryngoscope* 2003;113:1508–1514 [PubMed](#)
3. Taybi H, Lachman RS. *Radiology of Syndromes. Metabolic Disorder, and Skeletal Dysplasias*, 5th ed. Philadelphia: Mosby; 2007;913–915
4. Mendoza-Londono R, Lee B. Cleidocranial dysplasia. *Gene Reviews*. 2006. Updated August 29, 2013. <http://www.ncbi.nlm.nih.gov/books/NBK1513/>

Case 159

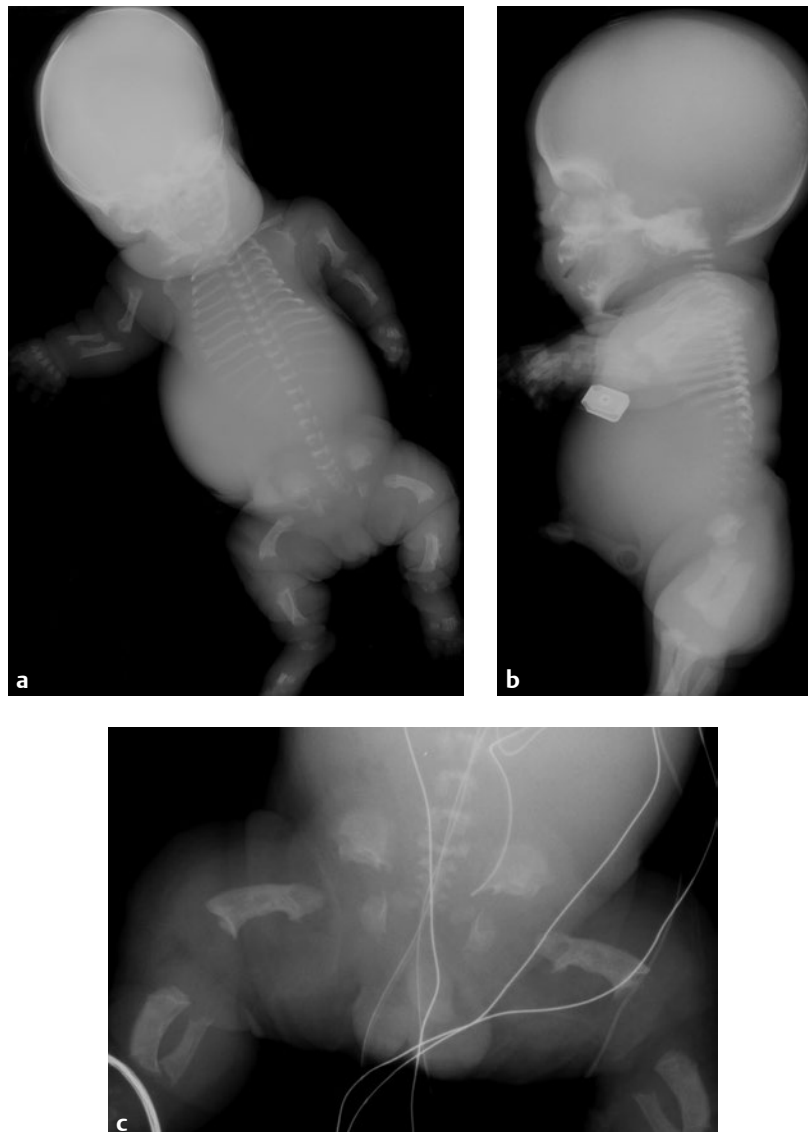
■ Clinical Presentation

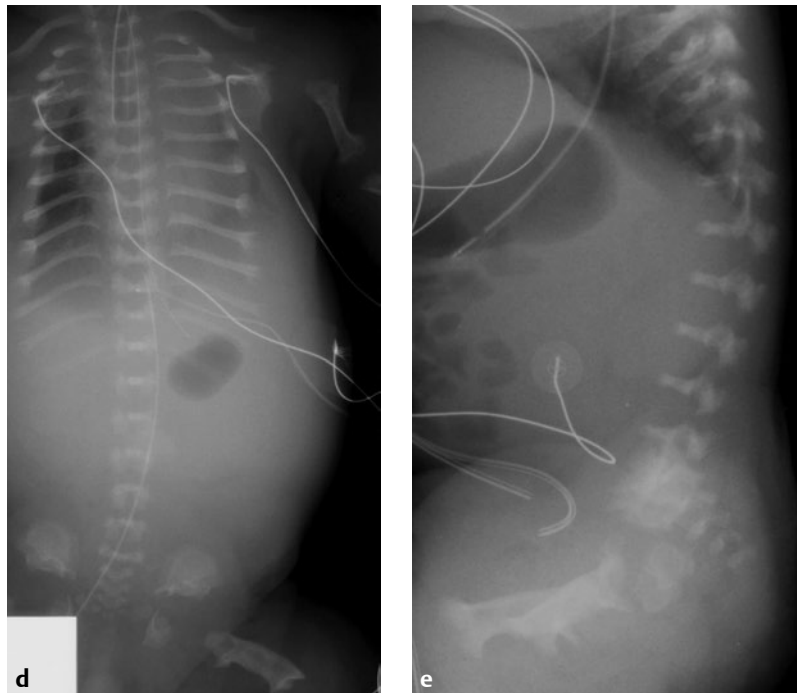
Two short-limbed dwarfs who died shortly after birth.

■ Radiographic Studies

Frontal and lateral radiographs (**Fig. 159.1a,b**) of the first infant show small chest and short ribs. Shortening and bowing of the long bones with metaphyseal widening and irregularity is seen. The tubular bones of the hands and feet are extremely short and broad. Pelvic/lower extremity radiograph (**Fig. 159.1c**) shows bowed femurs with a prominent medial spur of the proximal metaphysis. Small iliac wings, small sacro-

sciatic notches, and horizontal acetabular roofs are seen. Frontal and lateral radiographs of the second infant (**Fig. 159.1d,e**) show a small chest with short ribs. There is severe flattening of the vertebral bodies and generalized narrowing of the interpediculate spaces. This produces a u-shaped or h-shaped appearance of the vertebral bodies on the frontal projection.





■ Diagnosis

Thanatophoric Dysplasia

■ Discussion and Differential Diagnosis

Thanatophoric dysplasia is the most common lethal skeletal dysplasia in neonates, affecting 1 in 20,000 live births. It is characterized by marked short limb dwarfism with a large head, curved limbs, near-normal trunk length, small chest, and death shortly after birth.^{1–3} There are two types. Type 1 may have characteristic bowing of long bones (“French telephone receiver” appearance). Type 2 is associated with clover-leaf de-

formity of the skull, or kleeblattschädel.² Thanatophoric dysplasia is usually diagnosed in the second trimester with fetal ultrasound.⁴ 3D and 4D ultrasound may be used to enhance the precise diagnosis.⁵ Thanatophoric dwarfism may closely resemble homozygous achondroplasia. The history of two parents with achondroplasia should differentiate the two.

Pearls

- ◆ This disorder is a new autosomal dominant mutation; gene location is on chromosome 4p16.²
- ◆ Thanatophoric dysplasia, achondroplasia, and hypochondroplasia all share the same gene defect.

Pitfall

- ◆ Thanatophoric dwarf with kleeblattschädel usually has straight femurs.²

References

1. McAlister WH. Current concepts: an approach to skeletal dysplasias. In: Seibert JJ, ed. *A Categorical Course in Pediatric Radiology*. Chicago: RSNA; 1994:101
2. Taybi H, Lachman RS. *Radiology of Syndromes. Metabolic Disorder, and Skeletal Dysplasias*, 5th ed. Philadelphia: Mosby; 2007:1092–1095
3. Greenfield GB. *Radiology of Bone Diseases*. Philadelphia: JB Lippincott; 1990:276–277
4. Karczeski B, Cutting GR. Thanatophoric Dysplasia. In: Pagon RA, Adam MP, Ardinger HH, et al, eds. *Gene Reviews* [online]. Seattle: University of Washington; 2013
5. Achiron R, Gindes L, Zalel Y, Lipitz S, Weisz B. Three- and four-dimensional ultrasound: new methods for evaluating fetal thoracic anomalies. *Ultrasound Obstet Gynecol* 2008;32:36–43. [PubMed](#)

Case 160

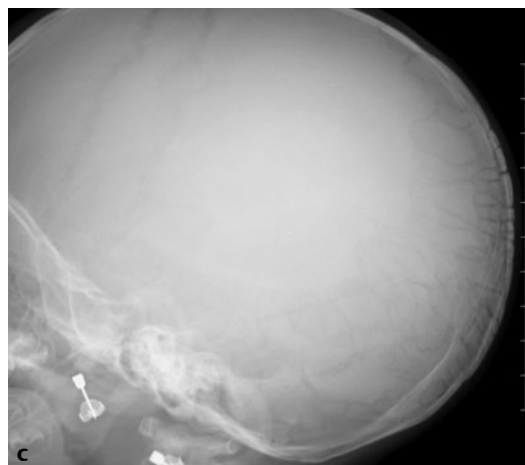
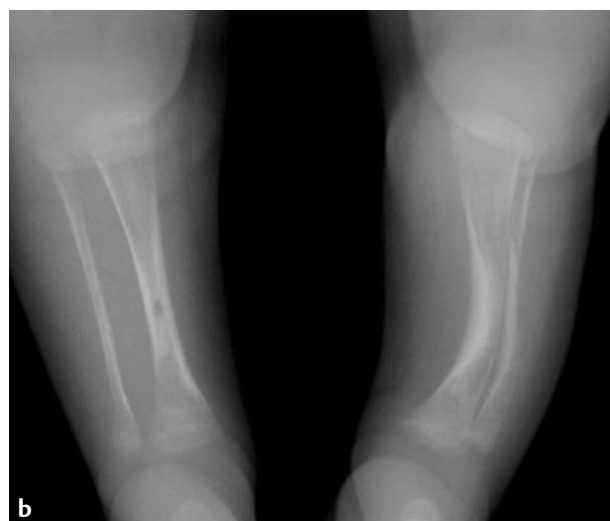
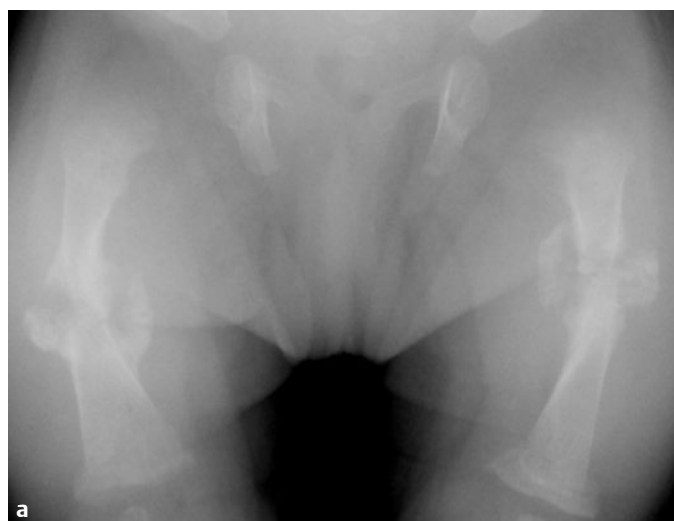
■ Clinical Presentation

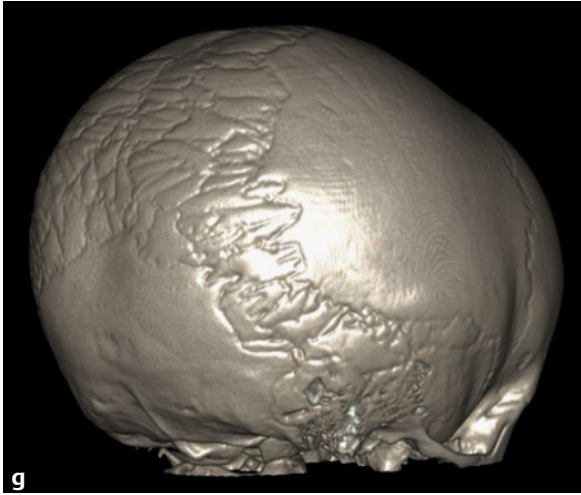
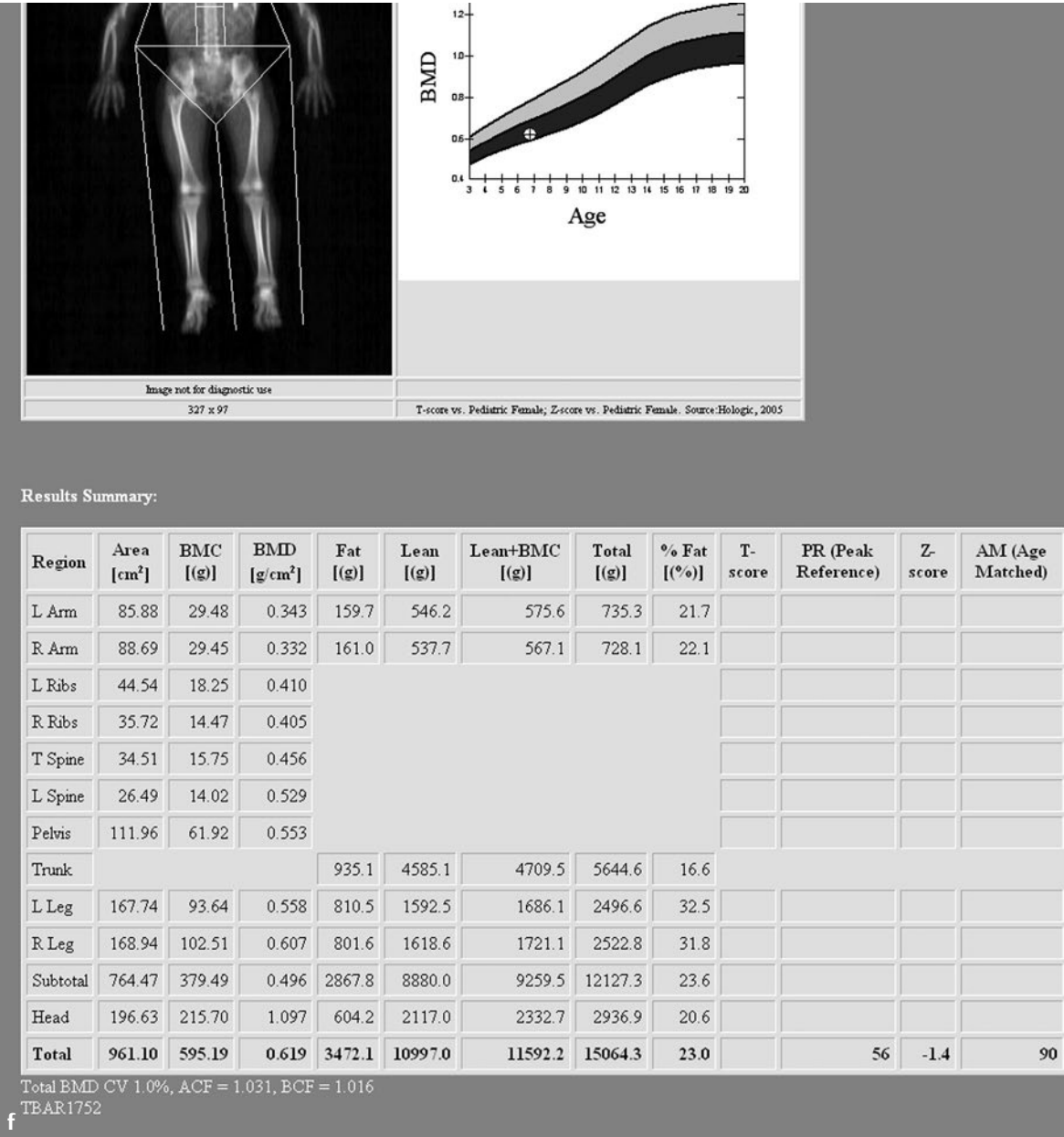
An infant with multiple healing fractures.

■ Radiographic Studies

Radiographs show healing femur fractures (**Fig. 160.1a**), bowed left tibia and fibula (**Fig. 160.1b**), and wormian bones (**Fig. 160.1c**). Radiographs in a different patient, a 13-month-old child (**Fig. 160.1d**) show healing rib fractures and healing frac-

ture of the left humerus. Spine radiograph (**Fig. 160.1e**) shows multiple vertebral body fractures. At 6 years of age this patient has decreased bone density (**Fig. 160.1f**) and wormian bones on 3D head CT (**Fig. 160.1g**).





■ Diagnosis

Osteogenesis Imperfecta

■ Discussion and Differential Diagnosis

Osteogenesis imperfecta (OI) is a genetic disorder characterized by fragile bones, frequent fractures, ligamentous laxity, easy bruising, blue sclera, deafness, poor dentition, and abnormal temperature regulation. There are four major types of OI. Type I is the most common type, with autosomal dominant inheritance, moderately severe bone fragility, blue sclera throughout life, and hearing loss (50% by age 40). Type IA has normal dentition and type IB has abnormal teeth.^{1,2} Type II usually represents a new dominant mutation and is usually lethal in the perinatal period. It is characterized by broad, crumpled, accordion-like long bones, no ossification of the skull, and variable rib beading. Type III is a rare autosomal recessive type that is progressive and nonlethal. It presents with fractures/limb deformities at birth, poor growth, and pulmo-

nary hypertension. Fractures are numerous by 2 years of age.³ Older children with type III may have metaphyseal and diaphyseal widening, “popcorn” calcifications, and hyperplastic callus.^{1,2} Patients affected with autosomal dominant type IV usually have normal sclera and are also divided into two groups depending on the presence of normal or abnormal dentition. Type IV is similar to type I except for the absence of bleeding disorder, less deafness, usually greater long bone deformity, and kyphoscoliosis.

The most frequent differential diagnosis for OI is child abuse. Other considerations would be steroid-induced osteoporosis, juvenile osteoporosis, camptomelic dysplasia, and copper deficiency.^{3,4}

Pearls

- ◆ Osteogenesis imperfecta is the most common diagnosis when short bent limbs are seen at second-trimester fetal ultrasound.^{3,5}
- ◆ Twenty-five percent of patients with OI (especially types I and IV) have basilar invagination.^{3,6}

Pitfall

- ◆ Mild cases of OI in patients with normal teeth may occasionally be difficult to distinguish from child abuse. Patients with OI may have corner metaphyseal fractures as seen in child abuse. Abused children are less likely to have the osteopenia, family history of fractures, or multiple wormian bones seen in OI.⁶

References

1. Campbell JB. Case report 217. Hyperostosis of the calvaria in osteogenesis imperfecta. *Skeletal Radiol* 1982;9:141–143 [PubMed](#)
2. Goldman AB, Davidson D, Pavlov H, Bullough PG. “Popcorn” calcifications: a prognostic sign in osteogenesis imperfecta. *Radiology* 1980;136:351–358. [PubMed](#)
3. Taybi H, Lachman RS. *Radiology of Syndromes. Metabolic Disorder, and Skeletal Dysplasias*, 5th ed. Philadelphia, PA: Mosby. 2007:1018–1024
4. Ablin DS, Greenspan A, Reinhart M, Grix A. Differentiation of child abuse from osteogenesis imperfecta. *AJR Am J Roentgenol* 1990;154:1035–1046 [PubMed](#)
5. Romero R, Pilu G, Jeanty P, et al. *Prenatal Diagnosis of Congenital Anomalies*. Norwalk, CT: Appleton and Lange; 1987:354–357
6. Steiner RD, Adsit J, Basel D. COL1A1/2-Related osteogenesis imperfecta. In: Pagon RA, Adam MP, Ardinger HH, et al, eds. *Gene Reviews* [online]. Seattle: University of Washington; 2005 [updated February 14, 2013]

Case 161

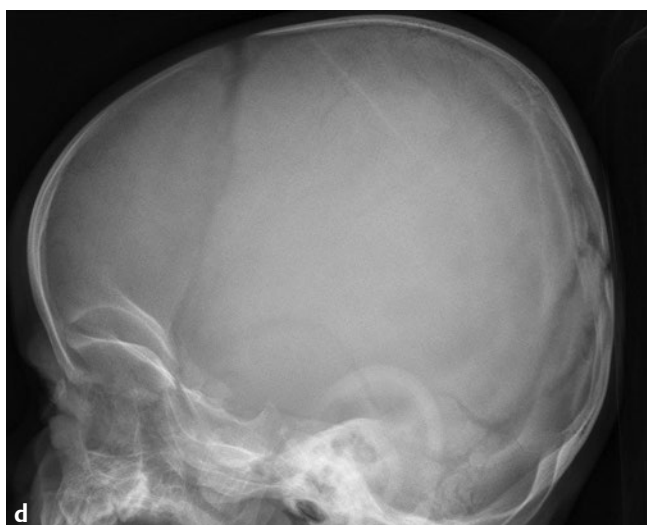
■ Clinical Diagnosis

A 6-month-old with coarse features and feeding difficulty.

■ Radiographic Studies

Radiograph of the chest/abdomen (**Fig. 161.1a**) shows thickened oar-shaped ribs and iliac bones shaped like a ping-pong paddle. Lateral radiograph of the spine (**Fig. 161.1b**) shows kyphosis with a hook dysplasia of the vertebral body at the apex of the gibbus. An AP hand radiograph (**Fig. 161.1c**) shows

osteopenia and diaphyseal widening of the metacarpals and phalanges with pointed proximal ends of the second through fifth metacarpals. Lateral view of the skull (**Fig. 161.1d**) shows a J-shaped sella turcica.



■ Diagnosis

Mucopolysaccharidosis Type I

■ Discussion and Differential Diagnosis

The mucopolysaccharidoses (MPSs) are a group of hereditary metabolic disorders caused by a deficiency of specific lysosomal enzymes that take part in the degradation of mucopolysaccharides. These lysosomal storage disorders result in subsequent intracellular accumulation of mucopolysaccharides in skin, connective tissue, bone, central nervous system tissue, and sometimes the heart and blood vessels. Excess excretion of mucopolysaccharides occurs in urine, and the specific enzyme deficiency is confirmed by fibroblast culture.^{1,2} MPS I or Hurler syndrome (dysostosis multiplex) is the most common of the mucopolysaccharidoses. This progressive autosomal recessive disease is detected clinically in patients by 2 years of age, and is identified by coarse facial features, gibbus spine deformity, rhinorrhea, recurrent respiratory infections, hepatosplenomegaly, and hernias.³ Death is typically caused by cardiorespiratory failure and usually occurs within the first 10 years of life in those with severe disease.⁴ The skull is large and thickened with a J-shaped sella turcica. Bones are expanded, shortened, and pointed at one end, resulting in short pointed metacarpals, “oar-shaped” ribs, steep acetabular roofs,

and a “ping-pong paddle” pelvis. Hunter syndrome (MPS II) has less severe findings than Hurler and is X-linked recessive. Sanfilippo syndrome (MPS III) presents with cognitive/neurologic impairment and behavior changes with little or no coarse facial features.⁵ Morquio syndrome (MPS IV) is detected between the first and third year of life with short-trunk dwarfism secondary to generalized platyspondyly with a characteristic central beak protruding from the vertebral bodies. Other features include ligamentous laxity, odontoid hypoplasia, atlantoaxial subluxation, and normal cognition.⁵ Maroteaux-Lamy syndrome (MPS VI) has normal cognition and somatic manifestations similar to those seen with MPS I, II and VII.⁵ It is characterized by kyphosis at thoracic lumbar regions with wedged-shaped vertebra and irregular fragmentation of the femoral head (avascular necrosis). Most affected children with a mucopolysaccharidosis disorder appear normal at birth, and later in infancy/childhood they begin to display signs or symptoms. One exception is that hydrops fetalis is a common presentation of MPS VII (Sly syndrome).⁶

Pearls

- ◆ Normal intelligence and corneal clouding may be seen in some types of mucopolysaccharidoses such as Morquio (MPS IV) and Maroteaux-Lamy syndromes (MPS VI).
- ◆ When neurologic decline occurs with MPS, odontoid hypoplasia with C1–2 instability or thickening of the dura mater with cord compression at the craniocervical junction should be considered.⁷
- ◆ Treatment modalities consist of bone marrow transplantation, enzyme replacement therapy, and gene therapy.⁸

Pitfalls

- ◆ Patients with mucopolysaccharidoses may be normal at birth except for joint stiffness.
- ◆ Beaking of the inferior vertebral bodies at the thoracolumbar junction (**Fig. 161.1e**) may be seen in mucopolipidosis type II (I-cell disease) and mimics Hurler syndrome.³

References

1. Eggli KD, Dorst JP. The mucopolysaccharidoses and related conditions. *Semin Roentgenol* 1986;21:275–294. [PubMed](#)
2. Grossman H, Dorst JP. The mucopolysaccharidoses and mucopoliposes. In: Kaufmann HJ, ed. *Progress in Pediatric Radiology, Vol 4: Intrinsic Diseases of Bones*. Basel: Karger; 1973:495–544
3. Lachman RS. Syndromes and metabolic disorders: mucopolipidosis II. In: Taybi and Lachman's *Radiology of Syndromes, Metabolic Disorders, and Skeletal Dysplasias*, 5th ed. Philadelphia: Mosby Elsevier; 2007:524–525
4. Clarke LA, Heppner J. Mucopolysaccharidosis type I. *Gene Reviews*. October 31, 2002. Updated July 21, 2011. <http://www.ncbi.nlm.nih.gov/books/NBK1162/>
5. Muenzer J. Overview of the mucopolysaccharidoses. *Rheumatology (Oxford)* 2011;50(5, Suppl 5):v4–v12. [PubMed](#)
6. Muenzer J. The mucopolysaccharidoses: a heterogeneous group of disorders with variable pediatric presentations. *J Pediatr* 2004;144(5, Suppl):S27–S34. [PubMed](#)
7. Taccone A, Tortori Donati P, Marzoli A, Dell'Acqua A, Gatti R, Leone D. Mucopolysaccharidosis: thickening of dura mater at the craniocervical junction and other CT/MRI findings. *Pediatr Radiol* 1993;23:349–352. [PubMed](#)
8. Fang-Kircher S. [Mucopolysaccharidoses—current aspects of diagnosis and therapy]. *Wien Klin Wochenschr* 1995;107:698–701. [PubMed](#)

Case 162

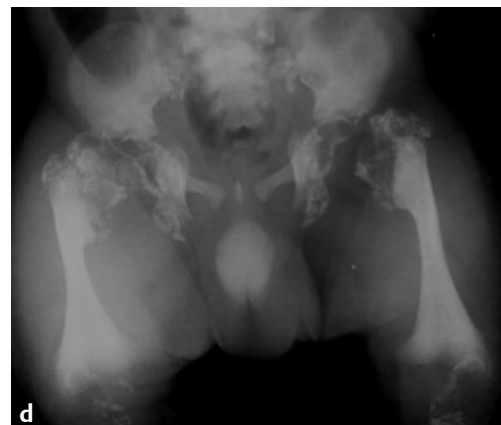
■ Clinical Presentation

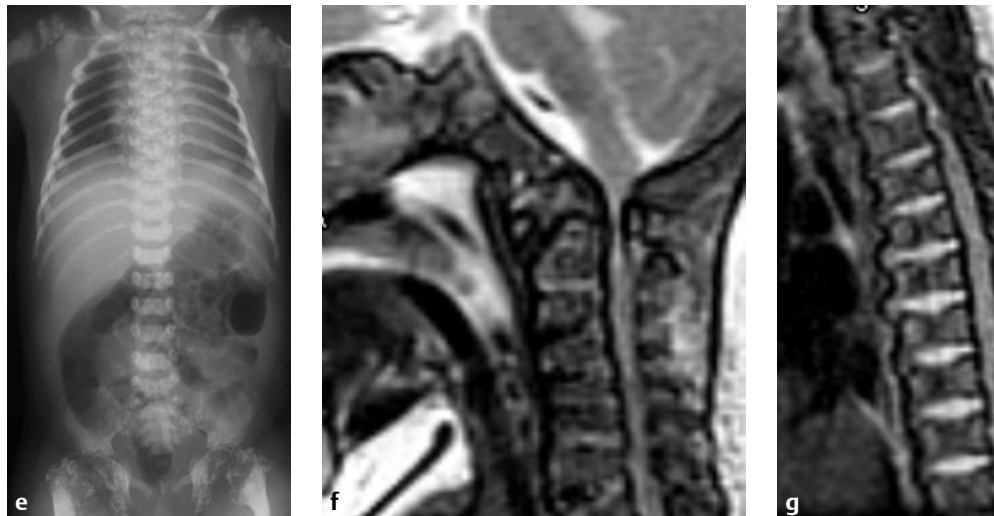
A newborn with limb shortening, flat nasal bridge, cataracts, high arched palate, and linear and blotchy skin lesions.

■ Radiographic Studies

Radiograph of the pelvis (**Fig. 162.1a**) shows stippled calcifications about the hips and knees with one femur shorter than the other. Lateral radiograph of the spine (**Fig. 162.1b**) shows punctate calcific deposits in the cartilaginous skeleton of the spinal column, sternum, and rib ends. Seven months later the stippling has greatly decreased (**Fig. 162.1c**). Radiographs in a

second newborn with alopecia and skin lesions (**Fig. 162.1d,e**) show symmetric shortening of the long bones, punctate calcifications in the periarticular regions, and mild stippling of the axial skeleton. Sagittal T2-weighted MRI (**Fig. 162.1f,g**) shows foramen magnum stenosis and coronal clefts in several thoracic vertebrae.





■ Diagnosis

Chondrodysplasia Punctata

■ Discussion and Differential Diagnosis

Chondrodysplasia punctata (stippled epiphyses syndrome) entails aberrant deposition of calcium during endochondral bone formation and results in abnormal cartilaginous stippling on radiographs.¹ Several classification systems of chondrodysplasia punctata have been suggested. The two major types are the more common genetically heterogeneous nonrhizomelic type (Conradi-Hünermann type) and the rare autosomal recessive rhizomelic type. The nonrhizomelic type is milder, with subtle anomalies; prenatal diagnosis is less common.^{1,2} This type is associated with normal intelligence, characteristic flat nose, asymmetrical shortening of the limbs, and lower incidence of cataracts (17%). Spinal stenosis, spinal instability, and tracheal stenosis may be later sequelae. In contrast, the rhizomelic type is typically lethal, with serious anomalies and a more confident prenatal diagnosis. It is characterized by severe psychomotor

retardation and a higher incidence of cataracts (72%). This type has symmetric limb shortening, less laryngeal/tracheal calcifications, and more commonly has coronal clefts in the vertebral bodies.

A milder form of chondrodysplasia punctata called the Sheffield type typically presents later in infancy as failure to thrive, typical facies, mild mental retardation, and diffuse calcaneus stippling.³ Radiographic stippling can be observed in a range of disorders, including fetal exposure to warfarin or alcohol, chromosome syndromes (18 and 21), and Zellweger syndrome.⁴ The stippled calcifications in Zellweger syndrome are primarily in the patellae.⁵ The epiphyseal calcifications in fetal alcohol syndrome are regularly located in the lower limbs and rarely found in the upper limbs.⁶

Pearl

- ◆ The recessive form of chondrodysplasia punctata is characterized by symmetrical short humeri compared with asymmetrical shortening in the Conradi-Hünermann type.

Pitfall

- ◆ The rhizomelic form of chondrodysplasia punctata may have mild or absent stippling of the axial skeleton. Coronal clefts of the vertebrae can be a real clue to the diagnosis.

References

1. Irving MD, Chitty LS, Mansour S, Hall CM. Chondrodysplasia punctata: a clinical diagnostic and radiological review. *Clin Dysmorphol* 2008;17:229–241. [PubMed](#)
2. Pryde PG, Bawle E, Brandt F, Romero R, Treadwell MC, Evans MI. Prenatal diagnosis of nonrhizomelic chondrodysplasia punctata (Conradi-Hünermann syndrome). *Am J Med Genet* 1993;47:426–431. [PubMed](#)
3. Sheffield LJ, Danks DM, Mayne V, Hutchinson AL. Chondrodysplasia punctata—23 cases of a mild and relatively common variety. *J Pediatr* 1976; 89:916–923. [PubMed](#)
4. Taybi H, Lachman RS. *Radiology of Syndromes, Metabolic Disorders, and Skeletal Dysplasias*, 5th ed. Philadelphia: Mosby; 2007:900–907
5. Poznanski AK. Punctate epiphyses: a radiological sign not a disease. *Pediatr Radiol* 1994;24:418–424, 436. [PubMed](#)
6. Leicher-Düber A, Schumacher R, Spranger J. Stippled epiphyses in fetal alcohol syndrome. *Pediatr Radiol* 1990;20:369–370. [PubMed](#)

Case 163

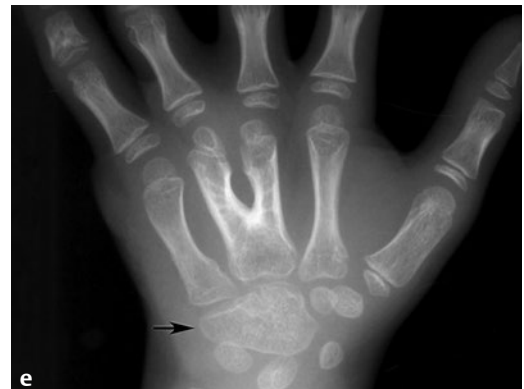
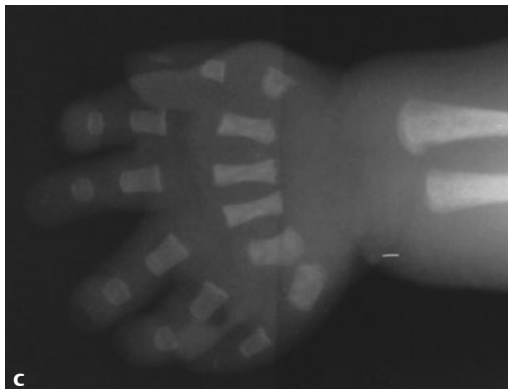
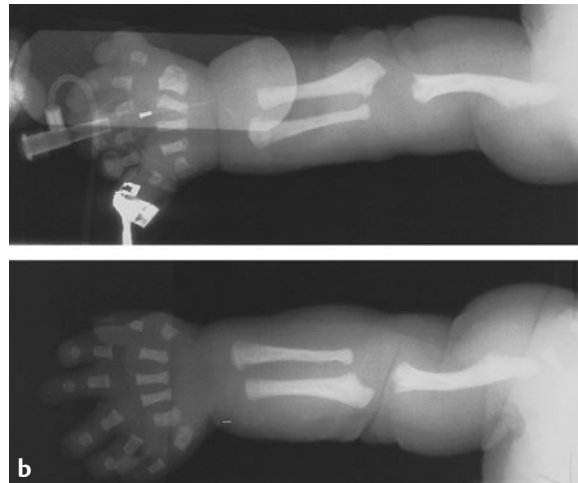
■ Clinical Presentation

A newborn with polydactyly, hypoplastic nails and teeth, sparse hair, and atrial septal defect (ASD).

■ Radiographic Studies

Radiograph of the chest/abdomen (**Fig. 163.1a**) shows a small chest compared with the abdomen, short ribs, and an enlarged heart. The sacrosciatic notch in the pelvis is small, and the acetabulum is saw-toothed. The proximal femoral epiphyses are prematurely present (normally appear at age 6 months). A radiograph of both shortened upper extremities (**Fig. 163.1b**) shows an enlarged proximal ulna and distal radius bilaterally,

polydactyly, and short tubular bones of the hands. There is a short medial and long lateral slope to the metaphysis of the proximal humerus. Radiograph of the hand (**Fig. 163.1c**) again shows polydactyly and short wide tubular bones. Radiograph of the lower extremity (**Fig. 163.1d**) shows mesomelic shortening (affecting the tibia and fibula more than the femur).



■ Diagnosis

Chondroectodermal Dysplasia

■ Discussion and Differential Diagnosis

Chondroectodermal dysplasia (Ellis–van Creveld [EVC] syndrome) is an autosomal recessive chondral and ectodermal dysplasia. Common abnormalities include short ribs, polydactyly, growth retardation, heart defects, and ectodermal abnormalities.¹ Ectodermal defects include dysplasia/hypoplasia of teeth and nails and sparse hair. Common skeletal manifestations include mesomelic dwarfism (shortening in the “middle” long bones) with shortening in the radius/ulna and tibia/fibula, as well as acromelic shortening (hands and feet).^{2,3} Middle phalanges of digits 2 to 5 may be cone-shaped. Polycarpaly or a ninth carpal bone is present in all patients older than 5 years. It is located in the distal carpal row, proximal to the fifth metacarpal and accessory sixth metacarpal.⁴

Chondroectodermal dysplasia is one of the short rib polydactyly syndromes. The diagnosis should be suspected on pre-

natal ultrasound when observing growth retardation, small chest, congenital heart disease (60%), short limbs, and polydactyly (100%).^{1,5} In EVC syndrome, unlike achondroplasia, the skull and spine are normal.⁶ The major postnatal differential diagnosis of EVC is asphyxiating thoracic dystrophy (ATD) or Jeune syndrome, which has similar radiographic findings.^{1–3} The presence of congenital heart disease (usually ASD or single atrium), supernumerary digits, carpal abnormalities, and ectodermal dysplasia favors the diagnosis of EVC syndrome over ATD.¹ The respiratory distress, small chest, hypoplastic lungs, and shortened ribs are usually more severe in ATD. Survivors with ATD develop a progressive nephropathy and hepatic dysfunction that are not seen in EVC syndrome.^{2,3}

Pearls

- ◆ The terminal phalanges in adults with chondroectodermal dysplasia are so short that affected persons cannot make a closed fist.
- ◆ Carpal fusion (**Fig. 163.1e**, arrow) is a frequent observation in older children.
- ◆ One of largest numbers of patients with EVC syndrome was first described by McKusick in the Amish population.⁶

Pitfall

- ◆ The characteristic pelvis seen in infancy becomes normal in childhood.⁷

References

1. Baujat G, Le Merrer M. Ellis-van Creveld syndrome. *Orphanet J Rare Dis* 2007;2:27 [PubMed](#)
2. Hanissian AS, Riggs WW Jr, Thomas DA. Infantile thoracic dystrophy—a variant of Ellis-Van Creveld syndrome. *J Pediatr* 1967;71:855–864 [PubMed](#)
3. Cortina H, Beltran J, Olague R, Ceres L, Alonso A, Lanuza A. The wide spectrum of the asphyxiating thoracic dysplasia. *Pediatr Radiol* 1979;8:93–99 [PubMed](#)
4. Taylor GA, Jordan CE, Dorst SK, Dorst JP. Polycarpaly and other abnormalities of the wrist in chondroectodermal dysplasia: the Ellis-van Creveld syndrome. *Radiology* 1984;151:393–396 [PubMed](#)
5. Qureshi F, Jacques SM, Evans MI, Johnson MP, Isada NB, Yang SS. Skeletal histopathology in fetuses with chondroectodermal dysplasia (Ellis-van Creveld syndrome). *Am J Med Genet* 1993;45:471–476 [PubMed](#)
6. Lachman RS. Syndromes and metabolic disorders: chondroectodermal dysplasia. In: Taybi and Lachman's *Radiology of Syndromes, Metabolic Disorders, and Skeletal Dysplasias*, 5th ed. Philadelphia: Mosby Elsevier, 2007:910–912
7. Silverman FN. A differential diagnosis of achondroplasia. *Radiol Clin North Am* 1968;6:223–237 [PubMed](#)

Case 164

Clinical Presentation

A 5-year-old with a swollen, hard, and red shoulder after minor trauma.

Radiographic Studies

Radiograph of the shoulder (**Fig. 164.1a**) shows swelling and early bone formation in the soft tissues overlying the proximal humerus. Follow-up radiographs (**Fig. 164.1b,c**) show progressive soft tissue bone formation. Radiograph of the hands (**Fig. 164.1d**) shows bilateral clinodactyly (*arrowhead*) and

hypoplastic first metacarpals. Radiographs of the feet (**Fig. 164.1e**) demonstrates short great toes bilaterally with bilateral hallux valgus. Joint space narrowing between the first metatarsal and a hypoplastic proximal phalanx is seen on the right; synostosis of this same joint is seen on the left (*arrow*).



■ Diagnosis

Myositis Ossificans Progressiva

■ Discussion and Differential Diagnosis

Myositis ossificans progressiva (fibrodysplasia ossificans progressiva) is an autosomal dominant mesodermal disorder characterized by swelling and progressive ossification of the fasciae, aponeuroses, ligaments, tendons, and connective tissue of skeletal muscle.¹ The average age at onset is 5 years, with the heterotopic ossification proceeding from the axial to appendicular skeleton as well as in a cranial to caudal and proximal to distal direction. Pain and stiffness of the spine or an inflammatory mass are common presenting features of myositis ossificans progressiva.² Radionuclide imaging and CT are sensitive for new bone formation; however, no effective

therapy is available.²⁻⁵ Diagnosis can be confirmed in patients with soft tissue swelling or ossification by the presence of the congenital osseous anomalies of the thumb and great toe. Hallux valgus is frequently found.

Circumscribed posttraumatic ossifying myositis is the most important differential diagnosis. It is characterized by the appearance of painful ossifications in young adults, following a trauma limited to one location.⁶ The diagnosis may also be confused with multiple exostoses, Klippel-Feil syndrome, dermatomyositis, and calcific myonecrosis.^{5,7}

Pearls

- ◆ Shortening of the great toe with ankylosis of the interphalangeal joint and ankylosis of the metatarsophalangeal joint with absence of one phalanx are the anomalies most commonly seen.
- ◆ The first metacarpal as well as many of the phalanges often are hypoplastic.^{8,9}

Pitfalls

- ◆ Biopsy should be avoided, as it may accelerate disease progression, and histology has been confused with malignancy.¹⁰
- ◆ Involvement of the spine often leads to complete fusion mimicking ankylosing spondylitis.²

References

1. Taybi H, Lachman RS. Radiology of Syndromes, Metabolic Disorders, and Skeletal Dysplasias, 5th ed. Philadelphia: Mosby; 2007:268–271
2. Bridges AJ, Hsu KC, Singh A, Churchill R, Miles J. Fibrodysplasia (myositis) ossificans progressiva. *Semin Arthritis Rheum* 1994;24:155–164 [PubMed](#)
3. Guze BH, Schelbert H. The nuclear medicine bone image and myositis ossificans progressiva. *Clin Nucl Med* 1989;14:161–162 [PubMed](#)
4. Reinig JW, Hill SC, Fang M, Marini J, Zasloff MA. Fibrodysplasia ossificans progressiva: CT appearance. *Radiology* 1986;159:153–157 [PubMed](#)
5. Baysal T, Elmali N, Kutlu R, Baysal O. The stone man: myositis (fibrodysplasia) ossificans progressiva. *Eur Radiol* 1998;8:479–481 [PubMed](#)
6. Trigui M, Ayadi K, Zribi M, Triki Z, Keskes H. Fibrodysplasia ossificans progressiva: diagnosis and surgical management. *Acta Orthop Belg* 2011; 77:139–144 [PubMed](#)
7. Seibert JJ, Morrissy RT, Fuller J, Young LW. Radiological case of the month: fibrodysplasia ossificans progressiva. *Am J Dis Child* 1983;137:77–78 [PubMed](#)
8. Singleton EB, Holt JF. Myositis ossificans progressiva. *Radiology* 1954;62: 47–54 [PubMed](#)
9. Thickman D, Bonakdar-pour A, Clancy M, Van Orden J, Steel H. Fibrodysplasia ossificans progressiva. *AJR Am J Roentgenol* 1982;139:935–941 [PubMed](#)
10. Rogers JC, Geho WB. Fibrodysplasia ossificans progressiva. A survey of forty-two cases. *J Bone Joint Surg Am* 1979;61:909–914 [PubMed](#)

Case 165

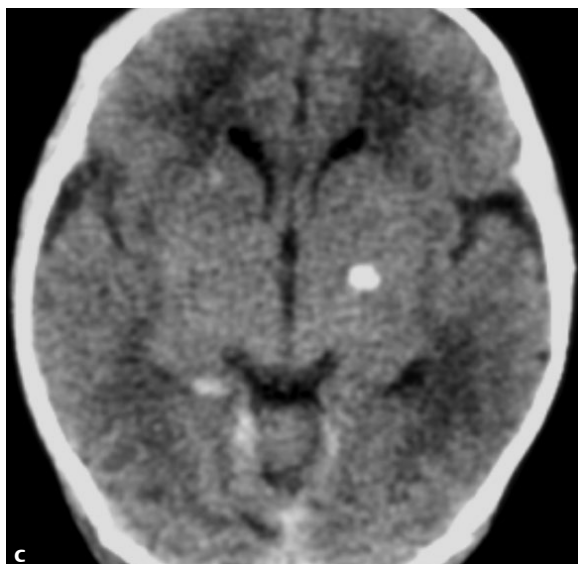
■ Clinical Presentation

An infant with thrombocytopenia and bilaterally deformed forearms and hands.

■ Radiographic Studies

Radiographs of both forearms and hands (**Fig. 165.1a,b**) show that both radii are absent, but the thumbs are present. Both hands are at right angles to the forearm. Noncontrast CT of the

head (**Fig. 165.1c**) demonstrates multiple sites of small high attenuation hemorrhage in the brain parenchyma.



■ Diagnosis

Thrombocytopenia–Absent Radius

■ Discussion and Differential Diagnosis

Thrombocytopenia–absent radius (TAR) syndrome is characterized by bilateral absent radii with associated thrombocytopenia secondary to leukemoid reaction, and hypercellular bone marrow with absent or markedly reduced megakaryocytes.¹ The prenatal diagnosis of TAR syndrome, utilizing ultrasound and cordocentesis, has been described.² Cardiac defects are common (22%) and cognitive development is normal.^{1,3,4}

Three other diseases should be included in the differential diagnosis: Fanconi anemia, Holt–Oram, and Roberts’ syndrome.³

Fanconi anemia patients have thrombocytopenia; absent, hypoplastic, or supernumerary thumbs; and renal anomalies. Patients with Holt–Oram have upper extremity/thumb anomalies and cardiac defects with no hematological disorder. Patients with Roberts’ syndrome have intellectual disability, cleft lip/palate, and reduction anomalies of the hands and feet (thumb aplasia or hypoplasia), but have no clinically significant thrombocytopenia.^{1,3,4}

Pearl

- ◆ The thumb is always present and nearly normal in size.⁴

Pitfall

- ◆ The humerus is absent in 5 to 10% of cases; digits may arise from the shoulder.¹

References

1. Taybi H, Lachman RS. Radiology of Syndromes. Metabolic Disorder, and Skeletal Dysplasias, 5th ed. Philadelphia: Mosby; 2007:781–783
2. Shelton SD, Paulysen K, Kay HH. Prenatal diagnosis of thrombocytopenia absent radius (TAR) syndrome and vaginal delivery. *Prenat Diagn* 1999;19: 54–57. [PubMed](#)
3. Hedberg VA, Lipton JM. Thrombocytopenia with absent radii. A review of 100 cases. *Am J Pediatr Hematol Oncol* 1988;10:51–64. [PubMed](#)
4. Toriello HV. Thrombocytopenia Absent Radius Syndrome. Gene Reviews. December 8, 2009. Updated May 29, 2014. <http://www.ncbi.nlm.nih.gov/books/NBK23758/>

Case 166

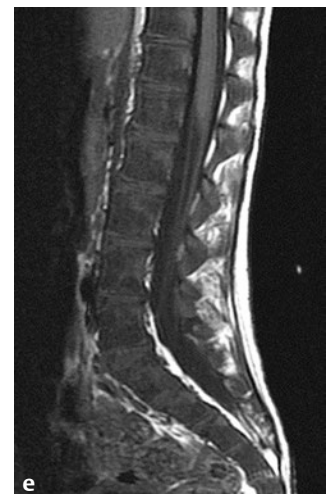
Clinical Presentation

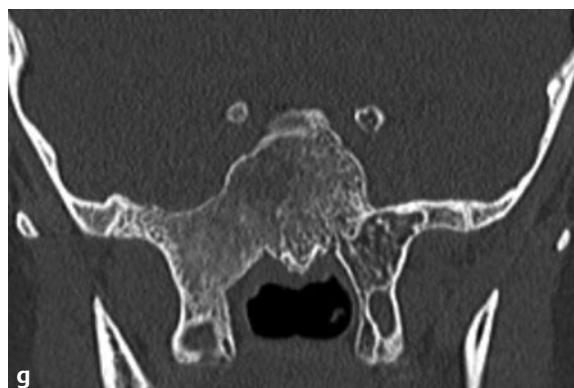
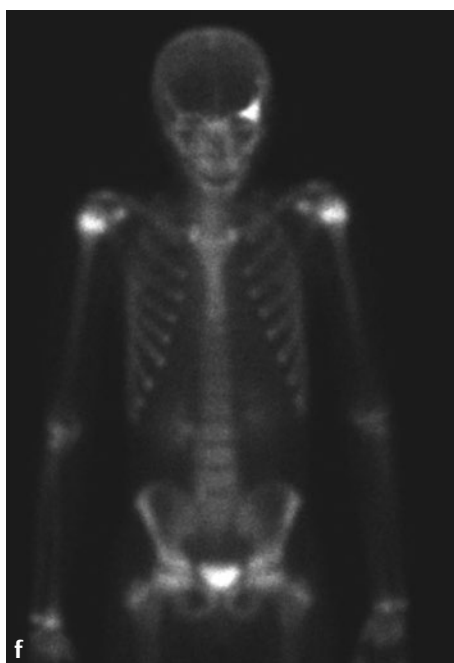
A 2-year-old with right tibial fracture, café-au-lait skins lesions, and hyperthyroidism.

Radiographic Studies

Right lower extremity radiographs (**Fig. 166.1a**) show patchy lucent lesions scattered throughout the long bones with some associated sclerosis. Healing pathological fracture of the proximal third right fibula (*arrowhead*) and “ground-glass” lesion of the distal third right tibia (*asterisk*) are noted. Follow-up radiographs at age 6 years (**Fig. 166.1b**) show progression of long lucent lesions in the long bones. Bony expansion and varus deformity of the proximal right femur is seen. Lateral skull ra-

diograph (**Fig. 166.1c**) shows expansion and deformity of the calvaria and mandible. The skull base thickening is sclerotic, whereas the remaining calvaria displays mottled oval lucencies and ground-glass diploic widening. Hand radiograph (**Fig. 166.1d**) shows medullary sclerosis and widening of multiple metacarpals and phalanges. Sagittal T1-weighted MRI (**Fig. 166.1e**) shows low signal marrow throughout the lumbosacral spine.





■ Diagnosis

Polyostotic Fibrous Dysplasia

■ Discussion and Differential Diagnosis

Fibrous dysplasia (FD) has been regarded as a developmental skeletal disorder characterized by replacement of normal bone with benign cellular fibrous connective tissue.¹ It can affect one bone (monostotic form) or multiple bones (polyostotic form). The latter form may be part of the McCune-Albright syndrome.¹ Originally, this syndrome was defined by the triad of polyostotic FD, café-au-lait skin pigmentation, and precocious puberty. It was later recognized that other endocrinopathies, including hyperthyroidism, acromegaly, hyperparathyroidism, and Cushing syndrome, could be found in association with the original triad.^{2,3}

The monostotic form of fibrous dysplasia is twice as common as the polyostotic form and typically affects the 20- to 30-year age group.¹ Patients with monostotic FD may be asymptomatic, with bony lesions detected as an incidental finding on radiological studies obtained for other reasons.³ Polyostotic FD has its onset generally before the age of 10 years; the lesions grow with the child, and usually stabilize after puberty. Polyostotic FD most commonly involves craniofacial bones, ribs, and metaphysis/diaphysis of the proximal femur or tibia. The craniofacial bones are affected in a majority of cases of polyostotic FD, and any cranial or facial bone can be affected. The clinical features depend on the bones affected. Signs and symptoms can include facial pain, headache, cranial asymmetry, facial deformity, tooth displacement, and visual or auditory impairment.¹

The radiological features of FD are diverse and are dependent on the proportion of mineralized bone to fibrous tissue in

the lesion. FD is the most common pediatric bone lesion, with both a lytic and sclerotic component. Characteristically, the softer dysplastic fibrous tissue slowly replaces, weakens, and deforms the normal bone, thinning and expanding the cortex. Involvement of the spine is rare. Early FD of craniofacial bones is typically radiolucent with either ill-defined or well-defined borders; these lesions may be unilocular or multilocular. As the lesions mature, the bony defects acquire a mixed radiolucent/radiopaque appearance, and established FD exhibits mottled radiopaque patterns often described as resembling ground glass, with ill-defined borders blending into normal adjacent bone.¹

Most lesions show increased uptake on bone scintigraphy; however, uptake becomes less intense as the lesions mature.^{4,5}

Fig. 166.1f shows a focal left sphenoid wing lesion (monostotic FD) in a patient evaluated for fever of unknown origin. CT scanning is the best technique for demonstrating the radiographic characteristics of fibrous dysplasia as well as defining the extent of the disease.^{4,6} Coronal reformatted CT image (**Fig. 166.1g**) shows an expansile ground-glass right sphenoid/pterygoid lesion in a patient with right-sided headaches and facial swelling. On MRI, the FD lesions are largely isointense with areas of hypointensity on T1-weighted images (**Fig. 166.1e**) and appear heterogeneously hyperintense on T2-weighted images. The MRI enhancement pattern is variable/patchy and reflects the variable tissue components of this entity.⁷

Differential diagnosis in children includes Langerhans cell histiocytosis, simple bone cyst, enchondroma, and aneurysmal bone cyst.

Pearls

- ◆ Fibrous dysplasia is typically a “long lesion in a long bone.”
- ◆ The proximal femoral lesion has the appearance of a shepherd’s crook deformity.
- ◆ Cherubism is a hereditary form of FD involving the mandible.
- ◆ Fibrous dysplasia is occasionally associated with hypophosphatemic vitamin D–resistant rickets (oncogenic rickets).

Pitfalls

- ◆ Epiphyseal involvement has been described in polyostotic FD before closure of the growth plate.⁸
- ◆ Fibrous dysplasia of the tibia often simulates ossifying fibroma and adamantinoma histologically and radiographically.⁹
- ◆ True chondrosarcomatous transformation of FD is rare (0.5%).⁸ An unusual complication of FD, especially in the femoral neck, is fibrocartilaginous dysplasia, which may be misdiagnosed as malignant. There is rapid growth of the lesion, with increased density and extensive calcifications.¹⁰

References

1. Feller L, Wood NH, Khammissa RA, Lemmer J, Raubenheimer EJ. The nature of fibrous dysplasia. *Head Face Med* 2009;5:22 [PubMed](#)
2. Dumitrescu CE, Collins MT. McCune-Albright syndrome. *Orphanet J Rare Dis* 2008;3:12 [PubMed](#)
3. Kransdorf MJ, Moser RP Jr, Gilkey FW. Fibrous dysplasia. *Radiographics* 1990;10:519–537 [PubMed](#)
4. DiCaprio MR, Enneking WF. Fibrous dysplasia. Pathophysiology, evaluation, and treatment. *J Bone Joint Surg Am* 2005;87:1848–1864 [PubMed](#)
5. Machida K, Makita K, Nishikawa J, Ohtake T, Iio M. Scintigraphic manifestation of fibrous dysplasia. *Clin Nucl Med* 1986;11:426–429 [PubMed](#)
6. Daffner RH, Kirks DR, Gehweiler JA Jr, Heaston DK. Computed tomography of fibrous dysplasia. *AJR Am J Roentgenol* 1982;139:943–948 [PubMed](#)
7. Shah ZK, Peh WC, Koh WL, Shek TW. Magnetic resonance imaging appearances of fibrous dysplasia. *Br J Radiol* 2005;78:1104–1115 [PubMed](#)
8. Nixon GW, Condon VR. Epiphyseal involvement in polyostotic fibrous dysplasia. A report of two cases. *Radiology* 1973;106:167–170 [PubMed](#)
9. Resnick D, Sartoris D. *Bone Disease*, vol IV. Reston, VA: American College of Radiology; 1989:637–638
10. Pelzmann KS, Nagel DZ, Salyer WR. Case report 114. *Skeletal Radiol* 1980;5:116–118 [PubMed](#)

Case 167

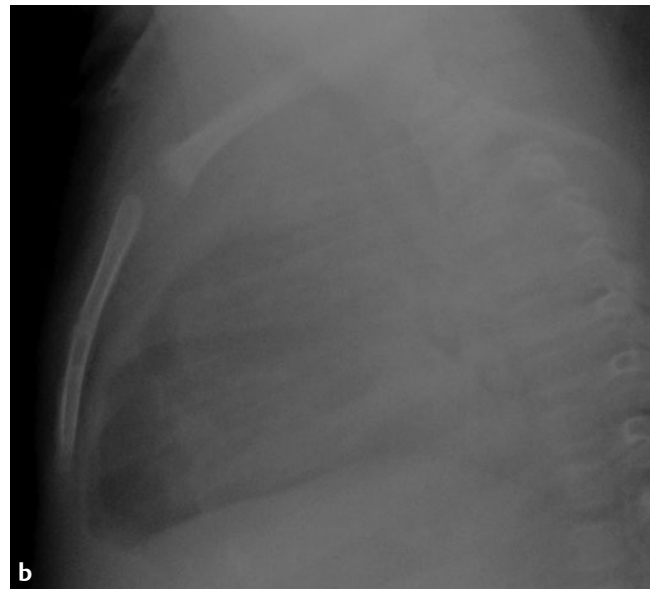
■ Clinical Presentation

An infant with chylothorax and cardiomyopathy.

■ Radiographic Studies

Anteroposterior chest radiograph (**Fig. 167.1a**) shows an enlarged heart and left pleural effusion. Lateral chest radiograph (**Fig. 167.1b**) shows pectus carinatum deformity with elonga-

tion of the manubrium. The body of the sternum is short, with premature fusion of ossification centers.



■ Diagnosis

Noonan Syndrome

■ Discussion and Differential Diagnosis

Noonan syndrome is an autosomal dominant syndrome characterized by short stature, congenital heart defect, developmental delay, and mild mental retardation. Unusual chest shape is frequent in over 90% of patients with superior pectus carinatum/inferior pectus excavatum.¹ The sternal abnormalities of manubrium elongation, short body, and premature fusion of the ossification centers of the sternum body is classic in Noonan syndrome. Other findings can include characteristic facies, broad/webbed neck, ocular abnormalities, lymphatic dysplasias, cryptorchidism, and coagulation defects.²⁻⁵ Congenital heart disease occurs in 50 to 80% of individuals, with right-sided lesions more common. Pulmonary valve stenosis is

the most common heart defect (20–50%), followed by hypertrophic cardiomyopathy (20–30%).^{2,3}

Noonan syndrome was initially called male Turner syndrome because the physical appearance is similar to that in Turner syndrome, but the karyotype is normal.² In Turner syndrome, renal anomalies are more common, developmental delay is less frequent, and left-sided heart defects such as aortic stenosis and coarctation predominate.³ Williams syndrome and cardiofaciocutaneous syndrome should also be considered in the differential diagnosis of Noonan syndrome. Williams syndrome patients have short stature, mild mental retardation, typical facies, normocalcemia or hypercalcemia, and, typically, supra-valvular aortic stenosis.²

Pearl

- ◆ Consider Noonan syndrome in a patient with lymphatic abnormality such as lymphedema, chylothorax, pulmonary or intestinal lymphangiectasia, or nonimmune hydrops.⁶⁻⁸

Pitfall

- ◆ Noonan syndrome is difficult to diagnose by facial appearance in the newborn.¹

References

1. Noonan JA. Noonan syndrome. An update and review for the primary pediatrician. *Clin Pediatr (Phila)* 1994;33:548–555. [PubMed](#)
2. Taybi H, Lachman RS. *Radiology of Syndromes, Metabolic Disorders, and Skeletal Dysplasias*, 5th ed. Philadelphia: Mosby; 2007:579–583
3. Allanson JE, Roberts AE. Noonan syndrome. *Gene Reviews*. November 15, 2001. Updated August 4, 2011. <http://www.ncbi.nlm.nih.gov/books/NBK1124/>
4. Romano AA, Allanson JE, Dahlgren J, et al. Noonan syndrome: clinical features, diagnosis, and management guidelines. *Pediatrics* 2010;126:746–759. [PubMed](#)
5. van der Burgt I. Noonan syndrome. *Orphanet J Rare Dis* 2007;2:4. [PubMed](#)
6. Hoeffel JC, Juncker P, Remy J. Lymphatic vessels dysplasia in Noonan's syndrome. *AJR Am J Roentgenol* 1980;134:399–401. [PubMed](#)
7. Hernandez RJ, Stern AM, Rosenthal A. Pulmonary lymphangiectasis in Noonan syndrome. *AJR Am J Roentgenol* 1980;134:75–80. [PubMed](#)
8. Allanson JE. Noonan syndrome. *Am J Med Genet C Semin Med Genet* 2007;145C:274–279. [PubMed](#)

Index

Note: Page numbers set *italic* indicate figures.

A

Abscess
 abdominal, 341, 341–342
 of brain, 53, 53–54
 Brodie's, 270
 epidermoid, 91, 91–92
 epidural, 65, 65–66, 80
 intracranial, 124
 orbital, 97, 97–98
 pelvic, 342
 psoas, 355
 retropharyngeal, 113, 113–114
 subperiosteal, 269, 270
N-Acetylaspartate (NAA), as Canavan
 disease marker, 31, 32
Achondroplasia, 367, 367–368
Acute chest syndrome, of sickle cell
 disease, 303, 303–304
Adenoids, in infectious mononucleosis,
 101, 102
Adenoma sebaceum, 60
Adnexal torsion, 217, 217–218
Adrenal glands, hemorrhage from, 187,
 187–188
Air reduction, of intussusception, 133,
 134
Albers-Schönberg disease. *See* Osteopetrosis
Alexander disease, 32
Alpha-fetoprotein, as hepatoblastoma
 marker, 182
Anemia, Fanconi, 388
Angiofibromas, juvenile nasopharyngeal,
 111, 111–112, 116
Angiography. *See also* Computed tomogra-
 phy angiography; Magnetic
 resonance angiography
 of juvenile nasopharyngeal angio-
 fibroma, 111, 112
Angiomatosis, Weber syndrome-related,
 51, 52
Angiomyolipomas, renal, tuberous
 sclerosis-related, 60
Angioplasty, of renal artery, 357, 358
Aniridia, 190
Ankle, fractures of, 273
Anorectal anomalies, 68
"Anteater sign," 249, 250
Anus, imperforate, 67, 67, 155–156,
 155–157
 cloacal anomalies associated with, 204
Aortic arch, double, 311, 311–312
Aortic coarctation, 335, 335–336
Aortic valve, bicuspid, 331, 331–332
Aortography, of renal artery stenosis, 357
Apert syndrome, 14, 100
Appendicitis, 159, 159–160
 differentiated from ovarian torsion, 218

Appendix testis, torsion of, 185, 185–186,
 242
Arrhythmogenic right ventricular
 dysplasia/cardiomyopathy, 320
Arteriovenous malformations, 326
 differentiated from hemangiomas, 120
 of vein of Galen, 3, 3–4
Arthritis
 juvenile idiopathic, 257–258, 257–259
 septic, 363, 363–364
Ascites
 chylous, 179
 necrotizing enterocolitis-related, 164
 posterior urethral valve-related, 197
Aspartoacylase deficiency, as Canavan
 disease cause, 32
Aspergillomas, differentiated from round
 pneumonia, 280
Aspiration
 of foreign body, 279–280, 279–281
 of meconium, 305, 305–306
Asplenia, 334
ASP triad, 68
Astrocytomas
 giant cell, 59
 hypothalamic, 37, 37–38
 neurofibromatosis type 1-related, 30
 pilocytic, 40
 cerebellar, 57–58, 58
 differentiated from medulloblasto-
 mas, 56
 of spinal cord, 93, 93–94
Atlantoaxial subluxation
 Down syndrome-related, 77, 77–78
 juvenile idiopathic arthritis-related,
 259
Atlantodental interval, 78
Atlanto-occipital dislocation, traumatic,
 71, 71–72
Atlanto-occipital subluxation, 77, 78
Atresia
 anorectal. *See* Anus, imperforate
 biliary, 162, 165, 165–166
 choanal, 99, 99–100
 duodenal, 167, 167–168
 with esophageal atresia, 170
 esophageal, with tracheoesophageal
 fistula, 169, 169–171
 of external auditory canal, 105, 105–106
 ileal, 142, 146, 148
 of small bowel, 145, 145–146
Atrial septal defects, 314
 chondroectodermal dysplasia-related,
 383–384
Autosomal dominant polycystic kidney
 disease, 212, 233, 233–234
Autosomal recessive polycystic kidney
 disease, 211, 211–212

B

Back pain
 epidural abscess-related, 65, 66
 vertebral osteomyelitis-related, 79
Barium studies
 of biliary atresia, 166
 "scout" radiograph in, 68
Beckwith-Wiedemann syndrome, 182
Bezoars, 138
Birth injury, as brachial plexopathy cause,
 63–64
"Blue-dot" sign, of torsed appendix testis,
 186
Bone radiology, 245–276
Bone scans. *See* Bone scintigraphy
Bone scintigraphy
 Ewing sarcoma, 251, 252
 osteomyelitis, 270
 osteosarcoma, 275
 polyostotic fibrous dysplasia, 390
 toddler fractures, 256
Bourneville's disease. *See* Tuberous
 sclerosis
Brachial cleft, type II cysts of, 103,
 103–104
Brachial plexopathy, birth injury-related,
 63, 63–64
Brain
 abscess of, 53, 53–54
 infarction of, 43, 43–44
 neuroimaging of, 3–60
Brain injury, child abuse-related, 15, 15–16
Brain radiology, 3–60
Brainstem anomalies, encephalocele-
 associated, 26
Brain tumors, neurofibromatosis type
 1-related, 30
Bronchiectasis, 299, 300

C

Café-au-lait skin lesions, 29, 30, 69, 390
Calcification
 craniopharyngioma-related, 11, 12, 38
 diffuse polymicrogyria/lissencephaly-
 related, 42
 periventricular, 19, 19, 20, 59, 60
 subcortical, 19, 19
 teratoma-related, 297, 298
 TORCH infection-related, 18
Calvaria, elongated, 5, 5–6
Canavan disease, 31, 31–32
Cardiac radiology, 311–336. *See also*
 X-rays, chest
Cardiomegaly, 313, 314, 323
Cardiomyopathy, 319, 319–321
Caroli disease, 162, 212
Caudal regression syndrome. *See*
 Currarino triad

- Cellulitis, orbital, 97, 97–98
 Central catheters, peripherally inserted, 355, 355–356
 Cephaloceles, 25, 25–26, 48
 Cerebral palsy, 8
 Cervical spine
 atlantoaxial instability of, 77, 77–78
 vertebral osteomyelitis of, 80
 CHARGE syndrome, 100, 170
 Chest radiology, 279–308. *See also* X-rays, chest
 Chiari I malformation, 82
 Chiari II malformation, 24, 81, 81–82
 Chiari III malformation, 26
 Child abuse, injuries associated with, 263–264, 263–264
 brain injuries, 15, 15–16
 differentiated from osteogenesis imperfecta, 377
 Choledochoceles, intraduodenal, 162
 Choledocholithiasis, 162
 Cholesteatomas, of the middle ear, 123, 123–124
 Chondroblastomas, 267, 267–268
 Chondrodysplasia punctata, 381–382, 381–382
 Chordomas, differentiated from sacrococcygeal teratomas, 74
 Classic metaphyseal injuries (CMLs), 265
 “Claw sign,” 189
 Clefts
 brachial, type II cysts of, 103–104, 103
 schizencephalic, 49, 49–50
 Cloacal anomalies, 156, 157, 204
 CLOVES syndrome, 360
 Coarctation of the aorta, 335, 335–336
 Colitis, ulcerative, differentiated from Crohn's disease, 176
 Colostography, of imperforate anus, 156, 156
 Colpocephaly, 23, 23
 Computed tomography
 abdominal abscess, 341, 342
 adrenal hemorrhage, 188
 antrochoanal polyps, 117, 117–118
 appendix/appendicitis, 159, 160
 atlantoaxial instability, 77, 77–78
 autosomal recessive polycystic kidney disease, 212
 brachial cleft type II cysts, 103, 103–104
 brain abscess, 53, 53–54
 bronchiectasis, 299, 300
 bronchogenic cysts, 293, 294
 cardiomyopathy, 321
 cerebellar pilocytic astrocytomas, 58
 Chance fractures, 75, 75–76
 child abuse-related brain injury, 15, 15, 16
 choanal atresia, 99, 99–100
 cholesteatomas, 123, 123–124
 chondroblastomas, 267, 268
 cleidocranial dysplasia, 371
 congenital pulmonary airway malformations (CPAMs), 287, 288
 coronal craniosynostosis, 13, 13
 craniopharyngiomas, 11, 11–12
 Crohn's disease, 175, 176
 cytomegalovirus encephalitis, 19, 19
 diastematomyelia, 83
 duodenal hematomas, 173, 174
 duplication cysts, 152
 ependymomas, 40
 external auditory canal atresia, 105, 105–106
 foreign body aspiration, 280
 hepatoblastomas, 181, 182
 imperforate anus, 67
 infectious mononucleosis, 101, 101–102
 juvenile nasopharyngeal angiofibroma, 111, 111–112
 L Leigh disease, 33, 33–34
 leukemia-related orbital metastases, 107, 107–108
 lymphatic malformations, 359
 medulloblastomas, 55, 55–56
 megaureter, 221
 mesoblastic nephromas, 225, 226
 nasal dermal sinus/dermoid cyst, 47, 47–48
 neuroblastomas, 207, 208, 296
 orbital cellulitis, 97, 97–98
 osteogenesis imperfecta, 376
 osteoid osteoma ablation, 349–350
 osteomyelitis, 270
 osteosarcoma, 275, 276s
 ovarian cysts, 205
 physeal fractures, 273, 274
 pulmonary sequestration, 291
 pyelonephritis, 224
 renal scarring, 232
 rhabdomyosarcomas, 115, 115–116, 236
 sagittal craniosynostosis, 5, 5–6
 Sturge-Weber syndrome, 52
 subdural empyema, 35, 35–36
 subependymal/intraventricular hemorrhage, 46
 tarsal coalition, 249, 250
 temporal bone fractures, 127, 127–128
 teratomas, 74, 298
 tethered spinal cord, 86
 tetralogy of Fallot, 318
 thyroglossal duct cysts, 129, 129–130
 traumatic atlanto-occipital dislocation, 71–72, 72
 tuberous sclerosis, 60
 urachal anomalies, 200
 ureteropelvic junction obstruction, 227
 urolithiasis, 219, 220
 Wilms' tumor, 189, 190
 Computed tomography angiography
 bicuspid aortic valve, 331, 332
 coarctation of the aorta, 336
 D-transposition of the great vessels, 323, 323–324
 hemoptysis, 343, 344
 hypoplastic left heart syndrome, 325, 326
 pulmonary sequestration, 292
 pulmonary sling, 327, 328
 renal artery stenosis, 357, 358
 tetralogy of Fallot, 317
 total anomalous pulmonary venous return, 329, 330
 vascular rings, 311, 312
 vein of Galen malformations, 3, 4
 Computed tomography enterography, of Crohn's disease, 176
 Congenital lobar overinflation, 307, 307–308
 Congenital megacystis/megaureter syndrome, 222
 Congenital pulmonary airway malformations (CPAMs), 287, 287–288, 302, 308
 Congestive heart failure, in neonates, 3, 3–4
 Contrast studies
 Hirschsprung disease, 147, 148
 imperforate anus, 156
 meconium ileus, 141, 142
 meconium plug syndrome, 149, 150
 necrotizing enterocolitis, 164
 small bowel atresia, 145, 146
 Conus medullaris, in tethered cord syndrome, 85, 86
 “Cord knot sign,” 242
 Corpus callosum, agenesis of, 23, 23–24, 25
 Cortex, “agryic,” differentiated from lissencephaly, 42
 Cortical scarring, 231, 231–232
 Cortical scintigraphy, of vesicoureteral reflux, 214
 Cowden syndrome, 56
 Craniocerebral injury, child abuse-related, 15, 15–16
 Craniocervical junction injury, 71, 71–72
 Craniopharyngiomas, 11, 11–12
 differentiated from hypothalamic/optic pathway gliomas, 38
 Craniosynostosis
 coronal, 13, 13–14
 sagittal, 5, 5–6, 14
 Crista galli, fat in, 48
 Crohn's disease, 175, 175–176
 Croup (laryngotracheobronchitis), 125, 125–126
 Crouzon syndrome, 14, 100
 Cryptorchidism, 190
 CT. *See* Computed tomography
 Currarino triad, 68, 74, 156, 157
 Cyanosis, 317–318, 323–324
 Cystic fibrosis, 299, 299–300
 as hemoptysis cause, 343–344
 as meconium ileus cause, 142
 meconium plug syndrome associated with, 150
 Cysts
 aneurysmal bone, 268
 arachnoid, 12
 autosomal dominant polycystic kidney disease-related, 233, 233–234
 biliary ductal, classification of, 162
 brachial cleft type II, 103, 103–104
 bronchogenic, 293, 293–294
 differentiated from congenital lobar overinflation, 308

- choledochal, 161, 161–162
 congenital pulmonary airway malformation-related, 288, 287
 craniopharyngioma-related, 12
 dermoid, 47, 48, 68
 differentiated from orbital abscess, 98
 duplication, 151, 151–152, 168
 differentiated from sacrococcygeal teratomas, 74
 enteric, 68
 epidermoid, differentiated from orbital abscess, 98
 intratumor, differentiated from spinal cord tumors, 94
 medulloblastoma-related, 57, 58
 mesenteric, 200, 204
 mucus retention, 118
 multicystic dysplastic kidney-related, 237–239, 238
 nasal dermoid, 47, 47–48
 ovarian, 205, 205–206
 differential diagnosis of, 200, 204
 perineal, 73, 73–74
 of Rathke cleft, 12
 subependymal, 8
 of superior vermian cistern, 4
 of thyroglossal duct, 129, 129–130
 of umbilical cord, 200
 urachal, 199, 200
 Cytomegalovirus infections, 19, 19–20, 42
- D**
- Dacryocystoceles, differentiated from orbital abscess, 98
 Dejerine-Klumpke palsy, 64
 Dens-basion distance, in children, 72
 Dermal sinus
 definition of, 92
 diastematomyelia-related, 83, 84
 with intraspinal epidermoid/infection, 91, 91–92
 nasal, 47, 47–48
 tethered cord syndrome-related, 86
 Dermoid. *See* Cysts, dermoid
 Diastematomyelia, 83, 83–84, 86
 Di George syndrome, 170
 Dolichocephaly, 6
 Doppler ultrasound
 of testicular torsion, 241, 242
 of vein of Galen malformations, 4
 “Double-bubble sign,” 168
 Down syndrome, 77, 77–78, 156, 157, 170
 “Drooping-lily sign,” 191, 192
 D-transposition of the great vessels, 323, 323–324
 Duchenne muscular dystrophy, 319, 320
 Duodenal-jejunal junction alignment, 177, 178, 179
 Duodenum
 atresia of, 167, 167–168, 170
 hematoma of, 173, 173–174
 stenosis of, 167, 168
 Duplication, gastrointestinal, 134
 Duplication cysts, 68, 74, 151, 151–152, 168
- Dwarfism
 Morquio syndrome-related, 380
 thanatophoric, 373–374
 Dysostosis multiplex, 380
 Dysplasia
 chondroectodermal, 383, 383–384
 cleidocranial, 371, 371–372
 polyostotic fibrous, 389–390, 389–391
 septo-optic, 9, 9–10
 thanatophoric, 88, 373–374
 Dysraphism, spinal, 86
- E**
- Echocardiography, of septal defects, 314
 Ectasia, dural, 70
 Edema, cerebral, differentiated from infarction, 44
 Eisenmenger syndrome, 314
 Elbow, fractures of, 245, 245–246
 Ellis-van Creveld syndrome. *See* Dysplasia chondroectodermal
 Empyema, subdural, 35, 35–36
 Encephalitis, cytomegalovirus-related, 19, 19–20
 Encephaloceles, occipital, 25, 25–26
 Endoscopic retrograde cholangiopancreatography (ERCP), of choledochal cysts, 162
 Ependymomas, 39, 39–40, 58
 hemorrhage associated with, 94
 neurofibromatosis type 2-related, 89, 90
 Epidermoid. *See* Cysts, epidermoid
 Epididymitis, 186
 Epididymitis/epididymo-orchitis, 186, 242
 Epidural space, abscess in, 65, 65–66, 80
 Epiglottitis, 121, 121–122, 126
 Epiphyses
 fractures of, 246, 273, 273–274
 ossified proximal humeral and/or coracoid, 306
 Epstein-Barr virus, 102, 286
 Erb-Duchenne palsy, 64
 Esophagus
 atresia of, with tracheoesophageal fistula, 169, 169–171
 duplication cysts of, 152
 foreign body in, 137–138, 137–139
 Ewing sarcoma, 251, 251–252
 External auditory canal, atresia of, 105, 105–106
- F**
- Familial adenomatous polyposis syndrome, 182
 Fibrodysplasia ossificans progressiva. *See* Myositis ossificans progressiva
 Fibromatosis colli, 109, 109–110
 Filum terminale, thickened, 85, 86
 Fistulae
 arteriovenous, 3, 3–4
 imperforate anus-associated, 155, 156–157
 labyrinthine, 124
 perilymphatic, 128
 tracheoesophageal, 169, 169–171
- Fluoroscopy
 duodenal hematoma, 173, 174
 esophageal atresia with tracheoesophageal fistula, 169
 Hirschsprung disease, 147, 148
 hydrocolpos, 203
 imperforate anus, 156
 malrotation with midgut volvulus, 177–178
 Foramen of Luschka, ependymoma extension through, 39, 40
 Foramen of Magendie, ependymoma extension through, 39, 40
 Foreign body
 aspiration of, 279–280, 279–281
 esophageal, 170, 171
 ingestion of, 137–138, 137–139
 “Four-artery” sign, 312
 Fractures
 “bucket handle,” 263, 265
 Chance, 75–76, 76
 child abuse-related, 16, 263, 264–265
 of the clavicle, 64
 “corner,” 263, 265
 elbow, 245, 245–246
 osteogenesis imperfecta-related, 375–376, 377
 physeal, 273, 273–274
 Salter-Harris classification of, 246, 274
 of the rib, 265
 of the skull, 16
 spinal, 75–76, 76
 of the temporal bone, 127, 127–128
 toddler, 255, 255–256
 Freckling, axillary, 30
 Fukuyama muscular dystrophy, 42
 Fungal infections, differentiated from round pneumonia, 280
- G**
- Gallbladder
 absent, 165
 in biliary atresia, 166
 normal, 161
 Ganglioneuroblastomas, 208, 296
 Ganglioneuromas, 296
 Gardner syndrome, 56, 182
 Gastrointestinal duplication cysts, 151, 151–152
 Gastrointestinal radiology, 133–182
 Gastrojejunostomy, 347, 347–348
 Genitourinary radiology, 185–242
 Germ cell tumors, 38
 mediastinal, 297, 297–298
 Gliomas
 of brainstem, 58
 hypothalamic, 37, 37–38
 nasal, 48
 of optic chiasm, 38
 of optic nerve, 30
 Glycogen storage disease, type 1, 182
 Goldenhar syndrome, 106
 Gray matter, heterotopia of, 17, 17–18, 42

H

Haemophilus influenzae vaccine, 122, 126

Hamartomas
mesenchymal, 182
presacral, 68
tuber cinereum, 38

Hand-Schüller-Christian disease, 248

"Harlequin eye" deformity, 14

Head and neck radiology, 97–130

Hearing loss, temporal bone fracture-related, 128

Hemangioblastomas, multifocal, 90

Hemangiomas
of the head and neck, 119, 119–120
tethered cord syndrome-related, 86

Hematomas
clival, 71, 72
duodenal, 173, 173–174
subdural, child abuse-related, 15, 15–16

Hemicords, 83, 83–84

Hemihypertrophy, 190

Hemoptysis, embolization of, 343, 343–344

Hemorrhage
adrenal, 187, 187–188
differentiated from pulmonary sequestration, 292
ependymoma-related, 94
retinal, child abuse-related, 263
subarachnoid, 71
subdural, child abuse-related, 263
subependymal/intraventricular, 45, 45–46

Henoch-Schönlein purpura, 134, 361

Hepatoblastomas, 181, 181–182

Hepatocellular carcinoma, 182

Heptomegaly, infectious mononucleosis-related, 102

Hernia, congenital diaphragmatic, 301, 301–302

Heterotaxy, 178, 333, 333–334

Heterotopia, of gray matter, 17, 17–18, 42

Hip
developmental dysplasia of, 253, 253–254
septic arthritis of, 363, 363–364

Hirschsprung disease, 147, 147–148, 150

Holoprosencephaly, 21, 21–22

Holt-Oram syndrome, 388

Hunter syndrome, 380

Hurler syndrome, 380

Hyaline membrane disease, 7–8, 45–46

Hydranencephaly, 22

Hydroceles, 186

Hydrocephalus
with absent septum pellucidum, 10
Chiari II malformation-related, 82
medulloblastoma-related, 56
posthemorrhagic, 46
tuberous sclerosis-related, 59

Hydrocephalus, achondroplasia-related, 368

Hydrocolpos, 157, 203, 203–204

Hydrometrocolpos, 204

Hydronephrosis, 156, 157, 214, 226, 361
differential diagnosis of, 206, 238
hydrocolpos-associated, 204
in neonates, 195, 196, 197

Hydroureters, hydrocolpos-related, 204

Hypertension, renovascular, 357, 357–358

Hypospadias, 190

Hypotonia, Leigh disease-related, 33, 34

I

I-cell disease, 380

Ileum, terminal, as appendix mimic, 160

Immotile cilia syndrome, 300

Infarction, cerebral, 43, 43–44

Infectious mononucleosis, 101, 101–102

Inferior vena cava, in heterotaxy, 333, 334

Internal carotid artery angiography, in moyamoya disease, 43

Interventional radiology, 341–364

Intramedullary tumors, neurofibromatosis type 2-related, 89, 90

Intussusception, 133, 133–135
differentiated from duodenal hematoma, 174

"Ivy sign," 44

J

Jaundice
biliary atresia-related, 165–166
differential diagnosis of, 166

K

Kaposiform hemangioendotheliomas, 120

Kasabach-Merritt syndrome, 120

Kidney
autosomal dominant polycystic disease of, 212, 233, 233–234
autosomal recessive polycystic disease of, 211, 211–212
fetal lobulation of, 232
multicystic dysplastic, 226, 237, 237–239

Klippel-Feil syndrome, 386

Klippel-Trenaunay syndrome, 360

L

Ladd's bands, surgical excision of, 178

Langerhans cell histiocytosis, 12, 38
with bone involvement, 247, 247–248
differential diagnosis of, 108, 248, 390
as vertebra plana cause, 87, 87–88

Laryngotracheobronchitis (croup), 125, 125–126

Left heart syndrome, hypoplastic, 325, 325–326

Legg-Calvé-Perthes disease, 261, 261–262

Leigh disease, 33, 33–34

Leptomeningeal angiomas, 51, 52

Leptomeningeal metastases, 40

Leukemia, acute myelogenous, 107–108

Leukoencephalopathy, vacuolating, 32

Leukomalacia, periventricular, 7, 7–8, 24

Lipomas, 74, 85, 86

Lisch nodules, 30

Lissencephaly, 28, 41, 41–42
type 1, 42
type 2, 42

Lumbar spine
fractures of, 75, 75–76, 76
vertebral osteomyelitis of, 79, 79–80

Lumbosacral spine
dermal sinus with intraspinal epidermoid/infection of, 91, 91–92
in neurofibromatosis type 2, 89, 89–90

Lymphatic malformations, sclerotherapy for, 359, 359–360

Lymphoceles, mesenteric, 179

Lymphoma, 285, 285–286
differentiated from teratoma, 298

M

Macrocephaly, Canavan disease-related, 31, 32

Magnetic resonance angiography
coarctation of the aorta, 335, 336
D-transposition of the great vessels, 324
renal artery stenosis, 358
total anomalous pulmonary venous return, 330
vascular rings, 312
vein of Galen malformations, 3, 3

Magnetic resonance cholangiography, of choledochal cyst, 161, 162

Magnetic resonance enterography, of Crohn's disease, 176

Magnetic resonance imaging
adrenal hemorrhage, 188
anorectal anomalies, 68
atlantoaxial instability, 77, 77–78
autosomal recessive polycystic kidney disease, 212
bicuspid aortic valve, 332
brachial cleft cysts type II, 104
brachial plexopathy, 63
brain abscess, 53, 54
bronchogenic cysts, 294
Canavan disease, 31–32, 32
cardiomyopathy, 319, 319–321
cerebellar pilocytic astrocytoma, 57–58, 58
Chance fractures, 75, 75–76
child abuse-related injuries, 15, 15, 16, 263
cholesteatomas, 124
chondroblastomas, 267, 268
congenital diaphragmatic hernia, 302
congenital lobar overinflation, 308
congenital pulmonary airway malformations (CPAMs), 288
coronal craniosynostosis, 13, 13
corpus callosum agenesis, 23, 23, 24
craniopharyngiomas, 11, 11–12
cytomegalovirus encephalitis, 19, 19
dermal sinus with intraspinal epidermoid/infection, 91, 91–92
diastematomyelia, 83, 83–84
duplication cysts, 151, 152
encephaloceles, 25, 25–26
epidural abscess, 65, 65–66
epiglottitis, 121, 121–122

- gray matter heterotopia, 17
hemangiomas, 119, 119–120
hepatoblastomas, 182
holoprosencephaly, 21, 21, 22
hypoplastic left heart syndrome, 326
hypothalamic astrocytomas, 37, 37–38
imperforate anus, 67
juvenile idiopathic arthritis, 258, 258
Langerhans cell histiocytosis, 247, 248
Legg-Calvé-Perthes disease, 261, 262
Leigh disease, 33, 33–34
leukemia-related orbital metastases, 107, 107–108
lissencephaly, 41, 41
medulloblastomas, 55, 55–56
moyamoya disease, 43
myelomeningocele/Chiari II malformation, 81, 81–82
myelomeningoceles, 82
nasal dermal sinus/dermoid cysts, 47, 48
neuroblastomas, 296
neurofibromatosis, 29, 29–30, 89, 89–90
osteoid osteoma ablation, 349
osteomyelitis, 269, 270
osteosarcoma, 275, 276
ovarian cysts, 205
periventricular leukomalacia, 7, 7–8
polymicrogyria, 27–28, 28
polyostotic fibrous dysplasia, 389, 389, 390, 390
pyelonephritis, 224
rhabdomyosarcomas, 115, 115–116, 235, 236
schizencephaly, 49, 49–50
septo-optic dysplasia, 9, 9–10
slipped capital femoral epiphysis, 271, 272
spinal cord astrocytomas, 93–94
Sturge-Weber syndrome, 51, 51–52
subdural empyema, 35, 35–36
subependymal/intraventricular hemorrhage, 45, 46
tarsal coalition, 250
teratomas, 73–74
tetralogy of Fallot, 318
tuberous sclerosis, 59, 59–60
vein of Galen malformation, 3, 3
venous malformations, 345, 346
vertebral osteomyelitis, 79, 79–80
vertebra plana, 87, 87–88
Magnetic resonance proton spectroscopy, of Leigh disease, 33, 33, 34
Magnetic resonance urography, 192
Magnetic resonance venography, of occipital encephaloceles, 25, 25
Magnets, ingestion of, 138
Malrotation
 duodenal, 168
 with midgut volvulus, 177–178, 177–179
Marble bone disease. *See* Osteopetrosis
Maroteaux-Lamy syndrome, 380
Maxillary sinus, antrochoanal polyps of, 117, 117–118
Meckel-Gruber syndrome, 26
Meckel's diverticulum, 153, 153–154
 differential diagnosis of, 152, 154
 as intussusception cause, 134
 rule of 2's for, 154
Meckel's scan, false-positive, 152
Meconium, absent, 155–156
Meconium ileus, 141, 141–142
 cystic fibrosis-related, 300
 differential diagnosis of, 146, 148
Meconium plug syndrome, 149, 149–150
Mediastinal lesions/masses, 285, 286
 bronchogenic cysts, 292–294, 293
 germ cell tumors, 297, 297–298
 neuroblastomas, 295, 295–296
 posterior, neuroblastomas as, 295, 295–296
Medulloblastomas, 55, 55–56, 58
 differentiated from ependymomas, 40
Megaureter, 221, 221–222
Melena, 179
Meningiomas, neurofibromatosis type 2-related, 89, 90
Meningitis, 54, 124
Meningoceles, sacral/presacral, 68, 74
Meningomyeloceles, 74, 84
Metaiodobenzylguanidine (MIBG) scintigraphy
 of gray matter heterotopia, 18
 of neuroblastoma, 207, 208, 209, 296
Middle ear, cholesteatomas of, 123, 123–124
Midsagittal ridge, palpable, 5, 5–6
Morquio syndrome, 88, 380
Moyamoya disease, 43, 43–44
MRI. *See* Magnetic resonance imaging
Mucopolysaccharidosis type 1, 379, 379–380
Mucus plugs, 280, 299
Muscle-eye-brain disease, 42
Muscular dystrophies, 320
 Becker, 320
 Duchenne, 319, 320
 type 2 lissencephalies associated with, 42
Myelomeningoceles, 81–82
Myocarditis, 320
Myositis
 circumscribed posttraumatic ossifying, 386
 ossificans progressiva, 385, 385–386
N
Nasal dermoid sinus, 47, 47–48
Nasal masses, congenital, 47, 47–48
Necrotizing enterocolitis, 163, 163–164
Neonates
 biliary ductal cysts in, 162
 brachial plexopathy in, 63–64
 choanal atresia in, 99, 99–100
 chondrodysplasia punctata in, 381–382, 381–382
 chondroectodermal dysplasia in, 383, 383–384
 congestive heart failure in, 3, 3–4
 D-transposition of the great vessels in, 323, 323–324
 esophageal atresia with tracheoesophageal fistula in, 169, 169–171
 hypoplastic left heart syndrome in, 325, 325–326
 imperforate anus in, 67
 myelomeningocele/Chiari II malformation in, 81, 81–82
 nasal obstruction in, 99–100
 necrotizing enterocolitis in, 163, 163–164
 osteomyelitis in, 80
 osteopetrosis in, 369–370
 posterior urethral valves in, 195–197
 ventricular septal defects in, 313, 313–314
Nephroblastomatosis, 190, 226
Nephromas, mesoblastic, 190, 225, 225–226
Nephrostomy, percutaneous, 361, 361–362
Neural migration anomalies, 27–28
Neuroblastomas, 207–208, 207–209
 differential diagnosis of, 188, 190, 292
 metastatic, 108
 thoracic, 295, 295–296
Neurofibromatosis type 1, 29, 29–30
 hypothalamic gliomas associated with, 38
 spinal radiographic findings in, 69, 69–70
Neurofibromatosis type 2, intramedullary tumors associated with, 89, 89–90
Noonan syndrome, 393, 393–394
Norwood II palliation procedure, 326
Nuclear medicine venography, of collecting system duplication/ectopic ureter/ureterocele, 191
O
Oligohydramnios, 156
Ophthalmoplegia, Leigh disease-related, 33
Opsoclonus-myoclonus, 209
Optic nerve, hypoplasia of, 9, 9–10
Orbit
 cellulitis of, 97, 97–98
 metastases to, 107, 107–108
 rhabdomyosarcoma of, 116
Osteogenesis imperfecta, 88, 375–376, 375–377
Osteoid osteoma, ablation of, 349–350, 349–351
Osteomyelitis, 269, 269–270
 differentiated from Ewing sarcoma, 252
 of the frontal bone, 48
 neonatal, 80
 osteopetrosis-related, 370
 vertebral, 79, 79–80
Osteopetrosis, 369, 369–370
Osteosarcomas, 252, 275, 275–276
Ovarian torsion, 217, 217–218
P
Pachygyria, 28
Papilledema, 55, 57
Paranasal sinus disease, 35, 36

- Patent ductus arteriosus, 314, 323, 324, 325
 left, 328
- Pelvis
 abscess in, 342
 “ping-pong paddle”-shaped, 379, 380
- Pericarditis, restrictive, 321
- Perineal masses, neonatal, 73, 73–74
- Perthes disease, 261, 261–262. *See also* Legg-Calvé-Perthes Disease
- PHACES syndrome, 120
- Pharyngitis, infectious mononucleosis-related, 101, 102
- Phleboliths, 345
- Pierre Robin sequence, 170
- Pinna, hypoplastic, 105
- Pituitary lesions, 12
- Plagiocephaly, 13, 13–14
- Platyspondyly, 88
- Pleural effusions, 285, 286, 304
 parapneumonic, 353, 353–354
- Pneumomediastinum, meconium aspiration-related, 306
- Pneumonia
 acute chest syndrome-related, 304
 differentiated from acute chest syndrome, 304
 as parapneumonic effusion cause, 354
 round, 289, 289–290
 as posterior mediastinal mass mimic, 296
- Pneumoperitoneum, necrotizing enterocolitis-related, 164
- Pneumothorax, 276, 305, 306, 308
- Pneumotosis, 164
- Polydactyly, 383, 384
- Polyhydramnios, 168
- Polymicrogyria, 27, 27–28, 42
- Polyps, antrochoanal, 117, 117–118
- Polysplenia, 334
- Port-wine stain, 51–52
- Positron emission tomography, of Ewing sarcoma, 252
- Posterior fossa tumors
 ependymomas, 39, 39–40
 most common, 58
- Precocious puberty, 12
- Premature infants
 dolichocephaly in, 6
 esophageal atresia with tracheoesophageal fistula associated in, 171
 heterotaxy in, 333, 333–334
 necrotizing enterocolitis in, 163, 163–164
 respiratory distress syndrome in, 283–284
 subependymal/intraventricular hemorrhage in, 45–46
- Primitive neuroectodermal tumors (PNETs), 56
- Probst bundles, 23
- Propranolol, as hemangioma treatment, 120
- Proptosis, acute myelogenous leukemia-related, 107, 107–108
- Prune-belly syndrome, 196, 222
- Pseudomeningoceles, 63, 64
- Pseudotumor, orbital inflammatory, 108
- Pulmonary artery
 enlarged, 325
 left, anomalous, 327
 stenosis of, 324
 transposition of, 323
- Pulmonary sequestration, 291, 291–292, 302
- Pulmonary sling, 327, 327–328
- Pulmonary venous return
 partial anomalous, 330
 total anomalous, 329, 329–330
- Pyelonephritis, 214, 215, 223, 223–224
- Pyloric spasm, 144
- Pyloric stenosis, 143, 143–144
- R**
- Radionuclide cystography, of vesico-ureteral reflux, 214
- Radius, thrombocytopenia-absent, 387, 387–388
- Rathe cleft, cysts of, 12
- Renal artery stenosis, 357, 358
- Renal scintigraphy, of pyelonephritis, 224
- Renal stones, as ureteropelvic junction obstruction cause, 229
- Renal tumors, multilocular cystic, 226
- Renal vein, thrombosis of, 188, 190
- Renography
 of multicystic dysplastic kidney, 237, 238
 of ureteropelvic junction obstruction, 227, 228, 229
- Respiratory distress syndrome, 99–100, 283, 283–284
- Retropharyngeal space, abscess of, 113, 113–114
- “Reverse-3” sign, 336
- Rhabdoid tumors, 190
- Rhabdomyosarcomas, 235, 235–236
 alveolar, 116
 differential diagnosis of, 102, 108, 236
 embryonal, 116
 of head and neck region, 115, 115–116
 orbital, 116
 pleomorphic, 116
- Rib, fractures of, 264, 265
- Roberts’ syndrome, 388
- S**
- Sacrum
 agenesis of, 68
 anomalies of, 68, 74
 “sickle deformity” of, 68
- Sagittal craniosynostosis, 5, 5–6
- Salter-Harris classification, of physeal fractures, 246, 274
- Sanfilippo syndrome, 380
- Sarcomas, granulocytic, 107, 107–108
- Scaphocephaly, 6
- Schizencephaly, 22, 28, 49, 49–50
 closed-lip, 50
- Schönlein-Henoch purpura, 134, 361
- Schwannomas, acoustic, 89, 90
- Scimitar syndrome, 330
- Scintigraphy. *See also* Bone scintigraphy
 hepatobiliary, 165, 166
 metaiodobenzylguanidine (MIBG)
 of gray matter heterotopia, 18
 of neuroblastoma, 207, 208, 209, 296
 technetium-99m
 of Meckel’s diverticulum, 153, 154
 of osteosarcoma, 275
 technetium-99m dimercaptosuccinic acid (DMSA), of renal scarring, 231, 232
 technetium-99m methylene diphosphate, of Ewing sarcoma, 251
- Sclerotherapy
 for lymphatic malformations, 359, 359–360
 for venous malformation, 345, 345–346
- Seizures
 corpus callosum agenesis-related, 23
 cytomegalovirus infection-related, 20
 gray matter heterotopia-related, 17–18
 Leigh disease-related, 34
 lissencephaly-related, 41
 neuronal migration anomaly-related, 27, 28
 schizencephaly-related, 49, 50
 Sturge-Weber syndrome-related, 51, 52
 subdural empyema-related, 35, 36
 tuberous sclerosis-related, 59, 60
- Septal defects, heterotaxy-related, 334
- Septum pellucidum, absent, 10
- Sickle cell disease
 acute chest syndrome of, 303, 303–304
 moyamoya disease associated with, 43–44
- “Signet ring sign,” 299, 300
- Single photon emission tomography (SPECT), of renal scarring, 232
- Sinus venosum defects, 314
- Situs, 334
- Skeletal surveys, of child abuse-related injuries, 264–265
- Skull fractures, child abuse-related, 16
- Slipped capital femoral epiphysis, 271, 271–272
- Sly syndrome, 380
- Small bowel
 atresia of, 145, 145–146
 duplication cysts of, 152
- Small left colon syndrome, 149, 150
- Spinal cord
 astrocytoma of, 93, 93–94
 split. *See* Diastematomyelia
 tethered. *See* Tethered cord syndrome
- Spinal dysraphism, 220
- Spine radiology, 63–94
- Spine. *See also* Cervical spine; Lumbar spine; Lumbosacral spine; Thoracic spine; Thoracolumbar spine
 imperforate anus-associated deformities of, 157
 stenosis of, 77, 78
- Spleen, infectious mononucleosis-related rupture of, 102
- Splenomegaly, infectious mononucleosis-related, 102

Staphylococcus aureus, as vertebral osteomyelitis causal organism, 80

Stenosis
anal, 74
rectal, 67, 69
spinal, 77, 78

Sternocleidomastoid muscle, fibromatosis colli of, 109–110, 110

Stevens-Johnson syndrome, 122

Stippled epiphyses syndrome. *See* Chondrodysplasia punctata

Stomach, duplication cysts of, 152

Streptococcal group B infection, as respiratory distress syndrome mimic, 280

Streptococcus pneumoniae, as round pneumonia cause, 290

Stridor, croup (laryngotracheobronchitis)-related, 125, 126

Sturge-Weber syndrome, 51, 51–52

Subependymal nodules, tuberous sclerosis-related, 59, 60

Subtalar joints, coalition of, 249, 249–250

Superior mesenteric artery and vein, in volvulus, 178

Superior vena cava
in heterotaxy, 333, 334
peripherally-inserted central catheter in, 355

Superior vermian cistern, cysts of, 4

Suprasellar masses, 11, 11–12
types of, 37, 37–38

Sutures, closure of, in sagittal synostosis, 5, 5–6, 13, 13–14

Syndromes, 367–394

Syringohydromyelia, 82

T

Tarsal coalition, 249, 249–250

TAR (thrombocytopenia-absent radius) syndrome, 387, 387–388

Technetium-99m dimercaptosuccinic acid (DMSA) scintigraphy, of renal scarring, 231, 232

Technetium-99m mercaptoacetyltriglycine (MAG3) tracer, 229

Technetium-99m methylene diphosphate scintigraphy, of Ewing sarcoma, 251

Technetium-99m scintigraphy
of Meckel's diverticulum, 153, 154
of osteosarcoma, 275

Temporal bone, fractures of, 127, 127–128

Teratomas
mediastinal, 297, 297–298
presacral, 68
sacroccygeal, 73, 73–74

Testicular torsion, 186, 241, 241–242

Tethered cord syndrome, 68, 85, 85–86

Tetralogy of Fallot, 317, 317–318

Thoracic spine
astrocytoma of, 93, 93–94
diastematomyelia of, 83, 83–84
epidural abscess of, 65, 65–66

Thoracolumbar spine, vertebra plana of, 87, 87–88

Thrombocytopenia-absent radius (TAR) syndrome, 387, 387–388

Thymic masses, 286

Thymolipomas, differentiated from teratomas, 298

Thymomas, differentiated from teratomas, 298

Thyroglossal duct, cysts of, 129, 129–130

Toddler fracture, 255, 255–256

Tonsils, in infectious mononucleosis, 101, 102

TORCH infections, 8, 18. *See also* Cytomegalovirus infections

Torsion, of appendix testis, 185, 185–186

Torticollis, 129, 130
congenital muscular (fibromatosis colli), 109, 109–110

Total anomalous pulmonary venous return, 329, 329–330

Trachea, stenosis of, 327, 328

Tracheal rings, 327, 328

Transposition of the great vessels, 323, 323–324

Treacher Collins syndrome, 100, 106

Trigeminal nerve, schwannomas of, 89, 90

Trisomy 18, 182

Trisomy 21, 148

Trisomy 21 (Down syndrome), 77, 77–78, 156, 157, 170

Tuber cinereum, hamartomas of, 38

Tuberous sclerosis, 59, 59–60
differential diagnosis of, 18, 20, 60

Turcot syndrome, 56

Turner syndrome, 394

U

Ulcerative colitis, differentiated from Crohn's disease, 176

Ultrasound
abdominal abscess, 341, 342
adrenal hemorrhage, 187, 188
appendix/appendicitis, 159, 159–160
autosomal recessive polycystic kidney disease, 211, 212
biliary atresia, 165, 166
brachial cleft cysts type II, 103, 104
choledochal cysts, 161, 162
collection system duplication/ectopic ureter/ureterocele, 191–192, 191–193
congenital lobar overinflation, 308
congenital pulmonary airway malformations (CPAMs), 288
corpus callosum agenesis, 24
developmental dysplasia of the hip, 253, 254
diastematomyelia, 84
duodenal hematomas, 174
duplication cysts, 151, 152
fibromatosis colli, 109–110, 110
hepatoblastomas, 181, 182
holoprosencephaly, 22
hydrocolpos, 203
hydronephrosis, 361
imperforate anus, 155, 156

intussusception, 133, 133–134, 133–135

juvenile idiopathic arthritis, 258

lymphatic malformations, 359

malrotation with midgut volvulus, 178

meconium ileus, 141, 142

megaureter, 221, 222

mesoblastic nephroma, 225, 226

multicystic dysplastic kidney, 237, 238

myelomeningoceles, 82

neuroblastomas, 207, 208

osteoid osteoma ablation, 351

ovarian cysts, 206

ovarian torsion, 217, 217–218

parapneumonic effusion, 353

periventricular leukomalacia, 7, 7–8

posterior urethral valves, 195, 196

pyelonephritis, 223, 224

pyloric stenosis, 143–144

renal scarring, 231, 232

rhabdomyosarcomas, 235, 236

septic arthritis, 363

spinal, in imperforate anus patients, 157

subependymal/intraventricular hemorrhage, 45, 46

thanatophoric dysplasia, 373–374

torsion of the appendix testis, 185, 186

tuberous sclerosis, 60

urachal anomalies, 199, 200

ureteropelvic junction obstruction, 227, 228, 229

urolithiasis, 219, 220

vesicoureteral reflux, 213

Wilms' tumor, 189, 190

Urachus, anomalies of, 199, 199–201

Ureterocele, 191–192, 191–193

Ureteropelvic junction obstruction, 196, 220, 227–228, 227–229

Ureterovesical junction obstruction, 196, 220, 221, 229

Ureters, ectopic, 191–192, 191–193

Urethral strictures, differentiated from posterior urethral valves, 196, 197

Urethral valves, posterior, 195–196, 195–197

Urinary collecting system, duplicated, 191–192, 191–193
Weigert-Meyer rule regarding, 193

Urinary tract infections
differentiated from acute pyelonephritis, 224
as renal scarring cause, 231–232
ureteropelvic junction obstruction-related, 228
as urolithiasis risk factor, 220
as vesicoureteral reflux cause, 214, 215

Urolithiasis, 219, 219–220

V

VACTERL syndrome, 156, 170

Vaginal outlet obstruction, 204

Vascular rings, 311, 312, 328

VATER anomalies, 228

VCUG. *See* Voiding cystourethrography

Vein of Galen, malformations of, 3, 3–4

Venography
 of collecting system duplication/ectopic ureter/ureterocele, 191
 of occipital encephaloceles, 25, 25
 Venous malformations, sclerotherapy for, 345, 345–346
 Ventricular septal defects, 313, 313–315, 317
 Ventriculomegaly, Chiari II malformation-related, 82
 Vertebral bodies
 malignancy-related destruction of, 80
 subluxation of, 76
 Vertebra plana, 87, 87–88
 Vesicoureteral reflux, 195, 197, 213, 213–215
 antimicrobial prophylaxis for, 224
 as renal scarring cause, 231, 232
 Voiding cystourethrography
 after febrile urinary tract infections, 224
 megaureter, 222
 multicystic dysplastic kidney, 238
 posterior urethral valves, 195, 196
 renal scarring, 231
 ureteroceles, 191, 192, 193
 vesicoureteral reflux, 213, 214, 231, 232
 Volvulus
 duodenal, 168
 midgut, with malrotation, 177–178, 177–179

W

Walker-Warburg syndrome, 26, 42
 “Whirlpool sign,” 178, 179, 242
 Whitaker test, 362
 Williams syndrome, 394
 Wilms’ tumor, 189, 189–190, 226

X

X-rays
 achondroplasia, 367
 appendix/appendicitis, 160
 chest
 acute chest syndrome, 303, 304
 bronchogenic cysts, 293
 cardiomegaly, 313, 314
 cleidocranial dysplasia, 371
 coarctation of the aorta, 336
 congenital diaphragmatic hernia, 301, 302
 congenital lobar overinflation, 307
 cystic fibrosis, 299, 300
 double aortic arch, 311
 esophageal atresia with tracheoesophageal fistula, 169, 169–170
 foreign body aspiration, 279
 heterotaxy, 333
 ingested foreign bodies, 137
 lymphoma, 285, 286
 meconium aspiration, 305, 306
 meconium ileus, 141, 142
 neonatal congestive heart failure, 3, 3–4
 neuroblastoma, 295, 296
 Noonan syndrome, 393
 osteopetrosis, 369
 pulmonary sequestration, 291, 292
 pulmonary sling, 327, 328
 respiratory distress syndrome, 283, 284
 round pneumonia, 289, 290
 teratoma, 297, 298
 total anomalous pulmonary venous return, 330
 ventricular septal defects, 313

child abuse-related injuries, 263, 264–265
 chondroblastomas, 267
 chondrodysplasia punctata, 381–382
 congenital diaphragmatic hernia, 301
 croup (laryngotracheobronchitis), 125, 125–126
 developmental dysplasia of the hip, 253, 254
 duodenal hematomas, 173, 174
 elbow fractures, 245
 epiglottitis, 121, 121–122
 Hirschsprung disease, 147
 imperforate anus, 155
 intussusception, 134
 juvenile idiopathic arthritis, 257, 258
 Legg-Calvé-Perthes disease, 261, 262
 meconium plug syndrome, 149, 150
 mucopolysaccharidosis type 1, 379
 myositis ossificans progressiva, 385
 necrotizing enterocolitis, 163, 164
 neuroblastomas, 296
 osteogenesis imperfecta, 375–376
 osteomyelitis, 269, 270
 osteosarcoma, 275, 276
 physeal fractures, 273, 274
 polyostotic fibrous dysplasia, 389, 390
 retropharyngeal abscess, 113, 113–114
 of round pneumonia, 290
 slipped capital femoral epiphysis, 271, 272
 small bowel atresia, 145, 146
 tarsal coalition, 249, 250
 thanatophoric dysplasia, 373–374
 toddler fractures, 255, 256

Z

Zellweger syndrome, 382